

RIKEN R-CCS  
Annual Report FY2019  
R-CCS Research Activities

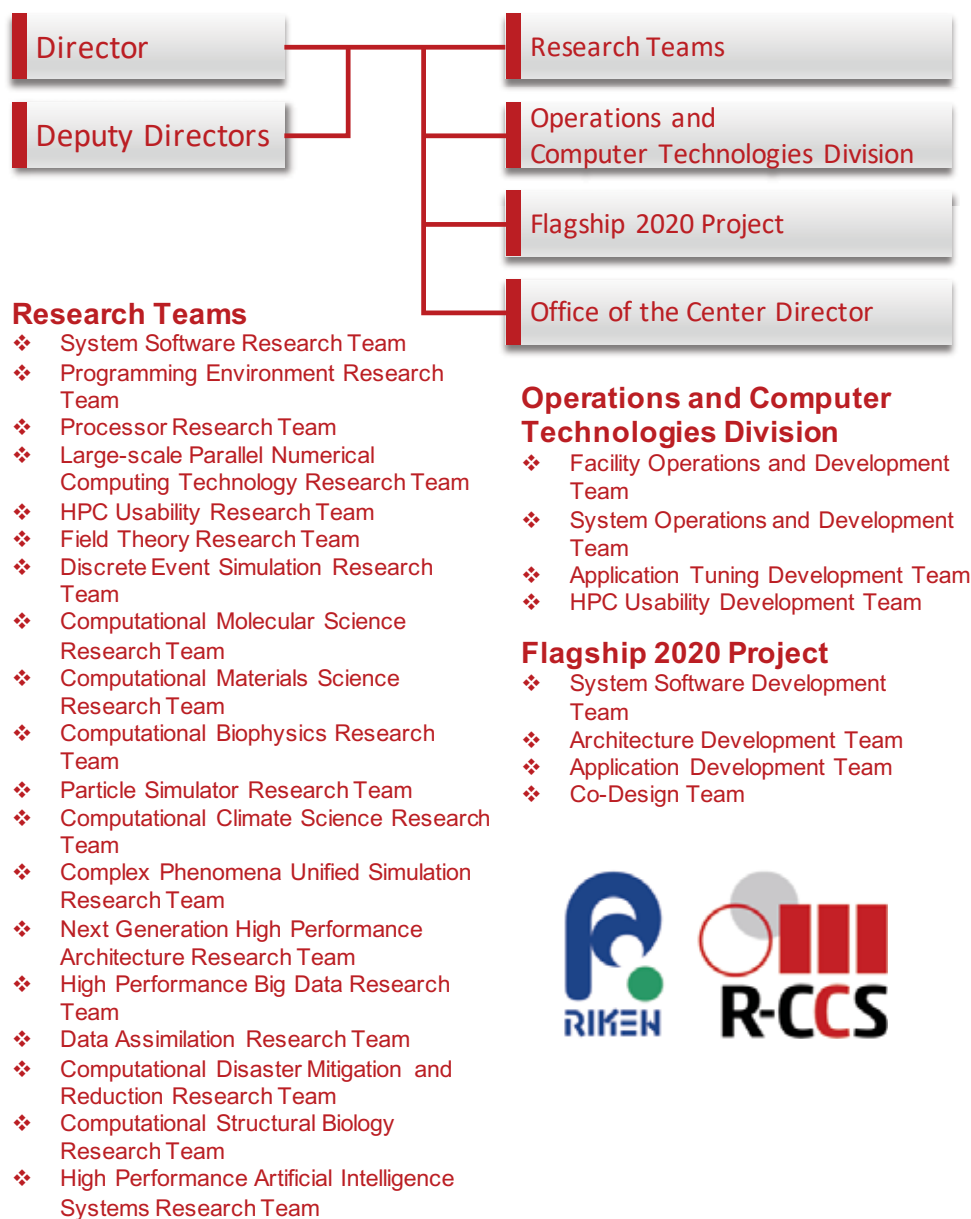
## Preface

The objectives of the RIKEN Center for Computational Science (R-CCS) are threefold, centered around supercomputing: one is to target high performance computation itself as a scientific objective, or namely, the “Science of Computing”; another is to apply the enormous computational power thus obtained to solve difficult scientific problems, or namely the “Science by Computing”; finally, to collaborate with other scientific disciplines that contribute to advances both sciences, or namely, the “Science for Computing”. Our goal is to be recognized as one of the global leadership research centers to advance high-end computational science in this regard.

Computational science employs multitudes of methodologies to essentially recreate various phenomena as computational activities inside machines, thereby allowing to challenge difficult problems encountered by mankind. For example, we could model a phenomenon by a set of physical/mathematical formulas, and the machine-driven solution to the formulas will result in direct ‘simulation’ of the phenomenon; alternatively, we could analyze the massive data measured on a phenomenon by scientific instruments, and further extrapolate future trends, or so-called ‘data science’ methodology; furthermore, we could train our ‘artificial intelligence’ to attain higher-level insights on the data, both simulated and/or analyzed. Here supercomputers will accelerate all such methodologies by many orders of magnitude, allowing synthesis of innovations to tackle the most difficult problems that are of interest to the greater society, and R-CCS intends to be at the forefront of such activities.

Moreover, innovative Information Technologies (IT) researched and developed to advance supercomputing is not only applicable to itself, but rather are the bleeding-edge technologies to advance the entire IT as a whole, from Clouds to the Edge, and thus will contribute to the massive improvement of the economy and our daily lives that are now heavily reliant on IT. We intend to collaborate with other leadership centers of the world to play a central role in advancing IT for the society at large.

## R-CCS Organization





# Contents

<b>I</b>	<b>Research Division</b>	<b>15</b>
<b>1</b>	<b>System Software Research Team</b>	<b>17</b>
1.1	Members	17
1.2	Overview of Research Activities	17
1.3	Research Results and Achievements	17
1.3.1	RIKEN-MPICH	17
1.3.2	Sharing Virtual Address Space	19
1.3.3	IHK/McKernel	21
1.3.4	Utility Thread Offloading Interface	22
1.4	Schedule and Future Plan	22
1.5	Publications	22
1.5.1	Articles/Journal	22
1.5.2	Conference Papers	24
1.5.3	Posters	24
1.5.4	Invited Talks	24
1.5.5	Oral Talks	24
1.5.6	Software	24
1.5.7	Patents	24
<b>2</b>	<b>Programming Environment Research Team</b>	<b>25</b>
2.1	Members	25
2.2	Overview of Research Activities	25
2.3	Research Results and Achievements	26
2.3.1	XcalableMP on Fugaku	26
2.3.2	Accuracy Improvement of Memory System Simulation for Modern Processor	28
2.3.3	Development optimization algorithm for grid graph in Order/Degree problem	31
2.3.4	HOPE: A Fault-Tolerant Parallel Execution Model Based on Hierarchical Omission	32
2.4	Schedule and Future Plan	33
2.5	Publications	34
2.5.1	Articles/Journal	34
2.5.2	Conference Papers	34
2.5.3	Posters	34
2.5.4	Invited Talks	34
2.5.5	Software	34
<b>3</b>	<b>Processor Research Team</b>	<b>35</b>
3.1	Members	35
3.2	Overview of Research Activities	35
3.2.1	Aim of Team	35
3.2.2	Overview of Research Activities FY2019	36
3.3	Research Results and Achievements	37
3.3.1	Investigation and exploration of coarse-grained reconfigurable architectures (CGRAs)	37
3.3.2	FPGA cluster	37
3.3.3	FPGA-based Applications	39
3.4	Schedule and Future Plan	40

3.5	Publications . . . . .	41
3.5.1	Articles/Journal . . . . .	41
3.5.2	Conference Papers . . . . .	41
3.5.3	Posters / Papers with Abstract Review . . . . .	41
3.5.4	Invited Talks (keynote, plenary talk, invited talk, panelist position talk) . . . . .	42
3.5.5	Other Publication Articles . . . . .	42
3.5.6	Oral Talks (with non-reviewed papers) . . . . .	42
<b>4</b>	<b>Large-scale Parallel Numerical Computing Technology Research Team</b>	<b>45</b>
4.1	Members . . . . .	45
4.2	Research Activities . . . . .	45
4.2.1	Application of the Jacobi Rotation Kernel for the eigen- and singular value computations	46
4.2.2	Parallel three-dimensional FFT on a massive-scale system like K . . . . .	47
4.2.3	Analysis and development of software of the HPL-AI benchmark . . . . .	47
4.2.4	Minimal-precision computing . . . . .	47
4.2.5	Accurate and reproducible BLAS routines and CG method . . . . .	48
4.2.6	DGEMM using Tensor Cores . . . . .	49
4.2.7	FPGA-based matrix multiplier with task parallelism . . . . .	49
4.2.8	FPGA-based acceleration of FDTD sound field rendering . . . . .	50
4.2.9	Other activities . . . . .	50
4.3	Schedule and Future Plan . . . . .	50
4.4	Publications . . . . .	51
4.4.1	Articles . . . . .	51
4.4.2	Oral talks and Poster presentations . . . . .	52
4.4.3	Award . . . . .	53
4.4.4	Other publication . . . . .	54
4.4.5	Software (released as of April 2020) . . . . .	54
<b>5</b>	<b>HPC Usability Research Team</b>	<b>55</b>
5.1	Members . . . . .	55
5.2	Research Activities . . . . .	55
5.2.1	Development of the Pyne Parallel Programming Framework . . . . .	55
5.2.2	A Digital Twin for Operation Planning of the Cooling Facility . . . . .	57
5.3	Schedule and Future Plan . . . . .	61
5.4	Publications . . . . .	61
5.4.1	Papers (refereed) . . . . .	61
5.4.2	Posters (refereed) . . . . .	62
5.4.3	Presentations . . . . .	62
5.4.4	Patents . . . . .	62
<b>6</b>	<b>Field Theory Research Team</b>	<b>63</b>
6.1	Members . . . . .	63
6.2	Overview of Research Activities . . . . .	63
6.3	Research Results and Achievements . . . . .	64
6.3.1	Lattice QCD codes and algorithms . . . . .	64
6.3.2	Finite Temperature QCD with domain wall fermions . . . . .	65
6.3.3	Proton decay matrix elements . . . . .	66
6.3.4	Miscellaneous LQCD developments . . . . .	67
6.4	Schedule and Future Plan . . . . .	68
6.4.1	Algorithm and code development for the chiral fermion simulation in QCD for Fugaku . .	68
6.4.2	QCD phase diagram with chiral fermion simulations . . . . .	68
6.4.3	Collaboration on physics applications . . . . .	68
6.5	Publications . . . . .	69
6.5.1	Articles/Journal . . . . .	69
6.5.2	Conference Papers . . . . .	69
6.5.3	Posters . . . . .	70
6.5.4	Invited Talks . . . . .	70

6.5.5	Oral Talks . . . . .	70
6.5.6	Software . . . . .	71
<b>7</b>	<b>Discrete-Event Simulation Research Team</b>	<b>73</b>
7.1	Members . . . . .	73
7.2	Research Activities . . . . .	73
7.2.1	Job management applications, OACIS and CARAVAN . . . . .	74
7.2.2	Traffic simulation and analysis . . . . .	74
7.2.3	Quantum computer simulation . . . . .	76
7.2.4	Other activities . . . . .	78
7.3	Schedule and Future Plan . . . . .	78
7.4	Publications . . . . .	79
7.4.1	Articles . . . . .	79
7.4.2	Invited talks . . . . .	79
7.4.3	Oral talks . . . . .	80
7.4.4	Poster presentation . . . . .	80
7.4.5	Other presentations . . . . .	80
7.4.6	Award . . . . .	80
7.4.7	Software . . . . .	80
<b>8</b>	<b>Computational Molecular Science Research Team</b>	<b>81</b>
8.1	Members . . . . .	81
8.2	Overview of Research Activities . . . . .	81
8.2.1	Development of Original Molecular Theory . . . . .	81
8.2.2	Quantum Chemistry Software NTChem . . . . .	82
8.3	Research Results and Achievements . . . . .	82
8.3.1	Trajectory Surface Hopping Molecular Dynamics Simulation by Spin-Flip Time-Dependent Density Functional Theory . . . . .	82
8.3.2	Quantum Mechanical/Molecular Mechanical Trajectory Surface Hopping Molecular Dynamics Simulation by Spin-Flip Time-Dependent Density Functional Theory . . . . .	83
8.3.3	Electron dynamics method using a locally projected group diabatic Fock matrix for molecules and aggregates . . . . .	83
8.3.4	Complexity Reduction in Density Functional Theory Calculations of Large Systems . . . . .	84
8.3.5	Molecular Design for Solar Cell Materials . . . . .	84
8.3.6	Molecular Design for Highly-functional Biopolymer Materials . . . . .	85
8.3.7	Construction of Molecular Orbital Method Consistent with Quantum Electrodynamics . . . . .	86
8.3.8	Multi-Scale Simulation to Predict Biodegradability of Plastics . . . . .	87
8.3.9	Theoretical and computational investigations of geometrical, electronic and spin structures of the $\text{CaMn}_4\text{O}_X$ ( $X=5, 6$ ) cluster in the Kok cycle $S_i$ ( $i = 0-3$ ) of oxygen evolving complex of photosystem II . . . . .	88
8.3.10	Domain-Based Local Pair Natural Orbital CCSD(T) Calculations of Strongly Correlated Electron Systems: Examination of Dynamic Equilibrium Models Based on Multiple Intermediates in $S_1$ State of Photosystem II . . . . .	88
8.3.11	Domain-Based Local Pair Natural Orbital CCSD(T) Calculations of Six Different $S_1$ Structures of Oxygen Evolving Complex of Photosystem II. Proposal of Multi-Intermediate Models for the $S_1$ State . . . . .	89
8.3.12	Domain-Based Local Pair Natural Orbital CCSD(T) Calculations of Fourteen Different $S_2$ Intermediates for Water Oxidation in the Kok Cycle of OEC of PSII. Re-visit to One LS-two HS Model for the $S_2$ State . . . . .	89
8.3.13	Quantum-Mechanical Study of Energies, Structures and Vibrational Spectra of the HF Complexed with Dimethyl Ether . . . . .	89
8.3.14	IR Spectra of Crystalline Nucleobases. Combination of Periodic Harmonic Calculations with Anharmonic Corrections Based on Finite Models . . . . .	90
8.3.15	A Comparison of the Hydrogen Bond Interactions Dynamics in the Guanine and Cytosine Crystals: Ab Initio Molecular Dynamics and Spectroscopic Study . . . . .	90
8.3.16	Conversion Reaction of Polyoxometalates from Anderson Structure to Keggin Structure . . . . .	90
8.4	Schedule and Future Plan . . . . .	92

8.4.1	Complexity Reduction in Density Functional Theory Calculations of Large Systems . . .	92
8.4.2	Molecular Design for Solar Cell Materials . . . . .	92
8.4.3	Molecular Design for Highly-functional Biopolymer Materials . . . . .	92
8.4.4	Construction of Molecular Orbital Method Consistent with Quantum Electrodynamics . .	92
8.4.5	Multi-Scale Simulation to Predict Biodegradability of Plastics . . . . .	92
8.5	Publications . . . . .	92
8.5.1	Articles/Journal . . . . .	92
8.5.2	Posters . . . . .	93
8.5.3	Invited Talks . . . . .	94
8.5.4	Oral Talks . . . . .	94
<b>9</b>	<b>Computational Materials Science Research Team</b>	<b>95</b>
9.1	Members . . . . .	95
9.2	Overview of Research Activities . . . . .	95
9.3	Research Results and Achievements . . . . .	96
9.3.1	Large-scale QMC simulations for interacting fermions . . . . .	96
9.3.2	Massively parallel DMRG algorithms for quantum many-body systems . . . . .	96
9.3.3	Controlled dynamics in quantum many-body systems . . . . .	97
9.3.4	Tensor network method for many-body systems . . . . .	98
9.4	Schedule and Future Plan . . . . .	98
9.4.1	Large-scale QMC simulations for interacting fermions . . . . .	98
9.4.2	Massively parallel DMRG algorithms for quantum many-body systems . . . . .	99
9.4.3	Controlled dynamics in quantum many-body systems . . . . .	100
9.4.4	Tensor network method for many-body systems . . . . .	100
9.5	Publications . . . . .	101
9.5.1	Articles/Journal . . . . .	101
9.5.2	Invited Talks . . . . .	101
9.5.3	Oral Talks . . . . .	102
9.5.4	Posters . . . . .	102
9.5.5	Software . . . . .	103
<b>10</b>	<b>Computational Biophysics Research Team</b>	<b>105</b>
10.1	Members . . . . .	105
10.2	Overview of Research Activities . . . . .	105
10.3	Research Results and Achievements . . . . .	106
10.3.1	Development of GENESIS on Fugaku supercomputer . . . . .	106
10.3.2	Investigatio of the Reaction Pathway on the E1/E2 transition of $\text{Ca}^{2+}$ -ATPase . . . . .	107
10.3.3	Simulating large-amplitude transitions in proteins with a coarse-grained Gō-model . . . .	107
10.3.4	Theoretical Study of Lateral Diffusion of Heme on Lipid Bilayer . . . . .	110
10.3.5	Implementation of CG models in GENESIS . . . . .	110
10.3.6	Development of a singularity-free dihedral angle potential in CG . . . . .	111
10.4	Schedule and Future Plan . . . . .	111
10.5	Publications . . . . .	111
10.5.1	Articles/Journal . . . . .	111
10.5.2	Posters . . . . .	111
10.5.3	Invited Talks . . . . .	112
10.5.4	Oral Talks . . . . .	112
10.5.5	Software . . . . .	112
10.5.6	Patents . . . . .	112
<b>11</b>	<b>Particle Simulator Research Team</b>	<b>113</b>
11.1	Members . . . . .	113
11.2	Overview of Research Activities . . . . .	113
11.3	Research Results and Achievements . . . . .	115
11.3.1	High-performance gravitational N-body solver. . . . .	115
11.3.2	Particle Simulation Platform. . . . .	115
11.4	Schedule and Future Plan . . . . .	117

11.5	Publications . . . . .	117
11.5.1	Articles/Journal . . . . .	117
11.5.2	Software . . . . .	118
11.5.3	Patents . . . . .	118
<b>12</b>	<b>Computational Climate Science Research Team</b>	<b>119</b>
12.1	Members . . . . .	119
12.2	Overview of Research Activities . . . . .	119
12.3	Research Results and Achievements . . . . .	120
12.3.1	Research and development of SCALE . . . . .	120
12.3.2	The Hyogo-Kobe COE establishment project . . . . .	120
12.3.3	Numerical convergence for simulation of atmospheric deep moist convection . . . . .	120
12.3.4	Self-organization of moist convection in the idealized radiative-convective equilibrium simulation . . . . .	121
12.4	Schedule and Future Plan . . . . .	122
12.5	Publications . . . . .	123
12.5.1	Articles/Journal . . . . .	123
12.5.2	Oral Talks . . . . .	123
12.5.3	Posters . . . . .	123
12.5.4	Books . . . . .	124
12.5.5	Software . . . . .	124
<b>13</b>	<b>Complex Phenomena Unified Simulation Research Team</b>	<b>125</b>
13.1	Members . . . . .	125
13.2	Overview of Research Activities . . . . .	125
13.3	Research Results and Achievements . . . . .	128
13.3.1	Empirical analysis using unified analysis framework CUBE . . . . .	128
13.3.2	Verification analysis of Eulerian finite volume formulation using Lagrangian marker particles for compressible solid . . . . .	133
13.3.3	Biomechanics CFD–Development of unified coupled analysis methods into practical problems . . . . .	139
13.3.4	Speed-up and scale-up of fundamental methodology targeting post-K system . . . . .	145
13.3.5	Strategic development and deployment of industrial software for the construction of digital engineering test beds . . . . .	147
13.4	Schedule and Future Plan . . . . .	159
13.5	Publications . . . . .	160
13.5.1	Articles/Journal . . . . .	160
13.5.2	Conference Papers . . . . .	160
13.5.3	Posters . . . . .	161
13.5.4	Invited Talks . . . . .	161
13.5.5	Oral Talks . . . . .	161
13.5.6	Software . . . . .	161
13.5.7	Patents . . . . .	161
<b>14</b>	<b>Next Generation High Performance Architecture Research Team</b>	<b>163</b>
14.1	Members . . . . .	163
14.2	Overview of Research Activities . . . . .	163
14.3	Research Results and Achievements . . . . .	163
14.3.1	Real-chip evaluation of a scalable accelerator core for deep neural networks . . . . .	163
14.3.2	Neuromorphic graph processing for minimum weight perfect matching . . . . .	164
14.3.3	Power consumption analysis for low-Precision floating-point arithmetic on numerical codes . . . . .	165
14.4	Schedule and Future Plan . . . . .	166
14.5	Publications . . . . .	167
14.5.1	Articles/Journal . . . . .	167
14.5.2	Conference Papers . . . . .	167
14.5.3	Posters . . . . .	167
14.5.4	Invited Talks . . . . .	167

<b>15 High Performance Big Data Research Team</b>	<b>169</b>
15.1 Members	169
15.2 Overview of Research Activities	169
15.3 Research Results and Achievements	169
15.3.1 Improving Data Compression with Deep Predictive Neural Network for Time Evolutional Data	169
15.3.2 Breakdown of Modern HPC Applications: Less Double-Precision Floating-Point Units and Faster Memory are Needed	171
15.3.3 The First Supercomputer with HyperX Topology: A Viable Alternative to State-of-the-Art Fat-Trees Topologies	172
15.3.4 Counter-based Performance Extrapolation Toolchain	173
15.3.5 Optimizing Asynchronous Multi-level Checkpoint/Restart Configurations with Machine Learning	173
15.3.6 Evaluating the Relationship between System Utilization and Benefits of Combining Different Scheduling Policies with Backfilling	174
15.4 Schedule and Future Plan	176
15.5 Publications	176
15.5.1 Articles/Journal	176
15.5.2 Conference Papers	176
15.5.3 Posters	177
15.5.4 Invited Talks	177
15.5.5 Oral Talks	178
<b>16 Data Assimilation Research Team</b>	<b>179</b>
16.1 Members	179
16.2 Overview of Research Activities	180
16.3 Research Results and Achievements	182
16.3.1 Development of a real-time workflow of the big data assimilation system	182
16.3.2 Model parameter estimation with data assimilation using NICAM-LETKF	184
16.3.3 Application of machine learning methods to model bias correction: idealized experiments with the Lorenz-96 model	184
16.4 Schedule and Future Plan	186
16.5 Publications	187
16.5.1 Awards	187
16.5.2 Articles	187
16.5.3 Invited Talks	188
16.5.4 Oral Presentations	190
16.5.5 Poster Presentations	194
<b>17 Computational Disaster Mitigation and Reduction Research Team</b>	<b>197</b>
17.1 Members	197
17.2 Overview of Research Activities	197
17.3 Research Results and Achievements	198
17.3.1 Urban model development	198
17.3.2 Performance enhancement of finite-element seismic ground motion simulation for many-core wide-SIMD architecture	198
17.3.3 Debris flow simulation	199
17.4 Schedule and Future Plan	201
17.5 Publications	201
17.5.1 Articles/Journal	201
17.5.2 Conference Papers	201
17.5.3 Invited Talks	201
17.5.4 Oral Talks	201
17.5.5 Software	201
17.5.6 Patents	202

<b>18 Computational Structural Biology Research Team</b>	<b>203</b>
18.1 Members	203
18.2 Overview of Research Activities	203
18.3 Research Results and Achievements	204
18.3.1 Developments of computational tools for XFEL experimental data	204
18.3.2 Developments of computational tools for analyzing cry-EM experimental data	205
18.3.3 Modeling from AFM images	207
18.3.4 Molecular dynamics simulations of Tim21 protein for interpretation of low-resolution X-ray crystallographic data	207
18.4 Schedule and Future Plan	208
18.5 Publications	208
18.5.1 Articles/Journal	208
18.5.2 Invited Talks	209
18.5.3 Oral Talks	209
18.5.4 Poster Presentations	209
<b>19 High Performance Artificial Intelligence Systems Research Team</b>	<b>211</b>
19.1 Members	211
19.2 Overview of Research Activities	211
19.2.1 Research Topics	211
19.3 Research Results and Achievements	212
19.3.1 Massive Scale Deep Learning on Fugaku	212
19.3.2 Accelerating DL with 2nd Order Optimization and Distributed Training	212
19.3.3 A Software Systolic Array on GPUs	213
19.3.4 Scaling Distributed Deep Learning Workloads beyond the Memory Capacity with KARMA	215
19.3.5 Optimizing Collective Communication in DL Training	215
19.3.6 Training Large 3D CNNs with Hybrid Parallelism	216
19.3.7 Advanced and Scalable NLP Models	217
19.3.8 Performance evaluation of deep learning software and systems	218
19.3.9 Predicting GPU Performance Using Collaborative Filtering	219
19.4 Schedule and Future Plan	220
19.5 Publications	220
19.5.1 Articles/Journal	220
19.5.2 Conference Papers	220
19.5.3 Posters	221
19.5.4 Invited Talks	221
<b>II Operations and Computer Technologies Division</b>	<b>223</b>
<b>20 Facility Operations and Development Unit</b>	<b>225</b>
20.1 Members	225
20.2 Overview of Research Activities	225
20.3 Research Results and Achievements	226
20.3.1 Optimum operation of electric power	226
20.3.2 Improvements to the power usage effectiveness (PUE)	227
20.3.3 Facility Expansion Work	227
20.4 Schedule and Future Plan	228
20.5 Publications	228
20.5.1 Conference Papers	228
20.5.2 Posters	228
20.5.3 Oral Talks	228

<b>21 System Operations and Development Unit</b>	<b>229</b>
21.1 Members	229
21.2 Overview of Research Activities	229
21.3 Research Results and Achievements	230
21.3.1 Activities for Stable System Operation	230
21.3.2 Analysis and Utilization of Operation Logs	231
21.3.3 Improvement of Information provided to Users	232
21.3.4 Power-aware System Operation	232
21.3.5 Information Exchanges among HPC Centers	233
21.4 User support	233
21.5 Schedule and Future Plan	233
21.6 Publications	234
21.6.1 Conference Papers	234
21.6.2 Posters	234
21.6.3 Oral Talks	234
21.6.4 Software	234
<b>22 Application Tuning Development Unit</b>	<b>235</b>
22.1 Members	235
22.2 Overview of Research Activities	235
22.3 Research Results and Achievements	235
22.3.1 Activities related to the R-CCS software	235
22.3.2 Activities to establish a deep learning environment on the K computer and Fugaku supercomputer	236
22.3.3 Power consumption of the job	238
22.3.4 Efforts in the development of the Fugaku supercomputer	238
22.4 Schedule and Future Plan	240
22.4.1 R-CCS software center activities	240
22.4.2 Activities to establish a DL environment on the Fugaku supercomputer	240
22.5 Publications	240
22.5.1 Articles/Journal	240
22.5.2 Conference Papers	240
22.5.3 Posters	241
22.5.4 Invited Talks	241
22.5.5 Oral Talks	241
22.5.6 Software	241
22.5.7 Patents	241
22.5.8 Book	241
<b>23 HPC Usability Development Unit</b>	<b>243</b>
23.1 Members	243
23.2 Overview of Research Activities	243
23.3 Research Results and Achievements	244
23.3.1 Software Center	244
23.3.2 Large Data Visualization and Analysis	244
23.3.3 Workflow Management Software (WHEEL)	246
23.3.4 K Pre-Post Cloud (Data Analysis Servers using Virtualization Technology)	246
23.3.5 HPCI Shared Storage	247
23.3.6 Oracle Cloud FastConnect Service	247
23.3.7 Other Activities	248
23.4 Schedule and Future Plan	248
23.5 Publications	248
23.5.1 Articles	248
23.5.2 Oral Talks	249
23.5.3 Posters	249
23.5.4 Software	250

**III Flagship 2020 Project 251**

**24 Flagship 2020 Project 253**

- 24.1 Members . . . . . 253
  - 24.1.1 System Software Development Team . . . . . 253
  - 24.1.2 Architecture Development Team . . . . . 253
  - 24.1.3 Application Development . . . . . 254
  - 24.1.4 Co-Design . . . . . 254
- 24.2 Overview of Research Activities . . . . . 254
- 24.3 Target of System Development and Achievements in FY2019 . . . . . 255
- 24.4 International Collaborations . . . . . 257
  - 24.4.1 DOE/MEXT Collaboration . . . . . 257
  - 24.4.2 CEA . . . . . 257
- 24.5 Schedule and Future Plan . . . . . 258
- 24.6 Publications . . . . . 258
  - 24.6.1 Articles/Journal . . . . . 258
  - 24.6.2 Conference Papers . . . . . 258
  - 24.6.3 Posters . . . . . 258
  - 24.6.4 Invited Talks . . . . . 258
  - 24.6.5 Oral Talks . . . . . 258
  - 24.6.6 Software . . . . . 259
  - 24.6.7 Patents . . . . . 259



**Part I**  
**Research Division**



# Chapter 1

## System Software Research Team

### 1.1 Members

Yutaka Ishikawa (Team Leader)

Atsushi Hori (Senior Scientist)

Masamichi Takagi (Senior Scientist)

Balazs Gerofi (Research Scientist)

Takahiro Ogura (Research & Development Scientist)

### 1.2 Overview of Research Activities

The system software research has been conducted in cooperation with the System Software Development Team in the Flagship 2020 project. The team focuses on the research and development of an advanced system software stack not only for the "K" computer but also for toward exa-scale computing including Fugaku.

We have been mainly focusing on scalable high performance communication and file I/O libraries and/or middlewares. The former research topics, sharing virtual address space and IHK/McKernel light-weight kernel, have been almost taken over by the System Software Development Team, but the research results are shown here.

### 1.3 Research Results and Achievements

#### 1.3.1 RIKEN-MPICH

We have been implementing an MPI library, based on MPICH developed by Argonne National Laboratory, for the Fugaku supercomputer under the DoE/MEXT collaboration in order to provide MPICH-based MPI for Fugaku.

The MPICH implementation has two layers, so-called MPID and device layers as shown in Figure 1.1. Basically, the MPID layer implements all the MPI functionalities using the device interface. The device layer CH4 is the latest device implementation. It consists of network and shared memory implementation layers, named "netmod" and "shmmmod," respectively. The netmod layer consists of OFI (OpenFabrics Interfaces), UCX (Unified Communication X), and Portal network drivers. We support the OFI driver for the Tofu-D implementation. The "tofu" provider in OFI is our Tofu-D implementation. The almost same capabilities but much simpler user API is also provided, named "UTF."

##### 1.3.1.1 OFI

OFI (OpenFabrics Interfaces) is a framework for high-performance communication, and Libfabric is its API. To make the libfabric interface available for a new network interface, we just implement the low-level implementation module, called "provider." The latest version at writing time is v1.10.1, but we have been using v1.8.0.

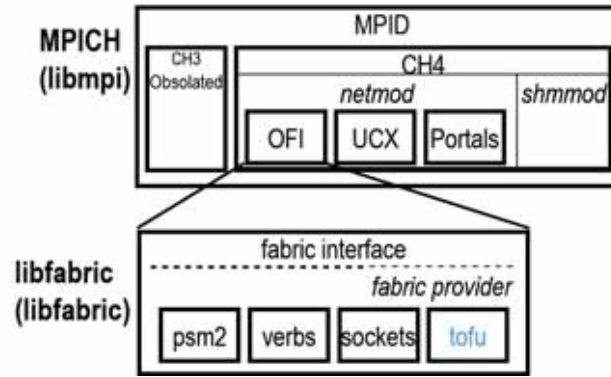


Figure 1.1: MPICH Software Architecture

The libfabric is capable of a point-to-point message passing function. A communication operation is divided into two phases: i) posting an operation, e.g., send, receive, and remote operation, and ii) receiving its completion. Those operations are non-blocking. There are four-type communication methods as follows:

1. **fi\_msg** (Message Queue), The message queue is a simple point-to-point message passing interface. Messages are enqueued and handled in the FIFO order. An interesting feature is a multi-receive capability. If a receive operation is issued with the multi-receive option, multiple messages can be received in the single receive operation. Incoming messages are sequentially stored in the receive buffer, and completion events are generated for received messages. In the MPICH implementation, this multi-receive feature is employed to realize an active message function for describing the MPI remote memory access feature such as MPI window.
2. **fi\_tagged** (Tagged Message Queue), The tagged message queue is the same concept of MPI communication. Each message has an integer value, called “tag.” The receive/send operation may specify the message tag. Sent messages are matched with its tag and receiver’s specified tag. MPICH uses this feature for the implementation of basic MPI point to point message function.
3. **fi\_rma** (Remote Memory Access), This is remote memory get and put features. MPI remote put and get operations can be implemented using this feature.
4. **fi\_atomic** (Atomic), Atomic operations are operations on the remote memory regions, such as atomic-add and compare-and-swap. Those operations can realize MPI atomic operations, such as MPI\_Fetch\_and\_op and MPI\_Compare\_and\_swap.

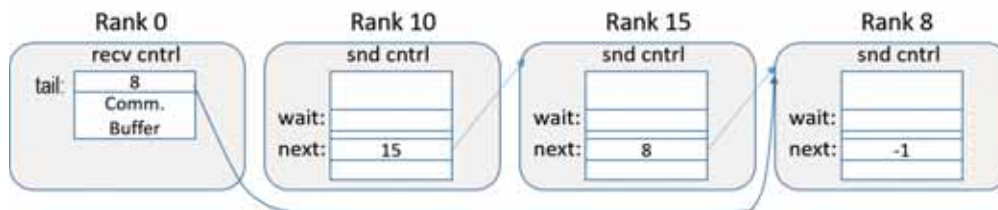


Figure 1.2: Chain Mode

### 1.3.1.2 uTofu and Tofu Provider

The “uTofu” library is the lowest user API for the Tofu-D interconnect interface. It provides the basic remote put and get operations, remote atomic operations, and barrier synchronization mechanisms. All memory regions, accessed by the Tofu-D interface, must be registered prior to the interface accessing. When a memory region is registered, the corresponding address defined by uTofu is associated with the registered virtual address. This address is called a “steering address.”

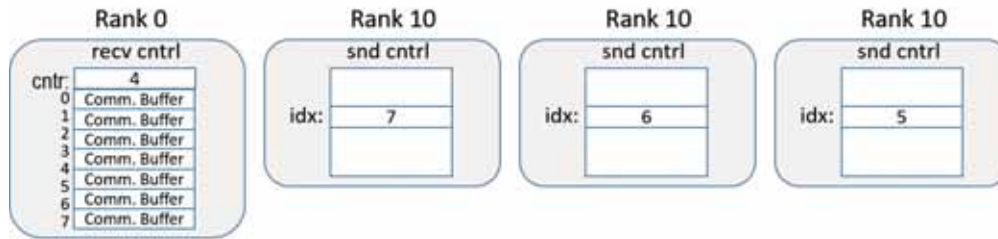


Figure 1.3: Reserve Mode

When a memory region is registered with a tag, an integer value, the steering address is identical over all other processes. We can create a common memory region over all processes using this feature without any extra processing. Unlike other interconnect interfaces, such as Infiniband, no message passing capability is provided in the Tofu-D interconnect. The `fi_msg` and `fi_tagged` operations are implemented in two ways as follows:

1. Chain mode

In this mode, the single receive buffer is shared by all the processes. The waiting processes form a distributed wait queue using the `uTofu` atomic operation as shown in Figure 1.2. In this figure, rank 10 is sending messages to rank 0, and rank 15 is waiting for completion of rank 10’s send operation, and rank 8 is the last process waiting for the other processes’ completions.

2. Reserve mode

Unlike the Chain mode, the limited common receive buffers are created to be accessed by other processes in the Reserve mode. Prior to send the first message to the receiver, the sender must reserve a receive buffer from the common receive buffers using the `uTofu` atomic operation. The reserved receive buffer is never freed. Figure 1.3 depicts the same situation of Figure 1.2. In this figure, the number of the common receive buffers is eight, and three of them have been reserved for ranks, 10, 15, and 8.

1.3.1.3 Implementation Status

The “`tofu`” driver and “`UTF`” have been implemented in FY2019. In FY2020, after evaluating those implementations, we will optimize those libraries.

1.3.2 Sharing Virtual Address Space

The two most common parallel execution models are multiprocess (MPI) and multithread (OpenMP). The multiprocess model allows each process to own a private address space, and the multithreaded model shares all address space by default. In the multiprocess model inter-process communication is inefficient because a process cannot access data owned by the other processes. In the multithread model threads share the same virtual address space and can access the all data which may incur lock contention overhead. Thus, both models have advantage and disadvantage. We propose a new implementation of the third model, called *Process-in-Process (PiP)* to take the best of two worlds, mutiprocess and multithread. In PiP, processes are mapped into a single virtual address space (VAS), but each process still owns its private storage. The idea of address-space sharing is not new. What makes PiP unique, however, is that its design is completely in user space, making it a portable and practical approach for large supercomputing systems.

In this fiscal year, we explore the potential of the PiP programming model. There are two research topics here, but both are close related with another. Unlike multithread model, PiP allows for two or more different programs to share the same virtual address space. Since they share the same virtual address space, a PiP task can context-switch to the another at user-level. This looks like another user-level thread (ULT) model and this is called user-level process (ULP). In ULT and ULP, some kernel threads schedules ULTs or ULPs. When a current task calls a systemcall to access the resource information resides in the OS kernel, it returns the information of the scheduling thread, not the one associated with the calling task. When a ULT or ULP migrates to the another kernel thread, then systemcalls return the information of the migrated kernel thread, not the information associated with the calling task. Thus there is no such consistency in the user-level implementations. In multithread model, regardless to its implementation of kernel-level or user-level, most kernel resources (e.g.,

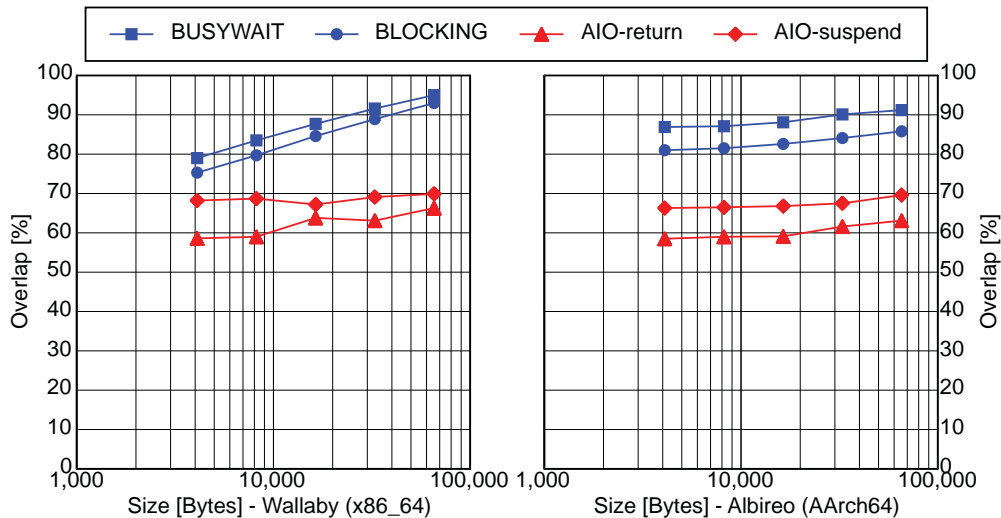


Figure 1.4: Comparing overlap ratio between Linux AIO and PiP/ULP (Wallaby: Intel Xeon E5-2650 v2, Albireo: AMD Opteron A1170 - Cortex-A57)

file descriptors) are shared and the systemcall consistency may not cause a severe problem. In multiprocess model, however, most of the kernel resources are not shared and the systemcall consistency can cause a big problem. To challenge this issue, PiP/ULP implements Bi-Level Thread/Task (BLT) where a user-level thread can become a kernel-level thread (KLT) and vice versa. When a ULP tries to call a systemcall, it becomes a KLT and the systemcall is called. When the systemcall returns it becomes a ULT again.

One of the well-known issues in ULT implementations is blocking systemcalls. In many cases, multithreads are oversubscribed to hide the systemcall latency. When a ULT calls a blocking systemcall, the scheduling task is blocked and there is no chance for the other eligible-to-run ULTs to be scheduled and wasting CPU resources. The above mentioned BLT on PiP can also solve this issue in addition to the systemcall consistency issue.

Figure 1.4 shows the overlap ratios of Linux AIO calls (`aio_write` followed by `aio_return` or `aio_suspend`) and PiP (blocking or busy-waiting kernel thread). As shown, PiP implementation outperforms the Linux AIO cases.

### 1.3.2.1 CEA-Riken Collaboration

CEA has been developing MPC which has the same goal to implement shared address space as PiP does. PiP's approach is to implement a user-level library while MPC's approach is to implement another programming language based on the multithread model. It is very natural to collaborate with the other since both have the same goal.

As described above, PiP has succeeded to implement BLT and ULP on PiP. CEA is very interested in those idea and they are working to have the similar functionalities of PiP's BLT and ULP in their MPC implementation.

### 1.3.2.2 DOE-MEXT Collaboration

Balancing communication workload among MPI processes is always a critical point during the development of High-Performance Computing (HPC) applications in order to avoid resource waste and achieve the best performance. However, because of many factors such as complex network interconnections and irregularity of HPC applications, fully achieving communication workload balance in practice is nearly impossible. Although inter-process work stealing is a promising solution, current shared-memory techniques that lack necessary flexibility or cause inefficiency during data access cannot provide an applicable and efficient process-level work-stealing solution; in addition, existing thread-based work stealing methods cannot be efficiently applied to MPI-layer task model. To solve this problem, we propose a new interprocess work-stealing method using PiP to balance communication workload among processes on MPI layers.

Figure 1.5 shows the performance comparison between the MPICH enhanced with the proposed technique and existing AMPI on the Minighost micron benchmark program. As shown in this figure, the proposed

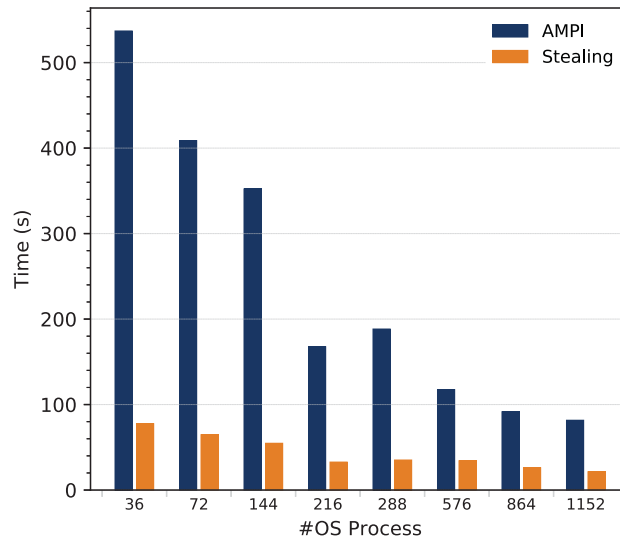


Figure 1.5: Performance comparison of AMPI and our method with Minighost strong scaling test. (Both use the same number of OS processes)

technique outperforms AMPI.

### 1.3.3 IHK/McKernel

This Section describes activities related to IHK/McKernel. Specifically, development items and results from a large-scale evaluation of a parallel multi-grid application on the Oakforest-PACS supercomputer are discussed.

#### 1.3.3.1 Development Activities

Most of the fiscal year 2019 has been spent on porting McKernel to the ARM architecture using Marvell's ThunderX-2 system as well as a prototype cluster of the Fujitsu A64FX platform. Some of the major development items are as follows.

- **Memory semantics:** The ARM architecture differs from x86 in many ways. Most notably ARM has a more relaxed memory semantics than x86 which implies the need for careful and more explicit inter-core synchronization. For example, as opposed to x86, during bringup of CPU cores one needs to ensure that contents of the last level cache must be flushed to memory before any secondary CPU accesses the corresponding memory area. Another implication of the relaxed memory semantics is the requirement for explicit usage of memory barriers in situations where on x86 the order of memory operations would otherwise proceed sequentially.
- **Overlay filesystem:** The overlay filesystem support that was originally implemented as modification to the Linux kernel overlayfs module has been moved to user-space so that portability across different Linux kernel versions is improved.
- **Performance counters:** Support for the ARM performance counters has been added via an implementation of the `perf_event_open()` system call and surrounding infrastructure.
- **Utility thread interface:** An implementation for for the utility thread interface for offloading helper threads to Linux cores has been added for the ARM architecture.
- **Live kernel debugger:** An extension to the `eclair` kernel dump inspection tool has been implemented that enables live debugging of McKernel with support for resuming execution.

### 1.3.3.2 Parallel Multigrid Methods

Multigrid is a scalable method for solving linear equations and preconditioning Krylov iterative linear solvers, and is especially suitable for large-scale problems. The parallel multigrid method is expected to be one of the powerful tools on exa-scale systems. We previously proposed a new format for sparse matrix storage based on sliced ELL, which optimized the serial communication on shared memory systems, and hierarchical coarse grid aggregation (hCGA) has been introduced for optimization of parallel communication by message passing. The proposed methods are implemented for pGW3D-FVM that solves ground-water flow in a three-dimensional heterogeneous porous medium by the finite volume method, and by using parallel conjugate gradient (CG) solver with multigrid preconditioner (MGCG).

With hCGA, high parallel performance can be achieved even when the number of MPI processes is on the order of ten thousands by introducing two layers of parallel hierarchical levels. However, if the number of MPI processes is orders of magnitude higher, e.g., on future exa-scale systems, the computational overhead of the coarse grid solver can become significant. In this publication, we proposed the adaptive multilevel hCGA (AM-hCGA) method that introduces three or more layers of parallel hierarchical levels. We evaluated the new method on the Oakforest-PACS (OFP) system (JCAHPC) and examined the impact of the IHK/McKernel operating system.

Figure 1.6 summarizes our application level results. Each plate shows computation time for weak scaling of optimum cases for hCGA, and AM-hCGA, with and without IHK/McKernel. Computation time for MGCG is normalized by the time of optimum case of hCGA without IHK/McKernel at each core number. Therefore, the values of Y-axis (Ratio) are always equal to 1.00 for hCGA without IHK/McKernel. Effects of IHK/McKernel for improvement of the performance of hCGA at 131,072 cores (2,048 nodes) is approximately 4% for Medium (m), 17% for Small (s), and 22% for Tiny (t) problem sizes.

### 1.3.4 Utility Thread Offloading Interface

The number of cores per node in HPC system has increased to the order of tens to hundreds. This abundance makes it possible to dedicate some cores to helper tasks to increase application performance. For example, MPI asynchronous progress threads can be put on those cores to parallelize a part of communication processing.

Putting those threads to appropriate cores is critical to the performance of this technique and needs the following additional cares. First, those threads should be identified as helper threads and treated in a special way so that they are put on the dedicated cores for the first place. Second, the thread-core mapping should be chosen to minimize the cost of the communication with those threads and the related components, e.g., the computation threads or the interconnect.

While there are the existing implementations, they are not done in an application transparent way, i.e., done by modifying application code or command line. In addition to that, they are not done in an easy way or in an across-systems-portable way because there is no simple and abstracted interface.

To solve those issues, we introduce an application-transparent and portable interface, called Utility Thread offloading Interface (UTI), and the library serving to runtime, e.g., MPI library. The library is given abstracted info by the runtime and performs the core allocation.

This is on-going work and the followings were done during this fiscal year.

1. Submit a paper about cross-layer resource coordinator which incorporating the UTI ideas. This is done with LLNL, Intel, CEA, INRIA people.
2. Improve prototype implementation of the library by getting the feedbacks from ANL people.

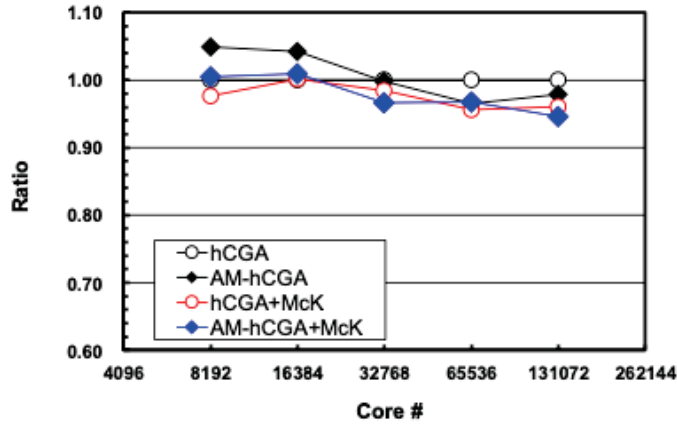
## 1.4 Schedule and Future Plan

We continue to enhance performance and functionality of our system software stack for Fugaku and other computer architectures, such as Intel Xeon.

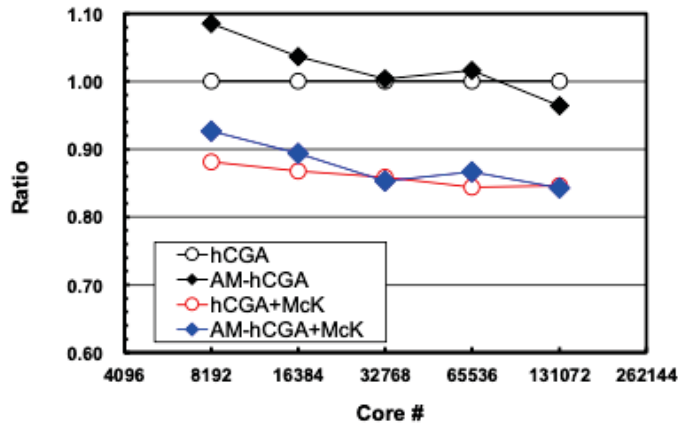
## 1.5 Publications

### 1.5.1 Articles/Journal

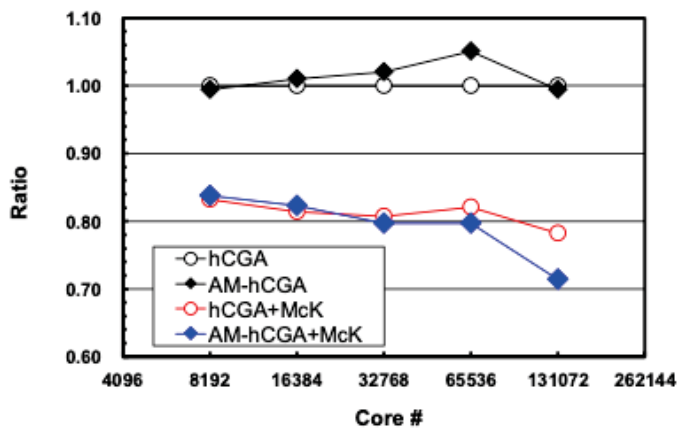
[1] A. Hori, K. Yoshinaga, T. Herault, A. Bouteiller, G. Bosilca, and Y. Ishikawa, Overhead of using spare nodes, International Journal of High Performance Computing Applications (IJHPCA), vol. 34(2) (2020).



(a) Medium



(b) Small



(c) Tiny

Figure 1.6: Computation time for MCGC solvers up to 2,048 nodes (131,072 cores) of OFP, normalized by computation time for hCGA at each core number, hCGA/AM-hCGA: without IHK/McKernel, hCGA/AM-hCGA+McK: with IHK/McKernel, (a) Medium (m), (b) Small (s), (c) Tiny (t)

### 1.5.2 Conference Papers

[2] A. Hori, G. Bosilca, E. Jeannot, T. Ogura, and Y. Ishikawa, Is Japanese HPC another Galapagos? - Interim Report of MPI International Survey -, IPSJ SIGHPC - SWoPP 2019, July, 2019.

[3] K. Nakajima, B. Geroft, Y. Ishikawa and M. Horikoshi, "Parallel Multigrid Methods on Manycore Clusters with IHK/McKernel," 2019 IEEE/ACM 10th Workshop on Latest Advances in Scalable Algorithms for Large-Scale Systems (ScalA), Denver, CO, USA, 2019, pp. 52-61, doi: 10.1109/ScalA49573.2019.00012.

### 1.5.3 Posters

### 1.5.4 Invited Talks

### 1.5.5 Oral Talks

[4] A. Hori, International Survey - MPI -, 9th JLESC Workshop, (Knoxville, USA, April, 2019) [5] A. Hori, A right decision is not always right, The All-RIKEN Workshop 2019 (Wako, Japan, Dec. 2019)

### 1.5.6 Software

<https://github.com/RIKEN-SysSoft> Distributing IHK/McKernel and PiP

### 1.5.7 Patents

## Chapter 2

# Programming Environment Research Team

### 2.1 Members

Mitsuhsisa Sato (Team Leader)

Yuetsu Kodama (Senior Research Scientist)

Hitoshi Murai (Research Scientist)

Miwako Tsuji (Research Scientist)

Masahiro Nakao (Research Scientist)

Jinpil Lee (Postdoc Researcher)

Tetsuya Odajima (Postdoc Researcher)

Manabu Yagi (Postdoc Researcher)

Itaru Kitayama (Technical Staff)

Masahiro Yasugi (Senior Visiting Researcher)

Hitoshi Sakagami (Senior Visiting Researcher)

Brian Wylie (Visiting Researcher)

Christian Feld (Visiting Researcher)

Hidetoshi Iwashita (Visiting Researcher)

Hiroko Takahashi (Assistant)

### 2.2 Overview of Research Activities

In order to exploit full potential computing power of large-scale parallel system such as the K computer to carry out advanced computational science, efficient parallel programming is required to coordinate these processors to perform scientific computing. Our team conduct researches and developments on parallel programming models and language to exploit full potentials of large-scale parallelism in the large-scale parallel system and increase productivity of parallel programming.

In 2019FY, in order to archive these objectives above, we carried out the following researches:

- (1) We continued working on the development and improvement of XcalableMP (XMP) programming languages. XcalableMP is a directive-based language extension, designed by XcalableMP Specification Working Group (XMP Spec WG) including some members from our team as a community effort in Japan. In this year, we have evaluated XcalableMP benchmark programming on Fugaku. The performance of XcalableMP on the Fugaku is enhanced by the manycore processor and a new Tofu-D interconnect. As an application for XcalableMP, we investigated the graph algorithm for the the Order/Degree problem. For an extension of XcalableMP to exascale computing, we are working on XcalableACC for emerging accelerator clusters, by integrating XcalableMP and OpenACC.
- (2) Since the Fugaku is a large-scale multicore-based system, we are investigating programming models for manycore-based parallel systems as XcalableMP 2.0. We focus especially on the integration of dynamic tasking with PGAS programming model. In this year, we continued the design of programming models for task parallelism and PGAS.
- (3) We investigated the programming model for accelerators including Field Programmable Gate Array (FPGA), which is expected as one of the promising technologies for future acceleration technology. In this year, we investigate OpenMP technologies for GPU and FPGA, and the task parallel programming model to combine several kinds of accelerators such as GPU and FPGA.
- (4) As a part of Flagship 2020 project, we are developing several tools for co-design, including performance analysis tools and simulators. In this year, we have improved the accuracy of the Gem5 simulator for Fujitsu A54FX used in the Fugaku system.
- (5) We conducted several collaborations on the performance evaluation with JSC, University of Tsukuba, Kyusyu Institute of Technology and other groups. In this year, we carried out the performance study on NEST brain simulator developed by JSC, using Scalasca. Prof. Yasugi's group of Kyusyu Institute of Technology developed a new approach to fault-tolerant language systems without a single point of failure for irregular parallel applications.

In addition to the research activities, we conducted promotion activities to disseminate our software. To promote XcalableMP as a means for parallelization of programs, we organized the XcalableMP workshop as follows:

- The 6th XcalableMP workshop (Nov. 1st, 2019, at University of Tsukuba)

## 2.3 Research Results and Achievements

### 2.3.1 XcalableMP on Fugaku

In this section, we report our early experience and the preliminary performance of XcalableMP on Fugaku. The Fugaku is a huge-scale system with general-purpose manycore processors. The node processor is a single chip, named Fujitsu A64FX, which consists of 48 cores with 2 or 4 cores dedicated for OS activities, 32 GiB HBM2 memory, with TofuD interconnect, and a PCI express controller in the chip together. The Fugaku system consists of 158,976 nodes in 432 racks. The Fugaku is scheduled to be put into operation for public service around 2021. In 2020, the installation is completed, and the system partially serves the early-access program.

XcalableMP is available as a parallel programming language for the Fugaku, supported by R-CCS team with Fujitsu. C and Fortran are supported as base languages with XcalableMP 1.2 compliant.

We report the preliminary performance of XcalableMP program running on the Fugaku <sup>1</sup>.

We used the following versions:

- Omni XcalableMP Version: 1.3.2, Git Hash:6d23f46
- Language specification: 1.2.25

The performance of XcalableMP on the Fugaku is enhanced by the manycore processor and a new Tofu-D interconnect.

---

<sup>1</sup> The reported results were obtained on the evaluation environment in the trial phase. Note that the performance is not guaranteed at the start of its operation.

### 2.3.1.1 Performance of XcalableMP Global View Programming

We executed the IMPACT-3D, described in Chapter 6, for the evaluation of XcalableMP global view programming in the Fugaku, using up to 512 nodes. The scalability on Fugaku is shown in Figure 2.1, comparing to the K computer. The program is parallelized by hybrid XMP-OpenMP parallel programming: An XMP node is assigned to a node, and 48 OpenMP threads are running within a node. The problem size is  $512 \times 512 \times 512$  with 3-dimensional block distribution. The compile option is “-Kfast”.

As shown in the figure, we found a good scalability in Fugaku, and the performance is better than that by MPI thanks to the optimized XMP runtime for communications in the stencil computation.

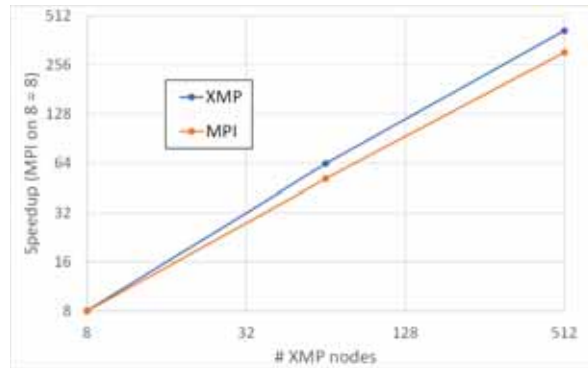


Figure 2.1: Speedup of Impact3D on Fugaku and Performance comparing to K computer

### 2.3.1.2 Performance of XcalableMP Local View Programming

Fugaku has a customized interconnection, called Tofu-D, which supports hardware-supported RDMA (Remote Direct Memory Access) operations. We implemented the XMP runtime library to make use of Tofu-D for one-sided communication for the XMP local view programming. The library is implemented by using a low-level communication layer, uTofu API, provided by Fujitsu.

For performance evaluation of XMP local view programming, we used CCS QCD and NTChem-MINI taken from the coarray version of Fiber Miniapp Suite.

To run CCS QCD mini-application, 8 XMP nodes are assigned to one node, running in a flat XMP mode. The size and conditions are as follows:

- Target data: Class 2 (32 x 32 x 32 x 32) (strong scaling)
- Compiler options: -Kfast,zfill,simd=2
- Timing region: sum of “Clover + Clover\_inv Performance” and “BiCGStab(CPU:double precision) Performance” of the built-in timing feature

Figure 2.2 shows the speedup of the Fugaku, comparing to the performance of the K computer. The XMP version archives almost same performance of the MPI version. Note that the reason of the performance degradation of the XMP version on the K computer is the overhead of allocation for allocatable coarray used as a buffer for communication. It is improved by removing this overhead by using the uTofu communication layer.

The NTChem-MINI is a mini-application taken from NTChem, a high-performance software package for molecular electronic structure calculation. An XMP node is assigned to one node, and within a node, BLAS functions are executed using 48 cores. The size and conditions are set as follows:

- Target data: taxol (strong scaling)
- Compiler options: -Kfast,simd=2
- Timing region: RIMP2.Driver of the built-in timing feature

As shown in Figure 2.3, the XMP versions archive almost the same performance of the original MPI versions.

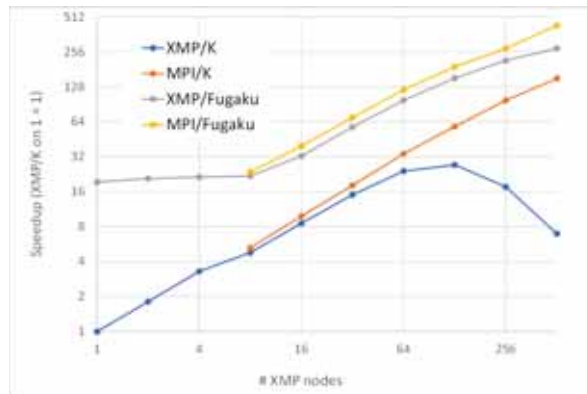


Figure 2.2: Speedup of CCS QCD on Fugaku and Performance comparing to the K computer

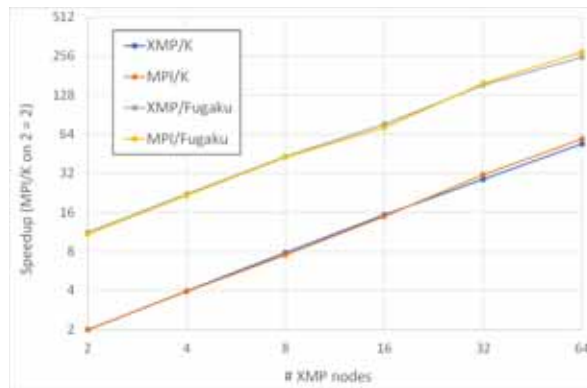


Figure 2.3: Speedup of NTChem-MINI on Fugaku and Performance comparing to the K computer

### 2.3.2 Accuracy Improvement of Memory System Simulation for Modern Processor

For the purpose of developing applications for supercomputer Fugaku at an early stage, RIKEN has developed a processor simulator. This simulator is based on the general-purpose processor simulator gem5. It does not simulate the actual hardware of a Fugaku processor. However, we believe that sufficient simulation accuracy can be obtained since it simulates the instruction pipeline of out-of-order execution with cycle-level accuracy along with performing detailed parameter tuning of out-of-order resources. In order to estimate the accurate execution time of a program, it is necessary to simulate with accuracy not only the instruction execution time, but also the access time of the cache memory hierarchy. Therefore, in the RIKEN simulator, we expanded gem5 to match the performance of the cache memory hierarchy to that of a Fugaku processor. In this simulator, we aim to estimate the execution cycles of one node application on a Fugaku processor with accuracy that enables relative evaluation and application tuning.

#### 2.3.2.1 RIKEN simulator for A64FX

The RIKEN simulator currently supports only one CMG simulation, and multithreaded execution of up to 12 cores is possible. In order to estimate the accurate execution time of a program, it is necessary to simulate with accuracy not only the instruction execution time, but also the access time of the cache memory hierarchy. Therefore, in the RIKEN simulator, we expanded gem5 to match the performance of the cache memory hierarchy to that of the A64FX. The main extensions are as follows. These functions were developed for the RIKEN simulator, but many of them are general functions and can be applied to other processors.

- The L1 cache and L2 cache capacity, associativity, line size and latency were set in the gem5 parameter file according to the actual settings of the A64FX.

- In gem5, it is assumed that load and store operations can access the L1 cache in the same cycle. On the other hand, the A64FX enables two load or single store operations in a cycle. The RIKEN simulator enabled the same controls as those of the A64FX.
- In gem5, the L1 cache access in order to maintain L2 cache such as cache fill from L2 cache to L1 cache and write-back from L1 cache to L2 cache is controlled independently of the L1 cache access from the core. Therefore, the performance of the L1 cache will be enhanced. By performing exclusive control between them, the RIKEN simulator was able to simulate the L1 cache performance of the A64FX accurately.
- In gem5, when the core accesses to the L1 cache exceeds cache alignment, the access is divided into multiple accesses, and the overhead occurs. The A64FX is designed so as not to cause performance degradation even when accessing across cache lines. The RIKEN simulator also supports the unaligned cache access without overhead.
- In gem5 for ARM ISA, software prefetch was supported, but only prefetch for read access targeting L1 cache was implemented. Prefetch for write access is important for optimizing memory access, so the RIKEN simulator supports it. This feature has already been reported to the gem5 developers and accepted. Software prefetch targeting L2 cache is also important for optimizing memory access. The RIKEN simulator also supports it.
- Gem5 has several hardware prefetching capabilities, but there are only simple prefetches such as queued prefetch and stride prefetch. Furthermore, they only support prefetch for read access from next level memory hierarchy. The A64FX supports the hardware prefetch which extended the prefetch of K computer, but the RIKEN simulator implements the following prefetch that is based on the prefetch of K computer with small modification matched to the A64FX. When a cache miss is detected, a prefetch entry is generated. When a subsequent memory access matches the prefetch entry, two consecutive prefetch requests are generated both for L1 cache and L2 cache. When the prefetch distance reaches a set value, it is switched to single prefetch. This prefetch distance is set individually for L1 cache and L2 cache. The hardware prefetch supports both read access and write access.
- Gem5 supports shared L2 cache with multiple cores, but since default L2 cache is a single bank, L2 access could be a bottleneck if the number of cores increases. Since the L2 cache is designed as a module in gem5, it is possible for users to set multiple banks of L2 cache by adding descriptions individually. The RIKEN simulator has been expanded so that the number of banks can be changed just by specifying parameters.
- In gem5, L2 cache requests are handled by FCFS (First Come First Serve) manner. In the A64FX, the L2 cache has a mechanism to keep fairness between requests from each core. In the RIKEN simulator, L2 cache has been extended to allow FCFS and RR (Round Robin) policies to be selected.
- In gem5, the bus width between L1 cache and L2 cache is one parameter, and it is assumed that the transfer throughput from L1 cache to L2 cache and that from L2 cache to L1 cache are the same. On the other hand, in the A64FX, these two transfers throughputs are different. The RIKEN simulator has been extended to specify these two bus widths as different parameters. The same applies to the bus width between the L2 cache and memory.
- Gem5 supports HBM1 as main memory, but HBM2 is not yet supported. The RIKEN simulator added HBM2 parameters based on the HBM1 parameters. Although standard features of gem5 could not completely match the memory interleaving method used with the A64FX, the RIKEN simulator achieved almost the same memory performance as that of the A64FX by combining this feature with other parameters, such as burst length.

### 2.3.2.2 Evaluation

The RIKEN simulator was evaluated using several programs to find out how accurate it is with the execution time of the A64FX. The evaluation target is the test chip of the A64FX prototype, and does not indicate the performance of the final Fugaku processor. Also, the compiler used for generating the program to be executed was a prototype version of the compiler for the Fugaku from Fujitsu, which is the April 2019 version. It is the same version of the compiler used with the test chip evaluation.

Listing 2.1: Example source code of the kernel program (double addition)

```

subroutine calc01_add_r8(n,iter ,dist ,y ,x1 ,x2)
  real*8 y(n), x1(n), x2(n)
  integer n, iter , i, j, dist
  do j = 1, iter
    do i = 1, n
      y(i) = x1(i) + x2(i)
    end do
  enddo
end subroutine calc01_add_r8

```

First, we compared the execution times of various kernel programs on a single core with that of the test chip. An example of a kernel program used for evaluation is shown in Listing 2.1. There are four types of kernels: basic arithmetic functions, type conversions, numerical functions, and mathematical functions. The basic arithmetic functions include seven arithmetic operations: addition, subtraction, multiplication, product-sum, division, reciprocal and square root. The type conversions include seven conversions: conversion from double precision to single precision and 32-bit integer and its inverse conversion, and conversion from the double precision of 'aint', 'nint' and 'anint' that are built-in functions of Fujitsu Fortran. The numerical functions include four functions of absolute value, maximum, minimum and sign. The mathematical functions include six functions of 'cos', 'sin', 'exp', 'exp10', 'log' and 'log10'. Evaluation was performed on a total of 24 kernels for double precision.

These kernel programs were compiled with the '-Kfast' option. We compared the execution time on the RIKEN simulator with that on the A64FX test chip. In the Fujitsu compiler, all of these kernels are executed by 8 SIMD for double precision and 16 SIMD for single precision, mathematical functions are inlined, and optimization by software pipeline is applied. Divisions and reciprocals are also calculated using reciprocal instructions that are pipelined rather than using non-pipelined division instructions.

The evaluation results are shown in Figure 2.4 for double precision. The bar graph represents the inverse of operation throughput (the number of cycles required for SIMD-length operation) evaluated by the RIKEN simulator, and corresponds to the left vertical axis. The orange point is the ratio of the difference in execution time between the test chip result and the RIKEN simulator result, and corresponds to the right vertical axis. An execution time difference of 10% indicates that the execution time of the RIKEN simulator is 10% longer than that of the test chip, and -10% indicates that the execution time of the test chip is 10% longer than that of the RIKEN simulator.

Next, in order to evaluate the L2 cache and memory performance in multithreaded execution, the performance of Stream Triad for two data sizes were compared by changing the number of threads.

The results for L2 cache throughput, using Stream Triad for the size within the L2 cache are shown in Figure 2.5. The left graph is results using hardware prefetch, and the right graph is results using software prefetch. The bar graph shows the total L2 cache throughput in the RIKEN simulator when the number of threads is changed from 1 to 12 for the same data size. The orange dots show the percentage difference in execution time between the RIKEN simulator and the A64FX test chip. The horizontal axis corresponds to the number of threads, the left vertical axis corresponds to the throughput, and the right vertical axis corresponds to the percentage difference.

Using hardware prefetch, although the result is relatively scalable with the increase in the number of threads, some of the difference are over 10%, and the variation is large. The A64FX results are more scalable up to 12 threads. When the number of threads is small, the RIKEN simulator is faster than the A64FX. This may be because the L1 hardware prefetch requests the L2 cache without checking the L1 cache in the RIKEN simulator, and the load on the L1 cache may be smaller. On the other hand, there is another problem on implementation of hardware prefetch for L2 cache in the RIKEN simulator. In the RIKEN simulator, the occupancy rate of crossbar between L1 cache and L2 cache is very high due to hardware prefetching to L2 cache, so we are continuing to develop to reduce it.

Using software prefetch, although the result is scalable with the increase in the number of threads, the throughput is saturated around 10 threads in the RIKEN simulator. On the other hand, the A64FX shows scalable performance up to 12 threads. As a result, the execution time difference for 12 threads is slightly larger at 8%, but otherwise it is 2% or less.

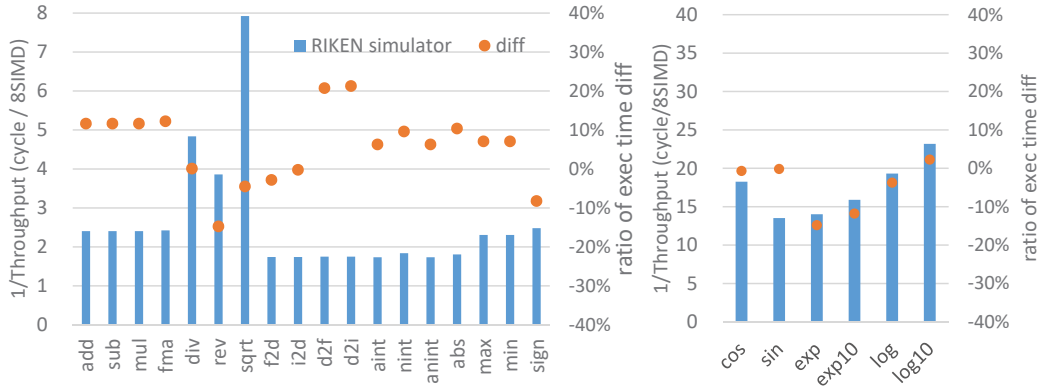


Figure 2.4: Execution throughput of kernel benchmark (double precision) in the RIKEN simulator and the execution time difference ratio of the test chip

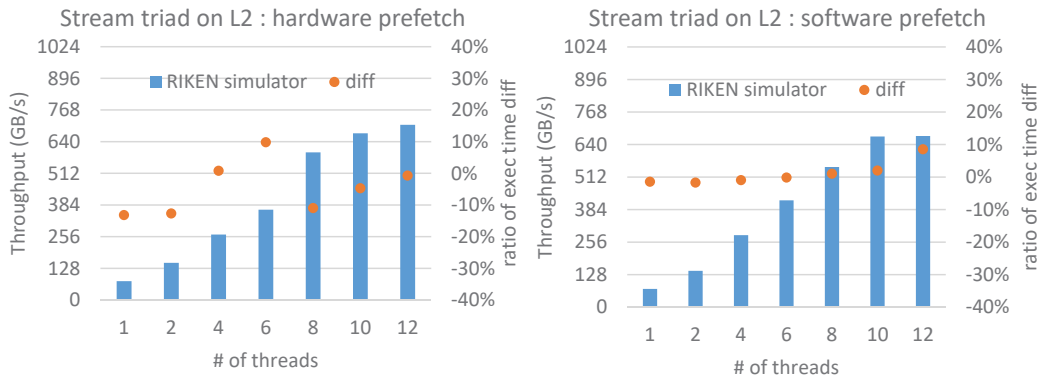


Figure 2.5: L2 cache throughput of Stream Triad in the RIKEN simulator and the difference in execution time with the test chip

### 2.3.3 Development optimization algorithm for grid graph in Order/Degree problem

We have developed a solver for the Order/Degree Problem as one of the real applications of XMP. The Order/Degree problem is the problem of finding the undirected graph with the smallest diameter and ASPL (Average Shortest Path Length) from the set of undirected graphs that satisfy a given number of vertices (Order) and degree (Degree). The problem is an abstraction of the network topology in large-scale systems such as supercomputers and data centers as a graph theory problem, and it is known that it can be used for designing a network with low latency. The categories of the Order/Degree problem include a general graph in which vertices can be arranged freely and a grid graph in which vertices are arranged on nodes of a two-dimensional grid. In the grid graph, the distance between vertices is defined as the Manhattan distance, which is because a parallel computer system or an intra-chip network that does not allow diagonal wiring is assumed. Since the maximum length of the edge can be set, the design can take into account the maximum length of the network cable, etc. Last year we tackled with general graphs, but this year we do with grid graphs.

We indicate that the symmetry of the graph can be used to improve both the solution search performance of Simulated Annealing and the calculation time. Figure 2.6 shows some examples of the symmetry. The graphs are 6 x 6 grid, degree is 3, and maximum length is 2. Hereinafter, it is represented as (width x height, degree, max length) = (6 x 6, 3, 2). When a graph is rotated (360/g) degrees and becomes the original graph, we define that the graph has the symmetry.

Figure 2.7 shows parts of the evaluation of the solution search performance for grid graph. The "number of groups" on the horizontal axis means the number of symmetries (g). The vertical axis is an ASPL of the actually found graph and a value in parentheses is the diameter. For comparison purpose, dot line is ASPL in random graph. The results show the solution search performance tends to be higher as the value of the number

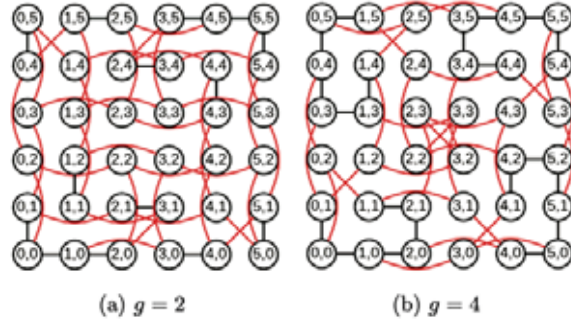


Figure 2.6: Examples of Symmetric Graph

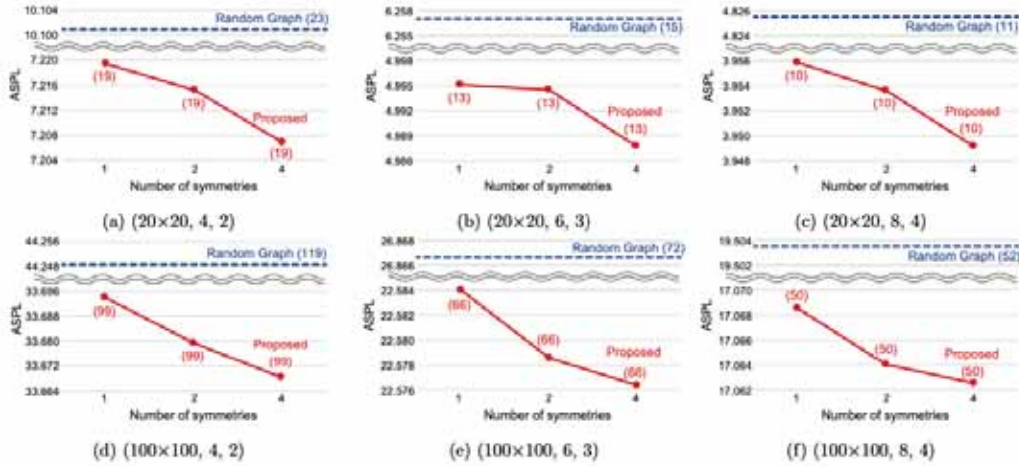


Figure 2.7: Evaluation results of the solution search performance for grid graph

of groups is larger.

We submitted the results to Graph Golf, an international competition on Order/Degree problem, and we won the award in 2019.

### 2.3.4 HOPE: A Fault-Tolerant Parallel Execution Model Based on Hierarchical Omission

This work presents a new approach to fault-tolerant language systems without a single point of failure for irregular parallel applications. Work-stealing frameworks provide good load balancing for many parallel applications, including irregular ones written in a divide-and-conquer style. However, work-stealing frameworks with fault-tolerant features such as checkpointing do not always work well.

This work proposes a completely opposite work omission paradigm and its more detailed concept as a hierarchical omission-based parallel execution model called HOPE. HOPE programmers' task is to specify which regions in imperative code can be executed in sequential but arbitrary order and how their partial results can be accessed. HOPE workers spawn no tasks/threads at all; rather, every worker has the entire work of the program with its own planned execution order, and then the workers and the underlying message mediation systems automatically exchange partial results to omit hierarchical subcomputations.

Figure 2.8 shows the results of HOPE with faults comparing to HPE and Tascell without faults. Efficiency (upper half) and execution times (lower half) of parallel systems using multiple workers on the K computer, in addition to execution times of serial C programs (lower half). We use 1 to 1024 nodes, each of which has eight cores and employs seven workers. HOPE FT(4) stands for HOPE with Fault injection into one out of 4 workers.

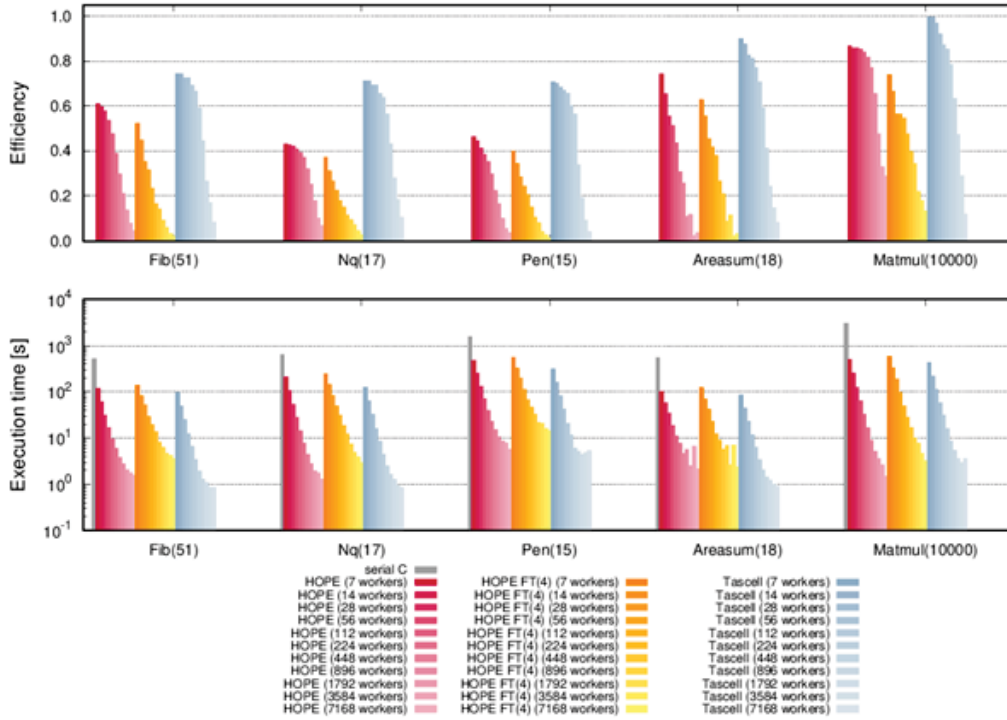


Figure 2.8: Results of HOPE with faults

Even with fault tolerance, the HOPE framework provides parallel speedups for many parallel applications, including irregular ones.

This work was done by Prof. Yasugi, Kyusyu institute of Technology, as a collaboration with our team.

## 2.4 Schedule and Future Plan

We have supported a production-level XcalableMP compiler, and evaluated a set of XcalableMP benchmark programs. XcalableMP (version 1.x) will be available for the Fugaku users.

We are working on the next version, XcalableMP 2.0, for cutting-edge high performance systems with many-core processors by multitasking with integrations of PGAS model and synchronization models for dataflow/multitasking executions. In this new programming model, the execution of the program is decomposed into several tasks executed according the dependency between tasks. This model enables less overhead of synchronization eliminating expensive global synchronization, overlap between computation and communication in manycore, and light-weight communication by RDMA in PGAS model. Especially for Fugaku, this model allows to exploit parallelism for both tasks and SIMD.

Our long-term goal is to establish the programming model for high-performance computing systems in Post-Moores era. Recently, the slow-down in progress of the semiconductor fabrication technologies is pointed out as a serious problem of the future computer system, and it is said that the post-Moore era is coming in near future after Moores low ends. Since modern high-performance computing systems has improved its performance by advanced semiconductor technologies, it is necessary to reconsider overall structure of computer architecture including hardware and software for the evolution the architecture of system, in order to improve performance in the post-Moores era.

We will extend the task parallel programming model to combine several kinds of accelerators such as GPU, FPGA and special-purpose processors with large-scale general-purpose manycore systems. It enables some task to be offloaded into the accelerators such as FPGA and accelerators as well as each core in modern manycore processor. We consider this configuration as a general global architecture of the future system as some part of system will be specialized for high performance and power efficiency. Our programming model will make it easy to adopt the existing computational science program to the new systems.

## 2.5 Publications

### 2.5.1 Articles/Journal

[1] Masahiro Nakao, Tetsuya Odajima, Hitoshi Murai, Akihiro Tabuchi, Norihisa Fujita, Toshihiro Hanawa, Taisuke Boku, Mitsuhisa Sato. "Evaluation of XcalableACC with Tightly Coupled Accelerators/InfiniBand Hybrid Communication on Accelerated Cluster," *International Journal of High-Performance Computing Applications*, 33(5) (2019).

[2] Ksander Ejjaouani, Olivier Aumage, Julien Bigot, Michel Mhrenberger, Hitoshi Murai, Masahiro Nakao, Mitsuhisa Sato. "InKS: a programming model to decouple algorithm from optimization in HPC codes", *The Journal of Supercomputing*, 76(6): 4666-4681 (2020)

### 2.5.2 Conference Papers

[1] Masahiro Nakao, Hitoshi Murai, Mitsuhisa Sato: Parallelization of All-Pairs-Shortest-Path Algorithms in Unweighted Graph. *HPC Asia 2020*: 63-72

[2] Yuetsu Kodama, Tetsuya Odajima, Akira Asato, Mitsuhisa Sato: Accuracy Improvement of Memory System Simulation for Modern Shared Memory Processor. *HPC Asia 2020*: 142-149

[3] Yutaka Watanabe, Jinpil Lee, Kentaro Sano, Taisuke Boku, Mitsuhisa Sato, "Design and Preliminary Evaluation of OpenACC Compiler for FPGA with OpenCL and Stream Processing DSL", *HPC Asia 2020*, workshops, pp. 10-16.

[4] Jinpil Lee, Yutaka Watanabe, Mitsuhisa Sato: OpenMP Task Generation for Batched Kernel APIs. *IWOMP 2019*: 262-273

[5] Masahiro Yasugi, Daisuke Muraoka, Tasuku Hiraishi, Seiji Umatani, and Kento Emoto: HOPE: A Parallel Execution Model Based on Hierarchical Omission. *Proceedings of the 48th International Conference on Parallel Processing (ICPP 2019)*, Kyoto, Japan. pp. 77:1-77:11, August 2019.

### 2.5.3 Posters

[1] Masahiro Nakao, Hitoshi Murai, Mitsuhisa Sato, Yoshimichi Andoh, Susumu Okazaki. "Performance improvement of MODYLAS using Remote Direct Memory Access on the K computer," *International Conference on Parallel Processing*, Kyoto, Japan, Aug. 2019.

### 2.5.4 Invited Talks

[1] Mitsuhisa Sato, "Challenges for Unified Parallel Programming Models for Accelerated Clusters", 4th International Workshop on Performance Portable Programming models for Manycore or Accelerators (P3MA) in ISC2019, Frankfurt, June 20th, 2019.

### 2.5.5 Software

- Omni XcalableMP compiler ver. 1.3.3, Nov. 27, 2020 (registered as an R-CCS-supported software)

# Chapter 3

## Processor Research Team

### 3.1 Members

Kentaro Sano (Team Leader)

Tomohiro Ueno (Postdoctoral Researcher)

Takaaki Miyajima (Postdoctoral Researcher)

Jens Christoph Huthmann (Postdoctoral Researcher)

Artur Podobas (Postdoctoral Researcher)

Atsushi Koshihara (Postdoctoral Researcher)

Antoniette Pangilinan Mondigo (Student Trainee)

Kohei Hijikata (Student Trainee)

Kouki Watanabe (Student Trainee)

### 3.2 Overview of Research Activities

#### 3.2.1 Aim of Team

The aim of the processor research team is to explore and establish data-flow-based parallel computing models and high-performance computer architectures which are promising and necessary as next-generation computing technologies in the forthcoming post-Moore era. We are researching and developing general-purpose processor architectures with their programming model different from existing multi/many-core processors, hardware and system software for reconfigurable computing, and any specific custom computing machines, as well as system software for data/task-flow-based high-performance computing to efficiently utilize large-scale parallel machines such as the supercomputer Fugaku.

In the next decade, sooner or later, the Moore's law as planar lithography-scaling is going to end and therefore we will be no longer able to rely on two-dimensional scaling of CMOS devices. In this "post-Moore" era, transistor integration, power consumption per transistor, and relative latency of data movement to the transistor's switching speed are not sufficiently improved. Consequently, it is predicted that the conventional approaches cannot increase the performance and performance per power, which have been so far improved mainly by the semiconductor scaling. Accordingly, we will need to more efficiently and effectively utilize available hardware resources, i.e., transistors on chips, to achieve target performance. In particular, the conventional many-core architectures and large-scale systems based on the parallel computing model and global synchronization will be confronted with limitation in increasing computing performance due to the following reasons:

- 1) dark silicon problem where most of transistors cannot be utilized due to the upper limit of on-chip power consumption. Since power per transistor does not decrease, we need to inactivate a large portion of transistors even if we have more transistors integrated on a chip,

- 2) relatively-increasing latency to transistor's switching speed. Due to the increasing latency, we can no longer shorten cycle time to update memory elements used for computing, cycle time to control computation based on some decision, and synchronization time among a large number of physically-distributed processor chips,
- 3) inefficient data-movement among on-chip cores via a memory subsystem or through a global network in a system, and
- 4) a large overhead in global synchronization for large-scale parallel computation which is affected by relatively-increasing delay of data transfer through a system-wide network.

That is, the existing approaches/architectures are not designed to scale the performance under these critical conditions. For example, the von-Neumann architecture is based on two cycles of "memory-element update" and "control" which cannot be accelerated any more, and therefore parallel processing is introduced as pipelining, super-scalar, and many cores as well as latency-hiding techniques of memory hierarchy with cache memories, speculative execution with branch prediction, and simultaneous multi-threading. These additional mechanisms make semiconductor resource utilization much worse for target processing and computing. In addition, the global barrier in parallel computation degrades overall performance as more nodes are utilized.

The custom computing/reconfigurable computing/spatially-mapped computing (spatial computing) allow us to efficiently utilize hardware resources for target computation while architectural overhead for reconfiguration, which can be seen in a field-programmable gate array (FPGA) device, is also suitable for the dark silicon problem. The spatial computing with the data-driven model (or data-flow model) allows us to avoid or mitigate cycles in processing. By spreading a sequence of operations onto space on hardware with a data flow, we can avoid instruction execution cycles with memory-element update and control so that we can increase a computing throughput with fine-grain parallelism increased naturally.

The data-flow or task-flow approach can also make it easier to avoid the global synchronization in large-scale parallel computing. If we automatically schedule and control task execution based on task-flow with task dependency, we can efficiently execute tasks without global synchronization when they become ready to be executed. Thus, we believe that the custom computing/reconfigurable computing/spatial computing with these localized control and synchronization is essentially necessary for future computer architectures in the post-Moore era, and therefore we are researching them.

Since researches on these themes require broad range of expertise, we are collaborating with other research teams in R-CCS, universities in Japan (Tohoku university, University of Tsukuba, Nagasaki university, Kumamoto university, Hiroshima city university, Kyoto university, and Japan advanced institute of science and technology; JAIST), and a research institute out of Japan, such as Argonne national laboratory, US.

### 3.2.2 Overview of Research Activities FY2019

Toward the aim of our team described above, we have conducted the following researches in the fiscal year of 2019.

1. Investigation and exploration of coarse-grained reconfigurable architectures (CGRAs)
2. Research and development of FPGA cluster
3. FPGA-based Applications

The background, motivation, objectives, and achievement of each research subject follow in the next section.

### 3.3 Research Results and Achievements

#### 3.3.1 Investigation and exploration of coarse-grained reconfigurable architectures (CGRAs)

As the achievement which was mainly published in [2], we conducted architectural investigation of CGRA with past related work for the last three decades. With the end of both Dennard’s scaling and Moore’s law, computer users and researchers are aggressively exploring alternative forms of computing in order to continue the performance scaling that we have come to enjoy. Among the more salient and practical of the post-Moore alternatives are reconfigurable systems, with CGRAs seemingly capable of striking a balance between performance and programmability.

In this work [2], we surveyed the landscape of CGRAs. We summarized nearly three decades of literature on the subject, with a particular focus on the premise behind the different CGRAs and how they have evolved. Next, we compiled metrics of available CGRAs and analyze their performance properties in order to understand and discover knowledge gaps and opportunities for future CGRA research specialized towards High-Performance Computing (HPC). We found that there are ample opportunities for future research on CGRAs, in particular with respect to size, functionality, support for parallel programming models, and to evaluate more complex applications.

As the achievement which was mainly published in [5], we also conducted architectural exploration framework by developing a CGRA simulator. CGRAs are being considered as a complementary addition to modern High-Performance Computing (HPC) systems. These reconfigurable devices overcome many of the limitations of the (more popular) FPGA, by providing higher operating frequency, denser compute capacity, and lower power consumption. Today, CGRAs have been used in several embedded applications, including automobile, telecommunication, and mobile systems, but the literature on CGRAs in HPC is sparse and the field full of research opportunities.

In this work [5], we introduced our CGRA simulator infrastructure for evaluating future HPC CGRA systems. The simulator is built on synthesizable VHDL and is highly parameterizable, including support for connectivity, SIMD, data-type width, and heterogeneity. Unlike other related work, our framework supports co-integration with third-party memory simulators, DRAMSim3, or evaluation of future memory architecture, which is crucial to reason around memory-bound applications. We demonstrated how our framework can be used to explore the performance of various kernels, showing the impact of different configuration and design-space options.

#### 3.3.2 FPGA cluster

We have been developed an FPGA Cluster of Fig.3.1 as a research platform for high-performance reconfigurable computing with FPGAs. We have conducted the following sub-topics for the FPGA cluster.

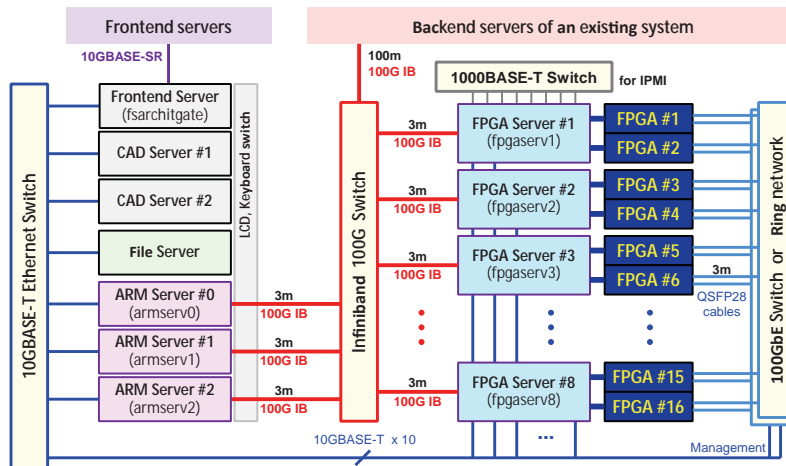


Figure 3.1: Organization of FPGA Cluster developed in Processor research team.

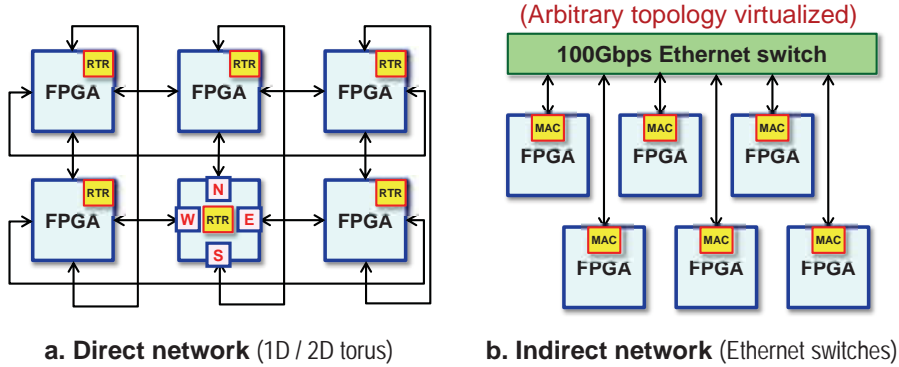


Figure 3.2: Two types of inter-FPGA networks considered.

### 3.3.2.1 Research on inter-FPGA networks

As the achievement which was mainly published in [6], we conducted the following research on inter-FPGA networks of Fig.3.2. As FPGAs become a favorable choice in exploring new computing architectures for the post-Moore era, a flexible network architecture for scalable FPGA clusters becomes increasingly important in high performance computing (HPC). In this work [6], we introduced a scalable platform of indirectly-connected FPGAs, where its Ethernet-switching network allows flexibly customized inter-FPGA connectivity. However, for certain applications such as in stream computing, it is necessary to establish a connection-oriented data-path with back-pressure between FPGAs. Due to the lack of physical back-pressure channel in the network, we utilized our existing credit-based network protocol with ow control to provide receiver FPGA awareness and tailored it to minimize overall communication overhead for the proposed framework.

To know its performance characteristics, we implemented necessary data transfer hardware on Intel Arria 10 FPGAs, modeled and obtained its communication performance, and compared it to a direct network. Results showed that our proposed indirect framework achieves approximately 3% higher effective network bandwidth than our existing direct inter-FPGA network, which demonstrates good performance and scalability for large HPC applications.

As the achievement which was mainly published in [7], we also researched hybrid utilization approaches with an inter-FPGA network and a host server network. A tightly coupled FPGA cluster is a promising approach for large-scale parallel processing with application specialized hardware. Along with the advantages of FPGA-based custom computing, such as high power efficiency, a customized network subsystem with efficient communication through direct Inter-FPGA links allows an FPGA cluster to be an effective platform for large-scale parallel processing. However, the cluster can suffer from substantial communication costs when a cluster becomes larger to obtain higher computing performance.

In this work [7], we propose to exploit the communication capacity of a host server network to improve communication performance. Besides, we show estimations for practical communication patterns on a network model in which we efficiently use both the FPGA and the host networks.

### 3.3.2.2 Research on software-bridged FPGA driver

As the achievement which was mainly published in [9], we researched and developed a remoted FPGA driver as a software bridge through a general-purpose network. A heterogeneous system with FPGAs is gathering attention in High-Performance Computing (HPC) area. When FPGAs are used as an accelerator attached to the host CPU, there can be many configurations such as network topology to construct FPGA cluster. Sustained data transfer bandwidth between FPGA memory and CPU memory on a distant node is one of the most important factors to decide a topology of FPGA cluster. In order to explore the best topology, a quantitative evaluation of bandwidth is required.

In this work [9], we developed a remoted FPGA driver as a software bridge through a Infiniband EDR (100 Gbps) network, which is commonly used as a general-purpose system network in HPC systems. We conducted bandwidth measurement on two host nodes; both nodes are connected via 100 Gbps Infiniband cable and one host node has PCIe Gen3 x8-based FPGA accelerator card. We implemented a Direct Memory Access (DMA) function on an FPGA-attached node and a software bridged data transfer function to transfer data between two nodes. The result shows that DMA function and software bridged data transfer function achieve 82.2 %

and 69.6 % of the theoretical bandwidth of PCIe Gen3 x8, a bottleneck of data transfer path, respectively.

### 3.3.2.3 Research on high-level synthesis (HLS) compiler for FPGA

As the achievement which was mainly published in [3], we researched and developed an extension of an existing HLS compiler with visualization and profiling tool. The recent maturity in High-Level Synthesis (HLS) has renewed the interest of using FPGAs to accelerate High-Performance Computing (HPC) applications. Today, several studies have shown performance- and power-benefits of using FPGAs compared to existing approaches for a number of application kernels with ample room for improvements. Unfortunately, modern HLS tools offer little support to gain clarity and insight regarding why a certain application behaves as it does on the FPGA, and most experts rely on intuition or abstract performance models.

In this work [3], we hypothesize that existing profiling and visualization tools used in the HPC domain are also usable for understanding performance on FPGAs. We extend an existing HLS tool-chain to support Paraver – a state-of-the-art visualization and profiling tool well-known in HPC. We describe how each of the events and states are collected, and empirically quantify its hardware overhead. Finally, we practically apply our contribution to two different applications, demonstrating how the tool can be used to provide unique insights into application execution and how it can be used to guide optimization.

As the achievement which was mainly published in [4], we also researched OpenMP-based task offloading for FPGA with an HLS compiler. Next to GPUs, FPGAs are an attractive target for OpenMP device offloading, as they allow to implement highly efficient, application-specific accelerators. However, prior approaches to support OpenMP device offloading for FPGAs have been limited by the interfaces provided by the FPGA vendors' HLS tool interface or their integration with the OpenMP runtime, e.g., for data mapping.

This work [4] presents an approach to OpenMP device offloading for FPGAs based on the LLVM compiler infrastructure and the Nymbler HLS compiler. The automatic compilation flow uses LLVM IR for HLS-specific optimization and transformation and for the interaction with the Nymbler HLS compiler. Parallel OpenMP constructs are automatically mapped to hardware threads executing simultaneously in the generated FPGA accelerator and the accelerator is integrated into `libomp-target` to support data-mapping. In a case study, we demonstrate the use of the compilation flow and evaluate its performance.

## 3.3.3 FPGA-based Applications

### 3.3.3.1 Highly-pipelined stream computation of Tsunami simulation with a ringed FPGAs

As the achievement which was mainly published in [1], we researched stream computation of Tsunami simulation with multiple FPGAs connected with a ring network. Since the hardware resource of a single FPGA is limited, one idea to scale the performance of FPGA-based HPC applications is to expand the design space with multiple FPGAs. In this work [1], we present a scalable architecture of a deeply pipelined stream computing platform, where available parallelism and inter-FPGA link characteristics are investigated to achieve a scaled performance.

For a practical exploration of this vast design space, a performance model was presented and verified with the evaluation of a tsunami simulation application implemented on Intel Arria 10 FPGAs. Finally, scalability analysis was performed, where speedup is achieved when increasing the computing pipeline over multiple FPGAs while maintaining the problem size of computation. Performance was scaled with multiple FPGAs; however, performance degradation occurred with insufficient available bandwidth and large pipeline overhead brought by inadequate data stream size.

Tsunami simulation results showed that the highest scaled performance for 8 cascaded Arria 10 FPGAs is achieved with a single pipeline of 5 stream processing elements (SPEs), which obtained a scaled performance of 2.5 TFlops and a parallel efficiency of 98%, indicating the strong scalability of the multi-FPGA stream computing platform.

### 3.3.3.2 Highly-pipelined stream computation of fluid simulation with a ringed FPGAs

As the achievement which was mainly published in [10], we researched stream computation of Fluid simulation with multiple FPGAs connected with a ring network. Stream computing is a suitable approach to improve both performance and power efficiency of numerical computations with FPGAs. To achieve further performance gain, temporal and spatial parallelism were exploited: the first one deepens and the latter duplicates pipelines of streamed computation cores. These two types of parallelism were previously evaluated with Arria 10 FPGA. However, it has not been verified if they are also effective for the latest FPGA, Stratix 10, which has a larger amount of logic elements (i.e., 2.4x of Arria 10) and is equipped with a new feature to improve the maximum

clock frequency (i.e., HyperFlex architecture). To show the scalability for such state-of-the-art FPGAs, in this paper, we firstly implemented a streamed fluid simulation accelerator with both parallelism types for Stratix 10.

We then thoroughly evaluated it by obtaining computational performance (FLOPS), power efficiency (FLOPS/W), resource utilization, and maximum clock frequency (Fmax). From the results, we found that this implementation excessively used DSP blocks due to inefficient mapping of floating-point operations, which reduced Fmax and the number of pipelined cores. To improve the scalability, we optimized the implementation to reduce the DSP block usage by utilizing a Multiply-Add function in a single DSP block. As a result, the optimized fluid simulation achieves 1.06 TFLOPS and 12.6 GFLOPS/W, which is 1.36X and 1.24X higher than the non-optimized version, respectively. Moreover, we estimate that the fluid simulation with Stratix 10 could outperform GPU-based implementation with Tesla V100 by optimizing it for HyperFlex architecture.

### 3.3.3.3 Scalable N-body stream computation with a ringed FPGAs

As the achievement which was mainly published in [8], we researched N-body stream computation with multiple FPGAs connected with a ring network. FPGAs offer a fairly non-invasive method to specialize custom architectures towards a specific application domain. Recent studies has successfully demonstrated that single-node FPGAs can be a rival to both CPUs and GPUs in performance. Unfortunately, most existing studies limit themselves to using a single FPGA devices, and their scalability requires more investigation.

In this work [8], we practically demonstrated how to scale the important n-body problem across a comparatively large FPGA cluster. Our design composed of up to 256 processing elements achieved near-linear strong scaling, with performance-levels comparable to that of custom Application-Specific Integrated Circuits (ASICs).

We further developed an analytical performance model, which we use to predict the performance of our solution onto future upcoming Intel Agilix FPGAs. Our system reached up to 47 Giga-Pairs/second, and using our performance model we predicted that we can reach up-to 0.142 Tera-Pairs/second peak performance with next-generation FPGAs.

## 3.4 Schedule and Future Plan

In addition to the researches and development done in FY2019, we are planning to conduct the following researches in the next fiscal year, some of which are newly started and some are continuous work to the present subjects.

1. Further exploration of CGRAs, and development of its place-and-route compiler. We will extend CGRAs and evaluate their performance by benchmarking with some computing kernels. For this, we will develop a compiler for our CGRAs.
2. Research and development of system hardware for FPGA cluster. We will develop a system-on-chip (SoC) on an FPGA device in the cluster, which is called AFU Shell. The developed AFU Shell will support fundamental data-movement among a host CPU and FPGA, and inter-FPGA networks of a direct and an indirect topologies. For the indirect topologies, SoC will provide a virtualized circuit switching mechanism on the top of the packet switching mechanism of 100 Gbps Ethernet.
3. Research and development of system software for FPGA cluster. We will develop an FPGA-object class library as a hardware-abstraction layer which allows us to easily use FPGAs. We are also developing a resource manager software for FPGA resources in the cluster. With this resource manager, we will be able to exclusively utilize a part of FPGA resources in a system with configuration of the Ethernet-based inter-FPGA network based on a request from a user program.
4. Research on utilization of FPGA cluster with an existing HPC machines without FPGAs. We will experimentally connect the FPGA cluster to the supercomputer Fugaku by using 100 Gbps Infiniband network and the software bridge of FPGA driver described in Section 3.3.2.2, so that we can offload tasks to the FPGA cluster from MPI processes running on Fugaku. This also demonstrates that the FPGA cluster with the software bridge is very flexible and available to extend no-FPGA machines.
5. Researches on more FPGA-based applications. We are going to develop and evaluate the following applications and benchmarks for FPGA cluster: 3D FFT, Genome sequence matching, stream computing of Fluid simulation in a different parallelism from deeper pipelining, breadth first search of a graph, and so on. We will mainly use Intel's HLS compiler to implement them.

## 3.5 Publications

### 3.5.1 Articles/Journal

[1] Antoniette Mondigo, Tomohiro Ueno, Kentaro Sano, and Hiroyuki Takizawa, "Scalability Analysis of Deeply Pipelined Tsunami Simulation with Multiple FPGAs," *IEICE Transactions on Information and Systems*(Special Section on Reconfigurable Systems), Vol.E102-D, No.5, pp.1029-1036,May. 2019.

[2] Artur Podobas, Kentaro Sano, and Satoshi Matsuoka, "A Survey on Coarse-Grained Reconfigurable Architectures from a Performance Perspective," *IEEE Access*, Vol.8, pp.146719-146743, DOI:10.1109/ACCESS.2020.3012084, 2020.

### 3.5.2 Conference Papers

[3] Jens Huthmann, Artur Podobas, Lukas Sommer, Andreas Koch, and Kentaro Sano, "Profiling and Visualizing Performance of FPGAs in High-Performance Computing Environments," *Proceedings of IEEE International Conference on Cluster Computing (CLUSTER)*, pp.371-380, DOI: 10.1109/CLUSTER49012.2020.00047.

[4] Jens Huthmann, Lukas Sommer, Artur Podobas, Andreas Koch, and Kentaro Sano, "OpenMP Device Offloading to FPGAs using the Nymbler Infrastructure," *Proceedings of the 16th International Workshop on OpenMP (IWOMP)*, Vol.12295, pp.265-279, 2020.

[5] Artur Podobas, Kentaro Sano, and Satoshi Matsuoka, "A Template-based Framework for Exploring Coarse-Grained Reconfigurable Architectures," *Proceedings of the 31st IEEE International Conference on Application-specific Systems, Architectures and Processors (ASAP)*, pp.1-8, DOI: 10.1109/ASAP49362.2020.00010, 2020.

[6] Antoniette Mondigo, Tomohiro Ueno, Kentaro Sano, and Hiroyuki Takizawa, "Comparison of direct and indirect networks for high-performance FPGA clusters," *Applied Reconfigurable Computing. Architectures, Tools, and Applications (ARC 2020)*, *Lecture Notes in Computer Science*, Vol.12083, 2020.

[7] Tomohiro Ueno, Takaaki Miyajima, Antoniette Mondigo, Kentaro Sano, "Hybrid Network Utilization for Efficient Communication in a Tightly Coupled FPGA Cluster," *Proceedings of 2019 International Conference on Field-Programmable Technology (FPT)*, pp. 363-366, December, 2019.

[8] Jens Huthmann, Shin Abiko, Artur Podobas, Kentaro Sano, and Hiroyuki Takizawa, "Scaling performance for N-Body Stream Computation with a ring of FPGAs," *Proceedings of the International Symposium on Highly-Efficient Accelerators and Reconfigurable Technologies (HEART)*, Article No.10, 6 pages, 2019.

[9] Takaaki Miyajima, Tomoya Hirao, Naoya Miyamoto, Jeongdo Son, and Kentaro Sano, "A Software Bridged Data Transfer on a FPGA Cluster by Using Pipelining and InfiniBand Berbs," *Proceedings of the International Symposium on Highly-Efficient Accelerators and Reconfigurable Technologies (HEART)*, Article No.11, 6 pages, 2019.

### 3.5.3 Posters / Papers with Abstract Review

[10] Atsushi Koshiba, Kouki Watanabe, Takaaki Miyajima, and Kentaro Sano, "Performance Evaluation and Power Analysis of Teraflop-scale Fluid Simulation with Stratix 10 FPGA," *Proceedings of 28th ACM/SIGDA International Symposium on Field-Programmable Gate Arrays (FPGA2020)*, abstract for poster, 1 page, Feb 2020.

[11] Takaaki Miyajima, Tomohiro Ueno, Atsushi Koshiba, Jens Huthmann, Kentaro Sano, "High-Performance Custom Computing with FPGA Cluster as an Off-loading Engine," *Proceedings of HPCAsia2020* (1 page), 2020.

[12] Atsushi Koshiba, Kentaro Sano, "System Software Support for Fast and Flexible Task Management on a Large-scale FPGA cluster," *Proceedings of HPCAsia2020* (1 page), 2020.

[13] Takaaki Miyajima, Tomohiro Ueno, Atsushi Koshiba, Jens Huthmann, Kentaro Sano, and Mitsuhsa Sato, "High-Performance Custom Computing with FPGA Cluster as an Off-loading Engine", International Conference for High Performance Computing, Networking, Storage and Analysis, SC'19, Denver, CO, USA RESEARCH POSTER, 2019.

### 3.5.4 Invited Talks (keynote, plenary talk, invited talk, panelist position talk)

[14] Kentaro Sano, "Data-flow Compiler for Stream Computing Hardware on FPGA," LSPANC, RIKEN R-CCS, Kobe, Jan 29, 2020.

[15] Kentaro Sano, "Networks of FPGA Cluster with High Flexibility of Resource Allocation," SC19 Booth talk of University of Tsukuba, Colorado Convention Center, Nov 20, 2019.

[16] Kentaro Sano, "May Pipelining Be with You," SC19 Panel:Reconfigurable Computing in HPC: Success Stories Today and Future?, Colorado Convention Center, Nov 19, 2019.

[17] Kentaro Sano, "FPGA Cluster as Off-loading Engine for Existing Machines," SC19 BOF:Reconfigurable/FPGA Clusters for High Performance Computing, Colorado Convention Center, Nov 20, 2019.

[18] 佐野 健太郎, "柔軟な資源割当てを可能とするFPGAクラスタシステムとそのネットワーク," 第12回FPGAエクストリームコンピューティング (FPGAX12), 東工大大岡山キャンパスくらまえホール, November 12, 2019.

[19] Kentaro Sano, "High-Performance Custom Computing with FPGA Cluster as Off-loading Engine for Supercomputers," 11th International Symposium on Discovery, Fusion, Creation of New Knowledge by Multidisciplinary Computational Sciences (held by CCS, University of Tsukuba), Tsukuba International Congress Center, Tsukuba, Japan, Oct 15, 2019.

[20] 佐野 健太郎, "FPGAを用いたカスタムコンピューティングと高性能計算の将来", 第12回総合科学を考えるセミナー, 東北大学大学院情報科学研究科, 宮城県仙台市, 9月27日, 2019.

[21] Kentaro Sano, "FPGA Cluster as Off-loading Engine for Supercomputers," 1st International Workshop on Reconfigurable High-Performance Computing (ReHPC), in conjunction with FPL, BSC in Barcelona, Spain, Sep 13, 2019.

[22] Kentaro Sano, "FPGA Cluster as Custom Computing Engine for Supercomputers," 5th workshop on Programming Abstractions for Data Locality (PADAL), INRIA in Bordeaux, France, Sep 9-11, 2019.

[23] Kentaro Sano, "FPGA-based High-Performance Custom Computing based Dataflow Approach," Workshop on Post Moore's Law HPC Computing in conjunction with ISC'19 June 20, 2019.

[24] Kentaro Sano, "Stratix10 FPGA Cluster as Off-loaded Custom Computing Engine for Supercomputers," Workshop of Intel eXtreme Performance Users Group (IXPUG) in conjunction with ISC'19 June 20, 2019.

### 3.5.5 Other Publication Articles

[25] 佐野 健太郎, "ソフトなハードで高性能," 日刊工業新聞, 朝刊19面, 2020年2月3日.

[26] 上野知洋, 佐野 健太郎, "FPGAクラスタとその相互結合網の研究動向," 電子情報通信学会誌 解説記事, vol.103, no.4, pp.421-425, 2020.

[27] 佐野 健太郎, "ピンチの中に勝機あり," 産経新聞連載エッセイ 科学の中身, 2019年4月20日.

### 3.5.6 Oral Talks (with non-reviewed papers)

[28] 小柴 篤史, 上野 知洋, 佐野 健太郎, "Stratix 10 FPGAクラスタにおける格子ボルツマン法のパイプライン並列化と性能評価," 電子情報通信学会リコンフィギャラブルシステム研究会 信学技法, Vol.120, No.168, pp.7-12, Sep 10-11, 2020.

- [29] 土方 康平, 上野 知洋, 江川 隆輔, 滝沢 寛之, 佐野 健太郎, "ベクトルプロセッサからFPGA へのタスクオフロードに関する一考察," 電子情報通信学会リコンフィギャラブルシステム研究会 信学技法, Vol.119, No.373, pp.7-11, Jan 22-23, 2020.
- [30] 小柴 篤史, 佐野 健太郎, "サーバレスコンピューティングにおけるハードウェアアクセラレータ仮想化機構の初期検討," 第31回コンピュータシステム・シンポジウム(ComSys2019), poster paper, 2 pages, 2019.
- [31] Jens Huthmann, Auter Podobas, Takaaki Miyajima, Atsushi Koshiba, and Kentaro Sano, "Multi-threaded High-Level Synthesis for Bandwidth-intensive Application," 電子情報通信学会リコンフィギャラブルシステム研究会 信学技法, Vol.119, No.208, pp.51-56, Sep 19-20, 2019.
- [32] 上野 知洋, 佐野 健太郎, 土方 康平, 滝沢 寛之, "RDMAを用いた密結合FPGAクラスタのメモリ間通信性能," 電子情報通信学会リコンフィギャラブルシステム研究会 信学技法, Vol.119, No.18, pp.7-10, May 9-10, 2019.



## Chapter 4

# Large-scale Parallel Numerical Computing Technology Research Team

### 4.1 Members

Toshiyuki Imamura (Team Leader)

Yiyu Tan (Research Scientist)

Daichi Mukunoki (Research Scientist)

Shuhei Kudo (Postdoctoral Researcher)

Takuya Ina (Technical Staff)

Tetsuya Sakurai (Senior Visiting Researcher, University of Tsukuba)

Daisuke Takahashi (Senior Visiting Researcher, University of Tsukuba)

Franz Franchetti (Senior Visiting Researcher, Carnegie Mellon University)

Yusuke Hirota (Visiting Researcher, Tokyo Denki University)

Sarah Huber (Visiting Researcher, Bergische Universtät Wuppertal)

Martin Galgon (Visiting Researcher, Bergische Universtät Wuppertal)

Andreas Marek (Visiting Researcher, Max-Plank Computing & Data Facility)

Takeyuki Harayama (Intern, University of Tsukuba)

Chen Yen-Chen (Intern, University of Tokyo)

Ryuki Shimotori (Intern, University of Yamaashi)

Aya Motohashi (Assistant)

### 4.2 Research Activities

The Large-scale Parallel Numerical Computing Technology Research Team conducts research and development of numerical software for the national flagship systems, K computer and the supercomputer Fugaku. In particular, we are focusing on significant technical issues when we face at extensive computing, such as, large-scale, highly parallel and high-performance. In general, simulation programs require various numerical techniques to solve systems of linear equations, to solve eigenvalue problems, to compute and solve non-linear equations, and to do fast Fourier transforms. From a mission critical point of view, it is natural for us to develop and deploy highly-parallelized and scalable numerical software integrated over a software framework dedicated on K and Fugaku as well, but not limited on a target platform. It comprises above-mentioned software components (numerical software) in order to run a specific simulation code which come from scientific and engineering domain problems.

Also, the K- and Fugaku- related issues were supposed to be also our challenging works such as communication reducing and avoidance, cooperation with advanced devices, fault detection and recovery, and precision-aware computing (higher-or-reduced/variable-or-mixed accuracy).

Since 2016, we have added three new research themes as recipes for long-term research goals;

1. investigation of unexplored and conventional numerical fields,
2. precision-aware computing and numerical reproducibility,
3. acceleration on some emerging devices such as an FPGA.

We are going to complete our mission through a tighter collaboration among trilateral communities from computational science (simulation), computer science (hardware and software), and numerical mathematics (scheme and theories). Our final goal is to establish fundamental techniques to develop numerical software libraries for next-generation supercomputer systems based on active and vigorous cooperation within R-CCS.

For the first topic to investigate the conventional numerical algorithm and new research on unexplored filed, we have investigated the eigen/singular-value solver, three-dimensional parallel FFT, and mixed-precision HPL kernel, namely HPL-AI benchmark, on the part of which is also related to the precision awareness. Three studies cover the second topic; minimal-precision computing, accurate and reproducible BLAS, and DGEMM emulated by Tensor Cores. For the third topic, we have conducted task-parallelism on an FPGA for matrix-matrix multiplier and a super-realistic acoustic simulation by the field-rendering method using FPGA's.

### 4.2.1 Application of the Jacobi Rotation Kernel for the eigen- and singular value computations

The Jacobi eigen-/singular value decomposition method (the Jacobi method) is accurate and also has a simple computation pattern, which is easy to parallelize. However, its high computational cost damages its benefits. In FY2019, we developed the Jacobi Rotation Kernel (JRK), which takes the core computation part of the Jacobi method with high efficiency and lower computational. Therefore, JRK can mitigate the defect of the Jacobi method. Since 2020, we have started to research to apply JRK to the Jacobi methods and evaluate its performance [11, 35]. Fig. 4.1 and 4.2 compare the performance of our implementations of the Jacobi method with that of LAPACK's eigen-/singular value solvers, respectively. The figures show that JRK improves the performance of the Jacobi methods and reduce the gap between other eigen-/singular value computation methods.

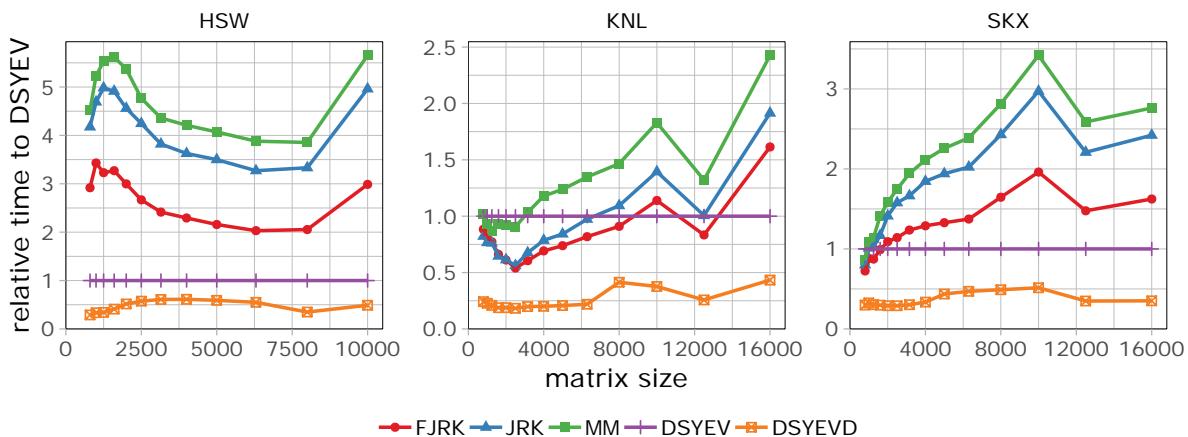


Figure 4.1: The relative computations time of eigenvalue solvers compared with the standard solver in LAPACK, DSYEV, on three different CPUs, Intel Haswell (HSW), Knights Landing(KNL), and Skylake-X (SKX). ‘FJRK’ and ‘JRK’ are the Jacobi method with JRK, and ‘MM’ refers to without JRK. ‘DSYEVD’ is the fastest solver in LAPACK. The Jacobi method is about 2–5 times slower than DSYEV without JRK. With the faster version of JRK, ‘FJRK’, the gaps reduce to about 1.5–3.

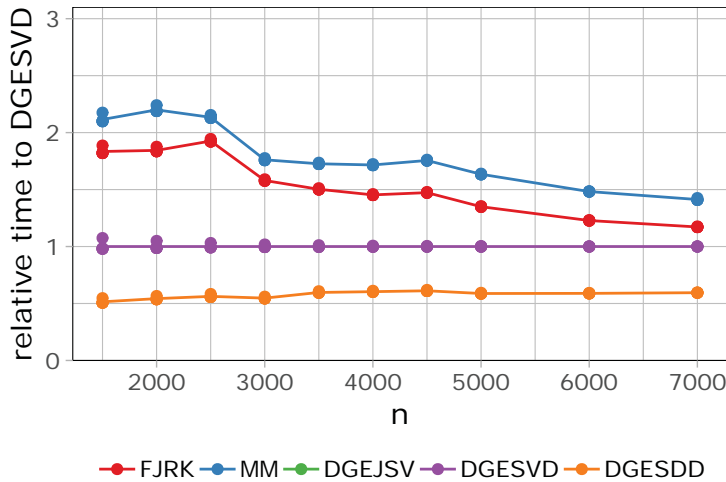


Figure 4.2: The relative computation time of singular solvers compared with the standard solver in LAPACK, DGESVD. The results are not as significant as the previous figure, Fig. 4.1, but we can observe the benefit of ‘FJRK’.

#### 4.2.2 Parallel three-dimensional FFT on a massive-scale system like K

The demand for large scale 3D FFTs will never change as we move from K to Fugaku. In order to overcome the weakness of the 3D FFT, we have been introducing a new implementation to enable the simultaneous execution of all-to-all and FFTs by proactively scheduling internal tasks with batching. This study’s results were presented in ParCo2019 [4], which was done collaboratively with Prof. Yokokawa from Kobe University, and partly under the leadership of visiting scholars; Prof. Franchetti from Carnegie Mellon University and Prof. Takahashi from University of Tsukuba.

The study showed that communication and computation are possibly comparable under the K computer’s specification, and communication and computation work concurrently overlapping each other. Our best achievement was a 45.9% improvement when the CFD domain’s grid size was  $2,048^3$ , and 128 processors on the K computer were utilized. On the other hand, the core of the work insists that the communication part tends to dominate as a steady-state even if the appropriate number of batches is guaranteed. Consequently, it revealed the difficulty in future systems. For example, we already know that the balance between computation and communication varies in Fugaku, which is more communication-intensive than the K computer. Thus, it must be necessary to apply optimizations for batch scheduling, communication methods, and investigation of other advanced methods for parallel/distributed FFTs.

#### 4.2.3 Analysis and development of software of the HPL-AI benchmark

The HPL-AI benchmark is a new benchmark for a supercomputer, similar to the well-known LINPACK benchmark but has been extended to reflect recent hardware’s capability for the AI applications. The HPL-AI allows us to use the lower-precision floating-point arithmetic by introducing the mixed-precision technique in the linear solver. Therefore, supercomputers can achieve much better FLOPS than with LINPACK. Although the enormous interest from the HPC communities, because it is new, there is no reference implementation of the HPL-AI benchmark for supercomputer environments. Therefore, we developed software for the benchmark from scratch, with analysis to avoid numerical difficulties in lower-precision arithmetic [43]. We plan to benchmark our software on supercomputer Fugaku in FY2020, and the results will be released at the top500 session during ISC2020.

#### 4.2.4 Minimal-precision computing

The mixed-precision technique utilizing fast low-precision operations is one of the promising approaches to improve the speed and energy efficiency of computations. In this FY, we have started a discussion on the precision-tuning scheme for existing mono-precision codes with RIKEN CCS, Sorbonne University (France),

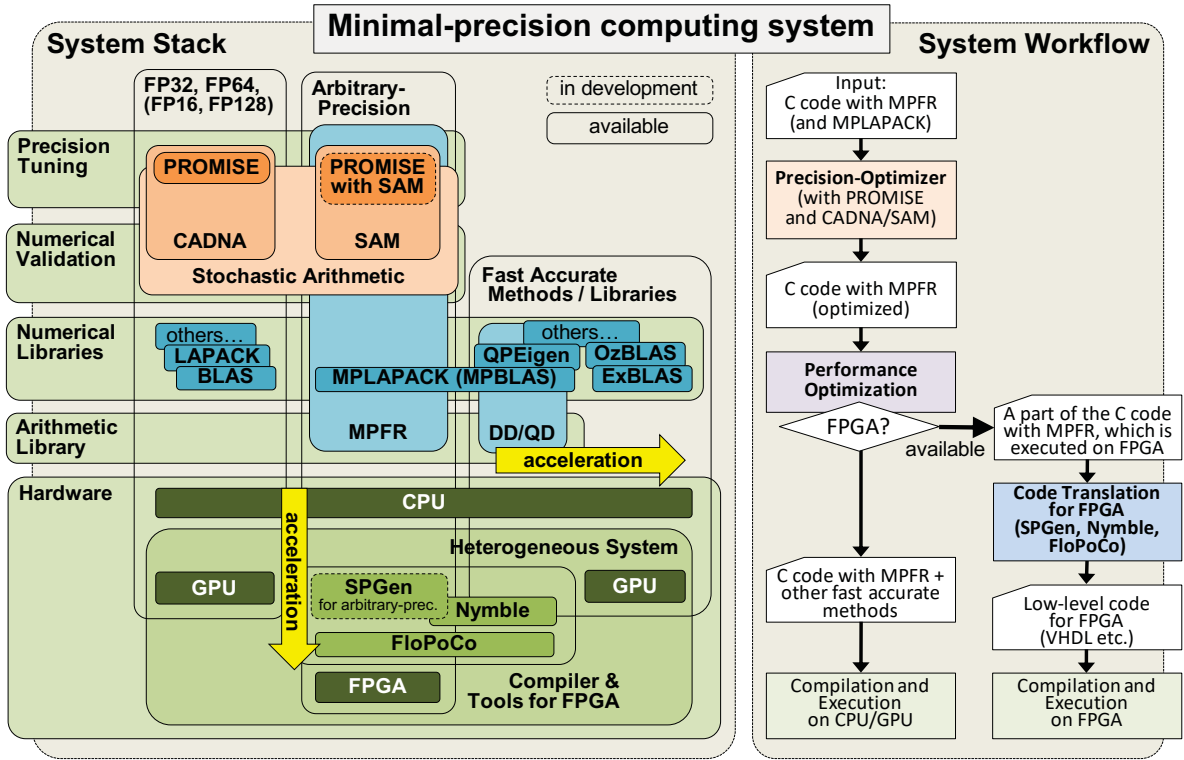


Figure 4.3: System overview required for Minimal-precision computing

and University of Tsukuba. As an intermediate result, we have proposed the minimal-precision computing system.

Figure 4.3 shows the system stack of the proposed minimal-precision computing system. Unlike the other existing precision tuning projects, it aims not only to optimize (minimize) the precision for each data in an input code but also to satisfy the demand for reliable computing – accurate and reproducible computations. Moreover, it is a system-level scheme involving both hardware and software stacks. In specific, it combines (1) a precision-tuning method based on a numerical validation method, (2) arbitrary-precision arithmetic libraries, (3) fast and accurate numerical libraries and (4) Field-Programmable Gate Array (FPGA) with high-level synthesis. Therefore, we ultimately aim to provide an arbitrary-precision computing platform with precision tuning.

One of the key technologies in our proposed scheme is the numerical validation based on Discrete Stochastic Arithmetic (DSA). The DSA enables one to obtain the number of correct digits in the computed result statistically by performing a code several times with random rounding. Then, the precision tuning is performed based on the validated result by DSA. Through numerical validation, the demand for reliable computing can be satisfied. This concept is applied even to obtain an accurate result whose accuracy is higher than that can be obtained using double-precision arithmetic. Currently, a DSA implementation for IEEE floating-point standards, CADNA, and a precision tuner based on CADNA, PROMISE, are available (both have been developed by Sorbonne University). We plan to extend and improve both libraries for our scheme.

Our proposed scheme has been presented and discussed in several international conferences (e.g., poster presentations at SC19 [21], HPC Asia 2020 [23] and 2nd R-CCS International Symposium [26], oral presentation at CRE2019 [13], SIAM PP20 [15] and others [20, 40]). Besides, we have organized two international workshops at R-CCS focusing on this topic (LSPANC 2019 June [33] and LSPANC 2020 January [41]). The white paper from the LSPANC2020 January workshop will be published (planned in FY2020 as "White Paper from Workshop on Large-scale Parallel Numerical Computing Technology (LSPANC 2020): HPC and Computer Arithmetic toward Minimal-Precision Computing", HAL-0253631).

### 4.2.5 Accurate and reproducible BLAS routines and CG method

Ozaki scheme is an accurate and reproducible dot-product/matrix multiplication algorithm based on the error-free transformation for dot-product/matrix multiplication proposed by Ozaki et al. in 2011. The scheme can

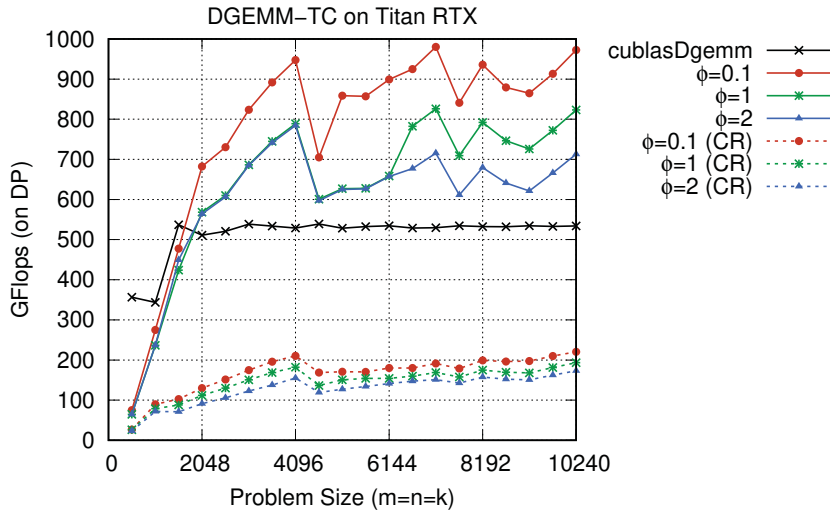


Figure 4.4: DGEMM using Tensor Cores on Titan RTX. “(CR)” is the correctly-rounded version, and without “(CR)” is the DGEMM equivalent accuracy version. The performance depends on the absolute range of the input values.  $\phi$  varies the range: it increases as  $\phi$  increases. When  $\phi = 0.1$ , the range is about  $1E+9$ .

realize tunable accuracy, including correct-rounding, and ensure bit-level reproducibility regardless of the computational environment, even between CPUs and GPUs. We have been developing accurate and reproducible linear algebra kernels using the Ozaki scheme on CPUs and GPUs since 2018 under the collaboration of Prof. Takeshi Ogita (Tokyo Woman’s Christian University) and Prof. Katsuhisa Ozaki (Shibaura Institute of Technology) (the development started when the main developer, Daichi Mukunoki worked at Tokyo Woman’s Christian University). In this FY2019-2020, we published a paper on accurate and reproducible BLAS routines on CPUs and GPUs based on the Ozaki scheme at PPAM2019 [6]. Also, a part of the results was presented at the poster session in Russian Supercomputing Days 2019 [18], LSPANC [34, 42], SIAM CSE19 [14], ATOS22 [31], and other domestic seminars [37, 38]. Moreover, in this FY2019-2020, we have developed accurate and reproducible sparse iterative solvers based on the conjugate gradient (CG) method using the Ozaki scheme on CPUs and GPUs. The result was presented at ENUMATH 2019 [10].

#### 4.2.6 DGEMM using Tensor Cores

We have developed a double-precision dense matrix multiplication routine (DGEMM) on NVIDIA Tensor Cores based on the Ozaki scheme. Tensor Cores are special processing units that perform  $4 \times 4$  matrix multiplications on FP16 inputs with FP32 precision and return the result on FP32. We have modified the Ozaki scheme for computing FP64 values using Tensor Cores. This study aims to enhance the potential of Tensor Cores or AI-oriented processors supporting fast low-precision operations for general-purpose workloads. In this FY2019-2020, we first developed a correctly-rounded implementation. The result was presented at the poster session in HPC Asia 2020 [25]. After that, we developed an enhanced implementation that can achieve standard DGEMM equivalent accuracy. The result was submitted as a paper to ISC2020 (which was accepted to publication in LNCS 12151). Figure 4.4 shows the performance of DGEMM using Tensor Cores on a Titan RTX.

#### 4.2.7 FPGA-based matrix multiplier with task parallelism

Matrix multiplication requires computer systems have huge computing capability and data throughput as problem size is increased. In this research, an OpenCL-based matrix multiplier with task parallelism is designed and implemented by using the FPGA board DE5a-NET to improve computation throughput and energy efficiency. The matrix multiplier is based on the systolic array architecture with  $10 \times 16$  processing elements, and all modules except the data loading modules are autorun to hide computation overhead. When data are single-precision floating-point, the proposed matrix multiplier averagely achieves about 785 GFLOPs in computation throughput (4.5(a)) and 66.75 GFLOPs/W in energy efficiency (4.5(b)). Compared with the Intel’s OpenCL example with data parallelism on an FPGA, software simulations with the Intel MKL and OpenBLAS

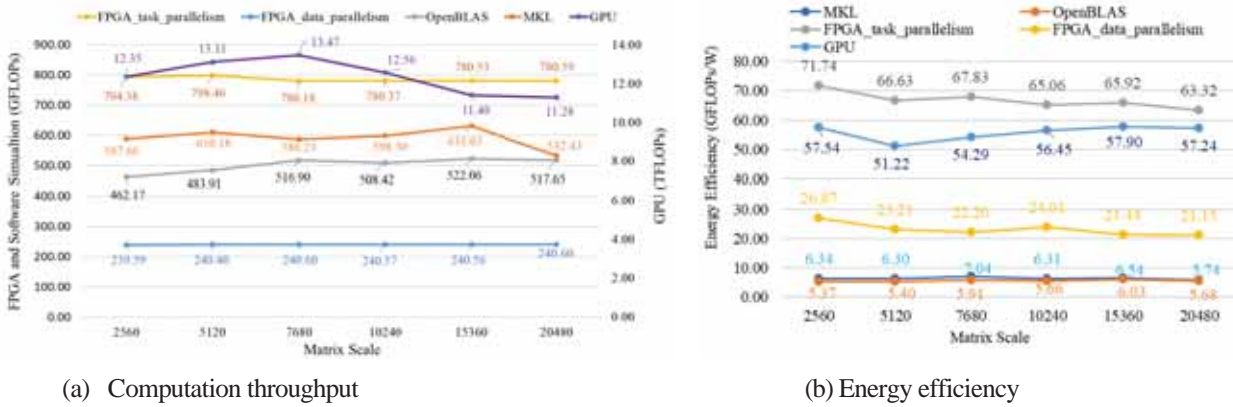


Figure 4.5: Performance of the FPGA-based matrix multiplier

libraries carried out on a desktop with 32 GB DDR4 RAMs and an Intel i7-6800K processor running at 3.4 GHz, the proposed matrix multiplier averagely outperforms by 3.2 times, 1.3 times, and 1.6 times in computation throughput, and by 2.9 times, 10.5 times, and 11.8 times in energy efficiency, respectively, even if the fabrication technology of the FPGA is 20 nm while it is 14 nm in CPU. Compared with the TITAN V GPU (12 nm), the proposed matrix multiplier is significantly defeated in computing performance, but it wins in energy efficiency. The related results were presented at the conference SIAM PP 2020 [16], ParCo 2019 [3], and ISC 2019 (poster) [17], CYGNUS project [19], and LSPANC2020Jan [44].

#### 4.2.8 FPGA-based acceleration of FDTD sound field rendering

Finite difference time domain (FDTD) schemes are widely applied to analyse sound propagation, but are computation-intensive and memory-intensive as sound space is increased. Current sound field rendering systems with FDTD schemes are mainly based on software simulations on personal computers (PCs) or GPUs. In this research, an accelerator is designed and implemented using FPGA for sound field rendering. Unlike software simulations on PCs and GPUs, the FPGA-based sound field rendering system directly implements wave equations by reconfigurable hardware. Furthermore, a sliding window-based data buffering system is adopted to alleviate external memory bandwidth bottlenecks. Compared to the software simulation carried out on a PC with 128 GB DDR4 RAMs and an Intel i7-7820X processor running at 3.6 GHz, the proposed FPGA-based accelerator takes half of the rendering time and doubles the computation throughput even though the clock frequency of the FPGA system is about 267 MHz and has only 8 GB DDR3 on-board RAMs. The related results were published on the conference USE 2019 [22], DAFx'19 [7], HPC Asia 2020 [24], R-CCS Intl.Sympo [27].

#### 4.2.9 Other activities

In FY2019-2020, the following studies were also conducted, and we published papers:

- Communication-avoiding PCG algorithm on a real-3D CFD code (ScaLA19 [1], R-CCS Intl.Sympo [28]),
- Performance optimization of GPU-based LOBPCG solver (ParCo19 [5]),
- Preliminary work on numerical linear algebra (JLESC [8], and [32]),
- Some of collaborative works with DL4Fugaku project (R-CCS Intl.Sympo [29]),
- Some review or summary talks for numerical libraries on Fugaku or other modern systems (JLESC [8, 9], JIFT [12], R-CCS Intl.Sympo [30], other domestic seminars [36, 39]).

### 4.3 Schedule and Future Plan

The most significant task in FY2019 and FY2020 was to complete the numerical software on the supercomputer Fugaku, and we recognized almost tasks were done in the final stage of development. As reported in the annual

report in FY2018-2019, we have updated the research milestone on a short-term and long-term as well. The must-do-topics should be rementioned again here.

- **Communication avoiding algorithm:**

We continue to investigate the communication avoiding algorithms and methods in any view of numerical linear algebra. The technologies will be applied on the algorithms of the existing CA-XX linear solvers, both dense and sparse eigenvalue solvers, the multi-dimensional FFT routines, and so on.

- **Precision-and-power aware computing:**

We have studied high/mixed/reduced-precision numerical software. Recently, reduced-precision computing enforced by deep-learning becomes a significant driving force not only on industry/consumer's market but the HPC community. What is more, other critical issue came from power-saving was pointed out in the annular report last year. We will incorporate with the stochastic and approximate approach and arbitrary precision arithmetic with the help of a reconfigurable device to reduce the cost of floating point operations and the total volume of the required hardware as well as energy consumption.

In addition to the above-mentioned issues, various international endeavors have been identified with the completion of the Fugaku project. For example, it is urgent to validate the numerical software developed in different parts of the world and to evaluate the performance of the standard software as the responsibility of the world's leading-edge computer institutions. In particular, the software products developed under the ECP initiatives in the US, SLATE and FFT-X will be actively implemented within the framework of DOE-MEXT, and through joint research agreements between CMU and R-CCS, respectively.

Furthermore, we also need to promote the log-term-ranged fundamental research on numerical algorithms that can be deployed on practical quantum computers, which will be available in ten years from now in the field of quantum computer science. In particular, it is thought to be one of the missions to explore the possibility of numerical computation on post-silicon generation computers by making full use of the emulator on Fugaku and the quantum computer programming environment developed by related organizations.

## 4.4 Publications

### 4.4.1 Articles

- [1] Y. Ali, N. Onodera, Y. Idomura, T. Ina, and T. Imamura: 'GPU Acceleration of Communication Avoiding Chebyshev Basis Conjugate Gradient Solver for Multiphase CFD Simulations,' Proc. 2019 10th Workshop on Latest Advances in Scalable Algorithms for Large-Scale Systems (ScalA), Nov. 2019
- [2] Daichi Mukunoki, Takeshi Ogita: 'Performance and Energy Consumption of Accurate and Mixed-precision Linear Algebra Kernels on GPUs,' Journal of Computational and Applied Mathematics, Volume 372, (Available online January 2020) July 2020.
- [3] Yiyu Tan, Toshiyuki Imamura, and Daichi Mukunoki: 'Design of an FPGA-based Matrix Multiplier with Task Parallelism,' International Conference on Parallel Computing, Prague, Czech, September 2019, Advances in Parallel Computing, Volume 36: Parallel Computing: Technology Trends, pp.241-250, IO-Press, April 2020
- [4] Toshiyuki Imamura, Masaaki Aoki, Mitsuo Yokokawa: 'Batched 3D-distributed FFT kernels towards practical DNS codes,' International Conference on Parallel Computing, Prague, Czech, September 2019, Advances in Parallel Computing, Volume 36: Parallel Computing: Technology Trends, pp.169-178, IO-Press, April 2020
- [5] Susumu Yamada, Toshiyuki Imamura, Masahiko Machida: 'High performance eigenvalue solver for Hubbard model: Tuning strategies for LOBPCG method on CUDA GPU,' International Conference on Parallel Computing, Prague, Czech, September 2019, Advances in Parallel Computing, Volume 36: Parallel Computing: Technology Trends, pp.105-113, IO-Press, April 2020
- [6] Daichi Mukunoki, Takeshi Ogita, Katsuhisa Ozaki: 'Reproducible BLAS Routines with Tunable Accuracy Using Ozaki Scheme for Many-core Architectures,' 13th International Conference on Parallel Processing and Applied Mathematics (PPAM2019), pp 516-527, LNCS, volume 12043, March 2020.
- [7] Yiyu Tan, and Toshiyuki Imamura, 'A FPGA-based Accelerator for Sound Field Rendering,' Proc. in the 22nd International Conference on Digital Audio Effects, Birmingham, UK, September 2019.

#### 4.4.2 Oral talks and Poster presentations

- [8] Toshiyuki Imamura, and Inge Gutheil: ‘Review on standard eigensolvers on a high-end GPU system,’ Project talk on ‘HPC libraries for solving dense symmetric eigenvalue problems,’ 9th JLESC workshop at ICL, Knoxville, TN, US. April 2019.
- [9] Toshiyuki Imamura: ‘Research advancement in autotuning in libraries and applications,’ BOS on Auto-tuning, 9th JLESC workshop at ICL, Knoxville, TN, US. April 2019.
- [10] Daichi Mukunoki, Takeshi Ogita, Katsuhisa Ozaki: ‘Accurate and Reproducible CG Method on GPUs,’ European Numerical Mathematics and Advanced Applications Conference 2019 (ENUMATH2019), Egmond aan Zee, Oct. 1, 2019.
- [11] S. Kudo, and T. Imamura: ‘A level-3 BLAS like kernel of the Jacobi rotations for the Jacobi’s eigenvalue algorithms,’ ParNum2019, Dubrovnik, Oct. 2019.
- [12] Toshiyuki Imamura: ‘Numerical software on Fugaku’, Joint US-Japan Workshop on PostK-ECP Collaboration and JIFT Exascale Computing Collaboration, October 28-29, 2019, at R-CCS, Riken, Kobe, Japan
- [13] Toshiyuki Imamura, Daichi Mukunoki, Fabienne Jézéquel, Stef Graillat, Roman Iakymchuk: ‘Numerical Reproducibility based on Minimal-Precision Validation,’ Computational Reproducibility at Exascale Workshop (CRE2019), in cooperation with SC19, 2019 (extended abstract).
- [14] Daichi Mukunoki, Takeshi Ogita: ‘High-performance Implementations of Accurate Linear Algebra Kernels on GPUs,’ 3rd International Conference on Modern Mathematical Methods and High Performance Computing in Science & Technology (M3HPCST), Jan. 9-11, 2020.
- [15] Daichi Mukunoki: ‘Minimal-Precision Computing for High-Performance, Energy-Efficient, and Reliable Computations,’ SIAM Conference on Parallel Processing for Scientific Computing (PP20), Seattle, Feb. 2020
- [16] Toshiyuki Imamura and Yiyu Tan: ‘Precision Tuning of the Arithmetic Units in Matrix Multiplication on FPGA,’ SIAM Conference on Parallel Processing for Scientific Computing (PP20), Seattle, Feb. 2020
- [17] Yiyu Tan, and Toshiyuki Imamura, ‘Design of an FPGA-based Matrix Multiplier with Task Parallelism,’ Poster presentation at the ISC High Performance Conference, Frankfurt, Germany, June 2019.
- [18] Daichi Mukunoki, Takeshi Ogita, and Katsuhisa Ozaki: ‘Accurate and Reproducible Linear Algebra Operations for Many-core Architectures,’ Poster presentation at Russian Supercomputing Days 2019 (RuSCDays 2019), Sep. 23 - 24, 2019.
- [19] Yiyu Tan, Daichi Mukunoki, Toshiyuki Imamura, et al, ‘Reduced and Extended-precision Computations on FPGAs and GPUs,’ Poster presentation at the 11th Symposium on Discovery, Fusion, Creation of New Knowledge by Multidisciplinary Computational Sciences, Tsukuba, Oct. 2019.
- [20] Daichi Mukunoki, Toshiyuki Imamura, Yiyu Tan, Atsushi Koshiba, Jens Huthmann, Kentaro Sano, Fabienne Jézéquel, Stef Graillat, Roman Iakymchuk, Norihisa Fujita, Taisuke Boku: ‘Minimal-Precision Computing for High-Performance, Energy-Efficient, and Reliable Computations,’ Poster presentation at France-Japan-Germany trilateral workshop: Convergence of HPC and Data Science for Future Extreme Scale Intelligent Applications, Nov. 7, 2019.
- [21] Daichi Mukunoki, Toshiyuki Imamura, Yiyu Tan, Atsushi Koshiba, Jens Huthmann, Kentaro Sano, Fabienne Jézéquel, Stef Graillat, Roman Iakymchuk, Norihisa Fujita, Taisuke Boku: ‘Minimal-Precision Computing for High-Performance, Energy-Efficient, and Reliable Computations,’ SC19 research poster session, The International Conference for High Performance Computing, Networking, Storage, and Analysis, Denver, USA, November 2019.
- [22] Tan Yiyu and Toshiyuki Imamura: ‘High-order FDTD Method for Room Acoustic Simulation,’ the 40th Symposium on Ultrasonic Electronics (USE 2019), Tokyo, November 2019.
- [23] Roman Iakymchuk, Fabienne Jézéquel, Stef Graillat, Daichi Mukunoki, Toshiyuki Imamura, Yiyu Tan, et al.: ‘Optimizing Precision for High-performance, Robust, and Energy-efficient Computations,’ Poster presentation at International Conference on High Performance Computing in Asia-pacific Region (HPC Asia), Fukuoka, January. 2020.
- [24] Yiyu Tan and Toshiyuki Imamura: ‘Sound Rendering and its Acceleration Using FPGA,’ Poster presentation at International Conference on High Performance Computing in Asia-pacific Region (HPC Asia), Fukuoka, January 2020.
- [25] Daichi Mukunoki, Katsuhisa Ozaki, Takeshi Ogita, and Toshiyuki Imamura: ‘Accurate DGEMM using Tensor Cores,’ Poster presentation at International Conference on High Performance Computing in Asia-pacific Region (HPC Asia), Fukuoka, January 2020.
- [26] Toshiyuki Imamura, Daichi Mukunoki, Yiyu Tan, Atsushi Koshiba, Jens Huthmann, Kentaro Sano, Fabienne Jézéquel, Stef Graillat, Roman Iakymchuk, Norihisa Fujita and Taisuke Boku: ‘Minimal-Precision

Computing for High-Performance, Energy-Efficient, and Reliable Computations,’ Poster presentation at the 2nd R-CCS International Symposium, Feb. 2020

[27] Yiyu Tan, Toshiyuki Imamura, and Daichi Mukunoki: ‘An FPGA-based Matrix Multiplier with Task Parallelism,’ Poster presentation at the 2nd R-CCS International Symposium, Feb. 2020

[28] Yasuhiro Idomura, Takuya Ina, Yussuf Ali, and Toshiyuki Imamura: ‘Optimization of Fusion Plasma Turbulence Code GT5D on FUGAKU and SUMMIT,’ Poster presentation at the 2nd R-CCS International Symposium, Feb. 2020

[29] Kento Sato, Akiyoshi Kuroda, Kazuo Minami, Jens Domke, Aleksandr Drozd, Mohamed Wahib, Shuhei Kudo, Toshiyuki Imamura, Kiyoshi Kumahata, Keigo Nitadori, Kazuo Ando, and Satoshi Matsuoka: ‘DL4Fugaku: Deep learning for Fugaku — Scalability Performance Extrapolation —,’ Poster presentation at the 2nd R-CCS International Symposium, Feb. 2020

[30] Toshiyuki Imamura, Yusuke Hirota, and Takuya Ina: ‘Re-design of parallel divide and conquer algorithm for a symmetric band matrix,’ Poster presentation at the 2nd R-CCS International Symposium, Feb. 2020

[31] 椋木大地: 尾崎スキームに基づく高精度かつ再現性のあるBLASルーチンの実装と自動チューニングの適用, 第22回AT研究会オープンアカデミックセッション (ATOS22), 東京大学情報基盤センター, 東京都, 2019年5月13日

[32] 工藤周平, 今村俊幸, “オンデマンドな行列計算カーネルの生成機構の構想,” 第24回計算工学講演会, 大宮市, 2019年5月.

[33] Toshiyuki Imamura: ‘High Precision Floating and Integer Arithmetic on Supercomputing Environment,’ Workshop on Largescale Parallel Numerical Computing Technology (LSPANC 2019 June), RIKEN R-CCS, Kobe, Jun. 7, 2019.

[34] Daichi Mukunoki: ‘High-Performance Implementations of Accurate and Reproducible BLAS Routines on GPUs,’ Workshop on Largescale Parallel Numerical Computing Technology (LSPANC 2019 June), RIKEN R-CCS, Kobe, Jun. 7, 2019.

[35] 工藤周平, 今村俊幸, “ヤコビ回転カーネルを用いたヤコビ固有値計算手法の性能評価”, 研究報告HPC, 2019-HPC-170, vol.35, pp.1-8 (2019).

[36] 今村 俊幸: 「「京」ならびに「富岳」に向けた並列固有値計算ソルバについて」, 第4回 High Performance Computing Physics (HPC-Phys) 勉強会, R-CCS, 2019年8月26日

[37] 椋木大地, 荻田武史, 尾崎克久, 今村俊幸: 尾崎スキームによる高精度かつ再現性のあるBLAS実装, 日本応用数理学会2019年年会講演予稿集, pp. 402-403, 2019 (extended abstract).

[38] 椋木大地, 荻田武史, 尾崎克久: 尾崎スキームによる高精度BLAS実装「OzBLAS」とその応用, 第3回 精度保証付き数値計算の実問題への応用研究集会 (NVR 2019), 高松市, 2019年12月1日

[39] 今村俊幸: エクサ時代の非同期タスクを応用した高性能高次元数値線形代数の研究, 第11回 自動チューニング技術の現状と応用に関するシンポジウム(ATTA2019), 東京大学, 2019年12月23日

[40] Daichi Mukunoki: ‘Minimal-Precision Computing for High-Performance, Energy-Efficient, and Reliable Computations,’ Sapporo Winter HPC Seminar 2020, Information Initiative Center, Hokkaido University, Jan. 24, 2020.

[41] Toshiyuki Imamura: ‘Overview of minimal-precision computing and (weak)-numerical reproducibility,’ Workshop on Largescale Parallel Numerical Computing Technology (LSPANC 2020 January), RIKEN R-CCS, Kobe, Jan. 30, 2020.

[42] Daichi Mukunoki: ‘Accurate BLAS implementations: OzBLAS and BLAS-DOT2,’ Workshop on Largescale Parallel Numerical Computing Technology (LSPANC 2020 January), RIKEN R-CCS, Kobe, Jan. 30, 2020.

[43] Shuhei Kudo: ‘How (not) to cheat in HPL-AI,’ Workshop on Largescale Parallel Numerical Computing Technology (LSPANC 2020 January), RIKEN R-CCS, Kobe, Jan. 30, 2020.

[44] Yiyu Tan: ‘Precision Tuning of the Arithmetic Units in Matrix Multiplication on FPGA,’ Workshop on Largescale Parallel Numerical Computing Technology (LSPANC 2020 January), RIKEN R-CCS, Kobe, Jan. 30, 2020.

#### 4.4.3 Award

[45] Daichi Mukunoki, Takeshi Ogita, Katsuhisa Ozaki: Best Research Poster Award, Russian Supercomputing Days 2019 (RuSCDays 2019), Sep. 2019 (Accurate and Reproducible Linear Algebra Operations for Many-core Architectures)

#### 4.4.4 Other publication

[46] 「固有値計算と特異値計算, 計算力学レクチャーコース」一般社団法人 日本計算工学会 編, 長谷川秀彦 今村俊幸 山田進 櫻井鉄也 荻田武史 相島健助 木村欣司 中村佳正 著, 丸善出版, 2019

#### 4.4.5 Software (released as of April 2020)

- [47] EigenExa, <http://www.r-ccs.riken.jp/labs/lpnctrtr/projects/eigenexa/>.
- [48] KMATH\_EIGEN\_GEV, <http://www.r-ccs.riken.jp/labs/lpnctrtr/projects/kmath-eigen-gev/>.
- [49] KMATH\_RANDOM, <http://www.r-ccs.riken.jp/labs/lpnctrtr/projects/kmath-random/>.
- [50] KMATHLIB\_API, <http://www.r-ccs.riken.jp/labs/lpnctrtr/projects/kmathlib-api/>.
- [51] KMATH\_FFT3D, <http://www.r-ccs.riken.jp/labs/lpnctrtr/projects/kmath-fft3d/>.
- [52] ASPEN.K2, <http://www.r-ccs.riken.jp/labs/lpnctrtr/projects/aspem-k2/>.
- [53] MUBLAS-GEMV, <http://www.r-ccs.riken.jp/labs/lpnctrtr/projects/mublas/>.

# Chapter 5

## HPC Usability Research Team

### 5.1 Members

Hiroya Matsuba (Team Leader)

Motohiko Matsuda (Research Scientist)

Masatoshi Kawai (Postdoctoral Researcher)

### 5.2 Research Activities

The mission of the HPC Usability Team is to develop a software platform that contributes to increasing the number of uses of K computer. This team focuses on Cyber-physical systems as potential new use cases of supercomputers, expecting that simulation of infrastructure facilities will provide valuable information for its operation. For example, if a simulator of a cooling facility is available, the operator can search for an energy-efficient combination of parameters such as a temperature of cooling water, power of pumps, and positions of valves. Simulation is especially valuable because it enables operators to test parameters that are impossible to apply to the real facilities because of safety reasons.

The main obstacles in utilizing simulation technologies in cyber-physical systems are the difficulties in developing simulation programs. Although there are many simulator products, many of them focus on a specific technical aspects such as fluid dynamics or structural analysis, whereas simulation of industrial facilities requires a combination of various simulation techniques, such as a 1-D circuit, discrete event, or agent simulations as well as fluid or structural simulations. No one commercial software covers such a wide range of simulation techniques. The HPC Usability Research Team aims to develop a new programming framework that enables rapid development of simulation programs or programs that connect existing simulators, especially those for parallel computers. We assume engineers of companies who provide, for example, consulting service for factory management, use this programming framework.

We also aim to contribute to improving operational efficiencies of the K computer by actually adopting the techniques of the cyber-physical systems. By developing a simulator of the cooling and electric facilities of the supercomputer K or Fugaku, we expect we can improve operational efficiencies by, for example, reducing safety margins while ensuring the safety of the operation by using the simulator.

#### 5.2.1 Development of the Pyne Parallel Programming Framework

We are developing a Pyne framework, which is a programming framework that enables ones to develop parallel programs as if they were sequential programs. The main objective of this framework is to improve the productivity of parallel programs, including simulation programs or programs for connecting existing simulators with another simulator or machine learning frameworks.

##### 5.2.1.1 Basic Concepts of Pyne

Pyne enables higher productivity of parallel programs by enabling programmers to write parallel programs as if they were sequential ones. Because parallelizing arbitrary sequential programs efficiently is almost impossible,

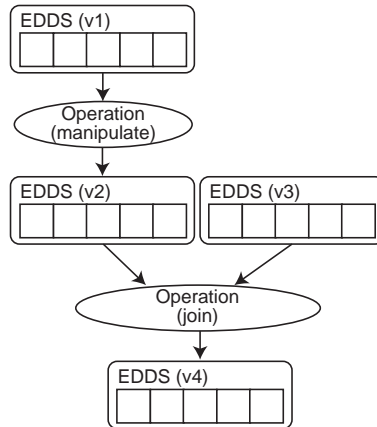


Figure 5.1: Example of Pyne's abstraction of a parallel program

```

1 def main:
2   v1 = edds.createVector(ini t=readStream)
3   v2 = v1.manipulate(nei ghSi ze=1, func=avgFunc)
4   v3 = edds.createVector(ini t=ini t3)
5   v4 = edds.join(operands=(v2, v3),
6                 nei ghSi ze=(0, 0), func=addFunc,
7                 di st=[1000])
8   v5 = v4.out(func=wri teStream)
9   edds.fi nal (v5)
10
11 def avgFunc(nei gh):
12   return (nei gh[0] + nei gh[1] + nei gh[2]) / 3.0
13
14 def addFunc(nei gh):
15   return nei gh[0][0] + nei gh[1][0]
  
```

Figure 5.2: Example source code of a Pyne program

Pyne introduces an appropriate restriction on the type of supported application while maintaining as much flexibility as possible. To be specific, Pyne applications are required to be a series of operations on the data structures called the implementation independent data structure (IIDS). Figure 5.1 shows an example of the structure of a simple Pyne program. In this program, after the creation of an IIDS called *v1*, which is a vector (creation is also an operation but omitted from the figure), manipulate operation is applied to this IIDS. This operation generates the resulting IIDS *v2*. What is done in this manipulate operation is specified by the programmer as a sequential procedure. Then, after the creation of another IIDS called *v3*, this program performs the join operation. Finally, the resulting IIDS, which is *v4*, is generated by this operation.

Figure 5.2 shows the source code to express this program (unimportant details are omitted). The above-described operations are written at Lines 2 to 7, which is the main part of the program. The functions *avgFunc* and *addFunc* are to specify the concrete calculation that should be done during the manipulate and join operations, respectively. The important point is the fact that this program can be run with a huge size of vectors. In such a case, vectors are automatically distributed across multiple nodes. How to distribute the vector is determined by Pyne, not by programmers. Therefore, programmers do not have to care about the parallel implementation of the vector, which is why the data structure of Pyne is named implementation independent data structure.

The problem of Pyne is that it is practically valuable only when many kinds of IIDS operations are provided as a library. If this were possible, Pyne would have become an attractive parallel application development framework. However, the team has been terminated due to management problems, and has not developed an actual library. Nevertheless, we think it is worthwhile to have designed a novel interface for the simple development of parallel applications.

### 5.2.1.2 Interface Improvement

This year, we tried to improve productivity of Pyne by allowing users to write pure Python programs. Last year, we developed Pyne using Cython, which is a technique to compile Python-like programs into native code. We used Cython, not pure Python, to obtain acceptable performance as an HPC infrastructure software. However, writing Cython programs requires knowledge of C language, which diminishes the productivity of Python.

The improved version of Pyne uses Numba, which is a Just-in-Time (JIT) compiler for Python. By specifying Python functions to be compiled at run-time, Numba generates native code using LLVM. The advantage of Numba over Cython is that it does not require users to rewrite their programs. Although Numba only supports a subset of Python language, its functionality is generally enough to compile the user-defined part of IIDS operations.

Numba is usually used by adding `@jit` annotation to Python functions that should be compiled. However, using Numba with Pyne is not straightforward. Adding the annotation to the user-defined part of IIDS operations provides no performance improvement because the overhead to pass Python objects to native code is involved at the innermost loop. Python specific objects are necessary when Pyne runtime library calls the user-defined functions. Specifically, because the number of arguments and return values varies with the function, a generic logic to call user-defined functions will have to manipulate variable-length lists, which incurs handling of Python-specific objects.

To avoid using Python-specific objects when Pyne runtime calls user-defined functions, Pyne dynamically generates an interface function, which is specific to each user-define function. Because the interface function is generated for a particular user-defined function, the number of arguments and return values is also fixed, and no variable-length data structure is required. Such an interface function can be compiled by Numba, and fast execution is realized.

Figure 5.3 shows the example of IIDS usage and generated code. Pyne generates the function named `caller_calcTentVelocity_1013`. This generated function embeds the information of, for instance, how many operands are necessary for user-defined part, or how many values are returned from the function. The generated function and the user-defined function are optimized by Numba (JIT). Because these functions generally include only simple loops and numerical calculations, these functions are efficiently converted to native code at run-time.

### 5.2.1.3 Performance Evaluation

We ran a fluid simulation application at two different sizes,  $2700 \times 900$  and  $900 \times 300$ , for large and small configurations, respectively. There is an obstacle in the space. Fluid flows around this object. We ran this simulation program for 10,000 time-steps so that we can see meaningful simulation results, the appearance of Kármán's vortexes. We used a 16-node cluster. Each node had an 8-core Xeon Platinum 8280 processor, with 376 GB of memory, and an Intel Omni-Path (100Gbps) interconnect.

Figure 5.4 shows the strong scaling performance obtained by executing the Pyne and PETSc versions with the two problem sizes and with 3, 12, 48, 75, and 108 processes. As shown in the figure, the Pyne version performed as well as the PETSc version when the number of processes is small, but Pyne performs worth than the PETSc version when the number of processes is large. This performance difference comes from the overhead of code generation. Because Pyne generates Python code as described above, and Numba generates native code at run-time, the time for code generation is included in the benchmark results.

## 5.2.2 A Digital Twin for Operation Planning of the Cooling Facility

HPC Usability Research Team is collaborating with Operations and Computer Technologies Division on creating a real cyber-physical system. Our target is the cooling facility of Fugaku. By reproducing the behavior of the cooling facility of Fugaku with a simulator, we can do trial and error in searching for efficient operation parameters, such as temperature settings of cooling water. The cyber-physical system that virtually experiment potentially dangerous operations is often called a digital twin. This project is to utilize a digital twin for contribution to the efficient operation of supercomputers. We also collaborate with AIST (National Institute of Advanced Industrial Science and Technology), who operates ABCI, to utilize the experiences of both parties for the efficient operation of the supercomputers.

### 5.2.2.1 Simulation Modeling of the Cooling Facility

The digital twin of the cooling facility will facilitate the mission of delivering a continuous operation of a supercomputer. It allows operation planning for efficiency optimizations and decision making at failure situations

```

# Global part
NX=900; NY=300
vT = gridInLoop.setNodeValue(
    func=calcTentVelocity,
    range=((1, 1), (NX-2,NY-2)),
    neigh=["v"], out=["vT"])

# Local part
def calcTentVelocity(cdn,myself,neigh):
    i, j = cdn
    uc, vc = neigh[0]
    ue, ve = neigh[1]
    .... (calculation) ...
    return (u, v)

# Generated code
def caller_calcTentVelocity_1013(
    exeFunc,n_0,n_1,o_0,o_1):
    for j in range(1, 299):
        for i in range(1, 899):
            r=exeFunc((i+0,j+0),(),((
                (n_0[j,i],n_1[j,i]),
                (n_0[j,i+1],n_1[j,i+1]),
                (n_0[j+1,i],n_1[j+1,i]),
                (n_0[j,i-1],n_1[j,i-1]),
                (n_0[j-1,i],n_1[j-1,i])))
            o_0[j,i]=r[0]
            o_1[j,i]=r[1]

```

Figure 5.3: IIDS Usage and Generated Code

which require a study on the behaviors of the cooling system. The key points of using the digital twin are the following.

- Cooling devices are slow and autonomous. That causes overshooting/undershooting of water temperatures. Minimizing deviations reduces energy consumption.
- Human operators need to prepare for faulty situations for prompt responses. Time bounds of tolerance are the keys to an operation protocol design.
- The facility designers, however, mainly concerns static, capacity-based limits. An analysis of dynamic behaviors is the responsibility of the operators.

We are working on simulation modeling with the focus on the dynamic behaviors, and performed some analysis on some artificial faulty situations. Figure 5.5 shows the simulation model of the cooling system modeled in Modelica. The model is still for K computer, currently. The enhancements of the cooling system from K to Fugaku are relatively minor, and the model will be updated for Fugaku after some actual operation data of Fugaku is collected.

### 5.2.2.2 Simulation result validation in failure situations

Figures 5.6 show temperature variations of the cooling water at an event of turning off a power generator at a time around 2,000 seconds. In the event, the absorption chillers stopped working due to the lack of the steam from the power generator. During the event, a human operator promptly responded by starting additional chillers, and canceled the all submitted jobs as an emergency safety measure. The figures show good matches between the model simulation (solid lines) and the actual measurement (dotted lines).

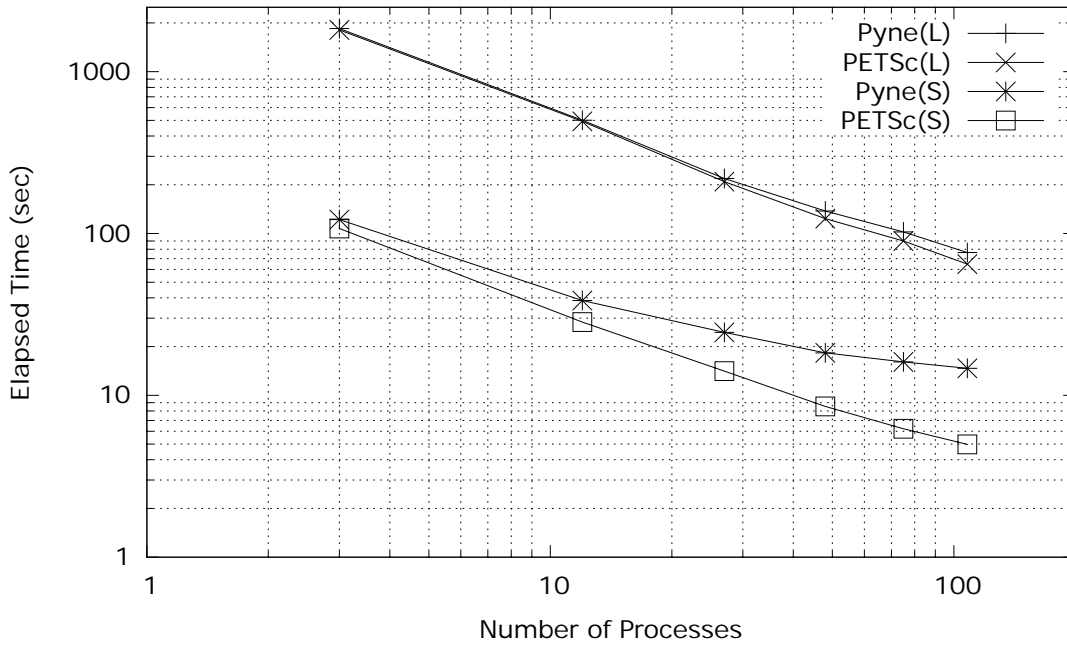


Figure 5.4: Performance (fluid simulation)

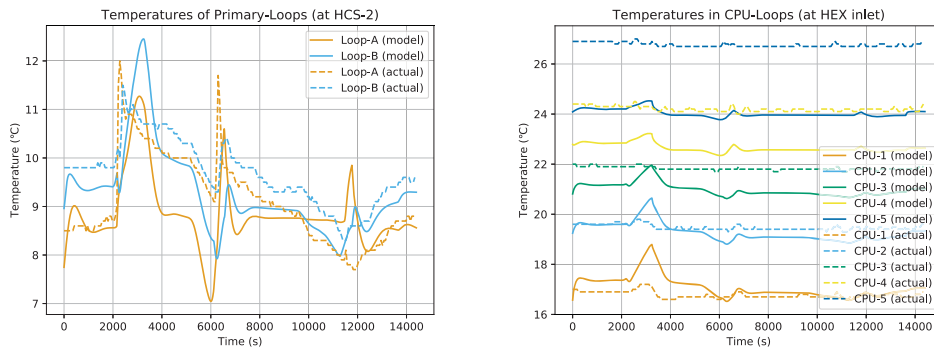


Figure 5.6: Water temperatures at a turning off event of a power generator

The model has well reproduced the behaviors in the situations of an event on a power generator as well as normal operations, where the temperature variations are unexpectedly complex. The next step is artificially sets up failure situations.

### 5.2.2.3 Case: An operator would not cancel jobs

The first artificially set-up case is that the jobs are not canceled at turning off a power generator. In the validation case above, a human operator took a safety measure of canceling the all submitted jobs. But it was not necessary as a hindsight. The temperature variations are very similar without a cancellation. The behaviors of the water temperatures when the job cancellation is skipped are shown in Figures 5.7.

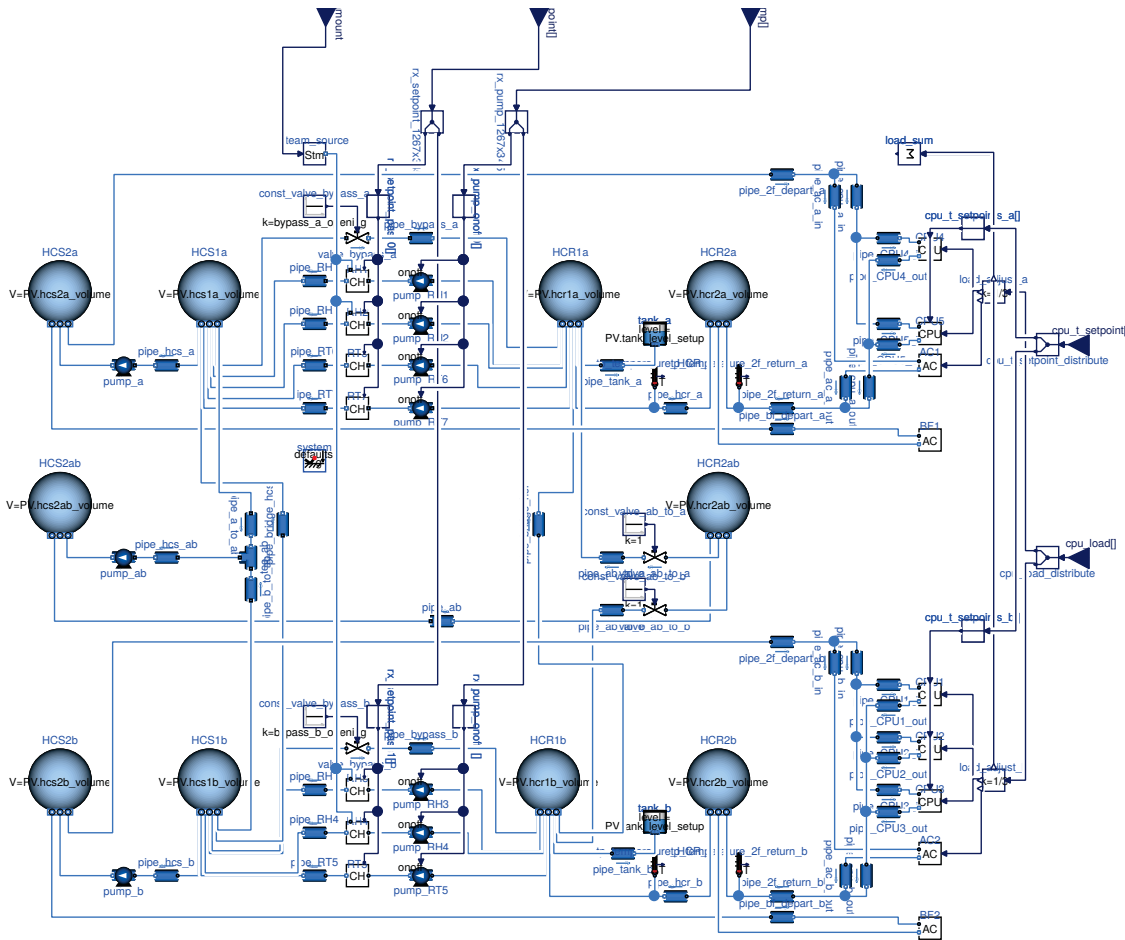


Figure 5.5: The model of the primary water loops in Modelica

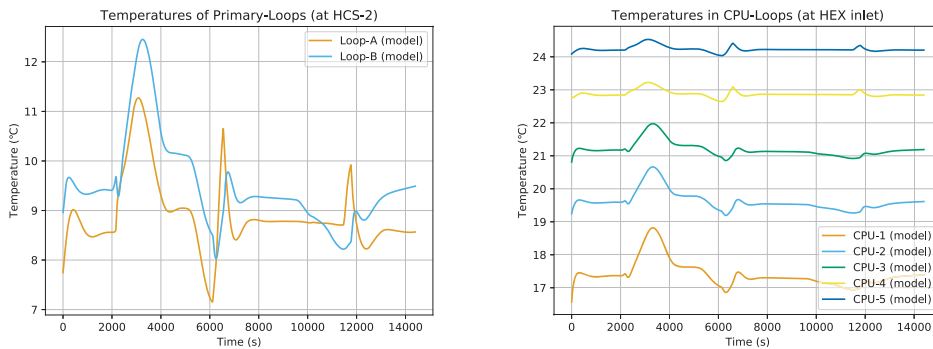


Figure 5.7: No cancellation of jobs at a turn off event

### 5.2.2.4 Case: An operator would not react forever

The second artificially set-up case is that a human operator would not react forever. In the validation case above, a human operator reacted very quickly in less than 10 minutes. The loss of a power generator is a fatal event for the cooling system, and the temperatures went higher quickly when an operator did not react at all. The simulation was stopped at a certain time before reaching the presupposed upper limit of the temperatures because that causes a simulation error (about 30 degrees Celsius). The behaviors of the water temperatures with no operator reactions are shown in Figures 5.8.

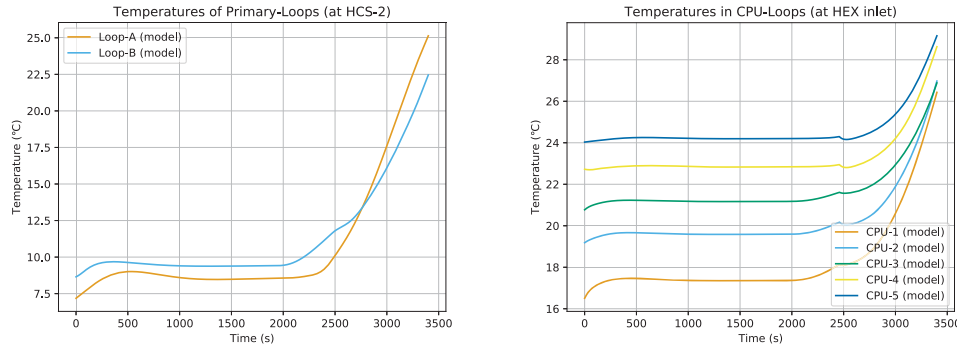


Figure 5.8: A human operator would not react

5.2.2.5 Case: An operator would react 30 minutes late

The third artificially set-up case is that a human operator reacted very late. Actually, the system could tolerate the delay of 30 minutes, keeping the water temperatures of CPU cooling below 30 degrees Celsius. The behaviors of the water temperatures with late operator reactions are shown in Figures 5.9.

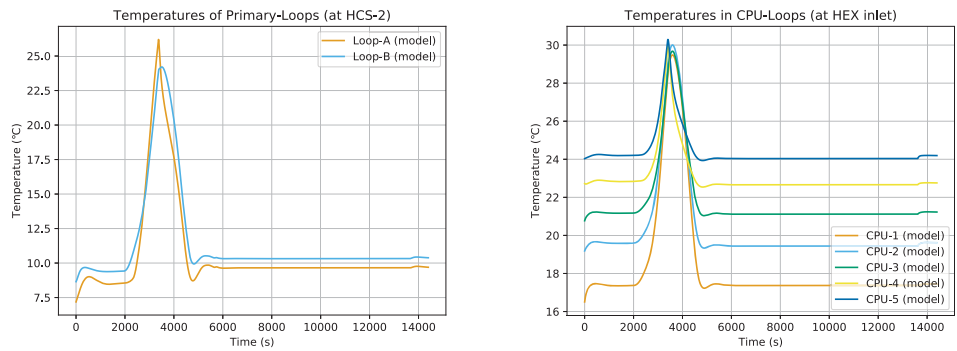


Figure 5.9: A human operator would react 30 minutes late

5.3 Schedule and Future Plan

This teams has been closed at the end of FY2019. There are no future plans.

5.4 Publications

5.4.1 Papers (refereed)

[1] M. Kawai, A. Ida, H. Matsuba, K. Nakajima, M. Bolten: "Multiplicative Schwartz-Type Block Multi-Color Gauss-Seidel Smoother for Algebraic Multigrid Methods". International Conference on High Performance Computing in Asia-Pacific Region 2020.

[2] H. Matsuba, M. Matsuda and M. Kawai: "Pyne: A programming framework for parallel simulation development". Workshop on Parallel Programming Models and Systems Software for High-End Computing (P2S2) 2019.

[3] M. Matsuda, H. Matsuba, J. Nonaka, K. Yamamoto, H. Shibata and T. Tsukamoto: "Modeling the Existing Cooling System to Learn its Behavior for Post-K Supercomputer at RIKEN R-CCS". Energy Efficient HPC State of the Practice Workshop (EE HPC SOP) 2019.

[4] K. Hayashi, N. Sakamoto, J. Nonaka, M. Matsuda, and F. Shoji: "An In-Situ Visualization Approach for the K computer using Mesa 3D and KVS". WOIV 2018 (ISC Workshop on In Situ Visualization <http://woiv.org/>).

### 5.4.2 Posters (refereed)

- [5] J. Nonaka, K. Ono, N. Sakamoto, K. Hayashi, M. Matsuda, F. Shoji, K. Oku, M. Fujita, K. Hatta: "A Large Data Visualization Framework for SPARC64 fx HPC Systems - Case Study: K Computer Operational Environment -", 2018 IEEE 8th Symposium on Large Data Analysis and Visualization (LDAV).
- [6] M. Kawai, A. Ida and G. Wellein, "ppOpen-SOL: Robust ILU Preconditioner for Exascale", HPC in Asia, ISC2018, Germany, 2018
- [7] M. Matsuda, J. Nonaka, K. Yamamoto H. Shibata, T. Tsukamoto, and H. Naemura, "R-CCS Facility Simulation Modeling for Assisting Operation Planning and Decision Making", The 2nd R-CCS International Symposium, 2020.

### 5.4.3 Presentations

- [8] N. Nomura, K. Nakajima, M. Kawai, A. Fujii, "The Analysis of SA-AMG Method by Applying Hybrid MPI/OpenMP Parallelization on Cluster Supercomputer System", 15th Copper Mountain Conference On Iterative Methods, US, 2019
- [9] N. Nomura, K. Nakajima, M. Kawai, A. Fujii, "The Evaluation of The SA-AMG Method By Applying Hybrid Parallelizaionon Cluster Computing System", ASE Seminar, Tokyo, 2019

### 5.4.4 Patents

- [10] M. Mase, T. Sakurai, and H. Matsuba, "Simulation execution method and computer system", Joint application by Riken and Hitachi, Ltd., May, 2018

# Chapter 6

## Field Theory Research Team

### 6.1 Members

Yasumichi Aoki (Team Leader)

Issaku Kanamori (Research Scientist)

Yoshifumi Nakamura (Research Scientist)

Sinya Aoki (Senior Visiting Scientist)

Shoji Hashimoto (Senior Visiting Scientist)

– close collaborators in R-CCS –

Keigo Nitadori (Technical Scientist at Operations and Computer Technologies Division)

### 6.2 Overview of Research Activities

Field theory research team performs researches related with the numerical computation of quantum field theory (QFT) in elementary particle and nuclear physics. The quantum field theory is the framework of quantum theory combined with Einstein's special relativity to describe the physical properties of elementary particles. The standard model (SM) of particle physics, which is scripted with QFT, represents the state-of-the-art understanding of the most basic physical law of the elements of matters in this world. This almost perfect law of nature is still incomplete in several reasoning: it does not explain the origin of dark matter; it does not explain the spectrum of elementary particles; it is not natural that highest energy scale in SM is seventeenth order of magnitude lower the Plank scale; etc. These motivate searches of new physics in various theoretical and experimental directions. Among these precision tests of SM and seeking answers of these questions in extensions of SM require precise information of the quantum chromo dynamics (QCD) which governs the strong interaction in SM. The involved QCD dynamics cannot be solved by hand. Computational approach with lattice QCD, discretized version of the QCD on the continuous space-time, is powerful and most effective. After the first lattice QCD simulation about 40 years ago, its technique has become sophisticated and matured to date by tremendous efforts. Realistic simulations with various parameters tuned as in the nature are becoming possible by use of supercomputer like K using a conventional version of the lattice QCD formulation. The required precision to many interesting quantities for the test of the standard model, however, has not been reached yet. In this situation, the breakthrough could be obtained by using methods which are ideal but computationally demanding. We believe using the next generation supercomputers like Fugaku with related developments makes this happen.

To maximize the power of the next generation supercomputers, multifaceted improvements are needed. First, algorithmic development for simulation technique and analysis of the large data set will be more than useful. Second, given the idea in algorithms, efficiency in the future HPC environment need to be maximized. The team conducts researches in such directions.

## 6.3 Research Results and Achievements

### 6.3.1 Lattice QCD codes and algorithms

Algorithm and code development of Lattice QCD (LQCD) for the supercomputer Fugaku is one of the most important missions of the team. The QCD Wide SIMD (QWS) Library is produced in the Flagship 2020 Project and open for public at github [40]. QWS provides libraries for most demanding numerical efforts in the Wilson fermion simulations. Namely the linear solvers for Wilson types are supported. The QWS library would be the most effective for those to simulate fermions in QCD on Fugaku. It has achieved  $[25+] \times$  speed up compared with the K supercomputer for the target application Wilson fermion solver.

In the particle physics applications, domain-wall fermions (DWFs), a most efficient chiral fermion formulation to date, are the promising framework for the Fugaku era. DWFs are variants of the Wilson fermions. It is a five dimensional Wilson fermion with a spacial boundary condition imposed in the fifth direction, which effectively makes domain walls in the both ends of the fifth direction. The four-dimensional physical degree of freedom is projected out from the wall positions. Each four-dimensional slice of the DWF at a fixed fifth dimensional position is a four dimensional Wilson fermion. The 5D DWF is superficially a connection of many 4D Wilson fermions. We may use QWS for numerical manipulations for 4D Wilson part where the most of the computational cycles are concentrated.

To make full use of QWS, LQCD package from which QWS is called is needed. The LQCD packages Bridge++ and Grid are the candidates for the use of DWF applications. Test and development of Grid is underway mainly using Intel Skylake processors at this stage through HPCI on Ito subsystem-A at Kyushu University and RIKEN Hokusai Big Waterfall, taking the finite temperature QCD with three degenerate quark flavors as a test case.

With relatively small size simulations for three degenerate quark flavors, a global search has been started as code and algorithm test. A pseudo-critical behavior in the susceptibility of plaquette (simplest observable in the gauge theory) has been found, which will be tested with changing parameters in future study.

One of the QCD package with Japanese initiative is Bridge++. Hybrid Monte Carlo for two-flavor QCD with domain-wall fermion algorithm is implemented in Bridge++ and tested at K-supercomputer. Tuning of the parameters of the molecular dynamics was done and realistic test runs were performed by taking the parameter set corresponding to those near the finite temperature transition but a bit above that. This code development appears to be successful. The knowledge acquired here for 2-flavor will be combined with the knowledge of the Grid development for 3-flavors and will be used for the development for 2+1-flavor simulations planned for the supercomputer Fugaku.

Large volume QCD simulations for Fugaku may suffer from extra slowing down. Multigrid algorithm is a promising method if implemented in efficient way. Applying it to domain-wall fermions may require special treatment as the physical light degree of freedom is not realized as simple as that of the Wilson fermion. First step to this direction is examined and is reported in the meeting of the Japan Physical Society [34] as well as in workshops [22][24].

A good pseudo random number generator for parallel computers are useful for LQCD computation and beyond that. Mersenne twister, which is one of this sort, is taken and its parameter set was searched for on K-supercomputer. The project, started with tuning of the program for this parameter mining, resulted finding about 180 million parameter sets.

Our team together with the Programming Environment Research Team organized an international workshop on the QCD coding for Fugaku <sup>1</sup>, calling related developers to participate. There knowledge and ideas acquired by domestic and international developers were shared, which encourages further research and development for the successful use of Fugaku for LQCD.

HPC-Phys workshops <sup>2</sup> are domestic meeting aiming to encourage exchanging ideas for high-performance computing especially research and developments for large scale numerical simulations in fundamental physics. This workshop in series are supported by the priority issue No. 9 to be tackled by the supercomputer Fugaku through the Joint Institute for Computational Fundamental Science (JICFuS). This year one of these workshops is held at R-CCS, and the other at Waseda University, organized by our team members together with the members in JICFuS. We plan to continue this activity taking main role of the organization in the future as well.

<sup>1</sup><https://www.r-ccs.riken.jp/labs/fttr/FugakuQCD.html>

<sup>2</sup><https://hpc-phys.kek.jp/>

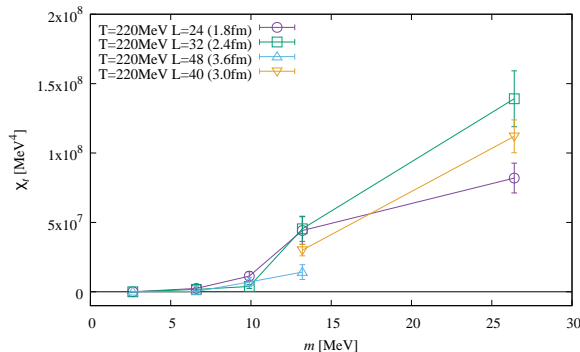


Figure 6.1: Preliminary result of the topological susceptibility as a function of ud-quark mass  $m$  for QCD with two dynamical quarks at system temperature about  $T=220$  MeV from JLQCD collaboration with a support of the priority issue 9 to be tackled by the supercomputer Fugaku. Use of a chiral fermion makes it possible to unambiguous definition of the topological charge, thus, of its susceptibility as well. Existence of the phase transition or cross-over around  $m=10$  MeV is implied. Figure is reproduced from Ref. [14].

### 6.3.2 Finite Temperature QCD with domain wall fermions

99% of the mass of the visible universe (and our body as well) is made of the energy dynamically generated by QCD interaction. The underlying mechanism of mass generation is the chiral symmetry breaking (Nambu-Goldstone mechanism): the chiral symmetry is spontaneously broken in the present universe. One can think of what happens if we unwind the history of the universe and with the temperature high enough, then the chiral symmetry should recover. If there has been a phase transition or just a crossover is a prime question whose answer would have had great influence on the history of the universe and the fate of the matters inside that. Furthermore, understanding the nature of the transition is necessary to judge the fate of one of the promising dark matter scenarios.

There is a long history of the research of QCD at finite temperature theoretically and experimentally. For theory side, as the strong coupling QCD is the target, numerical computation with lattice QCD is most useful. Because the target physics question is an involved interplay of the symmetry and its spontaneous breaking, we need the formulation which respects the symmetry in the first place. The lattice formulation which preserves exact “chiral symmetry”, thus being called as chiral fermions, is in our hands. However, it requires tremendous computational effort compared to the conventional lattice formulations, such as Wilson or staggered fermions, which respects only a part of the full chiral symmetry or does not at all. On the supercomputer Fugaku, we aim to conduct computations using chiral fermions and by that we can get rid of the compromises which we were not able to.

Along this line we employ domain-wall fermions as a practically best implementation of the chiral fermions to date. While ultimately the 2+1 flavor simulation, where lightest three quarks (up, down and strange flavors) enter, needs to be performed, we perform simulations of 2-flavor (without strange quark) QCD as a benchmark to the 2+1 flavor simulation. This is an approximation to 2+1 flavor world and actually known to be a very good approximation for low temperature systems. It is also expected to share crucial dynamical properties for finite temperatures near phase transition as well. This study is done in the JLQCD collaboration with a support of the priority issue No. 9 to be tackled by the supercomputer Fugaku to bridge to the 2+1 flavor simulations. Figure 6.1 shows a preliminary result of the topological susceptibility as a function of ud-quark mass  $m$  at temperature about  $T = 220$  MeV, which is our main target temperature and is 20-30% higher than the critical temperature expected for the chiral transition at mass-less limit. A sudden growth observed for  $m > 10$  MeV suggests a rapid transition. As there is no monotonic dependence on the volume, this is likely to be a crossover.

This quantity is related to the axial  $U(1)$  anomaly. The axial  $U(1)$  symmetry is intact in QCD at classical level, but, broken by quantum anomaly. There is a long history of debate as to whether this symmetry is effectively recovers above phase transition temperature. Chiral symmetric treatment of lattice QCD would provide the final answer to this question. Fig. 6.2 shows a preliminary results of the axial  $U(1)$  susceptibility, a measure of the breaking of axial  $U(1)$  symmetry, as a function of ud-quark mass  $m$ . Vanishing susceptibility in the  $m \rightarrow 0$  limit suggests the recovery of the symmetry at this temperature.

The fate of the axial  $U(1)$  symmetry is closely related to possible extended symmetries of the meson sector

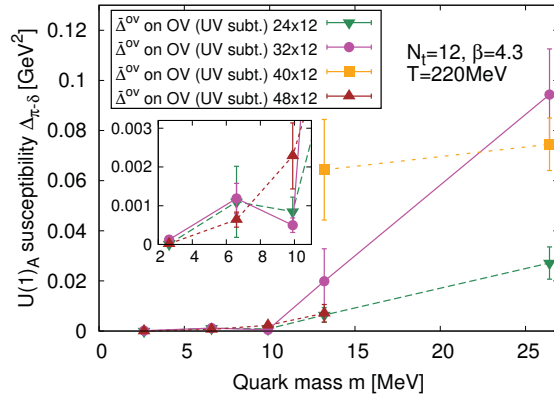


Figure 6.2: Preliminary result of the  $U(1)_A$  susceptibility as a function of ud-quark mass  $m$  for QCD with two dynamical quarks at system temperature about  $T=220$  MeV. Existence of the phase transition or cross-over around  $m=10$  MeV is implied. Figure is reproduced from Ref. [14]

in finite temperature. The meson correlation functions in spacial distance is examined using the chiral fermions in the temperature range above the critical temperature of the chiral phase transition. It has been found that the chiral-spin symmetry  $SU(2)_{CS}$  and further larger  $SU(4)$  symmetry are approximately recovered in the temperature range of  $T$  220 – 500 MeV [3][9]. This is taken as an indication of suppressed chromomagnetic interactions in QCD and systems at these temperatures are effectively described with color singlet object composed of the chirally symmetric quarks bound by the chromoelectric interaction of QCD. This new finding is made possible with the use of chiral fermions, and shows the power of using methods with large numerical cost but without compromise.

### 6.3.3 Proton decay matrix elements

Proton decay is a smoking gun evidence of new physics beyond the standard model of particle physics. It naturally takes place in grand unified theories (GUTs) which unifies the known forces in the nature except gravity. Ongoing experiments such as SuperKamiokande as well as the ones in preparation: HyperKamiokande in Japan, DUNE in USA and JUNO in China are aiming to detect the proton decay in deep underground as one of the core missions. Even without the signal of the decay, the lower bound of the proton lifetime will be prolonged with continuous operation of the experiments. That could impose severe constraint on the GUT models (ultimately leading to the way to finding the unique single theory of everything), provided that the proton decay matrix elements are determined in good precision. The underlying theory for the matrix elements is the quantum chromo dynamics, QCD, which describes the strong interaction among quarks, building blocks of proton. For the quantitative treatment for matrix elements, numerical computation using lattice QCD defined on the discrete space-time is only in our hands.

For long the numerical simulation of lattice QCD with physical value of light quark masses has not been possible due to its demanding computational cost. As such, extrapolations from simulations with unphysically heavy quark masses were performed. Use of K and other equivalent high performance computers and continuous improvement of the algorithms made it possible to now simulate QCD on top of the physical quark mass point. To cope with smaller quark mass, a larger volume needs to be used to control the finite volume error. Ever growing volume provides new room of improvement of the algorithm. All mode averaging (AMA), which one of our team member developed, is a promising new direction for accelerating the simulation for larger volumes. For most of the quantities calculated from QCD, the quark matrix inversion is the most computationally demanding part of the algorithm. The AMA framework guides the way to mix the exact low mode eigenvectors and many sloppy conjugate gradient solver with relaxed convergence criteria to minimize the computational cost for given precision using the covariance property of the matrix. This test is done using the Wilson fermion environment, with an outlook of using it to future chiral fermion simulations.

Using K at R-CCS and Hokusai BigWaterFall at Information System Division of RIKEN we have been testing the effectiveness of AMA technique using the gauge field configurations generated by PACS collaboration using a Wilson fermion formulation. With the success of the use of AMA for the low energy constants (LECs) of

proton decay matrix elements which has been achieved last year, we pushed forward to compute the form factors at the physical kinematics this year. The form factors of proton decay has more direct relation to the proton lifetime. But the computational effort needed to achieve the same precision with the LECs is almost an order of magnitude larger. Despite the cost the computation appears to be successful thanks to AMA. Figure 6.3 (a) shows the ratio as function of the position  $t$  of the baryon number violating operator with proton and pion interpolating field with distance  $t_s = 18, 20$  and  $24$ , for three different momentum injections (shown in different panels) to pion near the kinematics of physical process. The value for the form factor extracted from the plateau fit to them are plotted as a function of the squared momentum transfer in Fig. 6.3 (b). There three data points with open circle come from the three panels in (a). The cyan band is showing the results obtained with a long chiral extrapolation. Our new results with smaller error bar was made possible to utilize the physical pion mass, which does not require the chiral extrapolation, with larger computational effort with the help of AMA. The new result at the physical kinematics appears to be consistent with the old one within two standard deviations, which suggests that there is no surprise in the chiral extrapolation which could have lead to far small value thus prolongs the proton lifetime as suggested in a model estimate.

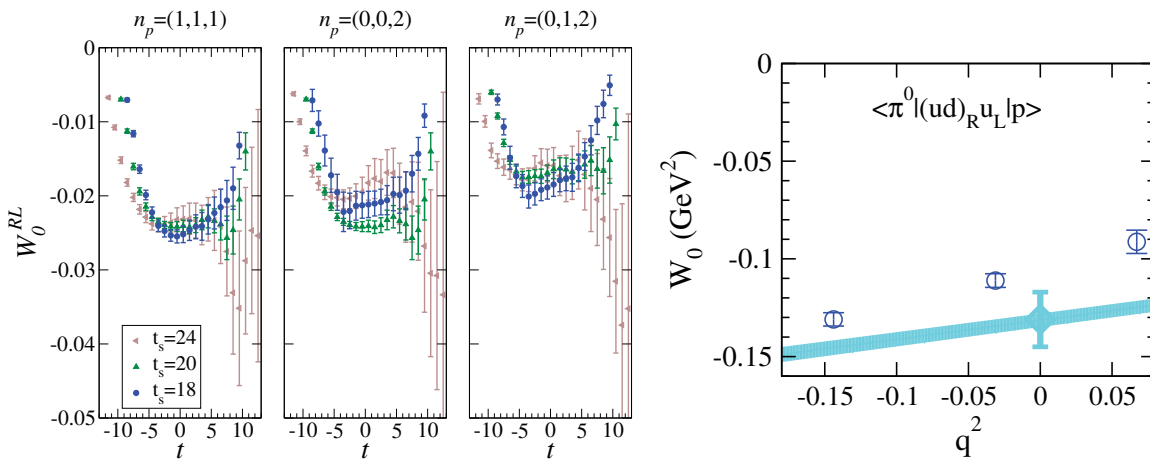


Figure 6.3: (a) (left panel) Relevant form factor of the  $p \rightarrow \pi^0$  decay with  $\mathcal{O}^I = \epsilon_{ijk}(u^{iT}CP_Rd^j)P_Lu^k$  in lattice units as a function of operator position  $t$ . (b) (right panel)  $W_0(q^2)$  for the same process (open symbol) compared against the chiral extrapolated results of domain-wall fermions shown as a cyan band. The figures are reproduced from Ref. [20].

### 6.3.4 Miscellaneous LQCD developments

There are LQCD related publications reported by members of the team with external collaborations. These works does not use K-computer, but, serve as possible seeds for future high performance computing on super-computer Fugaku and beyond that.

Yoshifumi Nakamura reported on works using Wilson fermions for QED and isospin breaking effects on the baryon spectrum [1][4], for the role of flavor symmetry on the hadronic matrix elements [2], and for system size effect on the vector meson and baryons [4]. A work for the single flavor optimization of the LQCD simulation algorithm was reported in [13]. He also worked on the tensor renormalization group as alternative algorithm to conventional Monte-Carlo, which have been reported in [11] and [12].

Issaku Kanamori reported on the application of the chiral random matrix model for two-color QCD [6], a toy-model but sharing several important properties with the real QCD. He also has published a work [7] on the numerical stochastic perturbation theory applied to the twisted Eguchi-Kawai model, a promising effective model for QCD in the limit of large number of colors.

The flavour lattice averaging group (FLAG) is establishing efforts to average LQCD results relevant to the phenomenological applications in particle physics and to provide them to community use. Yasumichi Aoki is taking a part of the activity and published the fourth edition “FLAG Review 2019” [8].

Our former member Eigo Shintani had been working on the hadronic vacuum polarization contribution to the muon  $g - 2$  in a big volume at physical point. This is done in collaboration with PACS Collaboration and published this year [10].

## 6.4 Schedule and Future Plan

The chiral fermion simulations of lattice QCD for the supercomputer Fugaku will eventually use 2+1 flavor (including the strange quark) physical point for heavy flavor physics targeting B mesons and the other precision tests of the standard model (SM). The same setting will also be used to explore the phase diagram of QCD at finite temperature which could end up simulating lighter quarks than physical. The Fugaku implementation of the existing algorithms are being developed this year and will further be extended to several LQCD packages in the coming years. Extended simulations to finer lattice, larger volume, and lighter quarks from the current ones, which would be the next stage on Fugaku as well as the post-Fugaku machines benefit from speedup with algorithmic development and tuning. There existing speedup techniques such as AMA or multigrid algorithm may serve as improvements. Developments in the methods beyond the conventional Monte-Carlo based on the molecular dynamics may find its use in the future simulations.

### 6.4.1 Algorithm and code development for the chiral fermion simulation in QCD for Fugaku

The chiral fermion simulations of two-flavor QCD uses Grid, the code set developed mainly by Edinburgh University. We are working on extending this to 2+1 flavor case. Through the co-design works for the supercomputer Fugaku involving members of our team, we foresee obstacles of simple extension of the Grid code set. The co-design software team is developing their version of Wilson fermion solvers, which can be used as main building blocks to simulate chiral fermions, too. A possible international collaboration with developers of Grid, which became one of the international standards, on the optimization for the supercomputer Fugaku, could benefit both sides and potential international users. The large volume and light quark simulations are computationally challenging. The AMA technique, being developed and tested seriously this year, will be useful. Independent of this technique, implementing and accelerating Multi-Grid algorithm would be a promising direction. In the lattice simulations, parameters not directly related with the physical setting, like the AMA and multi-grid specific ones or like tunable parameters in the hybrid Monte-Carlo potentially provide large rooms of improvement. There, optimizations assisted with deep learning could bring a significant speed up.

### 6.4.2 QCD phase diagram with chiral fermion simulations

As a test bed of new code development and new algorithms the degenerate three flavor simulation of QCD using chiral fermions can be used. The simulation is simpler than physical, non-degenerate, 2+1 flavor simulation, thus good for tests with situation close to the final target. But, it is also interesting on its own physical perspective. The phase diagram with respect to the change of the degenerate quark mass is one of the important boundary of 2+1 flavor QCD phase diagram. Recent results reported using conventional fermions suffer from huge discretization error. Use of the chiral fermions, thus being able to simulate with correct counting of the light degree of freedom, is expected to solve this problem. We started an experimental simulations with small size on existing HPC resources. Towards realistic simulations with larger volume and lighter quark mass, Fugaku-scale supercomputer is needed. Tests of the algorithm and codes for Fugaku will be immediate aim in the coming year. The knowledge acquired through these studies provide a base of the simulation of more challenging 2+1 flavor, where we would find further rooms for development on the algorithms and codes.

### 6.4.3 Collaboration on physics applications

We have a close collaboration with the priority issue No. 9 to be tackled by the supercomputer Fugaku. This project will be extended to the new “Program for Promoting Researches on the Supercomputer Fugaku” (Simulation for basic science: from fundamental laws of particles to creation of nuclei) next year. It will be continued for three years. We will start preparing the simulation on Fugaku in the first year and full scale simulations will be performed in the FY 2021 and 2022. Through this collaboration, we aim to maximize the scientific output of the issues for intensity frontier subjects including flavor physics, as well as for the QCD phase by cutting edge developments.

## 6.5 Publications

### 6.5.1 Articles/Journal

- [1] CSSM/QCDSF/UKQCD Collaboration: Z.R. Kordov, R. Horsley, Y. Nakamura, H. Perlt, P.E.L. Rakow, G. Schierholz, H. Stüben, R.D. Young, J.M. Zanotti, “Electromagnetic contribution to  $\Sigma - \Lambda$  mixing using lattice QCD+QED”, *Phys.Rev. D*101 (2020) no.3, 034517.
- [2] J.M. Bickerton, R. Horsley, Y. Nakamura, H. Perlt, D. Pleiter, P.E.L. Rakow, G. Schierholz, H. Stüben, R.D. Young, J.M. Zanotti, “Patterns of flavor symmetry breaking in hadron matrix elements involving  $u$ ,  $d$ , and  $s$  quarks”, *Phys.Rev. D*100 (2019) no.11, 114516.
- [3] C. Rohrhofer, Y. Aoki, L.Ya. Glozman, S. Hashimoto, “Chiral-spin symmetry of the meson spectral function above  $T_c$ ”, *Phys.Lett. B*802 (2020) 135245.
- [4] PACS Collaboration: K.I. Ishikawa, N. Ishizuka, Y. Kuramashi, Y. Nakamura, Y. Namekawa, E. Shintani, Y. Taniguchi, N. Ukita, T. Yamazaki, T. Yoshié, “Finite size effect on vector meson and baryon sectors in 2+1 flavor QCD at the physical point”, *Phys.Rev. D*100 (2019) no.9, 094502.
- [5] CSSM and QCDSF and UKQCD Collaborations: Z. Koumi, Y. Nakamura, H. Perlt, D. Pleiter, P.E.L. Rakow, G. Schierholz, A. Schiller, H. Stüben, R.D. Young, J.M. Zanotti, “Isospin splittings in the decuplet baryon spectrum from dynamical QCD+QED” *J. Phys. G*46 (2019) 11.
- [6] Hiroyuki Fuji, Issaku Kanamori, Shinsuke M. Nishigaki, “Janossy densities for chiral random matrix ensembles and their applications to two-color QCD”, *JHEP* 1908 (2019) 053.
- [7] Antonio González-Arroyo, Issaku Kanamori, Ken-Ichi Ishikawa, Kanata Miyahana, Masanori Okawa, Ryoichiro Ueno, “Numerical stochastic perturbation theory applied to the twisted Eguchi-Kawai model”, *JHEP* 1906 (2019) 127.
- [8] Flavour Lattice Averaging Group: S. Aoki, Y. Aoki, D. Bećirević, T. Blum, G. Colangelo, S. Collins, M. Della Morte, P. Dimopoulos, S. Dürr, H. Fukaya, M. Golterman, Steven Gottlieb, R. Gupta, S. Hashimoto, U.M. Heller, G. Herdoiza, R. Horsley, A. Jüttner, T. Kaneko, C.-J.D. Lin, E. Lunghi, R. Mawhinney, A. Nicholson, T. Onogi, C. Pena, A. Portelli, A. Ramos, S.R. Sharpe, J.N. Simone, S. Simula, R. Sommer, R. Van De Water, A. Vladikas, U. Wenger, H. Wittig, “FLAG Review 2019”, *Eur.Phys.J. C*80 (2020) no.2, 113.
- [9] C. Rohrhofer, Y. Aoki, G. Cossu, H. Fukaya, C. Gattringer, L.Ya. Glozman, S. Hashimoto, C.B. Lang, S. Prelovsek, “Symmetries of spatial meson correlators in high temperature QCD”, *Phys.Rev. D*100 (2019) no.1, 014502.
- [10] PACS Collaboration: Eigo Shintani, Yoshinobu Kuramashi, “Hadronic vacuum polarization contribution to the muon  $g - 2$  with 2+1 flavor lattice QCD on a larger than  $(10 \text{ fm})^4$  lattice at the physical point”, *Phys.Rev. D*100 (2019) no.3, 034517.
- [11] Daisuke Kadoh, Yoshinobu Kuramashi, Yoshifumi Nakamura, Ryo Sakai, Shinji Takeda, Yusuke Yoshimura, “Tensor network analysis of critical coupling in two dimensional  $\phi^4$  theory”, *JHEP* 1905 (2019) 184.
- [12] Yoshifumi Nakamura, Hideaki Oba, Shinji Takeda, “Tensor Renormalization Group Algorithms with a Projective Truncation Method”, *Phys.Rev. B*99 (2019) no.15, 155101.
- [13] Taylor Haar, Waseem Kamleh, James Zanotti, Yoshifumi Nakamura, “Single flavour optimisations to Hybrid Monte Carlo”, *Comput.Phys.Commun.* 238 (2019) 111-123.

### 6.5.2 Conference Papers

- [14] Kei Suzuki, Sinya Aoki, Yasumichi Aoki, Guido Cossu, Hidenori Fukaya, Shoji Hashimoto, “Axial U(1) symmetry, topology, and Dirac spectra at high temperature in  $N_f = 2$  lattice QCD”, *PoS CD2018* (2019) 085.
- [15] E. Shintani, Y. Kuramashi, “Analysis of systematic error in hadronic vacuum polarization contribution to muon  $g - 2$ ”, *PoS LATTICE2018* (2019) 060.
- [16] JLQCD Collaboration: Kei Suzuki, Sinya Aoki, Yasumichi Aoki, Guido Cossu, Hidenori Fukaya, Shoji Hashimoto, “Axial U(1) symmetry and Dirac spectra in high-temperature phase of  $N_f = 2$  lattice QCD”, *PoS LATTICE2018* (2018) 152.
- [17] Hiroshi Ohno, Yoshinobu Kuramashi, Yoshifumi Nakamura, Shinji Takeda, “Continuum extrapolation of the critical endpoint in 4-flavor QCD with Wilson-Clover fermions” *PoS LATTICE2018* (2018) 174.
- [18] Ryo Sakai, Daisuke Kadoh, Yoshinobu Kuramashi, Yoshifumi Nakamura, Shinji Takeda, Yusuke Yoshimura, “Tensor network study of two dimensional lattice  $\phi^4$  theory”, *PoS LATTICE2018* (2018) 232.
- [19] Sophie Hollitt, Roger Horsley, Paul D. Jackson, Yoshifumi Nakamura, Holger Perlt, Paul E.L. Rakow, Gerrit Schierholz, A. Schiller, Hinnerk Stüben, Ross D. Young, James M. Zanotti, “Control of SU(3) symmetry

breaking effects in calculations of B meson decay constant”, PoS LATTICE2018 (2018) 268.

### 6.5.3 Posters

- [20] Y. Aoki, Y. Kuramashi, E. Shintani, N. Tsukamoto, “Proton decay matrix elements with physical quark masses”, The 37th International Symposium on Lattice Field Theory (Lattice 2019) (June 16-21, 2019, Wuhan, China).
- [21] Y. Aoki, Y. Kuramashi, E. Shintani, N. Tsukamoto, “Proton decay matrix elements with physical quark masses”, Fugaku QCD coding workshop (Dec. 12-13, 2019, Kobe, Japan).
- [22] I. Kanamori, “Multigrid Solver with Bridge++ Code Set”, Fugaku QCD coding workshop (Dec. 12-13, 2019, Kobe, Japan).
- [23] Y. Aoki, Y. Kuramashi, E. Shintani, N. Tsukamoto, “Proton decay matrix elements with physical quark masses”, シミュレーションによる宇宙の基本法則と進化の解明に向けて (QUCS 2019) (Dec. 16-19, 2019, Kyoto, Japan).
- [24] I. Kanamori, “Multigrid Solver with Bridge++ Code Set”, シミュレーションによる宇宙の基本法則と進化の解明に向けて (QUCS 2019) (Dec. 16-19, 2019, Kyoto, Japan).
- [25] I. Kanamori, “Neighboring Communication with uTofu for LQCD Application”, The 2nd R-CCS International Symposium (Feb. 17-18, 2020, Kobe, Japan).
- [26] Y. Nakamura, “Nature of the finite temperature phase transition for three flavor QCD”, The 2nd R-CCS international symposium (Feb. 17-18, 2020, Kobe, Japan).
- [27] Y. Nakamura, “QCD Wide SIMD Library (QWS) for Fugaku”, The 2nd R-CCS international symposium (Feb. 17-18, 2020, Kobe, Japan).

### 6.5.4 Invited Talks

- [28] Y. Nakamura, “Phase diagram of finite temperature phase transition of QCD”, 2019 Autumn Meeting of Physical Society of Japan (Sep. 17-20, 2019, Yamagata, Japan).
- [29] Y. Nakamura, “Towards computing the standard model of particle physics by tensor renormalization group”, Tensor Network States: Algorithms and Applications (TNSAA) 2019-2020 (Dec, 4-6, 2019, National Cheng-Chi University, Taipei, Taiwan).

### 6.5.5 Oral Talks

- [30] Y. Nakamura, Y. Kuramashi, H. Ohno, S. Takeda, “Critical endpoints of the finite temperature QCD”, International Molecule-type Workshop, “Frontiers in Lattice QCD and related topics” (April 15-26, 2019 YITP Yukawa Institute for Theoretical Physics, Kyoto University, Japan).
- [31] C.-J. D. Lin, I. Kanamori, “chiral condensate and susceptibility of  $SU(2)$   $n_f = 8$  naive staggered system”, The 37th International Symposium on Lattice Field Theory (Lattice 2019) (June 16-21, 2019, Wuhan, China).
- [32] Y. Nakamura, Y. Kuramashi, H. Ohno, S. Takeda, “Critical endpoint in the continuum limit and critical endline at  $N_t = 6$  of the finite temperature phase transition of QCD with clover fermions”, The 37th International Symposium on Lattice Field Theory (Lattice 2019) (June 16-21, 2019, Wuhan, China).
- [33] Y. Aoki, “Proton decay matrix elements with physical quark masses”, 2019 Autumn Meeting of Physical Society of Japan (Sep. 17-20, 2019, Yamagata, Japan).
- [34] I. Kanamori, H. Matsufuru, “Implementation of multigrid solver for domainwall fermion with the common code Bridge++”, 2019 Autumn Meeting of Physical Society of Japan (Sep. 17-20, 2019, Yamagata, Japan).
- [35] Y. Aoki, “Toward Fugaku: Symmetries to be Unfolded”, R-CCS Cafe (Oct. 7, 2019, Kobe, Japan).
- [36] I. Kanamori, “Linear solvers in LQCD application”, R-CCS Cafe (Nov. 25, 2019, Kobe, Japan).
- [37] Y. Nakamura, “QCD Wide SIMD Library (QWS) for Fugaku”, Fugaku QCD coding workshop (Dec. 12-13, 2019, Kobe, Japan).
- [38] I. Kanamori, “Communication with Double Buffering” Fugaku QCD coding workshop (Dec. 12-13, 2019, Kobe, Japan).
- [39] C.-J. D. Lin, I. Kanamori, “About bulk phase transition of  $SU(2)$   $n_f = 8$  fundamental unimproved staggered fermion”, 75th Annual Meeting, The Physical Society of Japan (Mar. 16-19, 2020, Nagoya, Japan).

### 6.5.6 Software

[40] Y. Nakamura, Y. Mukai, K.-I. Ishikawa, I. Kanamori, “QCD Wide SIMD Library (QWS)”, <https://github.com/RIKEN-LQCD/qws>



## Chapter 7

# Discrete-Event Simulation Research Team

### 7.1 Members

Nobuyasu Ito (Team Leader)  
Yohsuke Murase (Research Scientist)  
Naoki Yoshioka (Research Scientist)  
Daigo Umemoto (Guest Researcher)  
Tomio Kamada (Guest Researcher)  
Takeshi Uchitane (Guest Researcher)

### 7.2 Research Activities

Discrete-event simulation comprise various kinds of models, for example, particles, agents, automata, games and so on, and their applications are from material and biomedical sciences to ecological and environmental problems. Furthermore, computer systems executing various simulations including discrete-event ones are also described as discrete-event systems and therefore design and construction of new computer requires discrete-event simulations. Discrete-event simulation research team (DESRT), only one research hub of discrete-event treatment in the Riken Center for Computational Science, has been challenging simulations for natural and social phenomena, and for future computer. Social designs and controls have becoming the more interesting target since so-called the "big data sciences" became popular. Continuous simulations are also becoming building block of discrete-event simulations. The DESRT aims to cultivate such applications of supercomputers.

One characteristic feature of discrete-event simulations is, of course, their discrete nature. Interpolation of two results from two parameter sets is not straightforward, but verification using results of simulations for parameter sets between them is expected. Discrete-event models often comprise with tens, hundreds, thousands, or more parameters which are often, again, discrete. So necessary number of simulations usually very large, and exhaustive parameter search in brute force way is not feasible even with a big supercomputer. One promising way is to use a Bayesian way: do best of what we observed. So-called the AI methods like multivariate statistical analysis, agent-based modeling, genetic method, and machine learning are expected to be powerful for the purposes.

Activities of the DESRT in the year 2019 are the following:

- development and support of job-management application software named OACIS and CARAVAN[1,2,24]
- simulation analysis of social phenomena[3-5,6-18]
- simulation analysis of nonlinear nonequilibrium physical phenomena[19]
- development an application software for quantum-computer simulation[20,21,25]

Some of their highlight achievements are in the following subsections.

	capability computing	←	→	capacity computing
class	A	B	C	D
manual execution	easy	tedious	troublesome	desperate
number of simulations	$\sim 10^1$	$\sim 10^4$	$\sim 10^7$	$\sim 10^{10}$ and more
(node · second ) per simulation	$\sim 10^{10}$ and more	$\sim 10^7$	$\sim 10^3$	$\sim 10^0$
output per simulation	$\sim$ TB and more	$\sim$ GB	$\sim$ MB	$\sim$ KB

Table 7.1: A classification of jobs in terms of necessary number of simulations. The OACIS is designed for jobs for class A, B and C, and the CARAVAN for C and D.

### 7.2.1 Job management applications, OACIS and CARAVAN

A characteristic feature of discrete-event models is their large and complex parameter spaces, and they often show qualitatively different various behaviors with different parameters. Supercomputers help to overcome such difficulty: their performance with extreme parallelism allows us to simulate huge number of parameter sets.

There are two kinds of computer jobs: one pursues computing capability and the other capacity. Discrete-event simulations are in the capacity computing, and many simulations are necessary to be prepared and executed efficiently. Table 7.1 shows a classification of computer jobs in terms of their capacity. But manual operation and orchestration of thousands and more jobs are hard, and application tools for the purpose are usually used. The OACIS and CARAVAN are applications developed and released in our team. OACIS since 2012 can manage most jobs interactively through web browser up to millions. CARAVAN since 2017 handles more jobs assuming that input and output size of each job be small. In this year 2019, eight releases of the OACIS[24] were made open for users, together with user-support activities and one tutorial meeting.

### 7.2.2 Traffic simulation and analysis

The DESRT has been developing a car-traffic simulator of the Kobe city. It is used to see how computer simulations contribute to analyze, predict and optimize modern traffic issues like efficiency, congestion and pollution. After reproducing and analyzing current Kobe traffic in the previous year, simulations of artificial traffic is now challenged. For one traffic situation of the Kobe city, thousands of parameter samples were needed to be simulated to achieve statistically significant analysis. So we had developed a simulator executing various artificial situations simultaneously using K computer. It is prepared by combining the CARAVAN and the simulator for each parameter. From these various simulation parameters, simulation results sometimes very smooth, and sometimes very congested. To identify and classify various outcome from the simulations, deep autoencoder using neural network models is prepared and trained to learn the simulation results(Fig. 7.1). After training, activities of ten neurons in the inner-most layer, which control the output layer activity, are classified using the K-mean methods. Five classes are identified, which turned out to correspond to congestion patterns.

One question arises from this success of the traffic classification using neural network. It is about behavior of the traffic model used in the simulation. From the fact that the neural model learned the traffic pattern, regime diagram of the model will be favorable for the neural learning. To see the regime-diagram morphology, a simplified model of car traffic on road network is proposed.

It is a flow model on directed graph  $G = (V, E)$  with a vertex set  $V = \{i, i = 1, 2, 3, \dots, N\}$  and an edge set  $E = \{e_k = (i_k, j_k), i_k \in V, j_k \in V, k = 1, 2, 3, \dots, M\}$  is treated in the following. Traffic flow of each edge with car density  $\rho$  is assumed to be governed by a single-peaked fundamental diagram,  $f(\rho)$ , where  $f(\rho) = 0$  for  $\rho \leq 0$  or  $\rho \geq \rho_m$  and  $f(\rho)$  takes maximum value  $f_m$  at  $\rho_p$  ( $0 < \rho_p < \rho_m$ ). This  $f(\rho)$  increases monotonically continuously in  $0 < \rho < \rho_{rmp}$  from 0 to  $f_m$ , and decreases monotonically continuously in  $\rho_p < \rho < \rho_m$  from  $f(\rho_m + 0)$  to 0 (Fig. 7.2). The edge is in free-run regime for  $0 < \rho < \rho_p$ , and it is in congested regime for  $\rho_p < \rho < \rho_m$ . Therefore a fundamental diagram here is characterized by three parameters  $\rho_p$ ,  $\rho_m$  and  $f_m$ . Each edge may have different FD, so the FD parameters of an edge  $e_k$  are denoted by  $\rho_{p,k}$ ,  $\rho_{m,k}$  and  $f_{m,k}$ .

Flow on this graph  $G$  obeying the FDs is considered. A divergent  $d_i$  (or sink if  $d_i < 0$ ) is assumed on each vertex  $i$ , and a positive flux  $f_k$  on each edge  $e_k$ . This flow is conserving in a sense that in-coming flux sum plus divergent and out-going flux sum are equal for all vertices(Fig. 7.3(a) ) and this relation is named as a "conserving condition". A flux  $f_k$  obeying a FD of a edge  $e_k$  so it should be in  $0 \leq f_k \leq f_m$  and this relation is named as "FD constraint".

Here an edge corresponds to a road segment, and a vertex to a crossing and/or parking. Only a steady traffic flow is considered with coarse-grained time scale averaged over movement of each car and signal change. A set of

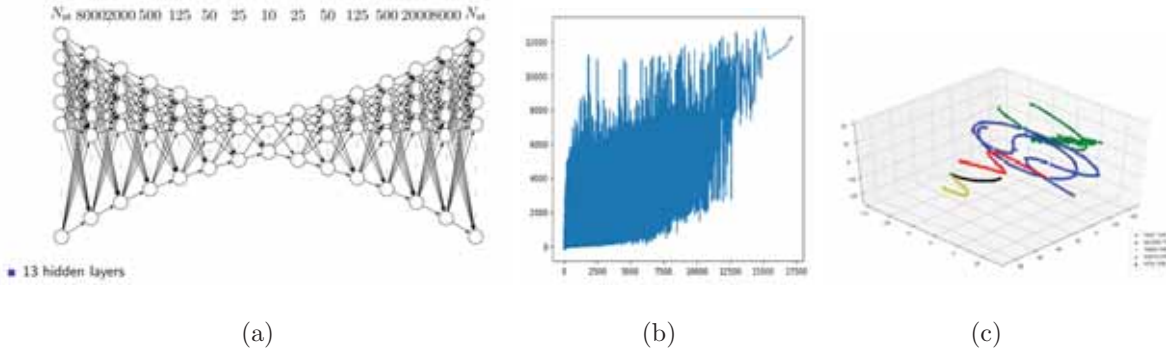


Figure 7.1: (a) A deep autoencoder network used to learn simulation results is shown. Each of left-most input layer and right-most has more than 30,000 neurons corresponding to road segments in Kobe traffic simulation. Quarter or four-times neurons are allocated for next layer, and the inner-most layer has ten neurons. (b) An example of training results Traffic flux for each road segment is shown. Horizontal axis shows traffic flux given in the input layer and vertical axis shows corresponding output from the output layer. The output signals reproduce statistically corresponding input flux and the network learned the simulation results. (c) K-mean classification results of the inner-most neuron activities is shown in three-dimensional plot. Five classes are identified.

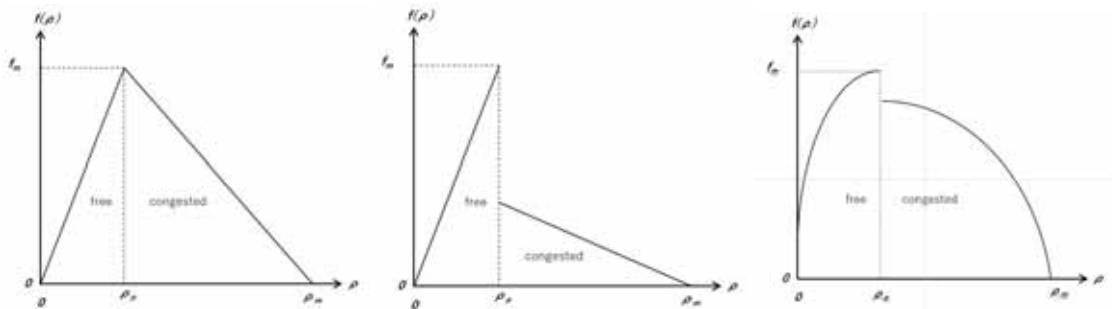


Figure 7.2: Some examples of fundamental diagram  $f(\rho)$  of each edge.

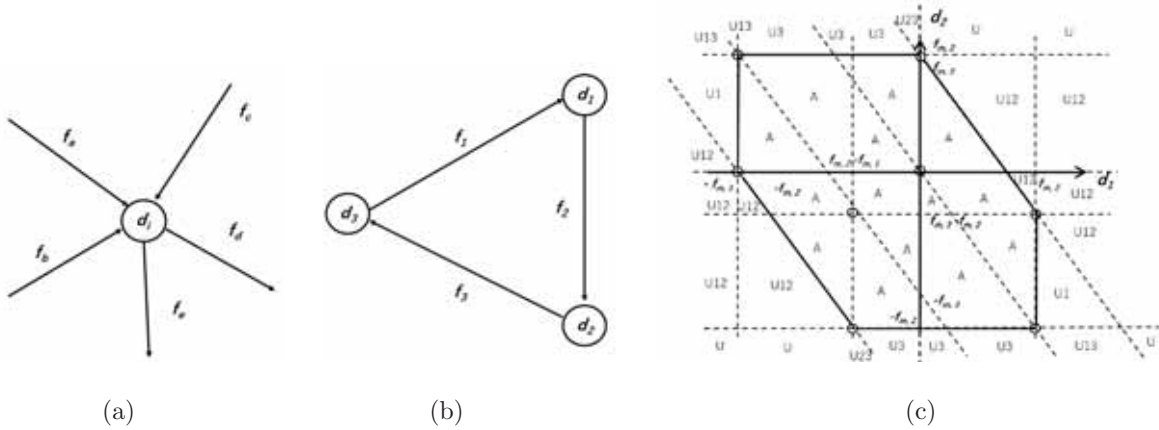


Figure 7.3: (a) Flow at vertex  $i$ . This flow and divergent satisfies a relation  $f_a + f_b + f_c + d_i = f_d + f_e$ . Even if a given graph and a set of divergence is accepted, it does not guarantee a possibility of routing for all cars. But if it is unacceptable, it is not possible to satisfy demand of all cars. (b) shows an example of a simple graph with three vertices with three edge,  $N = 3$  and  $M = 3$ . (c) shows regime diagram of this model for a graph (b). Area marked with "A" is acceptable and all cars can finish their drives. Area "U" is unacceptable and some cars cannot reach to their destinations, and number(s) with the "U" denote(s) overcapacity edge(s).

divergence  $\{d_i\}$  is called acceptable("A" regime), if a set of flow  $\{f_k\}$  satisfying the conserving condition and the FD constraint exists. Otherwise, it is called unacceptable("U" regime) and smooth traffic cannot be expected. The U regime can be classified further depending of which part of the considering graph is not unacceptable. It may be just one edge or some edges, or all edges. This classification is denoted by showing unacceptable edge(s), for example, U1, U23 and U123.

The FD constraint forms convex polyhedral domain and therefore each regime of this model is convex polyhedral, though some regimes will continue to infinity. As an example, regime diagram of a simple graph Fig. 7.3(b) with  $N = 3$  and  $M = 3$  and  $G = (V = \{1,2,3\}, E = \{e_1 = (3,1), e_2 = (1,2), e_3 = (2,3)\})$  is shown in Fig. 7.3(c). From the conserving condition,  $d_1 = f_2 - f_1$ ,  $d_2 = f_3 - f_2$  and  $d_3 = f_1 - f_3 = -d_1 - d_2$ . So the parameter space is two dimensional and here we take  $(d_1, d_2)$ . From the FD constraint, an acceptable regime in this parameter space is an area covering a point  $(d_1, d_2)$  when  $f_1, f_2$  and  $f_3$  take all acceptable flux values. Each of  $f_i (i \in V)$  may take any value between 0 and  $f_{m,i}$  independently, and therefore the acceptable regime is in a set of points which linearly interpolate the following eight points:  $(0, 0), (f_{m,2}, -f_{m,2}), (f_{m,2}, f_{m,3} - f_{m,2}), (0, f_{m,3}), (-f_{m,1}, 0), (f_{m,2} - f_{m,1}, -f_{m,2}), (f_{m,2} - f_{m,1}, f_{m,3} - f_{m,2})$  and  $(-f_{m,1}, f_{m,3})$ . When one or two of  $f_i$  are out of the range, corresponding unacceptable regime is named as  $U_i$  or  $U_{ij}$  using numbers of outranged edge,  $i$  and  $j$ .

This graph flow model is a simple one which will be a crude approximation of network traffic. But it will capture a basic feature of network traffic like jam and grid-lock. Regime diagram of this model will be a good starting point to design and control car traffic system using neural network AI.

### 7.2.3 Quantum computer simulation

Quantum information processing is expected to be a next breakthrough beyond current computers. Its growth is now reaching to a promising stage of device developments, and now a realistic design optimization will be a current issue. Simulation of quantum information processing will now be necessary to design a better quantum computers. The DESRT, together with global collaboration, had reached to a 48 qubits simulation which was the world-record scale<sup>1</sup>, and now we have developed further optimized algorithm for massively parallel computers. It is a way to prepare an optimal memory allocation, and it turned out to accelerate two to three times faster simulation. It was achieved using two optimization techniques which are proposed in order to improve performance of the simulator. The "page method" reduces unnecessary copies in each node. It is found that this method makes approximately 17% speed-up maximum. Initial permutation of qubits is also studied

<sup>1</sup> Hans De Raedt, Fengping Jin, Dennis Wilsch, Madita Nocon, Naoki Yoshioka, Nobuyasu Ito, Shengjun Yuan and Kristel Michielsen, "Massively parallel quantum computer simulator, eleven years later," Computer Physics Communications **237** (2019) 47-61.

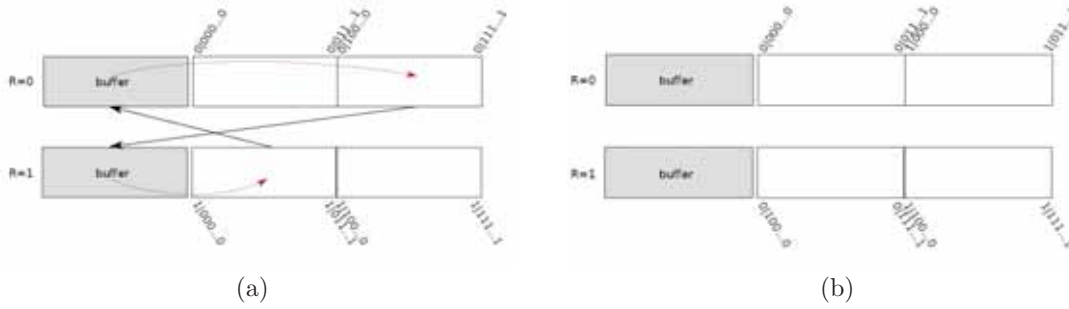


Figure 7.4: Naive data transfer procedure in memory of node R=0 and 1, without using the page method, is shown schematically. In this figure,  $i|ijkl \cdots z \rangle$  denotes a coefficient of a state  $|ijkl \cdots z \rangle$ . (a) Firstly, transferring halves of data were transferred into buffering areas in target nodes(black arrows), then data in buffering areas are copied in target areas(red broken arrows). (b) After (a) procedures, two-qubits interaction for  $|0jkl \cdots z \rangle$  and  $|1jlk \cdots z \rangle$  is simulated by operations on each node.

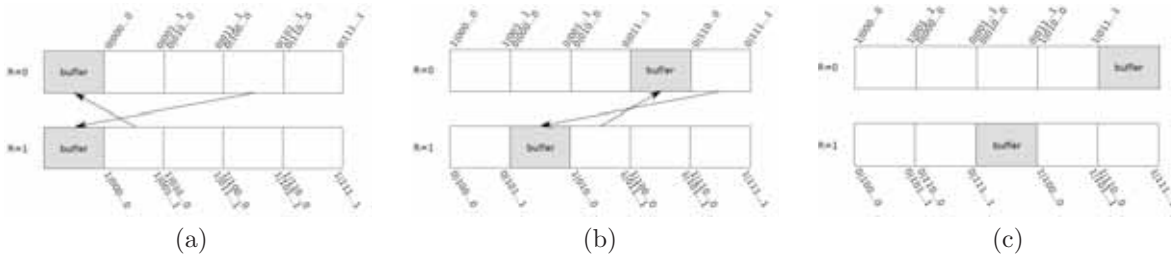


Figure 7.5: Data transfer procedure in memory of node R=0 and 1, using the page method, is shown schematically. (a) Firstly, transferring quarters of data were transferred into buffering areas in target nodes(black arrows) (b) After (a) procedures, data transferred areas are used as buffering areas and transferring quarters of data were transferred into this new buffering areas in target nodes (black arrows) (c) Then two-qubits interaction for  $|0jkl \cdots z \rangle$  and  $|1jlk \cdots z \rangle$  is simulated by operations on each node.

how it affects performance of the simulator. It is found that a simple permutation in ascending order of the number of operations for each qubit is sufficient in the case of simulations of quantum adder circuits.

On present classical computer, limitation of quantum-computer simulations treating quantum state exactly up to numeric precision of complex coefficients comes mainly from memory capacity. For  $N$  qubits simulation,  $2^N$  complex coefficients are necessary. If double precision for complex coefficients is used, necessary memory storage is  $16 \times 2^N = 2^{N+4}$  byte. A 45 qubits simulation, for example, uses 0.5EB storage. Massively parallel supercomputer can treat this 0.5EB in distributed main memory, and it was a key to achieve 45 qubits in double precision, 46 qubits in single, 47 qubits in half, and 48 qubits in one-byte precision. At every quantum gate operation or qubit interaction, simulator need to reorganize these coefficients so that all interacting coefficients are on the same node using inter-node data transfer. When interacting qubits are all on the same node, inter-node transfer is not necessary. When they are not, inter-node transfer of half of the coefficients for two-qubits interaction and three fourth for three-qubits interaction is necessary. Both of the two techniques optimize these data transfer.

The page method is a technique to omit in-node data transfer after inter-node transfer, and memory usage for data transfer reduced to half compared with a naive transfer described in Fig. 7.4. Procedure with the page method is described in Fig. 7.5. This page method usually reduces execution time because it reduces transfer from buffering area, but there is one drawback: it increases number of transfer operation. Though totally transferring data sizes are the same, increase of transfer call may cause additional waiting time for inter-node latency. Performance comparison on the K computer is given in Fig. 7.6. Slow-down around 41 qubits( $N=41$ ) will be caused by the increase of transfer call.

In this quantum computer simulation, data transfer cost is dominant. It is observed in Fig. 7.6(a), for example. In this simulation, each node holds up to 29 qubits using 8GB memory. And elapse time increases

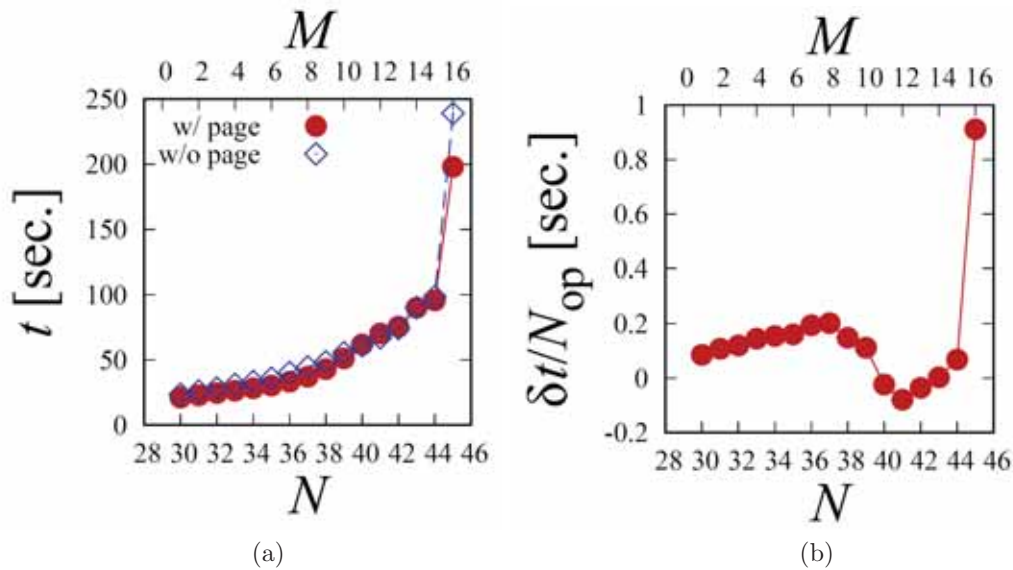


Figure 7.6: Performance of the page method is plotted. Elapse time of one Hadamard operation for each of  $N$  qubits is shown in cases with and without the page method.  $M$  on the top indicate number of qubits allocated over nodes, which implies that  $2^M$  nodes are used for simulation. (a) Elapse time with and without the page method is plotted. (b) Difference of the elapse time per Hadamard operation without and with the page method is plotted. Generally, this difference is positive and the page method improves the performance except around  $N = 41$ .

monotonically for the more qubits. Therefore, qubit allocation for the memory address and node number which minimizes inter-node transfer is expected. Transfer cost for one qubit allocations can be estimated easily, but number of possible allocation is factorial of qubit number. This transfer cost, which will be dominant cost for quantum computer simulation using huge number of nodes of massively parallel supercomputer, changes few times to few tens time depending of initial qubit allocation. Examples of the transfer-cost distribution is shown in Fig. 7.7. One way to find efficient allocation is to make a stochastic optimization. Instead, a simple method named "use-frequency method" is proposed. It is to allocate local address to node number from most frequently used qubit to least used one. This method seems to achieve relatively good performance in our simulation benchmark, and it is also observed in Fig. 7.7.

#### 7.2.4 Other activities

In the year of 2019, following subjects were studied in this team:

1. game theoretic study on cooperation and collaboration[8-10,16,18]
2. social network[3-5,15,17]
3. presursor of breakdown under subcritical stress[19]

### 7.3 Schedule and Future Plan

From the research activities of DESRT so far, following problems are becoming clearer:

1. Simulation models, typically social ones, comprise with large input parameters and output numbers, and their behaviors are strongly nonlinear with various regimes.
2. Social "big data" are often not big enough to picture details. It is clearly observed from our multivariate analysis of the traffic data. Thousands of samples are necessary to get minor traffic factors, but such repetitions are not expected in the real traffic. Weather, economics, calendar, accidents and other factors varies every day.

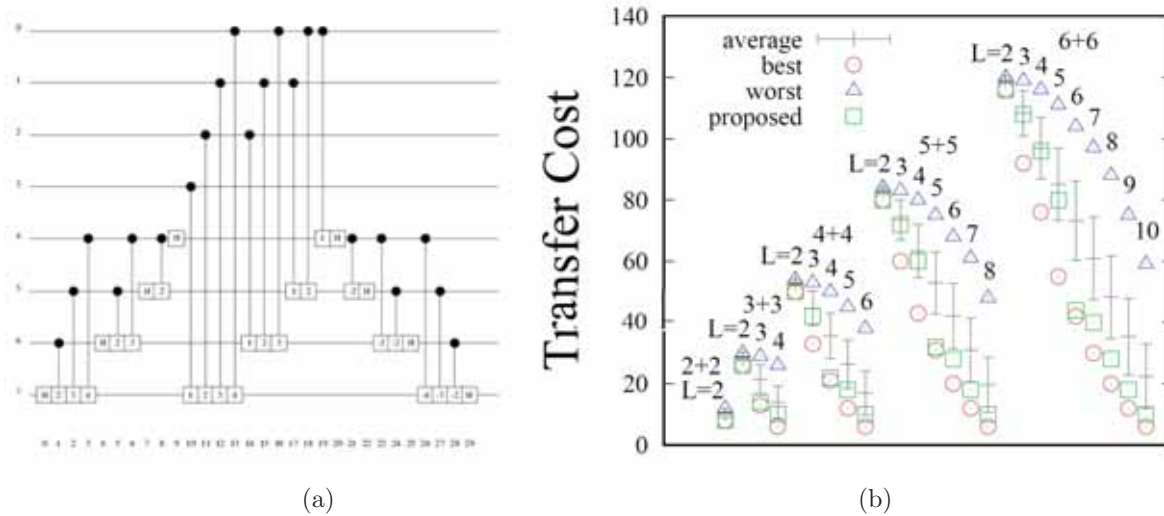


Figure 7.7: Distribution of total transfer costs of quantum addition of two registers, 2+2 to 6+6, obtained by enumerating all permutation  $L$  denotes number of in-node qubits. For example, in a case of  $L = 7$  of 6+6, totally 7 qubits are allocated to in-node address and  $6 + 6 - 7 = 5$  qubits to node number using  $2^5 = 32$  nodes. So there are  $12 = 4.8 \times 10^8$  ways of qubits allocation. Transfer cost is proportional to total data size of inter-node transfer. The best, worst, and average transfer costs are plotted for each case of the number of qubits per register and the number of local qubits. The empty squares are the results of the use-frequency method.

3. Development of multiscale social and economic models and simulations.
4. Bayesian AI will be useful to cultivate diverse behaviors of social phenomena.
5. Quantum information processing may become in near future.

## 7.4 Publications

### 7.4.1 Articles

- [1] Itsuki Noda, Yohsuke Murase, Nobuyasu Ito, Kiyoshi Izumi, Hiromitsu Hattori, Tomio Kamada, Hideyuki Mizuta "Project CASSIA - Framework for Exhaustive and Large-Scale Social Simulation," In: Sato M. (eds) Advanced Software Technologies for Post-Peta Scale Computing. Springer, Singapore, p271-299 (2019)
- [2] Yohsuke Murase, Hiroyasu Matsushima, Itsuki Noda, Tomio Kamada - CARAVAN: a framework for comprehensive simulations on massive parallel machines-"In: Lin D., Ishida T., Zambonelli F., Noda I. (eds) Massively Multi-Agent Systems II. MMAS 2018. Lecture Notes in Computer Science, vol 11422. Springer, Cham (2019).
- [3] Janos Kertesz, Janos Torok, Yohsuke Murase, Hang-Hyun Jo, Kimmo Kaski "Multiplex Modeling of the Society," A book chapter in "Multiplex and Multilevel Networks," edited by S. Battiston, G. Caldarelli, and A. Garas
- [4] Yohsuke Murase, Hang-Hyun Jo, Janos Torok, Janos Kertesz, Kimmo Kaski, "Structural transition in social networks: The role of homophily," Scientific Reports, 9, 4310 (2019)
- [5] Yohsuke Murase, Hang-Hyun Jo, Janos Torok, Janos Kertesz, Kimmo Kaski, "Sampling networks by nodal attributes," Physical Review E, 99, 052304 (2019)

### 7.4.2 Invited talks

- [6]33rd Workshop "Recent Developments in Computer Simulation Studies in Condensed Matter Physics" (The University of Georgia, Athens, U. S. A., February 17-21, 2020) Nobuyasu Ito, "Phase diagram of a traffic simulation model" (Kurt Binder Talk, Feb. 21).
- [7]X Brazilian Meeting on Simulational Physics (BMSP) (Belo Horizonte and Ouro Preto, Brazil, July 15-19, 2019) Nobuyasu Ito, "Simulation of Quantum Computer" (Jul.17, Invited).

- [8] Y. Murase et al., "Conservation of population size is required for self-organized criticality in evolution models," Roles of Heterogeneity in Non-equilibrium collective dynamics (RHINO 2019)
- [9] Y. Murase et al., "Computational Ethics for the Tragedy of the Commons," Self-Organization and Complexity in Social System (Satellite Session of CCS2019)
- [10] Y. Murase et al., "A large-scale search for successful strategies for social dilemma using the K-computer," The 5th Workshop on Self-Organization and Robustness of Evolving Many-Body Systems.

### 7.4.3 Oral talks

- [11] Nobuyasu Ito, "Social simulation with the Fugaku" (Invited, December 14), the 5th workshop on self-organization and robustness of evolving many-body systems (Kobe, December 13-14)
- [12] Nobuyasu Ito, "Social simulations and supercomputer" (Jul. 5), The big data on economy, science and technology Society Conference 2019 (July 5 - 7, 2019, Buenos Aires, Argentina)
- [13] Nobuyasu Ito, "Regime diagram of a traffic simulation model" (January 24, OS13-6), 25th International Symposium on Artificial Life and Robotics (AROB25th 2020) and 5th International Symposium on BioComplexity (ISBC5) (January 22 - 24, 2020, B-Con PLAZA, Beppu, Japan)
- [14] Luning Zhang, Naoki Yoshioka, Daigo Umemoto and Nobuyasu Ito, "Application of deep neural network to traffic simulation" (January 24, OS13-7), 25th International Symposium on Artificial Life and Robotics (AROB25th 2020) and 5th International Symposium on BioComplexity (ISBC5) (January 22 - 24, 2020, B-Con PLAZA, Beppu, Japan)
- [15] Y. Murase et al., "Sampling Networks by Nodal Attributes" NetSci 2019
- [16] Y. Murase et al., "Computational Ethics for the Tragedy of the Commons" FSP2019: Frontiers of Statistical Physics
- [17] Yohsuke Murase, "Network extraction from node attribution," Network Science Seminar (2019).
- [18] Y. Murase et al., "Successful strategies in the Tragedy of the Commons" Conference on Complex Systems 2019
- [19] Naoki Yoshioka, Ferenc Kun, and Nobuyasu Ito, "Jump distance of epicenters in thermally induced cracking of fiber bundles," FSP2019: Frontiers of Statistical Physics (Tokyo, Japan, Jun. 7-8, 2019)

### 7.4.4 Poster presentation

- [20] Supercomputing 19 (Nov. 17-22, 2019, Colorado Convention Center, Denver, U.S.A.) Naoki Yoshioka, Hajime Inaoka, Nobuyasu Ito, Fengping Jin, Kristel Michielsen and Hans De Raedt, "Optimization for Quantum Computer Simulation" (Nov. 19 Poster 69).

### 7.4.5 Other presentations

- [21] Nobuyasu Ito, "Simulation of quantum computer" (Osaka university, 2019, October 8).
- [22] Nobuyasu Ito, "Prediction science harmonizing global community and individuals" (May 24, 2019, Tokyo) the 6th forum of future strategy "Beyond human - machine taking over human".

### 7.4.6 Award

- [23] Yohsuke Murase, "Theoretical study on social activities and application of supercomputers", Outstanding performance award in social science of NTT Docomo mobile science

### 7.4.7 Software

- [24] eight releases of OACIS (v3.4.0 ~ v3.7.1)
- [25] Quantum computer simulator "braket", <https://github.com/naoki-yoshioka/braket>

## Chapter 8

# Computational Molecular Science Research Team

### 8.1 Members

Takahito Nakajima (Team Leader)  
Noriyuki Minezawa (Research Scientist)  
Takehiro Yonehara (Research Scientist)  
William Dawson (Research Scientist)  
Wataru Uemura (Postdoctoral Researcher)  
Nobuki Inoue (Postdoctoral Researcher)  
Takahide Matsuoka (Postdoctoral Researcher)  
Subrata Tewary (Postdoctoral Researcher)  
Eisuke Kawashima (Postdoctoral Researcher)  
Kizashi Yamaguchi (Visiting Scientist)  
Takashi Kawakami (Visiting Scientist)  
Marek Janusz Wójcik (Visiting Scientist)

### 8.2 Overview of Research Activities

#### 8.2.1 Development of Original Molecular Theory

An atomic- and molecular-level understanding of drug actions and the mechanisms of a variety of chemical reactions will provide insight for developing new drugs and materials. Although a number of diverse experimental methods have been developed, it still remains difficult to investigate the state of complex molecules and to follow chemical reactions in detail. Therefore, a theoretical molecular science that can predict the properties and functions of matter at the atomic and molecular levels by means of molecular theoretical calculations is keenly awaited as a replacement for experiment. Theoretical molecular science has recently made great strides due to progress in molecular theory and computer development. However, it is still unsatisfactory for practical applications. Consequently, our main goal is to realize an updated theoretical molecular science by developing a molecular theory and calculation methods to handle large complex molecules with high precision under a variety of conditions. To achieve our aim, we have so far developed several methods of calculation. Examples include a way for resolving a significant problem facing conventional methods of calculation, in which the calculation volume increases dramatically when dealing with larger molecules; a way for improving the precision of calculations in molecular simulations; and a way for high-precision calculation of the properties of molecules containing heavy atoms such as metal atoms.

## 8.2.2 Quantum Chemistry Software NTChem

Quantum chemistry software comprises immensely useful tools in material and biological science research. Widely diverse programs have been developed in Western countries as Japan has lagged. In fact, only a few programs have been developed in Japan. The mission of our research team is to provide K computer users with a high-performance software for quantum molecular simulation. In the early stage of the K computer project, no quantum chemistry software was available for general purpose and massively parallel computation on the K computer because not every program was designed for use on it. Therefore, we have chosen to develop a new comprehensive ab initio quantum chemistry software locally: NTChem. NTChem is completely new software that implements not only standard quantum chemistry approaches, but also original and improved theoretical methods that we have developed in our research work. The main features of the current version, NTChem2013, are the following:

1. Electronic structure calculation of the ground state of atoms and molecules based on Hartree–Fock (HF) and density functional theory (DFT) methods.
2. Linear-scaling or low-scaling DFT: Gaussian and finite-element Coulomb (GFC) resolution-of-the-identity (RI) DFT, pseudospectral DFT/HF, and dual-level DFT.
3. Low-scaling SCF calculation using diagonalization-free approaches: purification density matrix, pseudo-diagonalization, and quadratic convergence SCF.
4. Excited-state DFT calculation: time-dependent DFT (TDDFT) and transition potential (DFT-TP).
5. Accurate electron correlation methods for ground and excited states: Møller–Plesset perturbation theory, coupled-cluster (CC) theory, and quantum Monte Carlo (QMC) method.
6. Massively parallel computing on the K computer and Intel-based architectures: HF, DFT, resolution-of-the-identity second-order Møller–Plesset (RI-MP2) method, and QMC method.
7. Two-component relativistic electronic structure calculation with spin-orbit (SO) interactions: Douglas–Kroll (DK1, DK2 and DK3), zeroth- and infinite-order regular approximations (ZORA and IORA), and Relativistic scheme for Eliminating Small Components (RESC).
8. Model calculations for large molecular systems: quantum mechanics/molecular mechanics (QM/MM) and Our own N-layered Integrated molecular Orbital and molecular Mechanics (ONIOM).
9. Calculation of solvation effects: COnductor-like Screening MOdel (COSMO) (interfaced with the HONDO program), averaged solvent electrostatic potential/molecular dynamics (ASEP/MD), and QM/MM-MD.
10. Efficient calculation for chemical reaction pathway.
11. Ab initio molecular dynamics calculation.
12. Calculation of magnetic properties: nuclear magnetic resonance (NMR) chemical shifts, magnetizabilities, and electron paramagnetic resonance (EPR)  $g$  tensors.
13. Population analysis: Mulliken and natural bond orbital (NBO) analysis (interfaced with NBO 6.0).
14. Orbital interaction analysis: maximally interacting orbital (MIO) and paired interacting orbital (PIO) methods.

## 8.3 Research Results and Achievements

### 8.3.1 Trajectory Surface Hopping Molecular Dynamics Simulation by Spin-Flip Time-Dependent Density Functional Theory

This study presents the nonadiabatic molecular dynamics simulation combined with the spin-flip time-dependent density functional theory (SF-TDDFT). In contrast to the conventional single-reference electronic structure methods, which have difficulty in describing the  $S_0/S_1$  conical intersections, the SF-TDDFT can yield the correct topology of crossing points. Thus, one expects that the method can take naturally into account the  $S_1 \rightarrow S_0$  nonadiabatic transitions. We adopt Tully’s fewest switch surface hopping algorithm by introducing the

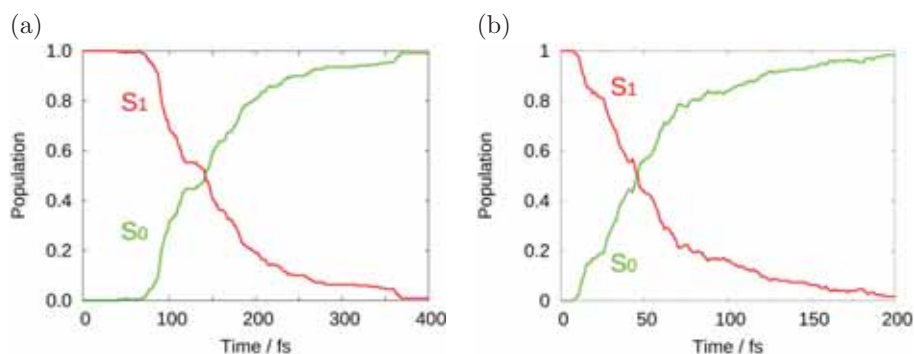


Figure 8.1: Time-dependent decay of (a) *E*-azomethane and (b) methanimine.

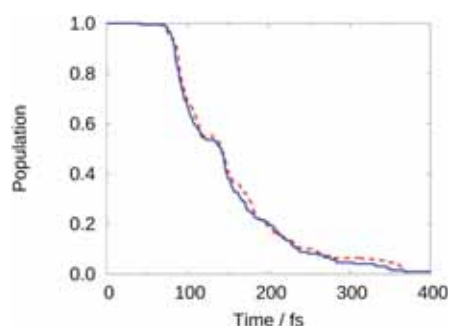


Figure 8.2: Time-dependent population decay of *E*-azomethane in vacuum (red dashed line) and water (blue solid line).

analytic SF-TDDFT nonadiabatic coupling vector. We apply the proposed method to the photoisomerization reactions of *E*-azomethane, methanimine, and ethene molecules and reproduce the results of previous studies based on the multireference methods (Figure 8.1). The proposed approach overcomes the ad hoc treatment of  $S_1 \rightarrow S_0$  transition at the single-reference calculation level and affords both the dynamics on the  $S_1$  state and the recovery of the  $S_0$  state with modest computational costs.

### 8.3.2 Quantum Mechanical/Molecular Mechanical Trajectory Surface Hopping Molecular Dynamics Simulation by Spin-Flip Time-Dependent Density Functional Theory

This study presents the nonadiabatic molecular dynamics simulation in the solution phase using the spin-flip time-dependent density functional theory (SF-TDDFT). Despite the single-reference level of theory, the SF-TDDFT method can generate the correct topology of  $S_0/S_1$  crossing points, thus providing a natural  $S_1 \rightarrow S_0$  nonadiabatic transition. We extend the gas-phase trajectory surface hopping simulation with the SF-TDDFT [N. Minezawa and T. Nakajima, *J. Chem. Phys.* 150, 204120 (2019)] to the hybrid quantum mechanical/molecular mechanics (QM/MM) scheme. To this end, we modify the code to evaluate the electrostatic interaction between the quantum and molecular mechanical, respectively QM and MM, atoms and to extract the classical MM energy and forces from the MM program package. We apply the proposed method to the photoisomerization reaction of aqueous *E*-azomethane and anionic green fluorescent protein chromophore in water and compare the results with those of the previous simulation studies based on the multireference methods (Figure 8.2).

### 8.3.3 Electron dynamics method using a locally projected group diabatic Fock matrix for molecules and aggregates

We propose a method using reduced size of Hilbert space to describe an electron dynamics in molecule and aggregate based on our previous theoretical scheme (Yonehara and Nakajima, 2017). The real-time time-dependent density functional theory is combined with newly introduced projected group diabatic Fock matrix. First, this projection method is applied to a test donor-acceptor dimer, namely, a naphthalene-tetracyanoethylene with

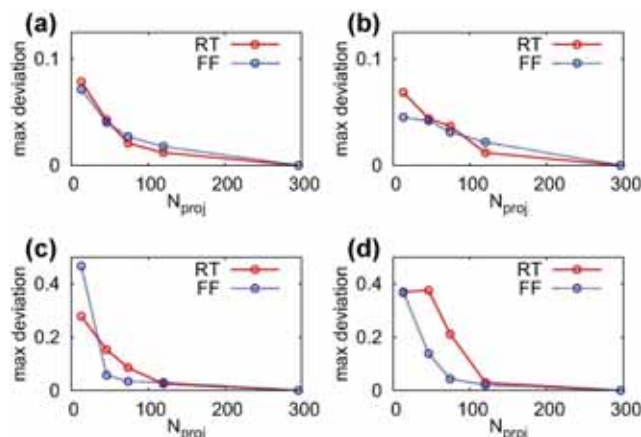


Figure 8.3:  $N_{\text{proj}}$  dependency of max deviations for donor molecule during dynamics from the results by full orbital calculation. Deviation is expressed as an absolute value but not relative one. The panels of (a), (b), (c) and (d) correspond to the results obtained by electron dynamics calculation using RT-TDDFT scheme considering the self-consistency and frozen Fock approximation.

and without initial local excitations and light fields. Secondly, we calculate an absorption spectrum of five-unit-polythiophene monomer. The importance of feedback of instantaneous density to Fock matrix is also clarified. In all cases, half of the orbitals were safely reduced without loss of accuracy in descriptions of properties (Figure 8.3). The present scheme provides one possible way to investigate and analyze a complex excited electron dynamics in molecular aggregates within a moderate computational cost.

### 8.3.4 Complexity Reduction in Density Functional Theory Calculations of Large Systems

The goal of this project is to develop new theory, algorithms, and workflows that enable the application of Density Functional Theory (DFT) to large systems. As we detailed in our recent review article, this will allow us to apply DFT to novel fields, such as the development of new enzymes for bioremediation. One of the challenges of large scale DFT is finding ways to extract chemical insight from complex systems. To this end, we have developed and evaluated a systematic complexity reduction framework which can break large systems down into fragments and quantify inter-fragmentation interaction.

To design our complexity reduction framework, we derived two measures from properties of the single particle density matrix: the fragment purity value and the fragment bond order. The purity value is a measure of fragment quality and the bond order of fragment interaction strength. We demonstrated how these two measures can be used to automatically partition a system into fragments at various levels of detail. At a suitable level of granularity, the observables of the full system can be reconstructed as a sum of fragment quantities. We further demonstrated this approach by using the fragment bond order to design QM/MM partitionings that preserve the observables of a target region (multipoles, forces, etc). Together, these two measures can be used to construct graph like views of molecular systems (Figure 8.4).

### 8.3.5 Molecular Design for Solar Cell Materials

Spiro-OMeTAD, a hole-transporting material (HTM) for perovskite solar cell, is known for its high power conversion efficiency (PCE). Its PCE for  $(\text{FAPbI}_3)_{0.92}(\text{MAPbBr}_3)_{0.08}$  perovskite is 23.4%, and the estimated cost for synthesizing Spiro-OMeTAD is approximately \$274/g. Although materials with cheaper synthesizing cost and fairly high PCE have been previously reported (X60: \$120/g, Py-C: \$192/g, etc), more cost-effective materials with higher PCEs are yet to be searched.

We trained deep neural network (DNN) model, which predicts PCEs of HTMs with molecular descriptors provided as inputs. Furthermore, we conducted Bayesian optimization by evaluating the acquisition function with Gaussian process regression (GPR). We employed discrete particle swarm optimization (DPSO) method to optimize the vast chemical space.

We constructed learning models to predict the PCEs of candidate HTMs, generated from fragments of

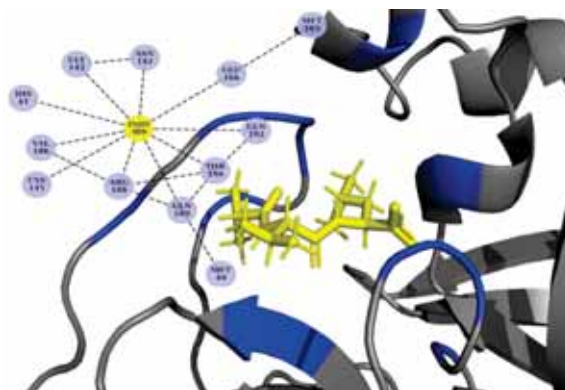


Figure 8.4: A graph view of the binding site of PDB:6lu7 based on the fragment bond order of protein residues with a potential inhibitor.

known HTMs. For training data, we collected 400 entries of experimental data of HTMs for perovskite solar cells. We employed HTMs (170 molecules), active layers (54 compounds, band gaps, valence band maximum, conduction band minimum), dopants, co-dopants, active area, and PCEs as input. 170 HTM molecules have been decomposed into three fragments, and the candidate HTMs have been generated from these fragments. The molecular descriptors have been calculated for each fragment with Mordred. We also prepared quantum descriptors (HOMO, LUMO, total energy, electronic energy, heat of formation, dispersion energy, dipole moment) using NTCHEM on K-computer. We constructed DNN model, which predicts PCEs, with combination of these descriptors, provided as input. The candidate HTMs have been chosen by GPR model with typical experimental conditions. As virtual experiment, the PCEs of the candidate HTMs have been predicted from the DNN model. The optimum candidates have been selected, while improving the GPR model by repeating the virtual experiment. Global optimization is unrealistic due to the vast chemical space (32,294,400 molecules). We searched for candidate HTMs with DPSO with the PCEs predicted by the constructed models, provided as the objective function. An  $n \times N$  bit matrix has been defined as coordinates of the particles, where  $n$  is number of fragments species and  $N$  is number of fragments contained in candidate HTMs. The coordinates are updated probabilistically. Softmax function has been selected as probability function to select single fragment.

TiO<sub>2</sub> electron-transporting layer and (FAPbI<sub>3</sub>)<sub>0.85</sub>(MAPbBr<sub>3</sub>)<sub>0.15</sub> active layer has been employed as typical experimental conditions. The PCEs of SAF structure HTMs and SFX structure HTMs has been predicted to be high (Figure 8.5). Among the SFX structure HTMs, X55(20.8%) and X26(20.2%) are known to show high PCEs. Therefore, we expect the SFX structure candidate HTMs will also show high PCEs. The predicted PCEs of selected SAF structure candidates are over 20%, which greatly improves from the known SAF structure HTMs, such as SAF-OMe(16.7%) and CW4(16.6%).

### 8.3.6 Molecular Design for Highly-functional Biopolymer Materials

The functionalities of typical biopolymers, such as poly(lactic acid), PLA, and poly(butylene succinate), PBS, remain equivalent to the ones of general polymers. Highly-functional biopolymer development technology is considered to be a powerful solution for realizing a recycling-oriented society and economic revitalization toward the achievement of SDGs. For developing highly-functional biopolymers, it is necessary to establish the basic technology for estimating the polymer structure from the desired functionality. In order to establish a method for predicting properties from a given structure, we searched for polymers with high heat resistance. The learning model was constructed by using an experimental database and quantum chemistry calculation, and implemented a data-driven search method.

For the glass transition point ( $T_g$ ) and melting point ( $T_m$ ), experimental data of 497 types and 421 types of polymers were collected, respectively. Mordred was used to calculate the molecular descriptors determined from the topology and structure of the repeating unit molecules (1501 descriptors for  $T_g$  and 1432 descriptors for  $T_m$ ). Furthermore, the molecule of the repeating unit was decomposed into two fragments, and the molecular descriptors were calculated for each fragment (1347 descriptors for  $T_g$  and 1286 descriptors for  $T_m$ ). Additionally, HOMO, LUMO, total energy, total electron energy, heat of formation, and dipole moment were calculated using NTCHEM on K-computer and included as quantum descriptors. The base-level learning model was constructed with partial least squares regression (PLSR), support vector machine (SVM), and  $k$ -nearest neighbor algorithm

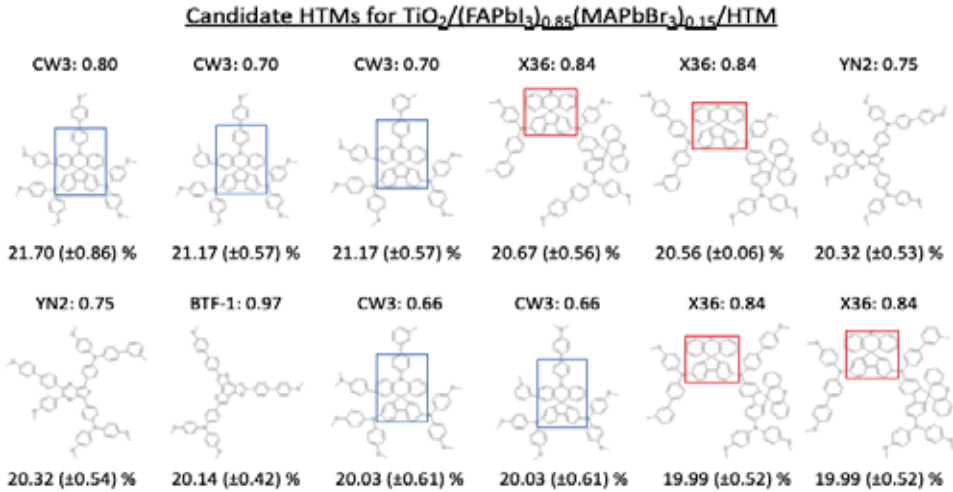


Figure 8.5: Hole-transporting material, HTM, candidates. Blue frames and red frames respectively indicate SAF structures and SFX structures.

( $k$ -NN), and a stacking model was constructed with DNN as meta-level model. We constructed 10 DNN learning models by  $K$ -fold cross-validation method. The above descriptors were calculated for all the molecules in the biosynthesizable monomer database (283 types of diols, 71 types of dicarboxylic acids, 307 types of diamines).

$T_g$  and  $T_m$  of 57,072 polyesters (combination of 283 diols and 71 dicarboxylic acids) and 18,573 polyamides (combination of 307 diamines and 71 dicarboxylic acids) were predicted from the learning model. As a result, 42 polyesters with predicted  $T_g$  of  $150^\circ\text{C}$  or higher and 391 polyamides of  $200^\circ\text{C}$  or higher were found, and 139 polyesters and 157 polyamides with predicted  $T_m$  of  $300^\circ\text{C}$  or higher were found (Figure ?? and ??). We found that aromatic polymers are promising as candidates for high heat resistant polymers. Although the biosynthesizable monomer database did not contain the para-dicarboxylic acid,  $T_g$  and  $T_m$  of the polymer synthesized from the para-dicarboxylic acid were predicted to be high.

### 8.3.7 Construction of Molecular Orbital Method Consistent with Quantum Electrodynamics

The relativistic molecular orbital (MO) method is commonly used today in the calculation of systems containing heavy elements. However, the relativistic quantum mechanics, which is the basic theory of the relativistic molecular orbital method, is incomplete in the treatment of antiparticles, and this point is the same in the relativistic molecular orbital method. To overcome this problem, the molecular orbital method should be reorganized based on quantum electrodynamics (QED), which is a “true” relativistic extension of quantum mechanics, and the relativistic MO method is extended to the QED-MO method. In this way, by rewriting the expression of quantum electrodynamics into a form that has a high affinity with the MO method, not only the theoretical rigor is increased, but also the quantum electrodynamics calculation of multi-electron systems can be executed by the program of the MO method. Therefore, in this study, we show that frequency-dependent Breit interaction

$$V^{\text{QED}}(r; \omega) = -\frac{\boldsymbol{\alpha} \cdot \boldsymbol{\alpha}}{4\pi\epsilon_0} \frac{e^{i\omega r/c}}{r} - \frac{(\boldsymbol{\alpha} \cdot \nabla)(\boldsymbol{\alpha}' \cdot \nabla')}{4\pi\epsilon_0} \frac{1 - e^{i\omega r/c}}{(\omega/c)^2 r} \quad (8.1)$$

is derived from the QED Hamiltonian of based on the first principle, and tried to formulate and implement the QED-MO method using this interaction.

First, we show that the frequency-dependent Breit interaction is derived from the QED Hamiltonian in the first principle. This interaction represents interactions between two electrons by a photon that transports energy  $\omega$  and can be obtained by applying Schrieffer–Wolff transformation to QED Hamiltonian of interaction representation. By this transformation, we can get the effective Hamiltonian (four-fermion(4f)-QED Hamiltonian)

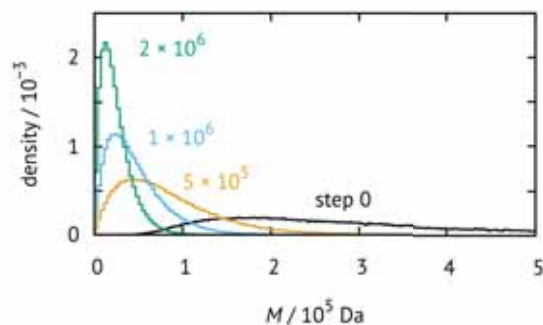


Figure 8.6: Molecular weight distribution of  $10^5$  poly(lactic acid) molecules under degradation. Molecular weights,  $M$ , at initialization follow a log-normal distribution; number- and weight-averaged molecular weights are  $2.56 \times 10^5$  and  $5.22 \times 10^5$ , respectively.

which has no photon external lines:

$$\hat{H}_2^{\text{4f-QED}} = \frac{1}{2} \sum_{ijkl} [ij | V^{\text{QED}}(r; \varepsilon_l - \varepsilon_k) | kl] \hat{b}_i^\dagger \hat{b}_k^\dagger \hat{b}_l \hat{b}_j. \quad (8.2)$$

Here,  $i, j, k$  and  $l$  are the indices of the molecular orbital, and  $\hat{b}^\dagger$  and  $\hat{b}$  are the electron creation and annihilation operators, respectively. This Hamiltonian depends on the orbital energy, and the Dirac–Hartree–Fock calculation using this Hamiltonian has a large calculation costs. For this reason, we treat it perturbatively, in other words, add the 4f-QED Hamiltonian after determining the orbitals by usual Dirac–Hartree–Fock calculations. 4f-QED Hamiltonian can be basically used as it is for the calculation of electron correlation method by adding it to ordinary two-electron Hamiltonian (Coulomb interaction). That is, the effect of QED can be calculated using the calculation program of the electron correlation method. That is, the QED-MO calculation can be realized if the two-electron integral of frequency-dependent Breit interaction can be evaluated. It is already known that the Obara–Saika method can be applied to two-electron integrals for arbitrary potentials in Cartesian Gaussian basis functions. However, it is necessary to newly create “molecular incomplete gamma function” for each potential. We have succeeded to develop methods for evaluating the “molecular incomplete gamma function” for frequency-dependent Breit interaction, which means that we provided the almost all tools necessary for QED-MO calculations.

### 8.3.8 Multi-Scale Simulation to Predict Biodegradability of Plastics

Biodegradable plastics are attracting attention to reduce environmental impact and achieve Sustainable Development Goals, SDGs. Biodegradable aliphatic polyesters—polymers or copolymers of hydroxyalkanoates, or copolymers of diols and dicarboxylic acids—eventually decompose into carbon dioxide and water by microbial metabolism. Examples of current commercial biodegradable polyesters are poly(lactic acid), PLA, poly(caprolactone), PCL, and poly(3-hydroxybutyrate-co-3-hydroxyhexanoate), PHBH. Skeleton structures of these materials determine mechanical and thermal properties and biodegradability, which restricts their application.

We are developing theoretical tools to estimate biodegradability of plastics to offer design guideline, by applying materials informatics. Density functional theory, DFT, calculations are employed as implemented in NTChem. Methylmethanoate,  $\text{CH}_3\text{COOCH}_3$ , was chosen as a model ester to guess structures for others. Reaction pathways of ester hydrolysis under base condition are investigated by nudged elastic band, NEB, and string method. Calculations are performed on HPC clusters including K computer, and activation energies and heats of reaction are obtained. A macroscopic Monte Carlo simulator is also implemented to estimate changes of molecular weight distributions under degradation. At initialization, polymers, whose molecular weights follow a probability distribution such as log-normal and inverse-gamma, are populated to reproduce experimental number- and mass-average molecular weights, and an ester bond is randomly cleaved at each Monte Carlo step (Figure 8.6).

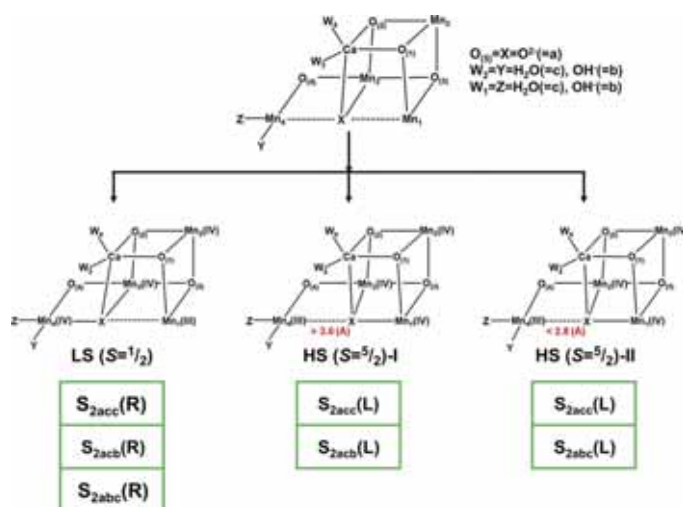


Figure 8.7: Structure of the  $\text{CaMn}_4\text{O}_5$  cluster in oxygen evolving cycle of PSII. Three different  $S_2$  structures, one R-opened LS ( $S = 1/2$ ) and two L-opened HS ( $S = 5/2$ ) structures are optimized by UB3LYP/TZVP methods.

### 8.3.9 Theoretical and computational investigations of geometrical, electronic and spin structures of the $\text{CaMn}_4\text{O}_X$ ( $X=5, 6$ ) cluster in the Kok cycle $S_i$ ( $i = 0-3$ ) of oxygen evolving complex of photosystem II

The optimized geometries of the  $\text{CaMn}_4\text{O}_X$  ( $X = 5, 6$ ) cluster in the oxygen evolving complex (OEC) of photosystem II (PSII) by large-scale quantum mechanics (QM) and molecular mechanics (MM) calculations are compared with recent serial femtosecond crystallography (SFX) results for the  $S_i$  ( $i = 0-3$ ) states. The valence states of four Mn ions by the QM/MM calculations are also examined in relation to the experimental results by the X-ray emission spectroscopy (XES) for the  $S_i$  intermediates. Geometrical and valence structures of right-opened Mn-hydroxide, Mn-oxo and Mn-peroxide intermediates in the  $S_3$  state are investigated in detail in relation to recent SFX and XES experiments for the  $S_3$  state (Figure 8.7). Interplay between theory and experiment indicates that the Mn-oxo intermediate is a new possible candidate for the  $S_3$  state. Implications of the computational results are discussed in relation to possible mechanisms of the oxygen-oxygen bond formation for water oxidation in OEC of PSII.

### 8.3.10 Domain-Based Local Pair Natural Orbital CCSD(T) Calculations of Strongly Correlated Electron Systems: Examination of Dynamic Equilibrium Models Based on Multiple Intermediates in $S_1$ State of Photosystem II

Domain-based local pair natural orbital (DLPNO) coupled cluster single and double (CCSD) methods with perturbative triples (T) correction with NormalPNO were used to compute energies for twelve different  $S_1$  structures of the  $\text{CaMn}_4\text{O}_5$  cluster in the oxygen evolving complex (OEC) of photosystem II (PSII). The DLPNO-CCSD( $T_0$ ) calculations with TightPNO for the important six structures among them revealed that the right (R)-opened  $S_{1XYZW}$  structures were more stable than the corresponding left (L)-opened structures ( $X = O_{(5)}$ ,  $Y = W_2$ ,  $Z = W_1$ , and  $W = O_{(4)}$ ) of  $\text{CaMn}_4\text{O}_5$ . The three different  $S_1$  structures belonging to the R-opened type ( $S_{1acca}$ ,  $S_{1bbca}$ , and  $S_{1abcb}$ , where  $O^{2-} = a$ ,  $OH^- = b$  and  $H_2O = c$ ) were found nearly degenerated in energy, indicating the possibility of the coexistence of different structures in the  $S_1$  state. The DLPNO-CCSD( $T_0$ ) calculations with TightPNO supported the proposal of a dynamic equilibrium model based on the multi-intermediate structures for the  $S_1$  state, which is also in agreement with EPR and other experimental and hybrid DFT computational results. Implications of the computational results are discussed in relation to scope and applicability of NormalPNO and TightPNO for the CCSD( $T_0$ ) calculations of strongly correlated electron systems such as 3d transition-metal complexes.

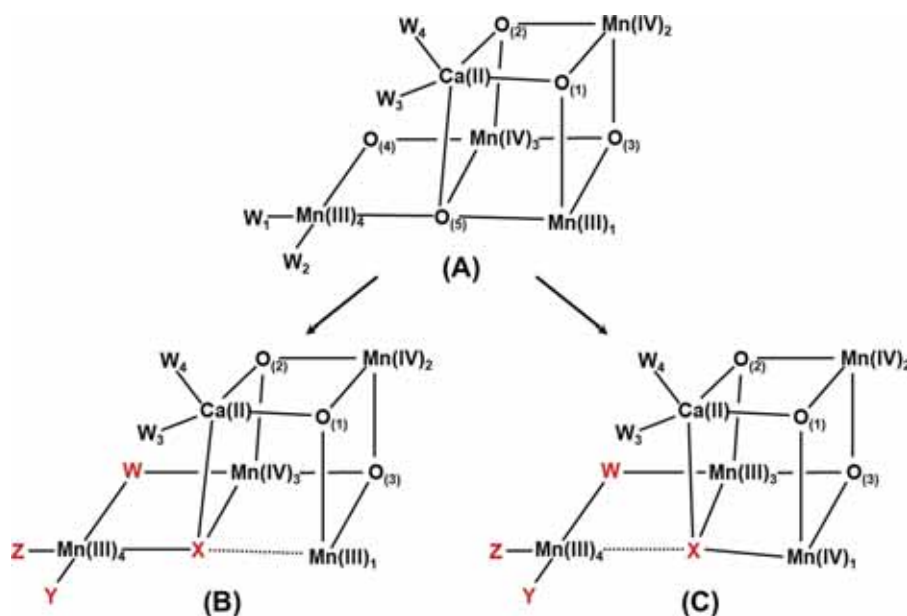


Figure 8.8: (A) Geometrical structure of the  $\text{CaMn}_4\text{O}_5$  cluster by the high-resolution XRD structure with central symmetry, (B) right (R)-opened optimized  $S_1$  structure and (C) left (L)-opened optimized  $S_1$  structure. The protonation states of water molecule in the  $S_1$  state are denoted as  $S_{1XYZ}$  where X, Y and Z are  $\text{O}^{2-}$  (=a),  $\text{OH}^-$  (=b) or  $\text{H}_2\text{O}$  (=c). Full geometry optimizations of six different structures; R- and L- $S_{1aca}$ , R- and L- $S_{1bba}$ .

### 8.3.11 Domain-Based Local Pair Natural Orbital CCSD(T) Calculations of Six Different $S_1$ Structures of Oxygen Evolving Complex of Photosystem II. Proposal of Multi-Intermediate Models for the $S_1$ State

Domain-based local pair natural orbital (DLPNO) coupled cluster single and double (CCSD) with triple perturbation (T) correction methods were applied for six different  $S_1$  structures of oxygen evolving complex (OEC) of photosystem II (PSII), showing that right-opened three  $S_1$  structures (Figure 8.8) were nearly degenerated in energy. The DLPNO-CCSD(T<sub>0</sub>) calculations support proposals of the multi-intermediate models for the  $S_1$  state in accord with the EPR, other experimental and DFT computational results.

### 8.3.12 Domain-Based Local Pair Natural Orbital CCSD(T) Calculations of Fourteen Different $S_2$ Intermediates for Water Oxidation in the Kok Cycle of OEC of PSII. Re-visit to One LS-two HS Model for the $S_2$ State

Domain-based local pair natural orbital (DLPNO) coupled cluster single and double (CCSD) with triple perturbation (T) correction methods were applied for fourteen different  $S_2$  structures of the  $\text{CaMn}_4\text{O}_5$  cluster in oxygen evolving complex (OEC) of photosystem II (PSII). The DLPNO-CCSD(T<sub>0</sub>) calculations elucidated that the right (R)-opened  $S_{2aYZ}$  structure (a =  $\text{O}^{2-}$  at the  $\text{O}_{(5)}$  site, Y = W<sub>2</sub> and Z = W<sub>1</sub>) with the low spin (LS) ( $S = 1/2$ ,  $g = 2$ ) state and two left (L)-opened  $S_{2aYZ}$  structures with the high spin (HS) ( $S = 5/2$ ,  $g = 4$ ;  $g > 4$ ) state were nearly degenerated in energy, supporting previous one LS-two HS model for the  $S_2$  state in compatible with recent EXAFS and EPR results.

### 8.3.13 Quantum-Mechanical Study of Energies, Structures and Vibrational Spectra of the HF Complexed with Dimethyl Ether

Interaction energies, geometry and vibrational frequencies of the gas-phase HF-dimethyl ether complex were obtained using quantum-chemical methods. Equilibrium and vibrationally averaged geometries, harmonic and anharmonic wavenumbers of the complex were calculated using second-order perturbation theory procedures with B3LYP, B2PLYP-D and MP2 methods with 6-311++G(2df, 2pd) basis set (Figure 8.9). Quantum-mechanical model describing anharmonic-type vibrational couplings within hydrogen bond was used to explain broadening, fine structure and temperature dependence of the F-H stretching IR absorption bands as effect of hydrogen

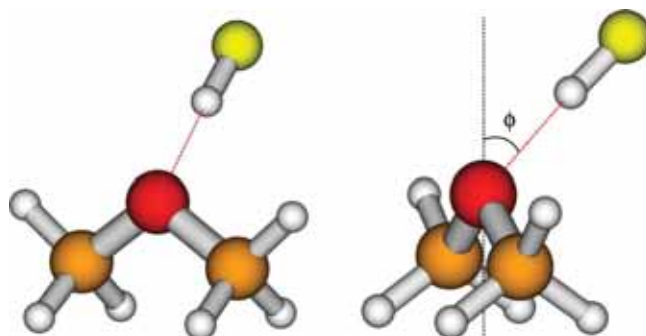


Figure 8.9: Equilibrium structure of the DME:HF complex with the  $C_s$  symmetry, optimized at the MP2/6-311++G(2df, 2pd) level, and the definition of the angle  $\phi$  between the O-H direction and the bisector of the C-O-C angle coplanar with this angle.

bond formation. Simulations of the rovibrational structure of the F-H stretching bands were performed for different temperatures. The results were compared with experimental spectra.

#### 8.3.14 IR Spectra of Crystalline Nucleobases. Combination of Periodic Harmonic Calculations with Anharmonic Corrections Based on Finite Models

This work reports a theoretical study of infrared (IR) spectra of four nucleobases (adenine, cytosine, guanine, and thymine) in the crystalline state. The effects responsible for the fine spectral features were revealed, and the nonfundamental bands significantly contributing to the IR fingerprint region were successfully reproduced. Additionally, we compared the fundamental bands simulated for periodic models in harmonic approximation with the results obtained for finite models in anharmonic approximation. On this basis, we concluded that accurate description of the chemical neighborhood is more essential for the IR fingerprint region than the anharmonicity (Figure 8.10). Comparison with previous results indicates that the vibrational properties and the nature of intermolecular interactions of nucleobases in the crystalline state remain similar to those in solution. Therefore, the conclusions obtained for well-defined crystalline structures of nucleobases are general and helpful in understanding the vibrational spectra and properties of nucleobases and their derivatives. Finally, this work evidences that anharmonic force field based on finite models may be applied as an inexpensive correction to the harmonic spectrum of an infinite periodic system.

#### 8.3.15 A Comparison of the Hydrogen Bond Interactions Dynamics in the Guanine and Cytosine Crystals: Ab Initio Molecular Dynamics and Spectroscopic Study

In this work, we present the comparison study of guanine and cytosine crystals based on the hydrogen bond (HB) dynamics. The ab initio molecular dynamics gave us a base for detailed analysis. The analysis of the trajectories by power spectrum generation, as well as the fluctuation of the interaction energies, showed large differences between HB networks in the considered crystals. The charge flow is present in the guanine molecule which forms the flat surfaces in the crystals. In the cytosine zigzag structure, the charge flow is blocked (Figure 8.11). The interaction energy is significantly less stabilizing in the cytosine structure than in the guanine. Finally, the possible influence of charge transfer on the melting temperature has been discussed.

#### 8.3.16 Conversion Reaction of Polyoxometalates from Anderson Structure to Keggin Structure

Aiming at developing synthetic methods of new Keggin-type polyoxometalates (POMs) that can mediate proton-conjugated multi-electron transfer reactions useful for efficient regeneration of fuels, we have investigated the reaction routes from Anderson-type POMs to Keggin-type POMs. The POM systems with various kinds of heteroatoms as their central cations were calculated using the Nudged Elastic Band (NEB) method as well as the first-principles electronic structure method (Figure 8.12). The effects of the heteroatoms on the reaction routes have been discussed.

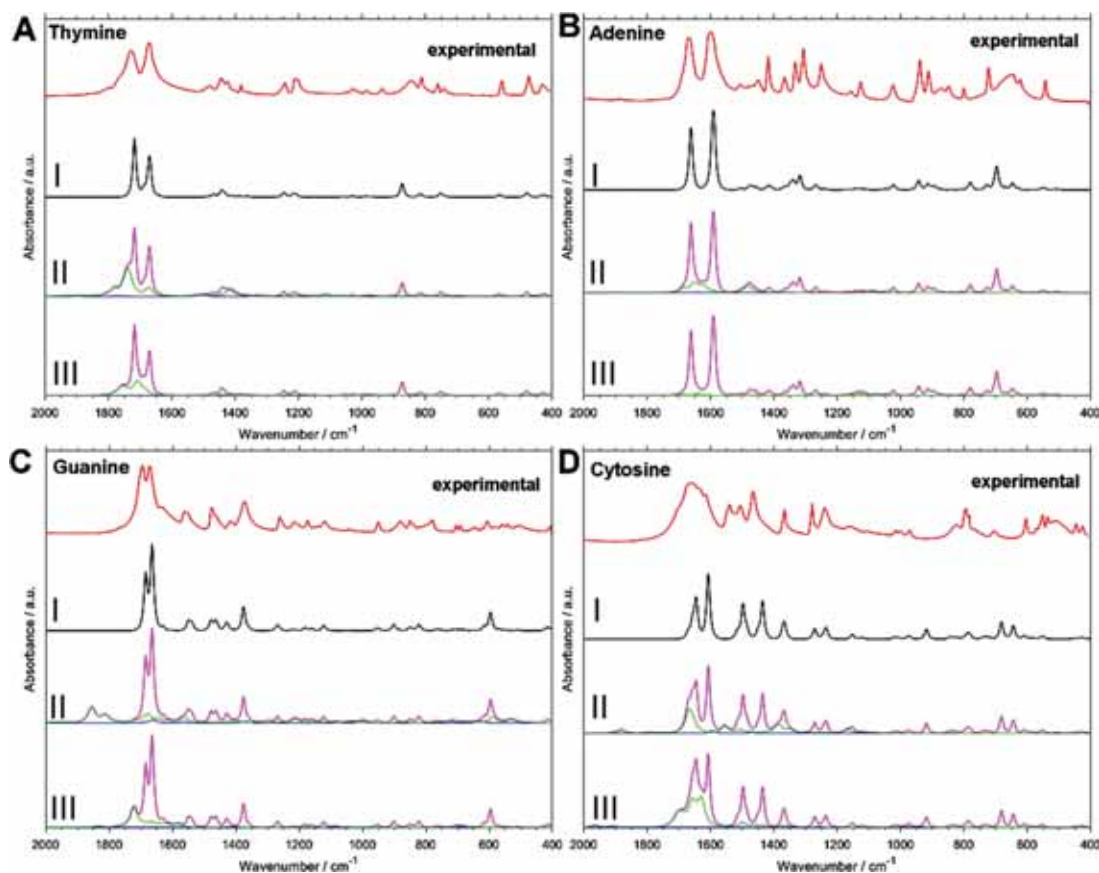


Figure 8.10: Experimental and simulated IR spectra of nucleobases in the fingerprint region ( $2000\text{--}400\text{ cm}^{-1}$ ). The harmonic spectrum (pdc./B3LYP/Gatti) in the 3D periodic system (I) and after additional anharmonic correction (II–III); II: DVPT2//B3LYP-GD3BJ/6-31++G(d,p) monomer; III: DVPT2//B3LYP-GD3BJ/6-31G(d,p) dimer. Green line, contribution from binary combinations; blue line, contribution from first overtones.

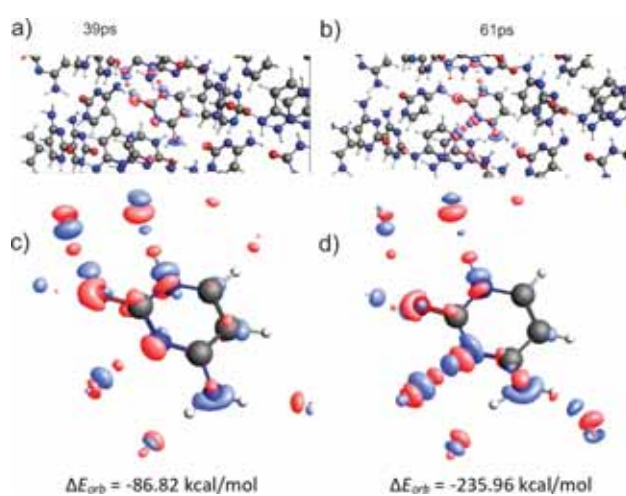


Figure 8.11: Analysis of deformation densities for the cluster of 27 molecules of cytosine. The blue and red colors show the accumulation and depletion of the electron density, respectively. Panel (a) shows the structure after 39 ps of simulation, while panel (b) after 61 ps. Panels (c) and (d) present the magnification of deformation density around the considered molecule in both snapshots, respectively.

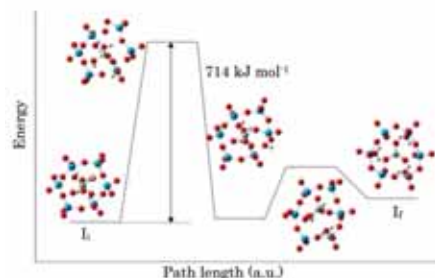


Figure 8.12: Exploration results of the conversion path between Anderson-type and Keggin-type six-membered rings  $I_A$  and  $I_K$ , for  $X = \text{Si}$ .

## 8.4 Schedule and Future Plan

### 8.4.1 Complexity Reduction in Density Functional Theory Calculations of Large Systems

In the following year, we plan to apply this framework to systems of practical interest including enzymes for bioremediation and important proteins of SARS-Cov-2. We further plan to use this framework in close collaboration with our newly developed version of NTChem aimed at computing large systems. In the previous year, we have worked on improving the robustness and ease of use of this new version of NTChem. Using the fragmentation information generated by our new framework, we hope to create accurate initial guesses for NTChem, further reducing the time to solution of hybrid DFT calculations.

### 8.4.2 Molecular Design for Solar Cell Materials

We found novel HTMs candidates by employing Bayesian optimization and DPSO. We will further expand our method by including quantum chemical calculation and improve our prediction model. Furthermore, we will improve our method by accelerating the Bayesian optimization process.

### 8.4.3 Molecular Design for Highly-functional Biopolymer Materials

Currently, we are investigating the experimental feasibility of synthesizing the candidate polymers. We will further improve our database by repeatedly reflecting the experimental results in simulation and informatics.

### 8.4.4 Construction of Molecular Orbital Method Consistent with Quantum Electrodynamics

The scheme of the QED-MO method developed this study has a high theoretical rigor, but has a demerit that the calculation cost is large. In the future, we will develop a program that can execute this QED-MO method stably and at low cost.

### 8.4.5 Multi-Scale Simulation to Predict Biodegradability of Plastics

The current MC simulator is not able to consider morphological effects and to evaluate real-time change in molecular weight distribution. We will implement Kinetic Monte Carlo, KMC, simulator to address above, which uses rates calculated by DFT and estimates time change of populations. We are also developing models to predict these values from monomer structures.

## 8.5 Publications

### 8.5.1 Articles/Journal

[1] K. Yamaguchi, S. Yamanaka, H. Isobe, M. Shoji, K. Miyagawa, T. Nakajima, T. Kawakami, and M. Okumura, "Theoretical and computational investigations of geometrical, electronic and spin structures of the  $\text{CaMn}_4\text{O}_X$

- (X=5, 6) cluster in the Kok cycle  $S_i$  ( $i = 0-3$ ) of oxygen evolving complex of photosystem II,” *Physiol. Plant.* 166, 44–59 (2019).
- [2] N. Minezawa and T. Nakajima, “Trajectory surface hopping molecular dynamics simulation by spin-flip time-dependent density functional theory,” *J. Chem. Phys.* 150, 204120 (2019).
- [3] L. Boda, M. Boczar, M. Z. Brela, M. J. Wojcik, and T. Nakajima, “Quantum-mechanical study of energies, structures and vibrational spectra of the HF complexed with dimethyl ether,” *Chem. Phys. Lett.* 731, 136590 (2019).
- [4] K. Miyagawa, T. Kawakami, Y. Suzuki, H. Isobe, M. Shoji, S. Yamanaka, M. Okumura, T. Nakajima, and K. Yamaguchi, “Domain-based local pair natural orbital CCSD(T) calculations of strongly correlated electron systems: Examination of dynamic equilibrium models based on multiple intermediates in  $S_1$  state of photosystem II,” *Mol. Phys.* 1666171 (2019).
- [5] K. Miyagawa, T. Kawakami, H. Isobe, M. Shoji, S. Yamanaka, K. Nakatani, M. Okumura, T. Nakajima, and K. Yamaguchi, “Domain-based local pair natural orbital CCSD(T) calculations of six different  $S_1$  structures of oxygen evolving complex of photosystem II. Proposal of multi-intermediate models for the  $S_1$  state,” *Chem. Phys. Lett.* 732, 136660 (2019).
- [6] K. Miyagawa, H. Isobe, T. Kawakami, M. Shoji, S. Yamanaka, M. Okumura, T. Nakajima, and K. Yamaguchi, “Domain-based local pair natural orbital CCSD(T) calculations of fourteen different  $S_2$  intermediates for water oxidation in the Kok cycle of OEC of PSII. Re-visit to one LS-two HS model for the  $S_2$  state,” *Chem. Phys. Lett.* 734, 136731 (2019).
- [7] K. Bec, J. Grabska, M. Czarnecki, C. Huck, M. Wójcik, T. Nakajima, and Y. Ozaki, “IR spectra of crystalline nucleobases. Combination of periodic harmonic calculations with anharmonic corrections based on finite models,” *J. Phys. Chem. B*, 123, 10001–10013 (2019).
- [8] M. Brela, O. Klimas, E. Surmiak, M. Boczar, T. Nakajima, and M. Wójcik, “A comparison of the hydrogen bond interactions dynamics in the guanine and cytosine crystals: Ab initio molecular dynamics and spectroscopic study,” *J. Phys. Chem. A*, 123, 10757–10763 (2019).
- [9] T. Yonehara and T. Nakajima, “Electron dynamics method using a locally projected group diabatic Fock matrix for molecules and aggregates,” *Chem. Phys.* 528, 110508 (2020).
- [10] N. Minezawa and T. Nakajima, “Quantum mechanical/molecular mechanical trajectory surface hopping molecular dynamics simulation by spin-flip time-dependent density functional theory,” *J. Chem. Phys.* 152, 024119 (2020).
- [11] T. Yamakawa, K. Eda, T. Osakai, and T. Nakajima, “Conversion reaction of polyoxometalates from Anderson structure to Keggin structure,” *J. Comput. Chem. Japan* 18, 257–258 (2020).

### 8.5.2 Posters

- [12] 米原大博, 中嶋隆人, “局所透熱表示と射影演算子を用いた自己参照型非線形電子動力学の効率的解法,” 第22回理論化学討論会, 札幌, 2019-05-27.
- [13] 井上頌基, 中嶋隆人, “Dirac-Fock 演算子の Douglas-Kroll 変換および IOTC 変換,” 第22回理論化学討論会, 札幌, 2019-05-28.
- [14] 川上貴資, 宮川晃一, 鈴木雄太, 磯辺寛, 庄司光男, 山中秀介, 奥村光隆, 中嶋隆人, 山口兆, “光合成酵素発生錯体 ( $\text{CaMn}_4\text{O}_5$  クラスター) の  $S_1$  状態での各構造と電子状態の LPNO-CC 法による解析,” 第13回分子科学討論会, 名古屋, 2019-09-17.
- [15] 神谷宗明, William Dawson, 中嶋隆人, “大規模分子の励起電子状態に対する時間依存密度汎関数法の開発,” 第13回分子科学討論会, 名古屋, 2019-09-17.
- [16] 嶺澤範行, 中嶋隆人, “太陽電池モデル分子の非断熱分子動力学シミュレーション,” 第13回分子科学討論会, 名古屋, 2019-09-18.
- [17] Takehiro Yonehara and Takahito Nakajima, “Computational study on quantum dynamics of excited electrons in molecular aggregates: Toward an efficient control of a conversion from light energy to chemical functionality,” The 2nd R-CCS International Symposium, Kobe, 2020-02-17.
- [18] William Dawson, Luigi Genovese and Takahito Nakajima, “Complexity Reduction in Density Functional Theory Calculations of Large Systems,” The 2nd R-CCS International Symposium, Kobe, 2020-02-17.
- [19] Nobuki Inoue and Takahito Nakajima, “Efficient calculation method considering charge distribution of nuclei in electronic structure theory,” The 2nd R-CCS International Symposium, Kobe, 2020-02-17.
- [20] Eisuke Kawashima and Takahito Nakajima, “Multi-Scale Simulation to Predict Biodegradability of Plastics,” The 2nd R-CCS International Symposium, Kobe, 2020-02-17.

### 8.5.3 Invited Talks

- [21] 中嶋隆人, “第一原理計算とスーパーコンピュータによる新材料設計,” 神戸大学開拓プロジェクト「階層縦断的アプローチによる革新的光エネルギー変換系の開拓」第1回シンポジウム, 神戸, 2019-04-16.
- [22] 中嶋隆人, “スーパーコンピュータを利用した第一原理シミュレーションによる新材料設計,” 新化学技術推進協会先端化学・材料技術部会講演会, 東京, 2019-05-10.
- [23] 中嶋隆人, “京を利用した第一原理計算とマテリアルズ・インフォマティクスによる新材料設計,” 高分子同友会勉強会, 東京, 2019-07-31.
- [24] T. Nakajima, T. Matsuoka, “Materials design of hole-transporting materials for perovskite solar cells,” Asia-Pacific Conference on Theoretical & Computational Chemistry 2019, Sydney, 2019-10-03.
- [25] 中嶋隆人, “シミュレーションとインフォマティクスの融合による新材料設計 -富岳に向けて-,” 第5回キャタリストインフォマティクスシンポジウム, 東京, 2019-11-12.
- [26] 中嶋隆人, “驚くべきスパコンの世界-その活用と未来展望-,” 量子科学技術研究開発機構学術情報流通講座, 稲毛, 2019-11-19.
- [27] 中嶋隆人, “分析・解析技術としての量子化学シミュレーションとインフォマティクスNMRを中心に (第一原理シミュレーションとマテリアルズ・インフォマティクスによる新材料設計),” 理研シンポジウム第20回 分析・解析技術と化学の最先端, 和光, 2019-12-11.
- [28] 中嶋隆人, “スーパーコンピュータを利用した分子シミュレーションとインフォマティクスによる新材料設計,” “AIと有機合成化学” 第4回公開講演会, 早稲田, 2020-02-03.

### 8.5.4 Oral Talks

- [29] 川嶋英佑, 中嶋隆人, “Virtual Screening of Non-Fullerene Acceptors for Organic Photovoltaics by Density Functional Theory and Dynamic Monte Carlo Method,” 重点課題5 第2回若手勉強会 (若手研究者によるワークショップ), 犬山, 2019-08-29.
- [30] Takahito Nakajima, “Molecular simulation on the K computer and towards Fugaku,” The 2nd R-CCS International Symposium, Kobe, 2020-02-17.

## Chapter 9

# Computational Materials Science Research Team

### 9.1 Members

Seiji Yunoki (Team Leader)

Yuichi Otsuka (Research Scientist)

Shigetoshi Sota (Research Scientist)

Tomonori Shirakawa (Research Scientist)

Hiroshi Ueda (Research Scientist)

Sandro Sorella (Guest Researcher)

Takami Toyama (Guest Researcher)

Michele Casula (Guest Researcher)

Tatsuya Shishidou (Guest Researcher)

Nauta Takemori (Guest Researcher)

Masako Hirata (Assistant)

Keiko Matsuoka (Assistant)

### 9.2 Overview of Research Activities

Strongly correlated quantum materials show great promise for next-generation electronic applications. In order to accelerate the development of functional strongly correlated quantum materials, a reliable theory with good predictability is required. However, the strong interactions that take place in this class of materials do not allow us to apply the traditional band theory based on the density functional theory, which played a major role in the advance of today's electronic technology based on semiconductors.

Consequently, we are developing large-scale numerical simulations for strongly correlated quantum systems, including strongly correlated quantum materials, where the many-body interactions are essential to induce novel phenomena and properties. We are interested particularly in the quantum Monte Carlo (QMC) method, the density matrix renormalization group (DMRG) method, and the tensor network method to simulate not only the ground state but also the dynamics (thermodynamics, excitation dynamics, and real time dynamics). We have established a platform for advanced research of strongly correlated quantum systems by developing state-of-the-art simulations.

## 9.3 Research Results and Achievements

### 9.3.1 Large-scale QMC simulations for interacting fermions

We develop a quantum Monte Carlo (QMC) method, which is one of the most reliable and efficient techniques for Hubbard-type lattice models of interacting electrons. Typical target systems we aim are of the order of 10,000 electrons unless the notorious minus-sign problem occurs. One of the main focuses in our QMC project is to clarify quantum criticality of quantum phase transitions in strongly-correlated electrons with high accuracy, which would be impossible without the power of super computers.

We have implemented a highly efficient QMC code based on the auxiliary field scheme for lattice fermion systems at zero temperature. Since numerical calculations involved in this formulation are mostly linear algebraic procedure such as matrix-matrix product and numerical orthogonalization, we can take advantage of the highly optimized numerical library on super computers such as K computer to calculate physical observables with a high degree of accuracy on unprecedentedly large systems.

In this fiscal year, we have revisited the quantum criticality of the phase transitions for the chiral-Heisenberg universality class in terms of the Gross-Neveu model. The linear dispersion of the Dirac fermions in the non-interacting limit, as shown in Fig. 9.1, is constructed by introducing a  $d$ -wave pairing field to the Hubbard model on the square lattice. The Hamiltonian we have studied reads

$$H = H_{\text{BCS}} + H_U, \quad (9.1)$$

where

$$H_{\text{BCS}} = \sum_{\langle i,j \rangle} \left\{ \begin{pmatrix} c_{i\uparrow}^\dagger & c_{i\downarrow} \end{pmatrix} \begin{pmatrix} -t & \Delta_{ij} \\ \Delta_{ij}^* & t \end{pmatrix} \begin{pmatrix} c_{j\uparrow} \\ c_{j\downarrow}^\dagger \end{pmatrix} + \text{h.c.} \right\} \quad (9.2)$$

and

$$H_U = U \sum_i n_{i\uparrow} n_{i\downarrow}. \quad (9.3)$$

It is noted that, the way of counting the number of fermion components being different, the effective model in the continuum limit is the same as that of the widely-studied Hubbard model on the honeycomb lattice, of which the critical exponents have been accurately determined in our previous study.

By exploiting large-scale quantum Monte Carlo simulations, we have calculated the correlation ratio of the spin structure factor, the staggered magnetization, and the quasiparticle weight. Based on these quantities, the antiferromagnetic phase transitions have been investigated by several methods such as the crossing-point analysis (Fig. 9.2) and the data-collapse fit (Fig. 9.3). The conservative estimates for the critical exponents obtained in this work are  $\nu=1.05(5)$ ,  $\eta_\phi=0.75(4)$ , and  $\eta_\psi=0.23(4)$ . These results improve our previous estimates, especially for the exponent  $\eta_\phi$ , which is now closer to the recent independent QMC calculation which features a quantum spin-Hall insulator transition [Nat. Commun. 10, 1 (2019)]. Indeed we have noticed that it is a cumbersome task to judge whether correction terms to the simple scaling ansatz should be included in a data-collapse fit of the Bayesian scaling analysis, and our previous estimates of  $\eta_\phi$  were eventually not accurate enough. We have also shown that the anisotropy of the Dirac cones does not affect the criticality, which suggests the emergent relativistic invariance at the quantum critical point.

### 9.3.2 Massively parallel DMRG algorithms for quantum many-body systems

The DMRG method is recognized as one of the most efficient numerical methods to investigate strongly correlated quantum systems. We have been developing four types of massively parallel DMRG programs, 2D-DMRG, DDMRG, paraDMRG, and QUARTZ. The 2D-DMRG is developed for the ground state calculations on two-dimensional strongly correlated quantum systems. The DDMRG is developed for quantum dynamics of strongly correlated quantum systems. The paraDMRG is developed for the full-CI calculations in *ab initio* simulations. The QUARTZ is developed to simulate quantum computers. Our developed massively parallel DMRG algorithm has achieved the extremely high peak performance ratio of 73.6% when 82,488 nodes are used on K computer, which is about 7.8 PFLOPS.

In this fiscal year, we have developed a new method using supervised machine learning (ML) and DMRG methods to construct phase diagrams in strongly correlated quantum systems. We usually find phase boundaries by detecting anomalous behaviors of physical quantities such as energy. However, these quantities sometimes exhibit little changes at the boundaries. Entanglement spectrum (ES) consisting of the eigenvalues of the entanglement Hamiltonian for the ground state has been suggested as an order parameter. For example, the absence

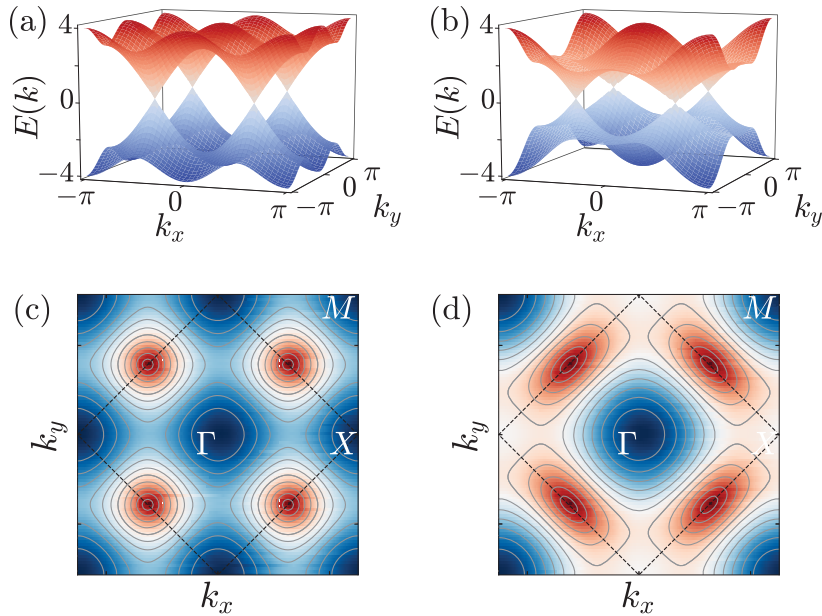


Figure 9.1: The noninteracting energy dispersion of the square lattice Hubbard model with the  $d$ -wave pairing field for (a)  $\Delta = 1$  and (b)  $\Delta = 0.5$ , and the corresponding contour plot of the lower band for (c)  $\Delta = 1$  and (d)  $\Delta = 0.5$ .

of a gap called Schmidt gap between the low-lying neighboring two levels of ES is characteristic of topologically ordered phase like the Haldane phase and Kitaev spin liquid phase. Especially, characterizing quantum states by using ES is useful in the DMRG calculations, since ES is always derived in the DMRG procedure. However, the Schmidt gap is not necessarily a good quantity for detecting phase transition between non-topological phases. Another strategy will be the use of ML. In fact, ML has been successful in characterizing ordered states, topological states, and photoexcited states. In the present study, we have used ES as a training dataset of neural network. We have demonstrated that the trained neural network can determine phase boundaries in the half-filled one-dimensional extended Hubbard model.

### 9.3.3 Controlled dynamics in quantum many-body systems

The recent extensive studies of photoinduced states of strongly correlated quantum systems have paved the way to find new states of matter. Indeed, those activities have found many intriguing phenomena, including the photoinduced transient superconducting states and the photoinduced insulator-to-metal transitions.

Motivated by these experimental activities, we have studied the photoinduced states in models of strongly correlated electron systems. Applying the exact diagonalization technique and the DMRG method, we have found that the pulse irradiation to the Mott insulating state in the Hubbard model can induce the enhancement of an unconventional superconductivity. This photoinduced superconductivity is due to the sequential generation of  $\eta$ -pairs, which is characterized by staggered pair-density-wave oscillations in the off-diagonal long-range correlation with a phase of  $\pi$  (see Fig. 9.4) and is associated with the transverse components of pseudospin  $1/2$  operators, first introduced by mathematical physicist C. N. Yang. We have also found that the  $\eta$  pairs are preferentially excited by the optical pulse field because of the beautiful mathematical structure forced by the symmetry of the pseudospin operators.

In our subsequent our works, we have also shown that the same mechanism can be applied to another class of models, the Kondo lattice model, known as an effective model to describe electronic states in heavy electron systems, potentially suggesting that this mechanism can be found ubiquitously. In addition, we have found that the spin dynamics changes drastically and becomes diffusive after pulse irradiation, which can be understood because the generation of the  $\eta$  pairs is equivalent to in-situ carrier doping for spin dynamics.

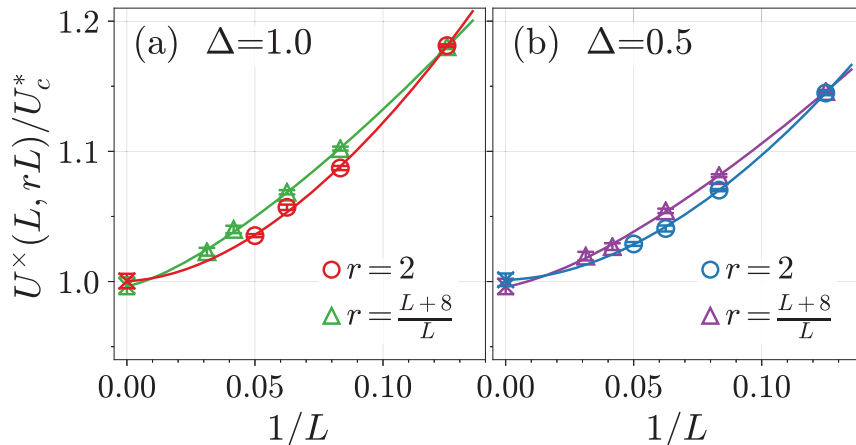


Figure 9.2: Crossing-point analysis of the correlation ratio  $R_{m^2}(U, L)$ .  $U^\times(L, rL)$  are obtained by interpolating data points of  $R_{m^2}(U, L)$  with second order polynomial functions. For ease of comparison, values of  $U^\times(L, rL)$  are normalized by  $U_c^* = 7.63$  and  $5.49$  for (a)  $\Delta = 1$  and (b)  $\Delta = 0.5$ , respectively. Ratios of two system sizes are  $r = 2$  (circles) and  $r = (L + 8)/L$  (triangles). Results of the fit with  $U^\times(L, rL) = U_c + dL^{-(\omega+1/\nu)}$  are (a)  $U_c=7.63(4)$  and  $\omega + 1/\nu=1.8(1)$  for  $r = 2$  and  $U_c=7.61(5)$  and  $\omega + 1/\nu=1.4(1)$  for  $r = (L + 8)/L$ , and (b)  $U_c=5.49(3)$  and  $\omega + 1/\nu=1.8(1)$  for  $r = 2$  and  $U_c=5.47(3)$  and  $\omega + 1/\nu=1.4(1)$  for  $r = (L + 8)/L$ . Note that  $U_c$ 's extrapolated in the thermodynamic limit are indicated by crosses at  $1/L = 0$ .

### 9.3.4 Tensor network method for many-body systems

We have investigated finite-temperature phase transitions in the dodecahedral (20 degrees of freedom) classical Heisenberg model on a two-dimensional square lattice using a large parallelized corner transfer matrix renormalization group (CTMRG) and revealed that the model has a single second-order phase transition with a non-trivial central charge in the conformal field theory between the order and disorder phases. We have also investigated the critical phenomena for intermediate phase associated with Berezinskii-Kosterlitz-Thouless (BKT) phase transitions in the classical six-state clock model on a square lattice using the CTMRG and a finite- $m$  scaling analysis to estimate the Tomonaga-Luttinger parameter. We have confirmed that the intermediate phase is successfully described by the  $Z_6$  dual sine-Gordon model.

In addition, we have optimized a class of tensor network states describable in quantum circuits on one-dimensional quantum spin systems in the thermodynamic limit and found that Suzuki-Trotter-like decomposed unitary operators including optimization parameters coupled with interaction parameters can effectively search the ground state energy rather than employing unitary gates describing an arbitrary unitary transformation. We have developed an MPI parallelized quantum circuit simulator for running these optimizations in a large-scale parallel computing, and succeeded in achieving more than 10 times faster than the existing non-parallelized simulator in a relatively large-scale quantum circuit simulation of 30 qubits.

## 9.4 Schedule and Future Plan

### 9.4.1 Large-scale QMC simulations for interacting fermions

The study of topological phenomena has already become a major trend in modern materials science. In order to establish further fundamental concepts and to yet develop new materials, it is important to clarify the correlation effects. In the systems with topological properties, some symmetries play crucial roles to preserve them, and these symmetries often enable us to perform the quantum Monte Carlo calculations without the notorious negative sign problem. We focus on this aspect and launch a new study to elucidate the topological phenomena brought by the strong correlation effect. Specifically, we plan to investigate the properties of high-order topological Mott insulators, which are predicted to exist when the strong correlation is added to the high-order topological insulators, the band insulator with non-trivial topological properties. In conventional topological insulators, when a  $d$ -dimensional bulk has a non-trivial topological order, a localized state appears at the edge of the  $(d - 1)$  dimension, which relation is known as the bulk-edge correspondence. In contrast, in

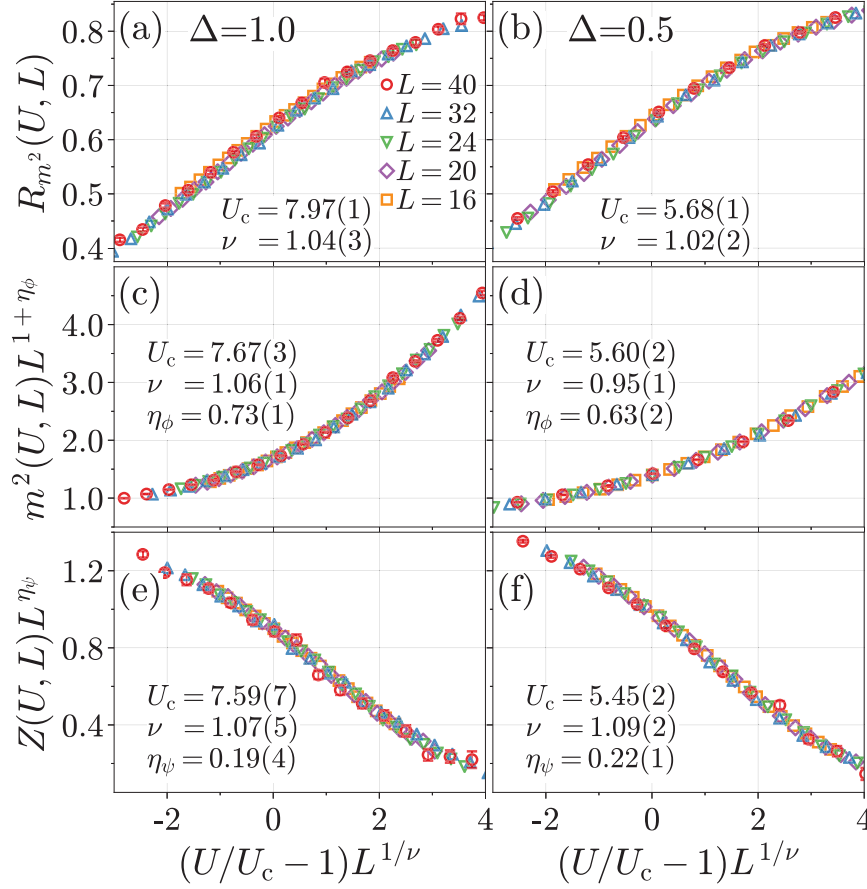


Figure 9.3: Data-collapse fits of correlation ratio [(a) and (b)], staggered magnetization [(c) and (d)], and quasiparticle weight [(e) and (f)]. For each observable, left and right figures show results of  $\Delta = 1$  and  $0.5$  with the same scale. Estimated critical points and exponents are indicated in each figure.

the higher-order topological insulators, localized states with lower dimensionality appear in the  $(d-2)$  or  $(d-3)$  dimension (e.g., a “corner” state with  $d = 0$  if  $d = 2$ ). It has recently been pointed out that although this localized state is band-insulator-like in the non-interacting systems, i.e., there is a gap in both the charge and spin sectors, the strong electron correlation qualitatively changes it to a Mott-like state with a gap opening only in charge [Phys. Rev. Lett 123, 196402 (2019)]. This proposal is based on the result of exact diagonalization for the Kagome lattice, which should be severely limited by finite-size effects and thus was unable to quantitatively estimate the gaps along with the topological phase transition or to determine a precise phase diagram. In this plan, we first aim to clarify the properties of corner states in the Kagome lattice system by the large-scale quantum Monte Carlo simulations. Preliminary calculations have confirmed that the QMC calculations on the Kagome lattice reproduce the results by the exact diagonalization with much fewer computer resources. We also plan to study the pyrochlore system, which is the original setup for the higher-order topological Mott insulators [Nat. Phys. 6, 376 (2009)].

### 9.4.2 Massively parallel DMRG algorithms for quantum many-body systems

We will optimize our massively parallel DMRG programs to perform calculations effectively and efficiently on Fugaku computer. In addition, we will develop our DMRG programs to perform calculations which are difficult

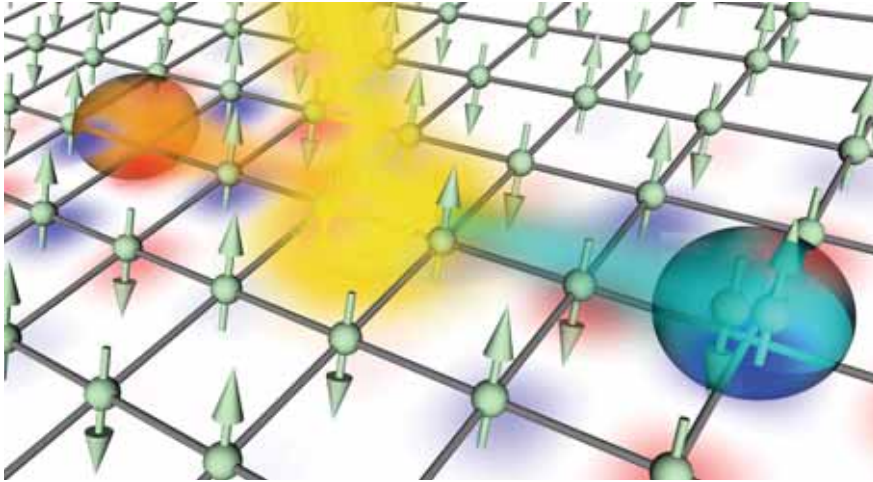


Figure 9.4: A schematic depiction of photoinduced  $\eta$ -pairing.

to perform on K computer, such as finite temperature calculations. Our developed finite temperature DMRG algorithm for higher-dimensional quantum many-body systems requires several ten times larger computational costs compared with those of the ground state calculations. Moreover, we will develop new massively parallel DMRG algorithms, such as the infinite DMRG method for quantum dynamics.

### 9.4.3 Controlled dynamics in quantum many-body systems

The numerical simulation of quantum dynamics of quantum many-body systems is one of important subjects to bridge the experimental observation and the theoretical prediction. Moreover, as demonstrated in the research results and achievements in this fiscal year, those are also promising fields to find new phenomena which can be controlled artificially. For example, one of application by using the controlled dynamics includes quantum computation, which has been attracted much attention not only in fundamental scientific fields but also in industrial fields.

In this fiscal year, we have developed a numerical technique to perform the numerically exact simulation in the complex systems composed of the quantum spins and fermion bath system by extending the method originally proposed by two of our members [T. Shirakawa and S. Yunoki, *Physical Review B* **90**, 195109 (2014)]. We plan to apply this method to study the spin current dynamics in the spin systems coupled to fermions with Rashba spin-orbit coupling, which finds important applications in the field of spintronics.

We also plan to develop quantum-classical hybrid algorithms for quantum computing in order to simulate quantum many-body systems by simulators developed by our team and also by quantum devices.

### 9.4.4 Tensor network method for many-body systems

We continuously implement the numerical code for calculating physical properties in our parallel CTMRG to clarify the non-trivial criticality in many-body systems and investigate a search algorithm for optimal tensor-network decomposition in non-uniform quantum states, which is important to accelerate the numerical methods based on tensor network algorithm.

We will also investigate quantum (inspired) algorithm with tensor network scheme and quantum circuits in the wake of recent rapid developments in quantum computing (QC). Especially, we focus on HPC-QC hybrid environments and try to accelerate numerical algorithm for simulating static/dynamical property of quantum spin systems.

## 9.5 Publications

### 9.5.1 Articles/Journal

- [1] B.-H. Kim, K. Seki, T. Shirakawa, and S. Yunoki, “Topological property of a  $t_{2g}^5$  system with a honeycomb lattice structure”, *Physical Review B* **99**, 155135/1–16 (2019).
- [2] R. Fujiuchi, T. Kaneko, Y. Ohta, and S. Yunoki, “Photoinduced electron-electron pairing in the extended Falicov-Kimball model”, *Physical Review B* **100**, 045121/1–14 (2019).
- [3] S. Ohmura, A. Takahashi, K. Iwano, T. Yamaguchi, K. Shinjo, T. Tohyama, S. Sota, and H. Okamoto, “Effective model of one-dimensional extended Hubbard systems: Application to linear optical spectrum calculations in large systems based on many-body Wannier functions”, *Physical Review B* **100**, 235134/1–15 (2019).
- [4] Y. Kawasaki, K. Seki, J. Pu, T. Takenobu, S. Yunoki, H. M. Yamamoto, and R. Kato, “Non-Fermi-liquid behavior and doping asymmetry in an organic Mott insulator interface”, *Physical Review B* **100**, 115141/1–7 (2019).
- [5] A. Masaki-Kato, S. Yunoki, and D. S. Hirashima, “Quantum Monte Carlo study of the superfluid density in quasi-one-dimensional systems of hard-core bosons: Effect of the suppression of phase slippage”, *Physical Review B* **100**, 224515/1–7 (2019).
- [6] T. Shirakawa, S. Miyakoshi, and S. Yunoki, “Photoinduced  $\eta$  pairing in the Kondo lattice model”, *Physical Review B* **101**, 174307/1–12 (2020).
- [7] C. C. Chang, A. Gambhir, T. S. Humble, and S. Sota, “Quantum annealing for systems of polynomial equations”, *Scientific Report* **9**, 10258/1–9 (2019).
- [8] Y. Kawasaki, K. Seki, S. Tajima, J. Pu, T. Takenobu, S. Yunoki, H. M. Yamamoto, and R. Kato, “Two-dimensional ground-state mapping of a Mott-Hubbard system in a flexible field-effect device”, *Sci. Adv.* **5**, eaav7282 (2019).
- [9] H. Watanabe, H. Seo, and S. Yunoki, “Mechanism of superconductivity and electron-hole doping asymmetry in  $\kappa$ -type molecular conductor”, *Nature Communications* **10**, 3167/1–8 (2019).
- [10] M. Khazaei, J. Wang, M. Estili, A. Ranjbar, S. Suehara, M. Arai, K. Esfarjani, and S. Yunoki, “Novel MAB phases and insights into their exfoliation into 2D MBenes”, *Nanoscale*. **11**, 11305 (2019).
- [11] M. Khazaei, A. Mishra, N. S. Venkataramanan, A. K. Singh, and S. Yunoki, “Recent advances in MXenes: From fundamentals to applications”, *Curr. Opin. Solid State Mater. Sci.* **23**, 164 (2019).
- [12] X. Yin, C. S. Tang, S. Zeng, T. C. Asmara, P. Yang, M. A. Naradipa, P. E. Trevisanutto, T. Shirakawa, B. H. Kim, S. Yunoki, M. B. H. Breese, T. Venkatesan, A. T. S. Wee, A. Ariando, and A. Rusydi, “Quantum correlated plasmons and their tunability in undoped and doped Mott-insulator cuprates”, *ACS Photonics* **6**, 3281–3289 (2019).
- [13] K. Shinjo, K. Sasaki, S. Hase, S. Sota, S. Ejima, S. Yunoki, and T. Tohyama, “Machine learning phase diagram in the half-filled one-dimensional extended Hubbard model”, *Journal of Physics Society of Japan* **88**, 065001/1–2 (2019).
- [14] K. Nishiguchi, T. Shirakawa, H. Watanabe, R. Arita, and S. Yunoki, “Possible Superconductivity Induced by a Large Spin-Orbit Coupling in Carrier Doped Iridium Oxide Insulators: A Weak Coupling Approach”, *Journal of the Physical Society of Japan* **88**, 094701/1–14 (2019).
- [15] F. Lange, S. Ejima, T. Shirakawa, S. Yunoki, and H. Fehske, “Block-Lanczos Density-Matrix Renormalization-Group Approach to Spin Transport in Heisenberg Chains Coupled to Leads”, *Journal of the Physical Society of Japan* **89**, 044601/1–6 (2020).
- [16] M. Khazaei, A. Ranjbar, Y. Liang, and S. Yunoki, “Electronic properties and applications of MXenes from ab initio calculations perspective”, Chap. 14 in “2D Metal Carbides and Nitrides (MXenes): Structure, Properties and Applications”, ed. by B. Anasori and Y. Gogotsi (Springer, 2019).
- [17] T. Kaneko, T. Shirakawa, and S. Yunoki, “Photo-induced  $\eta$ -pairing states in the Hubbard model”, *Kotai Butsuri* **55**, 1–9 (2020) (in Japanese).

### 9.5.2 Invited Talks

- [1] S. Sota, “Development of massively parallel DMRG method and its applications to quantum dynamics”, ISSP supercomputer center and CCMS collaboration workshop “Novel development of condensed matter physics”, April 2–3 (2019), Kashiwa (Japan).
- [2] S. Yunoki, “Correlation-driven dimerization and topological gap opening in isotropically strained graphene”, International Workshop: Topology the New Horizon of Materials Science and Nanophotonics, June 12-13 (2019), NIMS, Tsukuba (Japan).

- [3] S. Yunoki, “Photoinduced superconductivity by  $\eta$ -pairing mechanism in a Mott insulator”, 10th International Conference of the Asian Consortium on Computational Materials Science (ACCMS-10), July 22-26 (2019), City University of Hong Kong, Hong Kong (China).
- [4] H. Ueda, “Analysis of critical phenomena in classical spin systems using large-scale parallelized corner transfer matrix renormalization group”, the 4th HPC-Phys workshop, August 26 (2019), Kobe (Japan).
- [5] S. Yunoki, “Photoinduced superconductivity by  $\eta$  pairs in a Mott insulator”, International Conference Electron Correlation in Superconductors and Nanostructures (ECSN-2019), October 6-10 (2019), Odessa (Ukraine).
- [6] Y. Otsuka, “QMC study of the Gross-Neveu universality class; the chiral-Heisenberg class revisited”, Mini-workshop on “Fermion Quantum Criticality and beyond”, February 13–14 (2020), Würzburg (Germany).
- [7] S. Yunoki, “Relativistic Mott insulator, superconductivity, and other exotic states in  $5d$  electrons”, Mini-workshop on “Fermion Quantum Criticality and beyond”, February 13–14 (2020), Würzburg (Germany).

### 9.5.3 Oral Talks

- [1] H. Ueda, “Critical behavior of the two-dimensional dodecahedron model”, CAQMP 2019 (Computational Approaches to Quantum Many-body Problems), July 29 (2019), Kashiwa (Japan).
- [2] Y. Otsuka, K. Seki, S. Yunoki, and S. Sorella, “Numerical study of universal quantum criticality in strongly correlated Dirac electrons”, IMS workshop on “Topological physics and organic massless Dirac systems”, August 8–9 (2019), Okazaki (Japan).
- [3] Y. Otsuka, K. Seki, S. Yunoki, and S. Sorella, “Numerical study of Mott transition in the Hubbard model with d-wave superconducting order parameter”, Autumn Meeting of Physics Society of Japan, September 10-13 (2019), Gifu (Japan).
- [4] T. Tohyama, S. Sota, S. Yunoki, “Dynamical DMRG Study of spin dynamics on  $t - t' - J$  model”, Autumn Meeting of Physics Society of Japan, September 10–13 (2019), Nagoya (Japan).
- [5] T. Yamaguchi, K. Iwano, S. Ohmura, A. Takahashi, K. Shinjo, T. Tohyama, S. Sota, H. Okamoto, “Theoretical prediction for an optical conductivity of a charge model in the thermodynamic limit by constructing the many-body Wannier functions”, Autumn Meeting of Physics Society of Japan, September 10–13 (2019), Nagoya (Japan).
- [6] S. Ohmura, A. Takahashi, T. Yamaguchi, K. Iwano, K. Shinjo, T. Tohyama, S. Sota, H. Okamoto, “Charge model: An effective model for the one-dimensional extended Hubbard model, where spin-charge separation is compatible with charge fluctuations”, September 10–13 (2019), Nagoya (Japan).
- [7] K. Shinjo, S. Sota, T. Tohyama, “Time-dependent DMRG study of optical conductivity on one-dimensional and ladder lattice extended Hubbard model”, September 10–13 (2019), Nagoya (Japan).
- [8] H. Ueda, K. Okunishi, S. Yunoki, T. Nishino, “Finite- $m$  scaling of corner transfer matrix renormalization group for entanglement spectrum”, 2019 Autumn Meeting, The Physical Society of Japan, September 10-13 (2019), Nagoya (Japan).
- [9] H. Ueda, “Roles of easy-plane and easy-axis XXZ anisotropy and bond alternation in a frustrated ferromagnetic spin-1/2 chain”, the 14th quantum-spin-system workshop, January 8 (2020), Semboku (Japan).
- [10] T. Shirakawa, “Simulations of dynamics in quantum many-body systems”, The 190th R-CCS Cafe, February 3 (2020), Kobe (Japan).
- [11] S. Sota, T. Shirakawa, S. Yunoki, T. Tohyama, “Dynamical DMRG study of spin excitation dynamics in triangular lattice spin-1/2 antiferromagnet”, APS March Meeting 2020, March 2–6 (2020), Denver (USA).
- [12] T. Shirakawa, S. Miyakoshi, and S. Yunoki, “Photo-induced superconductivity in the Kondo lattice”, APS March Meeting 2020, March 2–6 (2020), Denver (USA).
- [13] H. Ueda, Y. Otsuka, M. Nakata, “Variational method using matrix product unitary state”, 75th Annual Meeting, The Physical Society of Japan, March 16-19 (2020), Nagoya (Japan).

### 9.5.4 Posters

- [1] S. Sota, S. Yunoki, “Kernel polynomial expansion method on quantum computer”, Autumn Meeting of Physics Society of Japan, September 10–13 (2019), Nagoya (Japan).
- [2] T. Shirakawa, S. Sota, S. Yunoki, and T. Tohyama, “Dynamical spin structure factor of the triangular-lattice Heisenberg model”, 2019 Autumn Meeting of the Physical Society of Japan, September 10–13 (2019), Gifu (Japan).
- [3] H. Watanabe, T. Shirakawa, K. Seki, H. Sakakibara, and S. Yunoki, “Study for magnetism and superconductivity in high- $T_c$  cuprates using 4-band  $d-p$  model”, 2019 Autumn Meeting of the Physical Society of Japan, September 10–13 (2019), Gifu (Japan).

[4] K. Seki, T. Shirakawa, and S. Yunoki, “Variational cluster approach to thermodynamic properties of interacting fermions at finite temperatures”, 2019 Autumn Meeting of the Physical Society of Japan, September 10–13 (2019), Gifu (Japan).

[5] S. Sota, T. Shirakawa, S. Yunoki, T. Tohyama, “Dynamical DMRG Study of Spin Excitation Dynamics on the Triangular Lattice Antiferromagnetic Heisenberg model”, International Conference on Strongly Correlated Electron Systems 2019, September 23–28 (2019), Okayama (Japan).

### 9.5.5 Software

[1] S. Sota, K. Morita, H. Matsueda, S. Yunoki, T. Tohyama, “DDMRG (Dynamical DMRG)”, R-CCS software.

[2] S. Sota, S. Yunoki, T. Tohyama, “2-D DMRG”, R-CCS software.

[3] S. Sota, Y. Imamura, T. Nakajima, S. Yunoki, T. Tohyama, “paraDMRG”, R-CCS software.

[4] S. Sota, S. Yunoki, “QUARTZ”, R-CCS software.



## Chapter 10

# Computational Biophysics Research Team

### 10.1 Members

Yuji Sugita (Team Leader (concurrent))\*

Jaewoon Jung (Research Scientist (concurrent)\*\*

Chigusa Kobayashi (Research Scientist)

Koichi Tamura (Special Postdoctoral Researcher)\*\*\*

Ai Shinobu (Postdoctoral Researcher)

Cheng Tan (Postdoctoral Researcher)

Hiromi Kano (Assistant)

Mitsunori Ikeguchi (Guest Scientist)\*\*\*\*

Michael Feig (Guest Scientist)\*\*\*\*\*

Takao Yoda (Guest Scientist)\*\*\*\*\*

Naoyuki Miyashita (Guest Scientist)\*\*\*\*\*

\* Chief Scientist in RIKEN CPR; Team leader in RIKEN BDR

\*\* Senior Technical Scientist in RIKEN CPR

\*\*\* Special Postdoctoral Fellow in RIKEN CPR

\*\*\*\* The main affiliation is Yokohama City University

\*\*\*\*\* The main affiliation is Michigan State University

\*\*\*\*\* The main affiliation is Nagahama Bio Institute.

\*\*\*\*\* The main affiliation is Kindai University.

### 10.2 Overview of Research Activities

We have developed GENESIS (Generalized-ensemble simulation system) software for high-performance molecular dynamics (MD) simulations of various chemical and biological systems. Using GENESIS, we can carry out MD simulations based on atomistic and coarse-grained molecular models. The atomistic model allows us to include accurate molecular interactions between biomacromolecules, while the available system size and simulation time are limited due to the required computational resources. We therefore consider combining simulations based on the atomistic model with those with coarse-grained models for simulating cellular-scale phenomena on Fugaku supercomputer. Now, in GENESIS, various coarse-grained models, such as AICG2+ for protein, the 3-site-per-nucleotide (3SPN) model for DNA, which were previously developed in CafeMol, a coarse-grained MD simulator.

GENESIS also includes various enhanced conformational sampling methods to explore wider conformational spaces of biomacromolecules. In collaboration with Laboratory for biomolecular function simulation, RIKEN BDR, we added Gaussian accelerated replica-exchange umbrella sampling (GaREUS) method and free-energy perturbation (FEP) calculations in the latest version of GENESIS. These methods will be applicable to in-silico drug discovery.

The performance of GENESIS has been greatly improved in the new non-bonded interaction kernels of the next major release (GENESIS 2.0 or later). This kernel was optimized to the ARM CPU architecture in Fugaku, allowing us to simulate slow conformational dynamics of biomolecules in cellular environments. We also used GENESIS for biological applications, such as Calcium ATPase and Heme transporters in biological membranes.

## 10.3 Research Results and Achievements

### 10.3.1 Development of GENESIS on Fugaku supercomputer

In the last fiscal year, we developed GENESIS MD software to carry out cellular scale molecular dynamics (MD) on Fugaku supercomputer. It includes the optimization of program algorithm and modeling of the system.

#### 10.3.1.1 Optimization of real-space non-bonded interaction

In MD with all atom model, there are bonded and non-bonded interactions. Bonded interactions include those of bond, angle, and dihedral angles. Non-bonded interactions consist of van der Waals and electrostatic interactions. Electrostatic interaction is separated into real- and reciprocal-space interactions. At moderate number of processors, the main bottleneck is the van der Waals and real-space electrostatic interactions. To accelerate the speed on Fugaku, we designed a new algorithm to minimize the operand waiting time. Array of Structure (AoS) and Structure of Array (SoA) types are appropriately assigned to maximize the overall performance. L1 cache prefetch is applied to minimize the memory access time. The new algorithm accelerates the speed on Fugaku more than twice compared to the algorithm used on K computer.

#### 10.3.1.2 Optimization of reciprocal-space interaction

The reciprocal-space electrostatic interaction can be understood by applying fast Fourier transform (FFT). Because FFT requires global communications, it becomes the main bottleneck for very large number of processors. To accelerate the reciprocal-space interaction, we developed new algorithm of charge grid data generation. With the new algorithm, we can reduce the number of operations before/after forward/backward FFTs. It also allows us to reduce the FFT grid points. In addition, we made a tool to decide the best FFT scheme automatically from given number of processors. These developments accelerate the speed of the reciprocal-space interaction more than twice.

#### 10.3.1.3 Optimization of multicopy enhanced sampling scheme on Fugaku

With multicopy enhanced sampling schemes, we prepare many replicas with different working conditions. To optimize the speed with these schemes, the communication among processors in the same replica should be minimized. For this, we defined three-dimensional indices of MPI ranks and replicas, and mapped these indices to multi-dimensional network topology of Fugaku.

#### 10.3.1.4 parallel file input/output for large scale MD simulations

Parallel file input/output (I/O) are used in GENESIS for large scale MD to avoid memory problem in reading and writing files. The original parallel file I/O in GENESIS has the problem that we need to regenerate parallel files whenever working conditions are changed. For example, when MPI processor number is changed, we should rewrite the parallel file by spending at least a few hours. In the newly developed parallel file I/O, we do not need to regenerate parallel files in spite of changed working conditions.

#### 10.3.1.5 modeling of cellular scale system

In living cells, a number of macromolecules such as proteins, nucleic acids, and lipids interact with each other. It is thought that their reactivity and stability are changed by recognizing each other. It is a fundamental issue to understand the mechanism of such processes. However, studying environments which include numerous

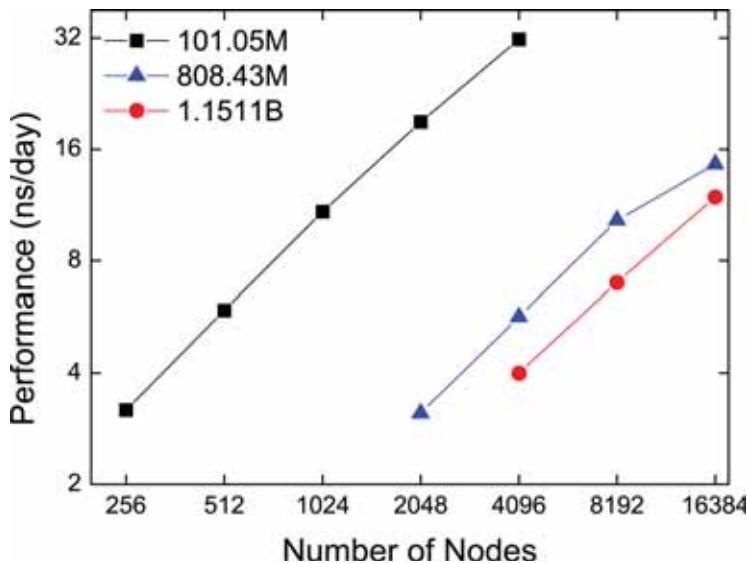


Figure 10.1: Strong scaling result of GENESIS on Fugaku.

macromolecules of different types is very difficult due to the enormous amount of calculation required. We previously developed a multi-scale modeling protocol that starts from coarse-grained (CG) model and increases the resolution step-by-step. This was applied successfully for assembling the first atomistic model of the cytoplasm of a small bacterium, *Mycoplasma genitalium*. We applied a very similar protocol as described previously for assembling proteins, nucleic acids, metabolites, ions, and water in a highly packed cytoplasmic model with much faster speed of equilibrium process. Finally, we could prepare the cytoplasmic systems with  $\sim 100$  million and  $\sim 1.5$  million atoms. This is used for a multi-copy enhanced sampling method on Fugaku.

#### 10.3.1.6 benchmark result on Fugaku

Due to the developments described above, we obtained 31.77 ns/day, 14.59 ns/day, and 11.88 ns/day for 101.05 million atoms (101.05M), 808.43 million atoms (808.43M) and 1.1511 billion atoms (1.1511B) systems (Figure 10.1). When we apply a multi-copy enhanced sampling scheme named the generalized REST (gREST) with 54 replicas, we could obtain 5.37 ns/day and 2.75 PFLOPS.

### 10.3.2 Investigatio of the Reaction Pathway on the E1/E2 transition of $\text{Ca}^{2+}$ -ATPase

Sarco(endo)plasmic reticulum  $\text{Ca}^{2+}$ -ATPase is a representative protein of P-type ATPases, which transports  $\text{Ca}^{2+}$  across membrane against a large concentration gradient (104 times) by utilizing ATP hydrolysis. The protein consists of three cytoplasmic domains and ten transmembrane (TM) helices. According to the E1/E2 theory, it exhibits at least two different states, E1 and E2. Structural and biochemical studies have suggested functional roles of coupled motions between the cytoplasmic domains and the transmembrane helices in the reaction step between the two states. It is, however, difficult to observe the atomistic information of reaction pathway for experimental studies. Therefore, we calculated the reaction pathway on the step and the free-energy profile by using GENESIS (Figure 10.2) We analyzed the conformational changes on the reaction pathway. As a result, we suggest a series of structural changes, domain motions of cytoplasmic domains, and rearrangement of transmembrane helices, and then gating motion.

### 10.3.3 Simulating large-amplitude transitions in proteins with a coarse-grained $\bar{G}\bar{o}$ -model

Molecular dynamics (MD) simulations of biomolecules are widely used to investigate conformational dynamics and structure-function relationship. All-atom (AA) models provide the most accurate description of the underlying dynamics. However at present, even with the fastest computers, the time-scale obtainable with

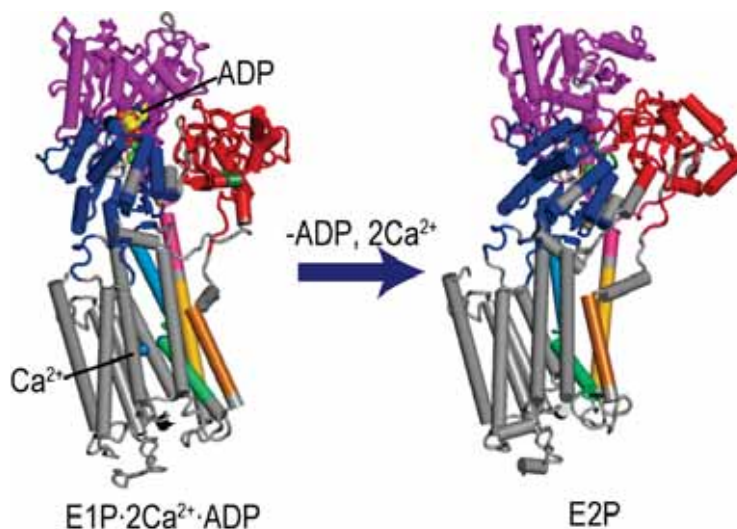


Figure 10.2: Reaction step between E1  $\sim$  P $\bullet$ 2Ca<sup>2+</sup>·ADP (left) and E2P (right) states of Ca<sup>2+</sup>-ATPase.

an atomistic simulation is up to a millisecond, whereas biologically relevant motions occur at the time scale of milliseconds to seconds. To overcome this, coarse-grained (CG) modeling can be utilized. The use of CG models reduces the computational time by several orders of magnitude, allowing access to biologically relevant time-scales.

In the first work (Figure 10.3), we used the dual-basin (DB)  $G\bar{o}$ -model, which is a structural-based CG model, for simulating conformational transitions between two known structures of a protein. The DB potential is formed by mixing two single-basin potentials and includes system-dependent parameters. The determination of parameters however, is usually not straightforward and can be time consuming.

We developed an efficient scheme to determine the mixing parameters using the Multistate Bennett Acceptance Ratio (MBAR) analysis method after short simulations with a set of parameters. In the scheme, MBAR allows us to predict observables at various unsimulated conditions, which are useful to improve the mixing parameters in the next round of iterative simulations. The number of iterations that are necessary for obtaining the converged mixing parameters is significantly reduced in the scheme.

We applied the scheme to several proteins, for showing the effectiveness in parameter determination. After obtaining the converged parameters, the proteins show frequent conformational transitions between open and closed states, providing the theoretical basis to investigate structure dynamics-function relationships of the proteins.

Next, we extended the DB model to a general multi-basin (MB) model for realizing conformational transitions in multi-domain protein with more than two labile domains. For such proteins, the previously developed DB model could not describe the structure of intermediate states because experimental structures are usually not available for them.

In our second work (Figure 10.4), we described intermediate structures by assuming that they have partial inter-domain contacts with respect to both reference structures, i.e. their potential can be described as some combination of the end-states potentials, thus obviating the need for obtaining their experimental structures. In addition, we use the MBAR analysis method for an efficient determination of mixing parameters.

We demonstrated the use of the MB  $G\bar{o}$  (MBGo) potential on the enzyme Adenylate Kinase. We sampled multiple transitions between its open, closed and the intermediate states, and characterized transition pathways and structural ensembles at each basin. We demonstrated that with the MBGo potential, unconstrained time-dependent dynamics can be obtained in a reasonable simulation time. The obtained trajectories can be analyzed in any desired reaction coordinate, serving as a ground for endless possibilities to study structure function relationship in proteins.

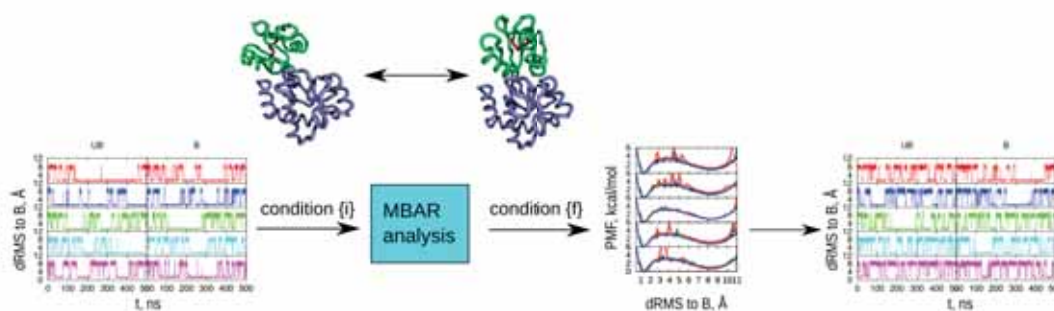


Figure 10.3: Top: Open and Closed conformations of the Glutamine-binding protein. Bottom: overall scheme describing mixing parameter optimization using MBAR analysis.

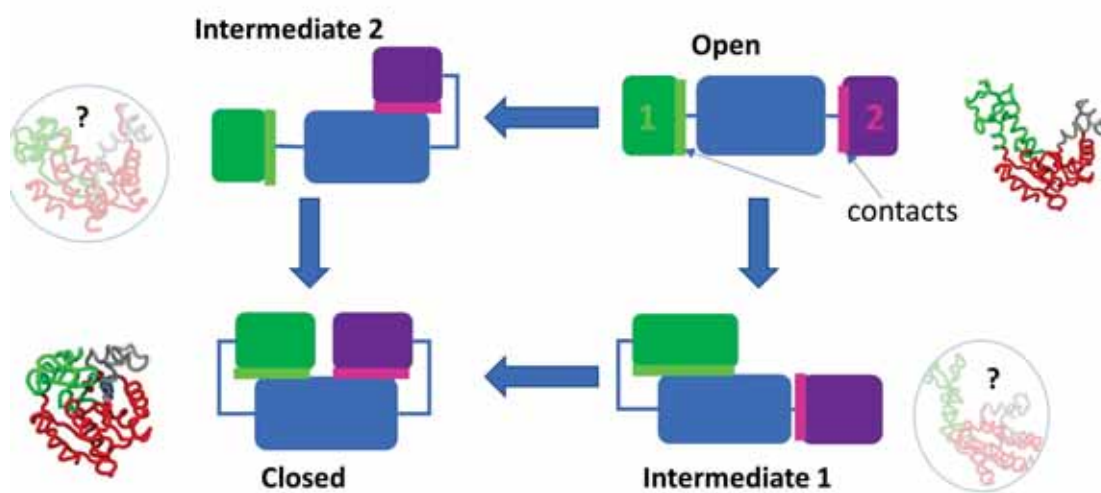


Figure 10.4: Schematic description of the conformational transition pathways of a protein with two labile domains.

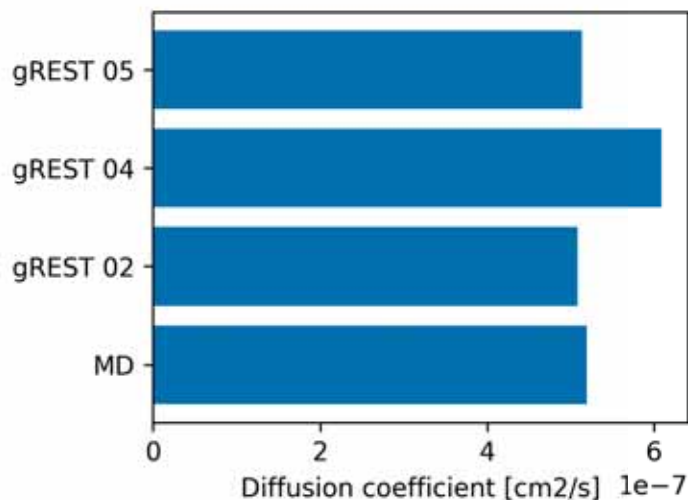


Figure 10.5: Comparison of diffusion coefficient calculated from the gREST and the conventional MD simulations.

### 10.3.4 Theoretical Study of Lateral Diffusion of Heme on Lipid Bilayer

In vertebrate, heme is abundant source of iron for infected bacterial pathogen. Bacteria have elaborated elegant system to acquire free heme from environment. Free heme that escape from the system tend to partition into the cell membrane and disrupt the structure of lipid bilayer. In this study, we aim to analyze the behavior of heme on the membrane. To this end, we adopted the gREST method to enhance lateral diffusion of heme. In the gREST simulation, the effective temperature of the specific part of the system (“solute region”) is increased and therefore can effectively simulate the diffusion process of heme. We considered several conditions for gREST simulation and selected three efficient ones for further sampling ( $\sim 50$  ns/replica). For comparison, we performed five independent conventional MD simulations (300 ns each). Figure 10.5 summarize diffusion coefficients calculated from the trajectories. Although gREST slightly enhanced diffusion, further consideration is obviously necessary to drastically increase its efficiency.

### 10.3.5 Implementation of CG models in GENESIS

One of the long-standing challenges in computational biophysics is to achieve the balance between force-field accuracy and sampling adequacy. Among the multiscale approaches, coarse-grained (CG) models have achieved great success in studying the long time-scale dynamics of large biomolecules. During the last year, we implemented the most popular CG models into GENESIS, to provide the biophysical society a versatile platform for running general purpose MD simulations. Specifically, we focused on the recently developed CG models at the resolution of roughly 10 atoms per bead, which have been shown to work consistently and compatibly with each other. These models include the atomic interaction-based CG model version 2+ (AICG2+) for protein, the 3-site-per-nucleotide (3SPN) model for DNA, and a structure-based model for RNA. In addition, we employed the hydrophobicity scale (HPS) model and the Kim-Hummer (KH) model for the intrinsically disordered regions in protein.<sup>5</sup> As for the inter-molecular interactions between protein and DNA, we considered the Debye-Huckel type electrostatics for the sequence-non-specific binding and the position-weight-matrix-complex-structure (PWMcos) integrated model for the sequence-specific recognition.<sup>6</sup> We have implemented and tested all the above-mentioned models in GENESIS.

After the implementation of the interactions, we determined a unified set of parameters such as cut-off values for short-ranged and long-ranged interactions, respectively. We also developed cell-linked list method for utilizing the pair-list method for each interaction term. Via these developments, the CG models in GENESIS are now ready for use.

### 10.3.6 Development of a singularity-free dihedral angle potential in CG

The classical dihedral angle potential has a singularity problem when three adjoining particles are colinearly aligned. The CG MD simulations are more susceptible to this problem. By introducing a modulating function as a multiplier and found suitable parameters based on statistics, we solved the singularity problem and combined the new potential with existing CG models seamlessly. By apply our new potential in the simulations of designed and real biomolecules, we showed that our method was not only computationally efficient, but also robust in practical numerical calculations.

## 10.4 Schedule and Future Plan

In the next fiscal year, we plan to design a better parallelization scheme of coarse-grained MD for cell-scale systems with large number of particles. We also consider further optimization to gain better performance on the Fugaku. As applications, we will use the current models to study the phase behaviors of biomolecules in physiological processes such as genome organization and gene expression.

## 10.5 Publications

### 10.5.1 Articles/Journal

- [1] Jung, J., Nishima, W., Daniels, M., Bascom, G., Kobayashi, C., Adedoyin, A., Wall, M., Lappala, A., Phillips, D., Fischer, W., Tung, C., Schlick, T., Sugita, Y. and Sanbonmatsu, K.Y., Scaling Molecular Dynamics beyond 100,000 Processor Cores for Large-Scale Biophysical Simulations, *Journal of Computational Chemistry*, vol. 40, 1919–1930 (2019)
- [2] Tamura, K., Sugitamoto, H., Shiro, Y. and Sugita, Y., Hemo-mechanical coupling in the transport cycle of a heme ABC transporter, *The Journal of Physical Chemistry B*, vol. 123, 7270–7281 (2019).
- [3] Shinobu, A., Kobayashi, C., Matsunaga, Y. and Sugita, Y., Building a macro-mixing dual-basin Gō model using the multistate bennett acceptance ratio, *Biophysics and Physicobiology*, vol. 16, 310–321 (2019).
- [4] Oshima, H., Re, S. and Sugita, Y., Replica-Exchange Umbrella Sampling Combined with Gaussian Accelerated Molecular Dynamics for Free-energy Calculation of Biomolecules, *Journal of Chemical Theory and Computation*, vol. 15, 5199–5208 (2019).
- [5] Matsunaga, Y. and Sugita, Y., Use of single-molecule time-series data for refining conformational dynamics in molecular simulations, *Current Opinon in Structural Biology*, vol. 61, 153–159 (2020).
- [6] Takada, S., Brandani, G. B. and Tan, C., Nucleosomes as allosteric scaffolds for genetic regulation. *Current Opinion in Structural Biology*, vol. 6, 93–101 (2020).
- [7] Tamura, K. and Sugita, Y., Free Energy Analysis of a Conformational Change of Heme ABC Transporter BhuUV-T, *Journal of Physical Chemistry Letter*, vol. 11, 2824–2829 (2020).

### 10.5.2 Posters

- [8] Shinobu, A., Simulating large-amplitude transitions in proteins with a coarse-grained model. Joint Annual Meeting of the 71st Japan Society for Cell Biology and 19th Protein Science Society of Japan, Kobe, Jun., 2019.
- [9] Jung, J., Oshima, H., Kasahara, K., Kobayashi, C., Mori, T. and Sugita, Y., A new MD integration enabling large time step from accurate temperature and pressure evaluations, The 57th Annual Meeting of The Biophysical Society of Japan, Miyazaki, Sep. 2019.
- [10] Shinobu, A., Simulating large-amplitude transitions in proteins with a coarse-grained model, The 57th Annual Meeting of the Biophysical Society of Japan, Miyazaki, Sep. 2019.
- [11] Tamura, K. and Sugita, Y., Free energy analysis of the conformational changes of a heme ABC importer BhuUV-T, The 57th Annual Meeting of The Biophysical Society of Japan, Miyazaki, Sep. 2019.
- [12] Kobayashi, C., Elucidation of a mechanism of ion transport in membrane transport protein, The 6th project report meeting of the HPCI system including K computer, Tokyo, Nov. 2019.
- [13] Tamura, K. and Sugita, Y., Free energy analysis of the conformational changes of a heme ABC transporter BhuUV-T, The 5th International Conference on Molecular Simulation (ICMS2019), Jeju, Korea, Nov. 2019.
- [14] Sugita, Y., Mori, T., Yagi, K., Oshima, H., Jung, J., Kobayashi, C. and Matsunaga, Y., Development of Molecular Dynamics Software, GENESIS 1.4 for Large Biological Systems, The 64th Biophysical Society Annual Meeting, San Diego, USA. Feb. 2020

### 10.5.3 Invited Talks

- [15] Sugita, Y., Machine Learning approach to link single-molecule FRET and MD simulations for understanding protein folding dynamics, Peking University Seminar, Beijing, China, May. 2019.
- [16] Tamura, K. and Hayashi, S., Atomistically deciphering alternation access mechanism of the mitochondrial ADP/ATP carrier with molecular simulations, The 2nd Tokyo ATPase Workshop, Tokyo, Sep. 2019.
- [17] Sugita, Y., Machine learning approach to link MD simulation with single-molecule experiment for understanding protein folding and dynamics, The Fifth Korean-Polish Conference on “Protein Folding: Theoretical and Experimental Approaches”, Seoul, Korea, Sep. 2019.
- [18] Sugita, Y., Enhanced Conformational Sampling Methods for Free Energy Calculation, CHARMM-GUI KIAS School, Seoul, Korea, Sep. 2019.
- [19] Sugita, Y., Free-Energy Calculations of Protein-Ligand Binding using GENESIS software, The 5th International Conference on Molecular Simulation (ICMS2019), Jeju, Korea, Nov. 2019.
- [20] Jung, J. and Sugita, Y., Optimal temperature and pressure evaluations for an MD integration with a large time step, The 5th International Conference on Molecular Simulation (ICMS2019), Jeju, Korea, Nov. 2019.
- [21] Sugita, Y., Free-energy landscapes of protein-ligand bindings along the positional and orientational ligand coordinates, Warsaw University CeNT Seminar, Warsaw, Poland, Nov. 2019.
- [22] Sugita, Y., Pushing forward the limit of molecular dynamics simulation by the development of GENESIS, ENS Seminar, Paris, France, Nov. 2019.
- [23] Sugita, Y., Development of GENESIS software for molecular simulations in cellular environments, Sorbonne University Seminar, Paris, France, Nov. 2019.
- [24] Tamura, K., Comprehensive analysis of a heme acquisition process by a heme transporter, The 6th project report meeting of the HPCI system including K computer, Tokyo, Nov. 2019.
- [25] Kobayashi, C., Development of Molecular Dynamics Software, 11th Symposium on Automatic Tuning Technology and its Application, Tokyo, Dec. 2019.

### 10.5.4 Oral Talks

- [26] Jung, J., Kobayashi, C., and Sugita, Y., The billion-atom simulation in biology with GENESIS on Intel Xeon Phi (KNL), The 33th Molecular Simulation conference, Nagoya, Dec. 2019
- [27] Shinobu, A., Building a macro-mixing Dual-basin Gō model using the Multistate Bennett Acceptance Ratio, The 64th Biophysical Society Annual Meeting, San Diego, USA. Feb. 2020

### 10.5.5 Software

- [28] Molecular dynamics and modeling software GENESIS, <https://www.r-ccs.riken.jp/labs/cbrt> (version 1.4)

### 10.5.6 Patents

# Chapter 11

## Particle Simulator Research Team

### 11.1 Members

Junichiro Makino (Team Leader)

Masaki Iwasawa (Research Scientist)

Daisuke Namekata (Postdoctoral Researcher)

Miyuki Tsubouchi (Technical Staff)

### 11.2 Overview of Research Activities

We are developing particle-based simulation software that can be used to solve problems of vastly different scales.

Simulation schemes for hydrodynamics and structural analysis can be divided into grid-based and particle-based methods. In grid-based methods, the computational region is mapped to regular or irregular grids. Continuous distributions of physical values are represented by discrete values at grid points, and the governing partial differential equation is approximated to a set of finite difference equations.

In the case of the particle-based methods, physical values are assigned to particles, while the partial differential equation is approximated by the interactions between particles.

Both methods are widely used, and they have their advantages and disadvantages. The computational cost of grid-based schemes is generally lower than that of particle-based methods with similar number of freedoms. Thus, if a near-uniform grid structure is appropriate for the problem to be solved, grid-based methods perform better.

The advantage of the particle-based methods comes from the fact that they use "Lagrangian" schemes, in which the particles move following the motion of the fluid in the case of the CFD calculation. In the case of grid-based methods, we generally use "Eulerian" schemes, in which the grid points do not move.

There are three points in which the Lagrangian schemes are better than Eulerian schemes. One is that the Lagrangian schemes are, to some extent, adaptive to the requirement of the accuracy, since when a low-density region is compressed to become high density, Second one is that the timestep criteria are quite different. In the case of the Lagrangian schemes, the timestep is determined basically by local sound velocity, while in the Eulerian scheme by global velocity. Thus, if a relatively cold fluid is moving very fast, the timestep for the Eulerian schemes can be many orders of magnitude shorter than that for Lagrangian schemes. Finally, in the case of fast-moving low-temperature fluid, the required accuracy would be very high for Eulerian scheme, since the error comes from the high velocity, while that error would be transferred to internal energy of the fluid element which is much smaller than that of the kinetic motion.

Of course, there are disadvantages of Lagrangian schemes. The primary one is the difficulty of construction of such schemes in two or higher dimensions. In the case of one-dimensional calculation, it is easy to move grid points following the motion of the fluid, but in two or higher dimensions, the grid structure would severely deform if we let the grid points follow the flow. Thus, we have to reconstruct the grid structure every so often. This requirement causes the program to become complex. Moreover, reconstruction of the grid structure (so called remeshing) means we lose numerical accuracy.

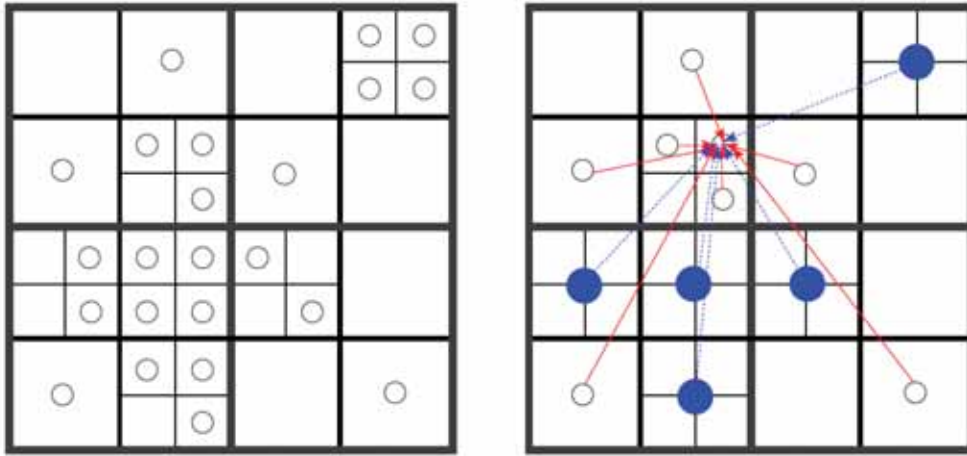


Figure 11.1: Basic idea of tree algorithm

Particle-based methods "solve" this difficulty by not requiring any mesh. In particle-based methods, particles interact with its neighboring particles, not through some connection through grid, but through distance-dependent kernel functions. Thus, there is no need of remeshing. As a result, particle-based schemes are simple to implement, and can give reasonable results even when the deformation is very large. Another important advantage is that it is relatively easy to achieve high efficiency with large-scale particle-based simulation.

In the case of grid-based schemes, in order achieve some adaptivity to the solution, we have to use either irregular grid or regular grid with adaptive mesh refinement. In both cases, adaptivity breaks the regularity of the mesh structure, resulting in non-contiguous access to the main memory. In the case of the particle-based schemes, it does require some irregular memory access, but it is relatively straightforward to make good use of spacial locality, and thereby achieving high efficiency. Similarly, very high parallel performance can be achieved.

However, it has its own problems. In the case of the SPH method, it has been known that the standard scheme cannot handle the contact discontinuity well. It also require rather strong artificial viscosity, which results in very low effective Reynolds number.

Thus, in many fields of computational sciences, many groups are working on implementation of high-performance particle-based simulation codes for their specific problem.

One serious problem here is that, high-performance, highly-parallel simulation codes for particle-based simulations are becoming more and more complex, in order to make full use of modern supercomputers. We need to distribute particles to many computing nodes in an appropriate way, so that the communication between nodes is minimized and at the same time near-optimal load balance is achieved. Within each nodes, we need to write an efficient code to find neighbor particles, rearrange data structure so that we can make good use of the locality, make good use of multiple cores and SIMD units within each core.

Even for the case of very simple particle-particle interaction such as the Lenard-Jones potential or Coulomb potential, the calculation code tends to be very large, and since the large fraction of the code is written to achieve a high efficiency on a specific architecture, it becomes very hard to port a code which is highly optimized to one architecture to another architecture.

Our goal is to develop a "universal" software that can be applied to a variety of problems whose scales are vastly different. In designing such universal software, it is important to ensure that it runs efficiently on highly parallel computers such as the K computer. Achieving a good load balance for particle-based simulations is a difficult task, since using a regular spatial decomposition method causes severe load imbalance, though this works well for grid-based software. Consequently, we have developed an adaptive decomposition method that is designed to work in a way that the calculation time on each node is almost the same, resulting in the near-optimal load balance.

The strategy to develop such a universal software is as follows.

We first construct an highly parallel and very efficient implementation of the TreePM algorithm for gravitational N-body problem. This is actually not a completely new implementation, but the GreeM code developed by researchers of the Strategic Program for Innovative Research (SPIRE) Field 5 "The origin of matter and the universe. In collaboration with the Field 5 researchers, we improve the efficiency of the code and study the

issues of the data structure, domain decomposition, load balance strategy etc.

In the second stage, we will develop a prototype of the parallel particle simulation platform. We will design the platform so that it can be used for multiple physical systems. In practice, we consider the following three applications as the initial targets.

1. Gravitational N-body simulation
2. Smoothed Particle Hydrodynamics
3. Molecular Dynamics

In the meantime, we will also investigate the way to improve the performance and accuracy of the current particle-based algorithms for hydrodynamics.

## 11.3 Research Results and Achievements

### 11.3.1 High-performance gravitational N-body solver.

We use the TreePM algorithm as the basic method for the evaluation of gravitational interaction between particles. TreePM is a combination of the tree method and the P<sup>3</sup>M (particle-particle particle-mesh) scheme. Figure 1 shows the basic idea of the tree algorithm. The space is divided into a hierarchical octree structure (quadtrees in the figure). Division is stopped when a cell contains one or no particle. When we calculate the force on a particle, we evaluate the force from a group of particles, with size larger for more distant particles. In this way, we can reduce the calculation cost from  $O(N^2)$  to  $O(N \log N)$ .

The tree algorithm is widely used, but when the periodic boundary condition is applied, we can actually use a more efficient scheme, since we can calculate the long-range, periodic term using FFT. The P<sup>3</sup>M scheme has been used for such problem, but it has the serious problem that when the density contrast becomes high, the calculation cost increases very quickly. The TreePM scheme solves this difficulty by using the tree algorithm to evaluate the forces from nearby particles. Even when there are very large number of neighbor particles, the calculation cost does not increase much, since the calculation cost of the neighbor force is proportional to the logarithm of the number of neighbors.

In order to map the problem to the distributed-memory parallel computer such as the K computer, we adopted the approach to divide the space into domains and assign particles in one domain to one calculation node. We used the orthogonal recursive multisection method developed by the team leader some years ago. It is the generalization of the orthogonal recursive bisection (ORB), which has been widely used in many parallel implementations of the tree algorithm.

With ORB, we recursively divide space into two halves, each with the same number of particles. An obvious disadvantage of the ORB approach is that it can utilize the computing nodes of integral powers of two. Thus, in the worst case we can use only half of the available nodes.

The difference between the multisection method and the ORB is that with the multisection method we allow the divisions to arbitrary number of domains, instead of bisection. This would allow too many possible divisions. In our current implementation, we limit the number of levels to three, and make the numbers of divisions at all levels as close as possible. Thus, our domain decomposition is topologically a simple three-dimension grid. This fact makes the multisection method well suited to the machines with the 3D torus network like the K computer.

We have developed a "reference code" for gravitational N-body simulation on the K computer. This code is fairly well optimized for the K computer, and shows quite good scalability for even for relatively small-size problems. The asymptotic speed per timestep for large number of nodes is around 7ms. This speed is comparable to that of highly optimized molecular dynamics codes on K, even though our code is designed to handle highly inhomogeneous systems.

We used this code as the reference implementation for more generalized particle simulation platform which will be described in the next subsection.

### 11.3.2 Particle Simulation Platform.

In FY 2014, We have completed and released Version 1.0 of the particle simulation platform, which we call FDPS (Framework for Developing Particle Simulator). In FY 2015, we have applied a number of improvements to FDPS.

The basic idea of FDPS is that the application developer (or the user) specified the way the particles interact with each other, and the rest is taken care by FDPS. Here, "the rest" includes domain decomposition and re-distribution of particles, evaluation of interactions between particles, including those in different domains (different MPI processes, for example).

In practice, there are many additional details the user should give. Consider a relatively simple case of particles interacting with softened  $1/r$  potential. There are a number of small but important points one has to decide on. For example, what algorithm should be used for the interaction calculation? Even if we limit the possibilities to reasonably adaptive schemes for open boundary problems, we have the choice between Barnes-Hut tree and FMM. For both algorithms, there are many different ways to parallelize them on distributed-memory parallel computers. Also, there are infinitely many variations for the time integration schemes.

The base layer of FDPS offers the domain decomposition based on the recursive multisection algorithm, with arbitrary weighting function for the load balancing. It also offers the parallel implementation of interaction calculation between particles.

The domain decomposition part takes the array of particles on each node as the main argument. It then generates an appropriate domain for each node, redistribute particles according to their locations, and returns.

The interaction calculation part takes the array of particles, the domain decomposition structure, and the specification of the interaction between particles as main arguments. The actual implementation of this part need to take into account a number of details. For example, the interaction can be of long-range nature, such as gravity, Coulomb force, and interaction between computational elements in the boundary element method (BEM). In this case, the user should also provide the way to construct approximations such as the multipole expansion and the way to estimate error. The interaction might be of short-range nature, with either particle-dependent or independent cutoff length. In these cases, the interaction calculation part should be reasonably efficient in finding neighbor particles.

We have successfully implemented all of these functionalities in FDPS version 1.0. (<https://github.com/FDPS/FDPS>). Using FDPS, a gravitational N-body simulation code can be written in 120 lines, and that code is actually fully scalable even to full-node runs on K computer. For SPH calculations, we have also achieved similar scaling.

FDPS is implemented as a class template library in C++ language. It receives the class definition of particles and a function (or multiple functions in the case of complex interactions) to evaluate the interaction between particles. When a user program is compiled with the FDPS library, the class template is instantiated with the user-specified definition of the particle class. Thus, even though the FDPS library functions are generic ones not specialized to a particular definition of particles, it behaves as if it is a specialized one.

The measured performance of applications developed using FDPS is quite good. Both for gravity-only calculation and SPH calculation, weak-scaling performance is practically perfect, up to the full-node configuration of K computer. Moreover, the measured efficiency, in terms of the fraction of the peak floating-point performance, is also very high. It is around 50% for gravity-only calculation. For SPH calculations, at the time of writing the performance is around 10%.

In FY 2015, we have extended FDPS in several important directions. The first one is the improvement of the strong scaling. The algorithm used for the domain decomposition contains one serial bottleneck. The "sampling" algorithm used in FDPS 1.0 works well only when the average number of particles per MPI process is significantly larger than the total number of MPI processes. We developed a new parallel algorithm, in which  $O(p^{1/3})$  MPI processes are used to decompose the computational domain. Here  $p$  is the total number of MPI processes. Thus now the requirement for the number of particle is relaxed from larger than  $p$  to larger than  $p^{2/3}$ . Now we can achieve pretty good performance for around 1 billion particles, on the full nodes of K computer. Previously we need near 100 billion particle to achieve good efficiency.

The second one is the addition of new interface method to interaction calculation function, which allows efficient use of accelerator hardware such as GPGPU or Intel MIC. In order to achieve high performance on accelerators, it is important to pass a large chunk of work at one time. In order to achieve this goal, in the current version of FDPS the CPU creates the list of multiple interaction lists, and send all of them at once so that the overhead of the initialization of the accelerator would not become a bottleneck. This interface has been tested on NVIDIA GPGPUs as well as the PEZY-SC processor.

In FY 2016, we have released FDPS 3.0. The most important new feature of this release is the interface to application programs written in Fortran. FDPS itself is implemented using C++. The reason why we adopted C++ is to use its "template" functions. Using templates, we can write library functions which accept user-defined data types as template arguments. This means we can effectively generate "specialized" libraries for user-specified particle data types, without knowing the data types beforehand.

In FY 2017, we have released several new versions of FDPS, up to 4.0a. There are a number of improvements, mostly for improved performance, For example, we have implemented the reuse of the interaction list. In the

case of the calculation of short-range interactions, the neighbor-list method or so-called bookkeeping method has been used in many applications. On the other hand, to our knowledge, such a method has not been applied to Barnes-Hut treecode or FMM. There is no fundamental difficulty in combining the two methods, and the reason why such a combination has not tried before is probably it was not really necessary. The calculation cost of constructing the tree structure and traversing the tree to construct the interaction lists is, in the case of Barnes-Hut algorithm, a small fraction of the total calculation cost. Thus, it is usually unnecessary to try to reduce the cost of the tree construction and tree traversal.

However, some of recent high-performance computers have rather extreme ratios in various aspects, and thus require the performance improvements which were not necessary. One example is the Sunway SW26010. Its architecture is rather extreme in two aspects. First, its “core group” consists of one MPE (management processing element) and 64 CPEs (computing processing elements). MPE has data cache and runs the primary thread, and CPEs do not have cache. Thus, it is difficult and very time-consuming to develop the program which runs on CPEs, in particular for complex operations like tree construction. On the other hand, MPE is very slow compared to CPE, and thus we need to minimize the computational work of MPE.

Another aspect is the rather low memory bandwidth. The B/F number of SW26010 is around 0.03, which is around 1/15 of that of K computer. Thus, in order to achieve reasonable performance on SW26010, we need to minimize the main memory access per timestep.

The reuse of the interaction list turned out to be very effective on SW26010 and other machines with relatively low memory bandwidth, such as NVIDIA P100/V100 and PEZY-SC2.

In FY 2018, we have improved the API of FDPS and also worked on further performance improvement. Concerning the improvement of API, we added the API in the C language in FDPS 5.0. Before 5.0, user programs should be written either C++ or Fortran. Although these two languages cover a fair fraction of the needs of HPC users, it is clearly desirable to have API in C language, since that would allow users to write programs not only in C languages but also in any other languages with FFI (foreign function interface), since FFI is usually defined in C. The C language API works much in the same way as Fortran API.

In FY 2019, we have worked mainly on new functionalities for FDPS. The first one is the support of PM<sup>3</sup> (Particle-Mesh Multipole) method. As its name suggests, PM<sup>3</sup> method is a combination of Particle-Mesh method and Fast Multipole method. In the Particle-Mesh method, long-range and short-range interactions are separated using smooth splitting function, and the long-range interaction is calculated using FFT. In the case of PM<sup>3</sup> method, long-range interaction is defined as the interactions calculated using the tree higher than a certain level in FMM. Then, instead of using hierarchical FMM method, the long-range interaction is obtained as the convolution of the multipole expansions and Green’s function, and then FFT is used to evaluate convolution. Compared to the traditional particle-mesh (or even particle-mesh Ewald) method, PM<sup>3</sup> method can achieve much higher accuracy with significantly smaller amount of communication, and thus suited to large-scale parallel machines with relative weak network. We also worked on the optimization of FDPS on Fugaku. Compared to K, Fugaku has relatively weak network and CPU core with large latency for arithmetic operations. Thus, bottlenecks appear in several unexpected places. We have implemented various new algorithms to remove these bottlenecks.

## 11.4 Schedule and Future Plan

We plan to improve the performance of FDPS further in FY 2020. The main issue will be the performance tuning on Fugaku supercomputer. Other issues include the automatic generation of high-performance computing kernel for particle-particle interactions.

## 11.5 Publications

### 11.5.1 Articles/Journal

- [1] Iwasawa, M., D. Namekata, K. Nitadori, K. Nomura, L. Wang, M. Tsubouchi, and J. Makino, *Accelerated FDPS: Algorithms to use accelerators with FDPS*, Publications of the Astronomical Society of Japan, 2020, **72**,.
- [2] Ebisuzaki, T., H. Katori, J. Makino, A. Noda, H. Shinkai, and T. Tamagawa, *INO: Interplanetary network of optical lattice clocks*, International Journal of Modern Physics D, 2019, **29**,.
- [3] Hirai, Y., S. Wanajo, and T. R. Saitoh, *Enrichment of Strontium in Dwarf Galaxies*, The Astrophysical Journal, 2019, **885**,.

[4] Hirai, Y., T. R. Saitoh, S. Wanajo, and M. S. Fujii, *Enrichment of Heavy Elements in Chemo-Dynamical Simulations of Dwarf Galaxies*, *Dwarf Galaxies: From the Deep Universe to the Present*, 2019, **344**, 197-200.

### 11.5.2 Software

[5] FDPS [github.com/FDPS](https://github.com/FDPS)

[6] Formura [github.com/Formura](https://github.com/Formura)

### 11.5.3 Patents

## Chapter 12

# Computational Climate Science Research Team

### 12.1 Members

Hirofumi Tomita (Team Leader)  
Yoshiyuki Kajikawa (Senior Research Scientist)  
Seiya Nishizawa (Research Scientist)  
Sachiho Adachi (Research Scientist)  
Tsuyoshi Yamaura (Research Scientist)  
Kenta Sueki (Postdoctoral Researcher)  
Toshiki Matsushima (Postdoctoral Researcher)  
Yuta Kawai (Postdoctoral Researcher)  
Tomoro Yanase (Junior Research Associate)  
Hiroaki Miura (Guest Researcher)  
Yoshiaki Miyamoto (Guest Researcher)  
Yousuke Sato (Guest Researcher)  
Shinichiro Shima (Guest Researcher)  
Kazuyoshi Kikuchi (Guest Researcher)  
Ryuji Yoshida (Guest Researcher)

### 12.2 Overview of Research Activities

The primary aim of Computational Climate Science Research Team is to indicate a direction of future climate modeling with a reliable suggestion for the age of high-performance computers. For this purpose, we intend to construct a basic library, in which model components and their numerical method are inter-exchangeable among multiple models. This work contributes directly to the climate modeling community for the enhancement of fast output/outcome creation. Using the library, we also develop a more advanced climate model with new techniques that is necessary for efficient climate simulation. We promote to develop them, considering the following issues; the readability of code, its convenience for users, and traceability of computational results. The second aim is to pursue the high efficiency of the climate model in massively parallel computers. Computational meteorology and climatology always require large-scale numerical experiments. However, it is recently pointed out that

conventional computer architecture with the straightforward extension of existing simulation codes would be a limitation in getting a higher performance. From the viewpoint of hardware and climate modeling, we consider the numerical method, algorithm, and their implementation to large-scale computers, cooperating with research teams of computational and computer sciences in R-CCS. The third aim is to apply our model to address the meteorological/climatological problems, collaborating with outside research institutes. Climate studies are widely spread from the basic understanding of phenomena to assessment of the environment. The former is more scientific and the latter is more practical for the requirement of the society. Several issues we currently focus on are as follows; feedback mechanism between cloud, aerosol, and radiation, theory for the moist process linked to the turbulence process, comprehensive understanding of our earth's particularity by investigation other planets, and so on. The assessment of future environmental change for disaster prevention at the regional scale level is also one of our targets. In this fiscal year, we improved the basic library for more reliable simulation results. We also evaluated characteristics of moist convections in high-resolution simulations, especially their dependence on simulation resolution.

## 12.3 Research Results and Achievements

### 12.3.1 Research and development of SCALE

SCALE (Scalable Computing for Advanced Library and Environment) is a basic library for numerical atmospheric calculations. For the next generation atmospheric simulations, we have been evaluating existing schemes and developing new schemes for higher resolution simulation. In this year, we have improved several components to improve the reproducibility of simulations, including the planetary boundary layer turbulent model, cumulus parameterization, ocean model, and land model. Three target phenomena were selected: the total amount of precipitation in the 2018 heavy rainfall event around Hiroshima, the climatological distribution of precipitation in the summer Asian region, and extratropical cyclone in the 1966 heavy rainfall event around Kobe. Several sensitivity simulations of model components and simulation configurations were performed to optimize them.

### 12.3.2 The Hyogo-Kobe COE establishment project

We continued to drive the subject "Computational Research on Estimation to Complex Disaster Risk for Better Urban Planning" in Hyogo-Kobe COE establishment project started in FY2018. In this year, we conducted the study of the rainfall system during the recent catastrophic heavy rainfall event in western Japan in July 2018 and attempted to build the framework of the urban model in our SCALE library.

During the heavy rainfall event in July 2018, it is found that the number of sediment disasters in the Hiroshima area was larger than that in Keihanshin area including Hyogo-Kobe although the rainfall amount did not show a significant difference over these two areas. In order to figure out the possible reasons for the difference, we examined the characteristics of rainfall systems striking above two areas based on the radar observations with a special focus on the size of the rainfall system. We found that significantly large rainfall systems with areas equal to or larger than 104 km<sup>2</sup> were dominant in the Hiroshima area, inducing rapid accumulation of the rainfall amount. Eventually, it enhanced the risk of deadly sediment disasters. In contrast, the relatively small rainfall system with moderate intensity was found to be dominant in the Keihanshin area. We suggested that the difference in the damage between the two areas was anchored by the size difference of the rainfall system. A high vertical wind shear environment was also suggested to be a preferable condition for the large rainfall system formation (Sueki and Kajikawa, 2019).

We also built the framework of the urban model to advance our climate model (SCALE library) by reducing the model uncertainty. We improved the model to give the roughness lengths for momentum and heat and artificial heat in each grid point; the model can describe the inhomogeneous heating in the urban area. In the case we set the parameters based on the observation instead of the default value we have used in previous, wind speed and temperature in the urban area tend to be suppressed.

### 12.3.3 Numerical convergence for simulation of atmospheric deep moist convection

Deep convective clouds are responsible for thermal convection with moist processes in the atmosphere and impact the Earth's climate significantly. However, their representation in climate models is imperfect, causing great uncertainty in climate prediction. Convective clouds often form self-organized systems with spatially hierarchical

structures, such as super cloud clusters associated with Madden–Julian oscillations. This self-organization of convective clouds makes it difficult to assess their impact on the climate. High-resolution simulations that correctly reproduce organized cloud systems are necessary to understand the role of deep moist convection in the Earth’s climate system. However, the numerical convergence for simulation of organized cloud systems remains debatable. To investigate the model resolution necessary for a reasonable simulation of deep moist convection, we conducted grid-refinement experiments using the SCALE-RM on the K computer. Figure 12.1 shows horizontal grid-spacing dependence of the statistics of convective updrafts in an organized cloud system. We found that both the number of updrafts (Figure 12.1a) and the mean distance between two adjacent updrafts (Figure 12.1b) converge at progressively smaller scales as the grid spacing is reduced. The gap between two adjacent updrafts converges to a particular distance when the grid spacing becomes as small as 1/20–1/40 of the updraft effective radius. We also found that the converged inter-updraft distance value is not significantly different between Reynolds-averaged Navier–Stokes simulations (dashed line in Figure 12.1) and large eddy simulations (solid line in Figure 12.1) for grid spacings in the terra incognita range.

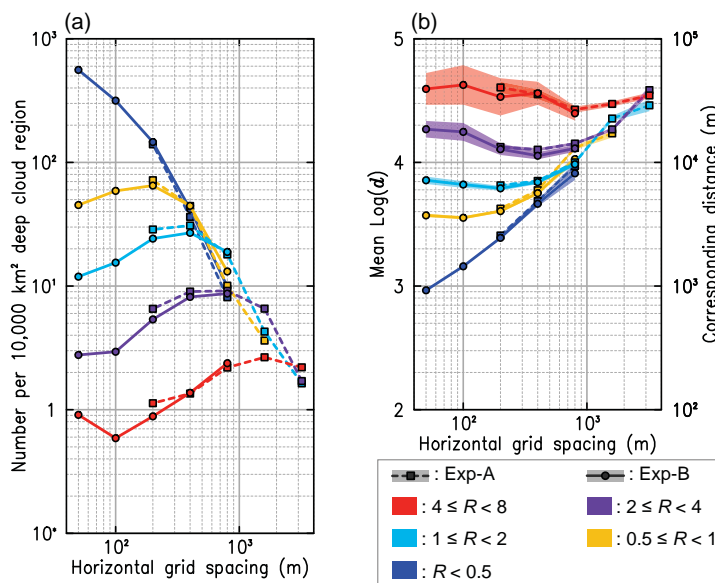


Figure 12.1: Horizontal grid-spacing dependence of the statistics of convective updrafts in an organized cloud system. (a) Number of updrafts per 10,000 km<sup>2</sup> deep cloud region. (b) Mean value of the logarithm of the distance,  $d$ , between two adjacent updrafts, denoted by mean  $\text{Log}(d)$ . The dashed and solid lines indicate the results of Reynolds-averaged Navier–Stokes simulations (Exp-A) and large eddy simulation (Exp-B), respectively. Different colors indicate different size classifications: Each updraft is classified by its effective radius,  $R$  (unit: km), which is defined as the square root of area  $S$  divided by  $\pi$ :  $R \equiv (S/\pi)^{1/2}$ . In (b), a confidence interval of 99% for mean  $\text{Log}(d)$  is indicated by the translucent color. (Figure 4 in Sueki et al. 2019, *Geophysical Research Letters*)

### 12.3.4 Self-organization of moist convection in the idealized radiative-convective equilibrium simulation

Atmospheric moist convection plays significant roles in the earth’s weather and climate system: it not only causes clouds and precipitation at a local scale but also organizes into a hierarchical structure extending to a global scale. Despite its importance being widely recognized, the representation of cloud-related processes is still insufficient and brings large uncertainties in climate model simulations. Recently, toward deepening basic understanding of the role of clouds, a numerical simulation framework of idealized climate, called radiative-convective equilibrium (RCE), is spotlighted in the climate modeling community. In the RCE simulation, it is known that moist convection can be organized into an aggregated cloud system even under a uniform boundary condition; that process is called convective self-aggregation (CSA) and is recognized as a key for the relationship of clouds and climate. Previous studies have shown that the CSA occurred if the simulation domain was larger than 200–300 km to a horizontal extent, which suggests the existence of critical length for the CSA onset. On

the other hand, the CSA onset also depends on the simulation resolution; only in the low-resolution simulation CSA have been found to spontaneously occur.

In this fiscal year, to investigate the characteristic length of CSA onset, we conducted systematic cloud-resolving simulations, with a scope covering the horizontal domain size and resolution, by using SCALE on the supercomputers including the K-computer. As a result, we updated an RCE regime diagram compared to Muller and Held (2012, MH12), as shown in Fig. 12.2. The main conclusions are summarized as follows: (1) CSA is unlikely to occur with a high resolution or small domain (the lines II and III, and MH12 reference line). (2) CSA occurs in sub-kilometer high-resolution cloud-resolving simulations with domain sizes larger than 500 km (line I).

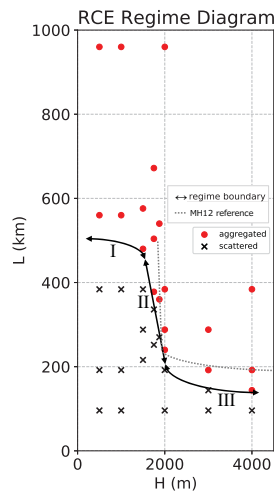


Figure 12.2: RCE regime diagram in a parameter space of horizontal domain size ( $L$  in kilometer) and grid spacing ( $H$  in meter). Red circles (black crosses) indicate aggregated (scattered) regime. (Figure 2b in Yanase et al. 2020 *Geophysical Research Letters*)

## 12.4 Schedule and Future Plan

The basic library SCALE is being advanced. At the moment, major processes such as dynamics and physics have already been comprehensively developed. In the future, we will pursue ease of use for external users. The advanced climate models based on the schemes continue to be improved in principle and provide a direction for future climate models. The key to advancement is the sub-grid scale models. A more accurate representation of cloud physics requires a turbulence model that takes into account moist processes. The combination of a turbulence-aware LES and Super Droplet Method (SDM) for cloud microphysics will be a useful tool for solving this issue. As well as developing accurate schemes for high-resolution simulations, there is also a need to improve parameterizations for coarser-resolution simulations. Data science techniques are useful for this purpose, including optimization of model parameters in the parameterizations and development of AI-based parameterization generated using a high-resolution simulation database.

One of our primary missions is to provide tools for the analysis of simulation results as well as improve the computational and physical performance of simulations. This is critical for accelerating scientific and social outcomes. Specifically, we will parallelize major analysis programs and make them suitable for massively parallel computer systems. In addition, we will continuously develop a short- and medium-range numerical weather forecasting system in collaboration with Data Assimilation Research Team. LETKF is an important application for data assimilation. Combining our models with LETKF, which combines high-resolution and large-scale ensemble simulations and observational big data, will enable us to take a new stage in numerical weather forecasting, especially for sudden and heavy rainfall. This has already begun as an applied research project under the AIP project and Program for Promoting Researches on the Supercomputer Fugaku (Issue 04).

## 12.5 Publications

### 12.5.1 Articles/Journal

- [1] Sato, Y., Y. Miyamoto, and H. Tomita (2019): Large dependency of charge distribution in a tropical cyclone inner core upon aerosol number concentration, *Prog Earth Planet Sci* 6, 62.
- [2] Sueki, K., and Y. Kajikawa (2019): Different precipitation Systems between Hiroshima and Keihanshin during extreme rainfall event in Western Japan in July 2018, *Journal of the Meteorological Society of Japan*, Volume 97 No.6.
- [3] Grabowski, W. W, H. Morrison, S. Shima, G. C. Abade, P. Dziekan, and H. Pawlowska (2019): Modeling of cloud microphysics: Can we do better?, *Bulletin of the American Meteorological Society*, Volume 100 No. 4.
- [4] Yamaura, T., S. Nishizawa, and H. Tomita (2019): Theoretical time evolution of numerical errors when using floating point numbers in shallow-water models, *Journal of Advances in Modeling Earth System*, Volume 11, Issue 10.
- [5] Sueki, K., T. Yamaura, H. Yashiro, S. Nishizawa, R. Yoshida, Y. Kajikawa, and H. Tomita (2019): Convergence of convective updraft ensembles with respect to the grid spacing of atmospheric models, *Geophysical Research Letters*, Volume 46, Issue 24.
- [6] Yoshida, R., and H. Fudeyasu (2020): How significant are low-level flow patterns in tropical cyclone genesis over the Western North Pacific?, *Monthly Weather Review*, Volume. 148 No.2.
- [7] Bai, L., K. Sueki, G. Chen, and R. Zhou (2019): Climatology of tropical cyclone tornadoes in China from 2006 to 2018, *Science China Earth Sciences*, Volume 63.

### 12.5.2 Oral Talks

- [8] 末木健太, 梶川義幸: 平成30年7月豪雨における広島と兵庫の降水特性の比較, 気象学会2019年度春季大会, Tokyo, Japan, May 15, 2019.
- [9] 柳瀬友朗: 高解像度公領域放射対流平衡実験における湿潤対流の自己組織化, 第6回マッデン・ジュリアン振動研究会, Kami, Japan, Sep 12, 2019.
- [10] 松嶋俊樹, 西澤誠也, 島伸一郎: 超水滴法を用いた雄大積雲のラージ・エディ・シミュレーション, 日本流体力学学会2019, Chofu, Japan, Sep 14, 2019.
- [11] Adachi, S. A.: Characteristics of Nonlinearity Between Climatology and Perturbation Components, 15th International Conference on Atmospheric Sciences and Applications to Air Quality, Kuala Lumpur, Malaysia, Oct.30, 2019.
- [12] 松嶋俊樹, 西澤誠也, 島伸一郎: 超水滴法を用いた雄大積雲のラージ・エディ・シミュレーション, 日本気象学会2019年度秋季大会, Fukuoka, Japan, Oct.31, 2019.
- [13] 山浦剛, 西澤誠也, 富田浩文: 浮動小数点演算エラーの理論的時間発展, 第21回非静力学モデルに関するワークショップ, Tsu, Japan, Nov. 21, 2019.
- [14] 山浦剛, 西澤誠也, 富田浩文: 浅水波モデルにおける浮動小数点演算誤差の理論的時間変化, 第33回数値流体力学シンポジウム, Sapporo, Japan, Nov.27, 2019.
- [15] 末木健太, 山浦剛, 八代尚, 西澤誠也, 吉田龍二, 梶川義幸, 富田浩文: 大気モデルの格子間隔に対する深い湿潤対流の収束性, 第11回熱帯気象研究会, Toyama, Japan, Dec. 26, 2019.
- [16] Yamaura, T.: The parameter estimation system in SCALE for reduced-precision floating-point numbers, The Second IMT-Atlantique & RIKEN Joint Workshop, Brest, France, Feb. 11, 2020.
- [17] Sueki, K.: Estimation of key parameters in cloud microphysics using ensemble Kalman filter, The Second IMT-Atlantique & RIKEN Joint Workshop, Brest, France, Feb. 11, 2020.
- [18] 松嶋俊樹: 超水滴法を用いた雄大積雲のラージ・エディ・シミュレーション, 2019年度 エアロゾル・雲・降水の相互作用に関する研究集会, Tachikawa, Japan, Feb. 19, 2020.

### 12.5.3 Posters

- [19] 足立幸穂, 西澤誠也, 安藤和人, 山浦剛, 吉田龍二, 梶川義幸, 八代尚, 富田浩文: 将来領域気候予測における不確定性の要因評価手法の提案, 気象学会2019年度春季大会, Tokyo, Japan, May 15, 2019.
- [20] 末木健太, 山浦剛, 八代尚, 西澤誠也, 吉田龍二, 梶川義幸, 富田浩文: 大気モデルにおける組織化した対流雲の数値的収束, 第6回メソ気象セミナー, Ise, Japan, Jul 14, 2019.
- [21] Adachi, S. A., and Hirofumi Tomita.: Characteristics of nonlinearity between mean state change and per-

turbation change, Latsis Symposium 2019, Zurich, Switzerland, Aug 21, 2019.

[22] Sueki, K., and Yoshiyuki Kajikawa.: Different Precipitation Systems between Hiroshima and Hyogo during the Extreme Rainfall Event in July 2018 Revealed by the Radar Observation, 39th International Conference on Radar Meteorology, Nara, Japan, Sep 17, 2019.

[23] Matsushima, T., Seiya Nishizawa, and Shin-ichiro Shima.: Large-Eddy Simulations of Cumulus Congestus Cloud Using Super Droplet Method, 39th International Conference on Radar Meteorology, Nara, Japan, Sep 17, 2019.

[24] 末木健太: 対流雲の大規模パラメータスイープ実験, 日本気象学会2019年度秋季大会, Fukuoka, Japan, Oct.30, 2019.

[25] Sueki, K.: Massive parameter-sweep warm bubble experiment on convective cloud environment, 10th European Conferences on Severe Storms, Krakow, Poland, Nov.7, 2019.

#### 12.5.4 Books

[26] 筆保弘徳, 山崎哲, 中村哲, 安成哲平, 吉田龍二, 釜江陽一, 下瀬健一, 大橋唯太, 堀田大介 (2019): ニュース・天気予報がよくわかる気象キーワード事典, ベレ出版, 276ページ, 2019/10/18出版.

#### 12.5.5 Software

[27] SCALE, Library and environment for Meteorological and Climate calculations, url<https://scale.riken.jp/>.

## Chapter 13

# Complex Phenomena Unified Simulation Research Team

### 13.1 Members

Makoto Tsubokura (Team Leader)

Keiji Onishi (Researcher)

Rahul Bale (Researcher)

Koji Nishiguchi (Postdoctoral Researcher)

Kazuto Ando (Technical Staff)

Hsueh-Jui Lu (Student Trainee)

Mehdi Badri (Student Trainee)

Chung-Gang Li (Visiting Researcher)

Ryoichi Kurose (Visiting Researcher)

Tetsuro Tamura (Visiting Researcher)

Shigeru Okazawa (Visiting Researcher)

Huilai Zhang (Visiting Researcher)

Leif Niclas Jansson (Visiting Researcher)

### 13.2 Overview of Research Activities

The objective of our research team is to propose a unified simulation method of solving multiple partial differential equations by developing common fundamental techniques such as the effective algorithms of multi-scale phenomena or the simulation modeling for effective utilization of the massively parallel computer architecture. The target of the unified simulation is supposed to be complex and combined phenomena observed in manufacturing processes in industrial cycles. Our final goal is to contribute to enhance Japanese technological capabilities and industrial process innovation through the high-performance computing simulation.

Most of the complex flow phenomena observed in manufacturing processes are relating to or coupled with other physical or chemical phenomenon such as turbulence diffusion, structure deformation, heat transfer, electromagnetic field or chemical reaction. While computer simulations are rapidly spreading in industry as useful engineering tools, their limitations to such coupled phenomena have come to realize recently. This is because of the fact that each simulation method has been optimized to a specific phenomenon and once two or more solvers of different phenomena are coupled for such a complicated target, its computational performance is seriously degraded. This is especially true when we utilize a high-performance computer such as Fugaku. In such

a situation, in addition to the fundamental difficulty of treating different time or spatial scales, interpolation of physical quantities like pressure or velocity at the interface of two different phenomena requires additional computer costs and communications among processor cores. Different mesh topology and hence data structures among each simulation and treatment of different time or spatial scales also deteriorate single processor performance. We understand that one of the keys to solve these problems is to adopt unified structured mesh and data structure among multiple simulations for coupled phenomena. As a candidate of unified data structure for complicated and coupled phenomena, we focused on the building-cube method (BCM) proposed by Nakahashi [1].

In summary, the overview of Research Activities in FY2019 was as followings.

In the research and development of unified simulation framework 'CUBE', an empirical analysis based on the actual vehicle aerodynamic problem has been conducted. The aerodynamic drag difference was predicted for the 11 specifications of the small vehicle model, and the results showed a generally good agreement with experiment. However, there were some cases where the size was reversed. The 16 specifications of SUV type automobile models was analyzed, including the rotation conditions of tires with tread patterns. Although it showed good agreement with the experiment in general, there were cases where the tendency could not be reproduced. In the future, we plan to continue working to improve accuracy by enhancing practical know-how together with our partners.

A study of the turbulence model was conducted that is important in the empirical vehicle aerodynamic analysis, the CSM turbulence model based on the coherent structure of the flow has been implemented. Based on the results of the turbulence energy decay spectrum of the uniform isotropic turbulence, it was confirmed that accurate modeling was done. This model has already begun to be applied to practical vehicle aerodynamic analysis. We are planning to proceed further research to improve its reliability.

As a prediction verification of narrow band noise generated in automobiles, the core technologies of the CUBE compressible unified solution method has been adjusted to create an improved results. A large-scale analysis of the real vehicle model has been conducted and successfully reproduced the acoustic vibration based on acoustic feedback. In addition, the grid resolution required to capture the correct peak was found from the basic verification study, and the required calculation scale has been estimated for the future study. In the future, we plan to realize analysis with this resolution in "Fugaku" and lead to the creation of results.

The fluid-structure unified analysis method with marker particles has been modified to deal with compressible solid analysis and verification analyses were conducted. The solid stress distribution in the tensile analysis and the shear analysis of the circular plate was compared and verified with the reference solution by the finite element method. The result that the ratio of the cell size to the diameter of the circular hole was 0.78% or less showed good agreement with the reference solution. It was also confirmed that the numerical solution by this method converged to the reference solution by making the cell size finer.

In the PIC (Particle in Cell) based Euler structural analysis method, the algorithm was applied to the rigidity analysis of the vehicle white-body by increasing the calculation scale. An analysis of about 210 million cells was performed on the real vehicle model, and the Mises stress distribution at each time obtained by LS-DYNA was compared. Qualitatively valid results were obtained, and it was confirmed that the calculation turn-around time could be significantly shortened by using large-scale computational resources. In the future, based on the results obtained in this research, we will strive to create further results through the activities of the automobile consortium.

As a deployment of the unified coupled analysis method to practical problems, the dolphin-kick swimming simulation has been conducted as the field of biomechanics and realized a moving boundary fluid simulation with smooth motion. By focusing on the width of the legs and the direction of the toes, it was clarified that the direction of the toes affects the dolphin-kick movement rather than the width of the legs. In the future, we will proceed with analysis of other athletes considering the difference due to body shape, analysis with increased resolution to improve visualization of vortices. We will continue to cooperate with related research institutes toward the 2020 Tokyo Olympic Games to create results.

As an application example in the field of biomechanics, an aerodynamic simulation considering the dynamic attitude change of ski jumping has been conducted, and realized numerical fluid analysis for a series of movements from takeoff movement to initial flight movement. This is probably the world's first achievement. In the future, we plan to continue research in order to analyze different jumpers and to solve the problem of clearly explaining the causal relationship between flight distance, aerodynamic force, and flow structure.

As an application example of the unified compressible solution, a sibilant fricatives pronunciation simulation of human mouse has been conducted. As an oral cavity model, simulations were performed on both a simplified flow channel and a realistic human model. The results of the sound source spectrum showed good agreement with the benchmarks in the references. In the future, we plan to clarify the effect of complex shapes on vocalization

and proceed with research to help support denture design.

A performance evaluation and tuning of the incompressible solver has been conducted on K-computer. The performance improvement of the entire program was obtained as 2.9 times faster at 8,192 nodes than the standard numerical scheme (Multigrid + CG method) used in the incompressible framework. The speedup is suitable for creating results in “Fugaku”. It has already been confirmed that the unified solution compressible solver is expected to improve the performance by 12.8 times per node and about 25 times in total in parallel performance compared to the K-computer by the estimation of the post-K computer performance evaluation tool. In the future, we plan to evaluate scaling performance further when the number of nodes is increased and deal with the expected increase in collective communication costs.

As a basic research for constructing a flow solution method using machine learning technology, the reconstruction of a flow mode using a neural network has been tried. When the original flow field was decomposed into two modes, and reconstructed it again, the flow field could be successfully reproduced with the same accuracy as the reference. We plan to extend this method in the future and evaluate the effectiveness of this method for 3D problems.

A feasibility study based on some well-known open source code including AMReX with the aim of implementing the adaptive mesh refinement has been conducted. Some basic simulations was conducted in search of new features suitable for our code, and gained important insights in investigating the low implementation effort and missing features in the available code. In the future, we plan to continue more detailed investigations and finally consider implementing it into CUBE.

A multi-objective optimization analysis framework has been developed and a genetic-evolutionary optimization up to the 12th generation with 4-objective functions has been conducted. From the Pareto solution in the obtained aerodynamic drag ( $C_d$ ) value and the difference in drag ( $\Delta C_d$ ) to the wind direction, it was confirmed that the tendency of the objective function value was similar to the knowledge obtained in the actual design field. Furthermore, using these results as training-data, a surrogate model construction was tried by machine learning with 9 design variables as inputs and  $C_d$  and  $\Delta C_d$  as outputs. The  $C_d$  value was predicted almost accurately in the prediction result by machine learning compared with the actual calculation result by CFD, and it was confirmed that the constructed neural network was appropriate. In the future, we plan to introduce design variables that reproduce more detailed shapes and improve the degree of freedom, which will lead to the creation of results in “Fugaku”.

A topology optimization framework for the Lagrangian marker particle method, which is a structural analysis method for Eulerian analysis, has been developed. The topology optimization results were verified by comparing them with those of a commercial finite element structural analysis software (LS-DYNA), and the formation of an optimized shape equivalent to the previous one was confirmed. In addition, topology optimization was performed on a design domain with 10 million design variables, which covers the white body frame of an automobile, and a frame shape close to the actual shape was obtained. In the future, we will continue to carry out various basic verification examples and optimization verifications for a large number of load cases that are assumed to be real problems, as well as to improve the optimization performance through collaboration with industry.

As part of the development of an automobile engine test bed, we performed a fuel-air mixing analysis that assumed a practical usage scenario. The simulation results of the standard engine shape showed the acceptable conservation of density, pressure and temperature comparing with the theoretical result. The comparison of the different shape of the piston showed the detailed insight of the flow mechanism for the strength of the tumble and swirl inside the engine. However, the calculation condition is still under the cold flow condition. In next step, we are planning to model the combustion inside the engine and conduct direct evaluation of combustion energy efficiency. And also we have started to provide this framework to the industrial user for the evaluation of the usability of the framework. We will continue to improve practicality through the consortium activities.

As a first step of the development of the combustion system test bed, the flow simulation of the jet engine combustor was performed. It can be inferred that the simulation qualitatively resolves the injector flow, though there was a qualitative difference at downstream section between the simulation and the PIV data which does not have depth component. In the next step, we are planning to develop the fuel spraying model and the combustion model which is specifically designed for the real engine combustors. We will continue to develop the functionality to reproduce the real state of engine combustion through the consortium activities.

As an issue of the architectural consortium, verification analysis of a test bed based on a unique fluid structure coupled analysis method was performed. First, the verification analysis for basic tower structure was performed. The results of wind pressure comparison with the wind tunnel experiments showed a well agreed profile. It proves the validity of the method that we have developed as a unique fluid-structure strong coupled unified solution that combines marker particles with the Euler-type structural analysis method. Next, the numerical stability was examined by performing analysis with various conditions of prismatic structures.

The numerical instability occurred near the prisms due to the numerical calculation method of solid strain. It revealed that it requires introducing a method that can stably calculate the solid strain without depending on the velocity field. Next, we conducted a simulation of wind resistance analysis of the dome roof of a stadium structure as an application to practical problems. We could realize the considerable world's first example of solving FSI problems at a high Reynolds number over hundred million by an Eulerian FSI method. The detailed analysis of the results has not been completed; however we plan to increase the resolution of calculation mesh to try to capture smaller flow structures and deformation modes. We will continue to develop the functionality to produce the practically useful framework for the strong-coupling fluid-structure interaction, and contribute to help users to apply this method into the practical cases through the consortium activities.

By combining aerodynamic analysis with vehicle motion analysis including suspension, steering mechanism, driver's operation reaction, etc., an analysis framework that can reproduce the actual driving state has been developed. The maneuver using a hatchback type real vehicle model has been realized and analyzed. By focusing on the roll motion and the steering input by the driver, the results consistent with the reports in the human-sensory test were obtained. In the future, we plan to carry out higher-resolution analysis and improve versatility while making improvements toward the creation results of "Fugaku".

[1] Nakahashi, K., "Building-cube Method for Flow Problems with Broadband Characteristic Length," In: Armfield S., Morgan R., and Srinivas K., editors. Computational Fluid Dynamics. (Springer, 2002, 2003), pp.77-81.

## 13.3 Research Results and Achievements

### 13.3.1 Empirical analysis using unified analysis framework CUBE

#### 13.3.1.1 Verification analysis for WLTP in vehicle aerodynamics

The WLTP (Worldwide harmonized Light vehicles Test Procedure) is an international new standard of fuel consumption test method in the automobile industry, and an evaluation test method for aerodynamic drag using computational fluid dynamics (CFD) has been established in automobile aerodynamic design. In Europe (and other member countries), a basic agreement on test methods between companies and certification agencies will be reached in 2019, and full-scale operation is expected to begin in 2020. On the other hand, in Japan, although the agreement has been obtained between companies, the situation is still in flux as the approval of the certification agency, that is the Ministry of Land, Infrastructure, Transport and Tourism, has not been obtained. It is still important for domestic automobile manufacturers to support WLTP, which expands opportunities for using CFD, they have requested us that we should continue this research activity. However, it may be a phase that requires more active lobbying to the certification agency. In this fiscal year, with the aim of further improvement of accuracy, Suzuki Motor Co., Ltd. and Nissan Motor Co., Ltd. provided us with new vehicle shapes and actual vehicle measurement data in multiple cases, and we conducted research to improve software practicality. The rate of improvement in accuracy has already slowed down, and more efforts are required for further improvement, so continuous efforts are important. In WLTP, it is expected that the aerodynamic drag measurement value by CFD is not an absolute value but only a relative value due to the specification difference. So in this research, the aerodynamic resistance difference  $\Delta C_d A [m]$  due to the specification difference has been mainly evaluated.

A total of 11 specifications were analyzed for the 2-box type small vehicle model provided by Suzuki Motor Corporation. Differences in specifications include not only large spoilers, but also consideration of combinations of optional parts such as mudguards, tow-bars, and door visors. The grid resolution is arranged with a minimum of about 1.5 mm in the necessary places such as near the grill, and adjusting it between about 1.5 to 6 mm according to the part of the car body. The number of grids is about 100 million, about 15 hours using 657 nodes of K-computer in each case for unsteady calculation of 300,000 time steps (equivalent to about 3 seconds of physical time), and 32 nodes in Oakforest-PACS that took about 43 hours to calculate. In addition, we plan to reduce the calculation time further in order to improve practicality. Figure 13.1 shows an example of the time-averaged flow velocity distribution obtained. It can be confirmed that the local change in the flow around each part affects the entire flow field such as the wake of the vehicle body and the flow in the engine room, and affects the aerodynamic performance.

Figure 13.2 shows the drag difference ( $\Delta C_d A$ ) due to the specifications of the obtained aerodynamics drag coefficient. Although the tendency is generally grasped, there are some cases where the tendency is reversed. Consideration of grid resolution dependency, aerodynamic drag accumulation graph, reproducibility of wind tunnel test, knowledge of analysis results by other commercially available software, consideration of deformation

for soft materials, CAD shape and actual vehicle shape comparison etc., the boundary conditions have been readjusted by Immersed Boundary and the turbulence model has been improved. Thus, some improvements have been obtained. However, it cannot be said that it has sufficient accuracy yet, so we plan to continue working to improve the accuracy in next year.

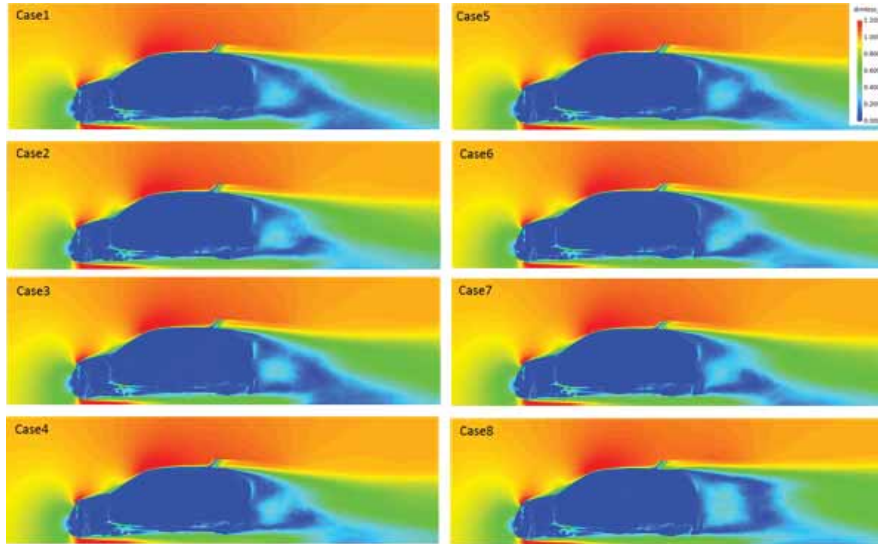


Figure 13.1: Profile of time-averaged dimensionless velocity magnitude in central section for several specifications of small vehicle simulation.

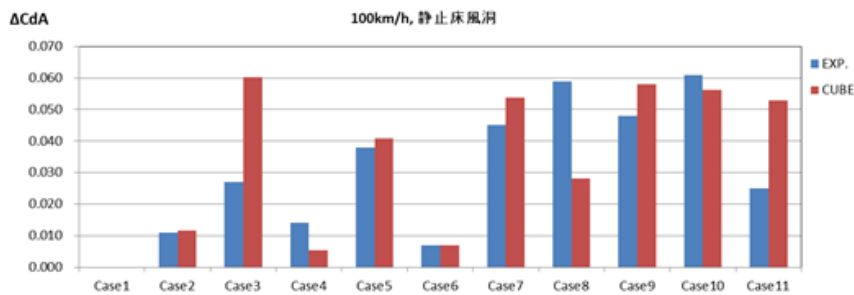


Figure 13.2: Predicted drag delta for all specifications of small vehicle simulation.

A total of 16 specifications were analyzed for the SUV type automobile model provided by Nissan Motor Co., Ltd. The actual measurement is conducted using a wind tunnel with a moving belt, and the analysis adopted that the condition involves tire/wheel rotation. Differences in specifications include a variety of aerodynamic add-on parts such as spoilers, deflectors, baffles, and grill covers. The grid resolution is adjusted to a minimum of about 1.5 mm near the grill and about 1.5 to 6 mm depending on the part of the car body. The number of analysis grids is about 120 million. Unsteady calculation of 150,000 time steps (equivalent to about 1.5 seconds of physical time) in each case required about 48 hours using Oakforest-PACS 32 nodes. Tire rotation provides a velocity boundary on the tire/wheel surface. In addition, the tire model is produced by a 3D scan technology which has the real shape, and the detailed shape including the tread pattern is reproduced. We succeeded in reproducing the rotation of the tire shape including the tread, but under this condition there are still problems that some calculations become unstable (the moment when the calculation point switches inside and outside the tire, etc.), so we will continue to improve. When this is completed, it will be the world's first case. Figure 13.3 shows an example of the time-averaged flow velocity distribution obtained. Figure 13.4 shows the difference ( $\Delta CdA$ ) due to the specifications of the obtained aerodynamic drag coefficient. Although

it shows good agreement with the experiment, there are cases where the tendency cannot be reproduced. In particular, since it was difficult to reproduce aerodynamic parts that affect the underfloor flow, we are reviewing the calculation conditions such as the modeling method of the wind tunnel floor surface and consideration of shape deformation. In this process, we are also preparing a group of post-treatment tools that contribute to flow evaluation, such as measuring surface pressure and creating an accumulation graph of aerodynamic drag. We will continue to work on improving accuracy in next year.

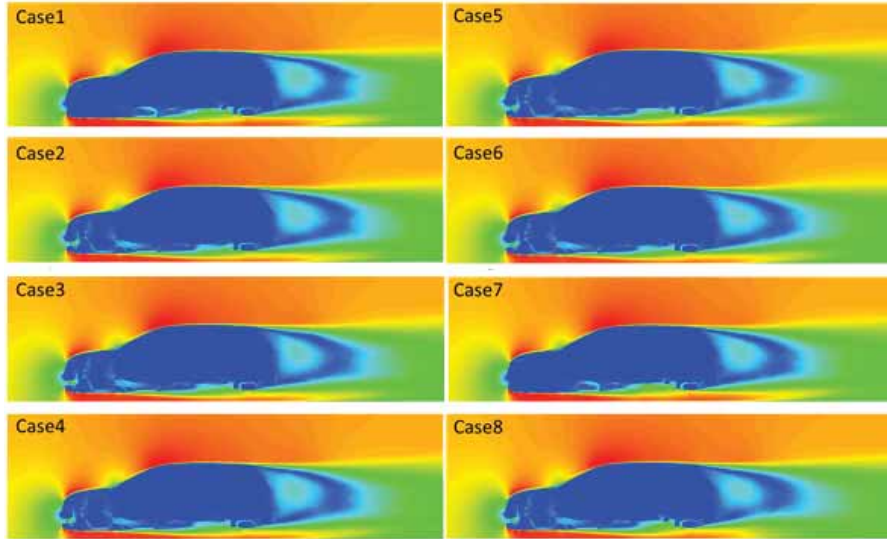


Figure 13.3: Profile of time-averaged dimensionless velocity magnitude in central section for several specifications of SUV vehicle simulation.

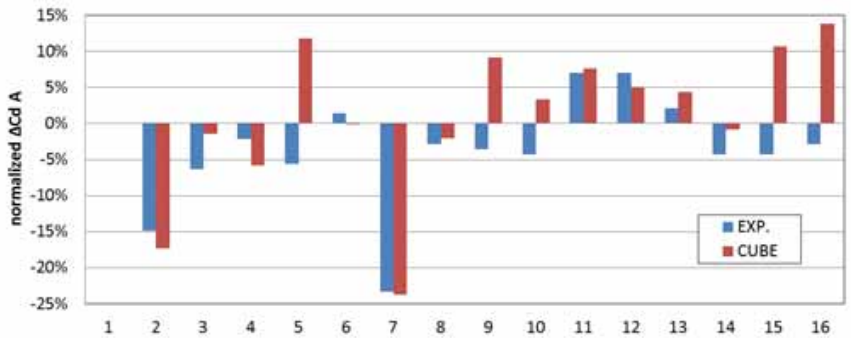


Figure 13.4: Predicted drag delta for all specifications of SUV vehicle simulation.

**13.3.1.2 Narrow-band noise analysis around the engine hood of the vehicle**

The narrow-band noise in automobile industries is caused by the quality problems and production issues and generally, it takes tremendous effort to solve this kind of problem in the design site. To improve the prediction accuracy, that the commercial software couldn't achieve by using the conventional methods, shorten the development period, and reduce the cost, the unified compressible solver installing in CUBE is under development. In this fiscal year, the knowhow and core technologies of the compressible solver have been summarized and the production of the results is under preparing.

For the resolution of the mesh, the finer resolution with a minimum width of 0.2 mm is located near the gap of the hood so that the acoustic feedback generated from the engine hood can be accurately captured. The total number of the grid is about 2 billion and 13,086 nodes in K-computer for about 50 hours are consumed. Figure

13.5 shows the contour of the propagation of the pressure fluctuation and the propagation with a circle shape emitting from the hood can be observed. This phenomenon is completely different from the usual acoustic noise caused by the vortex around the vehicle body. This kind of acoustic feedback can only be generated when the resonance appears. To capture this phenomenon, besides the much finer resolution compared with usual fluid simulation, a numerical scheme with extremely small dispersion and dissipation are also required. The resolution is determined by the flow velocity characteristics (the flow velocity, the gap of the hood, and the cavity length in the engine room), hence, it is necessary to perform the grid test to validate the current framework.



Figure 13.5: The propagation of the Pressure fluctuation.

In the second half of this year, because of the lack of computational resources, the large scale simulation couldn't be smoothly performed. Therefore, the basic validation of the cavity aeroacoustics problem has been conducted first. Figure 13.6 shows an example of the grid-dependent analysis of the frequency response for the simple cavity problem. From this result, the resolution required to capture the correct peak can be known, and the required computational resource can be also estimated. It can be seen that this simulation requires a resolution of around 0.5 mm (for a cavity width of 20 mm). Therefore, in the analysis equivalent to the real vehicle, it can be known that a resolution of 0.05 mm is required for the hood gap of 5 to 6 mm. In summary, 10 times the simulation time to h

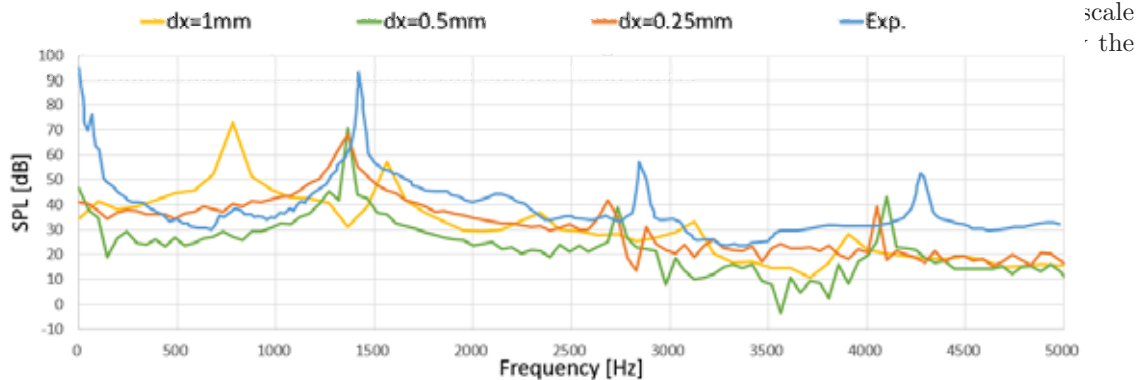


Figure 13.6: The comparison of the Frequency.

### 13.3.1.3 Research on turbulence models that contribute to large-scale aerodynamic analysis

In high Reynolds number turbulence analysis represented by automobile aerodynamics, it is important to select a suitable turbulence model for large-scale analysis. The Sub-grid-scale (SGS) model based on Smagorinsky (Smagorinsky, 1963) is widely used in the transient Large Eddy Simulation (LES), but it may be necessary to calculate the distance from the wall surface to the grid point (Van driest damping term of the standard Smagorinsky turbulence model). Or it requires operations that filter the model coefficients in a uniform direction to stabilize the solution (least squares operation of the dynamic Smagorinsky model [1]), and these methods has a high incidental calculation costs. In order to avoid this problem, in this study, we have mainly used the so-called "Implicit LES", which compares the artificial viscosity introduced by the stabilization method of

the numerical scheme with the physical viscosity and we have utilized it into practical simulation cases. In this year, we implemented a coherent structure turbulence model (CSM) based on the dominant vortical flow structures, which was derived by Kobayashi et al.[2]. In this model, in modeling vortex viscosity, the local constants of the Smagorinsky SGS model are dynamically determined based on the relationship between the second invariant of the velocity gradient tensor and the energy dissipation rate of the vortex. Unlike the dynamic Smagorinsky model, it does not require filtering and does not require distance calculation, which is advantageous for large-scale calculation and application to complicated shapes. The SGS model by Smagorinsky is expressed as follows:

$$\nu_t = C\bar{\Delta}^2|\bar{\mathcal{S}}|, \quad |\bar{\mathcal{S}}| = \sqrt{S_{ij}S_{ij}},$$

where  $\bar{\Delta} = (\bar{\Delta}_1\bar{\Delta}_2\bar{\Delta}_3)^{1/3}$  is the filter width, given by the grid width  $\bar{\Delta}_i$  in the  $i$ -th direction. In the CSM, the model coefficient  $C$  is determined as follows. The second invariant of the velocity gradient tensor  $Q$  is represented as:

$$Q = \frac{1}{2}(W_{ij}W_{ij} - S_{ij}S_{ij}),$$

$$\bar{\mathbf{W}} = \frac{1}{2}(\nabla\bar{\mathbf{u}} - (\nabla\bar{\mathbf{u}})^T), \quad |\bar{\mathbf{W}}| = \sqrt{W_{ij}W_{ij}},$$

where  $\bar{\mathbf{W}}$  is the vorticity tensor. This definition is termed the  $Q$ -criterion, and it is often used to visualize vortex structures [3]. Kobayashi determined the model coefficients (in non-rotating flow) independently of the flow properties and Reynolds number, as follows:

$$F_{CS} = Q/E,$$

$$E = \frac{1}{2}(W_{ij}W_{ij} + S_{ij}S_{ij}),$$

$$C = C_1|F_{CS}|^{3/2}, \quad C_1 = 1/20.$$

As a result, an eddy viscosity model is expressed, in which the coefficient is automatically zero in laminar flow, and is naturally damped in the wall direction. For details, refer to [2].

Figure 13.7 shows the basic verification results for this turbulence model on the isotropic turbulence decay energy spectrum. The homogeneous incompressible isotropic turbulence was generated in a three-dimensional cubic box using the random Fourier mode. The side length of the box was  $L = 0.09 \times 2\pi m$ , with a number of grid (cell) of  $128 \times 128 \times 128$  in three dimensions. The number of Fourier modes was 5000 and a generic dynamic viscosity  $\nu = 1.0 \times 10^{-5} m^2/s$  was chosen. The initial turbulence velocity field was generated from the energy spectrum table of Comte–Bellot et al. (CBC) [4], based on the method of Saad et al. [5]. A Fourier series of an arbitrary spatial velocity field  $\mathbf{u}$  at point  $\mathbf{x}$  is given by:

$$\mathbf{u}(\mathbf{x}) = 2 \sum_{m=1}^M q_m \cos(\kappa_m \hat{\mathbf{k}}_m \cdot \mathbf{x} + \psi_m) \hat{\boldsymbol{\sigma}}_m,$$

where  $M$  is the number of modes,  $q_m$  is the amplitude,  $\kappa_m$  is the  $m$ -th wavenumber, and  $\hat{\mathbf{k}}_m \equiv (k_{x,m}, k_{y,m}, k_{z,m})$  is a unit direction vector. The procedure consisted of choosing random  $\hat{\mathbf{k}}_m$  and  $\psi_m$  with  $q_m$  obtained from the energy spectrum such that  $q_m = \sqrt{E(\kappa_m)\Delta\kappa}$ . The modal direction vector  $\hat{\boldsymbol{\sigma}}_m$  was evaluated enforcing the divergence-free constraint; it was selected to be orthogonal to  $\hat{\mathbf{k}}_m$ ,

$$\hat{\mathbf{k}}_m \cdot \hat{\boldsymbol{\sigma}}_m = 0, \quad \forall m \in \{0, 1, \dots, M\}.$$

In Fig. 13.7, the input spectrum corresponds to the CBC data (solid lines). The simulated data are shown in filled circles and correspond to non-dimensional times of  $t^* = 42, 98, 171$ , respectively. The Nyquist limit is indicated via the vertical dashed line. The results of the initial spectrum and the decaying spectrum both well reproduced the results of the direct numerical simulation, confirming that accurate modeling was performed.

This model has already begun to be applied to practical vehicle aerodynamic analysis. From the results of initial studies, it has been confirmed that reasonable results with more suppressed numerical viscosity can be shown in areas that were previously sensitive to flow separation. In the next step, we plan to continue research to improve reliability by implementing a wide range of verification calculations and accumulating empirical calculation experiences.

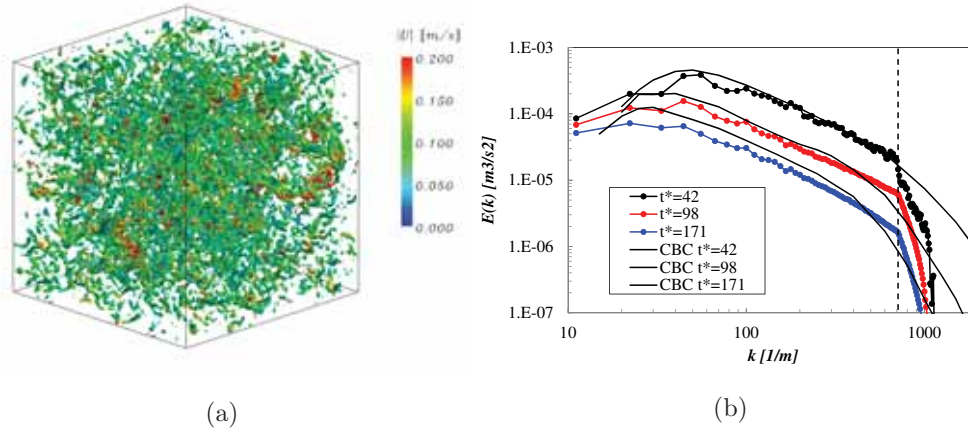


Figure 13.7: Isotropic turbulence decay energy spectrum for the CSM turbulence model. (a) The turbulence structures visualized by the Q-criterion. (b) The black circle represents the initial reference energy  $E(k)$  for each wavenumber  $k$ ; the red or blue colored circle shows simulation result. The solid line shows CBC data. The Nyquist limit is indicated via the vertical dashed line.

#### 13.3.1.4 References

- [1] M. Germano, U. Piomelli, P. Moin, W. H. Cabot, A dynamic subgrid-scale eddy viscosity model, *Physics of Fluids A: Fluid Dynamics* 3 (7), (1991), 1760-1765.
- [2] H. Kobayashi, The subgrid-scale models based on coherent structures for rotating homogeneous turbulence and turbulent channel flow, *Physics of Fluids* 17 (4), (2005), 045104.
- [3] M. Tanaka, S. Kida, Characterization of vortex tubes and sheets, *Physics of Fluids A: Fluid Dynamics* 5 (9), (1993), 2079-2082.
- [4] G. Comte-Bellot, S. Corrsin, Simple Eulerian time correlation of full-and narrow-band velocity signals in grid-generated “isotropic” turbulence, *Journal of Fluid Mechanics* 48 (2), (1971), 273-337.
- [5] T. Saad, D. Cline, R. Stoll, J. C. Sutherland, Scalable Tools for Generating Synthetic Isotropic Turbulence with Arbitrary Spectra, *AIAA Journal* 55 (1), (2017), 327-331.

### 13.3.2 Verification analysis of Eulerian finite volume formulation using Lagrangian marker particles for compressible solid

#### 13.3.2.1 Development of Eulerian finite volume formulation using Lagrangian marker particles for compressible solid analysis

In this study, in order to deal with large-scale structural analysis problems that reproduce complex shapes that are difficult to calculate with conventional methods, the Eulerian fluid-structure unified analysis method using Lagrangian marker particles has been developed. In this fiscal year, to deal with structural analysis problems with compressible materials, improvement of the fluid-structure unified analysis method with marker particles and implementation of an Eulerian finite volume formulation using Lagrangian marker particles for compressible solid analysis has been conducted. At this time, the conservation of mass and the equation of motion of compressible materials are expressed by the following equations [1].

$$\rho J = \rho_0$$

$$\rho \left\{ \frac{\partial \mathbf{v}}{\partial t} + (\mathbf{v} \cdot \nabla) \mathbf{v} \right\} = \nabla \cdot \boldsymbol{\sigma} + \rho \mathbf{b}$$

Here,  $\rho_0$  is the mass density at initial condition,  $\rho$  is the mass density,  $J$  is the volume ratio,  $\mathbf{v}$  is the velocity,  $\sigma$  is the Cauchy stress, and  $\mathbf{b}$  is the body force. In this study, the solid is modeled as a compressible neo-Hookean solid and the constitutive equation is given by [2]

$$\sigma = J^{-5/3}G \left\{ \mathbf{B} - \frac{1}{3}(\text{tr}\mathbf{B})\mathbf{I} \right\} + K(J-1)\mathbf{I},$$

where,  $G$  is the shear modulus,  $\mathbf{B}$  is the left Cauchy-Green deformation tensor,  $\mathbf{I}$  is a second-order unit tensor, and  $K$  is the bulk modulus.

In order to confirm the validity of the proposed method, the tensile analysis and the shear analysis of a flat plate with a circular hole were conducted and the solid stress distribution is compared with the reference solution obtained by the finite element method. Furthermore, by verifying the stress distribution when the mesh resolution is changed, the mesh resolution required to obtain the desired accuracy is clarified. In the following examples, the structure has Young's modulus and mass density of the steel, and the void region is given  $\rho_0 = 1.0\text{kg/m}^3$  to avoid numerical instability. The height of the flat plate(structure) is 1.0 m and the width is 0.5 m, and a circular hole with a diameter of 0.25 m is arranged in the center of the flat plate. The length of the plate in the direction perpendicular to the paper surface ( $y$ -direction) is assumed to be a unit length, and the plane strain state is assumed by setting the velocity in the  $y$ -direction to zero.

### 13.3.2.2 Verification analysis by the tensile analysis and the shear analysis of a flat plate with a circular hole

The lower end of the flat plate fixes the velocity component in all directions to zero, and the upper end of the flat plate gives a tensile velocity that increases linearly in the time direction in the positive  $z$ -axis direction. No restraint conditions are given to the other end faces. In the proposed method, the above velocity boundary conditions are given by the marker particles arranged in the region. In this example, the analysis time is up to 1 ms. Therefore, the displacement of the upper end of the flat plate is  $1\ \mu\text{m}$ , and this example can be regarded as a minute deformation problem. In the calculation by the proposed method, the time increment size is set so that the CFL number for the stress wave velocity is 0.1874 at each spatial resolution. In order to obtain the reference solution, a sufficiently fine finite element mesh is used, and the finite element size of the orthogonally divided region excluding the circumference of the circular hole is  $1/640$  m.

Figure 13.8 shows the reference solution at  $t = 1$  ms, the marker particles at each spatial resolution, and their Mises stress distribution. In this calculation, the number of marker particles in one cell is fixed at  $2 \times 2$ . The result that the ratio of the cell size to the diameter of the hole is 0.78% or less shows good agreement with the reference solution, and it can be seen that the stress concentration at the upper part and the lower part of the hole is particularly reproduced. In addition, in order to quantitatively verify the validity of the numerical solution, the time history of strain energy is compared with the reference solution. As shown in Figure 13.9, it can be confirmed that the numerical solution by this method converges to the reference solution by making the cell size  $h$  finer. In addition, Figure 13.10 shows the error  $\epsilon$  of the strain energy with respect to the reference solution at  $t = 1$  ms and its spatial convergence. It is confirmed that the error converges at the order of 0.025 and that the error is 0.27% at the cell size  $h = 1/1024$  m.

### 13.3.2.3 Verification analysis by shear analysis of a flat plate with a circular hole

The analysis conditions are the same as the example in the previous section, except that the upper end of the flat plate is given a shear rate that increases linearly in the time direction in the positive  $x$ -axis direction. Figure 13.11 shows the reference solution at  $t = 1$  ms, the marker particles at each spatial resolution, and their Mises stress distribution. The result that the ratio of the cell size to the diameter of the hole is 0.78% or less shows a good agreement with the reference solution, and it can be seen that the stress concentration around the hole is particularly reproduced. From Figure 13.12, it can be confirmed that the numerical solution by the proposed method converges to the reference solution by making the cell size  $h$  finer. Furthermore, Figure 13.10 also shows the error of strain energy with respect to the reference solution at  $t = 1$  ms and its spatial convergence. It is confirmed that the error converges at the order of 0.077 and that the error is 0.17% at the cell size  $h = 1/1024$  m.

When the ratio of the cell size to the diameter of the circular hole is 1.56% or more, it can be seen that the oscillation of stress occurs at the top corners of the flat plate in Figure 13.8 and Figure 13.11. This is because the velocity field is discontinuous between the cell to which the velocity boundary condition is given and the cells around it. Thus, the velocity gradient calculated from the velocity of these cells is overestimated.

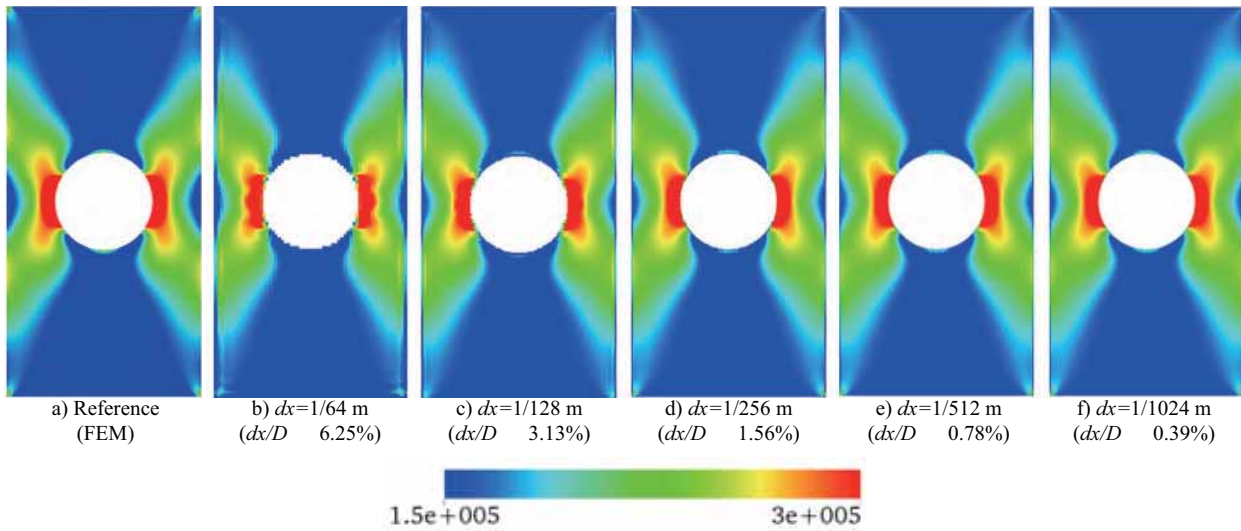


Figure 13.8: Tensile deformation problem of a flat plate with a circular hole: Distribution of Marker particles and their Mises stress distribution at  $t = 1\text{ms}$ .

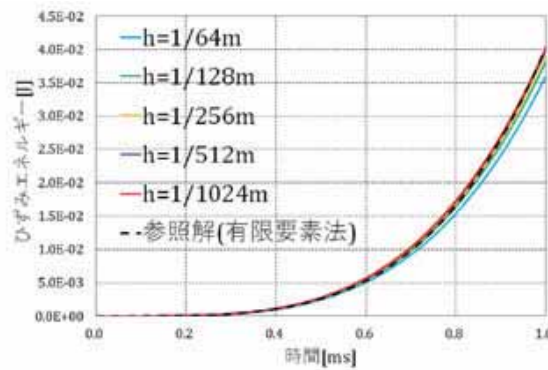


Figure 13.9: Tensile deformation problem of a flat plate with a circular hole: Time history of strain energy.

In order to avoid this numerical oscillation even when the spatial resolution is low, it is necessary to introduce a calculation method for solid deformation tensors that does not require velocity gradient calculation and we continue to work on development to improve analysis accuracy.

### 13.3.2.4 Large-scale real vehicle model structure analysis using Euler structure analysis framework

In this research, in order to conduct a large-scale structural analysis that reproduces detailed shapes of real vehicle model that are difficult to calculate with conventional methods, we are developing a unique fluid-structure unified solution method that combines an Euler-type structural analysis method with marker particles. We applied the algorithm to the stiffness analysis of the vehicle white-body by increasing the scale of calculation. In this report, steel is assumed as the solid material in all the numerical analysis examples, and  $\rho = 7850\text{kg/m}^3$ ,  $E = 200\text{GPa}$ ,  $\mu = 0.3$  are given as the material parameters of the solid. Here,  $E$  is Young's modulus and  $\mu$  is Poisson's ratio. In the region where no solid exists,  $\rho = 1.0\text{kg/m}^3$  is set to avoid zero division in numerical calculation. The shape of the automobile body and the hierarchical Cartesian grid based on the building cube method are shown in Fig. 13.13. The minimum cell size was 1.86 mm, and the total number of cells was about 210 million.  $32 \times 32 \times 32$  cells are evenly spaced in a cube. As shown in Fig. 13.14, the boundary conditions in the torsional stiffness test are reproduced by setting the velocity for the marker particles shown in red. The two marker particle groups at the rear of the vehicle body are completely fixed, and the two marker particle groups

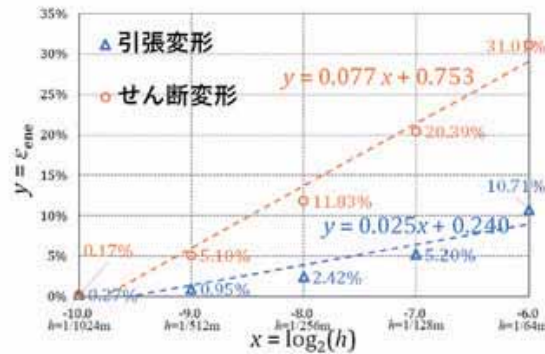


Figure 13.10: Error of strain energy at  $t = 1\text{ms}$  with respect to reference solution (finite element method) and its spatial convergence.

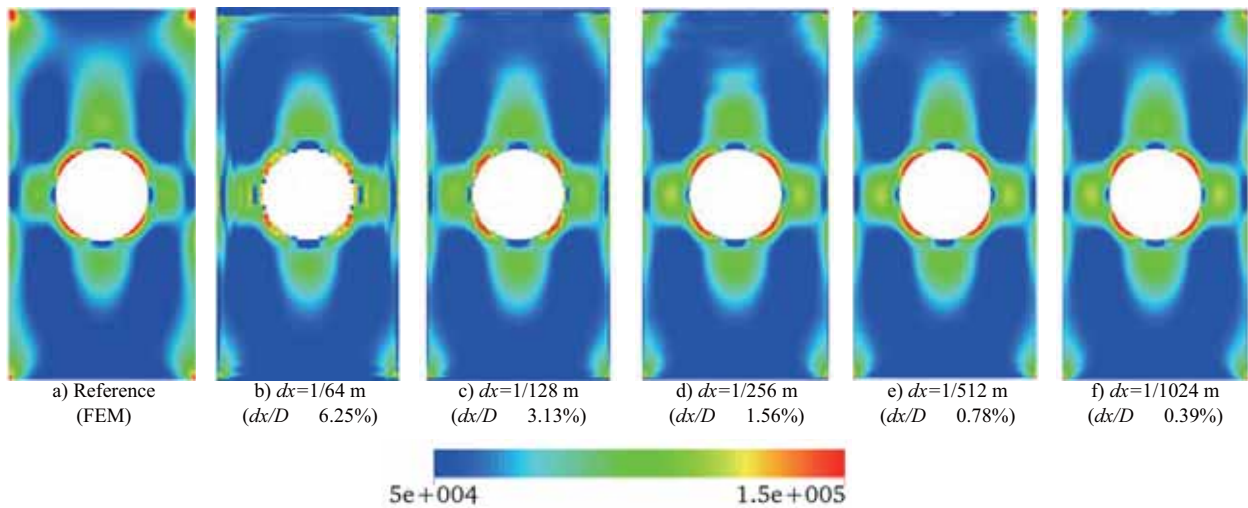


Figure 13.11: Shear deformation problem of a flat plate with a circular hole: Distribution of Marker Particle and its Mises Stress Distribution at  $t = 1\text{ms}$ .

at the front of the vehicle body give a velocity that increases linearly in the positive and negative directions of the  $z$ -axis. In this example, the time increment was set to  $6.25 \times 10^{-5}\text{ms}$ , and calculations were performed up to 4800 steps ( $t = 3.0\text{ms}$ ). 13,065 nodes of K-computer were used for this calculation. In order to compare and verify the numerical solutions by the proposed method, the reference solution was calculated using the commercial solid-structure analysis code LS-DYNA. The total number of elements of the finite element mesh in LS-DYNA was about 660,000, and it is consisted with about 580,000 shell elements, about 10,000 solid elements, 14 beam elements, and about 70,000 rigid body elements.

Figure 13.15 shows the Mises stress distribution at each time obtained by the proposed method and LS-DYNA. However, the color bar of Mises stress is normalized. From these figures, it could be confirmed that the Mises stress distribution obtained by the proposed method is qualitatively generally valid. Table.13.1 shows the turn-around time of the proposed method and LS-DYNA. The turn-around time could be significantly shortened in the calculation by the proposed method by using a large-scale computational resource (K-computer 13065 node  $\times$  2.4 hours). In the future, based on the results obtained in this research, we will continue to create further results through the activities of the automobile consortium organized by RIKEN.

### 13.3.2.5 References

[1] G. A. Holzapfel, "Nonlinear Solid Mechanics: A Continuum Approach for Engineering," Wiley, 2000.  
 [2] R. W. Ogden, "Non-linear elastic deformations," Courier Corporation, 1997.

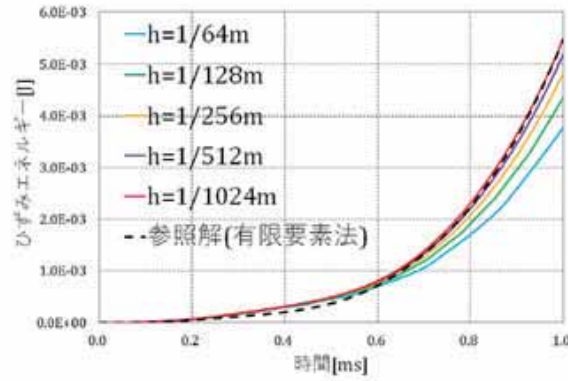


Figure 13.12: Shear deformation problem of a flat plate with a circular hole: Time history of strain energy.

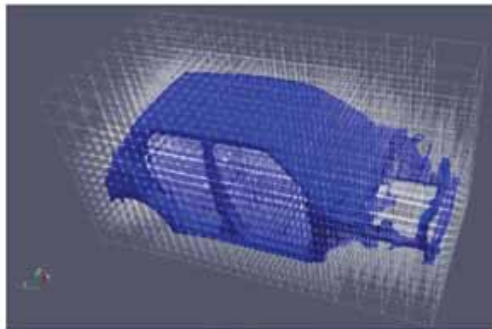


Figure 13.13: Overview of Euler grid and vehicle white body shape (finest size: 1.86mm, number of grids 210 million).

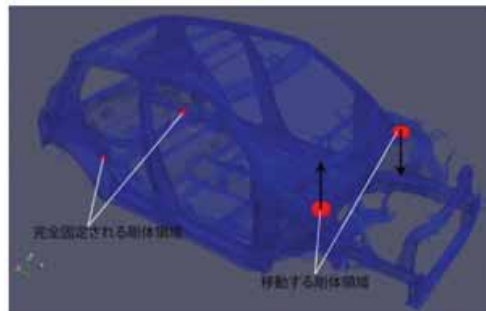


Figure 13.14: Geometric boundary conditions: (red) velocity boundary on a jig given by marker particles.

Table 13.1: Turn-around time comparison

	LS-DYNA	Proposed method
Grid generation	several weeks	10 minutes
Calculation	0.75 hours	2.4 hours
Visualization	1 hour	1 hour
Total (Turn-around time)	several weeks	3.6 hour

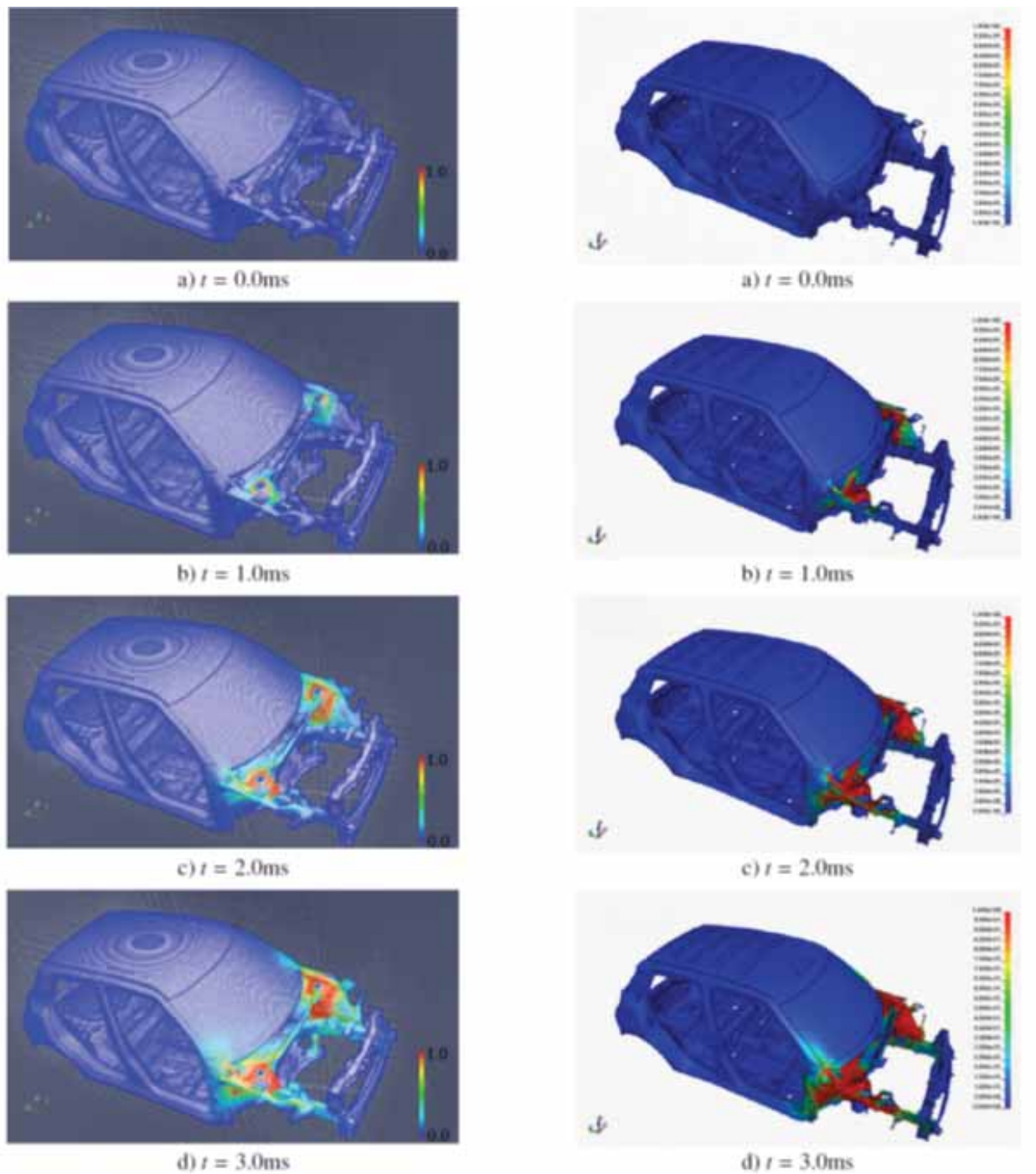


Figure 13.15: Analysis results by CUBE (left) and LS-DYNA (right) (Mises stress distribution).

### 13.3.3 Biomechanics CFD–Development of unified coupled analysis methods into practical problems

#### 13.3.3.1 Role of feet orientation on thrust generation in dolphin-kick swimming

In swimming competitions using the 50m pool, under water swimming is permitted up to 15m from the starting point and after turning back all swimming styles other than breaststroke. Generally, the swimming style employed for underwater swimming is known as dolphin kick. As a result, there is much interest in optimizing the swimming performance of the dolphin kick swimming.



Figure 13.16: The four feet orientations considered in this study.

Since it is difficult to measure the fluid forces generated unsteady swimming such as dolphin kick swimming experimentally, various studies using computational fluid dynamics have been conducted. The results of such studies suggest that lower limbs and feet account for major contribution to the propulsive forces, and that the joint angle of the lower body is important. However, most of the prior studies focus on a standard orientation of the legs and feet. Therefore, in this study, we investigate the role of feet orientation on the propulsive forces in dolphin kick swimming using numerical simulations. For that purpose, the position of the legs such as the width of the legs and the direction of the ankles was changed variously using the body shape data of the athlete measured using the 3D scanner. Experimentally obtained dolphin-kick motion was employed of the simulations. The movement of the lower body was converted into coordinates and given as motion data. The CAD model of the swimmer’s body was coupled with the motion capture data to generate CAD model based motion model.

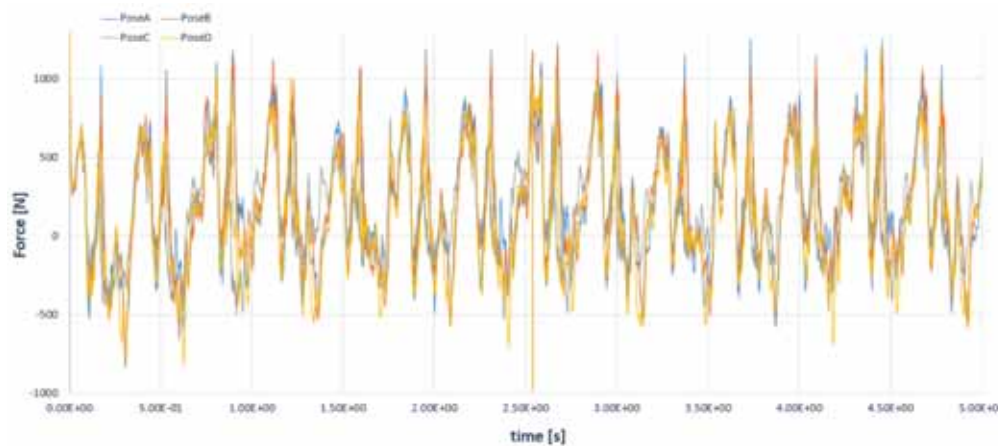


Figure 13.17: Instantaneous thrust generated by the four feet poses.

Numerical simulation was carried out using this setup for four different feet orientations, the results of which are shown in Fig.13.16. From the results of these simulations we find that there are differences in the flow velocity distribution, the vortex structure generated on the sole of the foot when the leg is kicked down, and the flow velocity vector. By comparing these results focusing on the width of the legs and the direction of the toes, it was confirmed that the direction of the toes rather than the width of the legs affects the diving

Table 13.2: Comparison of averaged thrust produced by the four feet orientations.

Pose	A	B	C	D
Thrust (N)	213	220	181	134

method movement. It was confirmed that collecting the flow velocity vectors generated on the sole of the foot more centrally and posteriorly with the toes facing the center has a large effect on propulsive forces.

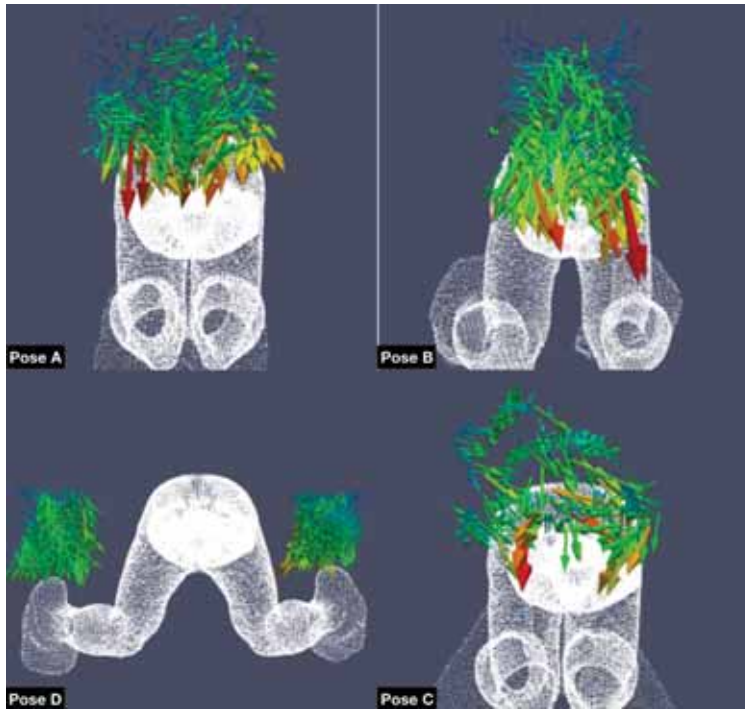


Figure 13.18: Visualization of the flow around the feet at the end of the power stroke.

Next, the thrust generated by the swimmer is plotted compared in Fig.13.17. The vertical axis is the force of the swimmer, and the horizontal axis is the time. For each leg orientation, the red circled area where the swimmer has the most propulsion. From the figure, it can be seen that Pose A and Pose B produce more thrust on average compared to the other two feet orientations. The time averaged thrust generated by each of the four feet orientations are shown in Table. 13.2.

PoseB has the most propulsion power, and PoseA also has a value close to PoseB, but PoseC and PoseD have relatively low values, and PoseD has the lowest propulsion power. From Fig.13.18, it can be seen that the flow velocity vector is generated in a circle on the sole of the foot.

In summary, we simulated the diving movement by intentionally changing the leg position for one athlete, and compared the effect of the leg position on the propulsive force. The following findings were obtained from the simulation results.

1. There was a difference in the flow velocity distribution and the force generated by the swimmer depending on the position of the legs.
2. The magnitude of the vorticity generated on the sole of the foot when the leg was kicked down greatly differed depending on the width of the leg opening and the direction of the toe.
3. There was a correlation between the vortex generated on the sole of the foot and the magnitude of the flow velocity vector.
4. The direction of the toes had the greatest effect on propulsion, followed by the width of the legs that had the greatest effect on propulsion.

From the above, it is considered that the position of the legs in the diving swimming method can be more propulsive by the posture in which the legs are closed and the toes are aligned with each other as in Pose B. In optimizing the diving method, as a future research subject, it is necessary to consider the difference due to body shape, perform the same analysis for other athletes, and perform more precise analysis with increased resolution to improve the visualization of vortices.

**13.3.3.2 Aerodynamic simulation of the dynamic flight posture in ski jumping**

In ski jumping competitions, take-off and flight posture are important movements that are greatly influence the flight distance. These two postures are closely related, and errors in the take off posture will adversely affect the flight posture and it is usually quite difficult to make adjustments during the flight. On the other hand, a jumper must dynamically adjust the flight posture taking into account the wind condition to prevent the increase in drag and the decrease in lift as much as possible. Failure to do so can result in the jumper stalling mid-flight, greatly reducing the jumping distance. Although these two movements are very important, there has been no study that aerodynamically investigated both movements together. This is because it is difficult to continuously reproduce both movements in a wind tunnel experiment, and it is also difficult to reproduce a large flight posture change in simulations that employ unstructured grid that that is typically used for such analysis. However, with the advent of local mesh refinement techniques in cartesian meshes and immersed boundary methods that can faithfully reproduce the dynamic motion of a ski-jump, for example, it is now possible to carryout such simulations. Therefore, the purpose of this study is to carry out aerodynamic simulation using the above framework for take-off motion to initial flight motion, and to investigate the characteristics of the aerodynamic force on the jumper. In this study, in order to reproduce more detailed movements before analysis, we asked for the cooperation of an active ski jumper and attached a motion sensor to the jumper to measure posture change data. In addition, a GPS device was attached to the jumper to measure the flight trajectory and instantaneous speed. Using these data, aerodynamic simulations were performed for movements from 0.3 seconds before takeoff to 0.7 seconds after takeoff.

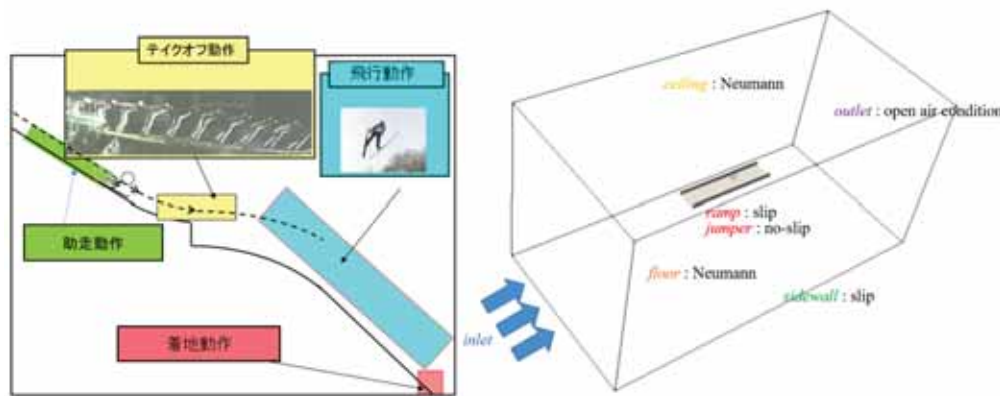


Figure 13.19: (Left) Schematic of ski jump. (Right) Computational domain setup.

The ski jumping competition is one of the Nordic skiing competitions held in the stadium, and is competed in two elements: distance and beauty of flying type. In ski jumping competitions, a series of movements can be classified into six categories: run-up, take-off, initial flight, stable flight, landing preparation, and landing (Fig.13.19). Of these movements, two important elements for extending the flight distance are take-off and flight posture (initial flight / stable flight). In the take-off motion, while maintaining the speed close to 90 m / s obtained during the approach run, the posture is changed significantly from the crouched position to the flight posture within a very short span of time, from 0.2 to 0.3 s. This movement, which involves a large change in posture in a short period of time, is considered to be a very difficult and important movement. In flight, jumper takes a posture to obtain a large lift and low drag. Although there is no significant change in posture during flight, it is necessary to fine-tune the posture taking into consideration of the wind conditions. In ski jumping competitions, once a stall occurs during flight, it is difficult to extend the flight distance, so stall prevention is also very important.

Table 13.3 shows the start gate, flight distance, Run time, and flight time of each trial measured in this

Table 13.3: Information obtained in each jump.

	Starting Gate	Flying Distance (m)	Run time (s)	Flight time (s)
First jump	26	112	6.1	4.2
Second Jump	17	90	5.7	3.2
Third Jump	22	113	5.8	4.1

study. In the measurement in this study, the largest gate is No. 26 and the smallest gate is No. 17, so there is a difference of 4.5 m in the maximum approach distance. In this study, the boundary conditions were set as shown in Fig.13.19.

From Fig. 13.20, in the first attempt, there was no significant increase in drag immediately after takeoff (around 0 s at time), which was seen in other attempts, and the drag decreased significantly between 0.3 s and 0.4 s after that. On the other hand, in the 2nd and 3rd trials, the drag increases immediately after the takeoff, then decreases and increases once, and then decreases again. At around 0.7 s time, there was no big difference between each attempt.

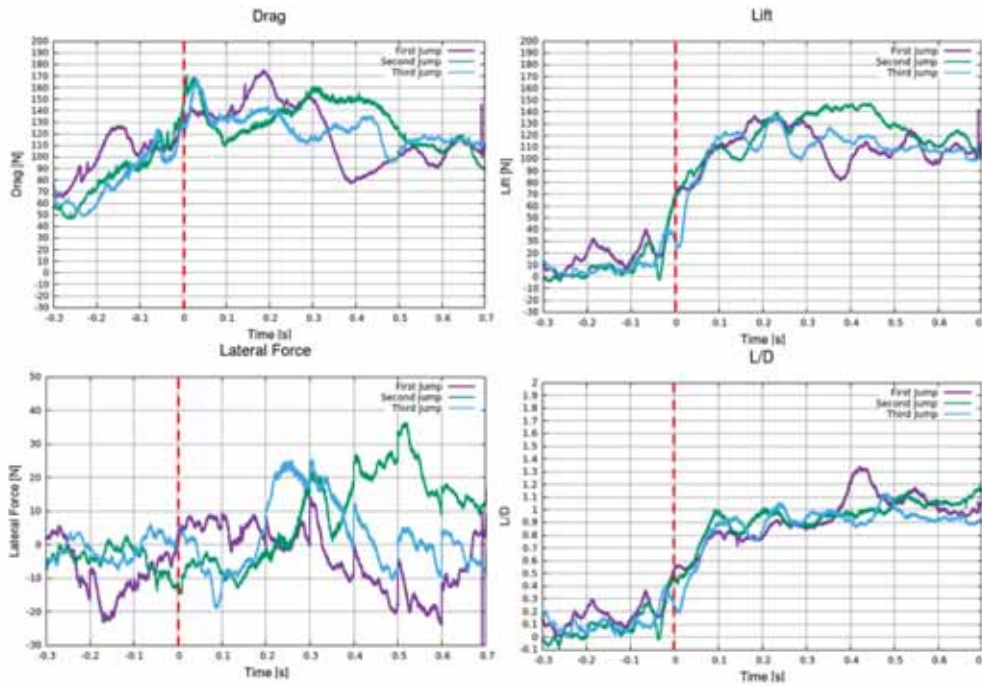


Figure 13.20: Evolution of drag, lift, lateral force and lift-drag ratio.

First, as with drag, lift has a low value before takeoff (before time 0 s) and tends to increase significantly by taking a flight attitude after takeoff (after time 0 s). However, in the first attempt, the lift was very high at time -0.2 s, and a fall similar to drag was seen at time 0.3 s to 0.4 s. On the other hand, it can be seen that in the second attempt, unlike the other attempts, the high value was maintained between the times of 0.3 s and 0.5 s. In the third attempt, there was no significant decrease after takeoff, but as with drag, it continued to decrease gradually. At 0.7 s, as with drag, there was no significant difference in lift between the three attempts. The lift to drag ratio is defined by the following equation.

$$L/D = \frac{\text{Lift}}{\text{Drag}} \tag{13.1}$$

Regarding the time transition of the lift-drag ratio, for each attempt, the value was close to 0 before the takeoff (before time 0 s), and after take-off L/D rapidly increases from 0 to 1 within a span of 0.1 s. As for the difference between the trials, it can be seen that the lift-drag ratio increases significantly only in the first run at around 0.4 s. A snapshot of the streamlines of the flow at 0.6s after take-off is presented in Fig.13.21.

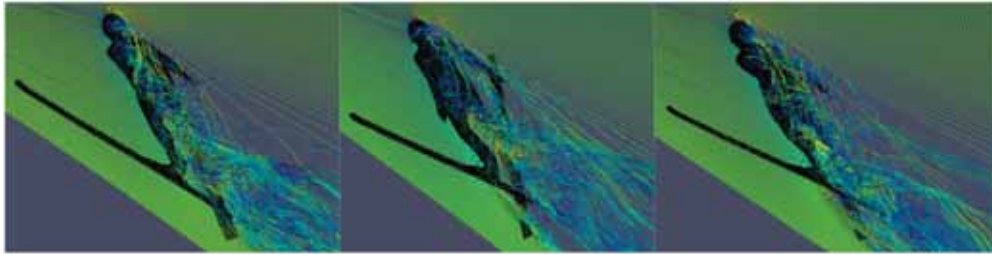


Figure 13.21: Streamlines at  $t = 0.6s$  for first, second and third jump, respectively.

### 13.3.3.3 Sibilant fricatives pronunciation simulation using a unified compressible solution

The simulation of human speech organ contributes to the dental application. For example, a well-designed denture enables patients speak better, especially improvement in pronouncing words containing sibilants or fricatives. However, human phonation process is a tough objective for the simulation because the fluctuation pressure which generates the sound is much smaller compare with the atmospheric pressure. Specifically, the amplitude of sound wave is only 0.01% of standard atmosphere. That means the simulation system is sensitive to the accuracy of the numerical scheme. Therefore, a numerical framework which is suitable for high-performance computing is built for modelling the sibilant fricative production in this study.

The implicit time scheme with immersed boundary method based on a hierarchical structure grid as well as the modified solution-limited time stepping method for the compressible flow are adopted. Firstly, the acoustic resonance generated from the flow around the single plate is simulated to validate the numerical scheme and the result shows that this framework is highly efficient and suitable for the massive parallelization system to tremendously save the calculation time. Then, the simulation for a simplified model of the sibilant /s/ is conducted and SPL profiles are in good agreement with the experimental results. Finally, the simulation for a realistic geometry of sibilant /s/ scanned from the human vocal tract is performed to demonstrate that this framework is capable of making a contribution to the dental application, such as helping designing the dental prosthesis.

The LUSGS implicit algorithm and the Unified Time Stepping scheme are applied for the time advancement. The Roe scheme with 5th order MUSCL is used to approximate the convective terms. And the second order central difference method is adopted to calculate the magnitudes of the viscous terms. The absorbing boundary condition is used at the outlet for avoiding the computational domain being polluted by the reflecting pressure waves. The immersed boundary method with the hierarchical structured grid is used to simulate the complex geometry surface. And the OpenMP and MPI are applied for parallel computation.

The resonance plays an important role in acoustics simulation, since it enhances the amplitude of sound wave and makes characteristics of sound clearly. Hence, the model of single plate is simulated to check the phenomenon of resonance with the benchmark [1] by present framework. In Fig. 13.22, the fluctuation pressure is indicated. The resonance occurs in a half-wavelength mode along the plate length at  $U = 44m/s$ , both of the wave length and intensity of the sound wave can be observed.

The sibilant fricative is the common consonant in each language produced by forcing air through a narrow channel inside the oral cavity. Nozaki et al. [2] replicated a realistic model of a subject pronouncing /s/ and used incompressible solver to simulate the flow field. Yoshinaga et al. [3] simulated the simplified sibilant fricatives model to investigate the mechanisms of the production process in the vocal tract. Both the simplified and realistic model are selected to be the validation by present framework. Fig. 13.23 is the instantaneous velocity magnitude. Observably, the flow is accelerated at the narrow channel and the turbulence is caused when the flow goes through the channel. As shown in Fig. 13.23, the sound source locates around the gap before the exit, which is the high RMS value region. The fluctuation pressure out of the oral cavity is shown in Fig. 13.24, the frequency of this sound wave is about 5kHz. The SPL spectrum sampling at 10 cm far from the exit of oral cavity is shown as Fig. 13.25. The result simulated by current framework has good agreement with the benchmark after 5kHz which is the first characteristic peak. Moreover, Fig. 13.26 is the instantaneous velocity of realistic model. Clearly, the flow is speed-up between the articulators, and then products the sound by turbulence. Besides, the SPL spectrum shown in Fig. 13.27 has good tendency with the benchmark.

Present framework applied the implicit time scheme with immersed boundary method to achieves the high accuracy and efficiency simulation in the computational acoustic of pronouncing sibilant fricatives. By validating with the benchmarks, the results have qualitatively good agreement. Moreover, the combination of immersed

boundary method and high-performance computing reduces the computational resource drastically. It indicates that this framework is a promising tool for human phonation problem. About the future work, the investigation of how the shape effect the phonation will conduct for helping designing the denture.

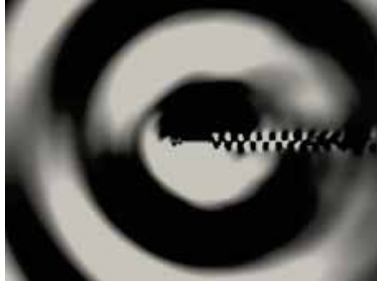


Figure 13.22: Contours of fluctuation pressure for phase- and spanwise-averaged flow fields.

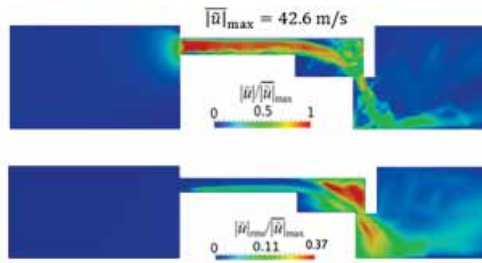


Figure 13.23: (Top) instantaneous and (bottom) RMS velocity magnitude.

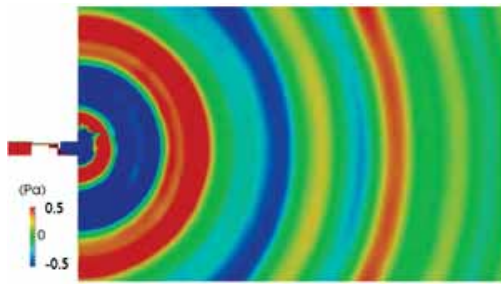


Figure 13.24: Fluctuation pressure of simplified model.

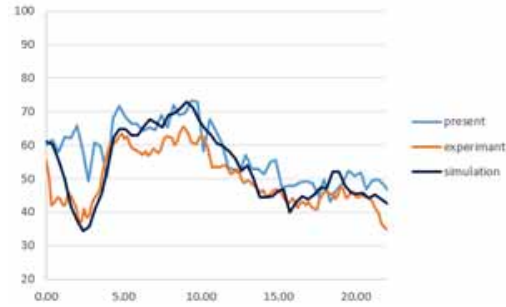


Figure 13.25: SPL spectrum of simplified model.

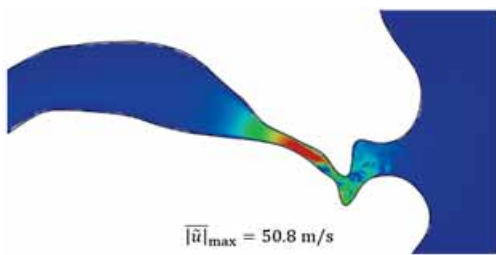


Figure 13.26: Instantaneous velocity magnitude of realistic model.

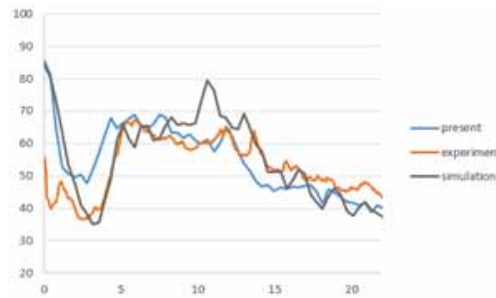


Figure 13.27: SPL spectrum of realistic model.

13.3.3.4 References

[1] Yokoyama, H., K. Kitamiya, and A. Iida. *Physics of Fluids*, 25.10, (2013), 106104.  
 [2] Nozaki K., Yoshinaga T., and Wada S., *J Dent Res*, 93(2), (2014), 207211.  
 [3] Yoshinaga, Tsukasa, Kazunori Nozaki, and Shigeo Wada. *Physics of Fluids*, 30.3, (2018), 035104.

### 13.3.4 Speed-up and scale-up of fundamental methodology targeting post-K system

#### 13.3.4.1 Performance optimization of incompressible solver of CUBE

This year, we evaluated and tuned the performance of the incompressible solver of CUBE on the K-computer. The target problem is a simple cavity flow, which targets a standard numerical scheme used for empirical analysis (Multigrid + CG method). The serial tuning of the relevant part was performed by cutting out the Poisson's equation solver by the multigrid method, which is the most costly part in the incompressible solver (accounting for 91% of the total). Specifically, the following measures were applied.

1. The integer operation for address calculation has been reduced by making the array referenced as a structure member directly referenced using a pointer.
2. Improved continuity of data access by swapping the dimensions of the array
3. The continuity of data access was improved by changing the array elements colored in red and black by Red-Black ordering so that they are stored in separate arrays.

As a result, a performance improvement of 9.8 times was obtained. Next, the following two tunings were applied as parallel tuning.

1. In the packing process for neighbor communication, the cost imbalance between threads has been improved by setting the division target of thread parallelization from each side of the subdomain to the cube (collection of cells) included in each side.
2. By changing the OpenMP thread scheduling scheme from dynamic to static for the computational loop included in the CG method, the cost balance between threads is improved and the overhead of dynamic scheduling is reduced.

As a result of these tunings (and the above-mentioned serial tuning), the performance of the entire program was improved by 2.9 times at 8,192 nodes in the K computer. As a result, it can be said that the speedup for creating results using "Fugaku" has been completed. However, there are still unknown parts about the evaluation of scaling when the number of nodes is further increased and the expected increase in collective communication cost, so we plan to deal with these in the result creation phase in the future.

#### 13.3.4.2 Basic research for constructing a flow solution method using a neural network

In preparation for the coming era of computational science with AI initiatives, we are conducting basic research on prediction technology based on neural networks, which is expected to be used in the future in this research project. This year, we tried to reconstruct the flow field for the two-dimensional flow calculated by the unified solution code CUBE based on the neural network (CNN) using the convolutional filter as a machine learning technology that can be used at present. The following network is constructed by following the method [1] of replacing POD (Proper Orthogonal Decomposition) with a neural network for the flow field of the flow around a cylinder.

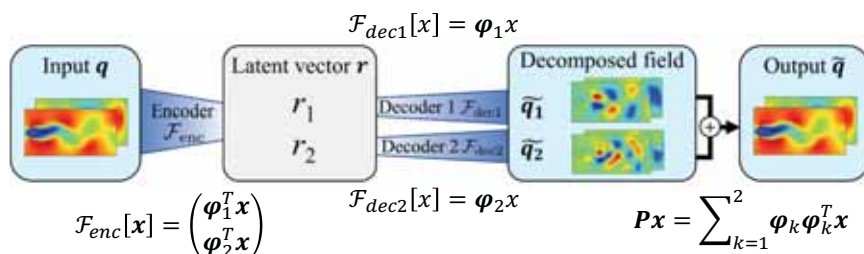


Figure 13.28: Structure of neural network (partially modified figure in paper [1]).

A neural network was trained for 10000 samples of snapshots as input, and the output was evaluated. As a result, the mode decomposition equivalent to that of reference [1], that is, the flow field was decomposed into two modes by a neural network, and the original flow field was reconstructed by synthesizing them, and the

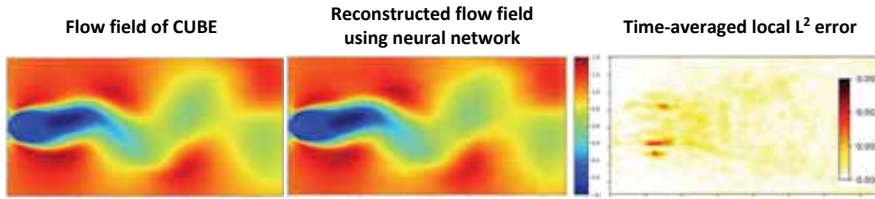


Figure 13.29: Example of flow field reconstruction results.

accuracy was equivalent to that of reference. It was confirmed that the flow field could be reconstructed. Figure 13.29 shows an example of the results.

Currently, only 2D is handled due to computational resources and technical restrictions, but we plan to expand this method in the future and evaluate the effectiveness of this method for 3D problems.

### 13.3.4.3 Unified solver extension using Adaptive Mesh Refinement (AMR)

Adaptive Mesh Refinement (AMR) has been found to be useful and effective for capturing fine structures in fluid analysis, such as where the gradient of a fluid state variable is steep, typically around a fluid-solid interface. Since the calculation grid is dynamically subdivided only where necessary for the solution and shape of the flow that changes quickly, it is not necessary to arrange a high-resolution calculation grid in the entire calculation domain. Costs are significantly reduced, especially in the unified multi-physics analysis such as the moving boundary problem. However, the calculation load balancing for high parallel computing is well known as a difficult task to implement.

The CUBE developed in this research project already has a hierarchical data structure, and has a solution for complex shapes, complex problems (heat, sound, chemical reaction, etc.) and moving boundaries. So, the best approach to introduce the AMR method is to build an extension of the solver. To examine the direction of the approach, we conducted a feasibility study based on several well-known open source softwares, including AMReX [2], which is being developed mainly by the Lawrence Berkeley National Laboratory in the United States. As a first step, we ran some basic simulations in search of new features suitable for our code. Figure 13.30 shows an example of the calculation applied to the vortex movement problem. It can be seen that as time progresses, the subdivided regions of the grid also move. Early studies provided important insights in investigating the low implementation effort and missing features in the available code. In the future, we plan to continue more detailed investigations and finally consider implementing it into CUBE.

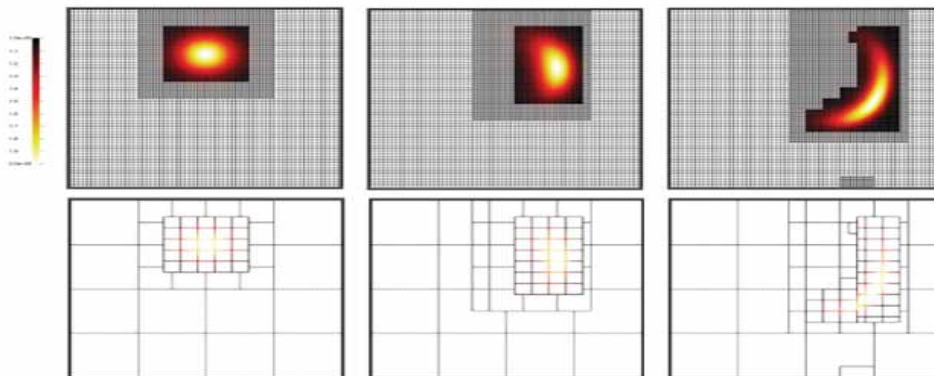


Figure 13.30: An adaptive mesh refinement solution for a typical advection problem.

#### 13.3.4.4 References

- [1] T. Murata, K. Fukami, and K. Fukagata, “Nonlinear mode decomposition with convolutional neural networks for fluid dynamics,” *J. Fluid Mech.* 882, A13 ,2020.  
 [2] AMReX-Codes, <https://amrex-codes.github.io/>, (cited 1st mar. 2020).

### 13.3.5 Strategic development and deployment of industrial software for the construction of digital engineering test beds

#### 13.3.5.1 Realistic automotive engine cycle simulation for the evaluation of the mixing efficiency

As part of the development of an automobile engine testbed, we performed a fuel-air mixing analysis that assumed a practical usage scenario. The fuel-air mixing efficiency plays an important rule for automotive engine design. Generally, through the observation of the fluid structures of the tumble and the swirl shown in Figure 13.31, the efficiency can be evaluated.

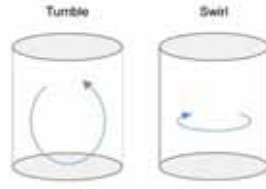


Figure 13.31: The tumble and the swirl.

However, this kind of the turbulent structure is not easy to obtain from the experience. Therefore, the aim of this study is to simulate the cold flow inside the engine using CUBE and visualize the turbulent structure to capture the tumble and swirl. Finally, the different shape of the piston is simulated to evaluate the performance to show that this framework is suitable for the industrial applications. The governing equation and numerical method of this study is as follows.

$$\frac{\partial U}{\partial t} + \frac{\partial F_1}{\partial x_1} + \frac{\partial F_2}{\partial x_2} + \frac{\partial F_3}{\partial x_3} = 0$$

The quantities included in  $U$  and  $F_i$  are

$$U = \begin{pmatrix} \rho \\ \rho u_1 \\ \rho u_2 \\ \rho u_3 \\ \rho e \end{pmatrix}, \quad F = \begin{pmatrix} \rho u_i \\ \rho u_i u_1 + P \delta_{i1} - \mu A_{i1} \\ \rho u_i u_2 + P \delta_{i2} - \mu A_{i2} \\ \rho u_i u_3 + P \delta_{i3} - \mu A_{i3} \\ \rho(e + P)u_i - \mu A_{ij}u_j - k \partial T / \partial x_i \end{pmatrix}$$

where  $A_{ij} = \partial u_i / \partial x_j + \partial u_j / \partial x_i - 2/3(\nabla u \delta_{ij})$  and  $P$  is the pressure given by the ideal gas equation,  $P = \rho RT$ . The low-Mach-fix for Roe (LMRoe) scheme [1] with 5th order MSUCL reconstruction [2] is utilized in convection term and second order central difference is used for the viscous term. For the moving geometry, the immersed boundary method (IBM) which has been implemented in CUBE [3,4] is adopted to the engine motion including intake valve, exhaust valve and piston movement. First, the standard shape of the engine is simulated and the conservation is calculated to validate the practicality of the framework. The computational parameter and the physical model are shown in Figure 13.32. Three different time steps are adopted.

The comparison of the results with the theoretical values from ideal gas state equation is shown in Fig. 13.33. According to the result, when the  $CFL < 10$ , the distribution of the density, pressure and temperature has acceptable agreement with the theoretical result. The suggested reason for the discrepancy is that using the IBM causes the leakage.

Next, the comparison of the different shape of the piston has been conducted. The computational parameter and the different shape of the piston are shown in Figure 13.35. The visualization result of the streamline with the contour of the velocity magnitude is utilized to evaluate the magnitude of the tumble and swirl.

Tab.1 Engine parameters

Engine type	4Cycle Single Cylinder
Bore [mm]	90.0
Stroke [mm]	98.0
Conrod length [mm]	157.5
Piston offset [mm]	9.2
Compression ratio	10.4
Rotational frequency [rpm]	2000

Tab. 2 Initial conditions

Pressure at inlet boundary $p_{in}$ [Pa]	97758.0
Pressure at outlet boundary $p_{out}$ [Pa]	107605.5
Pressure in cylinder $p_0$ [Pa]	107605.5
Viscosity $\mu$ [Pa·s]	$1.85 \times 10^{-5}$
Density $\rho$ [Kg/m <sup>3</sup> ]	1.1842
Gass constant $R$ [J/(K·kg)]	287
Specific heat ratio $\gamma$	1.4
Wall condition	Adiabatic

Tab.3 List of evaluated time steps

Time step $\Delta t$ [s]	$2.0 \times 10^{-5}$	$1.0 \times 10^{-5}$	$5.0 \times 10^{-6}$
Minimum cell size $\Delta x$ [mm]	0.5	0.5	0.5
Courant number	14.28	7.14	3.57
Cube number	4,912	4,912	4,912
Cell number	20,119,552	20,119,552	20,119,552



Shape of engine



Shape of Piston

Figure 13.32: The simulation conditions of the standard shape.

Figure 13.36 shows the results of the visualization result of the streamline with the contour of the velocity magnitude. The result shows that with the convex at the left side of the piston in shape2, the velocity will be decreased. On the other hand, shape1 and 3 still keep strong tumble. However, at the left side of the engine, the tumble in shape3 becomes very weak. Overall speaking, shape1 obtain the strongest tumble.

Figure 13.37 shows the results at CA270 (Crank angle at 270 degrees). The result shows the same trend as Fig. 5 that shape1 is the best shape. However, with the convex shape, the swirl will be enhanced because the flow field will not be symmetric anymore. The flow field in shape3 is not only in vertical direction but also in horizontal direction so the swirl structure can be confirmed.

The results show that the current framework can be a useful tool for the engine design by giving a detail insight of the flow mechanism. However, the calculation condition is still under the cold flow condition. In next step, we are planning to model the combustion inside the engine and conduct direct evaluation of combustion energy efficiency. And also we have started to provide this framework to the industrial user for the evaluation of the usability of the framework. We will continue to improve practicality through the consortium activities.

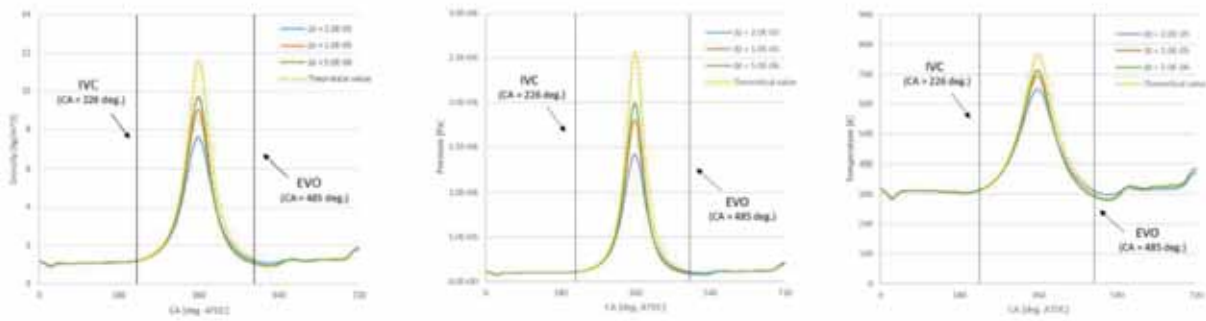


Figure 13.33: The comparison of the density, pressure and temperature.

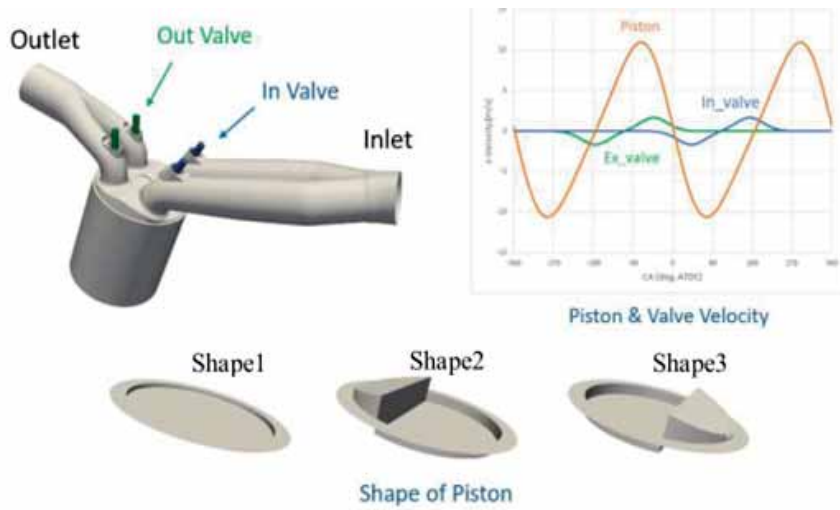


Figure 13.34: Engine cycle condition and piston shapes.

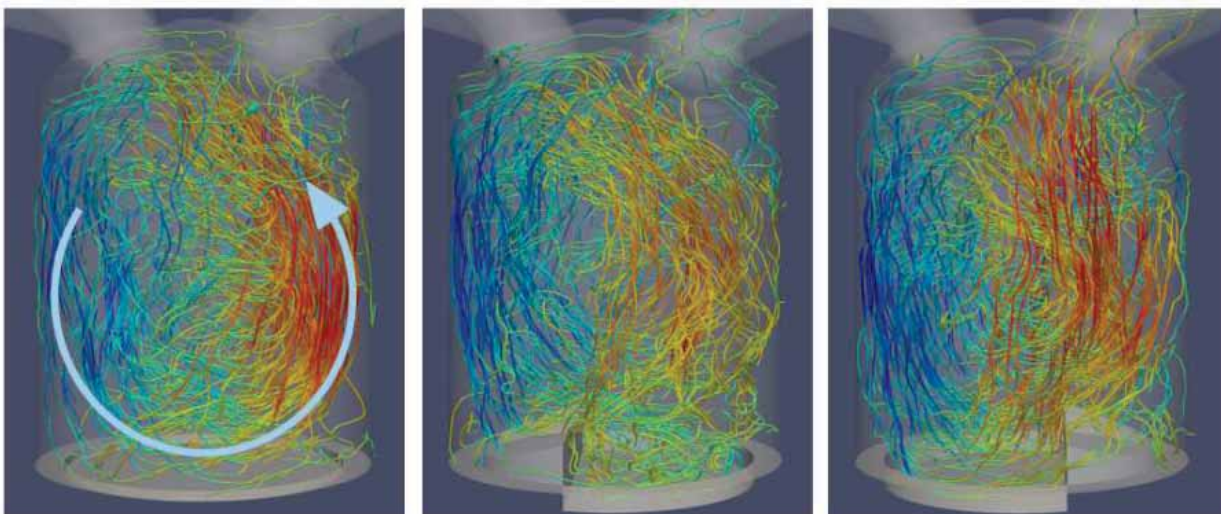


Figure 13.36: The streamline with the contour of the velocity magnitude at BDC.

Engine Type	4Cycle Single Cylinder		
Bore [mm]	78.0		
Stroke [mm]	83.6		
Conrod Length [mm]	133.0		
Piston Offset [mm]	0.5		
Rotational frequency [rpm]	2000		

	shape1	shape2	shape3
Time step $\Delta t$ [s]	$5.0 \times 10^{-6}$	$5.0 \times 10^{-6}$	$5.0 \times 10^{-6}$
Minimum cell size $\Delta x$ [mm]	0.5	0.5	0.5
Courant number	3.57	3.57	3.57
Cube number	3,305	3,285	3,289
Cell number	13,537,280	13,455,360	13,471,744

Figure 13.35: Engine simulation conditions.

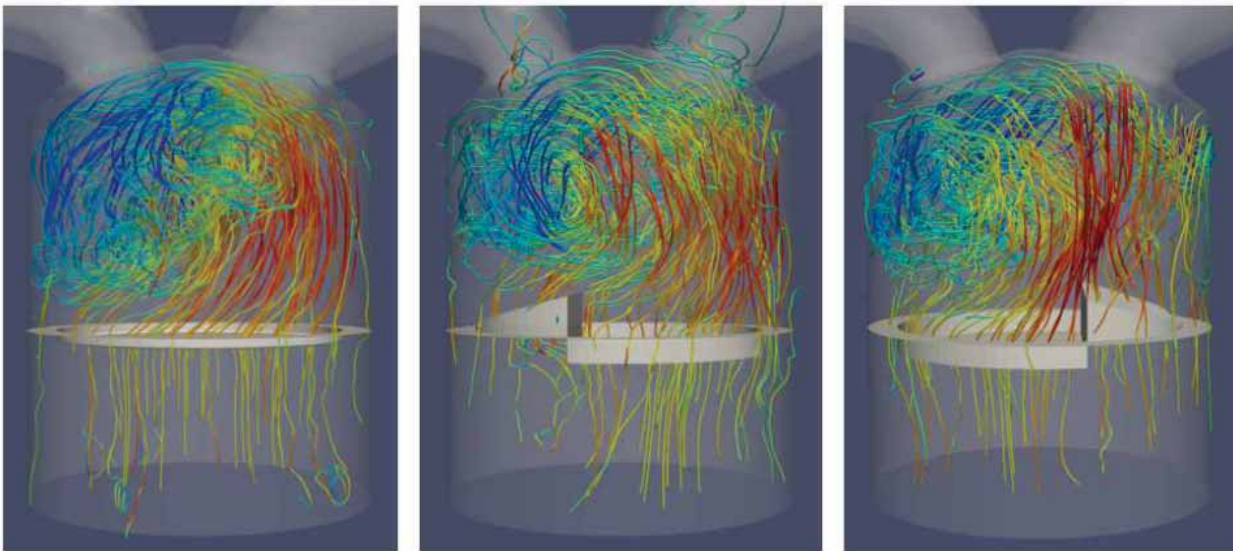


Figure 13.37: The streamline with the contour of the velocity magnitude at CA270.

### 13.3.5.2 Numerical simulation of flow in a fuel-injector of an aircraft engine

As a first step of the development of the combustion system test bed, the flow simulation of the jet engine combustor was performed. An investigation of grid sensitivity on local mesh refinement of numerical simulation of cold-flow in a fuel-injector of an aircraft engine was performed. In the case of an aircraft engine, a critical variable that governs emission, efficiency, and reliability is the equivalence ratio inside the combustion chamber. This value is transported by swirling turbulent flow from fuel-injector to the combustion chamber. Therefore, prior to precise prediction and appropriate control of the combustion characteristics of the engine, as a first step, the transport characteristics of flow through fuel-injector can be investigated through cold flow simulations. A complete evaluation of flow characteristics of the engine requires numerical simulation with the entire annular combustor geometry, which demands massive computational resources. Thus, an optimization strategy to minimize the computational cost through mesh optimization is warranted.

The cold flow simulations were carried out using CUBE, which is developed through this research. CUBE is a multiphysics simulation framework designed for large scale industrial simulations. A hierarchical meshing

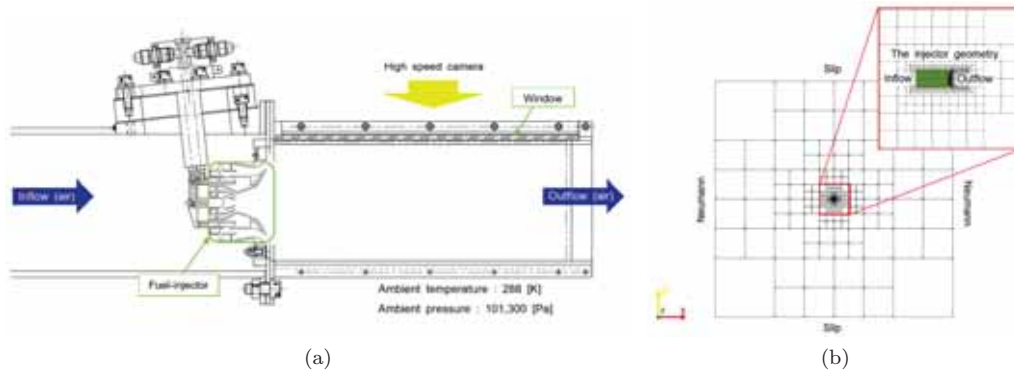


Figure 13.38: (a) The PIV measurement setup, (b) Numerical mesh and boundary condition

technique known as building cube method (BCM) is the foundation of CUBE over which numerical solvers are built. Even with the use of BCM for meshing the fuel-injector geometry, using a same near wall spacing mesh over the entire geometry results in excessively large numerical mesh. Consequently, relevant geometric components of the injector that strongly influence the flow have to be identified for mesh refinement while coarser mesh can be used for rest of the geometry. Then it is important to investigate the dependence of flow on the refined mesh and to minimize the total mesh size while ensuring accuracy. The governing equations used in this study are same as previous section. This is fully compressible flow approach. A 2D PIV measurement of air flow in a fuel-injector was conducted by Kawasaki Heavy Industries. The detail flow field results were compared with the measurement result. The experimental setup and the measurement window are shown in Fig. 13.38. In order to validate the accuracy, a very high-resolution mesh was used. The geometry used in the simulation is highlighted as the fuel injector in Fig. 13.38. The boundary conditions and the mesh are also shown in Fig. 13.38. The wall boundary condition, which means the boundary condition on the surface of geometry, was set as adiabatic condition. The inflow mass flow rate was set as the same value of PIV measurement and the ambient pressure 101,300 Pa, ambient temperature 288 K was set. The finest mesh resolution was 0.05 mm and the number of calculation mesh was 500 million. The 2048 nodes of K-computer was used and the calculation time was 48 hours to obtain the physical solution time of 2.7 s.

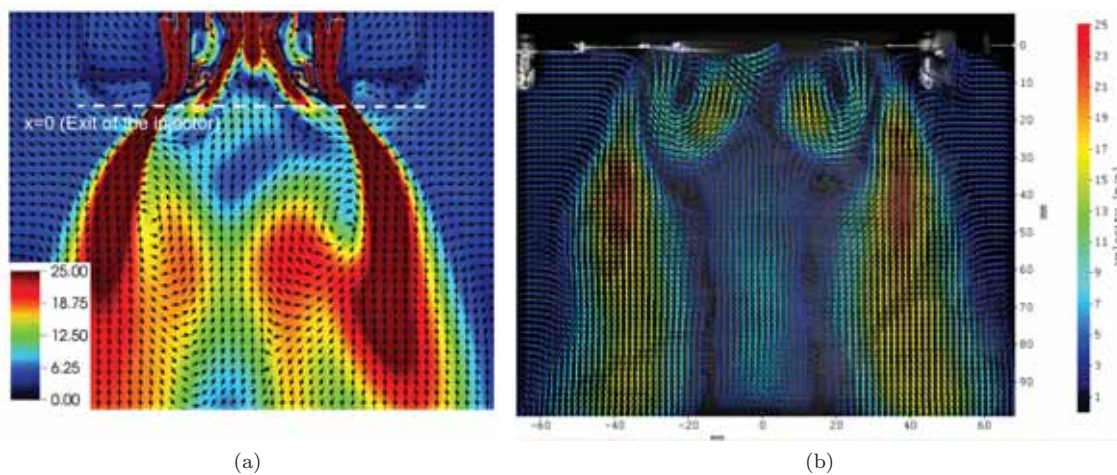


Figure 13.39: (a) Time averaged velocity magnitude high-resolution simulation, (b) Time averaged velocity magnitude 2D PIV data

Velocity magnitude contours on a mid-sectional plane from the PIV measurement and the numerical simulation are shown in Fig. 13.39. Four distinct identifiable flow signatures, in the exit plane are identified in

Fig. 13.40. The flow signatures are termed as A, B, C and D, in the PIV result, and A', B', C' and D' in the simulation result. First, A (and A') is the primary jet emanating out of the injector. A' shows greater velocity magnitude than A. In both cases, the flow gradually decelerates as it heads downstream. The flow signature B is the formed by the flows from the pilot region and air-silt nozzle. It is observed that B is separated from A and forms vortex. On the other hand, B' does not form any vortex but just joins into A', supplying momentum to A'. It is hypothesized that intrinsically, B' is just sucked into A' because of the large velocity magnitude in the exit-vicinity region of A'. Meanwhile, C' is more widely distributed although C is localized in narrow region. It is regarded that the absence of vortex in B and the intensity difference primary jet (A-A') may affect the distribution. Furthermore, the velocity magnitude of the flow in C' greater than the flow in C and it is likely that this is due to the difference in intensity of the primary jet, i.e. A-A', which induces C-C'. Finally, D' stretches longer than D up to the exit of the injector. It can be considered that the greater intensity in the region C' and the absence of vortex in B' assists the flow in D' stretching it longer than its PIV counterpart D.

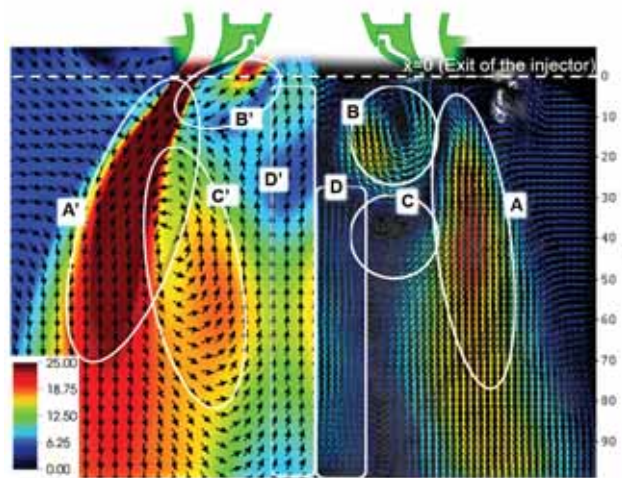


Figure 13.40: A comparison of the simulation and PIV results: 4 prominent features can be identified in each case.

To sum up, the overall difference of the velocity magnitude is due to that PIV data does not contain the depth component. Meanwhile, it is regarded that the local differences are mainly affected by the difference between B and B' induced by overestimation of A'. Therefore, this is the sole qualitative difference between the simulation and the PIV data. It can be inferred that the simulation qualitatively resolves the injector flow. In the next step, we are planning to develop the fuel spraying model and the combustion model which is specifically designed for the real engine combustors. We will continue to develop the functionality to reproduce the real state of engine combustion through the consortium activities.

### 13.3.5.3 Construction of surrogate model by aerodynamic multipurpose shape optimization analysis and machine learning

In this study, we have developed a multipurpose optimization analysis framework using CUBE for the purpose of efficiently optimizing aerodynamic performance at the initial design stages. This framework provides CHEETAH [5], a multipurpose evolution optimization software, in collaboration with the Japan Aerospace Exploration Agency. CUBE has a data structure with a hierarchical Cartesian grid, and MeshWorks [6] is applied, which is a shape morphing software by Detroit Engineered Products, Inc. It is a method that can be shared with a single calculation grid for a plurality of changing vehicle shapes, and can avoid problems related to calculation grid generation and morphing.

Continuing from last year, we performed genetic-evolutionary computation up to the 12th generation with a 4-objective function with the aim of obtaining an index of robustness against changes in the wind direction of sedan-type automobile models. The population size was 18, and a total of 252 cases of  $36 + 18 + 18 \times 12$  generations including individuals in the L36 orthogonal table for generating the initial generation population. And 2 wind directions for each needed to be calculated. Each case was calculated with 367 nodes of “K-computer” with 14 hours, and the total amount of calculation was about 2.6 million node-hours (including the

amount used last year). Figure 13.41 shows the Pareto solution for the difference between the aerodynamic resistance value ( $C_d$ ) and the resistance to the wind direction ( $\Delta C_d$ ). The tendency of the objective function value similar to the knowledge obtained in the actual design was reproduced, and the validity of the framework could be confirmed.

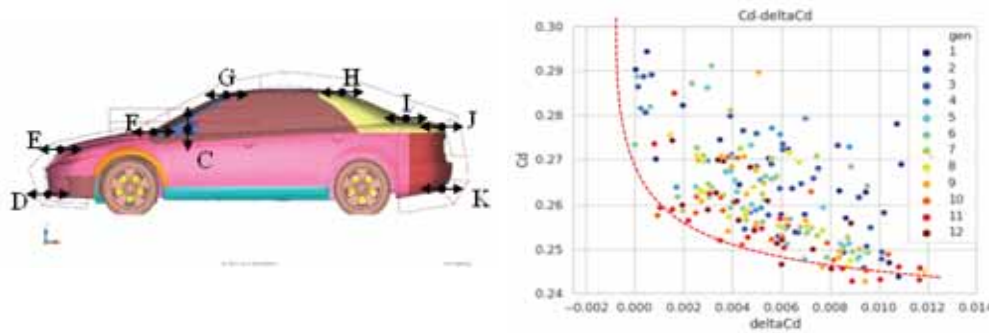


Figure 13.41: The geometry deformation parameters (left) and optimized results of Pareto solution on 12th generation (right).

In this physical year, we tried to build a surrogate model by machine learning utilizing these results as training-data. For neural networks constructed using Sony’s Neural Network Console [7], 18 individuals  $\times$  1 to 6 generations = 108 models were used for training-data, and 18 individuals  $\times$  7 to 12 generations = 108 models were used for evaluation-data. The input was 9 design variables, and  $C_d$  and  $\Delta C_d$  were targets. Figure 13.42 shows the aerodynamic drag obtained by calculation and the predicted result by machine learning. The  $C_d$  value was predicted almost accurately, and it could be confirmed that the constructed neural network was appropriate. It has also been confirmed that the Pareto solution based on this prediction result shows the same tendency as the solution obtained by the actual CFD calculation. This suggests that machine learning can be a powerful design tool in the future if appropriate design variables can be selected. However, there are some models whose prediction results are different with respect to the difference in aerodynamic drag, and there are also subtle differences in the obtained sedan-type optimum body shape. We are proceeding with consideration including investigation of the factors causing it. In the future, we plan to introduce design variables that reproduce more detailed shapes and improve the degree of freedom, which will lead to the creation of results in “Fugaku”.

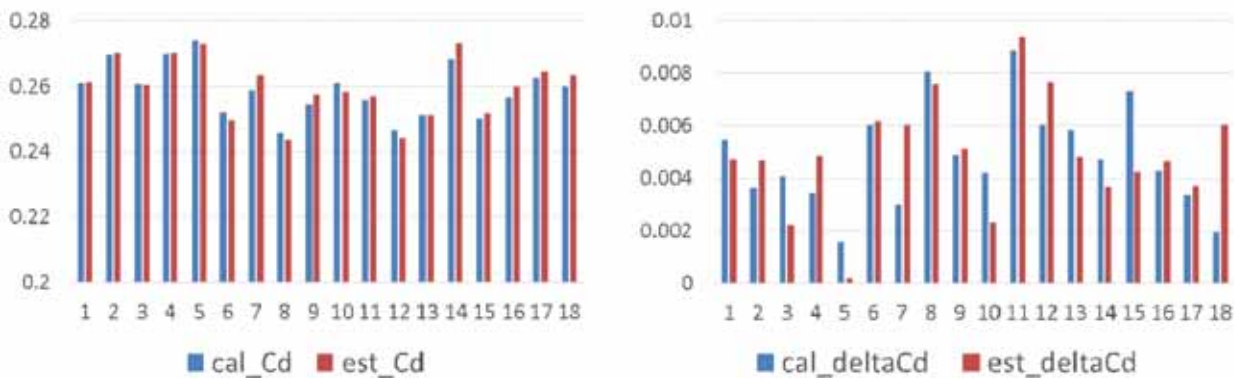


Figure 13.42: The prediction results using machine learning (left) drag (right) drag difference between 0 and -3 yawing angle.

#### 13.3.5.4 Wind resistant design of building structures – fluid structure coupled analysis of high-rise towers

As an issue of the architectural consortium, verification analysis of a test bed based on a unique fluid structure coupled analysis method was performed. In recent years, with the increase in the height of buildings and the reduction in the weight of construction materials, there have been increasing cases of construction of high-rise buildings and large-scale structures having roofs using light materials. Since the design of these structures requires low attenuation due to weight reduction, it is necessary to examine the wind resistance as well as the seismic resistance for earthquake. In particular, unstable aerodynamic vibrations caused by the interaction between the vibrations of the building itself and the flow field around the building due to the turbulence of the wind have a risk of causing a large amplitude leading to collapse of the building. Generally, a building is heavy and hard to be deformed as compared with a bridge or other structure. Therefore, conventionally, there has been no problem with dynamic vibration, and it has been a problem to secure the building resistance to a static wind load. However, with the emergence of such high-rise buildings, it has become important to study the problem of vibration when the buildings are subject to strong winds. Thus, it is important to grasp the structural characteristics in wind load evaluation. Figure 9 shows the mechanism of the generation of unstable vibration generated by the interaction between wind turbulence and the vibration of the building itself. Vigorous research has been conducted on the unstable vibration phenomenon of buildings in the past, however there are still many unknowns about the mechanism of occurrence and the influence of the interaction between them, and aerodynamic instability. It has been pointed out that when studying unstable phenomena such as vibration, the phenomena cannot be reproduced unless the structure and the surrounding flow field are treated as a strongly coupled problem. There is few software that can achieve this. In this project, we have developed a unique fluid-structure strong coupled unified solution that combines marker particles with the Euler-type structural analysis method. In order to prove the validity of the method, detailed verification analysis was performed using basic tower structure.

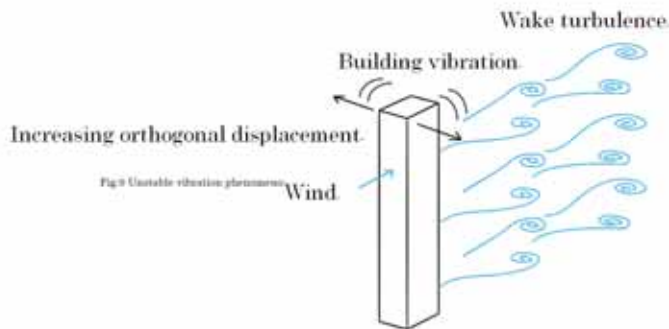


Figure 13.43: Unstable vibration phenomenon of high-rise building.

In order to verify the validity of this method, first, a fluid-structure interaction analysis with a rigid structure was performed. The structural shape is a quadrangular prism of  $0.1 \times 0.1 \times 0.1m$ . We compare it with the results of previous experiments. The calculation conditions, analysis mesh and inflow fluctuation wind are as follows.

Figure 13.48 shows a comparison with the results of previous wind tunnel experiments. The black line represents the result of the calculation by this method, and the blue line represents the result of the previous experiment, and it can be confirmed that the values agreed well.

Considering the introduction of this method to architectural structures, numerical stability was examined by performing analysis with various conditions of prismatic structures. Four cases were prepared in which the Reynolds number was fixed at 10, the mass density difference between the solid and the fluid, and the shear modulus of the solid has been changed. The analysis results are shown in Fig. 13.49-13.50. From these results, it was found that numerical instability occurred near the prisms in all models due to the numerical calculation method of solid strain. In the next step, we plan to introduce a method that can stably calculate the solid strain without depending on the velocity field. We will continue to develop the functionality to produce the practically useful framework for the strong-coupling fluid-structure interaction through the consortium activities.

Calculation region	X : -0.55~1.45 , Y : -0.5~0.5 , Z : 0~2.0 (m)
Mesh	About 36000000
Minimum cell size	0.000977(m)
Re	65846
Resolution	$\Delta t = 0.0005, 0.0050(\text{Minimum})$
Timeintegration	2nd order Crank-Nicolson
Spatial discretization	Convective term : 2nd order Central + 5% Upwind Diffusion term : 2nd order Central
Boundary condition	Inlet : Inflow turbulence Outflow : Convective Wall : Volume Constraint IBM , Side , Top : Slip
Iteration number	30
Pressure convergence	1d-5

Figure 13.44: Calculation conditions.

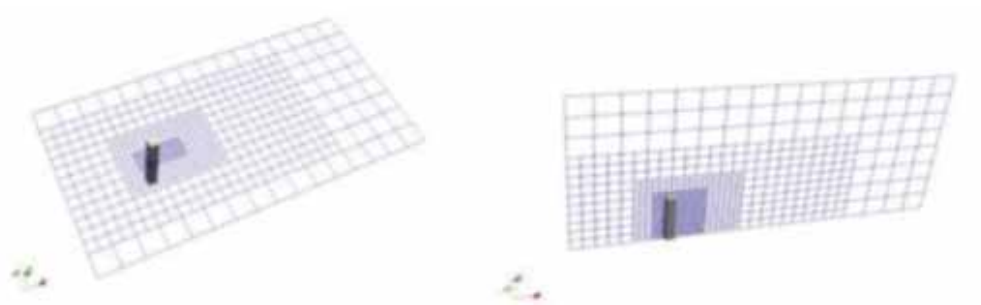


Figure 13.45: CUBE mesh.

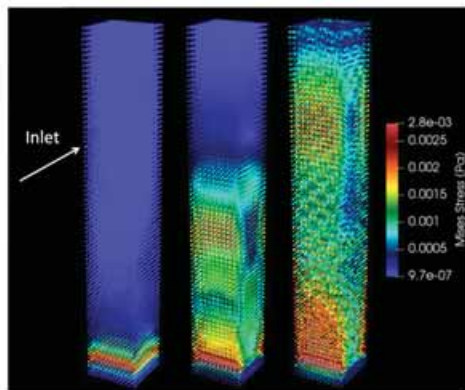


Figure 13.49: Mises stress distribution of CASE-D.

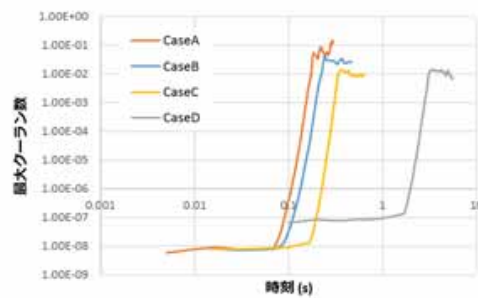


Figure 13.50: Comparison of calculation stability of each case.

Finally in this fiscal year, we conducted a simulation of wind resistance analysis of the dome roof of a stadium structure as an application to practical problems. The flow condition is 10 m/s of air wind, the Reynolds number is approximately 273 million, and the soft material property is set as 33,300 Pa of elastic modulus,  $300\text{kg}/\text{m}^3$  of the mass density of solid. The number of the cell was approximately 17 million, and the calculation time was 10 hours using 256 nodes of K-computer. Figure 13.51 shows a typical flow field coupled with the soft material deformation of the stadium roof. We cannot say anything about the validity of this result or its physics yet. However, this result may be the world's first example of solving FSI problems at a high Reynolds number over hundred million by an Eulerian FSI method. At least, we did not observe the unphysical deformation of the roof region (sponge) induced by wind force. In the next step, we plan to increase the resolution of calculation mesh to try to capture smaller flow structures and deformation modes. We will continue to contribute to help users to apply this method into the practical cases through the consortium activities.

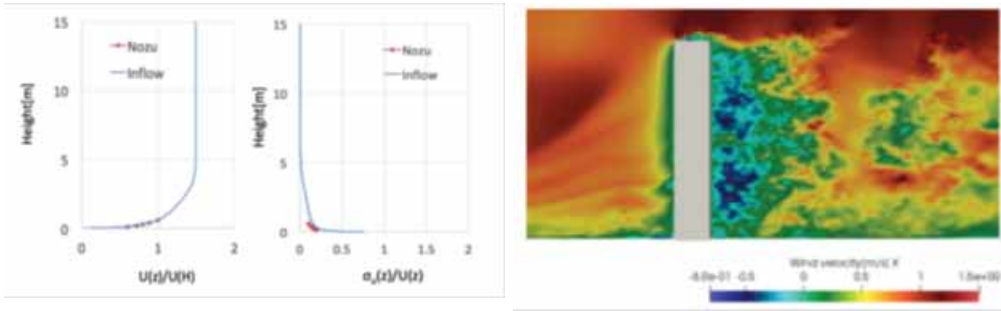


Figure 13.46: Inflow fluctuating wind profile. Figure 13.47: X-direction velocity distribution in vertical section of prism.

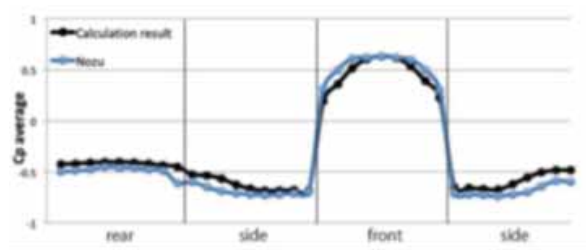


Figure 13.48: Horizontal mean wind pressure coefficient distribution of prism: comparison with previous experimental results.

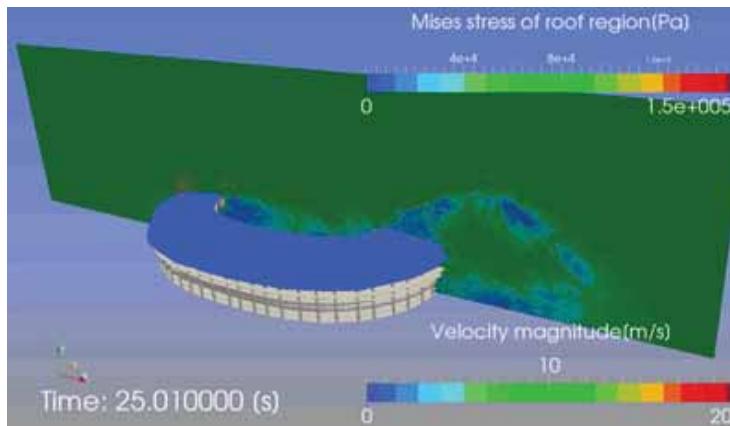


Figure 13.51: Example of flow and stress results on deformable roof analysis for a stadium structure.

**13.3.5.5 Topology optimization using Eulerian structure analysis**

Topology optimization [8] is a method to determine the arrangement of materials and components, including the voids, to maximize or minimize the objective function using a limited material volume in the design space. In recent years, industrial applications of topology optimization have been increasing as it provides effective suggestions to designers. On the other hand, when considering the application to a real product, the volume of the actual product material is usually less than 1% of the design area expected by the designer. In addition to this, the preparation of design-domain shape modeling, which includes many cases and trials in the upstream of the design process, requires a lot of time and effort. In this study, we are developing an original unified fluid-structure analysis method based on Eulerian methods combined with the Lagrangian marker particle method to solve a large-scale structural analysis problem which is difficult to be solved by conventional methods. The

marker particle method is one of the most promising methods to solve the topology optimization challenges mentioned above, because it is easy to achieve high parallelization efficiency and to reduce the time and effort of mesh generation in a massively parallel computing environment. In this year, we have developed a topology optimization framework using Eulerian structural analysis method. To verify the validity of the topology optimization, the optimization of the maximum amount of energy absorbed by a two-dimensional structure with a circular hole in the center of the design region under enforced velocity loading in the direction of shear was carried out. The results are comparable to those obtained by the finite element method, even when CUBE is used. In addition, the quantitative value of the objective function also approaches that of FEM by increasing the spatial resolution.

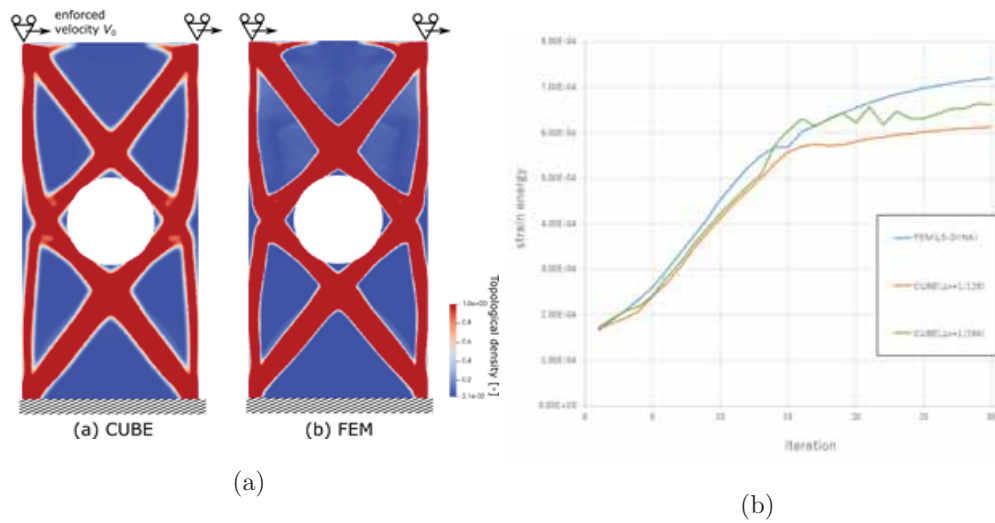


Figure 13.52: Optimal shape as a result of topology optimization to maximize absorption energy by shear enforced velocity load (left), and its objective function history (right).

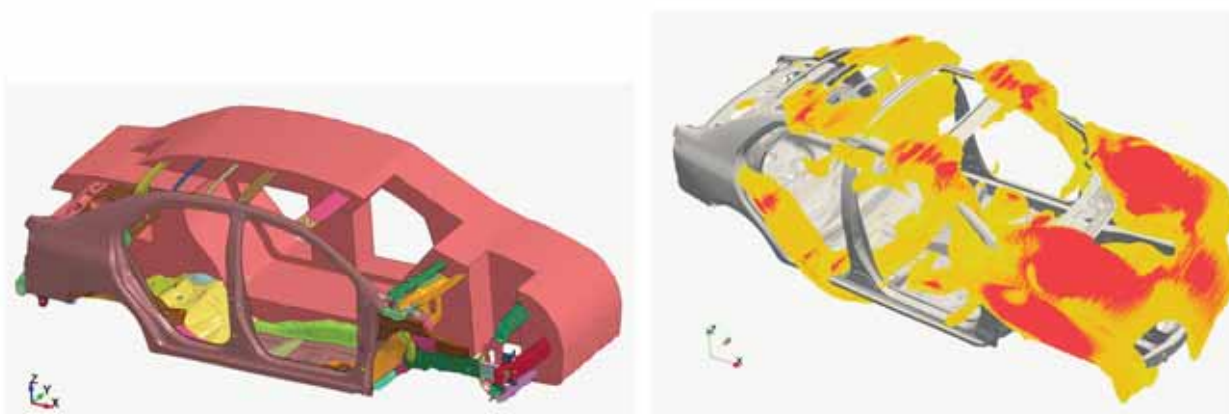


Figure 13.53: Design area which surrounds a conventional white body frame (left) and optimal shape as a result of topology optimization subject to torsional enforced velocity load (right).

Using this framework, we performed optimization trials for a car body frame with 10 million design variables, which is somewhat difficult to do with existing topology software (Fig. 2). A design domain was set up over the white body frame of an existing published body model (TOYOTA, Yaris 2010, [9]), and forced-velocity loads were applied to the design domain to maximize the amount of energy absorbed by the body torsion. As a result, a frame structure close to the intended white body frame was obtained. In the future, we will continue to carry out various basic verification examples and optimization verifications for a large number of load cases that are

assumed to be real problems, as well as to improve the optimization performance through collaboration with industry.

### 13.3.5.6 Implementation of aerodynamic body motion coupled analysis framework

In recent years, it has become clear that the evaluation of unsteady aerodynamic force that reproduced in the actual running state is indispensable for the aerodynamics parts design, since it affects the evaluation of steering stability of automobiles. In general, it is difficult to accurately capture the flow field around a vehicle during actual driving motion and to measure changes in vehicle attitude. And the actual driving test is affected by atmospheric disturbances, so the same situation should be reproduced. Additionally, it is difficult to evaluate the steering stability by quantitative evaluation depending on the driver's experience. Therefore, in this research, we constructed an analysis framework that can reproduce the actual driving state by combining aerodynamic analysis with vehicle motion on a supercomputer, which includes suspension, steering mechanism and driver's operation reaction, etc.

This framework adopts the implementation of the open source multibody dynamics analysis software, named Project Chrono [10], into the CUBE. It is possible to use commercial vehicle motion analysis software, but in order to operate it on a supercomputer, we have experienced problems such as binary support, license handling, and external communication of calculation nodes. So an open source framework is powerful solution, the significance of being able to do it is high rather than other researchers think. In this year, we succeeded in constructing this framework and implemented a practical example of vehicle motion analysis.

A hatchback type real vehicle shape model was used for the analysis. The model also reproduces detailed shapes such as underfloor and auxiliary equipment inside the engine room. We are comparing steering stability with and without aero parts mounted on the side of the vehicle. In this case, the suspension and steering mechanism of the same type as the actual vehicle could be used. Assuming a lane change movement to the overtaking lane-change maneuvering on the highway, the steering stability was evaluated for the movement to the right side 3 m at 100 km/h.

Figure 13.54 shows an example of visualization results of flow field and motion analysis. A correlation has been shown between the sensory evaluation of steering stability and the roll motion of the vehicle. When evaluated by focusing on the roll motion and the steering input by the driver (Fig. 13.55), both the angular velocity and the angular jerk (time change of acceleration) showed a decrease in peak and amplitude when the roll motion in the first half converged. Results consistent with the report were obtained in the driver's sensory test. In the future, we plan to make improvements to create results on "Fugaku" while conducting higher resolution analysis and improving versatility.

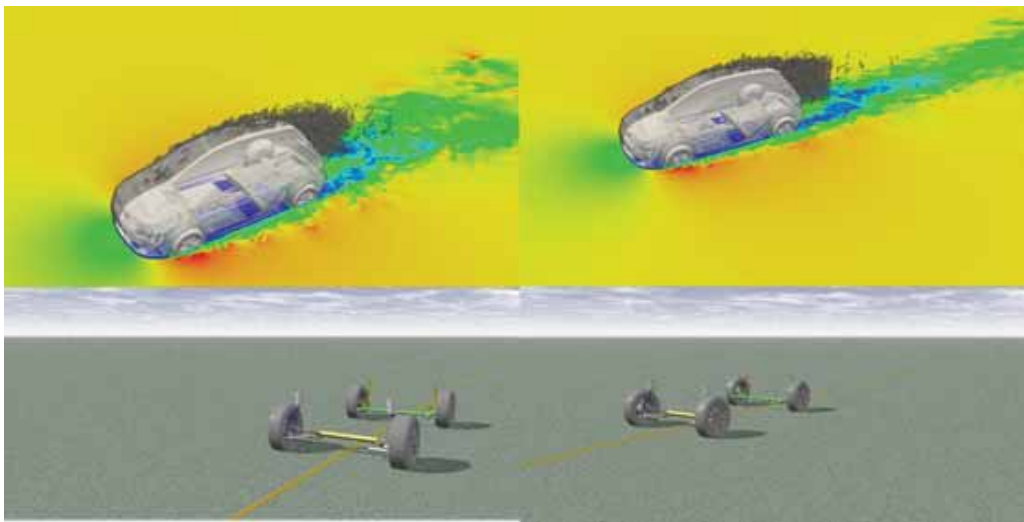


Figure 13.54: Analysis example of lane change maneuver (upper: CUBE result, lower: motion analysis visualization result).

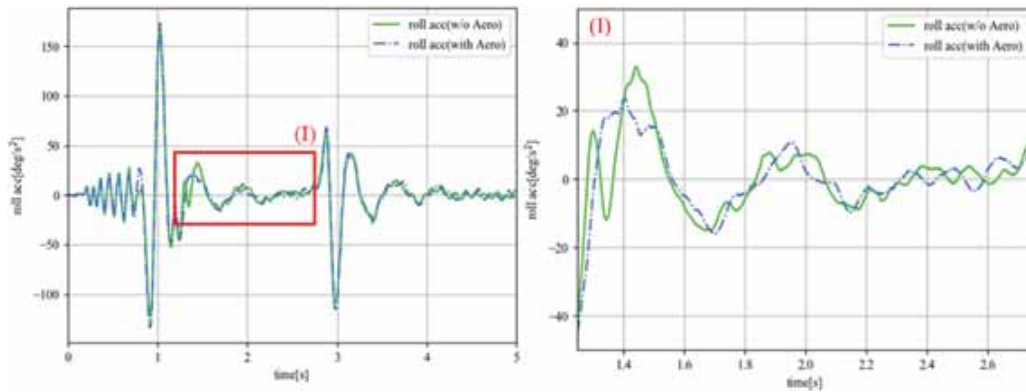


Figure 13.55: Results of roll angular velocity of vehicle motion.

### 13.3.5.7 References

- [1] F. Rieper, “A low-Mach number fix for Roe’s approximate Riemann solver,” *J. Comput. Phys.*, 230, pp. 52635287, (2011).
- [2] K.H. Kim, C. Kim, “Accurate, efficient and monotonic numerical methods for multi-dimensional compressible flows Part II: Multi-dimensional limiting process,” *J. Comput. Phys.*, 208, pp.570615, (2005).
- [3] C.-G. Li, M. Tsubokura, R. Bale, “Framework for simulation of natural convection in practical applications,” *Int. Commun. Heat Mass Transf.*, 75, pp.5258, (2016).
- [4] N. Jansson, R. Bale, K. Onishi and M. Tsubokura, CUBE, “A scalable framework for large-scale industrial simulations, International,” *Journal of High Performance Computing Applications*, Vol.33, pp.678-698, (2018).
- [5] A. L. Jaimes, A. Oyama, and K. Fujii, “A ranking method based on two preference criteria: Chebyshev function and e-indicator,” *Proceedings of 2015 IEEE Congress on Evolutionary Computation*, (2015).
- [6] MeshWorks WEB site, <https://www.depusa.com/meshworks/>, [cited 1 Mar 2020].
- [7] Neural Network Console WEB site, <https://dl.sony.com/ja/>, [cited 1 Mar 2020].
- [8] M.P. Bendsøe, N. Kikuchi: “Generating optimal topologies in structural design using a homogenization method,” *Comput.Methods in Appl.Mech.Eng.* Vol 71, No. 2, pp. 197 224 (1998).
- [9] Center for Collision Safety and Analysis: “2010 Toyota Yaris Coarse Finite Element Model Version 1l”, 2016 Dec. URL: <https://www.ccsa.gmu.edu/models/2010-toyota-yaris/>
- [10] Project Chrono WEB site, <https://projectchrono.org/>, [cited 1 Mar 2020].

## 13.4 Schedule and Future Plan

In the research and development of unified simulation framework ‘CUBE’ from 2012, the following goals has been achieved:

1. Construction and development of the simulation technology for bringing out the performance of K-computer
2. Validation and practical usage of industrial applications such as vehicle aerodynamics, aeroacoustics, unsteady motion aerodynamics, engine combustion, city area wind environment analysis, sport CFD, and structure analysis
3. Preparation of the simulation technologies of HPC toward EXA-scale

In the long-term objectives, the following target is considered:

1. Establishment of the research and development center for industrial simulation technology
2. Contribution to computer science by expanding the developed simulation technology to different fields

In terms of using Cartesian grids, the problems that the analysis accuracy in the vicinity of the wall surface decreases due to the limitation of immersed boundary method is becoming clear. In the future, through the

deployment of CUBE to the industrial applications, the introduction of higher order schemes, wall modeling and advance sophisticated research of immersed boundary method are planning.

In terms of structure analysis, to avoid this numerical oscillation even when the spatial resolution is low, we are going to introduce a calculation method for solid deformation tensors that does not require velocity gradient calculation and we continue to work on development to improve analysis accuracy.

In terms of using Hierarchical grid system, the problems that the interface communication in each halo of cubes will spoil the performance on future supercomputers is becoming clear. In the future, the enhancement to the current communication / calculation overlapping technique, or tuning for the interface communication, introduction of adaptive refinement scheme are planning.

From collaborative companies, including companies through the activities of the “Consortium for Next Generation Automotive CAE using HPC” and “Consortium for Next Generation Combustion CAE using HPC” organized by RIKEN, voices of surprises and expectation for software development have been received. We are planning to continue development for practical application in near future.

## 13.5 Publications

### 13.5.1 Articles/Journal

- [1] Rahul Bale, Neelesh A. Patankar, Niclas Jansson, Keiji Onishi, and Makoto Tsubokura, “Stencil Penalty approach based constraint immersed boundary method,” *Computers & Fluids*, Vol.200(30), 104457, (2020).
- [2] Koji Nishiguchi, Tokimasa Shimada, Masafumi Otaka, Shigenobu Okazawa, Makoto Tsubokura, “Eulerian finite volume formulation using Lagrangian marker particles for compressible solid analysis,” *Journal of Japan Society of Civil Engineers, Ser. A2 (Applied Mechanics (AM))*, 75(2), I\_237-I\_248, (2019).
- [3] Keiji Onishi, Makoto Tsubokura, “Topology-free immersed boundary method for incompressible turbulence flows: An aerodynamic simulation for ‘dirty’ CAD geometry”, arXiv preprint, arXiv:2002.06206, (2020)

### 13.5.2 Conference Papers

- [4] Keiji Onishi, Rahul Bale, Makoto Tsubokura, “Assessment of Rotating Wheel Vehicle Aerodynamics Simulation using Cartesian Grid Method and Open-grill Full Vehicle Models,” *SAE Technical Paper 2019-01-0660*, (2019).
- [5] Onishi Keiji, Jansson Niclas, Tsubokura Makoto, “In-situ visualization on large scale vehicle aerodynamics simulation,” In: *Proceedings of the 24th Conference on Computational Engineering and Science*, A-05, (2019).
- [6] Rahul Bale, Kazuto Ando, Yuki Hayashi, Keiji Onishi, and Makoto Tsubokura, “Analysis of underwater undulatory swimming using self-propulsion simulations,” In: *Proceedings of the 24th Conference on Computational Engineering and Science*, (2019).
- [7] Koji Nishiguchi, Tokimasa Shimada, Masafumi Otaka, Shigenobu Okazawa, Makoto Tsubokura, “Eulerian finite volume formulation using particle-in-cell method for large-scale parallel simulation of complex structures,” *Proceedings of ECCOMAS MSF 2019 THEMATIC CONFERENCE*, 4 pages, Sarajevo(Bosnia-Herzegovina), (2019).
- [8] Koji Nishiguchi, Rahul Bale, Tokimasa Shimada, Masafumi Otaka, Hirofumi Sugiyama, Shigenobu Okazawa, Makoto Tsubokura, “Eulerian finite volume formulation using Lagrangian marker particles for compressible solid analysis,” In: *Proceedings of the 22nd JSCE Applied Mechanics Symposium*, C000134, (2019).
- [9] Koji Nishiguchi, Tokimasa Shimada, Masafumi Otaka, Shigenobu Okazawa, Makoto Tsubokura, “Structure analysis with particle-in-cell method using hierarchical Cartesian mesh,” In: *Proceedings of the Conference on Computational Engineering and Science 24*, A-05-02, (2019).
- [10] Tokimasa Shimada, Koji Nishiguchi, Shigenobu Okazawa, Makoto Tsubokura, “Eulerian Unified Formulation Using Lagrangian Marker Particles for Fluid-Structure Interaction Problems,” In: *Proceedings of the 33th Computational Fluid Dynamics Symposium*, E11-4, (2019).
- [11] Hiromasa Kajimoto, Shunpei Koyama, Rahul Bale, Keizo Yamamoto, and Makoto Tsubokura, “Aerodynamics simulation framework for Ski-jumping take-off and its application to various jumpers,” In: *Proceedings of the 33th Computational Fluid Dynamics Symposium*, D01-4, (2019).
- [12] Yotaro Nomoto, Rahul Bale, Keiji Onishi and Makoto Tsubokura, “Construction of a Car Aerodynamic-Motion Coupled Analysis Framework Using Hierarchical Orthogonal Grid,” In: *Proceedings of the 33th Computational Fluid Dynamics Symposium*, B07-1, (2019).
- [13] Younghwa Cho, Rahul Bale, Chung-Gang Li, Tomonari Satoh, Ryusuke Matsuyama, Takeo Oda, Makoto

Tsubokura, Nobuyuki Oshima, “Numerical simulation of flow in a fuel-injector of an aircraft engine,” In: Proceedings of the 33th Computational Fluid Dynamics Symposium, (2019).

[14] Tetsuro TAMURA, Yong CAO, Yuki NAGAO, Hidenori KAWAI, Koji NISHIGUCHI, Makoto TSUBOKURA, “High performance computing of wind-induced pressures on various domes under real conditions,” Proceedings of the IASS Annual Symposium 2019 (FORM and FORCE 2019, Barcelona, Spain), pp.1185-1192, (2019).

### 13.5.3 Posters

[15] Kazuto Ando, Rahul Bale, Keiji Onishi, Kiyoshi Kumahata, Kazuo Minami, Makoto Tsubokura, “Optimizing Multigrid Poisson Solver of Cartesian CFD code,” SC19 - International Conference for High Performance Computing, Networking, Storage and Analysis, Denver(CO), (2019).

[16] Onishi Keiji, Bale Rahule, Tsubokura Makoto, “Research and development of automotive aerodynamic simulation method for WLTP,” Japan Society of Mechanical Engineers, the 97th Fluid Engineering Division Conference, (2019).

[17] Bale Rahul, Wang Wei-Hsiang, Li Chung Gang, Onishi Keiji, Uchida Kenji, Hidefumi Fujimoto, Tsubokura Makoto, “Numerical Simulation of Combustion in a Rapid Compression Machine (RCM),” Japan Society of Mechanical Engineers, the 97th Fluid Engineering Division Conference, (2019).

[18] Ando Yasunori, Li Chung Gang, Onishi Keiji, Tsubokura Makoto, “The Prediction of Narrowband Noise Emitted from Real Vehicle Shape,” Japan Society of Mechanical Engineers, the 97th Fluid Engineering Division Conference, (2019).

### 13.5.4 Invited Talks

### 13.5.5 Oral Talks

[19] Keiji Onishi, Yasunori Ando, Kosuke Nakasato, Makoto Tsubokura, “Assessment of Rotating Wheel Vehicle Aerodynamics Simulation using Cartesian Grid Method and Open-grill Full Vehicle Models,” WCX19: SAE World Congress Experience, Detroit (MI), (2019).

[20] Keiji Onishi, Makoto Tsubokura, “Toward Realization of Real-Time Vehicle Aerodynamics Simulation,” ASME-JSME-KSME Joint Fluids Engineering Conference (AJK Fluids2019), San Francisco, CA, (2019).

[21] Koji Nishiguchi, Rahul Bale, Tokimasa Shimada, Masafumi Otaka, Shigenobu Okazawa and Makoto Tsubokura, “Eulerian Finite Volume Formulation using Lagrangian Marker Particles for Deformable Solid-Fluid Interaction Problems,” Proceedings of the 7th Asia-Pacific Congress on Computational Mechanics (APCOM, Taipei), (2019).

[22] Koji Nishiguchi, Tokimasa Shimada, Rahul Bale, Shigenobu Okazawa, Makoto Tsubokura, “Particle-In-Cell Method using Hierarchical Cartesian Mesh for Deformable Solid-Fluid Interaction Problems,” Proceedings of VIII International Conference on Coupled Problems in Science and Engineering, 1 page, Sitges (Spain), (2019).

[23] Shunpei Oyama, Keizo Yamamoto, Hiromasa Kajimoto, Rahul Bale, Jun Ikeda, Makoto Tsubokura, “Unsteady aerodynamics simulation for the influence of difference in posture change on aerodynamics and flight distance in ski jump take-off motion,” JSME Symposium : Sports engineering and Human Dynamics, B-2, (2019).

[24] HsuehJui Lu, ChungGang Li, Akiyoshi Iida, Tsukasa Yoshinaga, Kazunori Nozaki, Makoto Tsubokura, “A framework for simulation of sibilant fricatives using implicit compressible flow solver,” The 72nd Annual Meeting of the American Physical Society’s Division of Fluid Dynamics (APSDFD)(Nov 23-26 2019, Seattle), C29.00005, (2019).

[25] HsuehJui Lu, ChungGang Li, Makoto Tsubokura, “The Simulation of Flow and Acoustics for Human Phonation System Using Implicit Compressible Flow Solver,” International Conference on Flow Dynamics(ICFD)(Nov 6-8 2019, Sendai), OS12-8, (2019).

### 13.5.6 Software

### 13.5.7 Patents



## Chapter 14

# Next Generation High Performance Architecture Research Team

### 14.1 Members

Masaaki Kondo (Team Leader)

Yiyu Tan (Research Scientist)

### 14.2 Overview of Research Activities

The next generation high performance architecture research team is conducting research and development of a next-generation high-performance computer architecture. Currently, we are mainly focusing on non-von Neumann architectures such as systolic arrays and neuromorphic computers based on the latest advances in device technologies, architectures that can integrate next generation non-volatile memories and/or various types of accelerators into a general-purpose processor, the advancement of scientific simulations by accelerating machine learning computations, and hybrid computing architectures that combine the benefits of quantum computing and classical computing. We are also performing detailed co-design evaluations of the computer architectures noted above as well as the co-design evaluations of algorithms that take advantage of them on the supercomputers K and Fugaku.

Another important aspect of designing future high-performance systems is power consumption. Power consumption is a prerequisite design constraint for developing exascale or next-generation computer systems. In order to maximize effective performance within a given power constraint, we need a new system-design concept in which the system's peak power is allowed to exceed maximum power provisioning using adaptively controlling power knobs incorporated in hardware components so that effective power consumption is maintained below the power constraint. This concept is recently known as hardware overprovisioning. In such systems, it is indispensable to allocate the power budget adaptively among various hardware component such as processors, memories, and interconnects, or among co-scheduled jobs, instead of fully utilizing all available hardware resources. We are researching strategies to improve the power efficiency and total system throughput for future hardware overprovisioned supercomputer systems.

In this fiscal year, we have conducted several researches including evaluations of domain-specific architectures, a prototype implementation of a systolic array in FPGAs, neuromorphic computing for graph processing, and power consumption analysis for low-precision floating-point arithmetic on numerical codes.

### 14.3 Research Results and Achievements

#### 14.3.1 Real-chip evaluation of a scalable accelerator core for deep neural networks

Recently, a Convolutional Neural Network (CNN) is utilized in many applications such as image recognition and object detection. One of the challenges for executing CNNs is developing a high-performance inference engine with high power efficiency. Several CNN accelerator architectures or LSI chips have been proposed so far for high-performance and low-power CNN executions.

Though existing CNN accelerator architectures can successfully achieve high energy efficiency, they typically focus on optimized execution for either of convolutional or fully connected layers. They also sometimes need to change the network structure which may limit the applicability to the variety of network structures. Since DNN algorithm and organization is now continuing to evolve, it is desirable for CNN accelerators to have flexibility to handle various types of network structure.

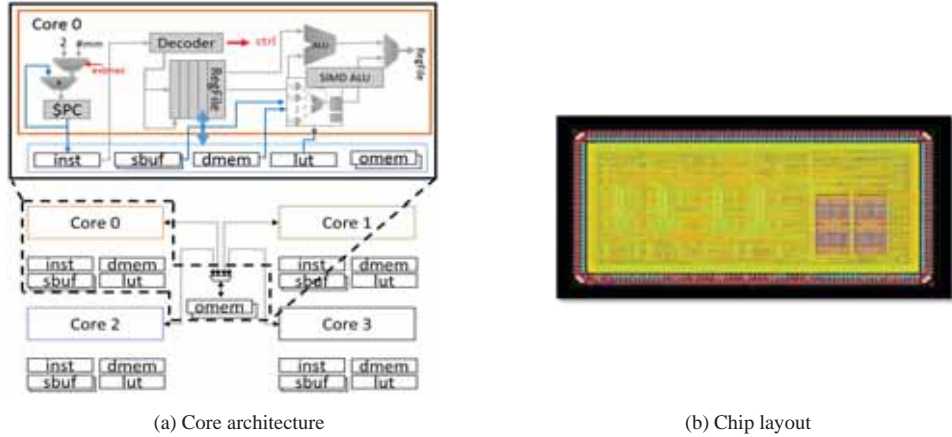


Figure 14.1: Core Microarchitecture and Chip Layout of Designed DNN Accelerator

To this end, we have been conducting research and development of the architecture and LSI design of a flexible and scalable DNN accelerator. This is a joint work with several universities in Japan. Our accelerator is a multi-core accelerator with several cores each of which consists of a micro-controller and a SIMD multiply and accumulate (MAC) unit. Figure 14.1 (a) presents the schematic view of the overall accelerator architecture with four cores, each of which has five scratch-pad memories, an instruction memory (inst), a stream buffer (sbuf), a temporal data memory (dmem), a lookup table (lut), and an output memory (omem).

We designed and implemented an accelerator core in real chip. we laid out the chip and taped out it with Renesas Electronics 65nm SOTB process technology. Figure 14.1 (b) shows the layout of the chip. The chip size is 3mm times 6mm with four cores. Due to the chip size limitation, only four cores were implemented on the chip. The chip contains 68-KB of distributed on-chip SRAMs. One core has 2KB instruction and 2KB lookup table memories. The size of dmem and sbuf is 4KB each. The four cores share the 4KB of omem. Each core has 18,8864 logic gates.

The prototype chip was successfully operated and we evaluated performance and power-efficiency of the prototype chip with the LeNet CNN model. We used the MNIST dataset as the image recognition workload. We found that the power consumption is less than 12mW at 50MHz clock frequency. As for performance, we compare the chip with a MIPS R3000 compatible embedded processor which was also developed by our collaborators using the same process technology. We found that our DNN accelerator can achieve 20x higher performance than the general purpose processor.

### 14.3.2 Neuromorphic graph processing for minimum weight perfect matching

The trend of exponential growth of processor performance known as Moore’s law is expected to end in the near future because semiconductor process advancement is almost reaching its physical limit. To achieve further performance improvement in post-Moore era, we need to make use of new types of computer architectures and computing models such as Neuromorphic Computing (NC). The computer systems with NC are attracting a lot of attention as a post-Moore architecture for various reasons. For example, it can potentially mitigate the von Neumann bottleneck and it is inherently power efficient.

In NC, many simple processing elements which are inspired by neurons of a human brain work as computation cores. The communication among them is relatively simple and based on the form of spikes. Therefore, NC has the potential to achieve higher computational efficiency and lower power consumption compared to traditional architectures. Although most of the applications of NC are typically based on neural networks, NC characteristic, massively parallel computation with many simple computational units, can be applied to other types of applications.

We studied on using NC for a graph problem specially a minimum weight matching problem. In particular, we proposed an approximate algorithm for minimum weight perfect matching with NC. We proposed a neuron-like unit named ‘‘Spike Delay Neuron’’ to solve MWPM problems. Figure 14.2 shows the Way to map a target graph to NC with Spike Delay neurons.

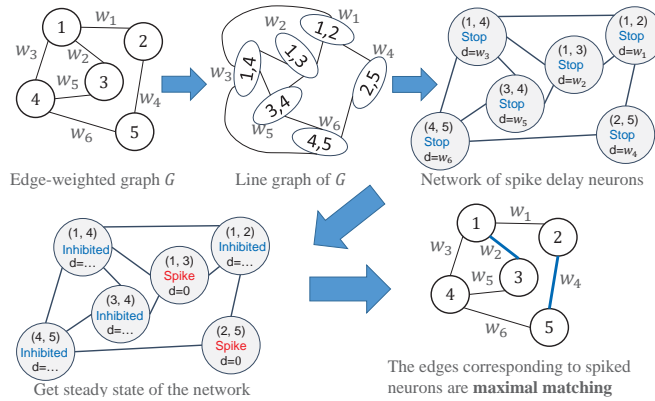


Figure 14.2: A way to solve matching problem by NC with Spike Delay neurons

We also implemented the proposed NC algorithm on an FPGA device. The overview of the hardware architecture is shown in Fig. 14.3. Assuming that the number of neuron units is  $E$ , an  $E$ -bits register named *spike register* holds spike information of all neuron units. An adjacent matrix and weights of the target graph are saved in a memory which can be either onchip SRAM or off-chip DRAM. The weights are used for the initial value of the spike delay of each neuron.

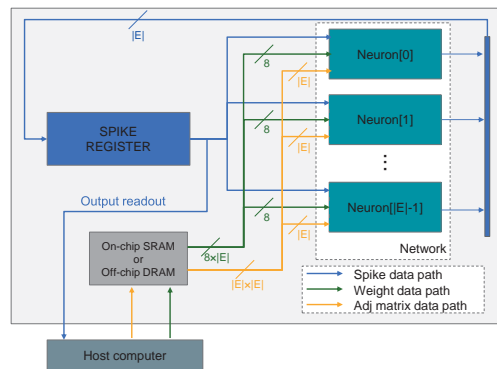


Figure 14.3: Overview of the hardware architecture

We applied it to several random graphs of different scales and concluded that the proposed algorithm is equivalent to a greedy algorithm whose approximation degree is  $\frac{1}{2}$ .

### 14.3.3 Power consumption analysis for low-Precision floating-point arithmetic on numerical codes

The low-precision floating point arithmetic that performs computation by reducing numerical accuracy with narrow bit-width is attracting since it can improve the performance of the numerical programs. Small memory footprint, faster computing speed, and energy saving are expected by performing calculation with low precision data. However, there have not been many studies on how low-precision arithmetics affects power and energy consumption of numerical codes. Therefore, we investigated the power efficiency improvement by aggressively using low-precision arithmetics for HPC applications. We analyzed power characteristics of the Poisson’s equation and the ground motion simulation programs with double precision and single precision floating point arithmetics.

We changed applications' codes written with double-precision to single-precision and measured execution time, power consumption, and the accuracy of the final result.

In the experiments, we used Reedbush-L supercomputer system installed in the Information Technology Center of the University of Tokyo. Since the effect of using low-precision arithmetics does not change even with parallel computation, we used only a single node. In addition, because power consumption may vary depending on compute nodes to be used due to manufacturing variations, we used a fixed node so that all evaluations are performed on the same compute node. To measure both CPU and DRAM power consumption, we used the Intel RAPL interface which provides power management functionality. It is possible to measure the power and energy consumption of CPU packages and DRAM modules. We create a power measurement library which supports measuring power and energy consumption of a Region of Interest (ROI) portion of the codes. In Poisson's equation solver, a kernel code of the ICCG method was measured. For the earthquake simulation, only the Adaptive CG part is measured. The Reedbush system has two Xeon processors, but we use only one of the processors. The application codes were compiled by Intel compiler with the -O3 option.

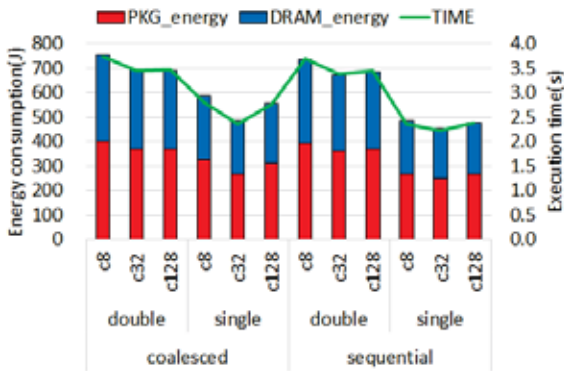


Figure 14.4: Comparison of energy consumption for ICCG solver

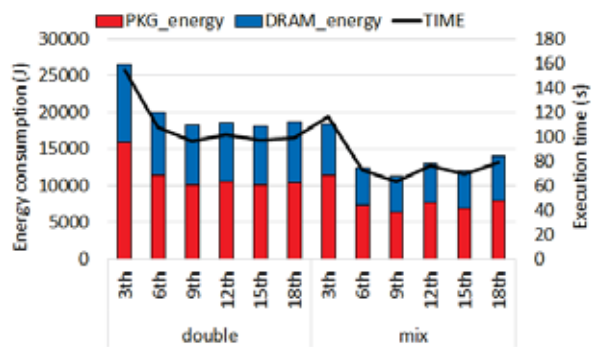


Figure 14.5: Comparison of energy consumption for Adaptive CG

we evaluated the average power, execution time, and the energy consumption comparing the cases of double-precision with single-precision. In the evaluation, for the ICCG solver, we varied the data arrangement method (Coalesced, Sequential) and the number of color divisions (8, 32, and 128 which are denoted as c8, c32, and c128, respectively). For the Adaptive CG code, six cases of the number of OpenMP threads, 3, 6, 9, 12, 15, and 18, were evaluated. Figure 14.4 and 14.5 show the results of the execution time and energy consumption for the ICCG solver and Adaptive CG, respectively.

From the figures, it is confirmed that the execution time is greatly shortened by lowering the compute precision. Since the average power consumption using single-precision did not change very much with the double-precision case, the energy consumption is greatly reduced by using single-precision. As for ICCG, in particular, when the number of colors is 8 (c8) and Sequential is used, energy saving becomes up to 34% in single-precision compared to double-precision. In the case of Coalesced, energy consumption can be reduced by 23.7% on average, whereas in the case of Sequential, energy was reduced by 32.1% on average. If the number of divisions is large, the execution time becomes longer causing the energy efficiency loss.

As for Adaptive CG, the execution time becomes minimum when the number of OpenMP threads is 9 in both cases of double-precision and single-precision even though the evaluated CPU has 18 physical cores per socket. As a result, the best energy efficiency was obtained by using 9 threads with single-precision. Overall, single-precision, we can reduce energy consumption by up to 38.3% and energy saving is 32.4% on average by utilizing single-precision arithmetics.

## 14.4 Schedule and Future Plan

In order to achieve further performance improvement for next generation HPC systems in post-Moore era, it is necessary to explore various types of devices, hardware architectures, system software/programming models, and algorithms that may contribute to the future system designs. We need to evaluate and analyze huge amount of possible scenarios varying the architectural parameters on wide variety of underlying system architecture. We plan to evaluate several benchmark applications which are expected to become important in future high-

performance computing including big-data and AI as well as traditional simulation applications. We will analyze their performance requirement and execution characteristics. We will also establish a performance model or performance simulation environment that enables to evaluate wide variety of future HPC architectures.

Beside exploring traditional CMOS-based computer systems, we will consider post-CMOS high-performance and low-power computing devices for post-Moore era. We also continue to study an ultra-high-performance accelerator system with an emerging device called SFQ (single-flux-quantum).

## 14.5 Publications

### 14.5.1 Articles/Journal

[1] 塚田 峰登, 近藤 正章, 松谷 宏紀, "OSUAD: FPGAを用いたオンライン逐次学習型教師無し異常検知器", 情報処理学会論文誌コンピューティングシステム (ACS65), Vol.12, No.3, pp.34-45, 2019年7月.

### 14.5.2 Conference Papers

[2] Rei Ito, Mineto Tsukada, Masaaki Kondo Hiroki Matsutani, "An Adaptive Abnormal Behavior Detection using Online Sequential Learning", In the 17th International Conference on Embedded and Ubiquitous Computing (EUC'19), Aug 2019.

[3] Ryohei Tomura, Takuya Kojima, Hideharu Amano, Ryuichi Sakamoto, and Masaki Kondo, "A Real Chip Evaluation of a CNN Accelerator SNACC", In the 22nd Workshop on Synthesis And System Integration of Mixed Information Technologies, Oct. 2019.

[4] Sayaka Terashima, Takuya Kojima, Hayate Okuhara, Kazusa Musha, Hideharu Amano, Ryuichi Sakamoto, Masaaki Kondo and Mitaro Namiki, "A Preliminary Evaluation of Building Block Computing Systems", In 13th International Symposium on Embedded Multicore/Many-core Systems-on-Chip (MCSoc-2019), pp.312-319, Oct. 2019.

[5] Shaswot Shresthamali, Masaaki Kondo, and Hiroshi Nakamura, "Power Management of Wireless Sensor Nodes with Coordinated Distributed Reinforcement Learning", In the 37th IEEE International Conference on Computer Design (ICCD2019), pp.638-647, Nov. 2019.

[6] Ryuichi Sakamoto, Masaaki Kondo, Kohei Fujita, Tsuyoshi Ichimura, and Kengo Nakajima, "The Effectiveness of Low-Precision Floating Arithmetic on Numerical Codes: A Case Study on Power Consumption", In International Conference on High Performance Computing in Asia Pacific Region (HPCAsia 2020), pp.199-206, Jan. 2020.

### 14.5.3 Posters

[7] Siddhartha Jana, Christopher Cantalupo, Jonathan Eastep, Masaaki Kondo, Matthias Maiterth, Aniruddha Marathe, Tapasya Patki, Barry Rountree, Ryuichi Sakamoto Martin Schulz, Carsten Trinitis, Josef Weidendorfer, "The HPC PowerStack: A Community-wide Collaboration Towards an Energy Efficient Software Stack", In ISC High Performance 2019 poster, June 2019.

[8] Siddhartha Jana, Stephanie Brink, Christopher Cantalupo, Jonathan Eastep, Masaaki Kondo, Matthias Maiterth, Aniruddha Marathe, Tapasya Patki, Barry Rountree, Ryuichi Sakamoto Martin Schulz, Carsten Trinitis, Josef Weidendorfer, "The HPC PowerStack: A Community-wide Collaboration Towards an Energy Efficient Software Stack", In the International Conference for High Performance Computing, Networking, Storage and Analysis (SC'19) poster, Nov. 2019.

[9] Yosuke Ueno and Masaaki Kondo, "Neuromorphic Graph Processing for Minimum Weight Perfect Matching", In the 2nd R-CCS international symposium poster, Feb. 2020.

### 14.5.4 Invited Talks

[10] Masaaki Kondo, "A Design of Scalable Deep Neural Network Accelerator Cores with 3D Integration", International Forum on MPSoc for Software-defined Hardware (MPSoc'19), July 2019.



## Chapter 15

# High Performance Big Data Research Team

### 15.1 Members

Kento Sato (Team Leader)

Jens Domke (Postdoctoral Researcher)

Jian Guo (Postdoctoral Researcher)

Takaaki Fukai (Postdoctoral Researcher)

Tonmoy Dey (Intern)

Rupak Roy (Intern)

Toshio Endo (Visiting Scientist)

Akihiro Nomura (Visiting Scientist)

Takashi Shimokawabe (Visiting Scientist)

### 15.2 Overview of Research Activities

The High Performance Big Data Research Team has been studying and developing software for accelerating “machine learning, deep learning and large-scale big data processing (AI techniques)” on the K and the Fugaku supercomputers (HPC for AI). We also study for accelerating HPC applications and HPC systems by using these AI techniques (AI for HPC). In FY2019, our team made several achievements which include: (1) Improving Data Compression with Deep Predictive Neural Network for Time Evolutional Data; (2) Breakdown of Modern HPC Applications: Less Double-Precision Floating-Point Units and Faster Memory are Needed; (3) The First Supercomputer with HyperX Topology: A Viable Alternative to State-of-the-Art Fat-Trees Topologies; (4) Counter-based Performance Extrapolation Toolchain; (5) Optimizing Asynchronous Multi-level Checkpoint/Restart Configurations with Machine Learning; (6) Evaluating the Relationship between System Utilization and Benefits of Combining Different Scheduling Policies with Backfilling.

### 15.3 Research Results and Achievements

#### 15.3.1 Improving Data Compression with Deep Predictive Neural Network for Time Evolutional Data

A lot of intermediate data has to be generated and transferred for further analysis in data science. A Large Hadron Collider (LHC) in CERN generated about 88PB of data in 2018 and foresees “Data archival is expected to be two-times higher during Run 3 and five-times higher or more during Run 4 (foreseen for 2026 to 2029).”.

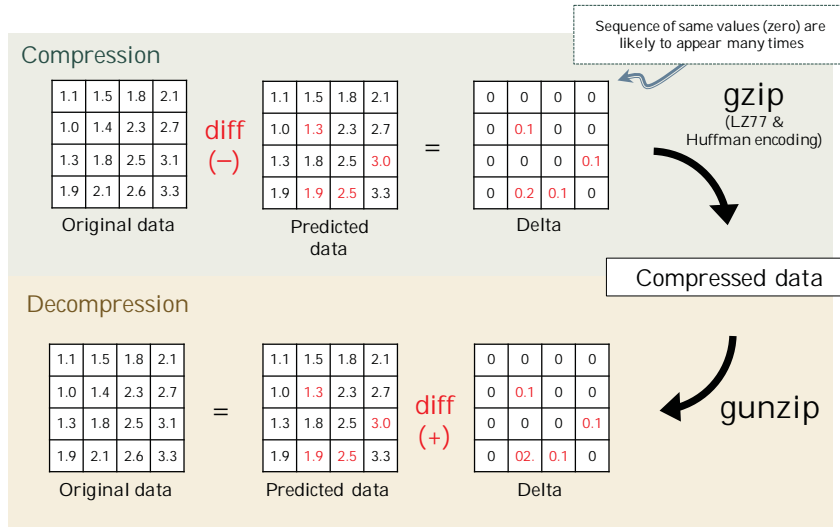


Figure 15.1: Predictive delta compression

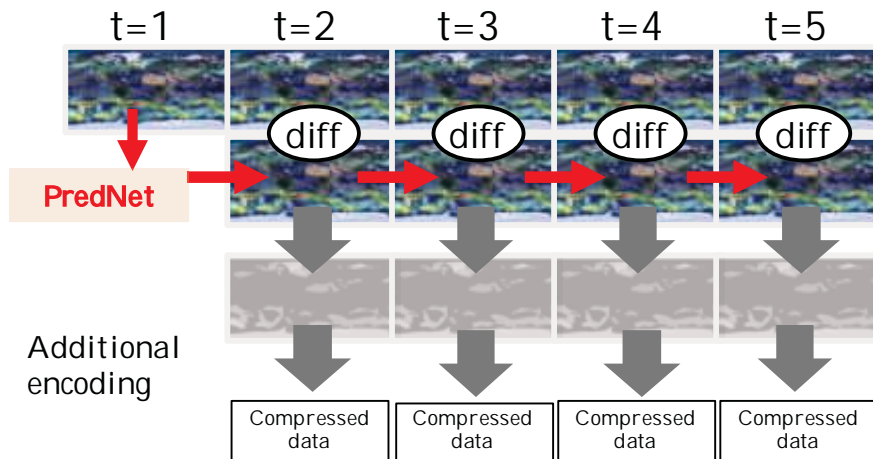


Figure 15.2: Data compression with predictive neural network

RIKEN also has a large synchrotron radiation facility (SPring-8). Spring-8 public beamline generated 0.32 PB/year in 2017. In 2025, with the next generation detector (CITISU), it is projected that a single beamline will generate 1.3 Exabytes of data per year. For the data analysis, checkpointing, debugging, visualization, etc., data generated by the scientific applications or simulations must be transferred from the sensors to computer systems. Fast transfer of such huge scale data from the sensors to computer systems is critical.

One of the approaches to accelerate data transfer is to reduce data size, i.e., data compression. However, existing compression algorithms show a low compression ratio for such kind of random evenly distributed floating-point data. As a result, achieving significant I/O acceleration is not possible with existing compressors. One of the promising approaches is predictive delta compression. Predictive delta compression is a technique to store only difference between original data and predicted data or the difference between consecutive predicted frames. Therefore, accurate prediction to the original data, which is data to compress, is important (Figure 15.1), both for increasing the compression ratio by making the delta values very small. Because the image data from sensors are time-evolutional images, we need a technique to accurately predict future image frames.

Predictive neural network is a predictive coding based deep convolutional neural network which learns to predict future frames of a video sequence. PredNet is such an architecture which is trained to predict the future movement of objects. We use PredNet to predict the future frames from the given time evolutionary frames. First, we train PredNet to learn movement of pixels by giving a number of time-evolutional frames generated from the sensor. In the example, in Figure 15.2, when we compress frames from t=2 to t=5, we predict future

frames from original frame ( $t=1$ ), we compute the difference and then apply conventional compressors such as gzip. Since we can always generate the predicted frames with the original frame at  $t=1$  with the help of trained neural network. we can restore the original frames by only storing (1) the original frame; (2) the trained neural network; (3) compressed frames from  $t=2$  and  $t=5$ . For compressing the frames we pass the delta data through two steps. The steps are spatial delta encoding and entropy coding.

In the evaluation, we observe that we can compress SPring-8 data by a factor of 40 compared to original size. Our approach shows 2.8x time better compression ratio compared to a recent compression algorithm SZ.

### 15.3.2 Breakdown of Modern HPC Applications: Less Double-Precision Floating-Point Units and Faster Memory are Needed

Historically, most of the compute silicon has been allocated to double-precision (DP; 64-bit) compute. Nowadays, in processors such as AA64FX and NVIDIA Volta, the trend (mostly driven by market/AI demands) is to replace some of the double-precision units with lower-precision units. Lower-precision units occupy less area (up to 3x going from double- to single-precision FMA), leading to more on-chip resources (more instruction-level parallelism), potentially lowered energy consumption, and a definitive decrease in external memory bandwidth pressure (i.e., more values per unit bandwidth). The gains: up to four times over their DP variants with little loss in accuracy are attractive and clear, but what is the impact on performance (if any) on existing HPC applications? What performance impact can HPC users expect when migrating their code to future processors with a different distribution in floating-point precision support? Finally, how can we empirically quantify this impact on performance using existing processors in an apples-to-apples comparison on real-life use cases without relying on tedious, slow, and potentially inaccurate simulators?

To answer these questions, we selected two processors with identical micro-architecture, where the main difference is in the relative allocation of double-precision units, namely Intel’s Knights Landing and Knights Mill architecture and a reference compute node which is commonly found in modern HPC systems. We stressed both processors with 22 HPC benchmarks and procurement application from the Exascale Computing Project and RIKEN’s R-CCS Fiber Miniapp Suite. An in depth analysis of various aspects for these applications revealed that most of them are either memory-bound or perform little FP64 operations, as can be seen in the roofline plot in Figure 15.3.

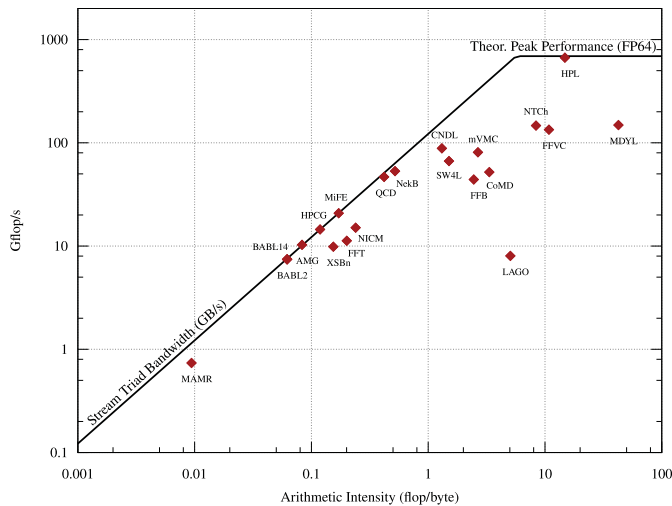


Figure 15.3: Roofline plot (w.r.t dominant floating-point operations and DRAM bandwidth) for Broadwell-EP reference system; Intel KNL/KNM results omitted to improve visual appearance (they showed similar behavior)

By studying a large number of HPC proxy application, we found no significant performance difference between these two processors, despite one having more double-precision compute than the other. Our study points toward a growing need to re-iterate and re-think architecture design decisions in high-performance computing, especially with respect to precision. Our versatile evaluation toolchain which we developed for this study has been publicly released, alongside the peer-reviewed publication [2], and will allow follow-up and replication studies by researchers and industry.

### 15.3.3 The First Supercomputer with HyperX Topology: A Viable Alternative to State-of-the-Art Fat-Trees Topologies

The recent generation of supercomputers underwent a drastic scale-out effect, e.g., reaching the extremes of K or Sunway TaihuLight with over 80,000 and over 40,000 nodes, respectively, to tackle the ending of Moore’s law. The interconnect in these HPC systems faces increasing demands for ultra-low latency from legacy HPC workloads, and new needs for high throughput of large messages from deep learning frameworks. Deploying Clos or Fat-Tree topologies will provide the needed throughput, but at a high cost. Furthermore, additional tree levels (to achieve this scale-out) will negatively affect the observable latency. Low-diameter, “electrically-optimized” topologies have been proposed, such as Dragonfly, Dragonfly+, or Slimfly. Another alternative is the HyperX which can provide high-throughput and low network dimensionality for ultralow latency.

We built the first large-scale HyperX prototype from the remains of the decommissioned TSUBAME2 supercomputer in collaboration with the Tokyo Institute of Technology and Hewlett Packard Enterprise. In a multi-months effort, we constructed the largest possible HPC system, given our hardware constraints, with HyperX network resulting in a 12x8 2D topology with 7 nodes per switch. The 672 compute nodes and 96 InfiniBand edge switches, composing our HyperX network, were distributed over 24 compute racks. The resulting system with two separate network rails, one of the old fat-trees and the new HyperX, see Figure 15.4, allowed for a near-perfect 1-to-1 comparison between the two topologies, which we published in two peer-reviewed conferences [3] and [4]. For these studies, we not only executed numerous MPI benchmarks and parallel HPC applications, but also developed a novel routing algorithm (PARX) to overcome the missing adaptive routing capabilities in the InfiniBand hardware.

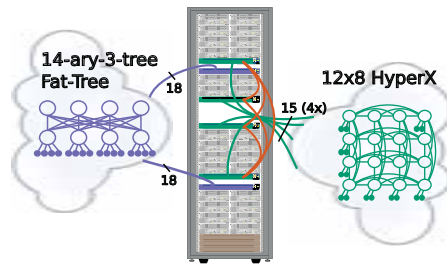


Figure 15.4: Depiction of one of 24 racks of our 672-node supercomputer with two edge switches connecting to the 3-level Fat-Tree and four switches for the 12x8 HyperX network (brown = rack-internal passive copper cables; gaps used for cable management)

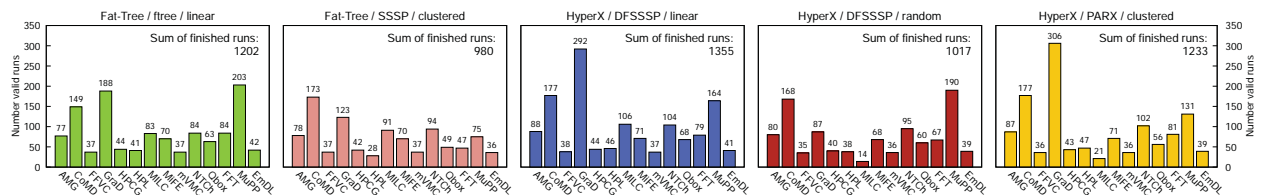


Figure 15.5: Capacity run for all five combinations over a 3 h time period for 14 concurrently running applications (using 32 or 56 nodes) while occupying 98.8% of the supercomputer; “HyperX / DFSSSP / linear” yields the highest number of finished compute jobs, outperforming the Fat-Tree by 12.7%, followed by PARX routing which yields 3% higher throughput.

The collected data from our 1-to-1 comparison implies that even a HyperX topology with roughly half-bisection bandwidth, and hence drastically reduced deployment costs, can compete with our 18-ary 3-tree, which theoretically offers more than full-bisection due to the reduced node count at the leaves. This result is even more astonishing, considering that we only had deprecated IB equipment (QDR type) available, which does not feature the required adaptive routing for the HyperX topology. We investigated two strategies: MPI rank placement and our novel PARX routing, which shows great potential as depicted in Figure 15.5, to circumvent the bottleneck arising from applying a shortest-path, static routing to a HyperX.

### 15.3.4 Counter-based Performance Extrapolation Toolchain

Nowadays, co-design efforts are aided by simulators, such as RIKEN’s gem5-based architecture simulator for Supercomputer Fugaku. However, such simulators have severe drawbacks. First, development cost (human time and labor) is substantial while still delivering runtime estimation errors in the lower double-digit percentage area. Second, this labor-intensity and required computer architecture knowledge means that a near-accurate simulation approach can only be used towards the end of a co-design effort, when the system deployment is only few years or months away. And lastly, simulator have reported slowdowns of 1000-10,000x compared to executing the program on real hardware, and therefore only small “toy-codes” or application hotspots can be tested, instead of full scientific programs running on future HPC systems.

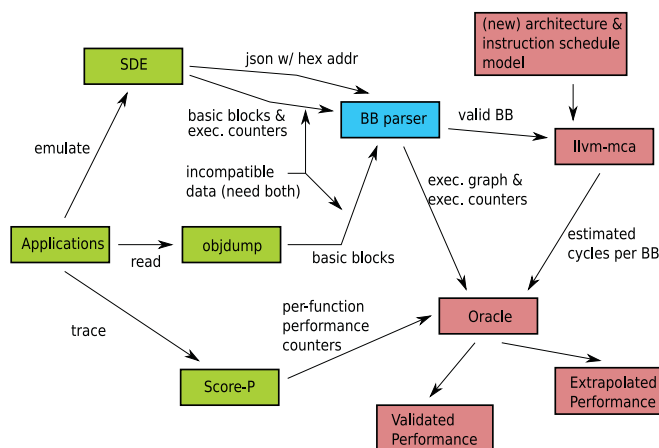


Figure 15.6: Counter-aided Performance Extrapolation Toolchain

We are currently exploring an alternative approach [8], by combining various tools into a framework designed to quickly test new ideas and extrapolate the performance of known/legacy application into the 5-to-10 year future. This toolchain, see Figure 15.6 shall aid processor and full-system architects in their early “what-if” stages to estimate the effect of a proposed architecture change for the full application runtime. Using existing hardware, we extract performance counters/data and internal information of the application, such as instruction- and memory-traces, and correlate this data with the basic blocks of the program. Defining a future node architecture and adjusting architecture characteristics, e.g., memory bandwidth and latency, can then be used to extrapolate the effects of such changes for individual basic blocks. Hence, knowing the speed up for each block yields an estimate of the performance benefit of the full application gained from a architecture.

### 15.3.5 Optimizing Asynchronous Multi-level Checkpoint/Restart Configurations with Machine Learning

To reliably run applications on current petascale systems in High-performance computing (HPC), a commonly used technique is checkpoint/restart(CR). In CR, the system writes a snapshot of the application’s state at fixed intervals to the different levels of storage hierarchy based on the configuration of the system. Though checkpoint and restart are useful for large scale systems, the checkpointing overhead can be enormous in an extensive system, which becomes one of the issues in the CR method.

One of approaches to reduce the overhead of CR is to determine the optimal checkpoint interval and checkpoint count. Poorly determined checkpoint interval makes system resilience worse. There are two approaches for obtaining the optimal checkpoint interval and checkpoint count values for any given configuration, namely the modeling approach and the simulation approach. The modeling approach mainly formulates an analytical solution to obtain optimal values, whereas the simulation approach runs the application across multiple failures to check different scenarios for obtaining the optimal values.

In this research, we try to use machine learning models in combination with an accurate simulation approach to determine the optimized checkpoint configuration. Specifically, the simulator has been developed to replicate the behavior of real-world scenarios when using a multi-level checkpoint for large scale systems. The simulator is provided with three critical parameters for each level, checkpoint overhead, check-point restart time, and failure rates as shown in Figure 15.7.

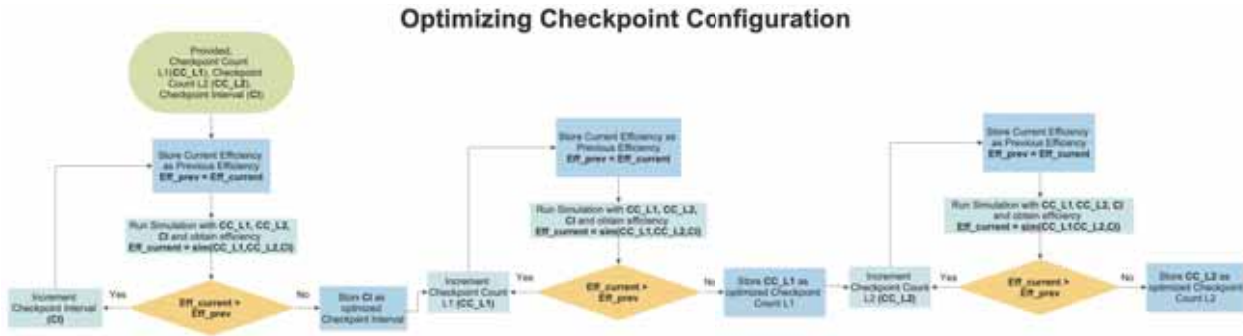


Figure 15.7: Workflow for Optimizing Checkpoint Configuration

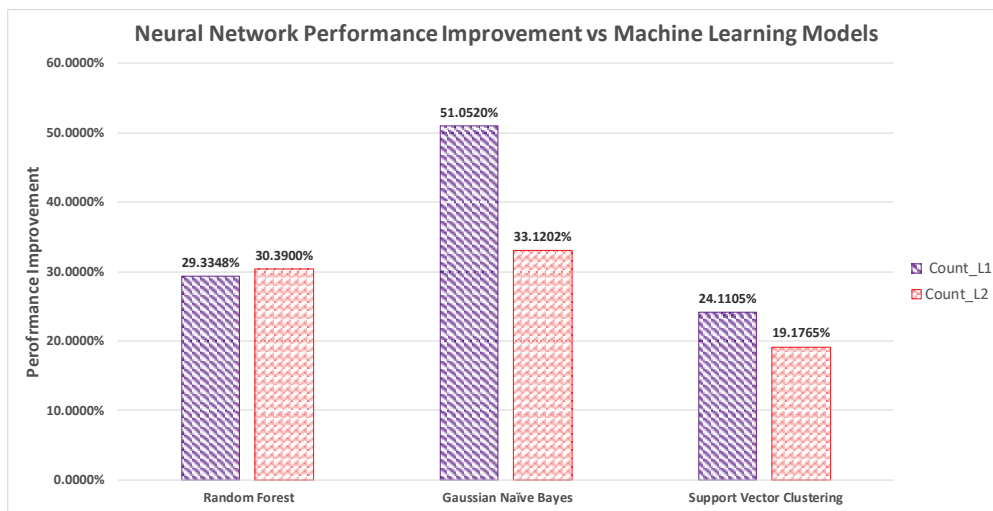


Figure 15.8: Neural Network Models Performance Improvement vs Machine Learning Models for three-level checkpoint model

The above simulation run provides the elapsed time and efficiency of a system with a specific configuration. The simulator we have developed not only provides the elapsed time and efficiency for a system but also performs simulation across different settings of the checkpoint system to determine the optimal checkpoint count for each level of the multi-level checkpoint system. The optimized configurations are obtained by modulating the checkpoint configuration values starting with checkpoint interval. After the peaks for all the configuration parameters are captured by the simulator, the user is provided with the optimized configuration for the given system based on the overhead, restart time, and failure rates. Once a significant amount of data is collected from the simulator, the information is passed on to different machine learning and neural network models to predict the optimized checkpoint configuration for other systems with different over-head, restart time, and failure rates.

we present an idea to combine the simulation approach with machine learning models to reduce the time taken to determine the optimized parameter values of check-point interval and checkpoint count for different configurations of CR. With our approach and design optimizations, we show that our models can predict the optimized parameter values when trained with the simulation approach. We have also demonstrated that using techniques such as neural networks can improve the performance over the machine learning models with neural network sometime exceeding the performance of a machine learning model by 50% as Figure 15.8 shows.

### 15.3.6 Evaluating the Relationship between System Utilization and Benefits of Combining Different Scheduling Policies with Backfilling

HPC users are required to estimate the job execution time and computing resource of their jobs before submitting, then the resource and job management systems (RJMSs) will submit jobs to HPC systems through

different scheduling policies for job execution. Related studies have shown that the EASY-Backfilling, also known as EASY-FCFS (EASY-First-Come-First-Served) is the most widely used scheduling policy in a lot of HPC systems due to its simple and robust implementation and increasing the overall utilization of the platform. On the other hand, because each of the HPC systems has its own scheduling policies, applications and users, which results in different system utilizations. Although with the same scheduling policy, there will be different benefits under different system utilizations of HPC systems. In this paper, we used real workload logs-based simulation to deep mining and analyze the relationship between system utilization and the benefits of combining different scheduling policy with backfilling for job scheduling in HPC systems.

In this research, we used real workload logs-based simulation to deep mining and analyze the relationship between system utilization and the benefits of different backfilling scheduling policies for job scheduling in HPC systems. Specifically, we would like to research the difference about the benefits of combining different scheduling policies with backfilling on different HPC systems. Meanwhile, we also want to explore and analyze how about the performance gap between different scheduling policies on low and medium utilization systems? And is a backfilling mechanism necessary on high utilization systems?

### 15.3.6.1 Current Progress

Currently, we have done a preliminary analysis on the three datasets (CEA Curie, LLNL Thunder and AIST AAIC): including the distribution of user estimated job execution time / real job execution time, the distribution of job states, etc. Firstly, we would like to check the real job execution time which was recorded after job execution to see whether the job execution time by a user conforms to a certain distribution law, e.g. a normal distribution? We analyse the distribution the real job execution time based-on the user-vector which is generated by combination of userID, groupID, queue, nodes, req\_walltime from SWF file (A file format for saving HPC system log). The reason why we use user-vectors for splitting jobs because we assume that vectors with the same information (same userID, groupID, queue, nodes and req\_walltime) represent that the user is submitting same applications for same purpose. Figure 15.9 is an example of distribution the real job execution time based-on the user-vector generated by using real workloads from CEA Curie dataset, we can see that the distribution the real job execution time of this user is random distribution which cannot be easily predicted.

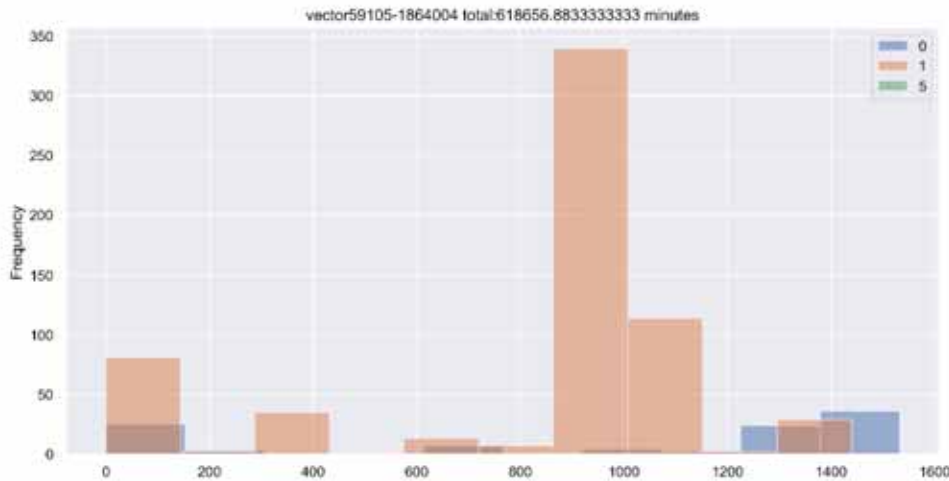


Figure 15.9: Histogram example of real job execution time from CEA Curie system, which is a user who submitted a total of 618,657 minutes.

Then, we also analyze the relationship between submit time and real job execution time base on user-vectors. We would like to see whether jobs submitted over a period of time by one user have the similar execution time. From Figure 15.10 we can see that job submitted over a period of time by one user has similar execution time. This phenomenon is common in other users. Generally speaking, job scheduling-related experiments cannot be performed directly on a real HPC system at the beginning. Most researchers choose to do their research with using job scheduling simulators. After deployment and adjustment of the simulators, we would like to start our

Experimental designing for our research. This research will base on a hypothesis that there is a relationship between different system utilization and the benefits of combining different scheduling policies with backfilling.

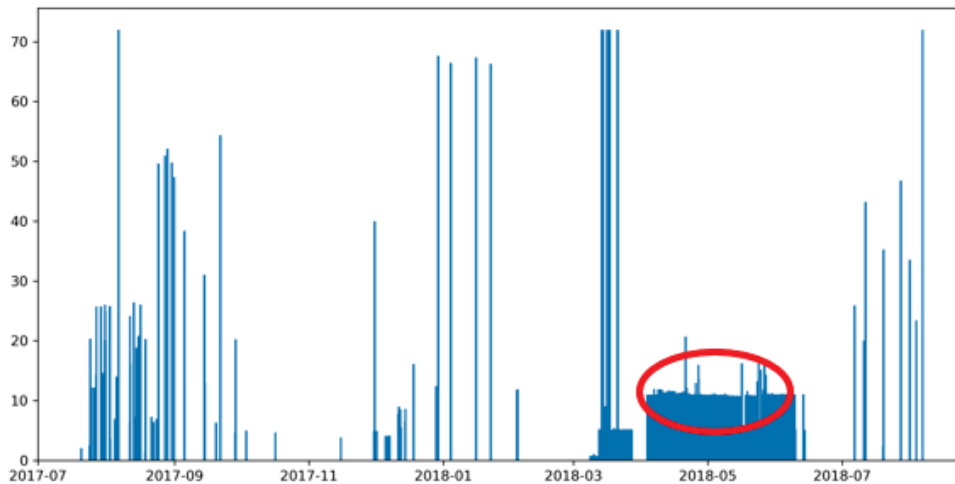


Figure 15.10: Jobs submitted over a period of time by one user have the similar execution time.

In this research, we also would like to conduct our experiments with simulation. After examining the popularity in recent research paper, updating frequency, functionality, and ease of use, we tentatively decided to use two simulators, BatSim and Slurm Simulator as our experiment platforms of job scheduling simulation in our research.

#### Future Plan

If everything goes well, we would like to follow tasks remain for the 2020 fiscal year:

- Extend this research to optimize job scheduling by predicting job execution time with AI
- Try to evaluate and test some of the latest AI-based (Machine Learning and Deep Learning-based) optimization studies for job scheduling in HPC systems

## 15.4 Schedule and Future Plan

In FY2020, we continuously work on HPC-for-AI, AI-for-HPC and many other researches and developments for HPC. These research topic include: (1) Fast and scalable parallel I/O by taking advantage of next-generation memory (e.g., Non-volatile memory) in big data processing and machine learning; (2) Scalable checkpointing for fault tolerance by taking advantage of next-generation memory (e.g., Non-volatile memory); (3) Scalable algorithms for deeply hieratical memory and storage architecture; (4) Fast data transfer technique for multi-petabyte of big data on high-speed network; (5) Integration of software stacks of big data, machine learning and HPC, and their optimization; (6) Visualization and UI techniques of big data; (7) Other research and software development related to big data, machine learning and I/O.

## 15.5 Publications

### 15.5.1 Articles/Journal

- [1] Chapp, D., Rorabaugh, D., Sato, K., Ahn, D. H., and Taufer, M. (2019). A three-phase workflow for general and expressive representations of nondeterminism in HPC applications. *The International Journal of High Performance Computing Applications*, 33(6), 1175–1184.

### 15.5.2 Conference Papers

- [2] J. Domke, K. Matsumura, M. Wahib, H. Zhang, K. Yashima, T. Tsuchikawa, Y. Tsuji, A. Podobas, S. Matsuoka, "Double-precision FPUs in High-Performance Computing: an Embarrassment of Riches?," in

Proceedings of the 33th IEEE International Parallel & Distributed Processing Symposium (IPDPS), (Rio de Janeiro, Brazil), IEEE Computer Society, May 2019.

- [3] J. Domke, S. Matsuoka, I.R. Ivanov, Y. Tsushima, T. Yuki, A. Nomura, S. Miura, N. McDonald, D.L. Floyd, N. Dube, "The First Supercomputer with HyperX Topology: A Viable Alternative to Fat-Trees?," peer-reviewed short paper presented at the 2019 IEEE 26th Symposium on High-Performance Interconnects (HOTI 26), Aug. 2019.
- [4] J. Domke, S. Matsuoka, I.R. Ivanov, Y. Tsushima, T. Yuki, A. Nomura, S. Miura, N. McDonald, D.L. Floyd, N. Dube, "HyperX Topology: First at-scale Implementation and Comparison to the Fat-Tree," in Proceedings of the International Conference for High Performance Computing, Networking, Storage and Analysis, SC '19, (Piscataway, NJ, USA), IEEE Press, Nov. 2019.
- [5] T. Dey, K. Sato, B. Nicolae, J. Guo, J. Domke, W. Yu, F. Cappello, K. Mohror, "Optimizing Asynchronous Multi-level Checkpoint/Restart Configurations with Machine Learning," accepted at the IEEE International Workshop on High-Performance Storage (co-located with 34th IEEE IPDPS), May 2020.

### 15.5.3 Posters

- [6] T. Dey, K. Sato, J. Guo, B. Nicolae, J. Domke, W. Yu, F. Cappello, K. Mohror, "Optimizing Asynchronous Multi-Level Checkpoint/Restart Configurations with Machine Learning," Poster presented at the International Conference for High Performance Computing, Networking, Storage and Analysis, SC '19, (Piscataway, NJ, USA), IEEE Press, Nov. 2019.
- [7] R. Roy, K. Sato, J. Guo, J. Domke, W. Yu, T. Hatsui, Y. Joti, "Improving Data Compression with Deep Predictive Neural Network for Time Evolutional Data," Poster presented at the International Conference for High Performance Computing, Networking, Storage and Analysis, SC '19, (Piscataway, NJ, USA), IEEE Press, Nov. 2019.
- [8] J. Domke, K. Sato, M. Kondo, "Counter-based Performance Extrapolation Toolchain – How far can we look into the Future?," Poster presented at The 2nd R-CCS International Symposium (RCCS-IS2), Kobe, Japan, Jan. 2020.
- [9] K. Sato, A. Kuroda, K. Minami, J. Domke, A. Drozd, M. Wahib, S. Kudo, T. Imamura, K. Kumahata, K. Nitadori, K. Ando, S. Matsuoka, "DL4Fugaku: Deep learning for Fugaku – Scalability Performance Extrapolation," Poster presented at The 2nd R-CCS International Symposium (RCCS-IS2), Kobe, Japan, Jan. 2020.
- [10] J. Guo and K. Sato, "Research on reproducibility and universality in machine learning-based optimizations for prediction job runtime in HPC systems," Poster presented at The 2nd R-CCS International Symposium (RCCS-IS2), Kobe, Japan, Jan. 2020.

### 15.5.4 Invited Talks

- [11] J. Domke "First At-Scale HyperX Implementation: A Compelling Alternative to Fat-Trees?" in High Performance Consortium for Advanced Scientific and Technical Computing (HP-CAST 32), June 2019.
- [12] 佐藤 賢斗, "高性能ビッグデータ処理とポストムーア時代に向けたアプリケーション解析", In JACORN (Japan Consortium for the Reconfigurable-hardware Next generation), October, 2019.
- [13] Kento Sato, "Convergence of AI/Big data and HPC", In 4th International Symposium on Research and Education of Computational Science (RECS), October, 2019.
- [14] Kento Sato, "AI for HPC - Data Compression and System Software Optimization", In France-Japan-Germany trilateral workshop: Convergence of HPC and Data Science for Future Extreme Scale Intelligent Applications, November, 2019.
- [15] Kento Sato, "High performance AI training on SVE/A64FX", In Arm HPC User Group (AHUG) at SC19, November, 2019.
- [16] 佐藤 賢斗, "「富岳」AI利用の展望", In 第14回 AI サービス研究会, December, 2019.

- [17] J. Domke "Double-precision FPUs in High-Performance Computing: an Embarrassment of Riches?" in Workshop on Large-scale Parallel Numerical Computing Technology (LSPANC 2020 January), Jan. 2020.
- [18] Kento Sato, "Convergence of AI/BD and HPC - Data compression and DL4Fugaku", Inauguration Meeting of Synchrotron for Neuroscience – an Asia Pacific Strategic Enterprise (SYNAPSE), Singapore, January, 2020)

### 15.5.5 Oral Talks

- [19] Kento Sato, "Model, Simulation and AI for Checkpointing", The 9th JLESC Workshop, April, 2019
- [20] Kento Sato, "ANL/RIKEN Collaboration on Lossy Compression", The DOE/MEXT Meeting, May, 2019
- [21] Kento Sato, "LLNL/UTK/RIKEN Collaboration — Data Analytics on System log —", The DOE/MEXT Meeting, May, 2019
- [22] Franck Cappello, Bogdan Nicolae, Kathryn Mohror, Rupak Roy, Weikuan Yu and Kento Sato, "ANL/F-SU/RIKEN Collaboration On C/R Optimization with AI", The DOE/MEXT Meeting, May, 2019
- [23] Kento Sato, "High Performance Big Data Research Team", The SPring-8 Meeting, August, 2019
- [24] Kento Sato, "Data Compression with Deep Predictive Neural Network", BDEC2, October, 2019
- [25] Kento Sato, Jens Domke, Jian GUO "Convergence of AI/Big data and HPC", R-CCS Cafe, November, 2019

# Chapter 16

## Data Assimilation Research Team

### 16.1 Members

Takemasa Miyoshi (Team Leader)

Koji Terasaki (Research Scientist)

Shigenori Otsuka (Research Scientist)

Shunji Kotsuki (Research Scientist/Visiting Scientist)

Takumi Honda (Postdoctoral Researcher)

Kohei Takatama (Postdoctoral Researcher)

James Taylor (Postdoctoral Researcher)

Arata Amemiya (Postdoctoral Researcher)

Maha Mdini (Postdoctoral Researcher)

Shun Ohishi (Postdoctoral Researcher)

Hironori Arai (Postdoctoral Researcher/Visiting Scientist)

Atsushi Okazaki (Special Postdoctoral Researcher/Visiting Scientist)

Yasumitsu Maejima (Research Associate)

Hazuki Arakida (Technical Staff/Visiting Scientist)

Marimo Ohhigashi (Technical Staff)

Hideyuki Sakamoto (Technical Staff)

Kenta Kurosawa (Technical Staff)

John C. Wells (Senior Visiting Scientist)

Shu-Chih Yang (Senior Visiting Scientist)

Juan Ruiz (Visiting Scientist)

Steve Penny (Visiting Scientist)

Yohei Sawada (Visiting Scientist)

Pierre Tandeo (Visiting Scientist)

Keichi Kondo (Visiting Scientist)

Shohei Takino (Visiting Scientist)

Yanqing Shen (Intern)

Tomoki Iwakiri (Intern)

Qiwen Sun (Intern)

Shlok Mohta (Intern/Student Trainee)

Tobias Necker (Student Trainee/Research Fellow)

Cheng Da (Student Trainee)

Paula Maldonado (Student Trainee)

Yukie Komori (Assistant)

Saeko Imano (Assistant)

## 16.2 Overview of Research Activities

Data Assimilation Research Team (DA Team) was launched in October 2012 and is composed of 22 research and technical staff including 11 visiting members as of March 2020. Data assimilation is a cross-disciplinary science to synergize computer simulations and real-world data, using statistical methods and applied mathematics. As computers become more powerful and enable more precise simulations, it will become more important to compare the simulations with actual observations. DA Team performs cutting-edge research and development on advanced data assimilation methods and their wide applications, aiming to integrate computer simulations and real-world data in the wisest way. Particularly, DA Team tackles challenging problems of developing efficient and accurate data assimilation systems for “big simulations” with real-world “big data” from various sources including advanced sensors. The specific foci include 1) theoretical and algorithmic developments for efficient and accurate data assimilation, 2) data assimilation methods and applications by taking advantage of powerful supercomputers and “big data” from new advanced sensors, and 3) exploratory new applications of data assimilation in wider simulation fields. These advanced data assimilation studies will enhance simulation capabilities and lead to a better use of supercomputers including the K computer and its successor “Fugaku.”

In FY2019, we continued on the ongoing data assimilation research in the following aspects: 1) theoretical research on challenging problems, 2) leading research on meteorological applications, 3) optimization of computational algorithms, and 4) exploratory research on wider applications. We also explored close collaborations with several research teams within the R-CCS. We have made substantial progress on the following research items:

### Theoretical research

- A particle filter was applied to the cellular automata of 3 state sheep model.
- Model bias correction using a machine learning method (Long Short Term Memory, LSTM) was explored with the Lorenz96 model.
- Denial of detrimental observations based on the Ensemble Forecast Sensitivity to Observation (EFSO) was investigated (1 paper in revision).
- Weight structure of the Local Ensemble Transform Kalman Filter (LETKF) was investigated with a simplified atmospheric general circulation model (GCM) (1 paper in revision).
- A local particle filter (LPF) was developed and tested with a simplified GCM.
- An LPF was developed for GPGPU.
- Ensemble Kalman filters (EnKFs) and LPFs were compared using the Lorenz96 model.
- Reservoir computing and EnKF were combined to predict spatio-temporal chaotic systems (1 paper in preparation).

### Leading research on meteorological applications

- A 30-second-update, real-time prediction system was developed with the SCALE-LETKF.
- The SCALE-LETKF realtime system toward a very short-term localized rainfall forecast was ported to Oakforest-PACS and tested in a realtime manner using the Multi-Parameter Phased Array Weather Radar (MP-PAWR) at Saitama University.
- The observational operator for PAWR in SCALE-LETKF was improved, and its impact on forecasts was investigated (1 paper published).
- An impact of a new observation system using a kite on a forecast of heavy rainfall was investigated.
- Impact of 30-second-update PAWR DA was investigated using the 100-m-mesh SCALE-LETKF for the west Japan heavy rainfall event in July 2018.
- An observation operator for high frequent lightning data assimilation was developed.
- Model acceleration by machine learning was investigated; convolutional neural networks were used to accelerate quasi-geostrophic model.
- To improve 3D precipitation nowcasting, neural networks were used to predict 3D radar images.
- Impact of assimilating lightning observations was investigated with the SCALE-LETKF.
- Efficient operation of water dam was investigated.
- Impact of assimilating Himawari-8 observations on precipitation events in Taiwan was investigated.
- Satellite observations at visible bands were simulated with the 1000-member SCALE-LETKF.
- Non-Gaussian PDF in DA was investigated using 1000-member, 1km-resolution assimilation experiments with assimilation windows ranging from 30 seconds to 5 minutes and assimilating PAWR observations in the SCALE-LETKF system. (1 paper in preparation)
- Conventional radar data assimilation experiments using the SCALE-LETKF system and RELAMPAGO field campaign observations. Analysis of the performance of the analysis and short range forecasts. (1 paper in preparation)
- Impact of dual phased array assimilation to severe convective weather forecasts investigated with the SCALE-LETKF was investigated.
- Sensitivity tests to optimize localization in the real-time SCALE-LETLF system were performed.
- We kept running the three-dimensional precipitation nowcasting system with the PAWR at NICT Kobe. A new system was developed for the MP-PAWR.
- A machine-learning system for the three-dimensional precipitation nowcasting system was developed with Convolutional LSTM.
- The sensitivity of a WRF-based convective-scale assimilation system on an afternoon thunderstorm in northern Taiwan was investigated (1 paper in press).
- Hybrid gain data assimilation using variational corrections in the subspace orthogonal to the ensemble was investigated (1 paper in press).
- Evaluation of stochastic perturbed parameterization tendencies on convective-permitting ensemble forecasts of heavy rainfall events in New York and Taiwan was performed (1 paper published).
- Convective-scale sampling error and its impact on the ensemble radar data assimilation system were investigated with a case study of heavy rainfall event on 16th June 2008 in Taiwan (1 paper in press).
- Impact of tropical cyclone initialization on its convection development and intensity was investigated with a case study of typhoon Megi (1 paper published).
- Convective-scale assimilation with the GNSS-ZTD and radar data was performed, and its impact on heavy rainfall prediction in Taiwan was investigated (1 paper published).
- Including the observation error correlation in DA was investigated with the NICAM-LETKF system. We found that reconditioning the observation error covariance matrix stabilizes the data assimilation and improves the analyses.
- Ensemble-based observation impact estimates was incorporated into the NICAM-LETKF (1 paper published).
- GPM/DPR-sensed heavy ice precipitation was compared with a 3.5-km NICAM simulation to design better cloud microphysics (1 paper in revision).
- We kept running the global precipitation nowcasting system with the Global Satellite Mapping of Precipitation (GSMaP) by JAXA, and the prediction was disseminated on our website and JAXA's website (1 paper published).
- Precipitation forecasts were improved by merging NICAM and spatio-temporal extrapolation forecasts (1 paper published).
- Spatially-varying model parameter was estimated with NICAM-LETKF (1 paper published).

- Survey of ensemble-covariance of CH<sub>4</sub>-emission and wind velocity with NICAM-RM-LETKF to evaluate unfavorable impacts of observation densities between PREPBUFR-wind and GOSAT-CH<sub>4</sub> data.
- An observation operator for a new space-borne precipitation radar was developed (1 paper accepted).
- Impact of oversampling observations from a geostationary precipitation radar satellite to tropical cyclone forecasts was investigated (paper to be submitted).
- An object-based verification method of precipitation pattern was investigated using pattern recognition techniques (1 paper published).
- An LETKF system to assimilate pattern features of precipitation areas was implemented with an intermediate atmospheric GCM. A feature based on the fractions skill score was investigated.
- Impact of the ocean mixed layer model in a regional atmospheric DA system was investigated for a case of typhoon Soudelor in 2015.
- Water level change in Lake Biwa under Typhoon Jebi in 2018 was reproduced by using SCALE and the Regional Ocean Modeling System (ROMS).
- Current filed in Lake Kinneret was simulated with 50-m mesh ROMS.
- A LETKF based ocean DA system was developed and tested with Argo assimilation in the western North Pacific.
- Bio-chemical fields in Tokyo-Bay are simulated to predict blue-green algae bloom.
- Relaxation methods of dynamical imbalance for ocean data assimilation systems were implemented.
- Performance of regional ocean data assimilation systems between 3D-VAR and LETKF was compared.
- Uncertainty quantification of a land surface model by machine learning based surrogate modelling was investigate (1 paper submitted).
- A prototype system of machine-learning-based dam operation optimization was developed in collaboration with Tokyo Electric Power Company Holdings, Incorporated.
- Land-atmosphere-coupled DA system was developed based on the NICAM-LETKF (1 paper in revision).
- Online- and offline-DA for paleoclimate reconstruction and its relation to the predictability were compared (1 paper in prep.).
- Observation operators for paleoclimate reconstruction were developed (1 paper accepted).

### Computational optimization

- The NICAM-LETKF system was developed for “Fugaku” as a target application in collaboration with the Computational Climate Science Research Team and FS2020 (1 application submitted to Gordon Bell).
- The just-in-time data transfer (JIT-DT) of PAWR observations from NICT and Saitama University to R-CCS was improved in collaboration with the System Software Development Team.

### Wider applications

- DA experiments were performed with the Moderate resolution Imaging Spectroradiometer (MODIS) leaf area index (LAI) observations and the Spatially-Explicit, Individual-Based Dynamic Global Vegetation Model (SEIB-DGVM) over Siberia.
- SEIB-DGVM DA experiments were performed with the MODIS LAI observations at Takayama Flux site in Japan.
- A particle filter was applied to a press-forming manufacturing simulation.

Several achievements are selected and highlighted in the next section.

## 16.3 Research Results and Achievements

### 16.3.1 Development of a real-time workflow of the big data assimilation system

In FY2019, we developed a 30-second-update, real-time prediction system assimilating the Phased Array Weather Radar (PAWR) observations by fully utilizing the Oakforest-PACS. In the previous fiscal year, we achieved a real-time execution of a 30-second-update PAWR DA cycle with a 250-m mesh on the supercomputer K. However, the computational domain was limited to the PAWR observation range of 60 km, and the boundary conditions for this domain were not provided in real time; a real-time system for the outer regions was yet to be developed. We also ported the entire system to the Oakforest-PACS in response to the upcoming shutdown of the K computer. In FY2019, we started to use the Oakforest-PACS as the main platform. Our

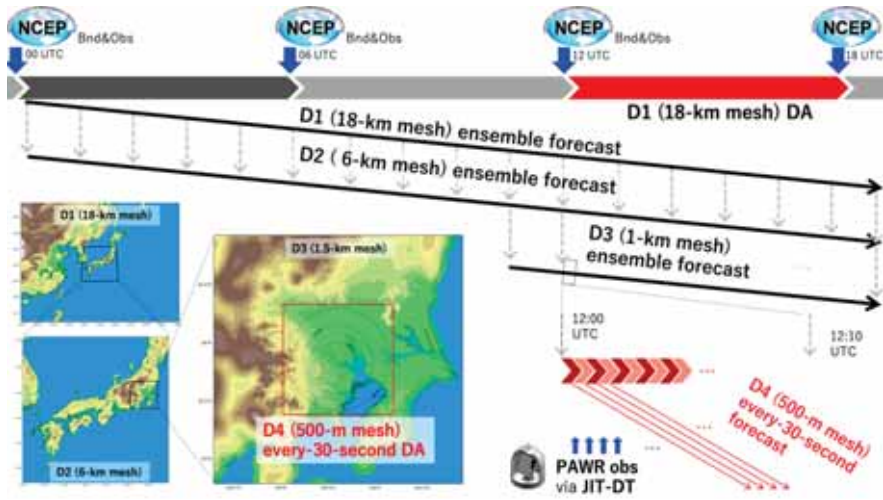


Figure 16.1: Workflow and computational domains of the 30-second-update, real-time SCALE-LETKF system.

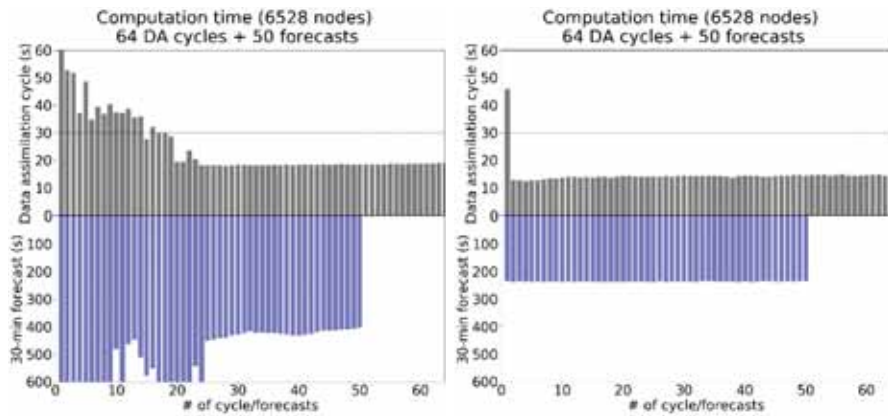


Figure 16.2: Elapse times of each DA and 30-minute forecast with a 250-m mesh. DA was performed for 64 cycles, and forecasts were performed for 50 initial conditions. Left: a test run in August 2019, right: a test run in November 2019.

system receives and assimilates PAWR observations every 30 seconds, and performs 30-minute deterministic forecasts from the analyses. Figure 16.1 presents the system design. The system consists of four computational domains. The outermost domain (D1, 18-km mesh) is the near-real-time SCALE-LETKF system developed by Lien et al. (2017), assimilating conventional observations provided by the National Center for Environmental Prediction (NCEP) every 6 hours. From the analyses by D1, ensemble forecasts over Japan (D2, 6-km mesh) and Kanto (D3, 1.5-km mesh) are performed to provide initial and boundary conditions for the innermost domain (D4). The D4 covers a region of 120 km × 120 km with a 500-m mesh or a 250-m mesh, assimilating observations of PAWR at Saitama University every 30 seconds. The data transfer of PAWR uses the Just-In-Time Data Transfer (JIT-DT) developed by the System Software Development Team, R-CCS.

In FY2019, the 30-minute deterministic forecasting from the analyses of D4 was implemented as follows. Here, 10 MPI processes are assigned to the 30-minute forecasts in addition to the MPI processes for the 52 ensemble members. MPI communicators are prepared for DA and the 30-minute forecasts separately; computations are independent except for the exchange of DA analyses. The SCALE and LETKF are combined as a single binary file to avoid data exchange via file IO; data are exchanged on memory. Figure 16.2 displays the execution time for DA and forecast. An earlier version of DA did not run stably in 30 seconds, and the corresponding 30-minute forecasts took long (left). The system was updated to solve these problems; the latest version runs stably within 30 seconds. The first cycle of DA takes longer to initialize the system, and from the second cycle, the DA finishes stably within 30 seconds. The 30-minute forecasts also runs in 4 minutes (right). This is a big step to the real time prediction. We will prepare a dissemination system and web page for this

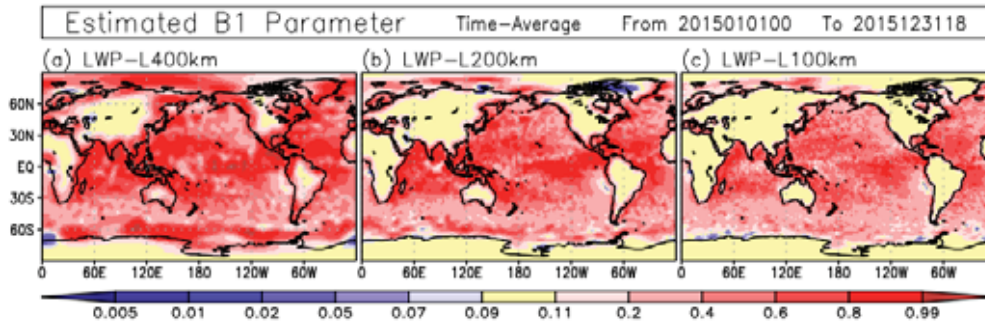


Figure 16.3: Spatial patterns of locally-estimated  $B_1$ , averaged over 12 months from January to December 2015 for the experiments with the horizontal localization scales of (a) 400, (b) 200, and (c) 100 km (LWP-L400km, LWP-L200km, and LWP-L100km, respectively). Red and blue colors indicate increases and decreases from the default value of  $B_1 = 0.10$  due to parameter estimation. Adopted from Kotsuki et al. (2020).

prediction. We also need to verify and improve the prediction accuracy.

### 16.3.2 Model parameter estimation with data assimilation using NICAM-LETKF

This study aims to improve forecasts of numerical weather prediction (NWP) models by optimizing model parameters with data assimilation. Kotsuki et al. (2018) succeeded in improving global precipitation forecasts at 112-km-resolution NICAM (Nonhydrostatic ICosahedral Atmospheric Model) by estimating a parameter called  $B_1$  of Berry (1967)’s large-scale condensation scheme using satellite-observed precipitation data and the Ensemble Transform Kalman Filter (ETKF).

Extending the previous study, this study explores to use the model parameter estimation for mitigating radiation bias. Kotsuki et al. (2020, JGR) estimated the parameter  $B_1$  as a global-constant parameter with cloud liquid water (CLW) data observed by GCOM-W/AMSR2. The parameter estimation successfully reduced excessive bias in CLW, and mitigated overestimated outgoing shortwave radiation (OSR) bias of the NICAM. In addition, Kotsuki et al. (2020, JGR) extended to estimate spatially-varying  $B_1$  parameters using the Local ETKF (i.e., LETKF) (Fig. 16.3). The local parameter estimation resulted in better cloud representations and improved OSR bias in regions where shallow clouds are dominant (Fig. 16.4).

### 16.3.3 Application of machine learning methods to model bias correction: idealized experiments with the Lorenz-96 model

Model bias correction has been studied as an important subject in data assimilation. Model bias can be effectively alleviated by statistical model bias correction methods combined with a variational or sequential (Kalman filter-based) data assimilation method (Dee, 2005). Conventional methods have assumed a bias correction term of simple functional form such as a constant or a linear dependence on model state variables (Dee and Da Silva, 1998, Danforth et al., 2007). Recently, the data-driven forecast and estimation of governing functions of the system in arbitrary form, known as ‘model detection’ or ‘system identification,’ has been rapidly developed with the use of machine learning (Brunton et al. 2016, Vlachas et al. 2018). The application of such machine learning methods to data assimilation is a potential solution to model bias correction with unknown complexity.

In this study, an application of Long-Short term memory (LSTM) on model bias correction problems is explored in the context of data assimilation using the Local Ensemble Transformed Kalman Filter (LETKF). The proposed method is applicable for model bias which is dependent on current and past model states in an arbitrarily nonlinear manner. Localization of bias correction treatment is also implemented. The new method is examined by idealized numerical experiments using a multi-scale Lorenz-96 model (Lorenz 1996; Wilks 2005).

As the first step, LSTM-based scheme is examined in the case of offline bias correction, where the network is trained with the pair of forecast and analysis time sequence produced by LETKF without correction. The bias correction with LSTM worked well and showed slightly better performance than simple polynomial fitting. However, the improvement is very subtle in the case of coupled Lorenz96 system, which have been used in previous studies. Therefore, experimental settings in which the use of LSTM has a clear advantage will be studied further. Figure 16.5 presents such an example; here, the ‘shear-Lorenz96’ by Pulido et al. (2018) is

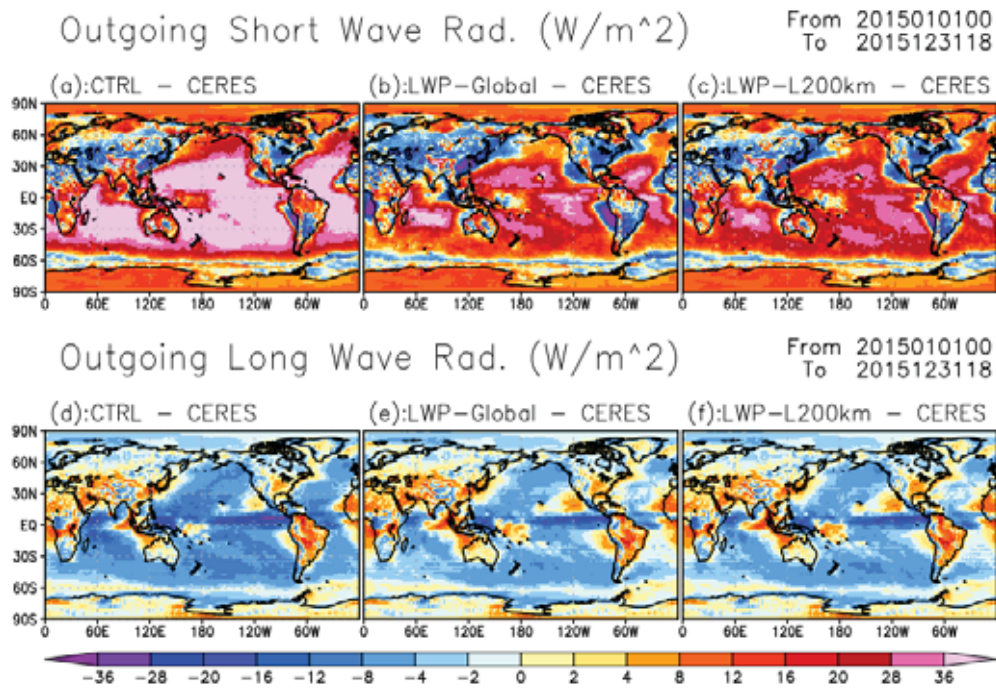


Figure 16.4: Global patterns of the time-mean bias relative to CERES data for (a, b, c) outgoing short wave radiation (OSR;  $W m^{-2}$ ), and (d, e, f) outgoing long wave radiation (OLR;  $W m^{-2}$ ), averaged over 12 months from January to December 2015. Panels (a, d), (b, e) and (c, f) show CTRL, LWP-Global (estimating  $B_1$  as a global constant), and LWP-L200km experiments, respectively. Warm (cold) color represents overestimated (underestimated) outgoing radiations relative to CERES data. Adopted from Kotsuki et al. (2020).

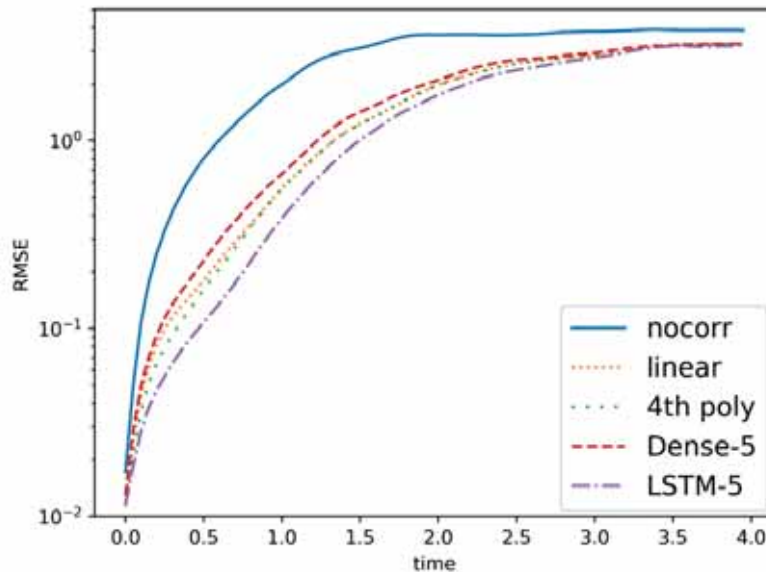


Figure 16.5: The comparison of average RMSE over 100 forecasts from different initial conditions in “shear-Lorenz96 (Pulido et al., 2018)” experiments. Each line corresponds to the experiment with different bias correction schemes; no correction, linear regression, 4th order polynomial regression, neural networks with dense layers, and LSTM. All bias correction schemes use the spatial localization with 5 neighboring grid points.

used. The next step will be the online bias correction, where the bias correction function is estimated with state variables by LETKF simultaneously, and the consideration of partial and noisy observation.

## 16.4 Schedule and Future Plan

DA Team aims to explore the frontier of large-scale DA problems, and to be a world’s leader in DA research. With the goals in mind, we plan to continue working on the three fundamental foci: 1) theoretical and algorithmic developments for efficient and accurate DA (core focus), 2) DA methods and applications by taking advantage of the Japan’s flagship supercomputer and “Big Data” from new advanced sensors (lead focus), and 3) exploratory new applications of DA in wider simulation fields (pioneer focus). We have very strong projects in weather forecast applications, and we will enhance the leading research to the world’s top level. Also, we will pioneer new application fields that have direct connection with societal benefits. For direct benefit to society, “real-time” application is essential with efficient computational algorithms, which are also an important aspect of our research.

“Big Data Assimilation” (BDA) is one of the major activities that we have developed in the past years. The prototype system showed promising results, but the physical performance for the 30-minute forecast of precipitation patterns can be improved. We will continue to work on the development of the BDA system to further improve the computational and physical performances toward the upcoming “Fugaku” era.

Beyond the direct future of the BDA effort, we can extend the idea of BDA to a broader perspective: integration of “Big Data” and “Big Simulation.” New sensors provide orders of magnitude more data, and simulations become more precise. Collaborative work with computer scientists will be essential to utilize the complex high-performance computer systems effectively. In addition, dense sensor data tend to have complicated error structures such as correlated errors, and the proper treatment is necessary to fully utilize the “Big Data.” The current DA methods usually assume no observation error correlation. Based on our previous theoretical research on the observation-error correlations, we plan to develop methods to consider the observation error correlations in realistic NWP applications.

Treating the model errors and non-Gaussian probability distribution has been grand challenges in DA. “Big Ensemble Data Assimilation” with the largest-ever 10240 samples was a milestone providing fundamental

data to investigate the non-Gaussian probability distribution. We have developed expertise and exclusive dataset to tackle these challenges. We have been pioneering a new implementation of Local Particle Filter (LPF) in collaboration with German Weather Service. We will continue the LPF development toward realistic applications.

DA is a cross-disciplinary science based on statistical mathematics and dynamical systems theory. In addition, DA connects simulations and real-world data. Therefore, it is naturally beneficial to enhance close collaborations with experts in mathematics, sensor technology, and various application fields. The current weather-forecast projects involve active collaborations with observation experts. In addition, we have been teaching semester-long courses on DA at the Department of Mathematics, Kyoto University, and this will lead to more collaborations with mathematicians. Moreover, TL Miyoshi has joint appointments at RIKEN iTHEMS (Interdisciplinary Theoretical and Mathematical Sciences Program) and RIKEN CPR (Cluster for Pioneering Research), and these will enhance broader collaborations. Collaborations with other R-CCS Research Teams will also be beneficial. The challenges for future DA systems require cross-disciplinary collaborations to most effectively use the massive supercomputers with more heterogeneous architecture design. Further, RIKEN's Engineering Network already gave us opportunities to collaborate among different disciplines among RIKEN centers. RIKEN President's Initiative for "DA innovation hub" also helped expand collaboration. We also started collaborations with industry partners for more direct benefit to society. Enhancing the broader collaborations is a key to success, i.e., to make a new scientific movement across the borders through DA as an innovation hub, to establish DA as a new scientific paradigm, and to change the world through innovation and education of DA.

## 16.5 Publications

### 16.5.1 Awards

- [1] Shigenori Otsuka, RIKEN Oubu Research Incentive Award, Development of a novel three-dimensional precipitation nowcast method and its real-time demonstration, 3/10/2020.

### 16.5.2 Articles

- [1] Takino, S., T. Honda, T. Miyoshi, and T. Tsukada 2019: Improving prediction of river-basin precipitation by assimilating every-10-minute all-sky Himawari-8 infrared satellite radiances – A case of Typhoon Malakas (2016). International Commission On Large Dams 2019 Symposium Proceedings, Volume 2, p339, ISBN:978-0-367-33422-2.
- [2] Kotsuki, S., K. Kurosawa, S. Otsuka, K. Terasaki, and T. Miyoshi, 2019: Global precipitation forecasts by merging extrapolation-based nowcast and numerical weather prediction with locally optimized weights. *Wea. Forecasting*, **34**, 701–714, <https://doi.org/10.1175/WAF-D-18-0164.1>.
- [3] 滝野晶平, 本田匠, 三好建正, 塚田智之, 2019: 10分毎のひまわり8号赤外輝度温度観測のデータ同化による流域雨量予測の改善-2016年9月台風16号の事例, *大ダム*, **248**, 79–82, ISSN0011-5347.
- [4] Okazaki, A., T. Honda, S. Kotsuki, M. Yamaji, T. Kubota, R. Oki, T. Iguchi, and T. Miyoshi, 2019: Simulating precipitation radar observations from a geostationary satellite. *Atmos. Meas. Tech.*, **12**, 3985–3996, <https://doi.org/10.5194/amt-12-3985-2019>.
- [5] Kotsuki, S., K. Kurosawa, and T. Miyoshi, 2019: On the properties of ensemble forecast sensitivity to observations. *Quart. J. Royal Meteorol. Soc.*, **145**, 1897–1914, <https://doi.org/10.1002/qj.3534>.
- [6] Kondo, K., and T. Miyoshi, 2019: Non-Gaussian statistics in global atmospheric dynamics: a study with a 10240-member ensemble Kalman filter using an intermediate atmospheric general circulation model. *Nolin. Processes Geophys.*, **26**, 211–225, <https://doi.org/10.5194/npg-26-211-2019>.
- [7] Okazaki, A. and K. Yoshimura, 2019: Global evaluation of proxy system models for stable water isotopes with realistic atmospheric forcing. *J. Geophys. Res. Atmos.*, **124**, 8972–8993, <https://doi.org/10.1029/2018JD029463>.
- [8] Kurosawa, K., Y. Uchiyama, and T. Kosako, 2020: Development of a numerical marine weather routing system for coastal and marginal seas using regional oceanic and atmospheric simulations. *Ocean Engineering*, **195**, 106706, ISSN 0029-8018, <https://doi.org/10.1016/j.oceaneng.2019.106706>.

- [9] Greybush, S. G., E. Kalnay, R. J. Wilson, R. N. Hoffman, T. Nehr Korn, M. Leidner, J. Eluszkiewicz, H. E. Gillespie, M. Wespetal, Y. Zhao, M. Hoffman, P. Dudas, T. McConnochie, A. Kleinböhl, D. Kass, D. McCleese, and T. Miyoshi, 2019: The ensemble Mars atmosphere reanalysis system (EMARS) Version 1.0, *Geoscience Data Journal*, **6**, 137–150, <https://doi.org/10.1002/gdj3.77>.
- [10] Awazu, T., S. Otsuka, and T. Miyoshi, 2019: Verification of precipitation forecast by pattern recognition, *J. Meteorol. Soc. Japan Ser. II*, **97**, 1173–1189, <https://doi.org/10.2151/jmsj.2019-066>.
- [11] 庄司悟, 岡崎淳史, 芳村圭, 2018: 気候プロキシデータ同化における観測インパクトの時空間偏在性に関する考察, 土木学会論文集B1(水工学), **74**, I\_49–I\_54, Online ISSN 2185-467X, [https://doi.org/10.2208/jscejhe.74.5\\_I\\_49](https://doi.org/10.2208/jscejhe.74.5_I_49).
- [12] Otsuka, S., S. Kotsuki, M. Ohhigashi, and T. Miyoshi, 2019: GSMaP RIKEN Nowcast: Global precipitation nowcasting with data assimilation. *J. Meteorol. Soc. Japan Ser. II*, **97**, 1099–1117, <https://doi.org/10.2151/jmsj.2019-061>.
- [13] Kotsuki, S., Y. Sato, and T. Miyoshi, 2020: Data assimilation for climate research: Model parameter estimation of large-scale condensation scheme. *J. Geophys. Res. Atmos.*, **125**, e2019JD031304, <https://doi.org/10.1029/2019JD031304>.
- [14] Necker, T., S. Geiss, M. Weissmann, J. Ruiz, T. Miyoshi, and G.-Y. Lien, 2020: A convective-scale 1,000-member ensemble simulation and potential applications. *Quart. J. Royal Meteorol. Soc.*, **148**, 1423–1442, <https://doi.org/10.1002/qj.3744>.
- [15] Chang, Y., S. Yang, K. Lin, G. Lien, and C. Wu, 2020: Impact of tropical cyclone initialization on its convection development and intensity: a case study of typhoon Megi (2010). *J. Atmos. Sci.*, **77**, 443–464, <https://doi.org/10.1175/JAS-D-19-0058.1>.
- [16] Amemiya, A., T. Honda, and T. Miyoshi, 2020: Improving the observation operator for the Phased Array Weather Radar in the SCALE-LETKF system, *SOLA*, **16**, 6–11, <http://dx.doi.org/10.2151/sola.2020-002>.
- [17] Maejima, Y. and T. Miyoshi, 2020: Impact of the window length of four-dimensional local ensemble transform Kalman filter: a case of convective rain event, *SOLA*, **16**, 37–41, <https://doi.org/10.2151/sola.2020-007>.
- [18] Yang, S., Z. Huang, C. Huang, C. Tsai, and T. Yeh, 2020: A case study on the impact of ensemble data assimilation with GNSS-zenith total delay and radar data on heavy rainfall prediction. *Mon. Wea. Rev.*, **148**, 1075–1098, <https://doi.org/10.1175/MWR-D-18-0418.1>.
- [19] Necker, T., M. Weissmann, Y. Ruckstuhl, J. Anderson, and T. Miyoshi, 2020: Sampling error correction evaluated using a convective-scale 1000-member ensemble. *Mon. Wea. Rev.*, **148**, 1229–1249, <http://doi:10.1175/MWR-D-19-0154.1>.

### 16.5.3 Invited Talks

- [1] Kotsuki S., Sato Y., Terasaki K., Yashiro H., Tomita H., Satoh M., and Miyoshi T.: Model Parameter Estimation with Data Assimilation using NICAM-LETKF. JpGU2019, Chiba, 5/29/2019.
- [2] Arakida, H., S. Kotsuki, S. Otsuka, Y. Sawada, T. Miyoshi, Data assimilation experiments with MODIS LAI observations and the dynamic global vegetation model SEIB-DGVM over Siberia, JpGU2019, Chiba, 5/29/2019.
- [3] Takemasa Miyoshi, Big data assimilation: A new science for weather prediction and beyond, 14TH INTERNATIONAL ENKF WORKSHOP IN VOSS, PARK HOTEL VOSSEVANGEN, VOSS, NORWAY, 6/4/2019.
- [4] Takemasa Miyoshi, Big Data Assimilation: A New Science for Weather Prediction and Beyond, Seminar, DWD, Frankfurt, Germany, 6/13/2019.
- [5] Takemasa Miyoshi, Big Data Assimilation: A New Science for Weather Prediction and Beyond, Seminar, LMU, Munich, Germany, 6/17/2019.

- [6] 三好建正、ビッグデータ同化：数値天気予報から予測科学へ、講演会（ショートセミナー）、日本工営株式会社、つくば, 7/4/2019.
- [7] 三好建正、ビッグデータ同化：数値天気予報から予測科学へ、社内講演会、株式会社先端力学シミュレーション研究所東京事業所、東京, 7/5/2019.
- [8] Takemasa Miyoshi, HPC challenges in numerical climate simulation and weather prediction, INTERNATIONAL HPC SUMMER SCHOOL 2019, R-CCS, Kobe, Japan, 7/10/2019.
- [9] 小槻峻司, 三好建正: 全球大気データ同化システムによる天気予報研究の最前線. 第14回名工大・核融合研合同セミナー、名古屋, 7/18/2019.
- [10] Takemasa Miyoshi, “Big Data Assimilation A New Science for Weather Prediction and Beyond”, 6th CREST “Big Data Application” Camp for Researchers, Kanagawa, Japan, 9/26/2019.
- [11] 三好建正、ビッグデータ同化：数値天気予報から予測科学へ、通信技術部会電波センサ専門部会講演会、三菱電機株式会社、尼崎, 10/3/2019.
- [12] Takemasa Miyoshi, Big Data Assimilation Incorporating Deep Learning with Phased Array Radar Data and Numerical Weather Prediction, BDEC2 San Diego, San Diego, USA, 10/16/2019.
- [13] 三好建正、ビッグデータ同化：「富岳」が拓く未来の天気予報、スーパーコンピュータ推進議員連盟総会、自民党本部、東京, 10/28/2019.
- [14] 三好建正、気象予報におけるビッグデータ同化とAIの協働に向けて、第6回「京」を中核とするHPCIシステム利用研究課題成果報告会、東京, 11/1/2019.
- [15] 大塚成徳・三好建正: データ同化技術について、HPCを活用した自動車用次世代CAEコンソーシアム第5回総会 基調講演, 神戸, 11/5/2019.
- [16] 三好建正、データ同化研究～ゲリラ豪雨予測から、予測科学へ～、精華寿大学第5回講座、精華町、京都, 11/8/2019.
- [17] Takemasa Miyoshi, Big Data Assimilation: 30-second-update Weather Forecasting and Perspectives toward DA-AI Integration, Big Data, Data Assimilation and Uncertainty Quantification, Institut Henri Poincaré, Paris, France, 11/12/2019.
- [18] 三好建正、ビッグデータ同化 ゲリラ豪雨予測から、予測科学へ、セミナー、独立行政法人酒類総合研究所、東広島, 11/20/2019.
- [19] Takemasa Miyoshi, Big Data Assimilation:A New Science for Weather Prediction and Beyond, seminar, ACADEMIA SINICA, Taipei, Taiwan, 11/27/2019.
- [20] Takemasa Miyoshi, Big Data Assimilation:A New Science for Weather Prediction and Beyond, seminar, National Taiwan University, Taipei, Taiwan, 11/28/2019.
- [21] 大塚成徳・三好建正: 最先端の気象予測技術：ゲリラ豪雨予測の実現に向けて、第45回（2019年度第2回）スーパーコンピューティング技術産業応用協議会セミナー、東京, 11/29/2019.
- [22] Takemasa Miyoshi, Big Data Assimilation:A New Science for Weather Prediction and Beyond, seminar, National Central University, Taoyuan City, Taiwan, 11/29/2019.
- [23] Otsuka, S. and T. Miyoshi: Overview of the rapid-update weather forecasting with the phased-array weather radar, 2019 6th KNU CARE Workshop on Phase array radar and Nowcasting, Daegu, Korea, 12/5/2019.
- [24] Otsuka, S., M. Ohhigashi, and T. Miyoshi: Three-dimensional precipitation nowcasting with the phased-array weather radar, 2019 6th KNU CARE Workshop on Phase array radar and Nowcasting, Daegu, Korea, 12/5/2019.
- [25] 大塚成徳・三好建正, 簡単モデルを用いたデータ同化, CREST 「ビッグデータ応用」第7回若手研究者合宿, 葉山, 1/16/2020.

- [26] 三好建正、ビッグデータ同化：「富岳」が拓く未来の天気予報、スーパーコンピュータ「富岳」を知る集い金沢、金沢歌劇座、金沢、1/25/2020.
- [27] 三好建正、ビッグデータ同化：ゲリラ豪雨予測から予測科学へ、CCSE ワークショップ、東海村産業・情報プラザ、東海村、2/21/2020.
- [28] 三好建正、「ビッグデータ同化」研究の最前線ゲリラ豪雨や台風の予測から、その先の予測科学へ、データマネジメント2020、東京、3/5/2020.

#### 16.5.4 Oral Presentations

- [1] Takemasa Miyoshi, Shigenori Otsuka, Takumi Honda, Guo-Yuan Lien, Yasumitsu Maejima, Yoshito Yoshizaki, Hiromu Seko, Hirofumi Tomita, Shinsuke Satoh, Tomoo Ushio, Tatiana V. Martsinkevich, Balazs Gerofi, and Yutaka Ishikawa, Big Data Assimilation: Past 5 Years and Perspectives for the Future, EGU2019, Vienna, Austria, 4/8/2019.
- [2] Takemasa Miyoshi, Shunji Kotsuki, Koji Terasaki, Kenta Kurosawa, Shigenori Otsuka, Kaya Kanemaru, Hisashi Yashiro, Masaki Satoh, Hirofumi Tomita, Kozo Okamoto, and Eugenia Kalnay, Enhancing Data Assimilation of GPM Observations: Past 6 Years and Future Plans, EGU2019, Vienna, Austria, 4/9/2019.
- [3] Takemasa Miyoshi, Big Data Assimilation: A New Science for Weather Prediction and Beyond, Japan – Israel meeting, Otsu, Japan, 4/14/2019.
- [4] Takatama, K., S. Kotsuki, K. Kurosawa, T. Miyoshi, and Y. Uchiyama: Progress on simulation research for Tokyo Bay and Lake Biwa using ROMS, SICORP Research Meeting, Shiga, Japan, 4/14/2019.
- [5] 岡崎淳史、本田匠、小槻峻司、James Taylor、三好建正、静止衛星による降水観測が台風予測に与えるインパクト評価、データ同化手法を活用した観測システムの影響評価に関する研究会、横浜、4/18/2019.
- [6] 小槻峻司、黒澤賢太、三好建正: Observation Diagnostics with NICAM-LETKF. データ同化手法を活用した観測システムの影響評価に関する研究会、横浜、4/18/2019.
- [7] 寺崎康児、三好建正、NICAM-LETKFの概要と観測誤差相関を考慮したデータ同化、データ同化手法を活用した観測システムの影響評価に関する研究会、横浜、4/18/2019.
- [8] 大塚成徳・栗津妙華・三好建正・Roland Potthast・Christian Welzbacher: Fractions Skill Scoreを用いたデータ同化、データ同化手法を活用した観測システムの影響評価に関する研究会、横浜、4/18/2019.
- [9] 雨宮新、本田匠、三好建正、SCALE-LETKFのフェーズドアレ イ気象レーダのデータ同化における観測演算子の改善のインパクト、データ同化手法を活用した観測システムの影響評価に関する研究会、横浜、4/19/2019.
- [10] 本田匠、三好建正、SCALE-LETKFの概要と衛星観測同化への適用例、データ同化手法を活用した観測システムの影響評価に関する研究会、横浜、4/19/2019.
- [11] 三好建正, Enhancing Precipitation Prediction Algorithm by Data Assimilation of GPM Observations, 「NICAM-LETKFと衛星観測データ同化に関する打ち合わせ」第17回会合、神戸、4/22/2019.
- [12] 菊地淳, 三好建正, 伊藤研悟, 高玉孝平, “海を耕す”新時代を創生する環境診断・予測技術の構築, エンジニアリングネットワークトリート2019, 和光, 4/23/2019.
- [13] 小槻峻司, 三好建正: Local Particle Filter: 低解像度全球大気モデルSPEEDY数値実験. 第10回 理研・京大データ同化研究会, 神戸, 4/26/2019.
- [14] 三好建正、非ガウスフィルタの実装理論：LETKFからLPFへ、第10回理研・京大データ同化研究会、神戸、4/26/2019.
- [15] 岡崎淳史、本田匠、小槻峻司、三好建正、次世代静止衛星搭載降水レーダ反射強度の観測システムシミュレーション実験、日本気象学会2019年度春季大会、東京、5/17/2019.
- [16] 前島康光、大塚成徳、三好建正 平成30年7月豪雨を対象とした高頻度・高解像度フェーズドアレ イ気象レーダーデータ同化実験、日本気象学会2019年度春季大会、東京、5/18/2019.

- [17] Arakida, H., S. Kotsuki, S. Otsuka, and T. Miyoshi, Data assimilation experiments with MODIS LAI observation and the dynamic global vegetation model SEIB-DGVM in Japan, JPGU2019, Chiba, Japan , 5/28/2019.
- [18] Okazaki, A., Isotope-enabled climate modeling and simulations: state of the art, next steps, Data Assimilation, Reanalyses and Proxy System Modeling in Paleoenvironmental Science, UMD, US., 5/29/2019.
- [19] Amemiya, A., T. Honda, and T. Miyoshi, Improving the observation operator for Phased Array Weather Radar in the SCALE-LETKF system, JPGU2019, Chiba, Japan , 5/29/2019.
- [20] Koji Terasaki and Takemasa Miyoshi, Data assimilation and forecast experiments for the record-breaking rainfall event in Japan in July 2018 with NICAM-LETKF at 112-km and 28-km resolution, JPGU2019, Chiba, Japan, 5/29/2019.
- [21] Takatama, K., T. Honda, T. Miyoshi. Regional atmospheric data assimilation coupled with an ocean mixed layer model: a case of typhoon Soudelor (2015), JPGU2019, Chiba, Japan , 5/29/2019.
- [22] 三好 建正、小槻 峻司、寺崎 康児、大塚 成徳、本田 匠、岡崎 淳史、高玉 孝平、「気象・海洋・陸面予測を革新する高頻度衛星観測網の設計事前評価プラットフォーム」、JpGU、千葉、5/29/2019.
- [23] Kotsuki S., Terasaki K., and Miyoshi T.: Ensemble-Based Data Assimilation of GPM/DPR Reflectivity into the Nonhydrostatic Icosahedral Atmospheric Model NICAM. JPGU2019, Chiba, Japan , 5/30/2019.
- [24] 高玉 孝平、小槻峻司、黒澤賢太、三好建正、内山雄介：“ROMS による東京湾の数値シミュレーション”，第1回理研-水研機構研究情報交換会，5/30/2019.
- [25] Hironori Arai, Development of Monitoring, Reporting and Verification system of Methane emissions from rice paddies in the Mekong delta, 15th International Workshop of Greenhouse Gas Measurements from Space, Sapporo, 6/5/2019.
- [26] 三好建正、Local Gaussian Mixture Particle Filter (LMCPF)の紹介、2019年度第1回高解像度豪雨予測とアンサンブル同化摂動手法に関する研究会（第7回アンサンブルデータ同化摂動に関する研究会）、苫小牧、6/28/2019.
- [27] 坂本英之、三好建正、プレスシミュレーションにおけるデータ同化（続編）、第四回ものづくりワークショップ：データ駆動型社会におけるものづくり設計の新潮流、日本橋 ライフサイエンスハブ、7/10/2019.
- [28] Takemasa Miyoshi, Advancing data assimilation as a science hub: from weather forecasting and beyond, ICIAM2019, University of Valencia, Valencia, Spain, 7/17/2019.
- [29] Arai, H., W.Takeuchi, K.Oyoshi, L.D. Nguyen, T.Tachibana, R.Uozumi, K.Terasaki, T.Miyoshi, H.Yashiro and K.Inubushi. Evaluation of methane emission status from tropical rice paddies with optical and SAR imagery and validation scheme using GHG observation data. Land cover/land use changes and impacts on environment in south/southeast asia – international regional science meeting, Johor Bahru, Malaysia, 7/22/2019.
- [30] Takemasa Miyoshi, Big Data Assimilation: Past 5 Years and Perspectives for the Future, AOGS, Singapore, 7/30/2019.
- [31] Takemasa Miyoshi, Enhancing Data Assimilation of GPM Observations: Past 6 Years and Future Plans, AOGS, Singapore, 8/2/2019.
- [32] 寺崎康児、三好建正：NICAM-LETKFを用いた観測誤差相関を考慮するデータ同化システムの開発。第3回 理研・気象庁データ同化研究会、東京、8/20/2019.
- [33] 三好建正、LETKFと融和的な粒子フィルタ実装方法について、第3回理研・気象庁 データ同化に関する情報交換会、気象庁、8/20/2019.
- [34] Takemasa Miyoshi, Big Data Assimilation: A New Science for Weather Prediction and Beyond, Seminar, CIMA, Buenos Aires, Argentina, 8/26/2019.
- [35] 三好建正、GPM観測データ同化による降水予測アルゴリズムの高度化、2019年度 第二回地球観測研究公募 降水観測ミッション サイエンスチーム国内キックオフ会合、東京、9/5/2019.

- [36] Takemasa Miyoshi, Shigenori Otsuka, Takumi Honda, Guo-Yuan Lien, Yasumitsu Maejima, Marimo Ohhigashi, Yoshito Yoshizaki, Hiromu Seko, Hirofumi Tomita, Shinsuke Satoh, Tomoo Ushio, Balazs Gerofi, Yutaka shikawa, Naonori Ueda, Kana Koike, Yasuhiko Nakada, Big Data Assimilation: Past 6 Years and Future Plans, 39th International Conference on Radar Meteorology, Nara, Japan, 9/17/2019.
- [37] 三好 建正, Enhancing Precipitation Prediction Algorithm by Data Assimilation of GPM Observations, 「NICAM-LETKFと衛星観測データ同化に関する打ち合わせ」第18回会合, 奈良, 9/18/2019.
- [38] Okazaki, A., Honda, T., Kotsuki, S., Taylor, J., Miyoshi, T., Impact assessment of Next Generation Rainfall Measuring Satellite on NWP: An Observation System Simulation Experiment for a typhoon case, 39th International Conference on Radar Meteorology, Nara, Japan, 9/19/2019.
- [39] 雨宮新、三好建正、雲微物理パラメタに依存するレーダー反射因子の観測演算子とパラメタ推定への展望、ポスト京重点課題4サブ課題A研究連絡会、東京、9/25/2019.
- [40] Takemasa Miyoshi, Big Data Assimilation and AI Creating New Development in Real-time Weather Prediction (AIP Acceleration Research), CREST Symposium on Big Data Application, Tokyo, Japan, 9/25/2019.
- [41] 小槻峻司, 三好建正: 低解像度全球大気モデルを用いた局所粒子フィルタ実験. 日本気象学会2019年度秋季大会, 福岡, 10/28/2019.
- [42] 黒澤賢太, 小槻峻司, 三好建正: 全球大気・水文結合データ同化システムの開発と土壌水分データ同化実験. 日本気象学会2019年度秋季大会, 福岡, 10/28/2019.
- [43] 小槻峻司, 三好建正: 低解像度全球大気モデルを用いた局所粒子フィルタ実験. 日本気象学会2019年度秋季大会, 福岡, 10/28/2019.
- [44] 黒澤賢太, 小槻峻司, 三好建正: 全球大気・水文結合データ同化システムの開発と土壌水分データ同化実験. 日本気象学会2019年度秋季大会, 福岡, 10/28/2019.
- [45] 近藤圭一、三好建正、背景誤差の非ガウス分布を考慮したアンサンブル同化手法、日本気象学会2019年度秋季大会、福岡、10/28/2019.
- [46] 大塚成徳, Viet Phi Huynh, 大東直利茂, Pierre Tandeo, 三好建正, 深層学習による三次元降水ナウキャスト手法の検討, 日本気象学会2019年度秋季大会, 福岡, 10/30/2019.
- [47] 雨宮新, 三好建正, Shlok Mohta, 機械学習によるモデルバイアス補正: Lorenz96 モデル実験, 日本気象学会秋季大会, 福岡, 10/30/2019.
- [48] 澤田洋平, データ駆動型アプローチが加速する地球科学シミュレーションの不確実性定量化, 日本気象学会秋季大会, 福岡, 10/30/2019.
- [49] 三好建正、気象学における AI 活用から AI 統合へ、日本気象学会2019年度秋季大会、福岡、10/30/2019.
- [50] Honda, T., Y. Sato, T. Miyoshi, Exploring the potential of assimilating three-dimensional lightning discharge observations with an ensemble Kalman filter , European Conferences on Severe Storms (ECSS), Krakow, Poland, 11/7/2019.
- [51] 坂本 英之, 三好 建正, 高村 正人, 見原 俊介, 第6回設計に活かすデータ同化研究会, プレスシミュレーションにおけるデータ同化, 鳥取, 11/11/2019.
- [52] 雨宮新, 本田匠, 三好建正, SCALE-LETKFのフェーズドレイ気象レーダのデータ同化における観測演算子の改善のインパクト, 第21回非静力学モデルワークショップ, 三重, 11/21/2019.
- [53] 寺崎康児、小槻峻司、三好建正: GSMaP降水データの観測誤差相関を考慮したデータ同化実験、第21回非静力学モデルに関するワークショップ、三重、11/21/2019.
- [54] 三好建正、小槻峻司、Roland Potthast、LETKFに基づいた局所粒子フィルタの簡易実装法の検討、第21回非静力学モデルに関するワークショップ、三重、11/21/2019.
- [55] 本田匠、佐藤陽祐、三好建正, SCALE-LETKF を用いた雷観測データ同化: 観測システムシミュレーション実験, 第21回非静力学モデルに関するワークショップ, 三重, 11/22/2019.

- [56] 三好建正、局所粒子フィルタの進展、2019年度第2回高解像度豪雨予測とアンサンブル同化摂動手法に関する研究会（第8回アンサンブルデータ同化摂動に関する研究会）、大洲市民会館、大洲、12/5/2019.
- [57] Takemasa Miyoshi, Local Particle Filter Implemented with Minor Modifications to the LETKF Code, AGU FALL MEETING, Moscone Center, San Francisco, USA, 12/9/2019.
- [58] Sawada, Y., Machine learning accelerates parameter optimization and uncertainty quantification of a land surface model, AGU Fall Meeting, San Francisco, USA, 12/9/2019.
- [59] Takemasa Miyoshi, Big Data Assimilation Incorporating Deep Learning with Phased Array Radar Data and Numerical Weather Prediction, AGU FALL MEETING, San Francisco, USA, 12/10/2019.
- [60] 雨宮新, 佐藤薫, アジアモンスーン高気圧（チベット高気圧）の形成と季節内変動の力学, 第2回高・低気圧ワークショップ, 京都大学防災研究所白浜海象観測所, 和歌山, 12/17/2019.
- [61] 三好建正、ビッグデータ同化とAIによるリアルタイム気象予測の新展開、ビッグデータ基盤/応用 合同領域会議、湯河原, 12/18/2019.
- [62] 三好建正, “Enhancing Precipitation Prediction Algorithm by Data Assimilation of GPM Observations”, 「NICAM-LETKFと衛星観測データ同化に関する打ち合わせ」第19回会合, 理研R-CCS、神戸, 12/20/2019.
- [63] 大塚成徳・三好建正: LSTMによる三次元降水ナウキャスト手法, 第11回理研・京大データ同化研究会, 京都, 12/24/2019.
- [64] 雨宮新, 三好建正, Shlok Mohta, 機械学習によるモデルバイアス補正: Lorenz96 モデル実験, 第11回理研・京大データ同化研究会, 京都, 12/24/2019.
- [65] Takemasa Miyoshi, “Big Data Assimilation: Real-Time Workflow for 30-Second-Update Forecasting and Perspectives Toward DA-AI Integration”, AMS 100th Annual Meeting, Boston, USA, 1/13/2020.
- [66] T. Miyoshi, S. Otsuka, H. Tomita, B. Gerofi, S. Satoh, Big Data Assimilation and AI Creating New Development in Real-time Weather Prediction. CREST International Symposium on Big Data Application, Tokyo, 1/13/2020.
- [67] 寺崎康児、三好建正、ビッグデータ同化に向けた観測誤差相関を考慮するデータ同化、NICAM開発者会議、沼津, 1/16/2020.
- [68] Takemasa Miyoshi, Enhancing Precipitation Prediction Algorithm by Data Assimilation of GPM Observations, The Joint PI Meeting of JAXA Earth Observation Missions FY2019, Tokyo, Japan, 1/24/2020.
- [69] 雨宮新、三好建正、Shlok Mohta, Application of machine learning methods to model bias correction: Lorenz-96 model experiments, 第10回データ同化ワークショップ、横浜, 1/30/2020.
- [70] 寺崎康児、三好建正、ビッグデータ同化に向けた観測誤差相関を考慮するデータ同化、ポスト京重点課題4成果報告会、東京, 1/31/2020.
- [71] Koji Terasaki and Takemasa Miyoshi, Accounting for the horizontal observation error correlation of satellite radiances in data assimilation, The Second IMT-Atlantique & RIKEN Joint Workshop, Brest, France, 2/10/2020.
- [72] Amemiya, A., T. Miyoshi, and M. Shlok, Application of machine learning methods to model bias correction: Lorenz-96 model experiments, The Second IMT-Atlantique & RIKEN Joint Workshop, Brest, France, 2/10/2020.
- [73] Shigenori Otsuka, Yasumitsu Maejima, and Takemasa Miyoshi, Toward hybrid NWP-AI system for precipitation nowcasting, The Second IMT-Atlantique & RIKEN Joint Workshop, Brest, France, 2/10/2020.
- [74] Maha Mdini, Toward model acceleration by ML, The Second IMT-Atlantique & RIKEN Joint Workshop: Statistical Modeling and Machine Learning in Meteorology and Oceanography, Brest, France, 2/10/2020.
- [75] Takemasa Miyoshi, Big Data Assimilation in Weather Prediction: From K to Fugaku, The 2nd R-CCS International Symposium, Kobe, Japan, 2/17/2020.

- [76] 三好建正、ビッグデータ同化による次世代気象予測、理研エンジニアリングネットワーク「気象予測データを再現する人工気象器利用した植物表現形質データ蓄積のための研究手法の開発」、東京、2/19/2020.
- [77] 高玉孝平、三好建正．東京湾の霧予報に向けた予備実験 大気-海洋-河川相互作用の役割，ポスト京重点課題4研究連絡会，神戸，2/22/2020.

### 16.5.5 Poster Presentations

- [1] Yasumitsu Maejima, Shigenori Otsuka and Takemasa Miyoshi Assimilating every 30-second phased array weather radar data in a torrential rainfall event on July 6, 2018 around Kobe city, JPGU2019, Chiba, Japan, 5/28/2019.
- [2] Honda, T., G.-Y. Lien, T. Miyoshi, Near-real-time SCALE-LETKF forecasts of the record breaking rainfall in Japan in July 2018, JPGU2019, Chiba, Japan, 5/29/2019.
- [3] Taylor, J., LienG.Y., Satoh, S., Miyoshi, T. Impact of Radar Artifacts from Phased Array Weather Radar to Short-Range Convective Forecasts, JPGU2019, Chiba, Japan, 5/29/2019.
- [4] Kotsuki S., Kurosawa K., Kanemaru K., Terasaki K. and Miyoshi T.: A New Evaluation Method for Cloud Microphysics Schemes Using GPM Dual-frequency Precipitation Radar. 39th International Conference on Radar Meteorology, Nara, Japan , 9/16/2019.
- [5] Otsuka, S., M. Ohhigashi, V. P. Huynh, P. Tandeo, and T. Miyoshi, A deep-learning approach to three-dimensional precipitation nowcasting. 39th International Conference on Radar Meteorology, Poster1-87, Nara, Japan, 9/16/2019.
- [6] Taylor, J., LienG.Y., Satoh, S., Miyoshi, T. The Use of Dual Phased Array Weather Radar Observations to Short-Range Convective Forecasts, 39th International Conference on Radar Meteorology, Nara, Japan, 9/16/2019.
- [7] Maejima, Y., S. Otsuka and T. Miyoshi, Assimilating every 30-second phased array weather radar data in a torrential rainfall event on July 6, 2018 around Kobe city, 39th International Conference on Radar Meteorology, Nara, Japan, 9/16/2019.
- [8] 寺崎康児，三好建正: NICAM-LETKFシステムを用いた平成30年7月豪雨再現性の解像度依存性について、日本気象学会秋季大会、福岡、10/30/2019.
- [9] 三好建正，ゲリラ豪雨予測を目指した「ビッグデータ同化」の研究，第6回「京」を中核とするHPCIシステム利用研究課題 成果報告会，東京，11/1/2019.
- [10] Keiichi Kondo, Takemasa Miyoshi, Non-Gaussian statistics in global atmospheric dynamics with a 10240-member ensemble Kalman filter experiment using an intermediate AGCM, AGU fall meeting 2019, San Francisco, USA, 12/10/2019.
- [11] Takemasa Miyoshi, “Local Particle Filter Implemented with Minor Modifications to the LETKF Code” , AMS 100th Annual Meeting, Boston, USA, 1/13/2020.
- [12] Taylor,J, Lien, G.Y., Satoh, S., T. Miyoshi, The use of dual phased array weather radar observations on short range convective forecasts, AMS 100th Annual Meeting, Boston, USA, 1/15/2020.
- [13] 高玉孝平，内山雄介，三好建正，アオコの分布予測に向けた湖の流動場シミュレーション琵琶湖とキネレット湖の事例．エンジニアリングネットワークリポート，和光，1/22/2020.
- [14] 三好建正、寺崎康児、小槻俊司、本田匠、雨宮新、James Taylor、高玉孝平、前島康光、坂本英之、観測ビッグデータ同化に向けた取り組み、ポスト京重点課題4成果報告会、東京、1/31/2020.
- [15] Kotsuki S., Terasaki K., Satoh M. and Miyoshi T.: Ensemble-Based Data Assimilation of GPM/DPR Reflectivity into the Nonhydrostatic Icosahedral Atmospheric Model NICAM. 4th workshop on assimilating satellite cloud and precipitation observations for NWP, ECMWF, Reading, UK , 2/3/2020.

- [16] Honda, T., S.-C. Yang, T. Miyoshi, Assimilating all-sky Himawari-8 radiances in the heavy rainfall event on 23 August 2018 in Taiwan, 4th workshop on assimilating satellite cloud and precipitation observations for NWP, ECMWF, Reading, UK, 2/3/2020.
- [17] T. Miyoshi, S. Kotsuki, K.Kondo, R. Potthast, Local Particle Filter Implemented with Minor Modifications to the LETKF Code, 4th workshop on assimilating satellite cloud and precipitation observations for NWP, ECMWF, Reading, UK, 2/5/2020.
- [18] Koji Terasaki and Takemasa Miyoshi, Towards big data assimilation in Fugaku by accounting for the horizontal observation error correlation of satellite observations, The 2nd R-CCS International Symposium, Kobe, Japan , 2/17/2020.
- [19] Honda, T., S.-C. Yang, T. Miyoshi, Assimilating all-sky Himawari-8 radiances in the heavy rainfall event on 23 August 2018 in Taiwan, The 2nd R-CCS International Symposium, Kobe, Japan , 2/17/2020.
- [20] Amemiya, A., T. Miyoshi, and M. Shlok, Application of machine learning methods to model bias correction: Lorenz-96 model experiments, The 2nd R-CCS International Symposium, Kobe, Japan , 2/17/2020.
- [21] Shigenori Otsuka, Marimo Ohhigashi, Viet Phi Huynh, Pierre Tandeo, and Takemasa Miyoshi, A deep-learning approach to three-dimensional precipitation nowcasting, The 2nd R-CCS International Symposium, Kobe, Japan, 2/17/2020.
- [22] Taylor,J, Lien, G.Y., Satoh, S., T. Miyoshi, The use of dual phased array weather radar observations on short range convective forecasts, The 2nd R-CCS International Symposium, Kobe, Japan , 2/17/2020.
- [23] Kohei Takatama, Yusuke Uchiyama, Takemasa Miyoshi, Simulations of lake currents toward the prediction of blue-green algae – cases of Lake Biwa and Lake Kinneret - The 2nd R-CCS International Symposium, Kobe, Japan, 2/17/2020.
- [24] M. Mdini, S. Otsuka, T. Miyoshi, Precipitation Nowcasting Based on Convolutional Neural Networks, The 2nd R-CCS International Symposium, Kobe, Japan, 2/17/2020.
- [25] Ohishi, S., T. Hihara, H. Aiki, J. Ishizaka, Y. Miyazawa, M. Kachi, An LETKF-based ocean reanalysis for the Asia-Oceania region using Himawari-8 SSTs and SMOS/SMAP SSS, Ocean Sciences Meeting 2020, San Diego, USA, 2/18/2020.
- [26] Otsuka, S., T. Awazu, and T. Miyoshi, Verification of precipitation forecast by pattern recognition. WCR-P/SPARC SATIO-TCS joint workshop on Stratosphere-Troposphere Dynamical Coupling in the Tropics, Kyoto, Japan, 2/22/2020.



## Chapter 17

# Computational Disaster Mitigation and Reduction Research Team

### 17.1 Members

Satoru Oishi (Team Leader)  
Muneo Hori (Senior Visiting Scientist)  
Hideyuki O-tani (Research Scientist)  
Yasuyuki Nagano (Senior Visiting Scientist)  
Masaaki Yabe (Senior Visiting Scientist)  
Tsuyoshi Ichimura (Visiting Scientist)  
Lalith Maddegedara (Visiting Scientist)  
Kohei Fujita (Visiting Scientist)  
Jian Chen (Visiting Scientist)  
Kazuki Yamanoi (Visiting Scientist)  
Hiroki Motoyama (Visiting Scientist)  
Tomohide Takeyama (Visiting Scientist)

### 17.2 Overview of Research Activities

Computational Disaster Mitigation and Reduction Research Team is aimed at developing advanced large-scale numerical simulation of natural disasters such as earthquake, tsunami, flood and inundation, for Kobe City and other urban areas in Hyogo Prefecture. Besides for the construction of a sophisticated urban area model and the development of new numerical codes, the team seeks to be a bridge between Science and Local Government for the disaster mitigation and reduction.

Computational Disaster Mitigation and Reduction Research Team is also conducting to integrate all kinds of geo hazards, water hazards and related hazards. Demand for natural disaster simulations increased related to growing number of disasters in recent years. Therefore, we are developing appropriate sets of programs which meet the demand of calculations. Computational Disaster Mitigation and Reduction Research Team is dealing with the following three kinds of research topics.

Urban model development: Research for urban hazards requires urban models which represent structure and shape of cities in numerical form. However, it takes very long time to create urban models consisting of buildings, foundations and infrastructures like bridges, ports and roads with ordinary way. Therefore, it is indispensable to invent methods which automatically construct urban models from existing data that is basically

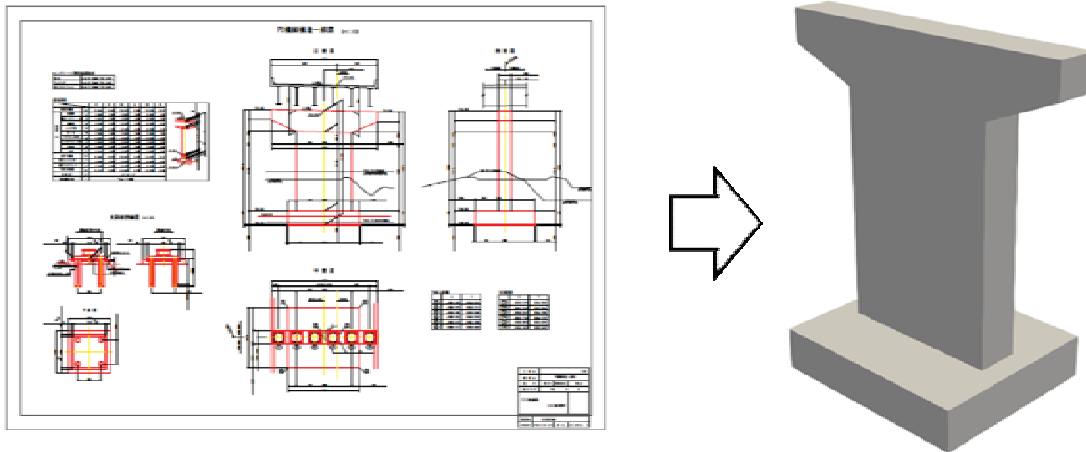


Figure 17.1: Automatically created three dimensional model of bridge pier.

ill-structured. Computational Disaster Mitigation and Reduction Research Team developed Data Processing Platform (DPP) for such purpose. By using DPP, construction of a national-wide urban model and 3D model construction from engineering drawings are achieved.

Performance enhancement of finite-element seismic ground motion simulation for many-core wide-SIMD architecture: We have been developing high-performance finite-element methods for the K computer and other CPU-based computational resources. In order to adapt the existing code to the Supercomputer Fugaku, we developed solver methods suitable for many-core wide SIMD architecture. An example of urban earthquake simulation using the developed finite-element method is conducted on the Intel Xeon Phi (Knights Landing)-based Oakforest PACS system.

Development of simulation-based assessment for debris-flow: To enable predictive simulation for debris-flow, we combined a 2D FVM simulation of debris flow and statistically-based landslide prediction. By using the numerous landslide data that was randomly generated based on the possibility distribution of landslides, 60 cases of the predictive simulations were simultaneously conducted on K computer. By this method, we numerically indicated that the variation of the estimated damage of debris-flow decreases in the downstream area of catchment topography. Additionally, we also started to use the debris-flow simulation as a generator of artificial damage map for machine learning training data.

## 17.3 Research Results and Achievements

### 17.3.1 Urban model development

In this year, we re-developed sets of programs for creating three dimensional urban model automatically. Those programs, namely Data Processing Platform (DPP) has been re-designed and implemented as Data Processing Platform Version 2 (DPP2). This program gives thematic elements on two dimensional computer aided design data (2D-CAD data) according to their levels of recognition, contexts of 2D-CAD data which come from arrangement of lines, figures and types of 2D-CAD data. Fig. 17.1 shows the result of three dimensional model of bridge pier from 2D-CAD data. The programs utilize rule-base processes for recognizing elements on the drawings in order to adopting the contexts and levels of recognition. However, the programs also utilize other kinds of process for recognizing elements, then it is possible to develop each software for many kinds of drawings using division of programming the software.

### 17.3.2 Performance enhancement of finite-element seismic ground motion simulation for many-core wide-SIMD architecture

We have been developing high-performance finite-element methods for the K computer and other CPU-based computational resources. Recent CPU systems such as the Arm SVE-based Fugaku system often equip many cores with wide-SIMD units; thus, changes in the algorithm and tuning designed for previous systems with lower

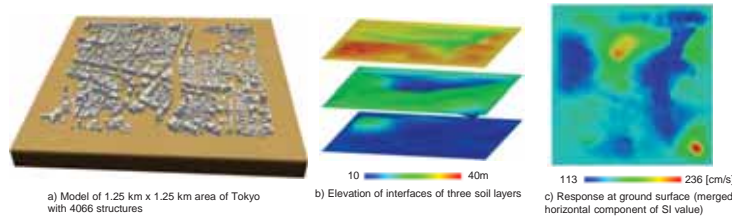


Figure 17.2: Application problem setting and results of finite-element seismic ground motion simulation. The ground is modeled with 252,738,195 second-order tetrahedral elements and 340,873,512 nodes.

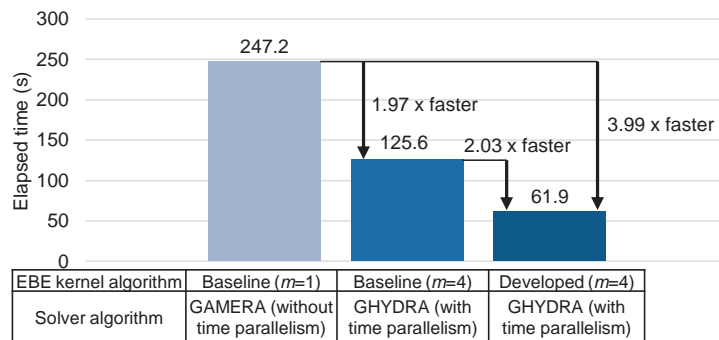


Figure 17.3: Performance of the developed finite-element solver on the application problem measured using 144 nodes of Oakforest-PACS.

core counts and narrower SIMD units are required to attain performance on recent systems. Indeed, when using the SC14 Gordon Bell Prize finalist solver, which attained high performance of 11.1% of peak FLOPS on the K computer, attained only 2.26% of peak FLOPS on the many-core wide-SIMD CPU-based Oakforest-PACS system at JCAHPC (Joint Center for Advanced High Performance Computing). Thus, we introduced a time-parallel solver algorithm and Element-by-Element kernel algorithms which can exploit performance of many-core wide-SIMD systems [1]. Here, based on the fact that the finite-element mesh is constant in time, the time-parallel solver algorithm rearranges the iterative solver such that random access is converted to sequential access in the matrix-vector product kernel. Cache-aware thread partitioning methods and SIMD-friendly blocking and loop splitting methods are introduced to accelerate the Element-by-Element based matrix-vector product kernel.

As an application example of the developed finite-element solver, we computed a 1.25 x 1.25 km area of Tokyo with a three-layered ground structure, discretized with 1 m sized elements (Fig. 17.2). Fig. 17.3 shows the elapsed time for solving the first 25 time steps of the input 1995 Kobe Earthquake wave with  $dt = 0.001$  s using 144 nodes of Oakforest-PACS. We can see that by using the time-parallel algorithm, the baseline solver (GAMERA: SC14 Gordon Bell Prize finalist solver) was accelerated by 1.97-fold. Combination with the developed Element-by-Element kernel algorithm leads to a further 2.03-fold speedup, leading to application performance of 11.6% of FP64 peak and a total of 3.99-fold speedup from the baseline solver. We can see that suitable algorithms and tuning for the many-core wide-SIMD CPU architecture has led to high-performance for the random access-dominated unstructured finite-element application. The developed method is expected to be effective for other many-core wide-SIMD CPU-based systems such as the Supercomputer Fugaku.

### 17.3.3 Debris flow simulation

Debris flow is a phenomenon that develops from landslide and is a catastrophic hazard that can cause human damages. To establish a widely-applicable debris-flow assessing scheme, firstly, we developed a parallelized numerical code based on the MacCoamack scheme, one of a scheme in finite difference method. To validate the simulation, we applied it to the heavy rainfall disaster that happened in Asakura city, Fukuoka prefecture, in 2017. In the simulation that uses actual landslide data as initiate locations of the debris flow, the damaged

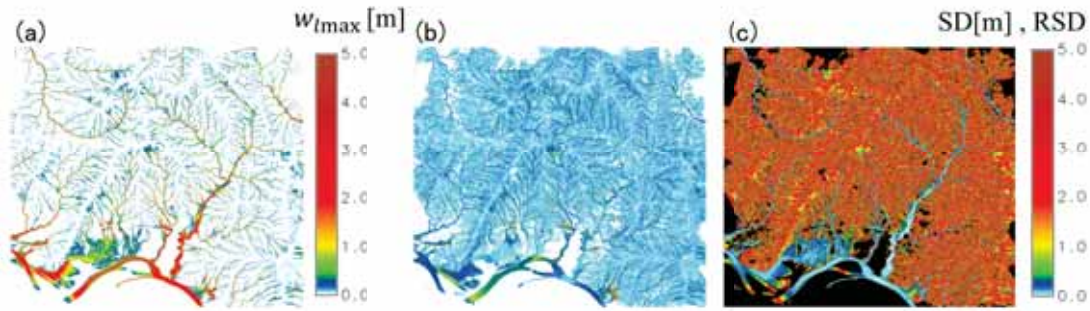


Figure 17.4: Average value, standard deviation, and relative standard deviation for maximum water level among 60 the simulation cases. [2].

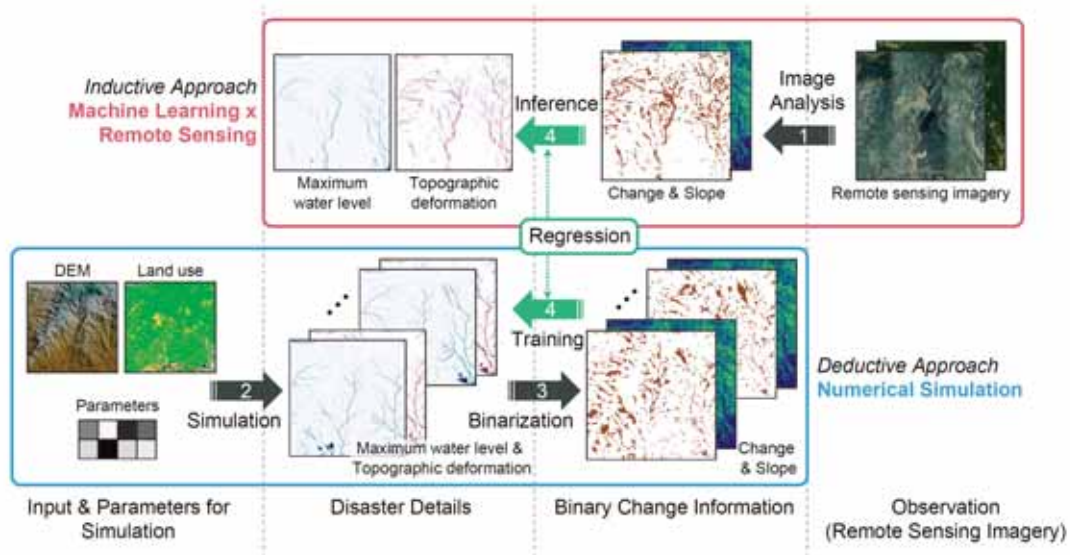


Figure 17.5: The overview concept of the proposed framework combining numerical simulation and machine learning [3].

area in the disaster was successfully reproduced. However, the landslide data can be obtained only in the post-disaster term; therefore, it was difficult to use the simulation for the prediction. To solve this problem, we generated the numerous artificial landslide data by applying the statistical landslide prediction method using logistic regression. We applied 60 cases of simulations using different artificial landslide data simultaneously using K computer. By summarizing all simulation outputs, we found that the variation of the maximum water levels and terrain deformation decreases as it flows to downstream in the catchment topography [2], see Fig 17.4. In other words, we numerically showed that the predictability of the debris-flow damages increases in the downstream area.

Another advantage of the proposed method is that it can generate numerous artificial damage maps for sediment-related disasters. To estimate the damage of disaster from the satellite imagery at an immediately following phase, AI trained with the actual disaster data seems to be very effective. However, the amount of training data is very limited because of the rarity of disasters. On the other hand, the proposed simulation can be used as a data generator to increase the amount of data. From this viewpoint, we started to collaborative work with the Geoinformatics Unit, RIKEN Center for Advanced Intelligence Project, to employ the simulation for the data generator. In this fiscal year, we succeeded in estimating the inundation depth and terrain deformation from remote sensing images by combining deep learning and numerical simulation[3], see Fig 17.5..

## 17.4 Schedule and Future Plan

1. Developing a national-wide real-time disaster simulation: We will enhance the automation of DPP2 to collect real-time seismic information and to perform an automated disaster simulation in a certain target area. This will reveal the extent to which speeding up is required for real-time characteristics.
2. Construction of templates for high fidelity models of highway network: In the template-based methodology, we need to ready the templates in beforehand, and the quality and quantity of templates will be critical to the output model.
3. Developing an algorithm for resolving the topographic error to improve the quality of the simulation and establish efficient data preparation on the large-scale simulation.
4. Testing the rapid extraction from SAR observation employing AI based method using the multiple simulation results as learning data.
5. Damage estimation of the sediment and water-related disasters in urban area considering the ground condition change due to an earthquake.

## 17.5 Publications

### 17.5.1 Articles/Journal

- [1] Fujita, K., Horikoshi, M., Ichimura, T., Meadows, L., Nakajima, K., Hori, M., Maddeggedara, L., “Development of Element-by-Element Kernel Algorithms in Unstructured Implicit Low-Order Finite-Element Earthquake Simulation for Many-Core Wide-SIMD CPUs.” *Computational Science - ICCS 2019, Lecture Notes in Computer Science*, vol 11536, 2019.
- [2] Yamanoi, K., Oishi, S., Kawaike, K., Nakagawa, H., “Predictive Simulation of Concurrent Debris Flow: How Slope Failure Locations Affect Predicted Damage”, *Preprints (2020)*,  
(doi: 10.20944/preprints202004.0118.v1).
- [3] Yokoya, N., Yamanoi K., He, W., Baier, G., Adriano, B., Miura, H., Oishi, S., “Breaking the Limits of Remote Sensing by Simulation and Deep Learning for Flood and Debris Flow Mapping”, *Arxiv (2020)*,  
(doi: arXiv:2006.05180)

### 17.5.2 Conference Papers

- [4] O-tani, H., Oishi, S., Hori, M., “FLEXIBLE AND ROBUST METHOD OF AUTOMATED DIGITAL BRIDGE CONSTRUCTION CORESPONDING TO THE QUANTITY AND QUALITY OF INFORMATION FROM ENGINEERING DRAWINGS”, *First i-Construction Symposium proceeding*, (2019).

### 17.5.3 Invited Talks

- [5] Oishi, S., “Large scale numerical simulation of earthquake, tsunami, weather, flood and sediment disaster”, *Advanced sensor symposium 2019*, (Osaka, July 24, 2019).

### 17.5.4 Oral Talks

- [6] Oishi, S., “Digital-Ensemble Concept for Making Resilient Society against Natural Hazard”, *JpGU Meeting 2019*, (Chiba, May 26, 2019).
- [7] O-tani, H., “A Study on Automated Type Definition in the System for Utilization of Heterogeneous Datasets Based on Automatic Conversions of Data formats”, *28th congress of GIS Association of Japan*, (Tokushima, October 20, 2019).
- [8] O-tani, H., Oishi, S. Hori, M., “FLEXIBLE AND ROBUST METHOD OF AUTOMATED DIGITAL BRIDGE CONSTRUCTION CORESPONDING TO THE QUANTITY AND QUALITY OF INFORMATION FROM ENGINEERING DRAWINGS”, *First i-Construction Symposium*, (Tokyo, July 30, 2019).

### 17.5.5 Software

- [9] O-tani, H., “Data Processing Platform”, (2019).

### 17.5.6 Patents

[10] O-tani, H., (2019) “Data interpretation device, method and program, data unification device, method and program and system to transform cites into digital twins”, 2019-139150. (2019).

## Chapter 18

# Computational Structural Biology Research Team

### 18.1 Members

Florence Tama (Team Leader)

Osamu Miyashita (Senior Scientist - October-March)

Bhaskar Dasgupta (Research Scientist - May-March)

Miki Nakano (Post-doctoral Researcher)

Sandhya Tiwari (Post-doctoral Researcher)

Loic Broyer (Intern – 3months from University of Grenoble)

Yumeno Kusahara (Assistant)

### 18.2 Overview of Research Activities

Biological molecular complexes of proteins and RNAs are of great interest in the area of molecular biology, as they are responsible for core biological functions such as cell replication, gene transcription, protein synthesis, regulation of cellular transport and numerous others. Those systems undergo large conformational transitions to achieve functional processes. Therefore, characterization of dynamical structures of these macromolecular complexes is crucial to understand their functional mechanisms and play an important role in the development of new drugs to treat human disease.

Experimentally, X-ray crystallography has been the primary tool to study protein conformations, providing high-resolution structures. Cryo-electron microscopy (EM) is becoming an important technique due to development of experimental apparatus as well as data analysis software. Although the structural resolution of the cryo-EM data tends to be at lower resolution, it has revealed critical information on structure and dynamics of large biological molecules. More recently, efforts like in RIKEN/SPring-8 have focused on developing intense X-ray free-electron laser (XFEL) light sources, which offer a new possibility to image single biological macromolecules. Since crystallization is not necessary for such a protein structure analysis, it would be possible to investigate the structure of biomolecules under various physiological conditions or to observe elementary steps of a biochemical function. However, at the current experimental condition, it cannot achieve atomic level resolution such as obtained by X-ray crystallography. High-speed atomic force microscopy (HS-AFM) is also a technique that is seeing growing number of biological applications. This technique enables observation of biological molecular complexes in motions in near-native environment, providing unique information regarding functional dynamics. However, due to the limitation of manufacturing process of the observation device, the structural resolution of the images are relatively low. Each experimental technique has its own strengths and weaknesses, and thus integration of computational simulations with experimental data is beneficial to obtain new and detailed information on the structure and dynamics of biological molecules.

Computationally, methods have been developed to predict structures from low-resolution experimental data such as from cryo-EM either using rigid body fitting or flexible deformations of known atomic structures. In addition, even when structures of the molecules are unknown, atomic models can be predicted using homology modeling and *ab initio* predictions, which could also be used for the modeling of new biomolecular complexes. Such hybrid approaches need to be extended further to integrate various available experimental data to determine the structures of important biomolecular complexes.

The ultimate line of our interdisciplinary research is development and applications of computational tools, through high performance computing, to integrate experimental data as obtained from various techniques such as X-ray crystallography, cryo-EM and XFEL with molecular modeling and simulations to acquire knowledge on the structure of a physiologically important protein complexes that are unattainable with existing experimental techniques.

## 18.3 Research Results and Achievements

### 18.3.1 Developments of computational tools for XFEL experimental data

Recent development of intense X-ray free-electron laser (XFEL) light sources offers a new possibility to image single biological macromolecules. Since crystallization is not necessary for such structure analysis, it would be possible to investigate the structure of macromolecular complexes under various physiological conditions or to observe elementary steps of a biochemical function. SPring-8/SACLA in Japan is one of the pioneering XFEL facilities in the world.

However, with current experimental conditions, atomic level resolution such as obtained by X-ray crystallography cannot yet be achieved. As XFEL experiments are very recent and still undergoing further development for routine study of biological molecules, computational algorithms and tools to understand and analyze experimental data need to be developed simultaneously. One focus of our research is the development of such computational tools. We have started to tackle these issues from multiple angles described below.

#### 18.3.1.1 3D Reconstruction from XFEL Diffraction Patterns – Applications to Experimental Data

In order to apply the XFEL single particle structure analysis algorithms we have been developing to experimental data, we are conducting joint research with Professor Yoshinori Nishino's research group at Hokkaido University. Pulsed coherent X-ray solution scattering (PCXSS), which is being developed by Nishino group, is a method that can observe samples in aqueous solution using XFEL, and with the continuous development of experimental methods, it is becoming possible to observe nano-scale samples.

This year, we have been analyzing the XFEL diffraction data of gold nanoparticles with a size of about 40-50 nanometers, aiming to reconstruct the three-dimensional structure the sample. Since experimental data include measurements in various situations, such as sample hits, multiple-sample hits, and misses, and furthermore the intensities of the diffraction patterns are not homogeneous due to fluctuations in the beam intensity during the measurements, we had to develop algorithms for selecting data that can be used for three-dimensional structure recovery (Figure 18.1). Filtered diffraction patterns are then assembled into 3D space using the algorithms we have been developing, with additional improvement to take into account the fluctuation of diffraction intensity strength resulting from beam intensity fluctuations. The model of nano-particle can be obtained from the obtained 3D diffraction intensity volume through phase-recovery procedure. The suitable condition for the procedure is currently investigated.

#### 18.3.1.2 “Idea generator” from 2D XFEL data of biological systems

Data analysis for XFEL data remains challenging. XFEL diffraction pattern is an unintuitive representation of the projection image of the sample in Fourier space. For biological systems, the current standard approach to reconstruct a real-space image of the sample, phase recovery, often fails due to the low diffraction power of biological samples. Therefore, we are developing a new hybrid approach to interpret diffraction patterns that utilizes image analysis with database search. More specifically, for a given set of XFEL diffraction patterns, we identify a plausible structures through searching database of possible 3D low-resolution shapes. We have previously shown the feasibility of such an approach with real space images from EM.

In the XFEL adaptation, we have had to overcome the challenge of aligning 2D image patterns that are in Fourier space, considering they do not contain phase information. Being in Fourier space, low-frequency (center)

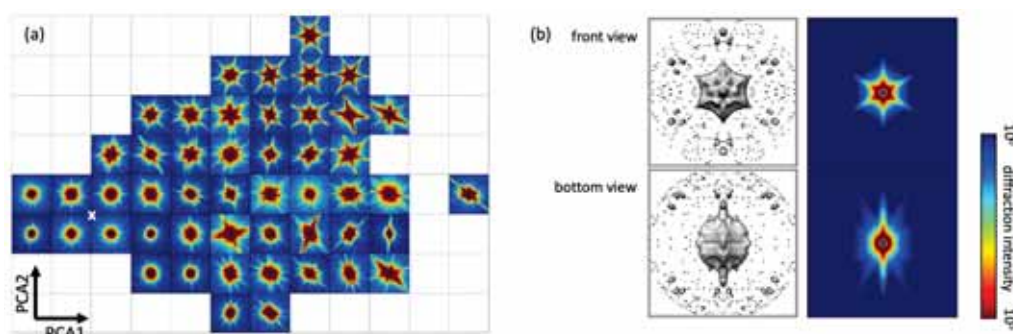


Figure 18.1: (a) Classification of experimental data. (b) A 3D diffraction intensity distribution reconstructed by slice matching algorithm. Isosurface plots from the top and the bottom view and the corresponding slice images are shown.

regions of diffraction patterns reflect the overall shapes of the molecule, while the details of the molecular structure is represented in high-frequency (outer) regions. Since our goal is to identify the low-resolution shapes that are consistent with target experimental data, we need to focus on the low-frequency regions. Furthermore, we are improving the algorithms so that it can deal with the diffraction patterns from actual experimental data. Diffraction patterns from biomolecules contain limited amount of signals due to the weak diffraction intensity, particularly being weak at high and strong at low wavenumber pixels, requiring careful selection of the matching region when aligning the diffraction images in Fourier space. Thus, only a certain region in the diffraction pattern (Region of Interest, ROI) can be used for the proposed match-finding algorithms, which poses a significant challenge in comparison to EM images. To automate the identification of ROI, we have developed an algorithm, in which the approximate size of the sample in the input image is estimated via fitting against a theoretical model, spherical form factors, and used to estimate the appropriate ROI. Using the estimated ROI, the match-finding algorithm to identify plausible candidate 3D models from a few XFEL diffraction patterns has been improved (Figure 18.2). In general, we find that the success of the strategy relies on the complexity of the shape and the diversity of input diffraction patterns. Nevertheless, the features of the shape in the input images are still captured within in the top matching hits.

### 18.3.2 Developments of computational tools for analyzing cry-EM experimental data

We have been developing a method to obtain detailed structural models from low resolution experimental data such as EM data using a molecular dynamics simulation. The three-dimensional image obtained from the cry-EM is given as data on a three-dimensional lattice. Here, the parameter that specifies the actual size of each lattice determines the size of the whole molecule and thus affects the modeling results. However, it is known that there can be an error of a few % in the estimation of this parameter. Therefore, in order to improve the accuracy of structural modeling, we have developed an algorithm that can estimate an accurate value for this lattice size parameter.

In this algorithm, many EM maps with different grid sizes are prepared and large number of models are created by performing structure refinement against these maps. Then, the correct lattice size is estimated by evaluating the "quality" of each of these structures. Here, evaluation of the "quality" of the obtained structures needs to be performed independent of the fitting procedure. The algorithm was tested using the maps created by simulation for several model systems, and various "quality" evaluation approaches were examined. First, we showed that the general correlation coefficient, which measures the degree of agreement between the structure and the map as corresponding electron densities, is not sufficient to detect correct grid size (Figure 18.3). It was also found that the Molprobit index, which is commonly used to evaluate X-ray crystal structure models, is insufficient because there is no physicochemical aspect in the evaluation of interatomic interactions. Finally, we found that GOAP, which is an index used for protein structure prediction, is effective in evaluating the local structure and interatomic distance in proteins, which is the "quality" of the structure necessary to identify correct grid size. We applied the developed algorithm to experimental data and demonstrated the usability of the algorithm.

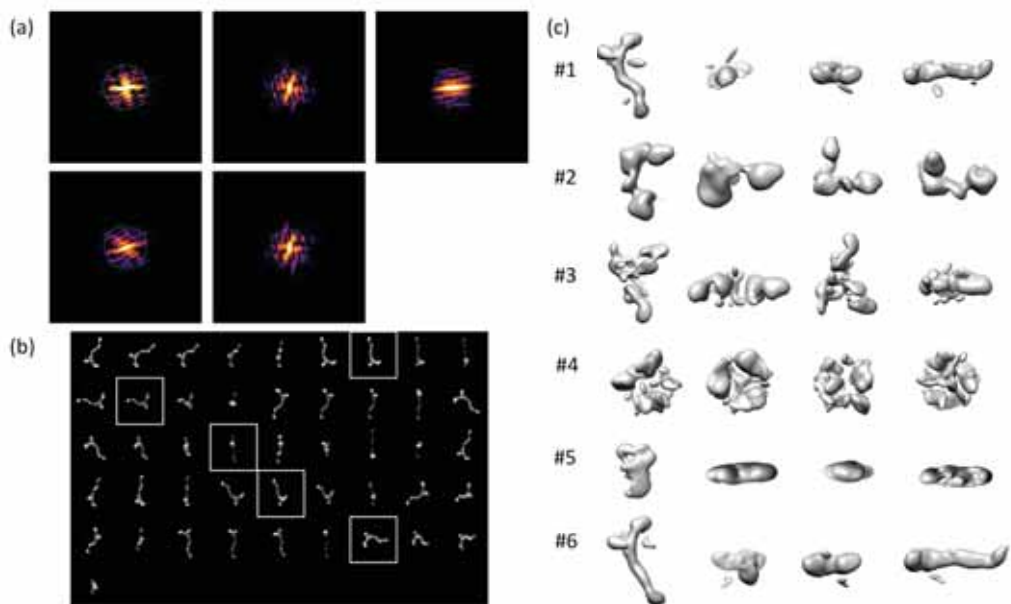


Figure 18.2: An example of the model finding algorithm outputs (a) Five simulated diffraction patterns that are used as the query inputs. Two circles on each pattern indicate the definition of Region of Interest that are determined using the newly developed algorithm. (b) Projection images of the “answer” structure. Five input patterns correspond to the input diffraction patterns. (c) Six cryo-EM maps that are identified as the models consistent with the input diffraction patterns.

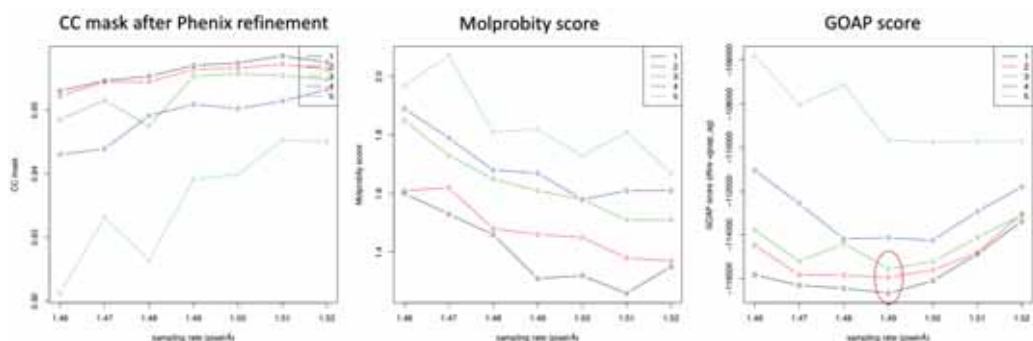


Figure 18.3: A variation of target EM maps were generated by changing the size of the grid lattice (X axis) and multiple structure refinement trials were performed against these EM maps. Then the “quality” of those structures was evaluated by several indicators (correlation coefficient CC, Molprobit score, GOAP score), and the GOAP score was most consistent with the ground truth (1.49). It was found that the structural model (circle) based on the cubic lattice size can be identified as the most correct.

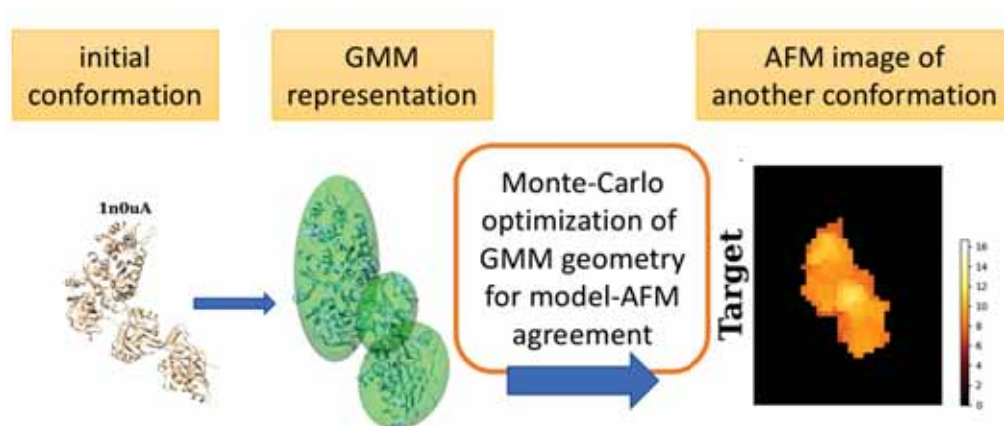


Figure 18.4: Overview of the new approach for conformational modeling of proteins based on AFM images. A structure of the target protein (initial conformation) is represented using Gaussian mixture model (GMM representation). The positions of the Gaussian kernels are optimized via Monte-Carlo optimization so that the agreement with the target AFM experimental image is maximized.

### 18.3.3 Modeling from AFM images

Atomic Force Microscopy (AFM) is an experimental technique which enables observation of biomolecules in near native condition. AFM uses mechanical device (cantilever) to trace the molecular surface and provides images of biomolecules at nanometer resolution. In particular, High-speed AFM experiments produce a series of images following live dynamics of biomolecules, which may provide a wealth of information regarding protein dynamics and functions. However, the information in the data is very limited, 2-dimensional and low-resolution. To further understand biomolecular functions, information on three-dimensional (3D) structures is beneficial.

We are developing algorithms to recover 3D information from AFM images by computational modeling. The AFM image includes only low-resolution representation of a molecule; therefore we represent the structures by a coarse grained model (Gaussian mixture model). Using Monte-Carlo sampling, candidate models are generated to increase the agreement between AFM images simulated from the models and target AFM image. We have tested the algorithm on two proteins which undergo large conformational transitions. AFM images were simulated from one conformation and used as synthetic target AFM image (Figure 18.4). We showed that, starting from another conformation, the algorithm can produce a low-resolution 3D model of the target molecule. Effect of molecular orientations captured in AFM images on the 3D modeling performance was also examined and it is shown that similar accuracy can be obtained for many orientations. The proposed algorithm can generate 3D low-resolution protein models, from which conformational transitions observed in AFM images can be interpreted in more detail.

### 18.3.4 Molecular dynamics simulations of Tim21 protein for interpretation of low-resolution X-ray crystallographic data

X-ray crystallography has been the major source of information on protein structures. It can provide detailed atomic level information, yet the sample needs to be crystallized and generally cryo-cooled, and the obtained data represents a frozen snapshot of proteins in crystal. Recently, new approaches to obtain dynamical information of biological molecules are actively studied. Professor Kohda group at Kyushu University proposed a method called CCFS, in which protein crystal is designed to have sufficient space inside so that molecules can still move inside the crystal. The electron density map from CCFS is at much lower resolution than conventional crystallography, due to the conformational flexibility, and as a result, analysis of such data also requires new computational approaches.

We have performed molecular dynamics simulations in order to interpret CCFS experimental data of a protein, Tim21, particularly regarding the conformation of a loop, L2. Tim21 is a subunit of a highly dynamic translocase of the inner mitochondrial membrane complex. A loop segment in Tim21, which is in close proximity of the binding site of Tim23, was recently studied by CCFS and the obtained electron density indicates the loop conformation that is different conformations obtained from conventional X-ray and NMR experiments, making

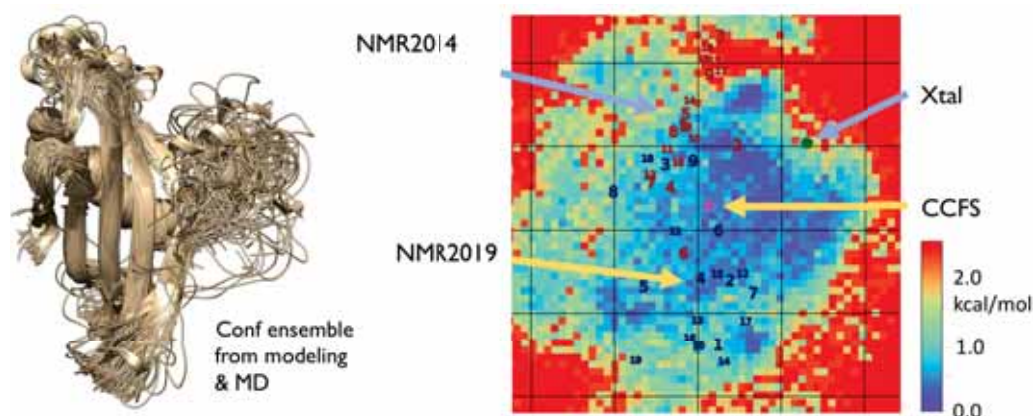


Figure 18.5: Conformational ensemble of loop L2 of Tim21 protein obtained by molecular dynamics simulation in solution environment (left). Free energy surface estimated from the results show that CCFS structural model is most consistent with the predicted solution conformations.

the analysis of the new experimental data difficult. Using MD simulations we can provide information on the structure and dynamics of the loop in solution to provide interpretation of these data.

We obtained the conformational ensemble of the loop using ab-initio loop modeling techniques and molecular MD simulations (Figure 18.5). MD simulations confirmed mobility of the loop. Multidimensional scaling and clustering were used to characterize the dynamic conformational ensemble of the loop. Free energy landscape showed that the CCFS crystal structure occupied a low energy region as compared to the conventional X-ray crystal structure. Analysis of crystal packing indicates that the CCFS provides larger conformational space for the motions of the loop. These methods in integration with experimental techniques such as CCFS has the potential to transform the studies on flexible regions of proteins.

## 18.4 Schedule and Future Plan

Cryo-EM experiments are quickly becoming an essential tool for studying biomolecular complexes. New XFEL facilities are getting into operation every year in the world, providing opportunities for new experiments. The amount of data from such experiments will continue to grow in numbers and analysis of such big datasets will increase the necessity of high-performance computing. Time-resolved experiments using high-speed AFM and XFEL serial femto-second crystallography also provides additional information of molecular movies. We aim to utilize high performance computer such as Fugaku to break the limitation of current data processing and hybrid computational modeling approaches to obtain a new level of structural information of biological complexes from various experimental data. For this goal, we plan to develop algorithms and software to analyze large dataset to obtain not only structural models but also dynamical information which is essential for understanding of the mechanisms of biomolecular functions. With these techniques, through collaborations with experimental groups, we aim to contribute to the structural biology community.

## 18.5 Publications

### 18.5.1 Articles/Journal

- [1] Bala S, Shinya S, Srivastava A et al. Crystal contact-free conformation of an intrinsically flexible loop in protein crystal: Tim21 as the case study. *Biochim Biophys Acta Gen Subj.* 2020;1864:129418.
- [2] Srivastava A, Bala S, Motomura H, Kohda D, Tama F, Miyashita O. Conformational ensemble of an intrinsically flexible loop in mitochondrial import protein Tim21 studied by modeling and molecular dynamics simulations. *Biochim Biophys Acta Gen Subj.* 2020;1864:129417.
- [3] Srivastava A, Bala S, Motomura H, Kohda D, Tama F, Miyashita O. Conformational ensemble of an intrinsically flexible loop in mitochondrial import protein Tim21 studied by modeling and molecular dynamics simulations. *Biochim Biophys Acta Gen Subj.* 2020;1864:129417.

- [4] Dasgupta B, Miyashita O, Tama F. Reconstruction of low-resolution molecular structures from simulated atomic force microscopy images. *Biochim Biophys Acta Gen Subj.* 2020;1864:129420.
- [5] Nakano M, Miyashita O, Tama F. Parameter optimization for 3D-reconstruction from XFEL diffraction patterns based on Fourier slice matching. *Biophys Physicobiol.* 2019;16:367-376.
- [6] Nagai T, Tama F, Miyashita O. Cryo-Cooling Effect on DHFR Crystal Studied by Replica-Exchange Molecular Dynamics Simulations. *Biophys J.* 2019;116:395-405.
- [7] Srivastava A, Tama F, Kohda D, Miyashita O. Computational investigation of the conformational dynamics in Tom20-mitochondrial presequence tethered complexes. *Proteins.* 2019;87:81-90.

### 18.5.2 Invited Talks

- [8] Tama F, “Hybrid approaches to reveal structure and dynamics of large biological complexes from single molecule experiments”, American Chemical Society National Meeting, 2019/3/31-4/3, Orlando, US
- [9] Miyashita O, “Hybrid Structure Modeling of Biomolecules from”, Chem-Bio Informatics Society(CBI) Annual Meeting 2019, 2019/6/17-19, Tokyo, Japan
- [10] Tama F, “Modeling conformational transitions of biomolecules from cryo-EM data”, French Electron Microscopy Society meeting, 2019/7/2-5, Poitiers, France
- [11] Tama F, “Kinase inhibitors for modulation of circadian rhythms”, American Chemical Society National Meeting, 2019/8/25-29, San Diego, US
- [12] Tama F, “Molecular mechanisms involved in the regulation of the Circadian Clock”, The 10th Toyota RIKEN international workshop on Science of Life Phenomena Woven by Water and Biomolecules, 2019/9/4-6, Nagoya, Japan
- [13] Tama F, “Integrative modeling to characterize structure and dynamics of biomolecules from single molecule experiments”, Integrative structural biology meeting, 2019/10/7-11, Toulouse, France
- [14] Miyashita O, “Hybrid Approach for Structural Biology: Simulation and Experimental Data”, CBI-society meeting 2019, 2019/10/22-24, Tokyo, Japan
- [15] Miyashita O, “Hybrid Structure Modeling of Biomolecules using Cryo-EM Data”, KINKA Chemical Society 106th Open Lecture - Structure Analysis of Biomolecules using Cryo-electron Microscopy, 2019/10/30, Osaka Japan
- [16] Miyashita O, “Reconstruction of Low-resolution (Bio) Molecular Structures from Simulated Atomic Force Microscopy Images”, The 1st International Conference on Big Data and Machine Learning in Microscopy, 2020/01/15-17, Kanazawa, Japan
- [17] Tama F, “Flexible fitting methods and applications”, EMBO workshop, CEM3DIP 2020: Single particle cryoEM of macromolecular-assemblies and cellular tomography, 2020/1/19-30, Kolkata, India

### 18.5.3 Oral Talks

- [18] Nakano M, Miyashita O, Tama F, “Effect of binning size of XFEL Diffraction Patterns on the resolution of reconstructed 3D-molecular structure”, Chem-Bio Informatics Society(CBI) Annual Meeting 2019, 2019/10/22-24, Tokyo, Japan

### 18.5.4 Poster Presentations

- [19] Tiwari SP, Miyashita O, Tama F, “COMPUTATIONAL PROTOCOL FOR OPTIMIZING THE PIXEL SIZE PARAMETER TO IMPROVE SINGLE PARTICLE CRYO-ELECTRON MICROSCOPY MAPS.”, Biophysical Society 64th Annual Meeting, 2020/2/17, San Diego, California, USA
- [20] Miki N, Tama F, Miyashita O, “Effect of binning size of XFEL Diffraction Patterns on the resolution of reconstructed 3D-molecular structure”, Chem-Bio Informatics Society(CBI) Annual Meeting 2019, 2019/10/22-24, Tokyo, Japan
- [21] Dasgupta B, Miyashita O, Tama F, “Hybrid Structural Modeling of Proteins Based on Atomic Force Microscopy (AFM) to Recover Conformational Transition Included in AFM Images”, The 2nd R-CCS International Symposium, 2020/2/17-18, Kobe, Japan



## Chapter 19

# High Performance Artificial Intelligence Systems Research Team

### 19.1 Members

Satoshi Matsuoka (Team Leader)

Jun Igarashi (Senior Scientist)

Aleksandr Drozd (Research Scientist)

Shweta Salaria (Postdoctoral Researcher)

Emil Vatai (Postdoctoral Researcher)

Toshio Endo (Senior Visiting Scientist)

Mohamed Wahib (Visiting Scientist)

Miquel Pericas (Visiting Scientist)

Akihiro Nomura (Visiting Scientist)

Tokyo Tech Matsuoka lab students

### 19.2 Overview of Research Activities

The High Performance Artificial Intelligence Systems Research Team focuses on convergence of HPC and AI, namely high performance systems, software, and algorithms research for artificial intelligence/machine learning. In collaboration with other research institutes in HPC and AI-related research in Japan as well as globally it seeks to develop next-generation AI technology that will utilize state-of-art HPC facilities, including Fugaku.

For the time being until Mar 31, 2022, team's research work is being sponsored by the JST-CREST "DEEP" AI Project "Fast and cost-effective deep learning algorithm platform for video processing in social infrastructure".

#### 19.2.1 Research Topics

- Extreme speedup and scalability of deep learning: Achieve extreme scalability of deep learning in large-scale supercomputing environments including the Fugaku extending the latest algorithms and frameworks for deep learning.
- Performance analysis of deep learning: Accelerate computational kernels for AI over the state-of-the-art hardware architectures by analyzing algorithms for deep learning and other machine learning/AI, measuring their performance and constructing their performance models.

- Acceleration of modern AI algorithms: Accelerate advanced AI algorithms, such as ultra-deep neural networks and high-resolution GAN over images, those that require massive computational resources, using extreme-scale deep learning systems.
- Acceleration of HPC algorithms using machine learning: Accelerate HPC algorithms, systems, and applications using empirical models based on machine learning.

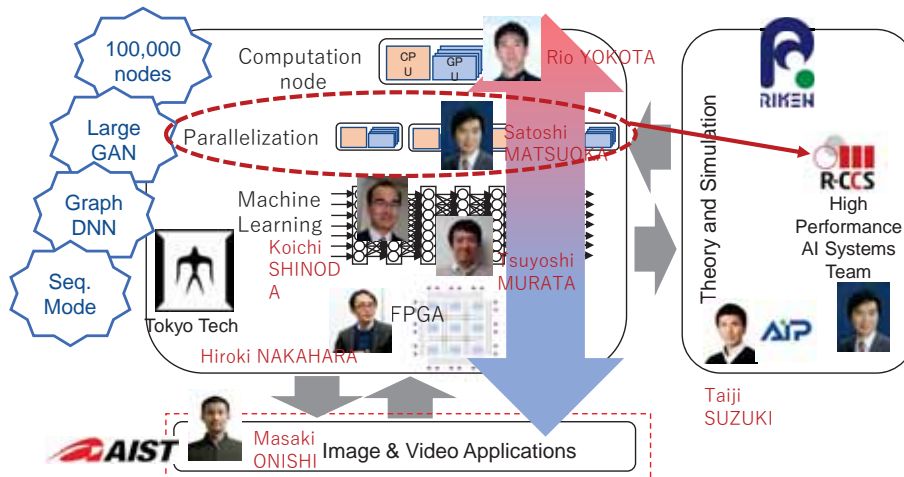


Figure 19.1: Structure of JST-CREST “DEEP” AI project

## 19.3 Research Results and Achievements

### 19.3.1 Massive Scale Deep Learning on Fugaku

The Fugaku supercomputer is an attractive platform for deep learning training and inference. A64FX CPU provided high FP16 and int8 compute performance as well as high memory bandwidth for memory-bound kernels such as certain implementations of convolutional operation. Additionally, high performance Tofu fabric enables efficient model-parallel and hybrid training schemes. We are exploring how unique features of the Fugaku supercomputer can be exploited in the most efficient ways in AI workloads, as well doing basic work to create deep learning software ecosystem on Fugaku. The later is done in collaboration with other research teams (Minami team and K. Sato team) as well as with industrial partners such as Arm, Fujitsu, and Linaro.

### 19.3.2 Accelerating DL with 2nd Order Optimization and Distributed Training

In this work, we proposed a large-scale distributed computational design for the second-order optimization using Kronecker-Factored Approximate Curvature (K-FAC) and showed the advantages of K-FAC over the first order stochastic gradient descent (SGD) for the training of ResNet-50 with ImageNet classification using extremely large mini-batches. We introduced several schemes for the training using K-FAC with mini-batch sizes up to 131,072 and achieved over 75% top-1 accuracy in much fewer number of epochs/iterations compared to the existing work using SGD with large mini-batch. Contrary to prior claims that second order methods do not generalize as well as SGD, we were able to show that this is not at all the case, even for extremely large mini-batches. Data and model hybrid parallelism introduced in our design allowed us to train on 1024 GPUs and achieved 74.9% in 10 minutes by using K-FAC with the stale Fisher information matrix (FIM). This is the first work which observes the relationship between the FIM of ResNet-50 and its training on large mini-batches ranging from 4K to 131K. There is still room for improvement in our distributed design to overcome the bottleneck of computation/communication for K-FAC – the Kronecker factors can be approximated more aggressively without loss of accuracy. One interesting observation is that, whenever we coupled our method with a well known technique that improves the convergence of SGD, it allowed us to approximate the FIM

more aggressively without any loss of accuracy. This suggests that all these seemingly ad hoc techniques to improve the convergence of SGD, are actually performing an equivalent role to the FIM in some way. The advantage that we have in designing better optimizers by taking this approach is that we are starting from the most mathematically rigorous form, and every improvement that we make is a systematic design decision based on observation of the FIM. Even if we end up having similar performance to the best known first-order methods, at least we will have a better understanding of why it works by starting from second-order methods. Further analysis of the eigenvalues of FIM and its effect on preconditioning the gradient will allow us to further understand the advantage of second-order methods for the training of deep neural networks with extremely

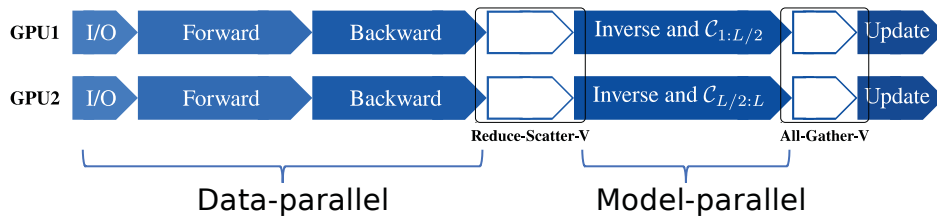


Figure 19.2: Design of hybrid parallel distributed K-FAC

### 19.3.3 A Software Systolic Array on GPUs

In this study, we build a software systolic array on the top of GPU architecture. Driven by the critical demands of intensive computation in a variety of fields, an old and heavily-researched parallel computer architecture, namely systolic array, is being revived in the post-Moore’s law era, e.g. Google’s Tensor Processing Unit (TPU), Nvidia’s Tensor Core. Such a kind of domain-specific processors can provide extremely high TOPS (TeraOps/Second) and TOPS/Watt for compute-intensive algorithms, i.e. convolution, dense matrix multiplication, AI-purposed computation, Discrete Cosine Transform (DCT). In the last decade, we witnessed the emergence of Graphics Processing Units (GPU). As one of the most popular accelerators recently, GPUs are adopted to speed up the computation in a wide range of fields, i.e. scientific, engineering. Taking the latest TOP500 rankings in High-Performance Computing (HPC) for instance, more than half of the FLOPS comes from the Nvidia Tesla GPUs.

As Figure 19.3 shown, a systolic array is a network of processing elements (PEs) that rhythmically compute, accumulate and transfer data through the system. In typical systolic arrays, all of the PEs are often nested as a two-dimensional mesh. The systolic array architecture is simple yet very effective to achieve both computation and energy efficiencies with very limited memory bandwidth. Inspired by the mechanism of the hard-wired systolic arrays, we innovate a versatile execution model on the top of CUDA architecture for optimizing applications on GPUs. More specifically, we mimic the behavior of systolic arrays by CUDA warp, register files, and shuffle instruction. It is noteworthy that the three key techniques contribute to our model. First, register cache; second, partial sums accumulation and transfer; third, in-register computation. Our model improves the performance of regular memory-bound kernels by taking advantage of thread-private registers as a cache to perform the efficient in-register computation and employing the shuffle intrinsic to exchange partial sums between CUDA threads within a single CUDA Warp. Our model can be viewed as Software Systolic Array Execution Model (SSAM).

Regarding most of the scientific applications (or kernels), the increasing flops-to-bytes ratio of GPUs makes their computational performances bounded by the memory bandwidth. Memory-bound kernels that have a regular pattern of computation are particularly challenging since they appear to be simple, yet they require very complex data reuse schemes to effectively utilize the CUDA memory hierarchy, e.g. global memory, shared memory, register memory, etc. Typically, advanced GPU implementations for memory-bound kernels on structured grids rely on the optimized use of fast on-chip scratchpad memory: the programmer uses this user-managed scratchpad memory for reducing the global memory access. Indeed, there exists a plethora of work proposing variations and combinations of the three locality schemes that rely on scratchpad memory: spatial blocking, temporal blocking, and a wavefront pipeline. Those complex locality schemes enabled strides in performance improvements. However, they essentially moved the bottleneck from the global memory to the faster, yet smaller, scratchpad. The objective of this study is to yet again move the bottleneck from the scratchpad to a faster resource: register files. Hence, we prioritize to use register files to cache data rather than

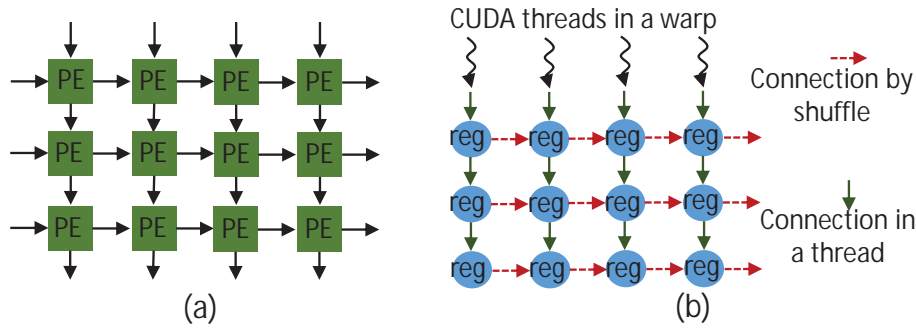


Figure 19.3: (a) Hardware 2D systolic array structure. PE is a processing element. (b) SSAM on CUDA (2D problem illustration: "reg" is a register). In the vertical direction, registers are in the same thread. In the horizontal direction, registers are exchanged by the shuffle instruction.

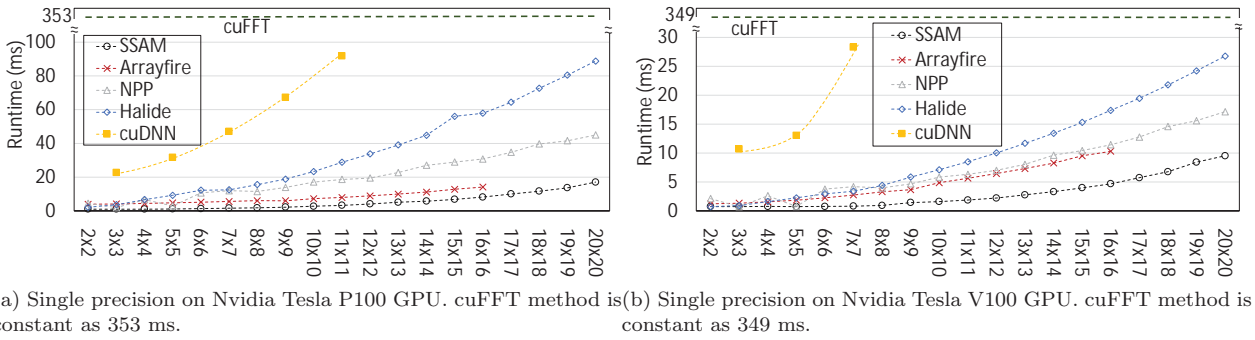


Figure 19.4: 2D Convolution performance and scalability. The image size is  $8192 \times 8192$ , the x-axis is filter size, the y-axis is execution time. Arrayfire, NPP, Halide, and cuDNN are state-of-the-art libraries.

shared memory, resulting in better data locality and higher computational efficiency.

A wide class of memory-bound kernels (or applications) can benefit from this execution model. In this study, we focus on mapping typical memory-bound kernels in SSAM, i.e. 2D convolution, 2D/3D stencils, Summed Area Tables (SAT). There is a strong motivation to optimize these kernels on GPUs. The 2D convolution and SAT computation become increasingly important in the Deep Learning workload. The stencil is a fundamental computation pattern in most of the scientific applications. To further improve the dependency graph in SSAM, we propose a novel algorithm to transpose the register cache locally (termed as BRLT). Unlike 2D convolution and stencils, we propose a collection of SSAM-based algorithms for SAT computation by the BRLT algorithm. To insight the performance advances of SSAM-based algorithms, we build performance models to analyze their mechanisms while using micro-benchmarking to measure some constant variables of GPUs.

The contributions in this study are as follows. *First*, we design and formulate a software systolic array on the top of CUDA architecture for speeding up the computation of memory-bound kernels with regular access on GPUs. *Second*, we analyze the data reuse and redundancy schemes to quantify the efficiency and limitations of SSAM. *Third*, we evaluate the proposed model for a wide variety of 2D/3D stencils, 2D general convolution (as in Figure 19.4), and SAT kernels on the latest Nvidia Tesla GPUs and demonstrate that SSAM-based algorithms outperform the top reported state-of-the-art libraries, e.g. NPP, Arrayfire, OpenCV. *Fourth*, we propose a novel algorithm to transpose the register matrix (used as register cache) locally and concurrently, resulting in improving the program dependency graph in SSAM for better locality and higher parallelism. *Finally*, we pave a novel way for code automation on GPUs due to the versatility and simplicity of SSAM for optimizing a large variant of algorithms.

### 19.3.4 Scaling Distributed Deep Learning Workloads beyond the Memory Capacity with KARMA

The dedicated memory of hardware accelerators can be insufficient to store all weights and/or intermediate states of large deep learning models. Although model parallelism is a viable approach to reduce the memory pressure issue, significant modification of the source code and considerations for algorithms are required. We propose a performance model based on the concurrency analysis of out-of-core training behavior, and derive a strategy that combines layer swapping and redundant recomputing. *KARMA* enables distributed training of DNNs beyond memory capacity. *KARMA* splits the layers to groups of blocks that optimize for reducing the total runtime. We reduce the total runtime by formulating a two-tier constrained optimization problem that maximizes the device occupancy, which in-turn requires an efficient strategy to reduce the stalls due to data movement to minimum. We use a novel scheduling strategy that involves a capacity-based layer swapping policy interleaved with recomputation. Next, *KARMA* generates an execution plan based on the identified optimal blocking and recompute strategy, and finally replaces the original model code with the new one.

Figure 19.5 shows the training performance (samples/second) of different batch sizes, for different models. As the batch size grows, the out-of-core effects start to appear. The performance begins to drop after the memory footprint exceeds the GPU memory capacity (starting from the second data point on each x-axis). We further conduct an experiment at which we use the same number of GPUs for the original implementation vs. data parallel *KARMA* (Figure 19.6). To get a fair comparison, we also compare to an optimized version of the original implementation for which we added the phased gradient exchange. Surprisingly, the pure data parallel *KARMA* outperforms the model-/data-parallel hybrid on 2,048 GPUs. Upon inspection it became clear that increasing the numbers of GPUs also increases the communication cost for the original version. Note that *KARMA* has fewer iterations (i.e. communication rounds) since it has a larger mini-batch size.

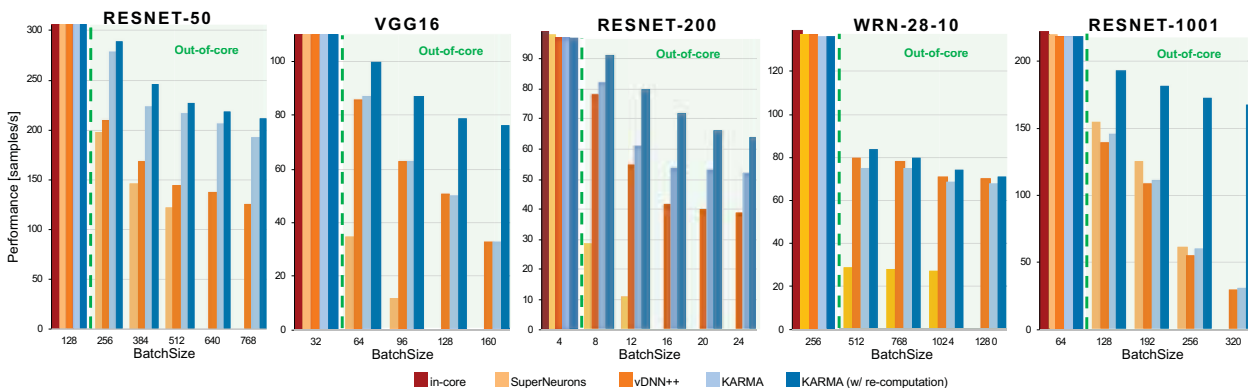


Figure 19.5: Performance using a V100 SMX2 (16GB) GPU. For all figures, only the first reported mini-batch size (x-axis) fits in memory for all models (state-of-the-art recompute strategy)

### 19.3.5 Optimizing Collective Communication in DL Training

Training models on large-scale GPUs-accelerated clusters are becoming a commonplace due to the increase in complexity and size in deep learning models. One of the main challenges for distributed training is the collective communication overhead for large message sizes: up to hundreds of MB. We have developed two hierarchical distributed memory multileader AllReduce algorithms optimized for GPU-accelerated clusters (named *lr\_lr* and *lr\_rab*), in which GPUs inside a computing node perform an intra-node communication phase to gather and store results of local reduced values to designated GPUs (known as node leaders). Node leaders then keep a role as an inter-node communicator. Each leader exchanges one part of reduced values to the leaders of the other nodes in parallel. Hence, we are capable of significantly reducing the time for injecting data into the inter-node network. We also overlap the inter-node and intra-node communication by implementing our proposal in a pipelined manner. We evaluate those algorithms on the discrete-event simulation Simgrid. We show that our algorithms, *lr\_lr* and *lr\_rab*, can cut down the execution time of an AllReduce microbenchmark that uses the logical ring algorithm (*lr*) by up to 45% and 51%, respectively. With the pipelined implementation, our *lr\_lr\_pipe* achieves 15% performance improvement when compared with *lr\_lr*. In addition, the simulation result also projects power savings for the network devices of up to 23% and 32%.

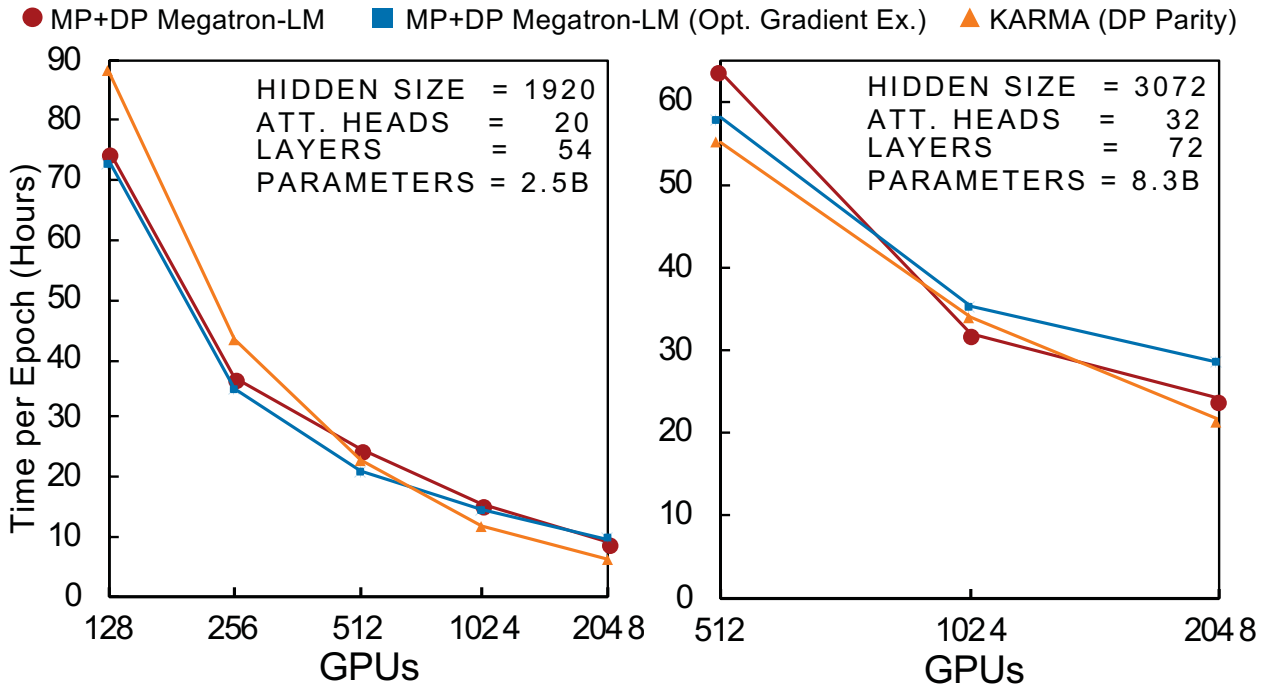


Figure 19.6: Parallelization performance of two Megatron-LM configurations. We compare using the same number of GPUs (parity<sup>1</sup>). Megatron-LM: we compare the original data-/model-parallel hybrid, the original plus our optimized phased gradient exchange, and data parallel KARMA

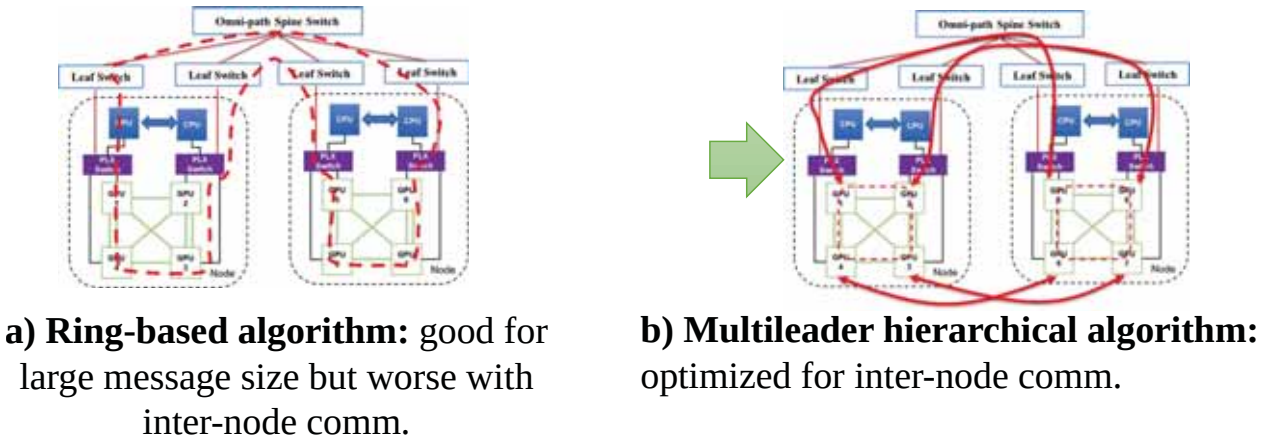


Figure 19.7: Multileader hierarchical reduction algorithm

### 19.3.6 Training Large 3D CNNs with Hybrid Parallelism

*This work is conducted among Yosuke Oyama (Satoshi Matsuoka lab, Tokyo Tech), Center for Applied Scientific Computing (CASC) at Lawrence Livermore National Laboratory, and National Energy Research Scientific Computing Center (NERSC) at Lawrence Berkeley National Laboratory.*

Recent advances in deep learning have demonstrated that deep neural networks, especially convolutional neural networks (CNNs), can solve a lot of real-world problems. Specifically, 3D convolutional neural networks have been applied to scientific workflows, including 3D medical images and simulation outputs, to perform end-to-end inference without prior knowledge of underlying research fields. However, the training of 3D CNNs requires much computational resources and time, especially GPU memory capacity, to store the networks' intermediate data due to their gigantic data volume. This problem worsens when higher-resolution data is fed to the networks, which can improve the inference accuracy of the networks. 3D CNNs can consume tens to

hundreds of gigabytes of memory, as exemplified in the cosmology and medical models evaluated in our work.

In our work, we present scalable hybrid-parallel algorithms for training large-scale 3D convolutional neural networks. Deep learning-based emerging scientific workflows often require model training with large, high-dimensional samples, which can make training much more costly and even infeasible due to excessive memory usage. We solve these challenges by extensively applying hybrid parallelism throughout the end-to-end training pipeline, including both computations and I/O. Our hybrid-parallel algorithm extends the standard data parallelism with spatial parallelism, which partitions a single sample in the spatial domain, realizing strong scaling beyond the mini-batch dimension with a larger aggregated memory capacity. We evaluate our proposed training algorithms with two challenging 3D CNNs, CosmoFlow and 3D U-Net. Our comprehensive performance studies show that good weak and strong scaling can be achieved for both networks using up to 2K GPUs. More importantly, we enable training of CosmoFlow with much larger samples than previously possible, realizing an order-of-magnitude improvement in prediction accuracy.

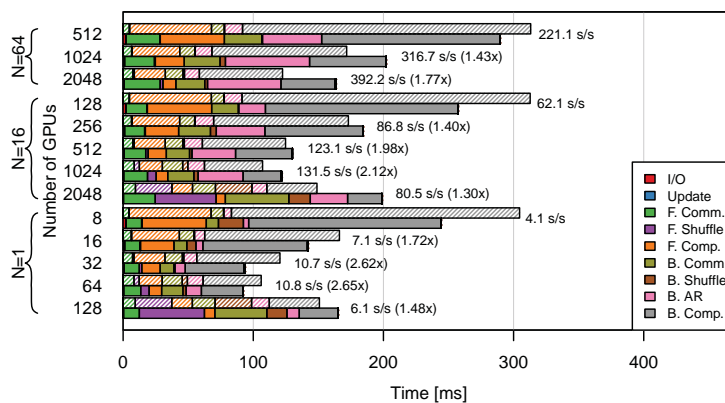


Figure 19.8: Strong scaling of the CosmoFlow network. Shaded bars show iteration time predicted by the performance model.

### 19.3.7 Advanced and Scalable NLP Models

Subword-level information is crucial for capturing the meaning and morphology of words, especially for out-of-vocabulary entries. We have proposed implementing linguistic compositionality using dedicated neural modules, based on CNN or RNN architecture. Additionally, we propose a hybrid training scheme in which a pure subword-level model is trained jointly with a conventional word-level embedding model based on lookup-tables. We have shown that morphological information can be captured efficiently by extremely compact models. Embeddings generated dynamically from just a few megabytes of parameters significantly outperform conventional (word2vec and FastText) models on morphology related tasks. Additionally, this indicates the vast limitation of the ability of conventional models to capture morphological information.

To model both morphological and semantic information, we have implemented two methods for combining strength of compact subword-level- and lookup-table based models: merging trained embeddings and training jointly. The resulting embeddings achieved high accuracy on a range of benchmarks and are particularly promising for datasets with high OOV rate.

We have showed that for languages with logographic scripts (fig. 19.10), such as Japanese, we can go even deeper than subword level and leverage sub-character information to improve accuracy of NLP applications with rare words.

Finally, we have identified that skewed distribution of different lexical elements in the training corpora is negatively affecting models' convergence dynamics under large minibatch sizes. We have introduced sample mining technique with which we prefetch more uniformly distributed training samples (with respect to involved linguistic phenomena) which allows us to train models with larger batch sizes and, in turn, enables better performance on a single GPU and scalability to multi-GPU clusters.

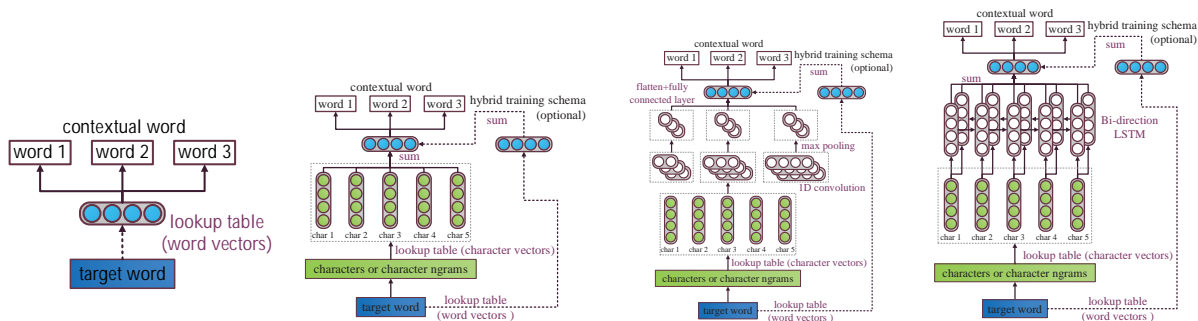


Figure 19.9: different neural nets as a compositional function

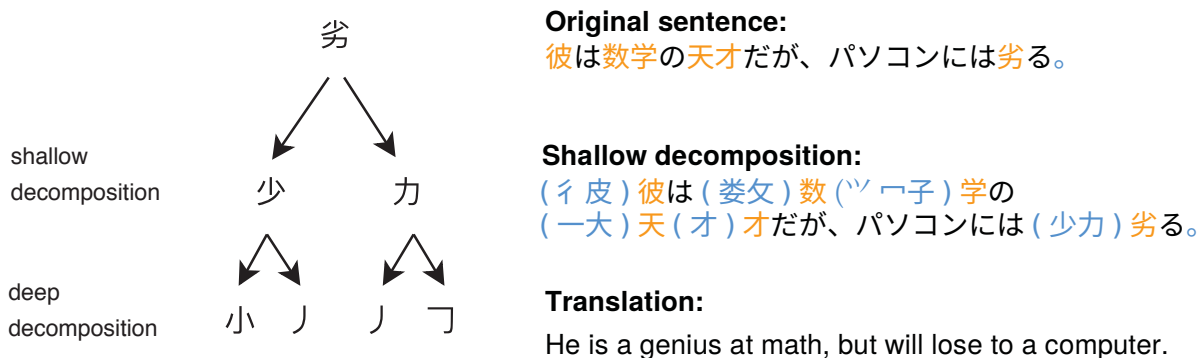


Figure 19.10: example of subcharacter information in Japanese characters

### 19.3.8 Performance evaluation of deep learning software and systems

The diverse tools used for the development and deployment of machine learning (ML) and deep learning (DL) applications makes benchmarking difficult. This diversity includes: different *hardware* (e.g. GPUs, TPUs, different CPUs such as A64FX of the Fugaku Supercomputer), multiple *frameworks* (e.g. TensorFlow, PyTorch), with numerous *backends* (e.g. BLAS, MKL, cuBLAS, cuDNN) executing different neural network neural network *architectures* (e.g. ResNet, BERT) running on various datasets synthetic or real (such as MNIST, ImageNet, COCO) and hyperparameters (e.g. batch size, precision).

We are developing *Benchmarker*, a modular benchmarking software, to tackle this problem. Benchmarker has well-defined interfaces, which enables easy addition of components at all levels mentioned above. It can generate logs in human- and machine-readable JSON format with detailed platform information. From these logs, it can generate visualisations, such as relative comparison over the any dimensions (frameworks, hardware, hyperparameter etc).

The purpose of such fine grained benchmarking, is to help pinpoint bottlenecks in the different implementations, but, more importantly, to provide insight into the reason behind the efficiency (or the lack of it) of certain implementations. Figure 19.11 shows the relative performance of 5 different deep learning models executed on 4 different hardware platforms with mixed and single precision.

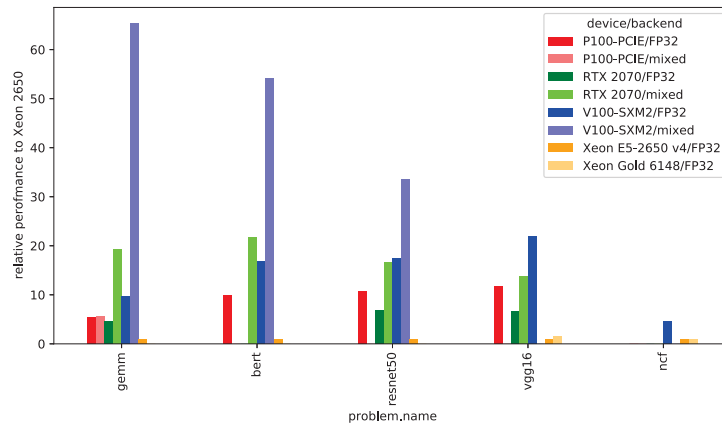


Figure 19.11: Relative performance of different models on various hardware

### 19.3.9 Predicting GPU Performance Using Collaborative Filtering

Graphical Processing Units (GPUs) are the de-facto source of performance in high performance computing. With the rapid increase in number and types of GPUs available, finding the best hardware accelerator for each application is a challenge. For that matter, it is time consuming and tedious to execute every application on every GPU system to learn the correlation between application properties and hardware characteristics. To address this problem, we use collaborative filtering to build an analytical model which can analyze and predict performance of applications across different GPU systems. Our model learns representations, or embeddings (dense vectors of latent features) for applications and systems and uses them to characterize the performance of various GPU-accelerated applications. We improve state-of-the-art collaborative filtering approach based on matrix factorization (MF) by building a multi-layer perceptron (MLP) as shown in figure 19.12.

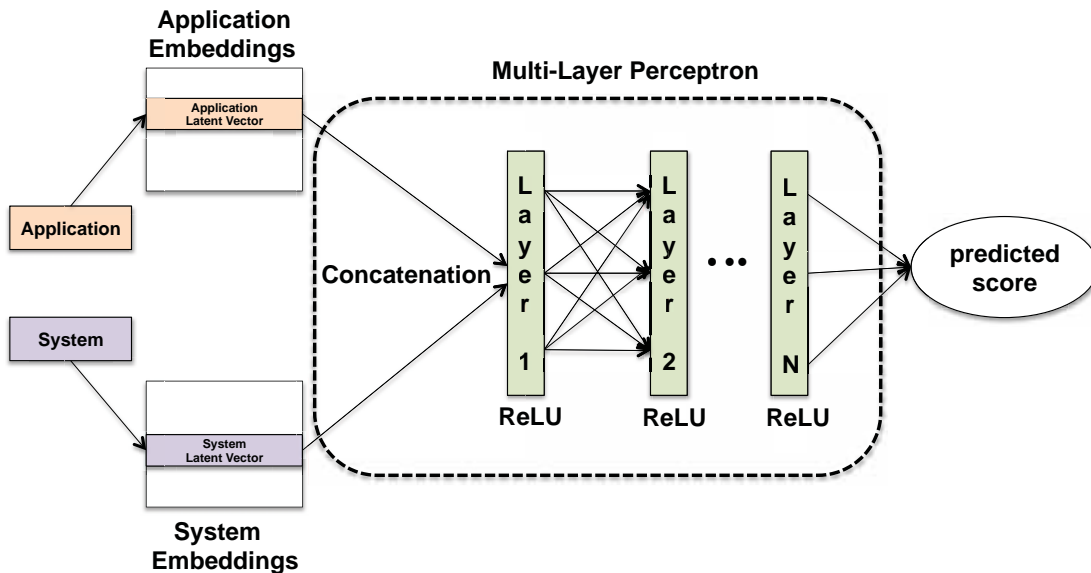


Figure 19.12: Multi-layer perceptron model using latent features

We evaluate our approach on a set of 30 well-known micro-applications and seven Nvidia GPUs of multiple generations. Figure 19.13 shows the prediction accuracy for MF and two variants of MLP when predicting instructions per second (IPS). As a result, we can predict expected IPS values with 90.6% accuracy in average.

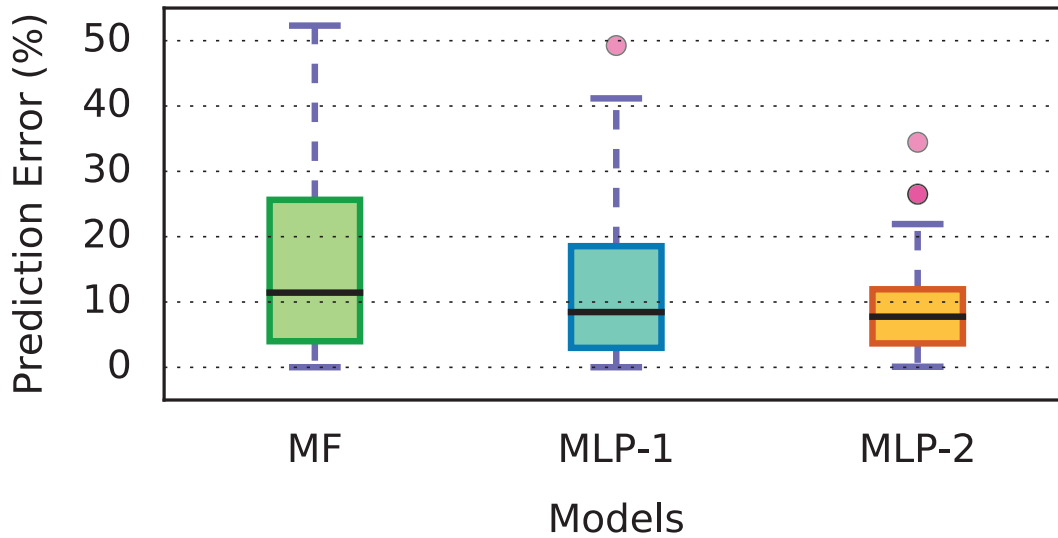


Figure 19.13: Prediction performance of MF, MLP-1 and MLP-2 using IPS dataset

## 19.4 Schedule and Future Plan

Activity within some of the existing research directions by the team are scheduled according to objective factors. For instance, creating deep learning ecosystem for Fugaku supercomputer is paced so that working solutions are ready for the general acceptance of the machine. Other directions are of more exploratory in nature and are being implemented depending on the current progress of the team and in the field in general. Such, withing natural language processing direction we incorporate large-scale experiments with transformer-based language models to reflect current trends in the field of NLP.

Within the general paradigm of the team, we are exploring new promising research direction as well. Two of such new directions are approximate computing and quantum computing.

## 19.5 Publications

### 19.5.1 Articles/Journal

- [1] Nagasaka, Yusuke; Matsuoka, Satoshi; Azad, Ariful; Buluc, Aydin "Performance optimization, modeling and analysis of sparse matrix-matrix products on multi-core and many-core processors" Parallel Computing
- [2] Bofang Li, Aleksandr Drozd, Yuhe Guo, Tao Liu, Satoshi Matsuoka and Xiaoyong Du "Scaling Word2Vec on Big Corpus"

### 19.5.2 Conference Papers

- [3] Jens Domke, Kazuaki Matsumura, Mohamed Wahib, Haoyu Zhang, Keita Yashima, Toshiki Tsuchikawa, Yohei Tsuji, Artur Podobas and Satoshi Matsuoka "Double-precision FPUs in High-Performance Computing: an Embarrassment of Riches?" IPDPS'19
- [4] Shweta Salaria, Aleksandr Drozd, Artur Podobas and Satoshi Matsuoka "Learning Neural Representations for Predicting GPU Performance"
- [5] Yusuke Nagasaka, Akira Nukada, Ryosuke Kojima and Satoshi Matsuoka "Batched Sparse Matrix Multiplication for Accelerating Graph Convolutional Networks"
- [6] Jens Domke, Satoshi Matsuoka, Ivan R. Ivanov, Yuki Tsushima, Tomoya Yuki, Akihiro Nomura, Shin'ichi Miura, Nic McDonald, Dennis L. Floyd and Nicolas Dube "The First Supercomputer with HyperX Topology: A Viable Alternative to Fat-Trees?"

- [7] Chen Peng, Wahib Mohamed, Takizawa Shinichiro and Matsuoka Satoshi “A Versatile Software Systolic Execution Model for GPU Memory Bound Kernels”
- [8] Chen Peng, Wahib Mohamed, Takizawa Shinichiro and Matsuoka Satoshi “iFDK: A Scalable Framework for Instant High-Resolution Image Reconstruction”
- [9] Hamid Reza Zohouri, Satoshi Matsuoka “The Memory Controller Wall: Benchmarking the Intel FPGA SDK for OpenCL Memory Interface”
- [10] Kazuki Oosawa, Youhei Tsuji, Yuichiro Ueno, Akira Naruse, Rio Yokota and Satoshi Matsuoka “Second-order Optimization Method for Large Mini-batch: Training ResNet-50 on ImageNet in 35 Epochs”
- [11] Youhei Tsuji, Kazuki Oosawa, Yuichiro Ueno, Akira Naruse, Rio Yokota, Satoshi Matsuoka “Performance Optimizations and Analysis of Distributed Deep Learning with Approximated Second-Order Optimization Method”
- [12] Hideyuki Jitsumoto, Yuya Kobayashi, Akihiro Nomura, Satoshi Matsuoka “MH-QEMU: Memory-State-Aware Fault Injection Platform”

### 19.5.3 Posters

- [13] Yosuke Oyama, Naoya Maruyama, Nikoli Dryden, Peter Harrington, Jan Balewski, Satoshi Matsuoka, Marc Snir, Peter Nugent, Brian Van Essen “Toward Training a Large 3D Cosmological CNN with Hybrid Parallelization” ICPP 2019 Kyoto, Japan
- [14] Haoyu Zhang, Wahib Mohamed, Pen Chen, Satoshi Matsuoka “Can Local Binary Convolutions Make Neural Networks Models Smaller?” ICPP 2019 Kyoto, Japan
- [15] Lingqi Zhang, Wahib Mohamed, Satoshi Matsuoka “Understanding the Overheads of Launching CUDA Kernels” ICPP 2019 Kyoto, Japan
- [16] Chen Peng, Wahib Mohamed, Takizawa Shinichiro, Matsuoka Satoshi “High resolution Image Reconstruction on Super computers” GTC 2020 Online (COVID-19), Originally San Jose, CA, USA
- [17] Ryan Barton, Wahib Mohamed, Artur Podobas, Satoshi Matsuoka “BITFLEX: A Dynamic Runtime Library for Bit-Level Precision Manipulation and Approximate Computing” HPCAsia 2020 Fukuoka, Japan
- [18] Chen Peng, Wahib Mohamed, Takizawa Shinichiro, Matsuoka Satoshi “A Software Systolic Array on GPUs GTC 2020” Online (COVID-19), Originally San Jose, CA, USA

### 19.5.4 Invited Talks

- [19] Satoshi Matsuoka, “Riken R-CCS, Fugaku and AI”, Shanghai Arm Symposium, 2019/07/11, Shanghai, China
- [20] Satoshi Matsuoka, “Fugaku: Co-Designing the first ‘Exascale’ Supercomputer with Real Application Performance as the Primary Target”, French-Germany-Japan HPC Workshop, 2019/11/06, Tokyo, Japan
- [21] Satoshi Matsuoka, “The first “exascale” supercomputer Fugaku & beyond”, HPC China Keynote, 2019/08/22, Hohhot, Inner Mongolia, China
- [22] Satoshi Matsuoka, “A64fx and Fugaku - A Game Changing, HPC / AI Optimized Arm CPU to enable Exascale Performance”, HPC User Forum, 2019/10/11, Edinburgh, UK
- [23] Satoshi Matsuoka, “Arm A64fx and Post-K: Game Changing CPU & Supercomputer for HPC and its Convergence of with Big Data / AI”, Hyperion HPC User’s Forum, 2019/04/03, Santa Fe, New Mexico
- [24] Satoshi Matsuoka, “Fugaku and its Facilities”, ICPP 2019 EEHC Workshop, 2019/08/05, Kyoto, Japan
- [25] Satoshi Matsuoka, “スーパーコンピュータ「京」「富岳」の概要”, JST-CRD 「社会革新を先導する量子科学技術」ワークショップ, 2019/06/14, 東京

- [26] Satoshi Matsuoka, “The first “exascale” supercomputer Fugaku – HPC, BD & AI”, JST Singapore 10th Anniversary Symposium, 2020/01/10, Biopolis, Singapore
- [27] Satoshi Matsuoka, “The first ”exascale” supercomputer Fugaku & beyond”, DoE Workshop on Modeling and Simulation (ModSim) 2019, 2019/08/15, Seattle, WA
- [28] Satoshi Matsuoka, “Fugaku as the Centerpiece of Society5.0 Revolution”, Multicore World 2020, 2020/02/20, Wellington, New Zealand
- [29] Satoshi Matsuoka, “RIKEN R-CCS OpenACC Presentation”, Annual OpenACC Meeting Presentation, 2019/09/02, Kobe, Japan
- [30] Satoshi Matsuoka, “Fugaku: The first ‘Exascale’ Supercomputer with Real Application Performance as the Primary Target, and Towards the Future”, PPAM 2019 Keynote, 2019/09/08, Bialystok, Poland
- [31] Satoshi Matsuoka, “Fugaku as the Centerpiece of Society5.0 Revolution”, 2nd Annual R-CCS Symposium Keynote, 2020/02/18, Kobe, Japan
- [32] Satoshi Matsuoka, “Post-K: the first ‘exascale’ supercomputer for convergence of HPC and big data/AI Numerical algorithms for high-performance computational science”, The Royal Society, 2019/04/09, London, UK
- [33] Satoshi Matsuoka, “AI for HPC and HPC for AI: Bidirectional Convergence Efforts of HPC and AI on the Fugaku Supercomputer”, Deep Learning on Supercomputers Workshop Keynote, Supercomputing 2019, 2019/11/18, Denver, Colorado, USA
- [34] Satoshi Matsuoka, “Toward Scaling Deep Learning to 100,000 Processors – The Fugaku Challenge”, Scala 2019 Workshop Keynote, Supercomputing 2019, 2019/11/18, Denver, Colorado, USA
- [35] Satoshi Matsuoka, “Fugaku: Co-Designing the first ‘Exascale’ Supercomputer with Real Application Performance as the Primary Target”, SPPEXA Final Symposium, 2019/10/23, Dresden, Germany
- [36] Satoshi Matsuoka, “Fugaku and AI”, HPC Summer School, 2019/07/08, Kobe, Japan
- [37] Aleksandr Drozd, “Deep Learning Ecosystem for ARM-Based Flagship Supercomputer”, Linaro Connect 2019, 2019/10/20, San Diego

## Part II

# Operations and Computer Technologies Division



## Chapter 20

# Facility Operations and Development Unit

### 20.1 Members

Toshiyuki Tsukamoto (Unit Leader)

Satoshi Matsushita (Technical Staff)

Katsuyuki Tanaka (Technical Staff)

Hajime Naemura (Technical Staff)

Fumio Tsuda (Technical Staff)

Makoto Igasaki (Technical Staff)

Hiroshi Shibata (Technical Staff)

### 20.2 Overview of Research Activities

Our facilities possess multiple features not found at other supercomputer sites. These features include an expansive and pillar-free computer room, a power supply system that consists of a co-generation system (CGS) and a high-speed current-limiting circuit breaker without uninterruptible power supply (UPS), distribution boards installed not on the computer-room walls but under a raised floor, extremely quiet and high-efficiency air conditioners, and a water-cooling system for the CPUs featuring precise temperature control.

To ensure stable operation of the K Computer and its peripherals, the facility operations and development unit (FODU) of the operations and computer technologies division, RIKEN R-CCS, is responsible for the operation and enhancement of the facilities. Furthermore, FODU conducts research on the advanced management and operations of the R-CCS facilities.

One of the most serious problems is the rapid and substantial increase in the electricity prices since 2011. Therefore, we are investigating the most suitable driving conditions to allow the R-CCS facilities to achieve effective cost reductions.

Another problem is the increased power consumption by R-CCS. The use of electricity by R-CCS is strictly limited by a contract between R-CCS and the local electric supply company. However, in the early stage of operation, the facility's power consumption exceeded the contract limit. This is important because the company requires us to accept an increase in the upper/lower power limit, which amounts to an increase in the electricity cost. To prevent this, we have investigated methods to control the power consumption of the K Computer using emergency job stopping together with the system operations and development unit and the application tuning development team of the operations and computer technologies division, RIKEN R-CCS.

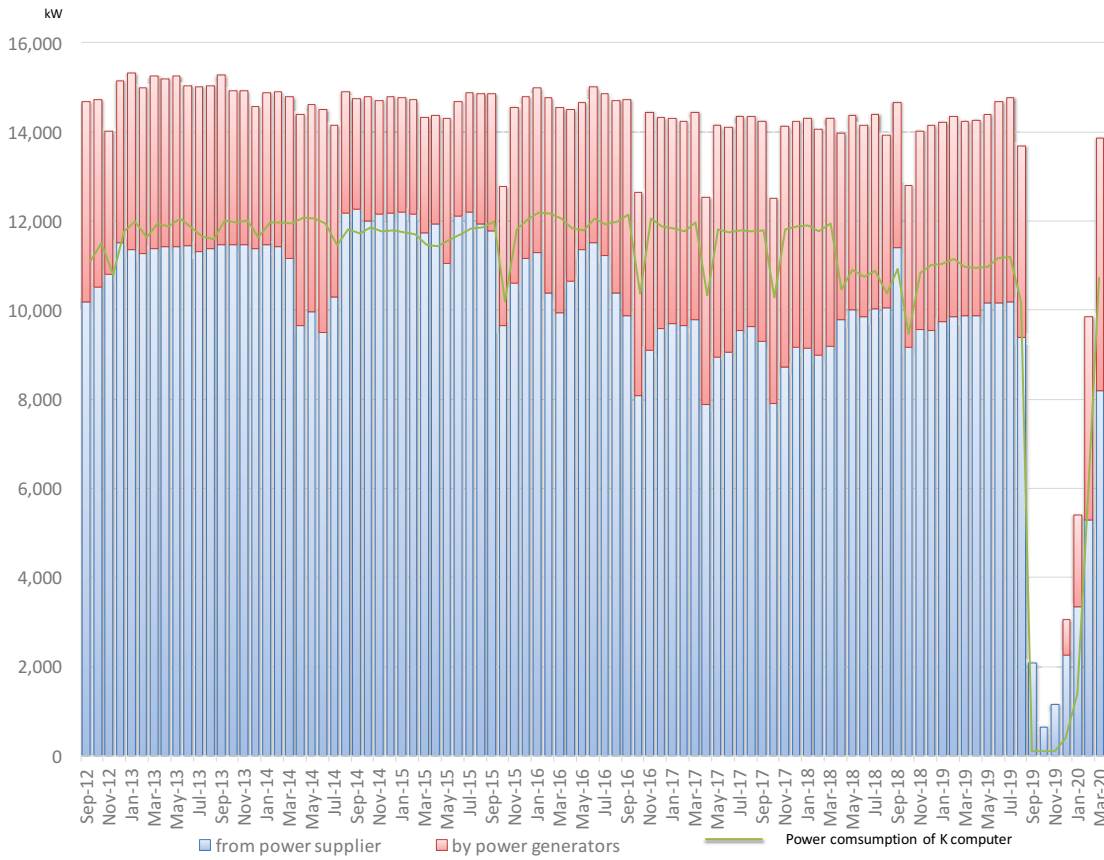


Figure 20.1: Monthly power supply and K computer power consumption.

## 20.3 Research Results and Achievements

### 20.3.1 Optimum operation of electric power

Figure 20.1 shows the monthly total power supply and power consumption of the K computer and the supercomputer Fugaku from September 2012 to March 2020. The power supply consists of commercial power purchased from a supply company and power generated by CGS.

The R-CCS power consumption is nearly synchronized with that of the K Computer. The power consumption of R-CCS is nearly 14,000 kW on average, and the power consumption of the K Computer accounts for approximately 80% (11,000 kW) of the total consumption of R-CCS.

As shown in Figure 20.1, the electric power supply of R-CCS consists of commercial and CGS power. There are two CGS systems at R-CCS, and they are used in turn for two weeks at a time. Therefore, at least one CGS is always in use. Commercial electric power is contractually set at approximately 12,500 kW, and the power consumption was approximately 11,000 kW (annual average), which corresponds to approximately a 90% load factor.

To minimize the cost, we try to optimize the ratio of the commercial and CGS electricity.

To investigate the optimized conditions that minimize the sum of the electricity and gas cost, we determined the costs of several ratios of commercial electricity to CGS electricity. We also constructed a model to describe the energy flow of the electric power supply and the cooling system. Then, we performed computer simulations using the model and the actual operating data. In the near future, we intend to identify the cost-optimized conditions that contribute to reducing costs.

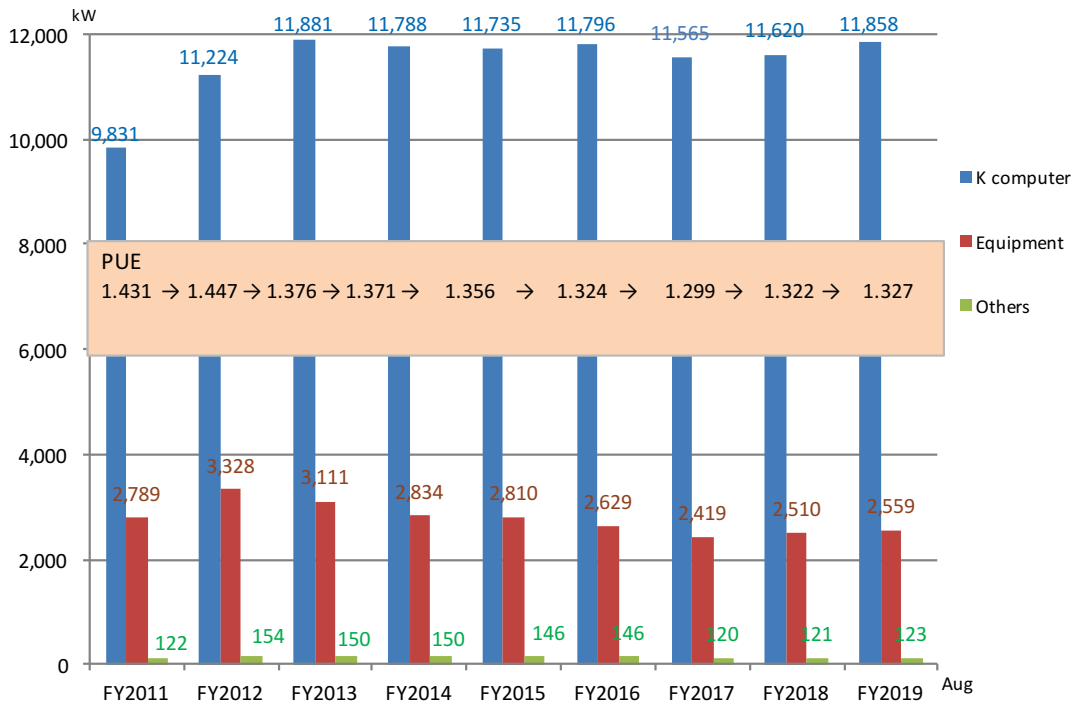


Figure 20.2: Trend in the annual average electric power consumption.

### 20.3.2 Improvements to the power usage effectiveness (PUE)

We have continued to work on improvements for the effective use of electricity. PUE is a well-known indicator of the effectiveness of electricity use.

To improve the PUE, we have attempted to optimize the operation of the cooling equipment (e.g., chillers and air-handlers) since FY2013.

Figure 20.2 indicates the change in the annual average power consumption of the K Computer (including the peripheral devices) and the cooling equipment. Since FY2013, the power consumption of the K Computer has been nearly flat at approximately 11,800 kW; however, the power consumption of the equipment decreased gradually from FY2013 to FY2017. Accordingly, the PUE of R-CCS improved to 1.322 in FY2018 from 1.447 in FY2012, contributing to the reduction in the electricity cost.

In FY2013, we reduced the electricity cost of the air conditioners by reducing the number of working air conditioners. The total cooling performance was maintained by lowering the air temperature. We achieved a reduction in the power consumption of 217 kW.

In FY2014, we focused on the fault-tolerance feature of the air-conditioning equipment. Each air conditioner has two motors for fault tolerance. We found that if one of the two motors could be stopped, the airflow could be maintained at approximately 60

In FY2016, we worked on improving the efficiency of the cooling tower. As a result, we achieved a reduction of 181 kW in the power consumption.

In FY2017, we focused on optimizing the operation control of the refrigerator using a heat storage tank. This reduced the power consumption by 210 kW.

In FY2018, we carried out the overhaul of a cooling tower and a large number of pumps. However, we were not able to operate CGS by the effective output because the electric equipment disorder caused by the typhoon occurred. Therefore, we were not able to improve PUE of FY2018 from last year.

### 20.3.3 Facility Expansion Work

This work was carried out between January 2019 and March 2020. We have greatly enhanced the power supply and cooling capacity for the Fugaku installation. Specifically, we doubled the number of 6000V/200V transformers, and tripled the cooling capacity per rack. In addition, the necessary chillers were added.

Since the work was to be carried out in parallel with the operation of the K computer until the end of August 2019, we had to be very careful not to affect our operation. In addition, a strict schedule was implemented to remove all the K computers by the end of September and to complete the under-floor facility work so that Fugaku could be installed in December.

## 20.4 Schedule and Future Plan

We will continue to improve the advanced management and operation of the R-CCS facilities and contribute to the user service of the K computer and Fugaku. We will work on reducing costs by investigating and applying the most suitable driving conditions to all the electric power supply and cooling equipment. Further, we will improve the electric power and cooling control of the entire R-CCS facility with the system operations and development unit to minimize the electric power consumption.

## 20.5 Publications

### 20.5.1 Conference Papers

[1] Motohiko Matsuda, Hiroya Matsuba, Jorji Nonaka, Keiji Yamamoto, Hiroshi Shibata, Toshiyuki Tsukamoto, “Modeling the Existing Cooling System to Learn its Behavior for Post-K Supercomputer at RIKEN R-CCS”, In proceedings of Energy Efficient HPC State of the Practice Workshop, 2019

### 20.5.2 Posters

[2] Fumiyoshi Shoji, Jorji Nonaka, Motohiko Matsuda, Hiroya Matsuba, Keiji Yamamoto, Yasumitsu Maejima, Toshiyuki Tsukamoto, “CPU Water Cooling Temperature Effects on the Performance and Energy Consumption”, ISC 2019 HPC in Aisa Poster, Frankfurt, Germany, 2019.

[3] Jorji Nonaka, Keiji Yamamoto, Akiyoshi Kuroda, Toshiyuki Tsukamoto, Kazuki Koiso, Naohisa Sakamoto, “View from the Facility Operations Side on the Water/Air Cooling System of the K Computer”, SC’19 Research Poster, Denver, USA, 2019.

[4] Jorji Nonaka, Toshiyuki Tsukamoto, Motohiko Matsuda, Keiji Yamamoto, Akiyoshi Kuroda, Atsuya Uno, Naohisa Sakamoto, “A Brief Analysis of the K Computer by using the HPC Facility’s Water Cooling Subsystem”, 2nd R-CCS International Symposium, Kobe, Japan, 2020.

[5] Motohiko Matsuda, Hiroshi Shibata, Jorji Nonaka, Toshiyuki Tsukamoto, Keiji Yamamoto, Hajime Naemura, “R-CCS Facility Simulation Modeling for Assisting Operation Planning and Decision Making”, 2nd R-CCS International Symposium, Kobe, Japan, 2020

### 20.5.3 Oral Talks

[6] Hiroshi Shibata, Hajime Naemura, Fumio Tsuda, Toshiyuki Tsukamoto, “Operations of Thermal Storage Tank for K Computer”, Proceedings of the 53th Japanese Joint Conference on Air-conditioning and Refrigeration(Tokyo). (In Japanese)

[7] Motohiko Matsuda, Hiroya Matsuba, Jorji Nonaka, Keiji Yamamoto, Hiroshi Shibata, Toshiyuki Tsukamoto, “Modeling the Existing Cooling System to Learn its Behavior for Post-K Supercomputer at RIKEN R-CCS”, Energy Efficient HPC State of the Practice Workshop (EE HPC SOP 2019) held in conjunction with ICPP 2019, Kyoto, Japan, 2019.

## Chapter 21

# System Operations and Development Unit

### 21.1 Members

Atsuya Uno (Unit Leader)

Hitoshi Murai (Research & Development Scientist)

Keiji Yamamoto (Technical Scientist)

Fumio Inoue (Research & Development Scientist)

Yuichi Tsujita (Senior Technical Scientist)

Mitsuo Iwamoto (Technical Staff)

Katsufumi Sugeta (Technical Staff)

### 21.2 Overview of Research Activities

K computer, a distributed-memory parallel computer comprising 82,944 computing nodes, played a central role in the High Performance Computing Infrastructure (HPCI) initiative granted by the Ministry of Education, Culture, Sports, Science and Technology. The HPCI has achieved the integrated operation of the K computer and other supercomputer centers in Japan. Further, it has enabled seamless access from user machines to a cluster of supercomputers that includes the K computer. Moreover, the HPCI has provided large-scale storage systems that are accessible from all over Japan.

The system operations and development (SOD) unit has conducted research and development on the advanced management and operations of the K computer. While analyzing operational statistics collected during shared use, the SOD has improved the system configuration, including aspects involving job scheduling, the file system, and user environments.

In the fiscal year 2019 (JFY2019), we primarily implemented improvements to the following operational issues:

- Advanced Disactivation of Faulty OSTs in the Global File System
- Active Termination of I/O Racing Jobs Towards High Compute Node Utilization
- Analysis and Utilization of Operation Logs
- Improvement of Information provided to Users
- Power-aware System Operation
- Information Exchanges among HPC Centers

### 21.3 Research Results and Achievements

The K computer was terminated at the middle of August, so the operation period of the K computer in JFY2019 is about 4.5 months. Figure 21.1 shows the resource usage details, and Table 21.1 indicates the major failures of the system down for JFY2019. The number of failures in JFY2019 was only 3 cases, and these suspended time were within 3 hours. The operation of the K computer in JFY2019 was very stable.

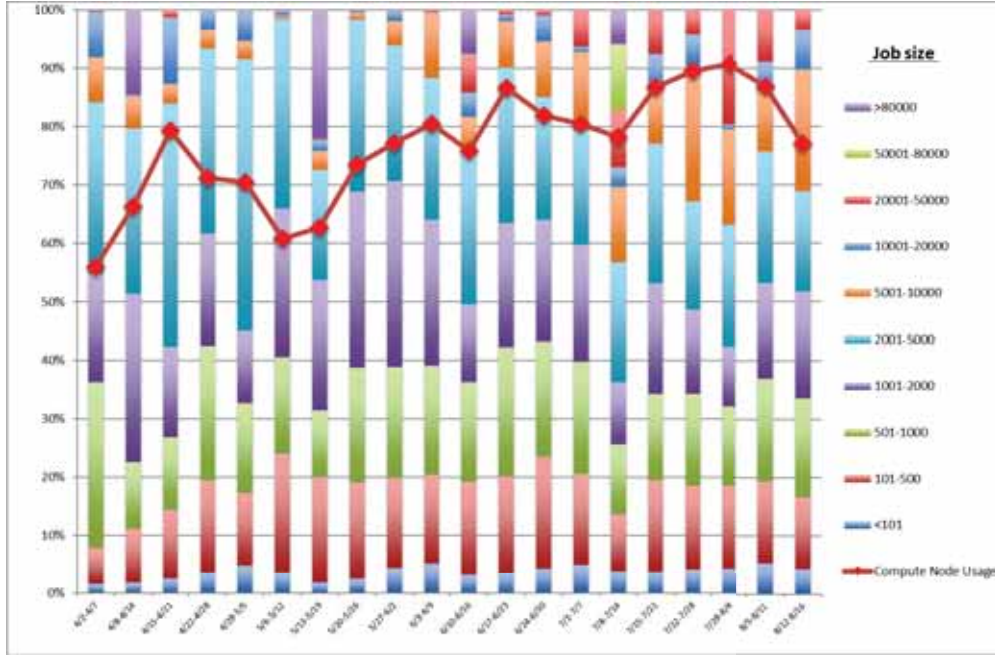


Figure 21.1: Resource usage in JFY2019

As usual, the resource usage is low at the beginning of the fiscal year, and the usage tends to increase towards the end of the term. The resource usage in JFY2019 was the same trend, and we maintained a high utilization rate, approximately 77%, which is nearly equal to that achieved in JFY2018 (77%).

Table 21.1: Major failures in JFY2019

Date	Details	Maintenance period (H)
2019/5/14	Tofu Network Trouble (SW trouble)	2.0
2019/5/26	Electrical facility trouble (CGS down)	3.0
2019/7/2	halt of pjstat command (SW trouble)	1.5

#### 21.3.1 Activities for Stable System Operation

##### 21.3.1.1 Advanced Disactivation of Faulty OSTs in the Global File System

Based on our study about faulty status of HDDs in the Global File System (GFS), we have carried out advanced disactivation of faulty Object Storage Targets (OSTs) that had high failure risks of HDDs inside the same RAID-6 configuration to avoid triple faults of HDDs at the same time. We have not met any severe incident losing a portion of data due to this kind of faults until the end of the K computer operation.

##### 21.3.1.2 Active Termination of I/O Racing Jobs Towards High Compute Node Utilization

We have deployed a client eviction scheme against the heavy Meta Data Server (MDS) load of the Local File System (LFS) caused by simultaneous I/O accesses at the same directory according to study done in

the last fiscal year. I/O operations took very long time in the above situation, and finally such situation led to exceeding elapse time limit and the system operation software could not terminate such job until its I/O operation completion. Terminating affected compute nodes was the promising way, however, it took long time until the nodes were ready, resulting in a loss in compute node utilization. Especially, such negative impact is very big if the number of affected compute nodes is very large. We have focused on client eviction which decline client I/O requests by servers in order to minimize the loss. We have deployed this scheme during the K computer operation as trial, and we have not met any serious problems until the end of the K computer operation.

Similar to the case above, we have considered to cope with the high MDS load due to simultaneous truncate operations from a large number of compute nodes. We demonstrated effectiveness of this approach which issued the client evictions once such truncate operations were observed.

### 21.3.2 Analysis and Utilization of Operation Logs

We collected various operation logs and analyzed them for the stable system operation of the K computer. As one example of this study, we have proposed an I/O characterization analysis framework for further I/O tuning. In this trial, we collected 1) stats of Object Storage Servers (OSSes) of the LFS, 2) I/O sizes at each OST of the LFS, 3) and packet transfer status on Tofu links among I/O nodes.

The analysis framework utilizes those log information with the help of a PostgreSQL database storing job information such as used compute nodes, start and end dates of jobs, and so forth (Figure 21.2, 21.3.) Evaluations of the framework at the K computer provide significant differences in I/O activities at OSTs and packet transfers on the Tofu links between the original MPI-IO implementation and the enhanced MPI-IO implementation named EARTH on K.



Figure 21.2: Configuration of Data collection framework for Operation log

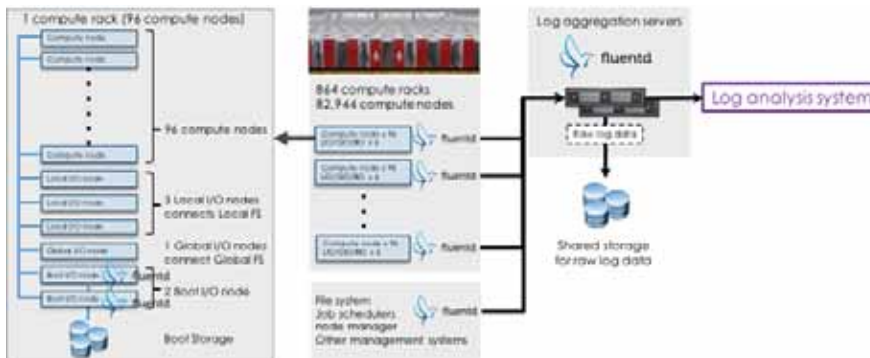


Figure 21.3: Configuration of System log collection

### 21.3.3 Improvement of Information provided to Users

We provided a tool that can display the scheduling status of the user's jobs in the three-dimensional views as the actual scheduling of the K computer. Users could download the scheduling information of the user's jobs from the K user portal, and could see the scheduling status of user's jobs on the local web-browser in the three-dimensional view (Figure 21.4.) We have a plan to provide this tool for the supercomputer Fugaku.

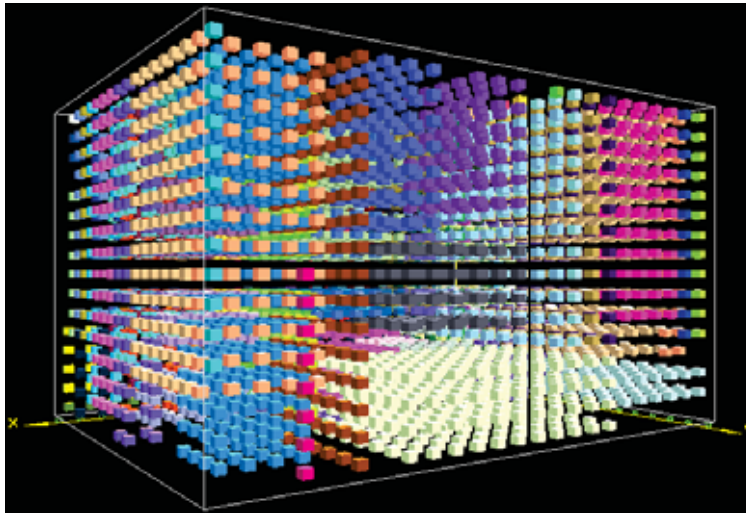


Figure 21.4: Example of 3D mapping of Job scheduling situation

### 21.3.4 Power-aware System Operation

We have studied the job scheduling considering power consumption of each job as excess power prevention. In this method, we estimate the time-series power consumption for each job from the submitted job's parameters and job scripts. In JFY2019, we have evaluated the estimation method using the similarity of job scripts. In this approach, we reclassify the jobs using the similarity of job scripts after classifying the jobs with job's parameters such as the number of compute nodes, declared limit time, and etc. We have found that this method improved estimation accuracy by several percent (Figure 21.5.)

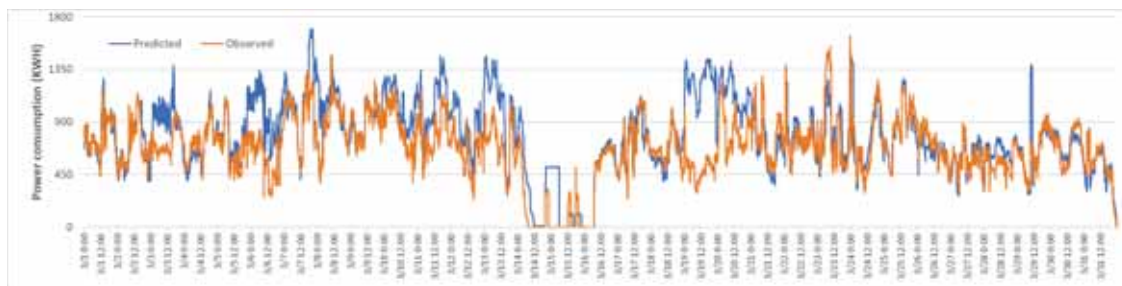


Figure 21.5: Prediction of system power consumption

In addition, we have developed the estimation model using the deep neural network system (Figure 21.6.) This model estimates the average power consumption of jobs, not the time-series power consumption at this time. We make the feature vector of the job script, user id, number of nodes and etc, and make the model with a one-dimensional convolutional neural network using them as input data. We also estimate the standard deviation in addition to the average power consumption, and give the confidence level of the estimated values. In the future, we plan to schedule jobs considering its power consumption on the supercomputer Fugaku.

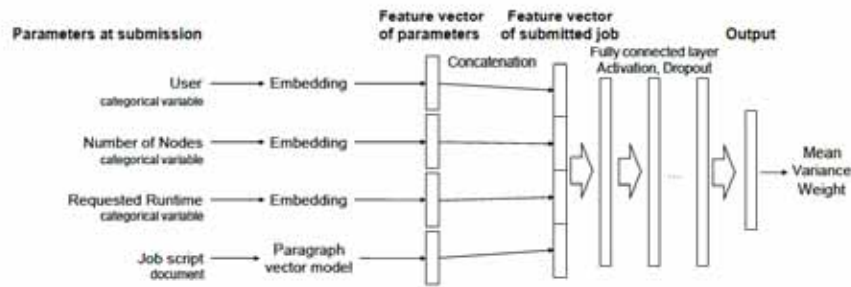


Figure 21.6: Layer structure of power prediction model using Deep Neural Network

### 21.3.5 Information Exchanges among HPC Centers

Recent growth in HPC systems has brings us complexity in HPC system operation. On the other hand, system operation is required to manage a high demand from a variety of HPC users. Each HPC center has been struggling to build own sophisticated operation environment and user support service system. To improve this situation, we started to make some information exchanges about HPC system operation and user support. As the first step of such inter-relationship, we started inter-relationship with the HPC centers at JAMSTEC and TITECH, and we have carried out file system performance evaluation in order to show characteristics of each HPC system in JFY2018. In this fiscal year, we held the workshop for the technical stuffs that are charge in the system operation in the domestic supercomputer centers to share the technical information. We have planned to share the technical information among world’s supercomputer centers as the next step.

## 21.4 User support

The K computer executed approximately 160 projects in JFY2019. The number of active daily users was approximately 90. We supported users through the K support desk and provided them with technical information regarding the K computer, including information regarding its system environment, system tools, and software libraries. In addition, we performed user registrations, failures investigation, software installation, etc. We offered our consulting services together with the HPC Usability Development Unit and Application Tuning Development Unit. Figure 21.7 presents the number of issues addressed in JFY2019, showing the number of new issues in JFY2019 to be approximately 85. The number of resolved issues was approximately 94.

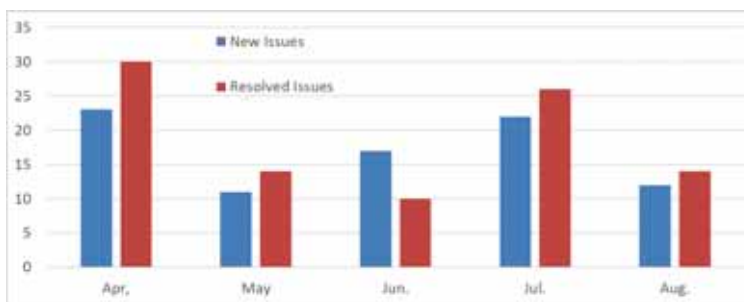


Figure 21.7: Number of issues addressed in JFY2019

## 21.5 Schedule and Future Plan

In this fiscal year, we analyzed the operation of the K computer and examined the operation improvement, and also studied the prediction method of the time series power consumption for each job about the power excess. In addition, we have proposed the framework that utilizes the operation logs and output information that in not obtained from the general profile, and we evaluated the difference in I/O activities at OSTs and packet transfer on the Tofu links between the original MPI-IO implementation and the enhanced MPI-IO implementation.

The operation of the K computer was terminated in this fiscal year. We will work for the stable operation of the supercomputer Fugaku with the experience we've gained through the operation of the K computer.

## 21.6 Publications

### 21.6.1 Conference Papers

[1] Motohiko Matsuda, Hiroya Matsuba, Jorji Nonaka, Keiji Yamamoto, Hiroshi Shibata, Toshiyuki Tsukamoto, Modeling the Existing Cooling System to Learn its Behavior for Post-K Supercomputer at RIKEN R-CCS, In proceedings of Energy Efficient HPC State of the Practice Workshop, 2019

### 21.6.2 Posters

- [2] Shigeto Suzuki, Michiko Hiraoka, Takashi Shiraishi, Hiroyuki Fukuda, Takuji Yamamoto, Shuji Matsui, Atsuya Uno, Power prediction with probabilistic topic modeling for HPC, ISC High Performance 2019, 2019
- [3] Jorji Nonaka, Keiji Yamamoto, Akiyoshi Kuroda, Toshiyuki Tsukamoto, Kazuki Koiso, Naohisa Sakamoto, A View from the Facility Operations Side on the Water/Air Cooling System of the K Computer, SC19
- [4] Jorji Nonaka, Motohiko Matsuda, Hiroya Matsuba, Keiji Yamamoto, Yasumitsu Maejima, Toshiyuki Tsukamoto, CPU Water Cooling Temperature Effects on the Performance and Energy Consumption, ISC19
- [5] Shigeto Suzuki, Michiko Hiraoka, Takashi Shiraishi, Enxhi Kreshpa, Takuji Yamamoto, Hiroyuki Fukuda, Shuji Matsui, Masahide Fujisaki, Atsuya Uno, Power Prediction for High-performance Computing, The International Conference for High Performance Computing, Networking, Storage, and Analysis (SC19), 2019

### 21.6.3 Oral Talks

- [6] Atsuya Uno, Approaches to the Power Consumption Problem on the K computer, PowerStack Seminar, 2019
- [7] Keiji Yamamoto, Operational Data Analytics, Birds of Feather at SC19, 2019

### 21.6.4 Software

- [8] Job scheduling 3D viewer
- [9] EARTH on K

## Chapter 22

# Application Tuning Development Unit

### 22.1 Members

Kazuo Minami (Unit Leader)

Akiyoshi Kuroda (Research & Development Scientist)

Kiyoshi Kumahata (Research & Development Scientist)

Kazuto Ando (Technical Staff I)

Keigo Nitadori (Technical Scientist)

### 22.2 Overview of Research Activities

In the case of the K computer, the collaboration between the system and the applications in use is the key to create innovative results. In order to maximize the performance and usability of both the system and such applications, the Application Tuning Development Unit conducted the following activities:

- (1) Activities related to the RIKEN Center for Computational Science (R-CCS) software center
- (2) Activities to establish a deep learning (DL) environment on the Fugaku supercomputer
- (3) Effort for the Fugaku supercomputer development

### 22.3 Research Results and Achievements

The application tuning development team has been conducting performance evaluation and enhancement aimed at popularizing the applications developed by the RIKEN Center of Computational Science (R-CCS) research team (i.e., R-CCS software) from applications on the K computer and the Fugaku supercomputer. By improving and enhancing the software, we expect industries and communities that have not used the R-CCS software to start using this software. Furthermore, along with the above activities, we are also trying to systemize performance optimization technology. Improving application performance will lead to a shortening of the elapsed time, which makes it possible to use more computational resources. This will help in the more effective utilization of resources. We kept these factors in mind while carrying out the following tasks.

#### 22.3.1 Activities related to the R-CCS software

The RIKEN R-CCS Software Center is developing and deploying high-quality software for numerous high-performance computers (HPCs), including the K computer and the Fugaku supercomputer. Up to now, we have focused on improving and using the following software product developed by R-CCS: NTChem.

### 22.3.1.1 Enhancement of the R-CCS software (NTChem)

This year, we implemented large-scale parallelization of NTChem in the R-CCS software. NTChem is the molecular chemistry software developed by RIKEN AICS. This application has been provided for the analysis of life science and material science and can be used to examine the electronic state of a material. The molecular orbital method and the density functional method are used in this software. We implemented a number of functions such as the various basis functions and several algorithms for acceleration of calculation. This application works well for calculations using the density functional theory that includes the relativistic effect.

Last year, the calculation of the linear optical response KAIN method was accelerated by the high parallelization of the I/O of the linear response time dependent density functional theory calculations. This revealed a new imbalance problem due to differences in atoms and the cutoff radius. This year, we attempted to improve the massive parallel performance by reducing the load-in balance of the DFT calculation by incorporating rearrangement in the atom division calculation, which was examined last year to solve this problem. Figure 22.1 shows the effect of distributing the elapsed time of the hot spots D1Rho\_Box and GGA\_Box. The total execution time was up to 42.81 [s] for the asis stage and up to 40.78 [s] for the tuned stage, and the imbalance was smoothed and reduced the elapsed time by approximately 4.98%. Based on these results, it is expected that the ratio of hotspot subroutines will increase for larger input data and that the load balancing effect will further increase.

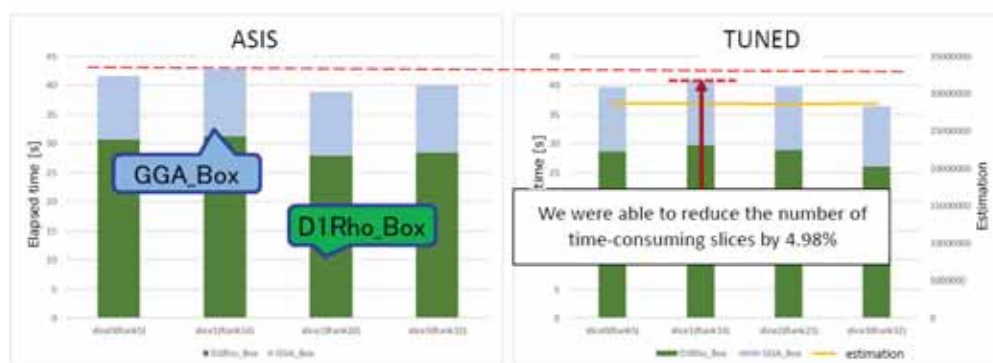


Figure 22.1: Improving imbalance for the KAIN method.

## 22.3.2 Activities to establish a deep learning environment on the K computer and Fugaku supercomputer

Recently, machine learning, especially deep learning (DL), has become commonplace. Deep learning calculation consists of a framework for flexibly handling complex network structures and a library (DNNL) for computing typical calculations with high performance. In addition, applications and research using graphics processing units (GPUs) are advancing in DL science fields. The GPU is said to be essential for DL. However, surveys up to last year have shown that even massively parallel computers, such as the K computer and the Fugaku supercomputer, can perform high-performance calculations by taking advantage of the massively parallel characteristics of the CPUs. Focusing on this point, we performed the following work this year, including the performance tuning of Chainer, which is a representative framework, with the goal of contributing to user convenience.

### 22.3.2.1 Building a development organization

The DL4Fugaku project, which began last year, has been further improved upon this year [8]. Within RIKEN, our unit cooperated to promote the project with the High Performance Big Data Research Team, led by Dr. Kento Sato, and the High Performance Artificial Intelligence Systems Research Team, led by Dr. Satoshi Matsuoka. We also collaborated continuing from last year with the Large-scale Parallel Numerical Computing Technology Research Team, led by Dr. Toshiyuki Imamura, to optimize the library used for calculations such as convolution. The cooperation with ARM and Linaro has been strengthened, and development is underway with the goal of committing to MLPerf benchmarks. The development of DNNL was promoted as a result of the cooperation with Fujitsu and Fujitsu Laboratories. We continued to contact Preferred Networks, Inc.

and provided technical cooperation on the issue of high parallelization for the utilization of DL on the Fugaku supercomputer.

#### 22.3.2.2 Performance evaluation and tuning of Chainer on the K computer

Continuing from last year, we optimized the performance of Chainer on the K computer this year. The MNIST problem required an original calculation time of approximately 10,300 [s]. Last year, we achieved a performance of  $16.2\times$  (635.2 [s]), and a performance efficiency of 15.8%. The floating point underflow and software pipelining inapplicability of Adam optimization were major factors in the efficiency decrease. This year, we found that a further factor is a non-parallel part, such as the Python control part. In addition, we could achieve a performance of  $36.4\times$  (283.4 [s]), and a performance efficiency of 35.9% using MPI process parallelization in a CPU. The results of the performance tuning were presented at a poster session [2,3,5,6]. We also provided and supported a tuned Chainer as R-CCS software.

#### 22.3.2.3 Performance evaluation and tuning of Chainer on the FX100

The performance tuning performed on the K computer was applied to FX100, and we identified the problems. The ASIS state on the FX100 took 49,200 [s] to calculate the MNIST sample problem, because the provided NumPy was built using gcc and the SSL2 library could not be linked. By applying Python know-how to the K computer, we finally achieved a performance of approximately  $1,030\times$  (47.8 [s]), and a performance efficiency of approximately 13.5%.

#### 22.3.2.4 Performance evaluation and tuning of Chainer on the ThunderX2

We evaluated and tuned the performance of Chainer on the ThunderX2 CPU, which was the previous chip used in the Fugaku supercomputer. The ASIS state on the ThunderX2 took 5,340 [s/core] to calculate the MNIST sample problem, but we finally achieved a performance of approximately  $4.8\times$  (1,100 [s/core]), and a performance efficiency of approximately 13.5%. Since the Fujitsu SSL2 library cannot be linked on the ThunderX2, convolution calculations are carried out with OpenBLAS. OpenBLAS tended to have good core performance but not thread scalability, so we evaluated the performance of processing parallelization. We also tuned the performance for the ImageNet problems on the ThunderX2. The calculation costs, such as the cost of batch normalization, have become large for ImageNet problems, so array calculations, which have large costs in NumPy, has been converted to Fortran and prepared as a kernel loop collection. The target kernels of the change were 10 files, 14 sections, and 83 lines, and there were only a few parts that needed to be modified. Based on this effect, ImageNet performance on the ThunderX2 achieved 0.748 [images per seconds (ips)] and a performance efficiency of 54.4% in core performance, and 11.95 [ips] and a performance efficiency of 31.0% in CPU performance.

#### 22.3.2.5 Performance evaluation and tuning of Chainer in the environment of the Fugaku early access program

We also evaluated the performance using the early access program environment of the Fugaku supercomputer. By combining the measurement results using one core Chainer overall calculation and thread parallel kernel performance using CMG, we estimated the performance to be approximately 44.7 to 63.6 [ips/cpu] on the Fugaku CPU. When the performance on the CPU was measured, the performance was approximately 16.3 [ips/cpu] in the first measurement. The cause of this performance difference was non-parallelism, such as the calculation of distribution, and we finally achieved a performance of 55.2 [ips/cpu] and a performance efficiency of 22.6% by rewriting and replacing these parts with Fortran kernels. Thus, the performance tuning of Chainer on the Fugaku supercomputer was almost completed, and it was then possible to promote the use of DL on the Fugaku supercomputer [Table 22.1]. In addition, the framework Chainer can now be provided to users on the Fugaku supercomputer. Since the development of Chainer will stop at Ver. 7, our performance tuning work will also be suspended.

#### 22.3.2.6 Performance evaluation and tuning of Chainer on the Apollo70+Volta

We also evaluated the performance of the ThunderX2 machine with two Volta GPUs provided by NVIDIA as a test user. Since ChainerX cannot be executed in parallel, we used Chainer-6.5.0 for evaluation. The maximum performance was 471.9 [ips], and the efficiency was 39.2%. On the Fugaku CPU, this performance is expected

to be approximately 102.7 [ips/cpu]. The performance of the Fugaku CPU is currently 55.2 [ips/cpu], but by replacing the convolution algorithm with a faster DNNL, we believe that approximately the same performance will be achieved.

Table 22.1: Summary of Chainer performance.

Performance of Chainer			ASIS	TUNED		
system name	unit	model	elapsed	elapsed	peak ratio	speedup rate
K computer	CPU	MNIST	10,300.0 [s]	283.4 [s]	35.9%	36.4 x
FX100	CPU	MNIST	49,200.0 [s]	47.8 [s]	13.5%	1030.0 x
ThunderX2	CORE	MNIST	5,340.0 [s]	1,100.0 [s]	35.7%	4.8 x
			performance	performance	peak ratio	speedup rate
ThunderX2	CORE	Resnet-50		0.75 [ips]	54.4%	
ThunderX2	CPU	Resnet-50		11.95 [ips]	31.0%	
Fugaku	CPU	Resnet-50	16.30 [ips]	* 55.20 [ips]	22.6%	3.4 x
Appolo70+Volta	GPU x2	Resnet-50		471.90 [ips]	39.2%	

\* estimation: 44.7-63.6 [ips]

### 22.3.3 Power consumption of the job

At the end of the operation of the K computer, we cooperated in research evaluation on temperature, failure rate, and performance. We created a job using the following kernels, executed the job as needed in a resource group with a low priority, and investigated the relationship between temperature, computational load, and failure rate.

- A basic kernel in which FMA operates at full capacity and is 90
- A kernel that also has large memory access and high power consumption.
- Stride array copy kernel with maximum memory access.
- Sleeping kernel.
- Adventure kernel having high power consumption due to use in real applications.

Although there is a clear relationship between the change in temperature and the calculation efficiency, it was found that there is no relationship between the temperature and the failure rate, which was reported in a poster session [4,7].

### 22.3.4 Efforts in the development of the Fugaku supercomputer

The FLAGSHIP2020 (FS2020) Project is engaged in research and development for the Japanese national flagship supercomputer "Fugaku", which is a post K computer. As part of the FS2020 project, the application tuning development unit applied co-design of the application and Fugaku supercomputer system through the performance optimization and sophistication of target applications. In particular, our unit is responsible for these three applications.

- ADVENTURE: A structural analysis application based on the finite-element method in Priority Issue No. 6
- RSDFT: A first-principles material simulation and optimization application based on density functional theory, in Priority Issue No. 7
- FrontFlow/Blue: A fluid analysis application based on the finite-element method in Priority Issue No. 8

For these applications, we have paid significant attention to the following efforts:

- Application performance tuning

- Establishing methods for estimating application performance on the supercomputer Fugaku.
- Establishing test kernel codes for evaluating the CPU and system of Fugaku.

The following subsections describe application tuning.

#### 22.3.4.1 Enhancement of the co-design application (ADVENTURE)

ADVENTURE, the structural analysis application based on the finite-element method, is composed of two major parts. One is a sub-domain solver, and the other is a coarse grid correction. The whole analysis domain is divided into multiple sub-domains. A sub-domain solver solves each sub-domain deformation. Coarse grid correction solves the inter-sub-domain relationship by representing a sub-domain as one point having six degrees of freedom. In both parts, a hot kernel is the multiplication of a dense matrix and a vector. Until last year, we continued to tune a hot kernel mainly by separating only the hot kernel source. In particular, we focused on the following issues:

- Avoiding unsuitable loop unrolling that caused cache thrashing to occur frequently
- Decreasing the number of data streams for effective cache memory utilization
- The essential procedure of multiplying a dense matrix and a vector is the taking the dot-product of two vectors. In order to apply SIMD instruction to the summation operation of the dot-product calculation effectively, we implemented a recursive summation operation and minimized the number of temporary arrays. Furthermore, we decreased the number of recursive summation operations to just one.

In previous years, the application used for evaluating performance on the Fugaku supercomputer was a limited version. For example, Fugaku omitted some functions and could only treat special input data. This year, we could evaluate a full-function application. Using this version, a successful run of a sample problem, namely, a 4,096-node-sized problem (16,384 processes, 65,536 sub-domains), was conducted on the Fugaku. Subsequently, in order to validate the performance on the Fugaku, timer routines and tuned kernel codes were implemented. As a result, on Fugaku supercomputer, the target problem achieved over 60× faster performance than the K computer. In addition, power consumption was significantly lower than estimated previously.

#### 22.3.4.2 Enhancement of the co-design application (RSDFT)

The main procedures in RSDFT are DGEMM, and collective communications are based on message passing interfaces (MPIs), such as MPI.Allreduce and MPI.Bcast. Owing to performance tuning conducted during K computer development, RSDFT achieved a performance efficiency of approximately 43.6% for the Si nano-wire problem and won the Gordon-Bell Award in 2011.

This year, we combined of the diagonal priority algorithm kernel into the application and confirmed that there are no problems in calculation and performance. We also evaluated the scalability of CPMD using the K computer. By changing the process mapping, MPI.bcast communication in the band direction became four times faster, and scalability was improved. In addition, we verified the small-scale calculations of the full RSDFT using the prototype Fugaku CPU. As a result, two thread parallelization problems and a problem involving parameter setting were found, but all of these problems were solved. For the power consumption evaluation of tread1 region of the EigenExa library, which is concerned with exceeding the power consumption in boost mode, it was confirmed that the full application can be used on the prototype Fugaku CPU using the development version ScaLAPACK. In addition, we compared the performance of the DGEMM kernel with the evaluation results of last year and found performance differences in some parameters. The cause was found to be due to a short measurement time, and the same performance of the evaluation result of last year was obtained by expanding the measurement time.

#### 22.3.4.3 Enhancement of the co-design application (FrontFlow/blue)

FrontFlow/blue is a fluid simulation code based on the finite-element method. Its major kernels are "kernels depending on memory bandwidth". The performance of these kernels is strongly dependent on the data transfer speed between the CPU and memory. Therefore, in order to tune the performance, it is necessary to obtain higher bandwidth rather than higher CPU calculation performance. In previous years, in order to effectively use the increased SIMD width of Fugaku, we performed a tuning in which list (or indirect) access storage, caused by the data structure of the finite-element method, was changed to sequential (or direct) access storage. Furthermore, last year we used the following tunings.

- Hiding the imbalance of cache memory latency, caused by the memory access pattern difference between threads, by prefetching the list access array.
- Obtaining maximum memory throughput using the SIMD prefetch instruction.
- Applying tuning for miscellaneous parts that were not considered in terms of performance.

Thus, the performance was significantly improved compared to the initial version, which is the version when starting co-design. For example, in the gradient calculation kernel, the elapsed time is improved from 27.4 [s] to 5.58 [s], the performance is improved from 11.18 [GFLOPS] to 59.29 [GFLOPS], and the memory throughput is improved from 53.6 [GB/s] to 195 [GB/s]. In addition, we contributed to environmental sophistication to enable standard use of the Fugaku supercomputer by identifying the problems listed below using FFB.

- Performance fluctuations
- Used memory increase corresponding to the calculated time

Finally, we submitted a paper for the ACM Gordon-Bell Prize, which was adopted as a finalist.

## 22.4 Schedule and Future Plan

### 22.4.1 R-CCS software center activities

Activities related to the following two areas should be continued for use with the Fugaku supercomputer after the service of the K computer ends this summer. One is application improvements from the viewpoint of both performance and usability, and the other is activities to promote the advancement of a utilization environment for R-CCS software users via demonstrations, tutorials, documents, and other methods. Although we focused on four R-CCS software products in our activities up to this point, it is undisputable that the focus could be expanded to additional software applications.

### 22.4.2 Activities to establish a DL environment on the Fugaku supercomputer

With regards to DL, we summarized the usage scenarios and performance levels of other computers. In the future, we intend to work to develop a high-performance DL library and scalable DL frameworks for use on the Fugaku supercomputer.

First, in order to improve the performance of the special DNN libraries developed by ARM Scalable Vector Extension (SVE), we intend to feed back knowledge gained during evaluations of the general DNN kernel prototyped herein. Furthermore, we intend to evaluate how much performance can be achieved for real training problems in order to build a general DNN kernel and special DNN library for use in a DL framework.

The elapsed time of a single convolution calculation depends on the DNN library performance, but the total training time of the scalable DL framework depends on the communication method. For this reason, the study of new communication algorithms will also be needed in order to facilitate high-performance training.

## 22.5 Publications

### 22.5.1 Articles/Journal

[1] Takahiro Yamasaki, Akiyoshi Kuroda, Toshihiro Kato, Jun Nara, Junichiro Koga, Tsuyoshi Uda, Kazuo Minami and Takahisa Ohno, "Multi-axis Decomposition of Density Functional Program for Strong Scaling up to 82,944 Nodes on the K Computer: Compactly Folded 3D-FFT Communicators in the 6D Torus Network", *Computer Physics Communications*, Vol.244, No.2019, (2019) pp.264-276, <https://doi.org/10.1016/j.cpc.2019.04.008>

### 22.5.2 Conference Papers

[1] Chisachi Kato, Yoshinobu Yamade, Katsuhiro Nagano, Kiyoshi Kumahata, Kazuo Minami, Tatsuo Nishikawa, "Toward Realization of Numerical Towing-Tank Tests by Wall-Resolved Large Eddy Simulation based on 32 billion grid Finite-Element", Finalist of ACM Gordonbel Prize for SC20, (2020).

[2] Hisashi Yashiro, Koji Terasaki, Yuta Kawai, Shuhei Kudo, Takemasa Miyoshi, Toshiyuki Imamura, Kazuo Minami, Hikaru Inoue, Tatsuo Nishiki, Takayuki Saji, Masaki Satoh and Hirofumi Tomita, "A 1024-member ensemble data assimilation with 3.5-km mesh global weather simulations", Finalist of ACM Gordonbel Prize for SC20, (2020).

### 22.5.3 Posters

[1] Kiyoshi Kumahata, Kazuo Minami, "Co-Designing of FEM based CFD code FrontFlow/blue for the Super-computer Fugaku", HPC Asia 2020, Fukuoka, Japan, (2020).

[http://sighpc.ipsj.or.jp/HPCAsia2020/hpcasia2020\\_poster\\_abstracts/poster\\_abstract\\_18.pdf](http://sighpc.ipsj.or.jp/HPCAsia2020/hpcasia2020_poster_abstracts/poster_abstract_18.pdf)

[2] Akiyoshi Kuroda, Kiyoshi Kumahata, Syuichi Chiba, Katsutoshi Takashina and Kazuo Minami, "Performance Tuning of Deep Learning Framework Chainer on the K computer.", Frontiers of Statistical Physics (FSP2019), Koshiba-Hall in Hongo Campus, The University of Tokyo, JAPAN, P-20 (2019.06.07-08).

[3] Akiyoshi Kuroda, Kiyoshi Kumahata, Syuichi Chiba, Katsutoshi Takashina and Kazuo Minami, "Performance Tuning of Deep Learning Framework Chainer on the K computer.", ISC High Performance (ISC2019), Research Posters/HPC in ASIA Research Posters, Frankfurt Messe, Germany, PR-28 (2019.06.18-19).

[4] Jorji Nonaka, Keiji Yamamoto, Akiyoshi Kuroda, Toshiyuki Tsukamoto, Kazuki Koiso, Naohisa Sakamoto, "A View from the Facility Operations Side on the Water/Air Cooling System of the K Computer", The International Conference for High Performance Computing, Networking, Storage, and Analysis (SC19), Research Posters, Denver, USA, Poster 82 (2019.11.17-22).

[5] Akiyoshi Kuroda, Kiyoshi Kumahata, Syuichi Chiba, Katsutoshi Takashina and Kazuo Minami, "Performance Tuning of Deep Learning Framework Chainer on the K computer.", HPC Asia 2020, ACROS Fukuoka, Japan, No.32 (2020.01.15-17).

[6] Akiyoshi Kuroda, Kiyoshi Kumahata, Syuichi Chiba, Katsutoshi Takashina and Kazuo Minami, "Performance Tuning of Deep Learning Framework Chainer on the K computer.", The 2nd R-CCS International Symposium, Kobe, JAPAN, No.26 (2020.02.17-18).

[7] Jorji Nonaka, Toshiyuki Tsukamoto, Motohiko Matsuda, Keiji Yamamoto, Akiyoshi Kuroda, Atsuya Uno and Naohisa Sakamoto, "A Brief Analysis of the K Computer by using the HPC Facility's Water Cooling Subsystem", The 2nd R-CCS International Symposium, Kobe, JAPAN, No.34 (2020.02.17-18).

[8] Kento Sato, Akiyoshi Kuroda, Kazuo Minami, Jens Domke, Aleksandr Drozd, Mohamed Wahib, Shuhei Kudo, Toshiyuki Imamura, Kiyoshi Kumahata, Keigo Nitadori, Kazuo Ando and Satoshi Matsuoka, "DL4Fugaku: Deep learning for Fugaku - Scalability Performance Extrapolation -", The 2nd R-CCS International Symposium, Kobe, JAPAN, No.42 (2020.02.17-18).

### 22.5.4 Invited Talks

[1] Kiyoshi Kumahata, "Achievement of the priority issue No.8 -summary of FFB tuning-", The 2nd meeting of application cooperation development, Institute of Industrial Science, The University of Tokyo, (2019).

### 22.5.5 Oral Talks

### 22.5.6 Software

### 22.5.7 Patents

### 22.5.8 Book

[1] Kazuo Minami, Kiyoshi Kumahata, "Case Studies of Performance Optimization of Applications", The Art of High-Performance Computing for Computational Science Vol.2, ed. Masaaki Geshi (Springer, Singapore, 2019), Chap. 1-3. [https://doi.org/10.1007/978-981-13-9802-5\\_3](https://doi.org/10.1007/978-981-13-9802-5_3), (2019).



## Chapter 23

# HPC Usability Development Unit

### 23.1 Members

Fumiyoshi Shoji (Unit Leader)

Masaaki Terai (Research & Development Scientist)

Hitoshi Murai (Research Scientist)

Jorji Nonaka (Technical Scientist)

Tomohiro Kawanabe (Technical Staff I)

Hiroshi Harada (Technical Scientist)

Hidetomo Kaneyama (Technical Staff I)

Megumi Takeuchi (Technical Staff I)

Kenji Ono (Senior Visiting Scientist)

Naohisa Sakamoto (Visiting Scientist)

Kazuki Koiso (Student Trainee)

Yoshiaki Yamaoka (Student Trainee)

### 23.2 Overview of Research Activities

The HPC Usability Development Unit has covered a wide range of topics including software, service, and infrastructure, aiming to improve the overall usability of the K computer environment, and of its successor (Fugaku). In addition, we also have some activities dedicated to one of the HPCI shared storage sites, located at the R-CCS, which is a commissioned project funded by the MEXT (Ministry of Education, Culture, Sports, Science and Technology). The official operation of the K computer was finished at August 16, 2019. As a consequence, we have joined in several projects related to the Fugaku operation and its application, and have aimed to prepare a useful environment for the Fugaku users. Targeting the start of the official service of Fugaku, we continued working on the already ongoing projects, and have focused on other related and relevant activities.

The summaries of our activities are listed below.

- **Software Center:** We have been running the *RIKEN R-CCS Software Center* to support and promote a set of software, also called “R-CCS software”, developed at the R-CCS.
- **Large Data Visualization and Analysis:** We have worked on tools and applications for assisting the visualization and analysis of large data sets generated from the K computer environment, which include traditional simulation results and the log data sets from the K computer facility and system. We have also worked on a scalable display system, named ChOWDER, for displaying high-resolution visualization results or simultaneous display of multiple data sets.

- **Workflow Management Software (WHEEL):** We have been working on WHEEL, a workflow management software. WHEEL was originally developed by the former Advanced Visualization Research Team, and continues being developed to enable more efficient capacity computing. In FY 2019, we have improved WHEEL in its usability, and it was used in trials by multiple research institutes, and verified the usefulness for capacity computing workflows in combination with practical application software.
- **K Pre-Post Cloud (Data Analysis Server using Virtualization Technology):** Data analysis has become an important topic in the field of HPC/Data Centers. However, the existing data analysis servers in the K computer environment are disproportionately small compared to the K compute nodes. Nowadays, the virtualization technology has sufficiently matured and can provide an ideal software environment for the users. Therefore, to accelerate the data analysis without compromising the usability, we have considered the application of OpenStack-based virtualization technology for data analysis and worked on the design and deployment of an experimental cloud system.
- **HPCI Shared Storage:** In the commissioned project of the HPCI shared storage, we have collaboratively worked with the University of Tokyo, which maintains the other shared storage. We have operated in the data-duplication mode to provide high availability, and to avoid the interruption of the service even if a serious failure occurs at one of the sites.
- **Oracle Cloud FastConnect Service:** We have developed a new secure and high-speed network infrastructure by using the “Oracle Cloud FastConnect Service” under the collaboration with Oracle. This infrastructure will enable the Fugaku users to transfer their data between the Fugaku/HPCI shared storage and their users’ environment on the Oracle Cloud Infrastructure (OCI), which is a public cloud service, via SINET (Science Information NETwork). This service will be available in FY 2020.

Furthermore, we have other activities that have been conducted in collaboration with universities and research institutes, in various fields of science and technology (e.g., Econophysics, Bioinformatics, and an analysis of the “hot-water” cooling method), and what they have in common is the investigation and exploration on how to enhance the usability, and to improve the productivity of the K computer environment. Although we have a wide variety of missions, we can say that our common objective is to improve the usability of the K computer environment as well as of the HPCI shared storage. Under this main goal, we have investigated and explored new usage for the K computer and the HPCI storage, trying to embrace not only the traditional HPC users but especially new users from various other fields. In the rest of this chapter, we will detail these aforementioned research and development projects carried out in FY 2019.

## 23.3 Research Results and Achievements

### 23.3.1 Software Center

We have been running the *RIKEN R-CCS Software Center*, since FY 2017, to support and promote *R-CCS software*, which is a set of applications, libraries, programming tools, and other software developed at the R-CCS.

The major achievements of the Center, in FY 2019, are as follows:

- Performance tuning of NTChem
- Development of Spack recipes for some of the R-CCS software, which include FrontFlow/red-HPC, SCALE, GENESIS, and EigenEXA

In addition, an overview and some use case examples of FrontFlow/red-HPC were also provided on the portal site, to promote its recognition and increase its usability.

### 23.3.2 Large Data Visualization and Analysis

The K computer environment includes pre- and post-processing oriented systems (K Pre/Post Server and K Pre-Post Cloud), in addition to the K computer itself, as shown in the Fig. 23.1. The target data for visualization and analysis includes those from the large-scale simulation as well as those generated from the K computer system and its facility, which are stored as log data [2]. Thanks to the availability of Mesa3D library, with its OSMesa (Off-screen Mesa) functionality, which was provided via OSS (Open-Source Software) porting effort

done in FY 2018, we started working on some applications and tools by using the KVS (Kyoto Visualization Software) library for both simulation data visualization and log data analysis. In order to facilitate the visual perception of high-resolution rendering results, we have extended our work on the ChOWDER, a VDA (Virtual Display Area) based scalable display system, for increasing its functionality and usefulness.

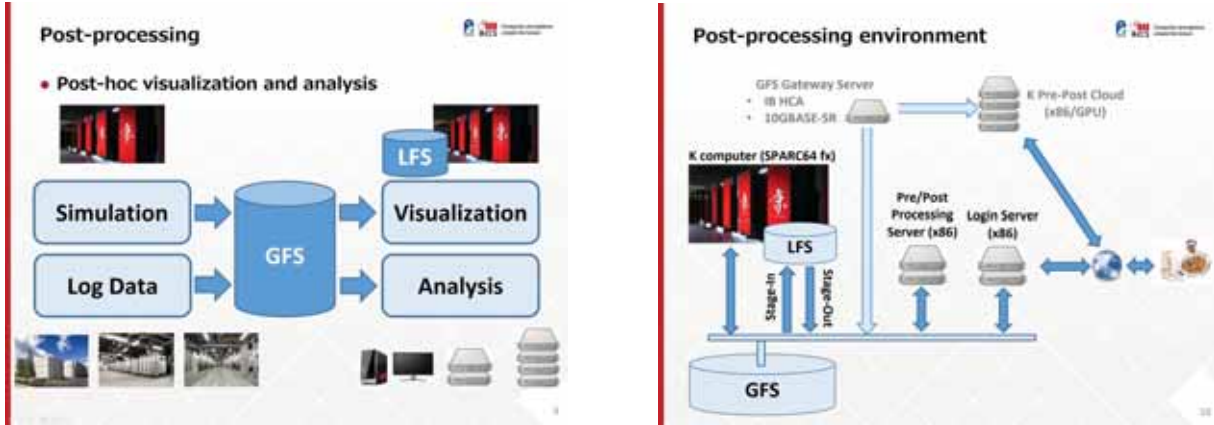


Figure 23.1: Post-processing environment for large data visualization and analysis.

### 23.3.2.1 Simulation Data

In addition to the traditional post-hoc visualization approach by reading and processing the data sets already stored in the disk, we have also developed a KVS-based in-situ visualization API for coupling to the simulation codes, in order to enable in-situ visualization processing simultaneously with the simulation. We have also proposed an adaptive time-step sampling method, based on the simulation data results, in order to improve the rendering throughput and reduce unnecessary data I/O, and we evaluated this in-situ API by integrating with OpenFOAM CFD simulation code [3, 4, 5, 11]. As an approach for analyzing ensemble computational climate simulation results, we have worked on a visualization approach which uses stochastic isosurface technique [6, 12].

### 23.3.2.2 Log Data

We have also worked on some visual data analysis techniques focusing on the operational improvements of the system and its facility. We have developed a KVS-based visual causal exploration framework to investigate the applicability of transfer entropy technique for analyzing the causality of hardware failure on the K computer system [13, 15]. We have also investigated the applicability of this visual exploration framework for the causal analysis of a severe rainfall event, simulated on the K computer, and a flash flood in a river situated at the Kobe-city [7, 14]. We have also analyzed some log data sets generated from experiments and from the K computer system and its facility, by using traditional Python-based data science tools, aiming to investigate the temperature changing behavior on air-cooled CPU [9] and compute rack [17, 18].

### 23.3.2.3 Scalable Display System (ChOWDER)

We are advancing the research and development of a scalable display system which was named ChOWDER (COoperative Workspace DrivER) [23]. It is also known as tiled display, which is a method that tiles multiple physical display devices to create one large pixel space. In recent years, it becomes possible to build tiled displays that connects multiple physical displays onto a single PC by using high-performance graphics cards. However, it can have limitations on the maximum achievable resolution, since it depends on the hardware and its middleware. In contrast, since ChOWDER is a software-based system, there is no logical upper limit regarding the maximum resolution it can provide. Since ChOWDER is a web-based software and requires only standard web browser, it can provide high availability. In addition, the server has a virtual pixel space called VDA (Virtual Display Area), and it enables the coexistence of tiled displays with physical displays possessing different resolutions and aspect ratios. It is also possible to use the ChOWDER as a remote collaboration tool

for displaying the same content on the tiled displays placed at multiple sites thanks to the web-based high availability functionality.

In FY 2019, to improve the display efficiency of ultra-high-resolution images on ChOWDER, we have introduced a new feature that split the visualization data at the sender-side, and send them to each corresponding display device. By using this feature, and in our tiled display environment, we have observed that the displaying speed of 16K resolution images can become up to 2.7 times faster [10, 20].

### 23.3.3 Workflow Management Software (WHEEL)

To easily handle many computational tasks on the HPC resources, we have developed a scientific workflow management system named WHEEL (Workflow in Hierarchical distributEd parallel) [24] jointly developed with Kyusyu University. WHEEL can support typical HPC simulation with a workflow consisted of pre-processing, simulation, and post-processing and can work on various HPC computing resources including not only the K computer but also other computing resources. In addition, this system is a web-based application written in JavaScript, and runs on common web browsers available for Windows, macOS, and Linux. WHEEL employs ordinary SSH and login shell to communicate with remote computers when it performs job submitting, monitoring, and file transfer. Therefore, the additional middleware is not required on the remote computers. In addition, WHEEL has the iteration/conditional branch functionality (e.g., For, Foreach, While, and If), and a parameter study functionality that allows multiple simulations simultaneously with the given parameter range specified by the user. By both features, the users can construct more complex workflows.

In FY 2019, WHEEL has been experimentally used in several research institutes and has been improved by their feedbacks. For example, at Kyushu University, WHEEL has been used for the VASP structural relaxation calculations for inorganic materials, and was performed with for capacity computing using the supercomputer ITO. At the University of Tokyo, WHEEL was also used to implement a shape optimization workflow for designing rotating machines. This workflow realizes two-objective optimization to maximize the performance and noise minimization of the rotating machine based on evolutionary calculations using genetic algorithms. In this workflow, WHEEL itself runs on a Linux PC, and the wing geometry creation and mesh generation programs are executed on a cluster computer owned by the University of Tokyo, and fluid dynamics and acoustic calculations are run on Kyushu University's ITO. Due to the limitation of the time period, the workflow running has not finished, however, this use case indicated the capability of WHEEL which is able to handle complex workflow among multiple computational resources.

### 23.3.4 K Pre-Post Cloud (Data Analysis Servers using Virtualization Technology)

The K Pre-Post Cloud is a private cloud system/service, and an experimental platform in the K computer and Fugaku environment, build to enhance the pre/post data processing features including data analysis and visualization. This system consists of 11 compute nodes and some auxiliary servers. Each compute node has 48 x86-based physical cores, and 384 GiB of RAM, and connects to other nodes with a 25 GiB Ethernet network switch. In addition, the system has an external Ceph-based 150 TiB storage. To improve the usability regarding OSS environment, we applied the server virtualization technology using the OpenStack framework. By using this framework, the users are able to install and uninstall any software on their own virtualized environment, including not only the OSS but even the operating system they want to use. Furthermore, we also added GPUs on some of the compute nodes to enhance and accelerate the data processing capabilities.

In the K computer environment, there exist auxiliary x86-based data-analysis servers, known as “Pre/Post Processing Servers,” where the users are allowed to submit jobs using large memory, and with longer duration than compared to those allowed on the K computer. The primary target usage of these servers is data preparation, analysis, and visualization, which are some of the essential processes needed in the early and/or late phases of a regular end-to-end scientific workflow. In addition, these servers were built using the traditional x86 architecture, in order to provide a readily available environment for the users to exploit various OSS packages.

On the other hand, the Pre/Post Processing Servers can currently be considered as outdated since they were installed several years ago. In addition, although data analysis is one of the significant topics in HPC/Data Centers, their computational resources have gradually become insufficient for the data analysis. As a result, there was a strong demand from the academic/industrial users to enhance the pre/post processing capabilities in the K computer environment. In FY 2018, to address the problem of the pre/post data processing by using OSS in the environment, we have launched a new experimental IaaS platform which was named “K Pre-Post Cloud.” In FY 2019, to improve the inbound and outbound connections between the system and external sites, we changed the routing configuration that directly connects the center's network infrastructure as well as the

K computer, and enhanced the network speed with 10GbE fiber cable in the inbound. Finally, we continued to provide the service for the users.

### 23.3.5 HPCI Shared Storage

In FY 2019, we operated the HPCI storage system with the clear operational goals listed below.

- 99.3 % or higher read-write service utilization
- No security incidents
- No data loss

In October 2019, due to the Fugaku installation, the HPCI shared storage was taken out of the operations for a month. At the time, by using the multiplexed data mechanism between the University of Tokyo and R-CCS, the entire service continued while the R-CCS equipment was out of service. In addition, the metadata server operated by the R-CCS maintained its continuous operation by failing over to the University of Tokyo. Thanks to the effectiveness of the data multiplexing operation, there was no service outage, no data loss, no security incidents in FY 2019 [21, 22]. As a result, we achieved all operational goals planned for FY 2019.

As a new attempt, the usability of the login servers was improved, and the monitoring function was strengthened. In order to occupy/submit batch jobs, a PBS batch scheduler was installed on the four login nodes installed at the R-CCS side. The PBS batch scheduler provides the queue optimization feature for MPI and other parallel execution jobs. Further, we improved the environment for using shared storage from Singularity containers. We also enhanced the service-level monitoring to provide a visual overview of the operational status. We will continue enhancing the monitoring capabilities so that users can quickly be informed of the service status.

Figure 23.2 shows the monthly operation rate of the HPCI shared storage system.



Figure 23.2: FY 2019 monthly utilization rate of the HPCI shared storage.

### 23.3.6 Oracle Cloud FastConnect Service

We have developed a new secure and high-speed network infrastructure by using the “Oracle Cloud FastConnect Service” under the collaboration with Oracle. This infrastructure enables the Fugaku users to transfer their data, without additional fee, between the Fugaku/HPCI shared storage and their users’ environment on the Oracle Cloud Infrastructure (OCI), which is as a public cloud service, via SINET (Science Information NETWORK). This service will be available in FY 2020.

As a background, various cloud services (e.g., data store, visualization) has recently matured sufficiently, and in the next decade, we expect that the Fugaku users will normally utilize the services in their research. Thus, one of the objectives for this infrastructure development is to promote the use of cloud services by the Fugaku users in order to improve usability in the supercomputing environment.

In FY 2019, we built and tested the service. The activities include many tasks: designing the service environment; designing the configuration of R-CCS main routers; setting up OCI tenant; create a user manual; and testing the network and service. Finally, we have connected the R-CCS and OCI data center with a private line, and have provided OCI tenant for service management. The overall of the new infrastructure is shown in Fig.23.3. This service is expected to be available to the users in FY 2020.

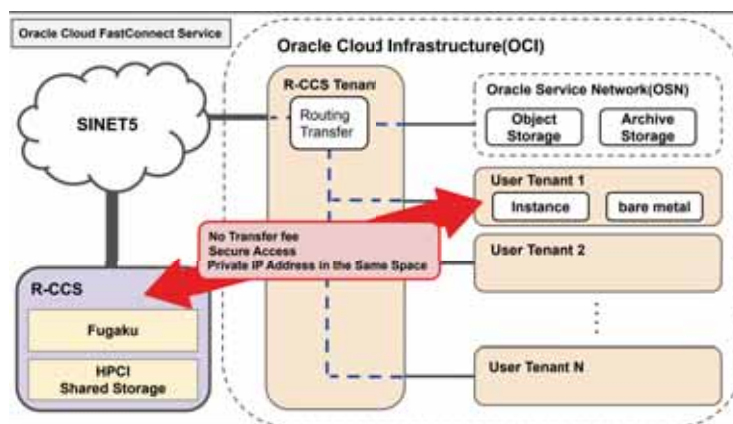


Figure 23.3: Oracle Cloud FastConnect Service Overall

### 23.3.7 Other Activities

In addition to those activities detailed in the previous subsections, we have also contributed to the following projects:

- Graph-based Economic Simulation under the Exploratory Challenges on Post-K computer (Studies of Multi-level Spatiotemporal Simulation of Socioeconomic Phenomena, Macroeconomic Simulations) [1]
- To share knowledge and actual usage regarding cutting-edge cloud resources in Bioinformatics and HPC, we started to collaborate with the Laboratory for Bioinformatics Research at the RIKEN Center for Biosystems Dynamics Research (BDR)
- Systematic and quantitative analysis of the “hot-water” cooling method, trying to better understand the impact of the higher cooling liquid temperature on the system and its facility. The investigations include the use of a portable water circulation equipment with chiller and heater [16], and Modelica-based cooling facility simulations [8, 19]

## 23.4 Schedule and Future Plan

FY2019 was a milestone year for us because the official operation of the K computer was finished in August, and was started the installation of the Fugaku, which is the successor of the K computer. Many of our members have been involved in the Fugaku project to prepare an easy-to-use environment and services for the Fugaku. In FY2020, we will have to accelerate our activities because the early access program for the Fugaku is planned to start before the beginning of the official operation. We will continue doing our best to investigate and explore new usage modes for the Fugaku environment, focusing not only on the traditional HPC users, but especially on potential new users from different fields. We also hope that Fugaku will produce many remarkable outcomes from the researchers and engineers, in the same manner as the K computer’s impressive achievements.

## 23.5 Publications

### 23.5.1 Articles

[1] Hazem Krichene, Yoshi Fujiwara, Abhijit Chakraborty, Yoshiyuki Arata, Hirasu Inoue, Masaaki Terai, “The emergence of properties of the Japanese production network: How do listed firms choose their partners?,” Social

Networks, Vol.59, pp.1-9, (2019).

### 23.5.2 Oral Talks

- [2] Jorji Nonaka, Yuichi Tsujita, “An Overview of the Storage and Post-Processing Environment at RIKEN R-CCS”, HPC I/O in the Data Center Workshop (HPC-IODC 2019) held in conjunction with ISC 2019, Frankfurt, Germany, 2019. (Oral Talk)
- [3] Yoshiaki Yamaoka, Kengo Hayashi, Naohisa Sakamoto, Jorji Nonaka, “In Situ Adaptive Timestep Control and Visualization based on the Spatio-Temporal Variations of the Simulation Results”, In Situ Infrastructures for Enabling Extreme-scale Analysis and Visualization (ISAV 2019) held in conjunction with SC’19, Denver, USA, 2019.
- [4] Yoshiaki Yamaoka, Kengo Hayashi, Naohisa Sakamoto, Jorji Nonaka, Tsukasa Yoshinaga, Kazunori Nozaki, “Adaptive Time-Step Sampling for In-Situ Visualization”, JSFM 33th CFD Symposium, Sapporo, Japan, 2019. (in Japanese)
- [5] Yoshiaki Yamaoka, Kengo Hayashi, Naohisa Sakamoto, Jorji Nonaka, Tsukasa Yoshinaga, Kazunori Nozaki, “Adaptive In-Situ Visualization Considering Spatio-temporal changes of Large-scale Numerical Simulation Results”, JSME 97th FED Meeting, Toyohashi, Japan, 2019. (in Japanese)
- [6] Go Tamura, Naohisa Sakamoto, Yasumitsu Maejima, Jorji Nonaka, “Stochastic Isosurface Visualization for Meteorological Ensemble Data Visual Analysis”, NIFS Visualization Research Meeting (VR 2019), Toki, Japan, 2019. (in Japanese)
- [7] Naohisa Sakamoto, Jorji Nonaka, Yasumitsu Maejima, Koji Koyamada, “Transfer Entropy based Visual Causality Analysis of a Severe Rainfall Event”, VizAfrica Data Visualization Symposium 2019, Gaborone, Botswana, 2019.
- [8] Motohiko Matsuda, Hiroya Matsuba, Jorji Nonaka, Keiji Yamamoto, Hiroshi Shibata, Toshiyuki Tsukamoto, “Modeling the Existing Cooling System to Learn its Behavior for Post-K Supercomputer at RIKEN R-CCS”, Energy Efficient HPC State of the Practice Workshop (EE HPC SOP 2019) held in conjunction with ICPP 2019, Kyoto, Japan, 2019.
- [9] Angelo N. C. Vieira, Paulo S. S. Souza, Wagner S. Marques, Marcelo S. Conterato, Tiago C. Ferreto, Marcelo C. Luizelly, Arthur F. Lorenzon, Antonio C. S. B. Filho, Fabio D. Rossi, Jorji Nonaka, “The Impact of Parallel Programming Interfaces on the Aging of a Multicore Embedded Processor”, IEEE International Symposium on Circuits and Systems (ISCAS 2019), Sapporo, Japan, 2019.
- [10] Tomohiro Kawanabe, Jorji Nonaka, Daisuke Sakurai, Kazuma Hatta, Shuhei Okayama, Kenji Ono, “Showing Ultra-High-Resolution Images in VDA-Based Scalable Displays”, International Conference on Cooperative Design, Visualization and Engineering (CDVE 2019), LNCS Vol. 11792, pp. 116-122, Mallorca, Spain, 2019.

### 23.5.3 Posters

- [11] Yoshiaki Yamaoka, Naohisa Sakamoto, Jorji Nonaka, “Adaptive Spatial and Temporal Sampling for In-Situ Visualization”, 2nd R-CCS International Symposium, Kobe, Japan, 2020. (Poster)
- [12] Go Tamura, Yasumitsu Maejima, Naohisa Sakamoto, Jorji Nonaka, “Visual Analysis of Meteorological Ensemble Data Sets by using Stochastic Isosurface Visualization Technique”, 2nd R-CCS International Symposium, Kobe, Japan, 2020. (Poster)
- [13] Kazuki Koiso, Naohisa Sakamoto, Jorji Nonaka, Fumiyoshi Shoji, Keiji Yamamoto, “BiClustering and Transfer Entropy for the Visual Analysis of Critical Hardware Failures on the K computer”, IEEE Pacific Visualization Symposium (PacificVis 2019), Bangkok, Thailand, 2019. (Poster)
- [14] Naohisa Sakamoto, Jorji Nonaka, Yasumitsu Maejima, Koji Koyamada, “Visual Causal Exploration with Transfer Entropy Applied to a Severe Rainfall Event”, IEEE Pacific Visualization Symposium (PacificVis 2019), Bangkok, Thailand, 2019. (Poster)
- [15] Kazuki Koiso, Naohisa Sakamoto, Jorji Nonaka, Keiji Yamamoto, Fumiyoshi Shoji, “A Visual Causality Exploration System for HPC Hardware Failure Analysis”, 2nd R-CCS international Symposium, Kobe, Japan, 2020. (Poster)
- [16] Fumiyoshi Shoji, Jorji Nonaka, Motohiko Matsuda, Hiroya Matsuba, Keiji Yamamoto, Yasumitsu Maejima, Toshiyuki Tsukamoto, “CPU Water Cooling Temperature Effects on the Performance and Energy Consumption”, ISC 2019 HPC in Aisa Poster, Frankfurt, Germany, 2019. (Poster)
- [17] Jorji Nonaka, Keiji Yamamoto, Akiyoshi Kuroda, Toshiyuki Tsukamoto, Kazuki Koiso, Naohisa Sakamoto, “View from the Facility Operations Side on the Water/Air Cooling System of the K Computer”, SC’19 Research Poster, Denver, USA, 2019. (Poster)

- [18] Jorji Nonaka, Toshiyuki Tsukamoto, Motohiko Matsuda, Keiji Yamamoto, Akiyoshi Kuroda, Atsuya Uno, Naohisa Sakamoto, “A Brief Analysis of the K Computer by using the HPC Facility’s Water Cooling Subsystem”, 2nd R-CCS International Symposium, Kobe, Japan, 2020. (Poster)
- [19] Motohiko Matsuda, Hiroshi Shibata, Jorji Nonaka, Toshiyuki Tsukamoto, Keiji Yamamoto, Hajime Naemura, “R-CCS Facility Simulation Modeling for Assisting Operation Planning and Decision Making”, 2nd R-CCS International Symposium, Kobe, Japan, 2020. (Poster)
- [20] Tomohiro Kawanabe, Jorji Nonaka, Kenji Ono, “ChOWDER: A VDA-Based Scalable Display System for Displaying High-Resolution Visualization Results”, HPC Asia 2020, Fukuoka, Japan, 2020. (Poster)
- [21] Hiroshi Harada, Osamu Tatebe, Toshihiro Hanawa, Isamu Koseda, Hidetomo Kaneyama, Noriyuki Soda, Akira Kondo, Takahiro Yugawa, “Introduction of HPCI shared storage that has achieved year-round non-stop operation”, HPC Asia 2020, Fukuoka, Japan, 2020. (Poster)
- [22] Hiroshi Harada, Hidetomo Kaneyama, Chihiro Shibano “Incident and operation analysis of HPCI Shared Storage System R-CCS hub”, 2nd R-CCS International Symposium, Kobe, Japan, 2020. (Poster)

#### 23.5.4 Software

- [23] WHEEL : Scientific workflow Management System. (<https://gitlab.com/aicshud/WHEEL>) (Currently managed as a private repository).
- [24] ChOWDER : Scalable Display System. (<https://github.com/SIPupstreamDesign/ChOWDER>).

**Part III**

**Flagship 2020 Project**



# Chapter 24

## Flagship 2020 Project

### 24.1 Members

Primary members are only listed.

#### 24.1.1 System Software Development Team

Yutaka Ishikawa (Team Leader)  
Masamichi Takagi (Senior Scientist)  
Atsushi Hori (Senior Scientist)  
Balazs Gerofi (Senior Scientist)  
Takahiro Ogura (Research & Development Scientist)  
Fumiyoshi Shoji (Research & Development Scientist)  
Atsuya Uno (Research & Development Scientist)  
Toshiyuki Tsukamoto (Research & Development Scientist)  
Toyohisa Kameyama (Technical Staff I)  
Jie Yien (Technical Staff I)

#### 24.1.2 Architecture Development Team

Mitsuhisa Sato (Team Leader)  
Yuetsu Kodama (Senior Scientist)  
Miwako Tsuji (Research Scientist)  
Masahiro Nakao (Research Scientist)  
Jinpil Lee (Research Scientist)  
Yutaka Maruyama (Research Scientist)  
Tetsuya Odajima (Postdoctoral Researcher)  
Hitoshi Murai (Technical Scientist)  
Motohiko Matsuda (Technical Scientist)  
Itaru Kitayama (Technical Staff)  
Toshiyuki Imamura (Research Scientist)  
Kentaro Sano (Research Scientist)

Table 24.1: Development Teams

Team Name	Team Leader
Architecture Development	Mitsuhsa Sato
System Software Development	Yutaka Ishikawa
Co-Design	Junichiro Makino
Application Development	Hirofumi Tomita

### 24.1.3 Application Development

Hirofumi Tomita (Team Leader)

Yoshifumi Nakamura (Research Scientist)

Soichiro Suzuki (Research & Development Scientist)

Kazunori Mikami (Research & Development Scientist)

Kiyoshi Kumahata (Research & Development Scientist)

Mamiko Hata (Technical Staff I)

Hiroshi Ueda (Research Scientist)

Naoki Yoshioka (Research Scientist)

Yiyu Tan (Research Scientist)

### 24.1.4 Co-Design

Junichiro Makino (Team Leader)

Masaki Iwasawa (Research Scientist)

Daisuke Namekata (Postdoctoral Researcher)

Kentaro Nomura (Research Associate)

Miyuki Tsubouchi (Technical Staff)

## 24.2 Overview of Research Activities

The Japanese government launched the FLAGSHIP 2020 project <sup>1</sup> in FY 2014 whose missions are defined as follows:

- Building the Japanese national flagship supercomputer, the successor to the K computer, Fugaku supercomputer, and
- developing wide range of HPC applications that will run on the post K computer in order to solve the pressing societal and scientific issues facing our country.

RIKEN is in charge of co-design of the Fugaku supercomputer and development of application codes in collaboration with the Priority Issue institutes selected by Japanese government, as well as research aimed at facilitating the efficient utilization of the Fugaku supercomputer by a broad community of users. Under the co-design concept, RIKEN and the selected institutions are expected to collaborate closely. The official name of the Fugaku supercomputer was decided in May 2019. It is now Fugaku.

As shown in Table 24.1, four development teams are working on Fugaku supercomputer system development with the FLAGSHIP 2020 Planning and Coordination Office that supports development activities. The primary members are listed in Section 24.1.

<sup>1</sup>FLAGSHIP is an acronym for Future LAtency core-based General-purpose Supercomputer with HIgh Productivity.

The Architecture Development team designs the architecture of the Fugaku supercomputer in cooperation with Fujitsu. And, the team designs and develops a productive programming language, called XcalableMP (XMP), and its compiler, and also specifies requirements of standard languages such as Fortran and C/C++ and mathematical libraries provided by Fujitsu.

The System Software Development team designs and specifies a system software stack such as Linux, MPI and File I/O middleware for the Fugaku computer in cooperation with Fujitsu and designs and develops multi-kernel for manycore architectures, Linux with light-weight kernel (McKernel), that provides a noise-less runtime environment, extendability and adaptability for future application demands. The team also designs and develops a low-level communication layer to provide scalable, efficient and portability for runtime libraries and applications.

The Co-Design team leads to optimize architectural features and application codes together in cooperation with RIKEN teams and Fujitsu. It also designs and develops an application framework, FDPS (Framework for Developing Particle Simulator), to help HPC users implement advanced algorithms.

The Application Development team is a representative of nine institutions aimed at solving Priority Issues. The team figures out weakness of target application codes in terms of performance and utilization of hardware resources and discusses them with RIKEN teams and Fujitsu to find out best solutions of architectural features and improvement of application codes.

## 24.3 Target of System Development and Achievements in FY2019

The Fugaku's design targets are as follows:

- A one hundred times speed improvement over the K computer is achieved in maximum case of some target applications. This will be accomplished through co-design of system development and target applications for the nine Priority Issues.
- The maximum electric power consumption should be between 30 and 40 MW.

The nine priority issues successfully finished at the end of March 2019. Since this fiscal year was the last of the priority projects, we have concentrated on more accurate performance estimation regarding the nine target application, using several nodes of Fugaku. Collaborating with compiler and system software groups, we conducted the tuning and improvement of the application algorithm. We confirmed that almost all of the nine target applications would obtain their target performance within the power cap.

In FY2019, the installation of Fugaku hardware started in December. Fujitsu continued to implement and test the Fugaku software stack. The major components system software is summarized as follows:

- Highly productive programming language, XcalableMP  
XcalableMP (XMP) is a directive-based PGAS language for large scale distributed memory systems that combine HPF-like concept and OpenMP-like description with directives. Two memory models are supported: global view and local view. The global view is supported by the PGAS feature, i.e., large array is distributed to partial ones in nodes. The local view is provided by MPI-like + Coarray notation. We finished the front-end for Fortran 2008 Standard for Omni XcalableMP compiler. In 2019, we have performed the performance evaluation using the test system of Fugaku. The results are reported in Section 2.3.1. We performed the performance improvement of the communication runtime using Tofu-D. We are still working on C++ Front-end based on LLVM clang. And, we are working on the research for XcalableMP 2.0 which newly supports task-parallelism with the integration of PGAS models for distributed memory environment.
- Domain specific library/language, FDPS  
FDPS is a framework for the development of massively parallel particle simulations. Users only need to program particle interactions and do not need to parallelize the code using the MPI library. The FDPS adopts highly optimized communication algorithms and its scalability has been confirmed using the K computer.
- MPI + OpenMP programming environment  
The current de facto standard programming environment, i.e., MPI + OpenMP environment, is supported. Two MPI implementations are being developed. Fujitsu continues to support own MPI implementation based on the OpenMPI. RIKEN is collaborating with ANL (Argonne National Laboratory) to develop

MPICH, mainly developed at ANL, for Fugaku supercomputer. Achievements of our MPI implementation have been described in Section 1.3.1.

- **New file I/O middleware**  
The Fugaku supercomputer does not employ the file staging technology for the layered storage system. The users do not need to specify which files must be staging-in and staging-out in their job scripts in the Fugaku supercomputer environment. The LLIO middleware, employing asynchronous I/O and caching technologies, has been being designed by Fujitsu in order to provide transparent file access with better performance. The implementation of LLIO started in FY2017 and was completed in FY2019.
- **Application-oriented file I/O middleware**  
In scientific Big-Data applications, such as real-time weather prediction using observed meteorological data, a rapid data transfer mechanism between two jobs, ensemble simulations and data assimilation, is required to meet their deadlines. A framework called Data Transfer Framework (DTF), based on PnetCDF file I/O library, that silently replaces file I/O with sending the data directly from one component to another over network was developed.
- **Process-in-Process**  
“Process-in-Process” or “PiP” in short is a user-level runtime system for sharing an address space among processes. Unlike the Linux process model, a group of processes shares the address space and thus the process context switch among those processes does not involve hardware TLB flushing. The detailed achievement has been described in Section 1.3.2.
- **Multi-Kernel for manycore architectures**  
Multi-Kernel, Linux with light-weight Kernel (McKernel) is being designed and implemented. It provides: i) a noiseless execution environment for bulk-synchronous applications, ii) ability to easily adapt to new/future system architectures, e.g., manycore CPUs, a new process/thread management, a memory management, heterogeneous core architectures, deep memory hierarchy, etc., and iii) ability to adapt to new/future application demands, such as Big-Data and in-situ applications that require optimization of data movement. In FY2019, McKernel was ported to Arm architecture machines, Marvell’s ThunderX-2 system and the Fugaku prototype system. Section 1.3.3 describes this effort.

The architecture development team carries out the research on co-design tools as well as the design of the Fugaku supercomputer:

#### **GEM5 processor simulator for the Fugaku processor**

We are developing a cycle-level processor simulator for the Fugaku processor based on GEM-5, which is a general-purpose processor simulator commonly used for the processor architecture research. ARM provided us the source code of GEM-5 Atomic-model processor simulator for ARM v8 with Scalable Vector Extension (SVE). The Atomic model enables an instruction-level simulation. We deployed and tested it, and extend it for the cycle-level Out-Of-Order(O3) model processor simulator with the Fugaku hardware parameters. It enables the cycle-level performance evaluation of application kernels. In 2019, we continued the service to provide “Fugaku performance evaluation environment” including this simulator for performance evaluation and tuning by potential Fugaku users. We investigated the adjustment of parameters and performance with Fujitsu-in-house processor simulator and a test chip of A64FX for more accurate performance evaluation. The result are described in Section 2.3.2.

#### **Performance estimation tools for co-design study**

We have tools for co-design study for future huge-scale parallel systems. The MPI application replay tool is a system to investigate a performance and behavior of parallel applications on a single node using MPI traces. SCAMP (SCAlable Mpi Profiler) is other system to simulate a large-scale network from a small number of profiling results.

#### **Study on performance metrics**

We have been developing a new metric, called Simplified Sustained System Performance (SSSP) metric, based on a suite of simple benchmarks, which enables performance projection that correlates with applications. In 2020 (FY2019), we organized the mini-symposium in SIAM PP20 titled ”Meaningful Performance Indicators for Scientific Computing” and presented our SSSP study for the dissemination of our proposed metrics.

In addition to co-design tools, we are working on the evaluation of compilers for ARM SVE. There are two kinds of compiler for ARM SVE: Fujitsu Compiler and ARM compiler. The Fujitsu compiler is a proprietary compiler supporting C/C++ and Fortran. The ARM compiler is developed by ARM based on LLVM. Initially, LLVM only supports C and C++, and supports Fortran recently by flang. We have been evaluating the quality of code generated by both compilers with collaboration of Kyoto University. Since these compilers are still immature, we gave several feedbacks by examining the generated code. And our team carried out several collaborations with ARM compiler team on LLVM.

## 24.4 International Collaborations

### 24.4.1 DOE/MEXT Collaboration

The following research topics were performed under the DOE/MEXT collaboration MOU.

- Efficient MPI for exascale  
In this research collaboration, the next version of MPICH MPI implementation, mainly developed by Argonne National Laboratory (ANL), has been cooperatively developed. The FY2016 achievements have been described in the previous section.
- Metadata and active storage  
This research collaboration, run by the University of Tsukuba as contract, studies metadata management and active storage.
- Storage as a Service  
This research collaboration explores APIs for delivering specific storage service models. This is also run by the University of Tsukuba.
- Parallel I/O Libraries  
This research collaboration is to improve parallel netCDF I/O software for extreme-scale computing facilities at both DOE and MEXT. To do that, the RIKEN side has designed DTF as described in the previous section.
- OpenMP/XMP Runtime  
This research collaboration explores interaction of Argobots/MPI with XscalableMP and PGAS models.
- Exascale co-design and performance modeling tools  
This collaborates on an application performance modeling tools for extreme-scale applications, and shared catalog of US/JP mini-apps.
- LLVM for vectorization  
This research collaboration explores compiler techniques for vectorization on LLVM.
- Power Monitoring and Control, and Power Steering  
This research collaboration explores APIs for monitoring, analyzing, and managing power from the node to the global machine, and power steering techniques for over-provisioned systems are evaluated.

### 24.4.2 CEA

RIKEN and CEA, Commissariat à l'énergie atomique et aux énergies alternatives, signed MOU in the fields of computational science and computer science concerning high performance computing and computational science in January 2017. The following collaboration topics are selected:

- Programming Language Environment
- Runtime Environment
- Energy-aware batch job scheduler

- Large DFT calculations and QM/MM
- Application of High Performance Computing to Earthquake Related Issues of Nuclear Power Plant Facilities
- Key Performance Indicators (KPIs)
- Human Resource and Training

While continuing these topics in 2019, two new topics of particular relevance emerged from the evolving HPC landscape:

- big data and AI became increasingly important in many sectors and applications. The combination of big data and AI with numerical simulation and HPC became increasingly important
- ARM-based processors made significant breakthroughs in the HPC ecosystem, in particular with the Fujitsu A64FX processor co-designed by RIKEN, arriving in 2019.

## 24.5 Schedule and Future Plan

A prototype implementation and its basic evaluation were completed in FY2018. The hardware will be installed from the end of 2019 and the development of the system software, conducted by Fujitsu, will be finished in September 2020. The service is expected to start public operation in 2021.

## 24.6 Publications

### 24.6.1 Articles/Journal

### 24.6.2 Conference Papers

### 24.6.3 Posters

### 24.6.4 Invited Talks

- [1] Yutaka Ishikawa, “An Overview of Fugaku Supercomputer,” Russian Supercomputing Days 2019, Sep.24, 2019.
- [2] Mitsuhsisa Sato, Arm-SVE enabled post-K processor for for energy-efficiency and sustained application performance, Linaro Connect Bangkok, Tuesday, April 2, 2019.
- [3] Mitsuhsisa Sato, The post-K system and ARM-SVE enabled A64FX processor or energy-efficiency and sustained application performance, IHPCF 2019, Chengdu, China, 17 May, 2019.
- [4] Mitsuhsisa Sato, FLAGSHIP 2020 project and Supercomputer Fugaku, Post-K activities sessi in ISC 2019, Frankfurt, 17th June 2019.
- [5] Mitsuhsisa Sato, Co-design for Post -K, ARM for HPC Co-design Opportunities, ISC 2018 BOF, June 25, 201
- [6] Mitsuhsisa Sato, The post-K project and Fujitsu ARM-SVE enabled A64FX processor, VCEW 2019, Vail CO, USA, 24th June 2019.
- [7] Mitsuhsisa Sato, Update of Fugaku and FLAGSHIP 2020 project, FTJI Meing, Kashiwa,T, 28 Oct 20.
- [8] Mitsuhsisa Sato, What We Did for Co-Design in Development of Fugaku, ORAP Forum Paris, France,November 29, 2019.
- [9] Mitsuhsisa Sato, Co-Design for Fugaku. HPCAsia 2020@ Fukuoka, Jap, , Jan 17th 2019

### 24.6.5 Oral Talks

- [1] Yoshifumi Nakamura, Y. Kuramashi, H. Ohno, S. Takeda: Critical endpoints of the finite temperature QCD, Frontiers in Lattice QCD and related topics, Kyoto, Japan, Apr. 2019

[2] Yoshifumi Nakamura, Y. Kuramashi, H. Ohno, S. Takeda: Critical endpoint in the continuum limit and critical endline at  $N_t = 6$  of the finite temperature phase transition of QCD with clover fermions, the 37th international conference on lattice field theory, Wuhan, China, Jun. 2019

[3] Yoshifumi Nakamura: Towards computing the standard model of particle physics by tensor renormalization group, Tensor Network States: Algorithms and Applications (TNSAA) 2019-2020, Taipei, Taiwan, Dec. 2019

[4] Yoshifumi Nakamura: QCD Wide SIMD Library (QWS) for Fugaku, Fugaku QCD coding workshop, Kobe, Japan, Dec. 2019

#### **24.6.6 Software**

#### **24.6.7 Patents**